The Role of the M−PR_2 Fragment in Hydrophosphination: From Mechanisms to Catalysis

by

Roman Belli
B. Sc. (Honors), University of Toronto, 2014

A Thesis Submitted in Partial Fulfillment
of the Requirements for the Degree of

DOCTOR OF PHILOSOPHY

in the Department of Chemistry

Supervisory Committee

The Role of the M−PR_2 Fragment in Hydrophosphination:
From Mechanisms to Catalysis

by

Roman Belli
B.Sc. (Honors), University of Toronto, 2014

Supervisory Committee

Dr. Lisa Rosenberg, Department of Chemistry
Supervisor

Dr. Cornelia Bohne, Department of Chemistry
Departmental Member

Dr. Scott McIndoe, Department of Chemistry
Departmental Member

Dr. Rogério de Sousa, Department of Physics and Astronomy
Outside Member

Abstract

Supervisory Committee
Dr. Lisa Rosenberg, Department of Chemistry
Supervisor
Dr. Cornelia Bohne, Department of Chemistry
Departmental Member
Dr. Scott McIndoe, Department of Chemistry
Departmental Member
Dr. Rogério de Sousa, Department of Physics and Astronomy
Outside Member

In this thesis, the synthesis and reactivity of metal complexes containing phosphido (PR_2^-) and phosphenium (PR_2^+) ligands for the hydrophosphination of alkenes were investigated. The mechanisms of hydrophosphination mediated by these M-PR_2 fragments were explored.

Based on previous work in the Rosenberg group, Ru(η^5-indenyl) complexes were explored and developed as catalysts for hydrophosphination. It was determined that Ru-phosphido complexes are key intermediates in the hydrophosphination of electron-deficient alkenes. A detailed study on the mechanisms of hydrophosphination catalyzed by the phosphido complexes Ru(η^5-indenyl)(PPh_2)(L)(PPh_3) (**4a**, L = NCPh; **b**, L = PPh_2H; **c**, L = CO) was performed. Evidence for product inhibition was found for this catalyst system using Reaction Progress Kinetic Analysis. Product inhibition is consistent with the observed catalyst resting state of a complex containing product phosphines and the determination that substitution of the product phosphine from Ru is rate-limiting. The ancillary ligands (L) of **4** were found to influence catalytic activity by enabling catalyst deactivation (L = NCPh) or off-cycle processes including alkene telomerization (L = CO).

Proposed mechanisms for catalysis were devised based on these findings. These results are important mechanistic insights that will be useful for designing new catalysts for hydrophosphination.

The unprecedented viability of metal phosphenium complexes as intermediates in hydrophosphination was also explored. Three Mo phosphenium complexes were synthesized via P-H bond hydride abstraction from coordinated secondary phosphines, PR_2H. These complexes were found to mediate the stoichiometric hydrophosphination of alkenes and ketones. In particular, *trans*-$[Mo(CO)_3(PPh_2H)_2(PPh_2)]^+$ (**13**) mediates the hydrophosphination of a wide scope of alkenes that includes ethylene, propene and 1-hexene, which are challenging substrates for metal-catalyzed hydrophosphination. Preliminary attempts were conducted to render this synthetic phosphenium-mediated hydrophosphination catalytic. These results provide evidence for the putative steps of a hydrophosphination cycle utilizing metal phosphenium complexes as intermediates.

The phosphenium complexes *trans*-$[Mo(CO)_4(PR_2H)(PR_2)]$ (**12a** R = Tol^p_2, **b** R = Ph) were also investigated as Lewis acid catalysts for hydrosilylation. A tentatively-assigned η^1-$HSiEt_3$ adduct of **12a**, $[Mo(CO)_4(PTol^p_2H)(PTol^p_2\{HSiEt_3\})]$ (**20a**), was observed by low temperature $^{31}P\{^1H\}$ NMR and was studied computationally. Complex **12b** is proposed to behave as a Lewis acid catalyst for hydrosilylation. An off-cycle equilibrium is proposed that results in the formation of $EtSi^+$. This work is a unique example of P(III) Lewis acid catalysis, of which there are few examples in the literature.

Table of Contents

List of Tables

List of Figures

List of Schemes

List of Abbreviations

Å	Angstrom (1 x 10^{-10} m)
AIBN	azobisisobutyronitrile
Anal.	analysis
atm	atmosphere
Ar	aryl
BINAP	2,2'-bis(diphenylphosphine)-1,1'binaphthyl
br	broad
Bu^n	butyl, $-CH_2CH_2CH_2CH_3$
Bu^t	tert-butyl, $-C(CH_3)_3$
°C	degrees Celsius
C*	centroid
C_{ipso}	*ipso*-carbon
C_{meta}	*meta*-carbon
C_{ortho}	*ortho*-carbon
C_{para}	*para*-carbon
Calcd	calculated
cat	catalyst
$^{13}C\{^1H\}$	observed carbon while decoupling proton
ChiraPhos	(2S,3S)-(−)-bis(diphenylphosphino)butane
cm^{-1}	wavenumber
COSY	correlation spectroscopy
Cp	cyclopentadienyl group, $C_5H_5^-$
Cp*	1,2,3,4,5-Pentamethylcyclopentadienyl, $C_5(CH_3)_5^-$
Cy	cyclohexyl group, $-C_6H_{11}$
d	doublet *or* days
DBU	1,8-diazabicyclo[5.4.0]undec-7-ene
dd	doublet of doublets
ddd	doublet of doublet of doublets
dec	decomposes
deg(or °)	degrees
Δ	solid state indenyl slip parameter *or* heat
$\Delta\delta(C_{3a,7a})$	solution phase indenyl slip parameter
DEPT	distortionless enhanced polarization transfer
DFT	density functional theory
δ	NMR chemical shift in parts per million
DIPAMP	(2-methoxyphenyl)-2-[(2-methoxyphenyl) -phenylphosphino]ethyl]-phenylphosphine)
E	Element (usually main group)
equiv	equivalent(s)
ESI	electron spray ionization
Et	ethyl group, $-C_2H_5$
EXSY	exchange spectroscopy
g	gram
GEI	Global Electrophilicity Index

η^n	hapticity
h	hour(s)
^1H	observed proton
H_m	*meta*-proton
H_o	*ortho*-proton
H_p	*para*-proton
HMBC	heteronuclear multiple-bond connectivity
HMDS	bis(trimethylsilyl)amide
HSQC	heteronuclear single quantum coherence
Hz	hertz
i	iso
IR	infrared
J	scalar nuclear spin-spin coupling constant (NMR)
κ^n	denticity
K	Kelvin
kcal	kilocalorie(s)
L	liter *or* neutral donor ligand
M	molarity *or* metal
M^+	parent ion
m	mutiplet (NMR)
Me	methyl,-CH_3
Me-DuPhos	1,2-bis-((2R,5R)-2,5-dimethylphospholano)benzene
Mes	Mesitylene (1,3,5-trimethylbenzene)
mg	milligram(s)
MHz	megahertz
min	minutes(s)
mL	milliliter
mm	millimeter
mmol	millimole(s)
mol	mole(s)
mp	melting point (°C)
MS	mass spectromertry
m/z	mass to charge ratio
µL	microliter
n	normal
NMR	nuclear magnetic resonance
nOe	nuclear Overhauser effect
NOESY	nuclear Overhauser effect spectroscopy
o	ortho
om	Overlapping multiplet
^{31}P	observed phosphorus
$^{31}P\{^1H\}$	observed phosphorus wihle decoupling proton
p	para
Ph	phenyl group, -C_6H_5
ppm	parts-per-million
q	quartet

R	alkyl *or* aryl group
RPKA	Reaction Progress Kinetic Analysis
rt	room temperature
s	singlet (NMR)
T	temperature
t	triplet (NMR)
t	tertiary
td	triplet of doublets
θ	Tolman cone angle
TEPO	triethylphosphine oxide
THF	tetrahydrofuran
Tol	tolyl group, $-C_6H_4CH_3$
Tol^p	*para*-tolyl group
VT	variable temperature
VTNA	Variable Time Normalization Analysis
$\omega_{1/2}$	line width at half height
X	anionic donor ligand
X_i	Tolman electronic factor

List of Numbered Compounds

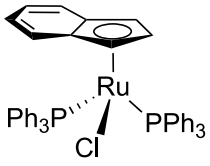

1

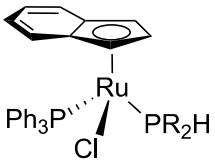

2a R = Ph
2b R = Cy

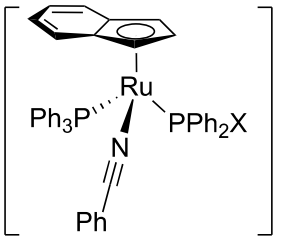

3a (X = Ph)
3b (X = H)

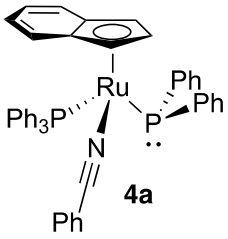

4a

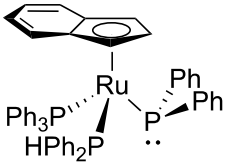

4b

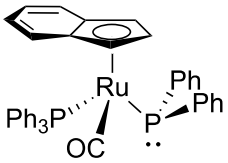

4c

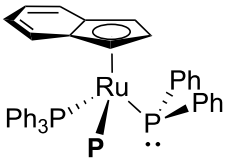

4d

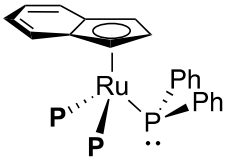

4e

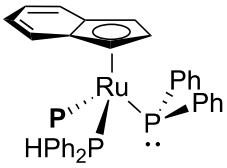

4f

P = 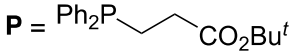

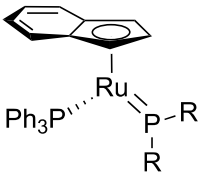

5a R = Ph
5b R = Cy

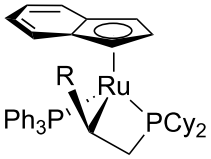

6a R = Bu^n
6b R = CN
6c R = Ph

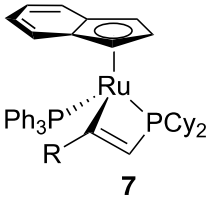

7

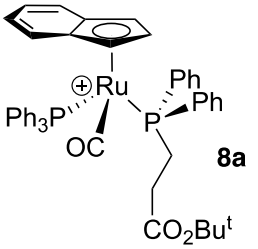

8a

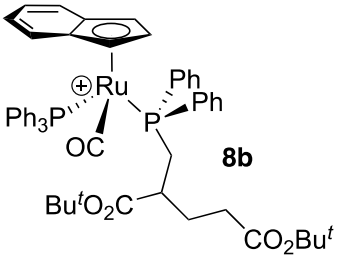

8b

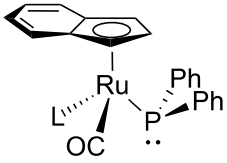

9a L = PPh_2H
9b L = **P**

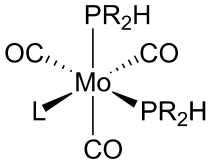

10a R = Tol^p, L = CO
10b R = Ph, L = CO
10c R = Cy, L = CO
11 R = Ph, L = PPh_2H

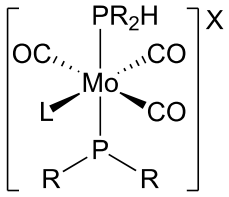

X = $B(C_6H_3Cl_2)_4$

12a R = Tol^p, L = CO
12b R = Ph, L = CO
13 R = Ph, L = PPh_2H

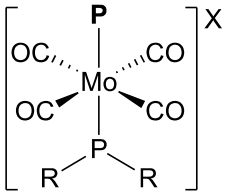

P = 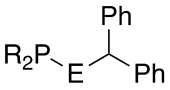

14a R = Tol^p, E = CH_2
14b R = Ph, E = CH_2
15a R = Tol^p, E = O
15b R = Ph, E = O

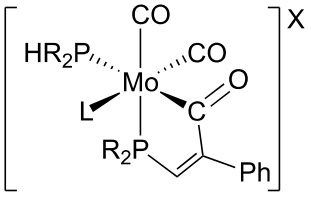

16a R = Tol^p, L = CO
16b R = Ph, L = CO
17 R = Ph, L = PPh_2H

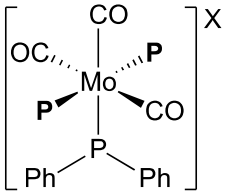

18a-h

P = 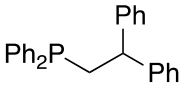

18a

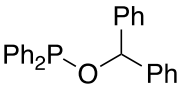

18b

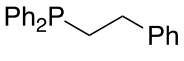

18c

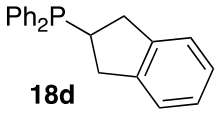

18d

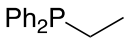

18e

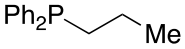

18f

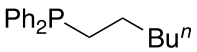

18g

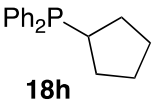

18h

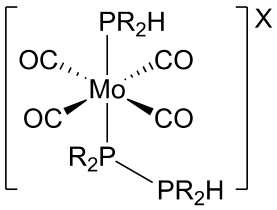

19a R = Tol^p
19b R = Ph

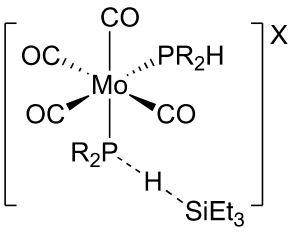

20a R = Tol^p
20b R = Ph

Acknowledgments

There are many people whom I would like to express my deepest gratitude towards for contributing to and enriching my PhD experience. First and foremost, my PhD supervisor, Dr. Lisa Rosenberg. I am extremely grateful for the knowledge she has shared with me, her thought-provoking discussions as well as her unwavering guidance and support. I am truly indebted to her for the incredible impact she has had on shaping the scientist that I have become. I would also like to thank the wonderful, past and present, Rosenberg group members whom I have had the pleasure of working with throughout my time at the University of Victoria. I would especially like to thank Jin Yang, who has been by my side from the very beginning, for his constant generosity, support and words of encouragement.

My sincere thanks also goes to my committee members. In particular, I thank Dr. Cornelia Bohne, for her helpful discussions regarding reaction kinetics, and Dr. Scott McIndoe, for his collaboration and use of his lab's electrospray-ionization mass spectrometer. I am grateful to Dr. Chris Barr for his assistance with NMR spectroscopy as well as his mentorship throughout my PhD. I would like to thank Dr. Dimitrios Pantazis from the Max Plank Institute of Catalysis for performing theoretical calculations and Dr. Robert McDonald at the University of Alberta for solving the crystal structures presented in this thesis.

Last, but not least, I am also grateful to my family and friends for their encouragement, love and support.

Chapter 1 Introduction

1.1. **Thesis Overview**

Phosphines have immense application in the fine chemicals industry (synthesis of pharmaceuticals, fragrances, agrochemicals etc.) as ligands in homogenous catalysis.[1] Despite their widespread use, traditional methods of synthesizing value-added phosphines are stoichiometric, wasteful and often require multiple steps. An attractive alternative is hydrophosphination, which is an atom economical method of synthesizing and functionalizing phosphines. Moreover, performing hydrophosphination via metal catalysis would be an efficient method of preparing phosphines. The number of examples of metal catalysts for hydrophosphination is growing, but more detailed and comprehensive studies of the mechanisms of metal-catalyzed hydrophosphination are needed in order to address current challenges in the field (activity, substrate scope, selectivity). The goal of my PhD research was to explore, investigate and develop catalytic systems for hydrophosphination. The insight gained will be useful for improving and developing future catalysts as well as for exploring new methodologies for metal-catalyzed hydrophosphination. Although outside the scope of this thesis, the insight gained from the work presented herein will also be useful for developing metal catalysts for asymmetric hydrophosphination to selectively synthesize chiral phosphines.

1.2. **Application and Value of Phosphines**

1.2.1. **Applications and Properties of Phosphines**

Phosphines (PR_3) are a ubiquitous and important class of molecules that have widespread application. These compounds are used everywhere from teaching to research laboratories and are even prepared through and used for industrial processes.[2] Arguably, the most important application of phosphines is their use as ligands in homogenous metal catalysis.[1] Other applications of phosphines include organic electronics[3,4] and organocatalysis.[5]

Phosphines are commonly used as ligands for metals because, through tuning the steric and electronic properties, by modifying the substituents (R) at P, the desired properties and reactivity of a metal centre in a catalyst can be achieved. The most well-known parameters of phosphines are the Tolman cone angle and electronic factor.[6–8] These parameters describe the ability of phosphines to influence the spatial environment around a metal and the ability of phosphines to donate/accept electron density to/from a metal, respectively. Recent examples of extensive parametrization of the steric and electronic properties of phosphines in order to accomplish desired reactivity of metal catalysts are described by Sigman[9,10] and Doyle.[11]

Besides the steric and electronic influence at a metal centre, phosphines are also important as ligands because they can introduce chirality in metal complexes. Chiral phosphines have found widespread use as ligands for stereoselective, asymmetric metal-catalyzed reactions.[12] Asymmetric catalytic reactions utilize a chiral catalyst in order to

direct the formation of one stereoisomer of a chiral product, which is of utmost importance for the fine chemicals industry. Many chiral phosphine ligands have garnered the distinction of being "privileged" ligands[13] (e.g. Figure 1.1) because of the high enantioselectivities over a wide range of reactions that are achieved when these ligands are employed in asymmetric catalysis.

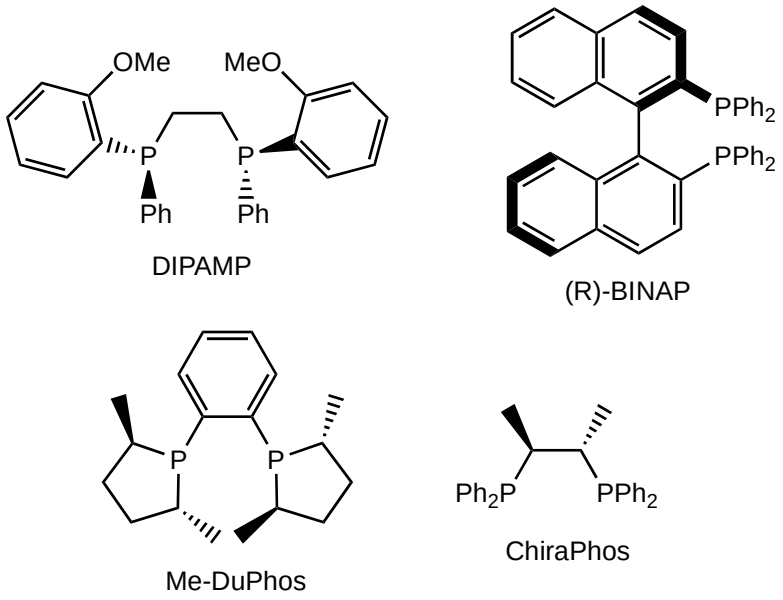

Figure 1.1. Examples of "privileged" chiral phosphine ligands for asymmetric catalysis.

1.2.2. **Value of Phosphines**

Phosphine ligands, especially "privileged" phosphines, are value-added compounds. The high cost of these ligands often originates from the syntheses of the phosphines, which are usually multistep and involve wasteful separations. Many of these ligands are also patent-protected (intellectual property rights, licensing), which also increases the cost.[14] In some cases, the phosphine ligands are just as, if not more, expensive

than the metals used in asymmetric catalysis. This is demonstrated through comparing the cost of a chiral catalyst with the cost of the chiral phosphine ligand used in the catalyst. For example, the catalyst for Noyori asymmetric hydrogenation, $RuCl_2${(S)-BINAP}[15] is $112/250 mg, whereas (S)-BINAP is $57.6/250 mg from Sigma-Aldrich; the ligand accounts for approximately half the cost of the catalyst!

1.3. **Synthesis of Phosphines**

The literature on the synthesis of P-containing compounds is vast and contains many synthetic routes.[16,17] This section focuses on methods of forming P-C bonds in the synthesis of P(III) compounds. The methods discussed are salt metathesis, cross-coupling and hydrophosphination (sections 1.3.1, 1.3.2 and 1.3.3, respectively). It is worth noting that other methods of forming P-C bonds exist. A notable example is the Michaelis-Arbuzov reaction that produces P(V) compounds, which can be subsequently reduced to P(III) compounds.[18]

1.3.1. **P-C Bond Formation via Nucleophilic Substitution**

A classic method of preparing organophosphines is stoichiometric phosphination via salt metathesis reactions using chlorophosphines, $ClPR_2$ (Scheme 1.1a) or metal phosphido reagents, MPR_2, (M = Li, Na, K) (Scheme 1.1b).[19] In both cases, P-C bond formation occurs via nucleophilic substitution, either through displacement of a halogen from phosphorus by an organometallic reagent, or substitution of a halogen from carbon by a phosphido. This chemistry has stood the test of time and is a robust, practical protocol to construct challenging P-C bonds. Many important phosphines are synthesized through

salt metathesis. For example, Buchwald phosphine ligands are prepared via salt metathesis using chlorophosphines and Grignard reagents (Scheme 1.1a).[20,21] Some of the value-added, "privileged" phosphines are also prepared through this method (Scheme 1.1b).[22]A disadvantage of the salt metathesis method is that stoichiometric amounts of metal halides are generated, which introduces an additional separation step to isolate the phosphine product.

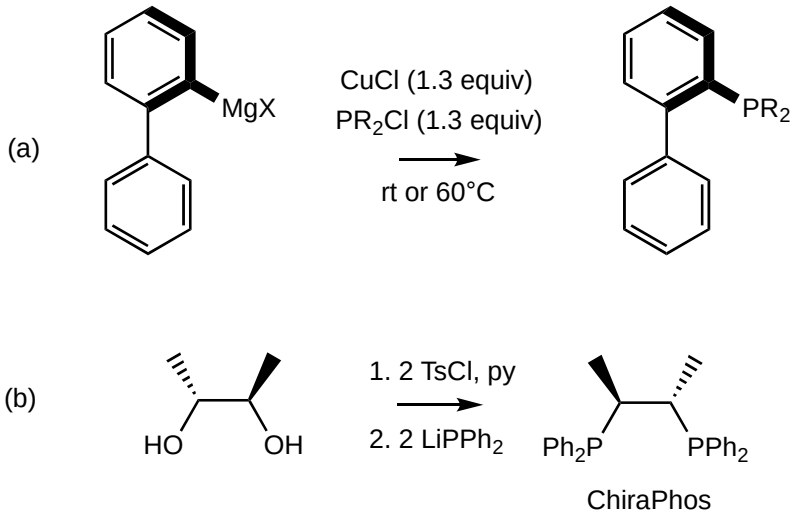

Scheme 1.1. Synthesis of (a) Buchwald phosphine ligands with a chlorophosphine, ClPR2,[20,21] and (b) ChiraPhos with $LiPPh_2$ via salt metathesis.[22]

1.3.2. **P-C Bond Formation via Metal-Catalyzed Phosphination**

Another method of preparing phosphines is metal-catalyzed phosphination via cross-coupling.[23–26] Cross-coupling of aryl- and alkyl- halides or triflates with a host of organophosphorus compounds, including primary (PRH_2) and secondary (PR_2H) aryl- and alkylphosphines,[27–33] have been reported. The metals often used are Pd, Pt or Ni.

The general proposed mechanism for metal-catalyzed phosphination (Scheme 1.2) involves oxidative addition of the organic halide to the metal (step A).[24,27] Deprotonation of a P-H bond of a metal-bound secondary phosphine generates a complex containing a phosphido ligand and a carbon-based ligand (step B). P-C bond formation via reductive elimination generates the phosphination product and regenerates the catalyst (step C). Metal-catalyzed phosphination is a powerful and useful method to prepare phosphines, but is not the most atom economical reaction. Cross-coupling reactions are usually accompanied by the formation of salt by-products ([BaseH]X in Scheme 1.2).

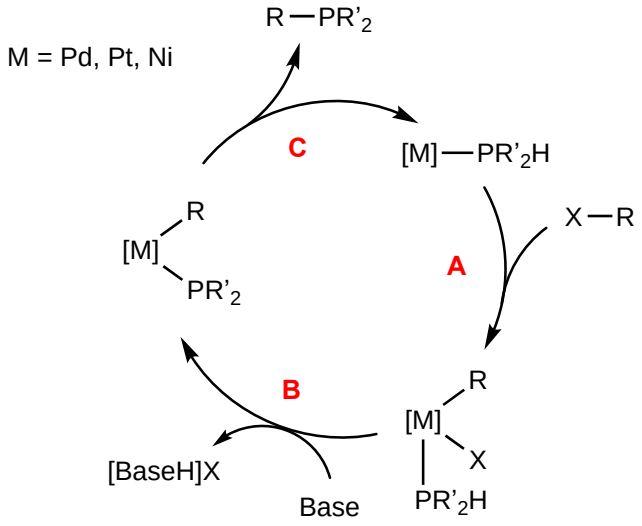

Scheme 1.2. General mechanism for metal-catalyzed phosphination.

1.3.3. **P-C Bond Formation via Hydrophosphination**

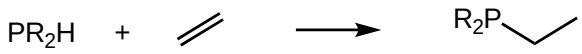

Scheme 1.3. General reaction scheme for the hydrophosphination of an alkene.

Hydrophosphination is an attractive alternative to the methods described above because it is an atom economical synthesis of phosphines (Scheme 1.3). This reaction involves the addition of a P-H bond of a primary or secondary phosphine to an unsaturated organic substrate, which results in no by-products.[34] Moreover, synthesizing phosphines through the hydrophosphination of unsaturated hydrocarbons is also advantageous because alkenes and alkynes are a large chemical feedstock.

Hydrophosphination is a facile reaction[35] in that it can occur thermally[36–38] or photochemically[39,40] or through initiation by radicals,[41–44] acids[45] or bases.[46–48] Thermal, photochemical and radical-initiated hydrophosphination occurs via homolytic cleavage of the P-H bond of a primary or secondary phosphine (Scheme 1.4, step A). The resulting phosphinyl radical adds to an alkene, which generates a carbon-centred radical (step B). The reaction propagates by hydrogen-atom abstraction from a P-H bond by the carbon-centred radical (step C). An example of this is the radical-initiated synthesis of 2-(pyrrol-1-yl)propyl-dialkylphosphines (Scheme 1.4, top).[49]

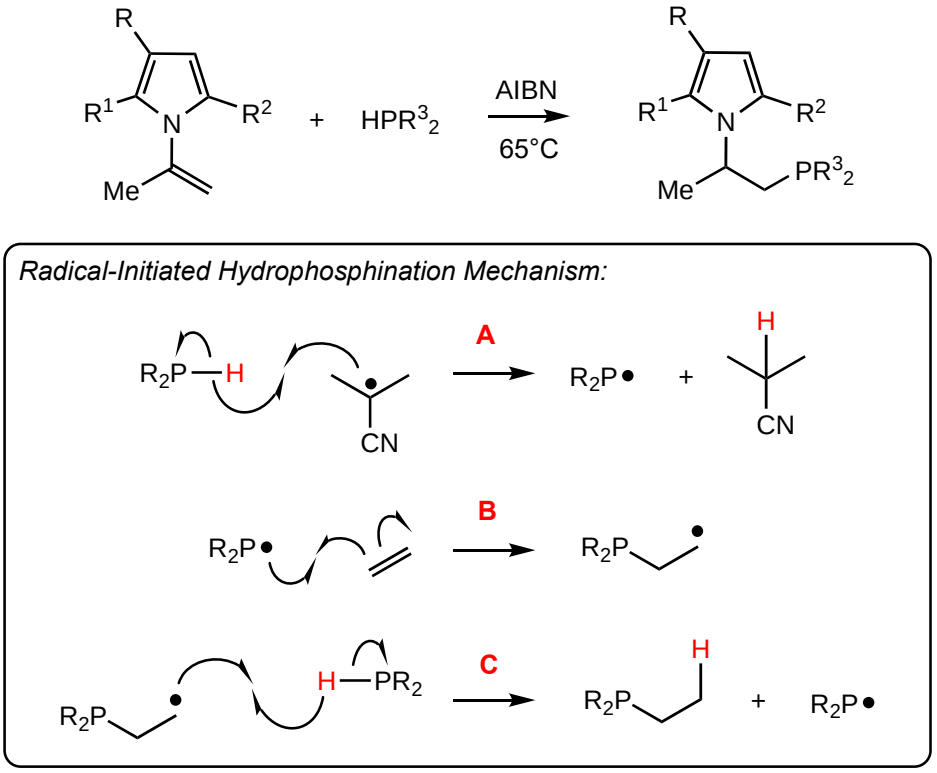

Scheme 1.4. Synthesis of 2-(pyrrol-1-yl)propyl-dialkylphosphines via radical-initiated hydrophosphination.[49]

Base-catalyzed hydrophosphination proceeds via heterolytic cleavage of the P-H bond of a primary or secondary phosphine (Scheme 1.5, step A). Deprotonation of a P-H bond generates a phosphido anion that can form P-C bonds with unsaturated substrates through conjugate addition (step B). An example of this is the base-catalyzed hydrophosphination of alkynes with PPh_2H reported by Webster *et al* (Scheme 1.5).[50] In this case, hydrophosphination of alkynes with PPh_2H resulted in the 1,1-diphosphine products.

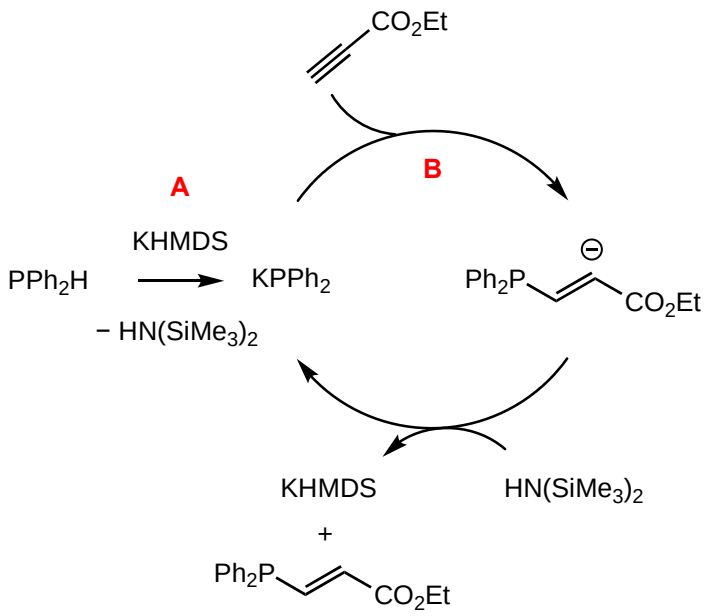

Scheme 1.5. Base-catalyzed hydrophosphination of alkynes with PPh2H. The product of the reaction shown can undergo a subsequent hydrophosphination by the same mechanism to give the 1,1-diphosphine product.[50]

These hydrophosphination methods, although facile, often lack the stereo- and regioselectivity needed for an efficient synthesis of phosphines. As shown in Scheme 1.6, P-H bond addition to unsaturated substrates can result in many products depending on the substrate. An unselective reaction would introduce additional separation steps to isolate the desired phosphine product. Thus, a metal-catalyzed hydrophosphination, which could ultimately allow for stereo- and regioselective syntheses of phosphines, would be an ideal (sustainable, efficient, cheaper) method to prepare phosphines.

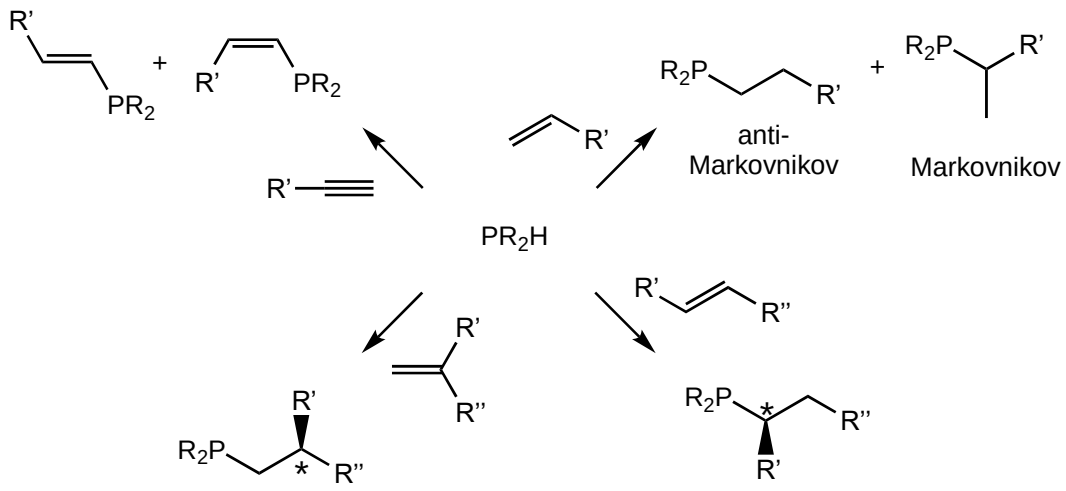

Scheme 1.6. Stereo- and regiochemical outcomes for the hydrophosphination of a variety of unsaturated substrates.

1.4. **Metal-Catalyzed Hydrophosphination**

The number of reports of metal-catalyzed hydrophosphination have been rapidly growing and recent examples have been thoroughly reviewed.[23,51–58] The proposed mechanisms of these reported examples vary with respect to how the P-H bond of the substrate phosphine is activated and how the P-C bond is formed.[59] Common to many of these examples, though, are intermediates that contain phosphido (PR_2^-) ligands. P-C bond formation with metal-phosphido (M-PR_2) complexes occurs either via inner-sphere or outer-sphere mechanisms (Scheme 1.7). Inner-sphere P-C bond formation usually involves 1,2-insertion of the unsaturated substrate into the M-PR_2 bond and is typically observed for electron-deficient metal catalysts. Outer-sphere P-C bond formation normally occurs via conjugate addition of the phosphido ligand to the unsaturated substrate and is typically observed with electron-rich metal catalysts. There is variation in the proposed mechanisms even among this dichotomy of P-C bond formation. The inner-, outer-sphere and additional

mechanisms of metal-catalyzed hydrophosphination will be discussed in sections 1.4.1, 1.4.2 and 1.4.3, respectively.

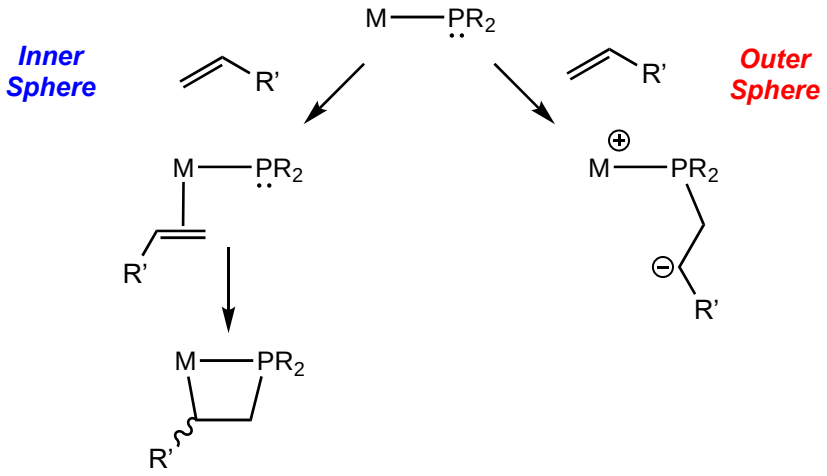

Scheme 1.7. P-C bond formation at metal-phosphido complexes via inner-sphere insertion or outer-sphere via nucleophilic attack.

1.4.1. Inner-Sphere Mechanism for Metal-Catalyzed Hydrophosphination

P-C bond formation via insertion of the unsaturated organic substrate into the M-P bond of a phosphido ligand typically occurs for the s- and f-block metal hydrophosphination catalysts (Ca, La, Sm, Y, Lu). This inner-sphere mechanism was first demonstrated for the intramolecular hydrophosphination of *α*,*ω*-alkenyl- and alkynylphosphines by lanthanide complexes reported by Marks *et al* (Scheme 1.8).[60–63]

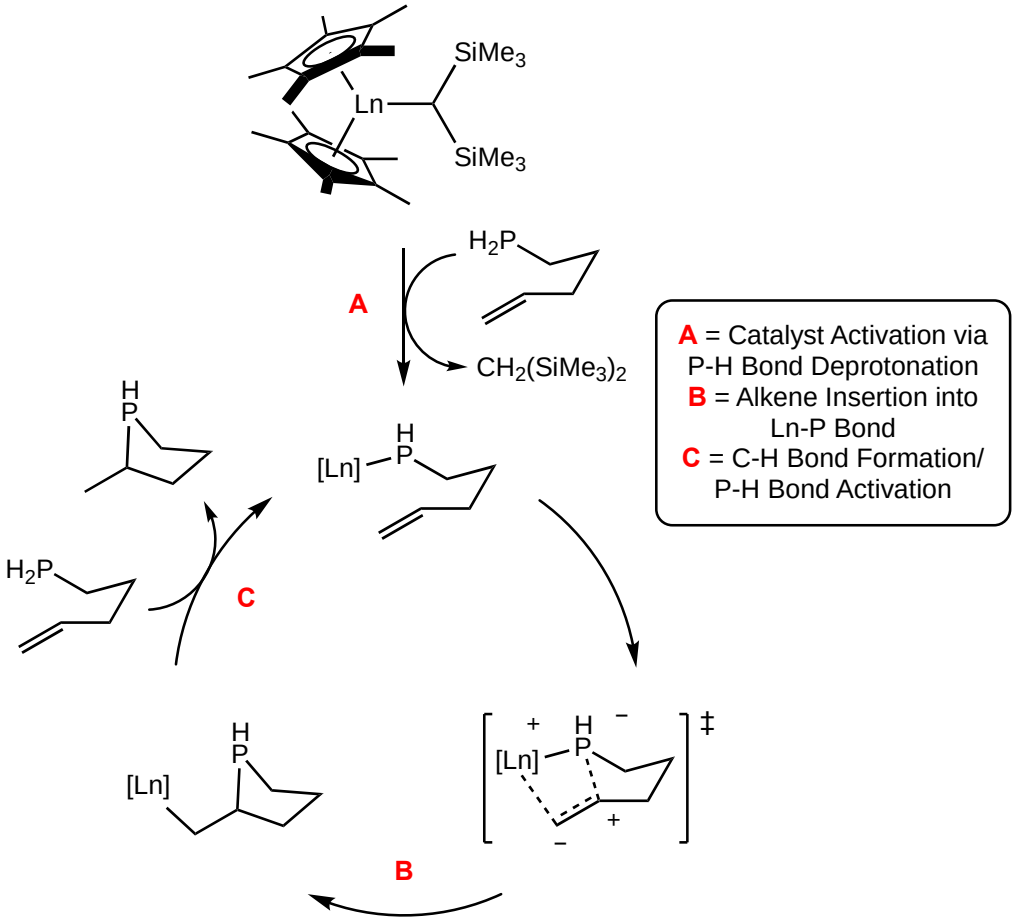

Scheme 1.8. General mechanism for the inner-sphere hydrophosphination of alkenes catalyzed by early metals.[60-63]

The proposed mechanism for Ln-catalyzed hydrophosphination involves activation of the Ln-alkyl precatalyst via σ-bond metathesis with substrate phosphine, which generates a phosphido ligand at the metal (step A). Intramolecular insertion of the pendent alkene into the Ln-P bond generates a P-C and Ln-C bond (step B). Protonolysis of the Ln-C bond via σ-bond metathesis with the P-H bond of a substrate phosphine regenerates the catalyst and liberates the hydrophosphination product. Based on a computational analysis, the authors determined that the rate-limiting step of this proposed mechanism is protonolysis of the Ln-C bond with substrate phosphine (step C).[64] This contrasts

hydroamination catalysis by this same precatalyst, which proceeds through a similar mechanism, but where alkene insertion into a Ln-imido (Ln-NR_2) is rate-limiting. The authors also determined, using a variable temperature NMR study, that the resting state of catalysis consisted of Ln phosphido complexes with either substrate or product phosphine coordinated (Scheme 1.9).[63] In order for alkene insertion to occur, the substrate or product phosphine must dissociate from Ln. This has a direct impact on the activity of catalysis and manifested in the observed product inhibition for this system, especially at high conversions.

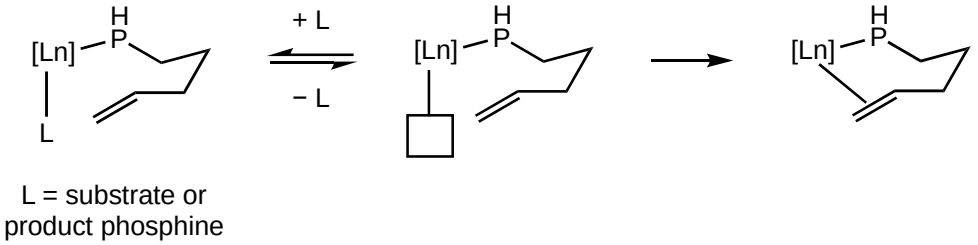

Scheme 1.9. Competition between the coordination of substrate or product phosphine with alkene.

Similar mechanisms have been proposed for the intermolecular hydrophosphination of alkenes and alkynes using other organolanthanide[57] and alkaline earth metal[65] catalysts. Intermolecular hydrophosphination differs from the intramolecular mechanism shown in Scheme 1.8 in that insertion of the unsaturated organic substrate into the M-PR_2 bond is typically rate-limiting (step B). For example, in alkaline earth metal-catalyzed hydrophosphination there is no reaction rate dependence on the concentration of substrate phosphine, which is consistent with protonolysis (step C) that precedes a rate-limiting insertion step (step B).[66] Furthermore, the reaction rates for the

hydrophosphination of *para*-substituted styrenes increases with more electron-deficient styrenes. The barrier of insertion is lower for the electron-deficient alkenes because these alkenes are pre-polarized for insertion into the polar M-P bond.

Early d-block metals are often proposed to participate in hydrophosphination catalysis via this inner-sphere mechanism. An example of this is Ti-catalyzed 1,4-hydrophosphination of 1,3-dienes with PPh_2H.[67] This example differs from the mechanism shown in Scheme 1.8 because the Ti-PPh_2 intermediate is not generated through σ-bond metathesis of the substrate phosphine with a metal-bound ligand. Instead, oxidative addition of the P-H bond of PPh_2H to Ti and subsequent H-atom transfer to another equivalent of the precatalyst generates the active Ti-PPh_2 intermediate and a Ti-H complex (Scheme 1.10).[68] The active phosphido complex is Ti^{3+}, which also distinguishes this mechanism from the others because the active species is d^1, not d^0.

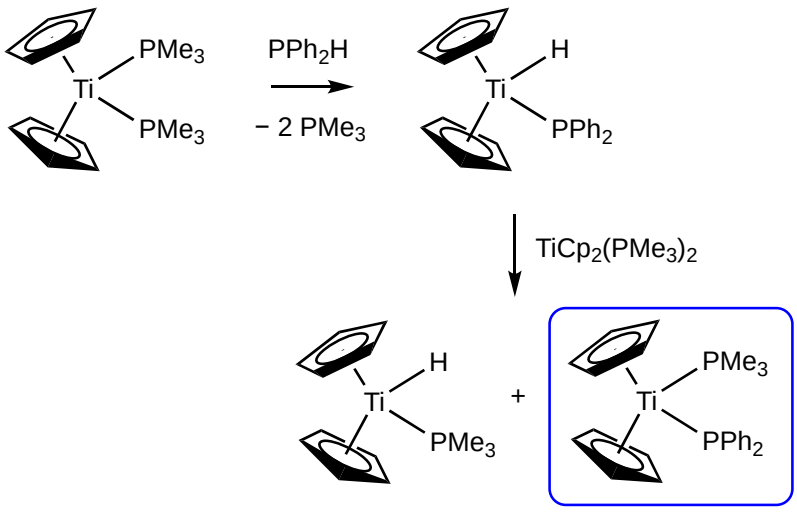

Scheme 1.10. Generation of a Ti(III)-phosphido complex.[68]

A reported zirconium-catalyzed hydrophosphination of unsaturated substrates is proposed to occur via an inner-sphere mechanism (Scheme 1.11).[69] In this case, the catalyst contains a phosphido ligand and a triamidoamine ligand. Unsaturated substrate inserts into the Zr-P bond to give a Zr-alkyl complex (step A). However, the product phosphine is not liberated via protonolysis by the substrate phosphine. Instead, protonolysis by a methyl C-H bond of a pendant N($SiMe_3$) generates the product phosphine (step B). The catalyst is regenerated by protonolysis of the resulting ligand-metallated complex with PPh_2H (step C). This catalyst can generate the secondary phosphine (single hydrophosphination) and tertiary phosphine (double hydrophosphination) products when phenylphosphine, $PPhH_2$, is used.[70] This system can be used to selectively generate the products that results from a single hydrophosphination because protonolysis (step C) is slower with secondary phosphines than with primary phosphines.

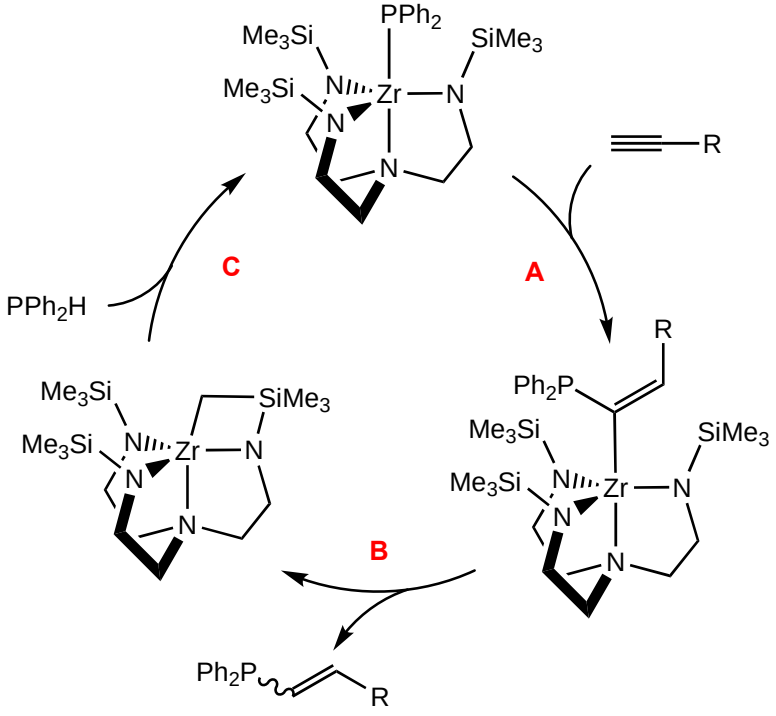

Scheme 1.11. Proposed mechanism for Zr-catalyzed hydrophosphination of alkynes.[69,70]

The authors found that the rate of the Zr-catalyzed hydrophosphination described above is increased under photocatalytic conditions.[71–73] Under irradiation, an n → d charge transfer from a P-based orbital to a Zr-based orbital occurs. The authors determined computationally that the Zr-P bond is lengthened upon this charge transfer, which they attribute to the improved activity of catalysis by lowering the barrier for insertion. Moreover, hydrophosphination is observed with challenging substrates, like unactivated alkenes, which the authors also attribute to the Zr-P bond lengthening under these conditions.

The inner-sphere mechanism for P-C bond formation discussed above is commonly proposed for catalysts that contain electron-deficient metals. Although rare, late-metal phosphido complexes can also participate in inner-sphere P-C bond formation. For example, the Rosenberg group showed that a wide scope of alkenes and alkynes (electron-rich and electron-deficient) can insert into a Ru-phosphido π-bond (Scheme 1.12).[74,75] The authors found that the insertion resulted from two distinct mechanisms.[76] Activated alkenes, which already have a polarized π-bond, can undergo direct cycloaddition to the Ru-P π-bond. Simple and electron-rich alkenes are polarized through coordination to Ru, which then undergo insertion. However, this inner-sphere insertion of unsaturated substrates into a Ru-P π-bond is not catalytic (discussed further in Chapter 2).

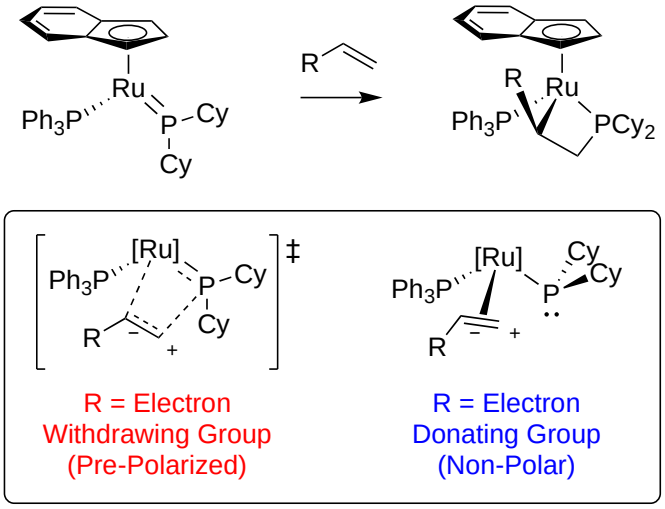

Scheme 1.12. Inner-sphere P-C bond formation of alkenes with the Ru-PR2 π-bond.[74-76]

Inner-sphere P-C bond formation has also been proposed for Fe-catalyzed hydrophosphination reported by Webster *et al* (Scheme 1.13).[77] This is an example of a d^6 metal participating in inner-sphere hydrophosphination. The proposed mechanism resembles the Ln-catalyzed hydrophosphination, but is a simplified picture as the authors also acknowledge that a radical process is operative. Addition of a radical clock, (chloromethyl)cyclopropane, to these catalytic reactions slowed down the catalysis, which suggests that radical intermediates are involved. Radical clocks are compounds that form radical intermediates on a given timescale and are used to determine the lifetime of radicals generated in reactions. The authors also used this Fe catalyst for the hydrophosphination of alkynes. The selectivity of this reaction could be tuned through the choice of solvent (Scheme 1.14).[78] The Markovnikov product forms when the reaction is performed in benzene, whereas in dichloromethane, the anti-Markovnikov product forms. The authors propose an inner-sphere mechanism for this reaction when performed in benzene and again, provide evidence for a radical process. The Markovnikov product is unusual as the

intermolecular insertion mechanisms discussed above usually give the anti-Markovnikov products. The authors propose an outer-sphere mechanism for the reaction when performed in dichloromethane that leads to the anti-Markovnikov product.

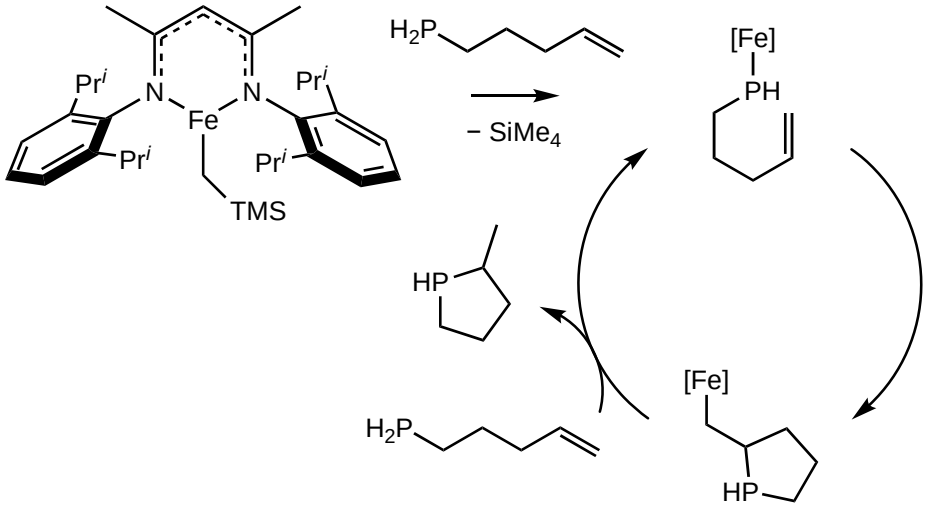

Scheme 1.13. Proposed mechanism for Fe-catalyzed intramolecular hydrophosphination.[77]

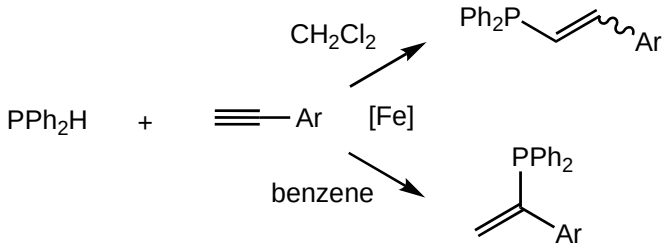

Scheme 1.14. Selectivity of Fe-catalyzed hydrophosphination of alkynes.[78]

1.4.2. **Outer-Sphere Mechanism for Metal-Catalyzed Hydrophosphination**

Phosphido ligands on late d-block metal complexes are very nucleophilic because these metals are electron-rich. Since these phosphido ligands are very nucleophilic, P-C bond formation typically occurs via outer-sphere, conjugate addition of the phosphido ligand to the unsaturated substrate. This mode of P-C bond formation usually limits the unsaturated substrate scope for these catalytic systems to activated, electron-deficient alkenes and alkynes; these are substrates that are susceptible to nucleophilic attack. Despite this outer-sphere P-C bond formation being common to many late d-block metal hydrophosphination catalysts, the other steps of catalysis (P-H bond activation, C-H bond formation) vary.

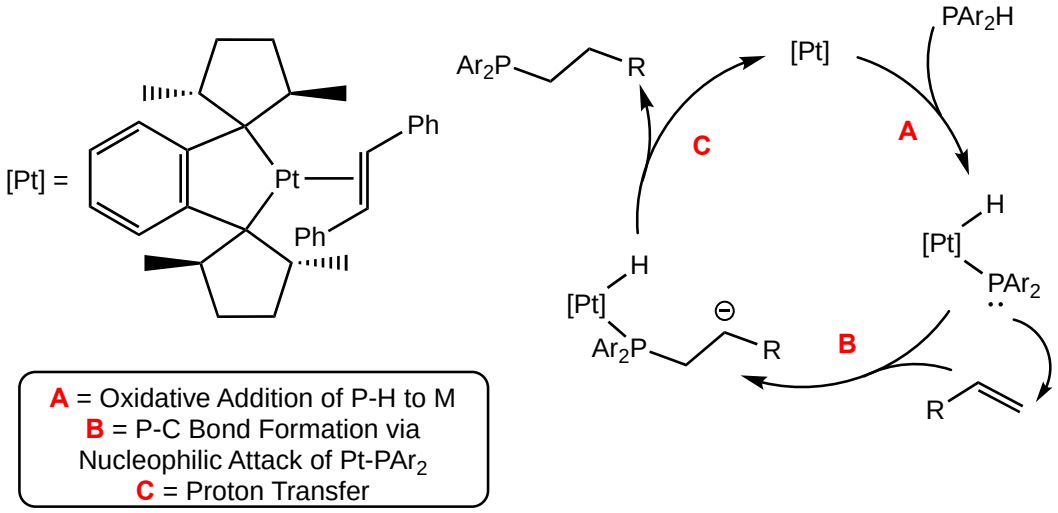

Scheme 1.15. Proposed mechanism for Pt-catalyzed hydrophosphination.[79,80]

The outer-sphere hydrophosphination mechanism was first delineated through an investigation of Pt-catalyzed hydrophosphination reported by Glueck *et al* (Scheme 1.15).[79,80] The proposed mechanism involves oxidative addition of the P-H bond of

substrate phosphine to the Pt(0) catalyst, which generates a Pt(II) intermediate with a phosphido ligand and a hydride ligand (Scheme 1.15, step A). The phosphido ligand of this intermediate participates in conjugate addition to activated alkenes, which generates a zwitterionic intermediate (step B). The carbanion of this zwitterionic intermediate is quenched by a 1,4-proton shift from Pt-H, which regenerates the Pt(0) catalyst (step C). Evidence for this outer-sphere mechanism came from the observation of telomerized hydrophosphination products (products that result from the addition of multiple equivalents of alkene) during catalysis. These products would form if, after conjugate addition of the phosphido ligand to alkene, the carbanion participates in nucleophilic attack at another equivalent of alkene (Scheme 1.16a). The authors went to great length to show that these telomerized products do not form from an alternative mechanism whereby alkene inserts into the Pt-P bond; they prepared the intermediate that would have formed from insertion of alkene into Pt-P bond and showed that additional alkene does not insert into the Pt-C bond (Scheme 1.16b). Furthermore, the authors showed that telomerization could be suppressed by the addition of a proton source ($HOBu^t$) to the catalytic reactions, which quenches the carbanion before it can participate in conjugate addition to alkene.

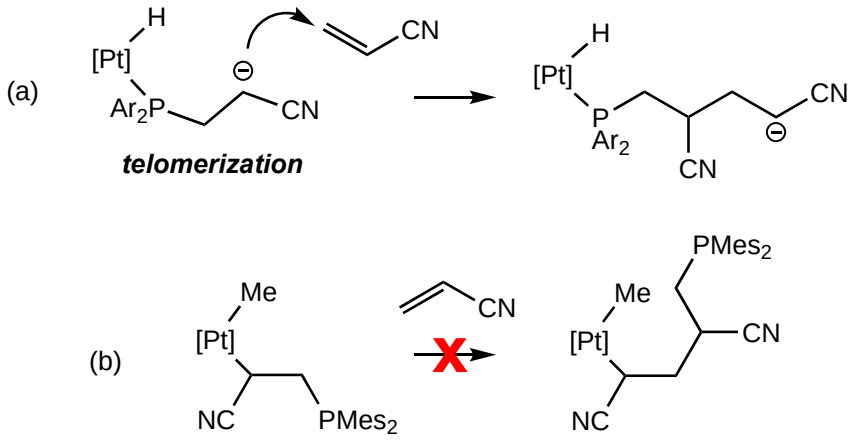

Scheme 1.16. Generation of telomerized hydrophosphination products through the outer-sphere P-C bond formation with alkenes.

A Pd-catalyzed hydrophosphination that is proposed to proceed via a similar outer-sphere mechanism has been reported and extensively exploited by Leung *et al* for the synthesis of new phosphines (Scheme 1.17).[81] The proposed mechanism differs from the mechanism reported by Glueck in that the P-H bond of the substrate phosphine is not activated via oxidative addition. In this case, P-H bond activation occurs via deprotonation of a Pd-coordinated PPh_2H by an external base co-catalyst (step A). This generates a phosphido ligand at Pd, which can participate in outer-sphere, conjugate addition to alkenes (step B). The resulting intermediate is quenched by redelivery of H^+ from the conjugate acid of the base used in step A (step C). It is worth noting that the oxidation state of Pd remains the same throughout the proposed cycle. This system has been employed for the synthesis of chiral phosphines through the asymmetric hydrophosphination of α,β- and $\alpha,\beta,\gamma,\delta$- conjugated esters and amides using chiral Pd catalysts.[82–85] The authors reports enantiomeric excesses (ee's) as high as 99 %, which are the highest reported enantioselectivities for metal-catalyzed hydrophosphination of activated alkenes.[83,86,87]

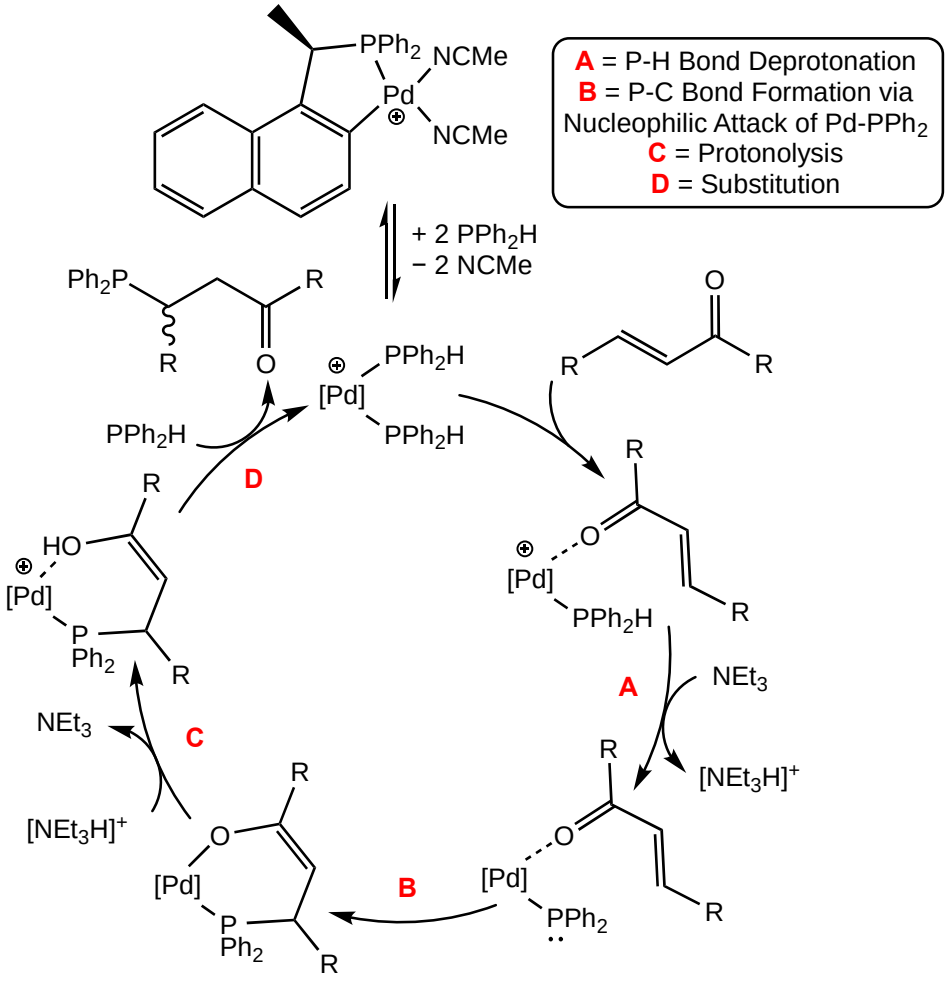

Scheme 1.17. Proposed mechanism for Pd-catalyzed hydrophosphination.[81]

A Ru-catalyzed hydrophosphination that is proposed to proceed via an outer-sphere mechanism has also been reported (Scheme 1.18).[88] In this example, the P-H bond of the substrate phosphine is activated via deprotonation, but not by an external base co-catalyst. It is proposed that the carbanion of the zwitterionic intermediate (resulting from nucleophilic attack of the Ru-PPh_2 at alkene, step A) acts as the base to deprotonate the P-

H bond of uncoordinated PPh_2H (step B). This would generate PPh_2^-, which can substitute the product phosphine from Ru to regenerate the catalyst (step C).

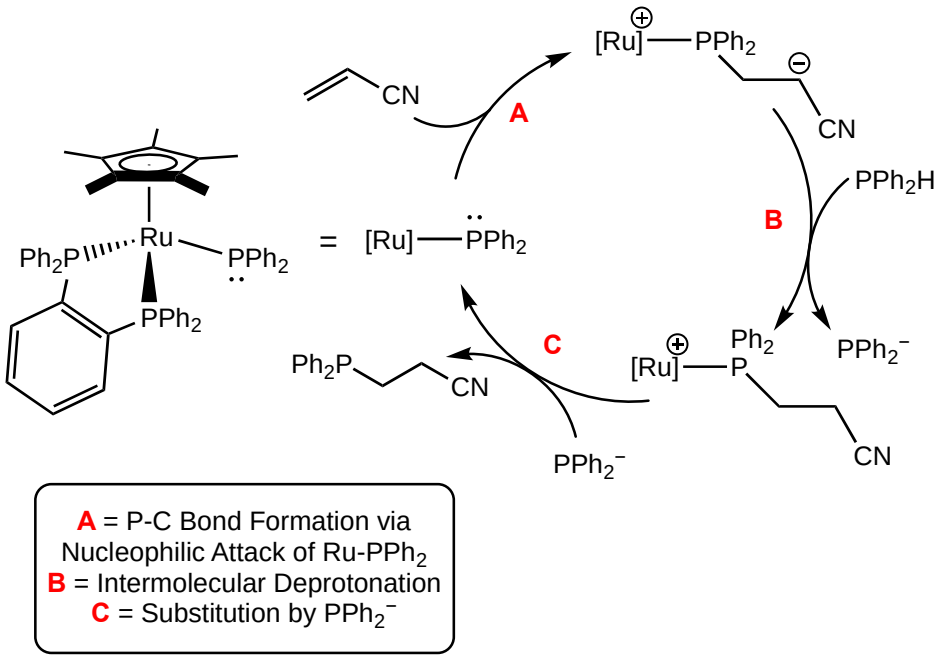

Scheme 1.18. Proposed mechanism for Ru-catalyzed hydrophosphination.[88]

1.4.3. **Other Mechanisms of Metal-Catalyzed Hydrophosphination**

The mechanisms described in sections 1.4.1. and 1.4.2. are the prevalent inner- and outer-sphere mechanisms proposed for metal-catalyzed hydrophosphination. Other mechanisms that are also considered inner- and outer-sphere are known, but deviate from the common mechanisms described above.

Inner-sphere hydrophosphination can also occur via insertion of unsaturated substrates into a M-H bond. This mechanism was first proposed for group 10 metal catalysts. An

example is the Ni(0)- and Pd(0)-catalyzed hydrophosphination reported by Beletskaya *et al* (Scheme 1.19).[89–92] Oxidative addition of the P-H bond of substrate phosphine to the M(0) catalyst generates a M(II) complex with a phosphido ligand and a hydride ligand (step A). Alkene insertion into the M-H bond generates a M-alkyl complex with a phosphido ligand (step B). Subsequent reductive elimination forms the P-C bond, which generates the hydrophosphination product and regenerates the catalyst (step C). Evidence for this mechanism comes from a computational investigation of Pd-catalyzed hydrophosphination of acetylene by PMe_2H.[93] The authors found that the barrier for insertion of acetylene into the Pd-H bond ($\Delta G^{\ddagger}$ = 0.3 kcal/mol) is lower than the barrier for insertion into the Pd-P bond ($\Delta G^{\ddagger}$ = 5.7 kcal/mol). This mechanism has also been proposed for Co[94] and Rh[95,96] catalysts.

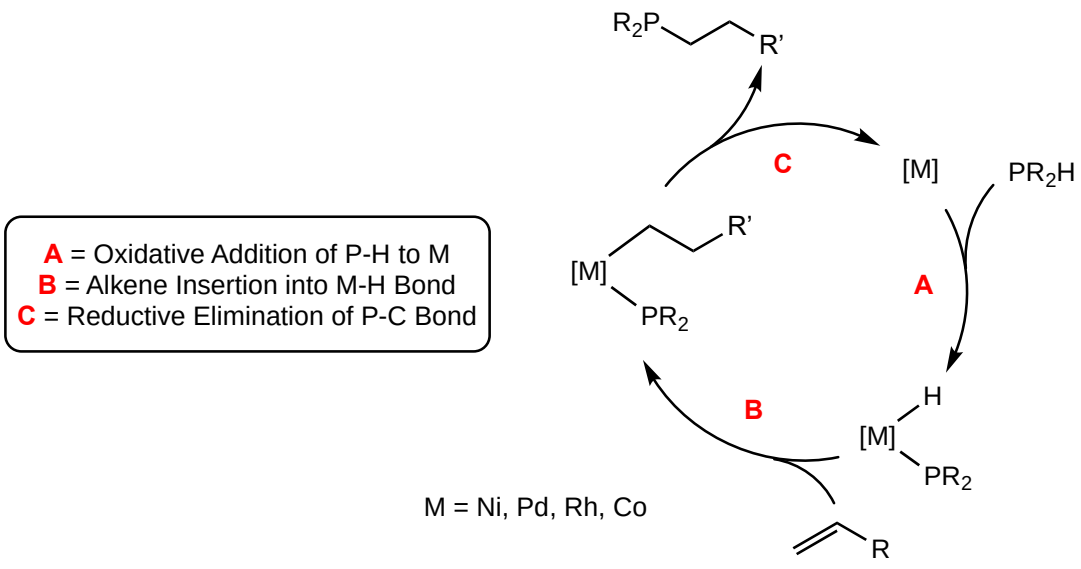

Scheme 1.19. Proposed mechanism for the hydrophosphination of alkenes involving insertion of alkene into a M-H bond (left).[89-92]

An outer-sphere mechanism is possible that does not involve phosphido ligands. An example of this is the asymmetric Ni-catalyzed hydrophosphination of methacrylonitrile reported by Togni *et al* (Scheme 1.20).[97,98] In this case, the unsaturated substrate coordinates to Ni through the nitrile N. Nucleophilic attack of the substrate phosphine at the terminal C of the coordinated substrate generates a phosphonium intermediate (step A). Subsequent proton-transfer (step B) and substitution by methacrylonitrile regenerates the catalyst (step C). This was proposed based on the author's study of hydroamination with the same Ni catalyst. Other systems that are proposed to operate through this outer-sphere mechanism have been reported (Fe, Ru, Ni, Pd).[99–101]

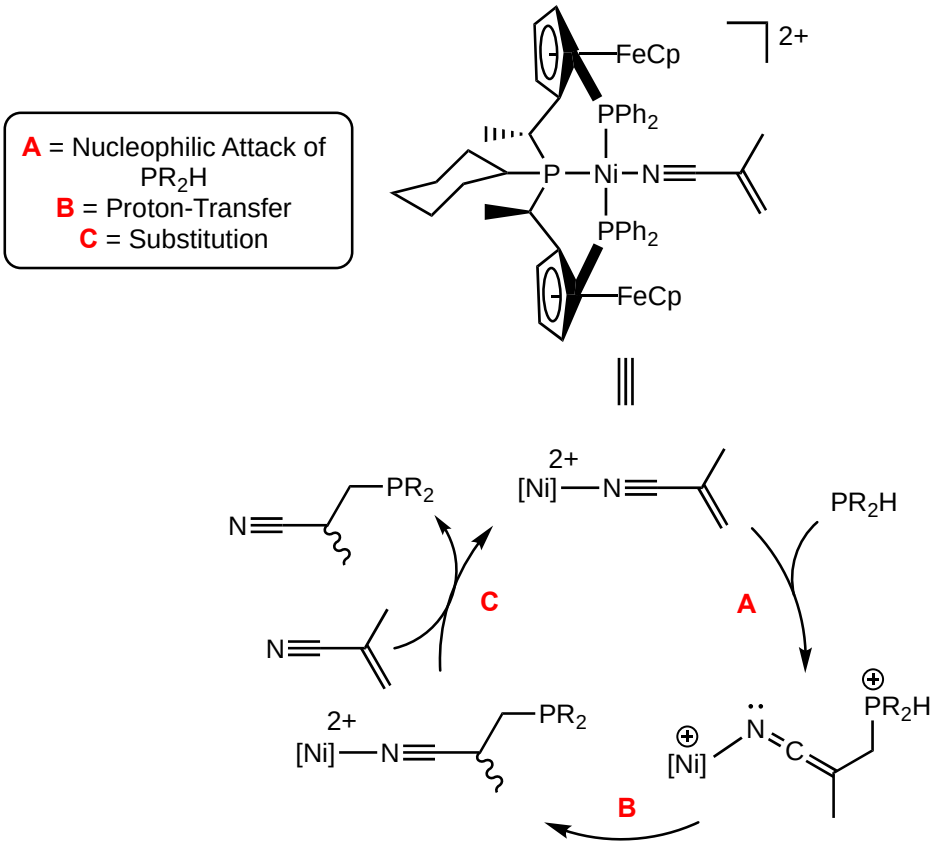

Scheme 1.20. Proposed mechanism for the asymmetric Ni-catalyzed hydrophosphination of methacrylonitrile.[97,98]

A Th-catalyzed hydrophosphination is a unique example in that insertion into a P-H bond is proposed (Scheme 1.21).[102] In this example, the precatalyst is a bis(phosphido) Th-complex that undergoes cyclometallation via elimination of mesitylphosphine, $PMesH_2$, which generates a mono(phosphido) complex (step A). Insertion of alkyne into the P-H bond of the phosphido ligand generates a new Th-complex with the functionalized phosphido ligand (step B). Protonolysis with the substrate phosphine releases the hydrophosphination product and regenerates the catalyst (step C). The direct insertion of alkyne into the P-H bond of the phosphido ligand is an unusual mechanism. Support for this insertion comes from the fact that no hydrophosphination is observed when using secondary phosphines, the phosphido derivatives of which would not have an available P-H bond for insertion.

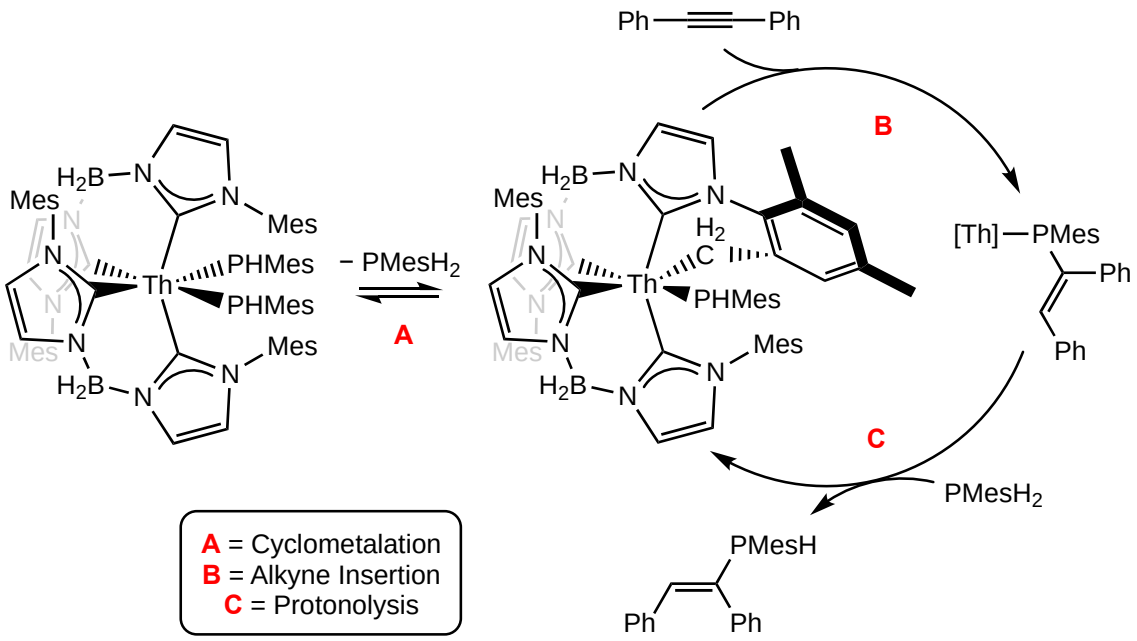

Scheme 1.21. Proposed mechanism for Th-catalyzed hydrophosphination of diphenylacetylene.[102]

Last, phosphinidenes (PR) are another low-valent P ligand that are known to participate in P-C bond formation.[103–107] An example of this is the Ti-catalyzed hydrophosphination of diphenylacetylene that employs a Ti phosphinidene intermediate (Ti=PR) reported by Mindiola *et al* (Scheme 1.22).[108] The proposed mechanism involves two σ-bond methathesis steps of the precatalyst with $PPhH_2$, which generates the active Ti phosphinidene intermediate (step A). P-C bond formation is proposed to occur via a [2+2]-cycloaddition of diphenylacetylene to the Ti=PPh bond (step B). Protonolysis of the metallacycle by $PPhH_2$ generates an intermediate containing two phosphido ligands (step C). A 1,3-proton transfer generates the product phosphine and regenerates the Ti phosphinidene intermediate (step D).

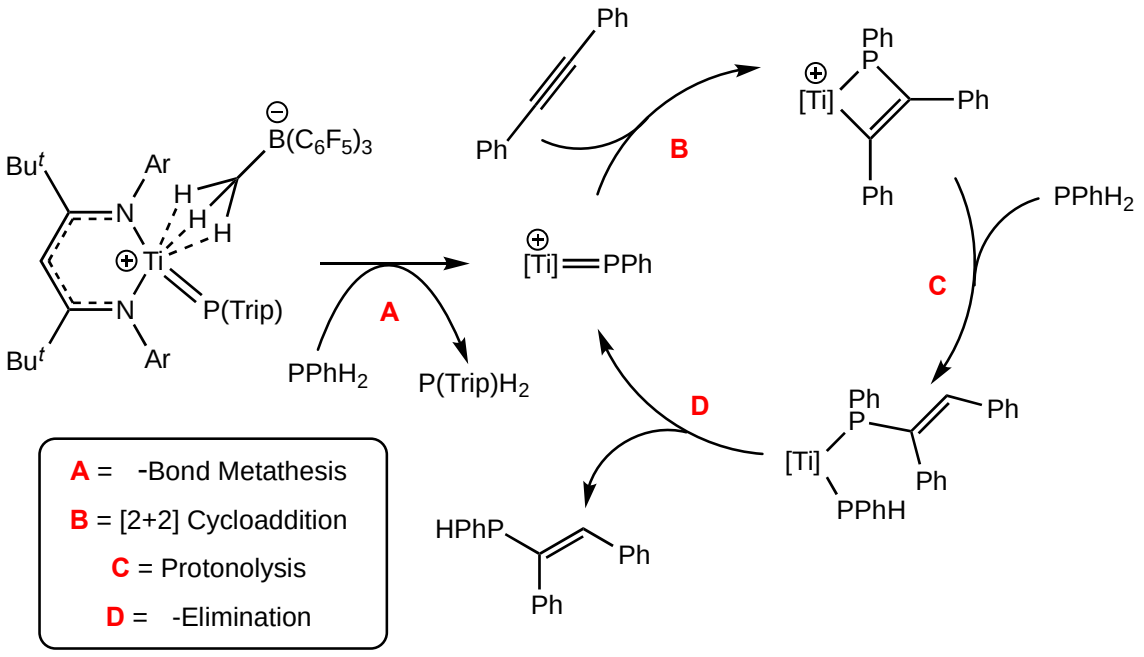

Scheme 1.22. Proposed mechanism for the Ti-catalyzed hydrophosphination of diphenylacetylene that involves a Ti phosphinidene intermediate.[108]

1.5. **Challenges in Metal-Catalyzed Hydrophosphination**

One of the earliest examples of metal-catalyzed hydrophosphination was the Pt-catalyzed hydrophosphination of acrylonitrile reported by Pringle *et al* in 1990.[109] Since this seminal report, as demonstrated in this Chapter, the field has progressed to include a growing number of metal catalysts that participate in hydrophosphination through an array of proposed mechanisms. Despite the progress made, many challenges still exist for metal-catalyzed hydrophosphination, which can only be addressed through a thorough understanding of the mechanism of catalysis.[110] Addressing these challenges represents areas for growth in this field and is paramount to improving the breadth and application of metal-catalyzed hydrophosphination.

A particular area for growth is the limited scope of both unsaturated substrates and phosphines that have been reported for metal-catalyzed hydrophosphination. Many examples of metal-catalyzed hydrophosphination use activated, electron-deficient alkenes and alkynes. This is particularly true for late-metal catalysts that participate in P-C bond formation via the outer-sphere, conjugate addition mechanism described in section 1.4.2. In terms of the phosphine substrates, almost all examples are reported using aromatic phosphines like PPh_2H. Thus, developing a metal catalyst system that can perform the hydrophosphination of a wide scope of unsaturated substrates with a variety of phosphines is of utmost importance.

Examples of metal-catalyzed hydrophosphination, in general, suffer from low catalytic activities, which is conceivably due to product inhibition. As discussed in section 1.2.1.

phosphines are good ligands for metals. Thus it is plausible that the product phosphine and substrate phosphine could coordinate to the metal catalysts used. Addressing product inhibition may be crucial for developing highly active catalysts for hydrophosphination.

Another challenge to tackle is selectivity in hydrophosphination. In terms of regioselectivity, most examples of metal-catalyzed hydrophosphination of alkenes and alkynes afford the anti-Markovnikov products. The field lacks examples of stereoselective hydrophosphination, which is needed to develop metal-catalyzed hydrophosphination for the synthesis of chiral phosphines. That being said, Leung *et al* have made considerable contributions to this area in their reports of asymmetric Pd-catalyzed hydrophosphination of electron-deficient alkenes (discussed in section 1.4.2).

New methodologies (new catalyst designs, different reactive intermediates, different reaction conditions etc.) are needed in order to address the challenges discussed. Discovering and developing these innovative methodologies is only possible through a thorough and deep understanding of the fundamental mechanisms that are operative. The Zr-photocatalyzed hydrophosphination described in section 1.4.1. is an example of using mechanistic insight to address a challenge. Through studying the photophysical properties of a catalytic intermediate, the authors were able to improve the activity and breadth of catalysis under photocatalytic conditions. Furthermore, mechanistic insight can address issues of selectivity. This is demonstrated by the Fe-catalyzed hydrophosphination discussed in section 1.4.1. where the authors could tune the selectivity of the hydrophosphination by accessing different mechanisms in different solvents.

1.6. **Scope of Thesis**

The overall goal of this thesis was to address challenges in metal-catalyzed hydrophosphination through understanding the mechanisms of catalysis. Through undertaking this work, I attempted to address issues related to low activity and limited alkene substrate scope in metal-catalyzed hydrophosphination.

Chapter 2 describes the identification and development of Ru(η^5-indenyl) complexes for the catalytic hydrophosphination of activated alkenes. In this work, I determined that Ru complexes that contain phosphido ligands are key intermediates and viable catalyst precursors for the hydrophosphination of activated alkenes. In Chapter 3, a detailed kinetic and mechanistic analysis of three Ru(η^5-indenyl) complexes that contain phosphido ligands is described. Through this work, I definitively showed that the Ru catalysts studied are susceptible to product inhibition. I also demonstrated that ancillary ligands can impact catalysis by enabling deactivation and off-cycle pathways.

Chapter 4 explores the viability of using metal phosphenium complexes as intermediates in metal-catalyzed hydrophosphination. Phospheniums are PR_2 ligands, like phosphido ligands, but are electrophilic rather than nucleophilic. The purpose for this shift in focus was to investigate whether metal complexes that contain electrophilic phosphenium ligands could participate in hydrophosphination with simple and electron-rich alkenes. The synthesis of three Mo complexes containing phosphenium ligands is described. These complexes undergo stoichiometric hydrophosphination with simple, unactivated alkenes. Attempts to exploit this for catalytic hydrophosphination are

described. Chapter 5 describes the use of these metal-phosphenium complexes as Lewis acid catalysts for the hydrosilylation of alkenes.

The final chapter, Chapter 6, provides plans for completing and publishing the projects presented in Chapter 3, 4 and 5. Furthermore, ideas for future work for each of the projects described in this thesis is presented.

1.7. **References**

(1) Pignolet, L. M. *Homogeneous Catalysis with Metal Phosphine Complexes*; Plenum Publishing Corporation: New York, 1983.

(2) Svara, J.; Weferling, N.; Hofmann, T. Phosphorus Compounds, Organic. *Ullmann's Encyclopedia of Industrial Chemistry*. December 15, 2006.

(3) Shameem, M. A.; Orthaber, A. Organophosphorus Compounds in Organic Electronics. *Chem. Eur. J.* **2016**, *22*, 10718–10735.

(4) Duffy, M. P.; Delaunay, W.; Bouit, P.-A.; Hissler, M. π-Conjugated Phospholes and Their Incorporation into Devices: Components with a Great Deal of Potential. *Chem. Soc. Rev.* **2016**, *45*, 5296–5310.

(5) Guo, H.; Fan, Y. C.; Sun, Z.; Wu, Y.; Kwon, O. Phosphine Organocatalysis. *Chem. Rev.* **2018**, *118*, 10049–10293.

(6) Tolman, C. A. Steric Effects of Phosphorus Ligands in Organometallic Chemistry and Homogeneous Catalysis. *Chem. Rev.* **1977**, *77*, 313–348.

(7) Tolman, C. A. Electron Donor-Acceptor Properties of Phosphorus Ligands. Substituent Additivity. *J. Am. Chem. Soc.* **1970**, *92*, 2953–2956.

(8) Bartik, T.; Himmler, T.; Schulte, H.-G.; Seevogel, K. Substituenteneinflüsse Auf Die Basizität von Phosphorliganden in R_3P-$Ni(CO)_3$-Komplexen. *J. Organomet. Chem.* **1984**, *272*, 29–41.

(9) Niemeyer, Z. L.; Milo, A.; Hickey, D. P.; Sigman, M. S. Parameterization of Phosphine Ligands Reveals Mechanistic Pathways and Predicts Reaction Outcomes. *Nat. Chem.* **2016**, *8*, 610.

(10) Zhao, S.; Gensch, T.; Murray, B.; Niemeyer, Z. L.; Sigman, M. S.; Biscoe, M. R.

Enantiodivergent Pd-Catalyzed C–C Bond Formation Enabled through Ligand Parameterization. *Science* **2018**, *362* (6415), 670 – 674.

(11) Wu, K.; Doyle, A. G. Parameterization of Phosphine Ligands Demonstrates Enhancement of Nickel Catalysis via Remote Steric Effects. *Nat. Chem.* **2017**, *9*, 779.

(12) Crépy, K. V. L.; Imamoto, T. New P-Chirogenic Phosphine Ligands and Their Use in Catalytic Asymmetric Reactions. In *New Aspects in Phosphorus Chemistry III*; Majoral, J.-P., Ed.; Springer Berlin Heidelberg: Berlin, Heidelberg, 2003; pp 1–40.

(13) Zhuo, Q.-. L. *Privileged Chiral Ligands and Catalysts*; WILEY-VCH Verlag: Weinheim, 2011.

(14) Thommen, M.; Blaser, H.-U. Sourcing Chiral Ligands - Issues and Solutions *Chimica Oggi*, **2003**, *21*, 6−8.

(15) Takaya, H.; Ohta, T.; Sayo, N.; Kumobayashi, H.; Akutagawa, S.; Inoue, S.; Kasahara, I.; Noyori, R. Enantioselective Hydrogenation of Allylic and Homoallylic Alcohols. *J. Am. Chem. Soc.* **1987**, *109*, 1596–1597.

(16) Wauters, I.; Debrouwer, W.; Stevens, C. V. Preparation of Phosphines through C-P Bond Formation. *Beilstein J Org Chem* **2014**, *10*, 1064–1096.

(17) Balueva, A. S.; Musina, E. I.; Karasik, A. A. Phosphines: Preparation, Reactivity and Applications. In *Organophosphorus Chemistry;* The Royal Society of Chemistry, 2018; pp 1–49.

(18) Bhattacharya, A. K.; Thyagarajan, G. Michaelis-Arbuzov Rearrangement. *Chem. Rev.* **1981**, *81*, 415–430.

(19) Pietrusiewicz, K. M.; Zablocka, M. Preparation of Scalemic P-Chiral Phosphines

and Their Derivatives. *Chem. Rev.* **1994**, *94*, 1375–1411.

(20) Tomori, H.; Fox, J. M.; Buchwald, S. L. An Improved Synthesis of Functionalized Biphenyl-Based Phosphine Ligands. *J. Org. Chem.* **2000**, *65*, 5334–5341.

(21) Kaye, S.; Fox, J. M.; Hicks, F. A.; Buchwald, S. L. The Use of Catalytic Amounts of CuCl and Other Improvements in the Benzyne Route to Biphenyl-Based Phosphine Ligands. *Adv. Synth. Catal.* **2001**, *343*, 789–794.

(22) Fryzuk, M. D.; Bosnich, B. Asymmetric Synthesis. Production of Optically Active Amino Acids by Catalytic Hydrogenation. *J. Am. Chem. Soc.* **1977**, *99*, 6262–6267.

(23) Glueck, D. Recent Advances in Metal-Catalyzed C–P Bond Formation. In *C-X Bond Formation*; Vigalok, A.; Springer Berlin Heidelberg, 2010; pp 65–100.

(24) Schwan, A. L. Palladium Catalyzed Cross-Coupling Reactions for Phosphorus–Carbon Bond Formation. *Chem. Soc. Rev.* **2004**, *33*, 218–224.

(25) Zhang, H.; Zhang, X.-Y.; Dong, D.-Q.; Wang, Z.-L. Copper-Catalyzed Cross-Coupling Reactions for C–P Bond Formation. *RSC Adv.* **2015**, *5*, 52824–52831.

(26) Tappe, F. M. J.; Trepohl, V. T.; Oestreich, M. Transition-Metal-Catalyzed C-P Cross-Coupling Reactions. *Synthesis* **2010**, *18*, 3037–3062.

(27) Chan, V. S.; Chiu, M.; Bergman, R. G.; Toste, F. D. Development of Ruthenium Catalysts for the Enantioselective Synthesis of P-Stereogenic Phosphines via Nucleophilic Phosphido Intermediates. *J. Am. Chem. Soc.* **2009**, *131*, 6021–6032.

(28) Chan, V. S.; Bergman, R. G.; Toste, F. D. Pd-Catalyzed Dynamic Kinetic Enantioselective Arylation of Silylphosphines. *J. Am. Chem. Soc.* **2007**, *129*, 15122–15123.

(29) Chan, V. S.; Stewart, I. C.; Bergman, R. G.; Toste, F. D. Asymmetric Catalytic Synthesis of P-Stereogenic Phosphines via a Nucleophilic Ruthenium Phosphido Complex. *J. Am. Chem. Soc.* **2006**, *128*, 2786–2787.

(30) Anderson, B. J.; Guino-o, M. A.; Glueck, D. S.; Golen, J. A.; DiPasquale, A. G.; Liable-Sands, L. M.; Rheingold, A. L. Platinum-Catalyzed Enantioselective Tandem Alkylation/Arylation of Primary Phosphines. Asymmetric Synthesis of P-Stereogenic 1-Phosphaacenaphthenes. *Org. Lett.* **2008**, *10*, 4425–4428.

(31) Blank, N. F.; Moncarz, J. R.; Brunker, T. J.; Scriban, C.; Anderson, B. J.; Amir, O.; Glueck, D. S.; Zakharov, L. N.; Golen, J. A.; Incarvito, C. D.; et al. Palladium-Catalyzed Asymmetric Phosphination. Scope, Mechanism, and Origin of Enantioselectivity. *J. Am. Chem. Soc.* **2007**, *129*, 6847–6858.

(32) Hosseinian, A.; Hosseini Nasab, F. A.; Ahmadi, S.; Rahmani, Z.; Vessally, E. Decarboxylative Cross-Coupling Reactions for P(O)–C Bond Formation. *RSC Adv.* **2018**, *8*, 26383–26398.

(33) Julienne, D.; Delacroix, O.; Gaumont, A.-C. An Overview of the Synthesis of Alkenylphosphines. *Curr. Org. Chem.* **2010**, *14*, 457–482.

(34) Quin, L. D. *A Guide to Organophosphorus Chemistry*; Wiley: Hoboken, NJ, 2000.

(35) Delocroix, O. Hydrophosphination of Unactivated Alkenes, Dienes and Alkynes: A Versatile and Valuable Approach for the Synthesis of Phosphines. *Curr. Org. Chem.* **2005**, *9*, 1851–1882.

(36) Alonso, F.; Moglie, Y.; Radivoy, G.; Yus, M. Solvent- and Catalyst-Free Regioselective Hydrophosphanation of Alkenes. *Green Chem.* **2012**, *14*, 2699–2702.

(37) Moglie, Y.; González-Soria, M. J.; Martín-García, I.; Radivoy, G.; Alonso, F. Catalyst- and Solvent-Free Hydrophosphination and Multicomponent Hydrothiophosphination of Alkenes and Alkynes. *Green Chem.* **2016**, *18*, 4896–4907.

(38) Gusarova, N. K.; Chernysheva, N. A.; Trofimov, B. A. Catalyst- and Solvent-Free Addition of the P-H Species to Alkenes and Alkynes: A Green Methodolody for C-P Bond Formation. *Synthesis* **2017**, *49*, 4783–4807.

(39) Jimenez, M. V.; Perez-Torrente, J. J.; Bartolome, M. I.; Oro, L. A. Convenient Methods for the Synthesis of a Library of Hemilabile Phosphines. *Synthesis* **2009**, *11*, 1916–1922.

(40) Stiles, A. R.; Rust, F. F.; Vaughan, W. E. The Preparation of Organo-Phosphines by the Addition of Phosphine to Unsaturated Compounds. *J. Am. Chem. Soc.* **1952**, *74*, 3282–3284.

(41) Arbuzova, S. N.; Gusarova, N. K.; Trofimov, B. A. Nucleophilic and Free-Radical Additions of Phosphines and Phosphine Chalcogenides to Alkenes and Alkynes. *ARKIVOC* **2006**, 12–36.

(42) Trofimov, B. A.; Malysheva, S. F.; Parshina, L. N.; Gusarova, N .K.; Belogorlova, N. A. Metal-Free Hydrophosphanation of 1-Vinylimidazoles with Secondary Phosphanes: A Straightforward Atom-Economic Route to Tertiary Phosphanes with Imidazolyl Substituents. *Synlett* **2011**, *1*, 94–98.

(43) Daeffler, C. S.; Grubbs, R. H. Radical-Mediated Anti-Markovnikov Hydrophosphonation of Olefins. *Org. Lett.* **2011**, *13*, 6429–6431.

(44) Leca, D.; Fensterbank, L.; Lacôte, E.; Malacria, M. Recent Advances in the Use of

Phosphorus-Centered Radicals in Organic Chemistry. *Chem. Soc. Rev.* **2005**, *34*, 858–865.

(45) Dombek, B. D. Acid-Catalyzed Addition of Secondary Phosphines to Vinyl Ethers. *J. Org. Chem.* **1978**, *43*, 3408–3409.

(46) Semenzin, D.; Etemad-Moghadam, G.; Albouy, D.; Diallo, O.; Koenig, M. Dual Radical/Polar Pudovik Reaction: Application Field of New Activation Methods. *J. Org. Chem.* **1997**, *62*, 2414–2422.

(47) Perrier, A.; Comte, V.; Moïse, C.; Richard, P.; Le Gendre, P. NBuLi-Mediated Hydrophosphination: A Simple Route to Valuable Organophosphorus Compounds. *European J. Org. Chem.* **2010**, *2010*, 1562–1568.

(48) Bunlaksananusorn, T.; Knochel, P. T-BuOK-Mediated Hydrophosphination of Functionalized Alkenes: A Novel Synthesis of Chiral P,N- and P,P-Ligands. *J. Org. Chem.* **2004**, *69*, 4595–4601.

(49) Trofimov, B. A.; Gusarova, N. K.; Sukhov, B. G.; Malysheva, S. F.; Tarasova, O. A.; Belogorlova, N. A.; Maximova, M. A.; Tunik, S. P. Atom-Economic, Solvent-Free, High Yield Synthesis of 2-(Pyrrol-1-yl)Propyldiorganylphosphines. *Synthesis* **2005**, *6*, 965–970.

(50) Coles, N. T.; Mahon, M. F.; Webster, R. L. 1,1-Diphosphines and Divinylphosphines via Base Catalyzed Hydrophosphination. *Chem. Commun.* **2018**, *54*, 10443–10446.

(51) Pullarkat, S.; Leung, P.-H. Chiral Metal Complex-Promoted Asymmetric Hydrophosphinations. In *Hydrofunctionalization*; Ananikov, V. P., Tanaka, M.; Springer Berlin Heidelberg, 2013; pp 145–166.

(52) Koshti, V.; Gaikwad, S.; Chikkali, S. H. Contemporary Avenues in Catalytic PH Bond Addition Reaction: A Case Study of Hydrophosphination. *Coord. Chem. Rev.* **2014**, *265*, 52–73.

(53) Greenhalgh, M. D.; Jones, A. S.; Thomas, S. P. Iron-Catalysed Hydrofunctionalisation of Alkenes and Alkynes. *ChemCatChem* **2015**, *7*, 190–222.

(54) Bezzenine-Lafollée, S.; Gil, R.; Prim, D.; Hannedouche, J. First-Row Late Transition Metals for Catalytic Alkene Hydrofunctionalisation: Recent Advances in C-N, C-O and C-P Bond Formation. *Molecules* **2017**, 1901−1930.

(55) Rodriguez-Ruiz, V.; Carlino, R.; Bezzenine-Lafollee, S.; Gil, R.; Prim, D.; Schulz, E.; Hannedouche, J. Recent Developments in Alkene Hydro-Functionalisation Promoted by Homogeneous Catalysts Based on Earth Abundant Elements: Formation of C-N, C-O and C-P Bond. *Dalton Trans.* **2015**, *44*, 12029–12059.

(56) Pullarkat, S. A. Recent Progress in Palladium-Catalyzed Asymmetric Hydrophosphination. *Synthesis* **2016**, *48*, 493–503.

(57) Trifonov, A. A.; Basalov, I. V; Kissel, A. A. Use of Organolanthanides in the Catalytic Intermolecular Hydrophosphination and Hydroamination of Multiple C–C Bonds. *Dalton Trans.* **2016**, *45*, 19172–19193.

(58) Hill, M. S.; Liptrot, D. J.; Weetman, C. Alkaline Earths as Main Group Reagents in Molecular Catalysis. *Chem. Soc. Rev.* **2016**, *45*, 972–988.

(59) Rosenberg, L. Mechanisms of Metal-Catalyzed Hydrophosphination of Alkenes and Alkynes. *ACS Catal.* **2013**, *3*, 2845–2855.

(60) Douglass, M. R.; Ogasawara, M.; Hong, S.; Metz, M. V; Marks, T. J. "Widening the Roof": Synthesis and Characterization of New Chiral C1-Symmetric

Octahydrofluorenyl Organolanthanide Catalysts and Their Implementation in the Stereoselective Cyclizations of Aminoalkenes and Phosphinoalkenes. *Organometallics* **2002**, *21*, 283–292.

(61) Douglass, M. R.; Marks, T. J. Organolanthanide-Catalyzed Intramolecular Hydrophosphination/Cyclization of Phosphinoalkenes and Phosphinoalkynes. *J. Am. Chem. Soc.* **2000**, *122*, 1824–1825.

(62) Kawaoka, A. M.; Douglass, M. R.; Marks, T. J. Homoleptic Lanthanide Alkyl and Amide Precatalysts Efficiently Mediate Intramolecular Hydrophosphination/Cyclization. Observations on Scope and Mechanism. *Organometallics* **2003**, *22*, 4630–4632.

(63) Douglass, M. R.; Stern, C. L.; Marks, T. J. Intramolecular Hydrophosphination/Cyclization of Phosphinoalkenes and Phosphinoalkynes Catalyzed by Organolanthanides: Scope, Selectivity, and Mechanism. *J. Am. Chem. Soc.* **2001**, *123*, 10221–10238.

(64) Motta, A.; Fragalà, I. L.; Marks, T. J. Energetics and Mechanism of Organolanthanide-Mediated Phosphinoalkene Hydrophosphination/Cyclization. A Density Functional Theory Analysis. *Organometallics* **2005**, *24*, 4995–5003.

(65) Sarazin, Y.; Carpentier, J.-F. Calcium, Strontium and Barium Homogeneous Catalysts for Fine Chemicals Synthesis. *Chem. Rec.* **2016**, *16*, 2482–2505.

(66) Liu, B.; Roisnel, T.; Carpentier, J.-F.; Sarazin, Y. Heteroleptic Alkyl and Amide Iminoanilide Alkaline Earth and Divalent Rare Earth Complexes for the Catalysis of Hydrophosphination and (Cyclo)Hydroamination Reactions. *Chem. Eur. J.* **2013**, *19*, 13445–13462.

(67) Perrier, A.; Comte, V.; Moïse, C.; Le Gendre, P. First Titanium-Catalyzed 1,4-Hydrophosphination of 1,3-Dienes. *Chem. Eur. J.* **2010**, *16*, 64–67.

(68) Shu, R.; Hao, L.; Harrod, J. F.; Woo, H.-G.; Samuel, E. Heterodehydrocoupling of Phosphines and Silanes Catalyzed by Titanocene: A Novel Route to the Formation of Si−P Bonds. *J. Am. Chem. Soc.* **1998**, *120*, 12988–12989.

(69) Roering, A. J.; Leshinski, S. E.; Chan, S. M.; Shalumova, T.; MacMillan, S. N.; Tanski, J. M.; Waterman, R. Insertion Reactions and Catalytic Hydrophosphination by Triamidoamine-Supported Zirconium Complexes. *Organometallics* **2010**, *29*, 2557–2565.

(70) Ghebreab, M. B.; Bange, C. A.; Waterman, R. Intermolecular Zirconium-Catalyzed Hydrophosphination of Alkenes and Dienes with Primary Phosphines. *J. Am. Chem. Soc.* **2014**, *136*, 9240–9243.

(71) Bange, C. A.; Waterman, R. Zirconium-Catalyzed Intermolecular Double Hydrophosphination of Alkynes with a Primary Phosphine. *ACS Catal.* **2016**, *6*, 6413–6416.

(72) Bange, C. A.; Conger, M. A.; Novas, B. T.; Young, E. R.; Liptak, M. D.; Waterman, R. Light-Driven, Zirconium-Catalyzed Hydrophosphination with Primary Phosphines. *ACS Catal.* **2018**, *8*, 6230–6238.

(73) Novas, B. T.; Bange, C. A.; Waterman, R. Photocatalytic Hydrophosphination of Alkenes and Alkynes Using Diphenylphosphine and Triamidoamine-Supported Zirconium. *Eur. J. Inorg. Chem.* **2019**, *2019*, 1640–1643.

(74) Derrah, E. J.; Pantazis, D. A.; McDonald, R.; Rosenberg, L. Concerted [2+2] Cycloaddition of Alkenes to a Ruthenium–Phosphorus Double Bond. *Angew.*

Chem. Int. Ed. **2010**, *49*, 3367–3370.

(75) Derrah, E. J.; McDonald, R.; Rosenberg, L. The [2+2] Cycloaddition of Alkynes at a Ru-P π-Bond. *Chem. Commun.* **2010**, *46*, 4592–4594.

(76) Burton, K. M. E.; Pantazis, D. A.; Belli, R. G.; McDonald, R.; Rosenberg, L. Alkene Insertions into a Ru–PR_2 Bond. *Organometallics* **2016**, *35*, 3970–3980.

(77) Espinal-Viguri, M.; King, A. K.; Lowe, J. P.; Mahon, M. F.; Webster, R. L. Hydrophosphination of Unactivated Alkenes and Alkynes Using Iron(II): Catalysis and Mechanistic Insight. *ACS Catal.* **2016**, *6*, 7892–7897.

(78) King, A. K.; Gallagher, K. J.; Mahon, M. F.; Webster, R. L. Markovnikov versus Anti-Markovnikov Hydrophosphination: Divergent Reactivity Using an Iron(II) β-Diketiminate Pre-Catalyst. *Chem. Eur. J.* **2017**, *23*, 9039–9043.

(79) Scriban, C.; Kovacik, I.; Glueck, D. S. A Protic Additive Suppresses Formation of Byproducts in Platinum-Catalyzed Hydrophosphination of Activated Olefins. Evidence for P−C and C−C Bond Formation by Michael Addition. *Organometallics* **2005**, *24*, 4871–4874.

(80) Scriban, C.; Glueck, D. S.; Zakharov, L. N.; Kassel, W. S.; DiPasquale, A. G.; Golen, J. A.; Rheingold, A. L. P−C and C−C Bond Formation by Michael Addition in Platinum-Catalyzed Hydrophosphination and in the Stoichiometric Reactions of Platinum Phosphido Complexes with Activated Alkenes. *Organometallics* **2006**, *25*, 5757–5767.

(81) (a) Yap, J. S. L.; Li, B. Bin; Wong, J.; Li, Y.; Pullarkat, S. A.; Leung, P.-H. Development of a Novel Chiral Palladacycle and Its Application in Asymmetric Hydrophosphination Reaction. *Dalton Trans.* **2014**, *43*, 5777–5784. (b) Tay, W.

S.; Yang, X.-Y.; Li, Y.; Pullarkat, S. A.; Leung, P.-H. Investigating Palladium Pincer Complexes in Catalytic Asymmetric Hydrophosphination and Hydroarsination. *Dalton Trans.* **2019**, *48*, 4602–4610. (c) Yang, X.-Y.; Jia, Y.-X.; Tay, W. S.; Li, Y.; Pullarkat, S. A.; Leung, P.-H. Mechanistic Insights into the Role of PC- and PCP-Type Palladium Catalysts in Asymmetric Hydrophosphination of Activated Alkenes Incorporating Potential Coordinating Heteroatoms. *Dalton Trans.* **2016**, *45*, 13449–13455. (d) Chew, R. J.; Teo, K. Y.; Huang, Y.; Li, B.-B.; Li, Y.; Pullarkat, S. A.; Leung, P.-H. Enantioselective Phospha-Michael Addition of Diarylphosphines to β,γ-Unsaturated α-Ketoesters and Amides. *Chem. Commun.* **2014**, *50*, 8768–8770, and referenences therein.

(82) Yang, X.-Y.; Gan, J. H.; Li, Y.; Pullarkat, S. A.; Leung, P.-H. Palladium Catalyzed Asymmetric Hydrophosphination of α, β- and α, β,γ,δ- Unsaturated Malonate Esters - Efficient Control of Reactivity, Stereo- and Regio-Selectivity. *Dalton Trans.* **2015**, *44*, 1258–1263.

(83) Li, X.-R.; Yang, X.-Y.; Li, Y.; Pullarkat, S. A.; Leung, P.-H. Efficient Access to a Designed Phosphapalladacycle Catalyst via Enantioselective Catalytic Asymmetric Hydrophosphination. *Dalton Trans.* **2017**, *46*, 1311–1316.

(84) Yang, X.-Y.; Tay, W. S.; Li, Y.; Pullarkat, S. A.; Leung, P.-H. Versatile Syntheses of Optically Pure PCE Pincer Ligands: Facile Modifications of the Pendant Arms and Ligand Backbones. *Organometallics* **2015**, *34*, 1582–1588.

(85) Li, X.-R.; Chen, Y.; Pang, B. P.; Tan, J.; Li, Y.; Pullarkat, S. A.; Leung, P.-H. Efficient Synthesis of Malonate Functionalized Chiral Phosphapalladacycles and Their Catalytic Evaluation in Asymmetric Hydrophosphination of Chalcone. *Eur.*

J. Inorg. Chem. **2018**, *2018*, 4385–4390.

(86) Yen Wong, E. H.; Jia, Y.-X.; Li, Y.; Pullarkat, S. A.; Leung, P.-H. Catalytic Asymmetric Synthesis of Pt- and Pd-PCP Pincer Complexes Bearing a Para-N Pyridinyl Backbone. *J. Organomet. Chem.* **2018**, *862*, 22–27.

(87) Yang, X.-Y.; Tay, W. S.; Li, Y.; Pullarkat, S. A.; Leung, P.-H. Asymmetric 1,4-Conjugate Addition of Diarylphosphines to α,β,γ,δ-Unsaturated Ketones Catalyzed by Transition-Metal Pincer Complexes. *Organometallics* **2015**, *34*, 5196–5201.

(88) Sues, P. E.; Lough, A. J.; Morris, R. H. Reactivity of Ruthenium Phosphido Species Generated through the Deprotonation of a Tripodal Phosphine Ligand and Implications for Hydrophosphination. *J. Am. Chem. Soc.* **2014**, *136*, 4746–4760.

(89) Shulyupin, M. O.; Kazankova, M. A.; Beletskaya, I. P. Catalytic Hydrophosphination of Styrenes. *Org. Lett.* **2002**, *4*, 761–763.

(90) Kazankova, M. A.; Shulyupin, M. O.; Borisenko, A. A.; Beletskaya, I. P. Synthesis of Alkyl(Diphenyl)Phosphines by Hydrophosphination of Vinylarenes Catalyzed by Transition Metal Complexes. *Russ. J. Org. Chem.* **2002**, *38*, 1479–1484.

(91) Ananikov, V. P.; Makarov, A. V; Beletskaya, I. P. Catalytic Hydrofunctionalization of Alkynes through P-H Bond Addition: The Unique Role of Orientation and Properties of the Phosphorus Group in the Insertion Step. *Chem. Eur. J.* **2011**, *17*, 12623–12630.

(92) A. Kazankova, M.; V. Efimova, I.; N. Kochetkov, A.; V. Afanas'ev, V.; P. Beletskaya, I.; Dixneuf, P. New Approach to Vinylphosphines Based on Pd- and Ni-Catalyzed Diphenylphosphine Addition to Alkynes. *Synlett*, **2001**, 497−500.

(93) Ananikov, V. P.; Beletskaya, I. P. Alkyne Insertion into the M-P and M-H Bonds

(M=Pd, Ni, Pt, and Rh): A Theoretical Mechanistic Study of the C-P and C-H Bond-Formation Steps. *Chem. Asian J.* **2011**, *6*, 1423–1430.

(94) Rajpurohit, J.; Kumar, P.; Shukla, P.; Shanmugam, M.; Shanmugam, M. Mechanistic Investigation of Well-Defined Cobalt Catalyzed Formal E-Selective Hydrophosphination of Alkynes. *Organometallics* **2018**, *37*, 2297–2304.

(95) Di Giuseppe, A.; De Luca, R.; Castarlenas, R.; Pérez-Torrente, J. J.; Crucianelli, M.; Oro, L. A. Double Hydrophosphination of Alkynes Promoted by Rhodium: The Key Role of an N-Heterocyclic Carbene Ligand. *Chem. Commun.* **2016**, *52*, 5554–5557.

(96) Geer, A. M.; Serrano, Á. L.; de Bruin, B.; Ciriano, M. A.; Tejel, C. Terminal Phosphanido Rhodium Complexes Mediating Catalytic P-P and P-C Bond Formation. *Angew. Chem. Int. Ed.* **2015**, *54*, 472–475.

(97) Sadow, A. D.; Haller, I.; Fadini, L.; Togni, A. Nickel(II)-Catalyzed Highly Enantioselective Hydrophosphination of Methacrylonitrile. *J. Am. Chem. Soc.* **2004**, *126*, 14704–14705.

(98) Sadow, A. D.; Togni, A. Enantioselective Addition of Secondary Phosphines to Methacrylonitrile: Catalysis and Mechanism. *J. Am. Chem. Soc.* **2005**, *127*, 17012–17024.

(99) A. Kazankova, M.; O. Shulyupin, M.; P. Beletskaya, I. Catalytic Hydrophosphination of Alkenylalkyl Ethers. *Synlett*, **2003**, 2155-2158.

(100) Routaboul, L.; Toulgoat, F.; Gatignol, J.; Lohier, J.-F.; Norah, B.; Delacroix, O.; Alayrac, C.; Taillefer, M.; Gaumont, A.-C. Iron-Salt-Promoted Highly Regioselective α and β Hydrophosphination of Alkenyl Arenes. *Chem. Eur. J.*

2013, *19*, 8760–8764.

(101) Jérôme, F.; Monnier, F.; Lawicka, H.; Dérien, S.; Dixneuf, P. H. Ruthenium Catalyzed Regioselective Hydrophosphination of Propargyl Alcohols. *Chem. Commun.* **2003**, 6, 696–697.

(102) Garner, M. E.; Parker, B. F.; Hohloch, S.; Bergman, R. G.; Arnold, J. Thorium Metallacycle Facilitates Catalytic Alkyne Hydrophosphination. *J. Am. Chem. Soc.* **2017**, *139*, 12935–12938.

(103) Courtemanche, M.-A.; Transue, W. J.; Cummins, C. C. Phosphinidene Reactivity of a Transient Vanadium P≡N Complex. *J. Am. Chem. Soc.* **2016**, *138*, 16220–16223.

(104) Waterman, R.; Hillhouse, G. L. Group Transfer from Nickel Imido, Phosphinidene, and Carbene Complexes to Ethylene with Formation of Aziridine, Phosphirane, and Cyclopropane Products. *J. Am. Chem. Soc.* **2003**, *125*, 13350–13351.

(105) Waterman, R.; Hillhouse, G. L. Formation of Phosphirenes by Phosphinidene Group-Transfer Reactions from (Dtbpe)NiP(Dmp) to Alkynes. *Organometallics* **2003**, *22*, 5182–5184.

(106) Zhao, X.; Lu, Z.; Wang, Q.; Wei, D.; Lu, Y.; Duan, Z.; Mathey, F. Blocking Intramolecular Cycloadditions between C≡C Triple Bonds and Electrophilic Phosphinidene Complexes: Generation of Intermediates Able To React with Arenes. *Organometallics* **2016**, *35*, 3440–3443.

(107) Rani, M. Application of Terminal Electrophilic Phosphinidene Complexes. *Synlett* **2008**, *13*, 2078–2079.

(108) Zhao, G.; Basuli, F.; Kilgore, U. J.; Fan, H.; Aneetha, H.; Huffman, J. C.; Wu, G.; Mindiola, D. J. Neutral and Zwitterionic Low-Coordinate Titanium Complexes Bearing the Terminal Phosphinidene Functionality. Structural, Spectroscopic, Theoretical, and Catalytic Studies Addressing the Ti−P Multiple Bond. *J. Am. Chem. Soc.* **2006**, *128*, 13575–13585.

(109) Pringle, P. G.; Smith, M. B. Platinum(0)-Catalysed Hydrophosphination of Acrylonitrile. *J. Chem. Soc. Chem. Commun.* **1990**, 23, 1701–1702.

(110) Bange, C. A.; Waterman, R. Challenges in Catalytic Hydrophosphination. *Chem. Eur. J.* **2016**, *22*, 12598–12605.

Chapter 2 Investigation of Indenyl Ruthenium Complexes as Hydrophosphination Catalysts

2.1. Chapter Overview

In this chapter, the development and competency of indenyl ruthenium complexes as catalysts for the hydrophosphination of electron-deficient alkenes with secondary phosphines is described. All catalyst precursors were prepared from Ru(η^5-indenyl)Cl(PPh_3)$_2$ (**1**) and Ru(η^5-indenyl)Cl(PPh_2H)(PPh_3) (**2a**). The four catalyst precursors are [Ru(η^5-indenyl)(NCPh)(PPh_3)$_2$][B(C_6F_5)$_4$] (**3a**), [Ru(η^5-indenyl)(NCPh)(PPh_2H)(PPh_3)][B(C_6F_5)$_4$] (**3b**), Ru(η^5-indenyl)(PPh_2)(NCPh)(PPh_3) (**4a**) and Ru(η^5-indenyl)(PPh_2)(PPh_2H)(PPh_3) (**4b**). The new complexes **3a**, **3b** and **4b** were synthesized, isolated and fully characterized. The results presented in this chapter are reproduced with permission from Belli, R. G.; Burton, K. M. E.; Rufh, S. A.; McDonald, R.; Rosenberg, L. Inner- and Outer-Sphere Roles of Ruthenium Phosphido Complexes in the Hydrophosphination of Alkenes. *Organometallics* **2015**, *34*, 5637–5646.[1] Copyright 2015 American Chemical Society. This Chapter includes contributions from Stephanie Rufh and Dr. Robert McDonald. Supplementary spectra are presented in Appendix E.

2.2. Introduction

2.2.1. Considerations in Designing and Selecting Catalyst Precursors for Hydrophosphination

A previous graduate student in the Rosenberg group, Eric Derrah, synthesized Ru(η^5-indenyl)(PCy_2)(PPh_3) (**5b**), a Ru complex bearing a terminal, planar phosphido

ligand, via dehydrohalogenation of Ru(η^5-indenyl)Cl(PCy_2H)(PPh_3) (**2b**) (Scheme 2.1).[2] Eric Derrah and Krista Burton (another previous graduate student in the Rosenberg group) showed that a wide scope of alkenes and alkynes (both electron-deficient and electron-rich alkenes and alkynes) insert into the Ru-P π-bond of complex **5b**, which generates the respective metallacycles **6** (with alkenes) and **7** (with alkynes) (Scheme 2.1).[3,4,5]

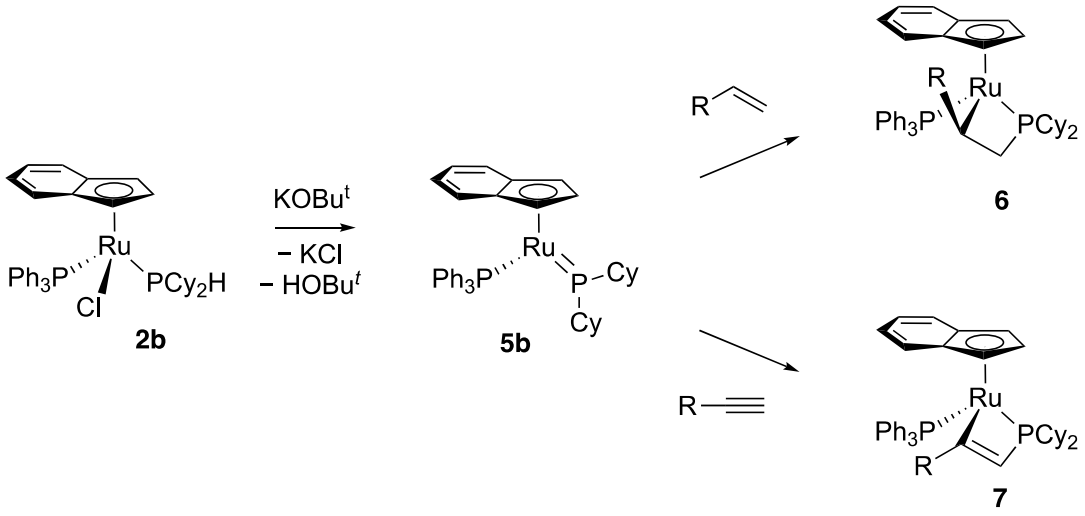

Scheme 2.1. Dehydrohalogenation of 2b and insertion reactions of alkenes (top) and alkynes (bottom) into the Ru-P bond of the phosphido ligand.

Formation of metallacycles **6** and **7** from complex **5b** demonstrated the potential of this system for the synthesis of phosphines *via* hydrophosphination of alkenes and alkynes. Moreover, the wide scope of substrates that could participate in this insertion chemistry highlights the potential of this system to allow for the hydrophosphination of a wide scope of unsaturated substrates. A potential synthetic cycle is shown in Scheme 2.2. A base deprotonates the P-H bond of a Ru-bound secondary phosphine, which generates complex **5** (step A). Complex **5** can participate in P-C bond formation with alkenes or alkynes *via* insertion into the Ru-P π-bond, which generates metallacycles **6** or **7** (step B). The

conjugate acid generated from step A protonolyzes the Ru-C bond of the metallacycle intermediate, which generates a complex with the hydrophosphination product bound to Ru and regenerates the base (step C). The hydrophosphination product is substituted by the secondary phosphine (step D), possibly rendering this cycle catalytic.

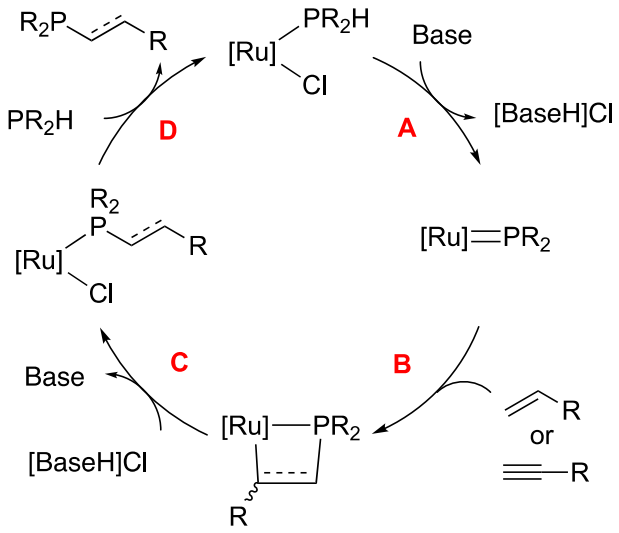

Scheme 2.2. Possible synthetic cycle for the hydrophosphination of alkenes

A key feature of this proposed cycle is a base that acts as a proton shuttle; a conjugate base/acid pair is needed that can participate in both steps A and C, respectively. In my previous work in the Rosenberg group as an undergraduate summer research student, I showed that a variety of organic acids can protonolyze the Ru-C bond of complexes **6a-c** (Scheme 2.3; Scheme 2.2, step C).[1] Pyridine and lutidine hydrochlorides (pK_a = 5.25 and 6.70 (H_2O), respectively)[6] are strong enough acids to protonolyze the Ru-C bond of **6a-c**. Triethylamine hydrochloride (pK_a = 10.7 (H_2O))[7] is the weakest acid tested that could protonolyze the Ru-C bond, but could do so only for **6a**. Unfortunately, the respective

conjugate bases of these acids are not basic enough to participate in step A. Neither the secondary phosphine substrate PCy_2H (pK_a = 35.7 (THF))[8] nor $HOBu^t$ (pK_a = 19.2 (H_2O))[9] are acidic enough to protonolyze the Ru-C bond of metallacycles **6a-c**.

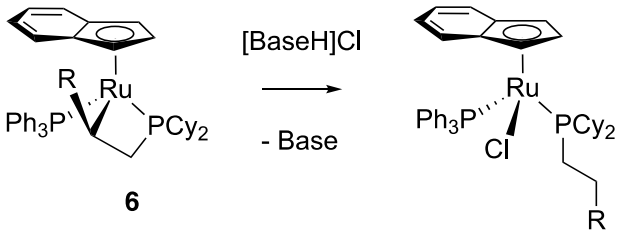

6

R = Bu^n (**a**), CN (**b**), Ph (**c**)

Scheme 2.3. Protonolysis of the Ru-C bonds of metallacycles 6a-c generating Ru complexes with hydrophosphination products as ligands.

A previous undergraduate student Chris Huang in the Rosenberg group showed that coordinated secondary phosphines in cationic complexes have more acidic P-H bonds. This allows for the use of weaker bases to deprotonate the coordinated secondary phosphines; a weak base for step A would afford a strong conjugate acid for step C. In particular, he showed that the base 1,8-diazabicyclo[5.4.0]undec-7-ene (DBU, pK_a = 13.5 (H_2O))[10] deprotonates the coordinated PCy_2H in the cationic complex [Ru(η^5-indenyl)(NCMe)(PCy_2H)(PPh_3)$_2$][PF_6].[11]

Based on the results described above, we proposed that using halide-free, cationic analogues of these Ru complexes would simplify the proposed cycle in Scheme 2.2. First, the role of the base is exclusively to deprotonate the coordinated secondary phosphine for the halide-free cationic complexes, rather than dehydrohalogenate the Ru complexes.

Second, by removing the Cl^- there would be less competition for coordination of the secondary phosphine or alkene at Ru. Furthermore, for the study presented in this Chapter, PPh_2H was used as the substrate phosphine because it has a lower pK_a than PCy_2H (PPh_2H, pK_a = 21.7 (THF)).[8,12,13]

2.3. Identification and Isolation of Catalyst Precursors

This section describes how [Ru(η^5-indenyl)(NCPh)(PPh_3)$_2$][$B(C_6F_5)_4$] (**3a**), [Ru(η^5-indenyl)(NCPh)(PPh_2H)(PPh_3)][$B(C_6F_5)_4$] (**3b**) and Ru(η^5-indenyl)(PPh_2)(PPh_2H)(PPh_3) (**4b**) were synthesized. It also describes why these complexes, as well as Ru(η^5-indenyl)(PPh_2)(NCPh)(PPh_3) (**4a**), were chosen as potential catalysts for hydrophosphination.

2.3.1. Synthesis and Characterization of [Ru(η^5-indenyl)(NCPh)(PPh_3)$_2$][$B(C_6F_5)_4$] and [Ru(η^5-indenyl)(NCPh)(PPh_2H)(PPh_3)][$B(C_6F_5)_4$]

Complexes **3a**,**b** were prepared from precursors **1** and **2a** (Scheme 2.4), respectively. The synthesis of complex **1** is well established[14] since it is commonly used as a catalyst for different types of reactions, such as C-C bond formation,[15] redox isomerizations[16] and alkyne insertions.[17,18] Previous graduate student, Eric Derrah, synthesized complex **2a**, as well as a variety of analogous complexes containing other secondary phosphine ligands, via substitution reactions of **1** with secondary phosphines.[19] Complexes **3a**,**b** were prepared by a halide abstraction of complexes **1** and **2a**, respectively, with K[$B(C_6F_5)_4$] in the presence of NCPh (Scheme 2.4). The synthesis of **3a** was performed by a previous undergraduate student Stephanie Rufh. I modified and optimized

her procedure to use fewer equivalents of $K[B(C_6F_5)_4]$ and NCPh. I used this modified procedure to prepare **3b**. Complexes **3a** and **3b** were isolated in 70 and 63 % yields, respectively.

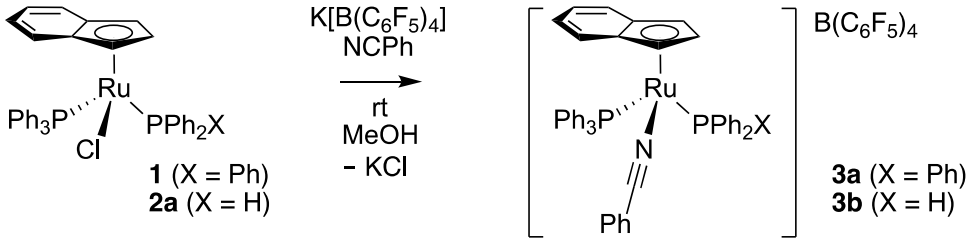

Scheme 2.4. Synthesis of $[Ru(\eta 5\text{-indenyl})(NCPh)(PPh_3)_2][B(C_6F_5)_4]$ (**3a**) and $[Ru(\eta 5\text{-indenyl})(NCPh)(PPh_2H)(PPh_3)][B(C_6F_5)_4]$ (**3b**)

Single crystals of **3a**,**b** were obtained and X-ray diffraction analysis was performed. The resulting structures are shown in Figure 2.1 and selected interatomic bond distances and bond angles are summarized in Table 2.1. The structures of both complexes show a *pseudo*-octahedral geometry at Ru. Indenyl metal complexes often show a distortion from the classical η^5-coordination mode of the indenyl ligand toward an η^3-coordination mode (Figure 2.2). This deviation is parametrized by the crystallographic indenyl slip factor (Δ). Δ is a defined as the difference between the average bond lengths of the metal to the ring junction carbons ($C_{3a,7a}$) and of the metal to the adjacent carbons in the five-membered ring ($C_{1,3}$).[20] A crystallographic slip factor of less than 0.25 Å indicates η^5-coordination and a Δ between 0.69 – 0.80 Å is typical of η^3-coordination. The crystallographic slip factors of **3a** and **3b** are 0.16 and 0.11 Å respectively, which are typical of η^5-coordination of the indenyl ring. These are smaller than the crystallographic slip factors for **1** and **2a**, which are 0.21 and 0.16 Å, respectively.[19,21] The spectroscopic slip factors, which I calculated

using $^{31}C\{^{1}H\}$ NMR data, are also consistent with η^5-coordination of the indenyl ligand in **3a**,**b** (summarized in section 2.6.5, Table 2.5). Complex **3a** is more sterically crowded than **3b**. This is seen in the larger bond angles at Ru between the phosphorus and nitrogen atoms in **3a** compared to **3b** as well as loss of linearity of the Ru-N-C10 bond angle in **3a**.

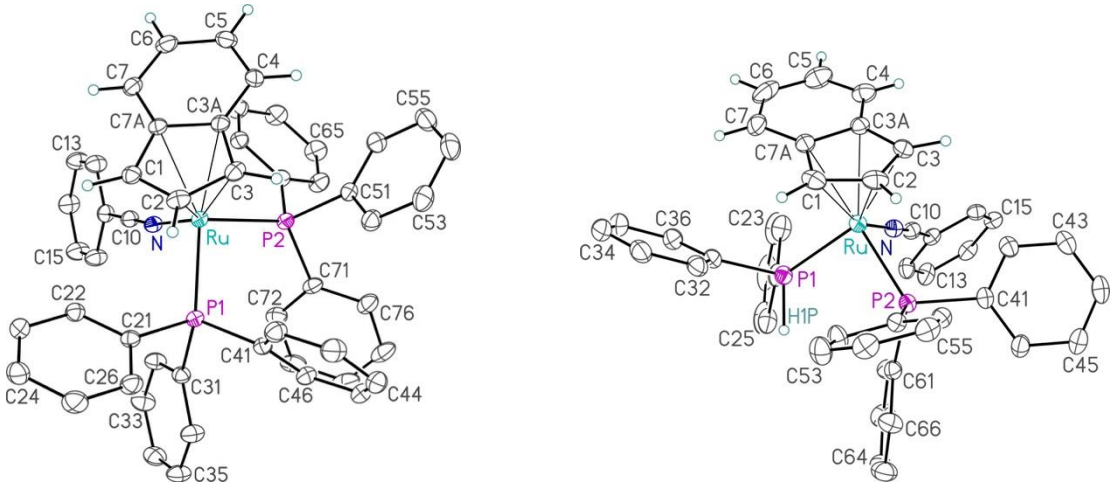

Figure 2.1. Molecular structure of the cation from [Ru(η^5-indenyl)(NCPh)(PPh_3)$_2$][$B(C_6F_5)_4$] (**3a**) left and [Ru(η^5-indenyl)(NCPh)(PPh_2H)(PPh_3)][$B(C_6F_5)_4$] (**3b**) right. Non-hydrogen atoms are represented by Gaussian ellipsoids at the 30% probability level. For **3b**, the hydrogen atom attached to P1 is shown with an arbitrarily small thermal parameter; all other hydrogen atoms are not shown.

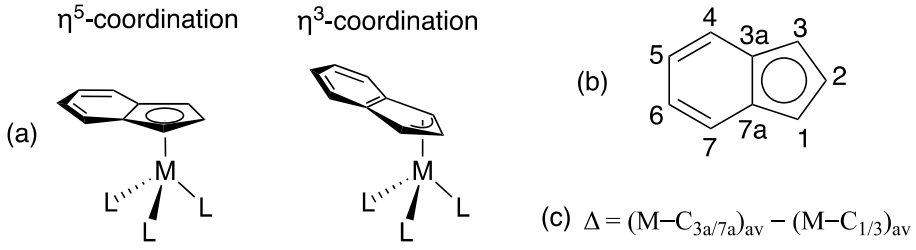

Figure 2.2. η^5- and η^3-coordination modes of the indenyl ligand (a) the labelled structure of indenyl ligand (b) and the crystallographic slip factor (Δ) equation (c).

Table 2.1. Selected Interatomic Distances (Å) and Bond Angles (°) for the Molecular Structures of the Cations in [Ru(η^5-indenyl)(NCPh)(PPh_3)$_2$][$B(C_6F_5)_4$] (**3a**), and [Ru(η^5-indenyl)(NCPh)(PPh_2H)(PPh_3)][$B(C_6F_5)_4$] (**3b**)

	3a	**3b**
Ru-P1	2.3123(5)	2.3148(5)
Ru-P2	2.3664(5)	2.2889(5)
Ru-N	2.0426(16)	2.0310(16)
Ru-C*	1.904	1.893
Ru-H1P	-	1.34(2)
Δ	0.16	0.11
P1-Ru-P2	98.240(17)	92.932(19)
P1-Ru-N	96.82(5)	91.07(5)
P2-Ru-N	91.84(5)	89.61(5)
Ru-P1-H1P	-	117.4(9)
Ru-N-C10	169.95(16)	178.66(17)
P1-Ru-C*	120.4	124.4
P2-Ru-C*	121.2	124.1
N-Ru-C*	121.9	124.8

[a] C* is centroid of the 5-membered ring of the indenyl ligand. Ru-C* is the distance from Ru to the centroid of the 5-membered ring of the indenyl ligand.

The structures of complexes **3a**,**b** were confirmed and characterized by 1D NMR (^{1}H, ^{31}P{^{1}H}, ^{31}P, ^{13}C{^{1}H} and ^{13}C DEPT 135) and 2D NMR (^{1}H COSY, ^{1}H/^{31}P{^{1}H}-HSQC, ^{1}H/^{31}P{^{1}H}-HMBC, ^{1}H/^{13}C{^{1}H}-HSQC and ^{1}H/^{13}C{^{1}H}-HMBC), ESI mass spectrometry, IR spectroscopy and elemental analysis. The syntheses of **3a**,**b** are described in section 2.6.2.1 and 2.6.2.2. ^{1}H and ^{13}C{^{1}H} NMR data for complexes **3a**,**b** is summarized in section 2.6.5, Table 2.4 and 2.5. ^{1}H, ^{31}P{^{1}H} and ^{13}C{^{1}H} NMR spectra of **3a**,**b** are in Appendix E.

2.3.2. Synthesis and Characterization of Ru(η^5-indenyl)(PPh_2)(PPh_2H)(PPh_3) (4b)

The phosphido complexes **4a**,**b** were prepared from precursor **2a**. Previous graduate student Eric Derrah determined that addition of a strong base ($KOBu^t$) to complex **2b**, and to analogous secondary phosphine complexes, results in a dehydrohalogenation reaction that generates coordinatively unsaturated Ru complexes with planar phosphido ligands (**5**). For the dehydrohalogenation of complex **2a**, the coordinatively unsaturated complex **5a** was only observed at low temperature and decomposed at high temperature.

A previous undergraduate student Marc-Andre Hoyle was able to trap **5a** as **4a** by performing the dehydrohalogenation of complex **2a** in the presence of NCPh (Scheme 2.5, top).[22] Complex **4a** is coordinatively saturated and the phosphido ligand is in a *pseudo*-tetrahedral geometry. Due to the lability of NCPh, complex **4a** acts as a "masked" form of **5a**. I was able to isolate complex **4b** by addition of PPh_2H to **4a**, which results in substitution of NCPh by PPh_2H. Complex **4b** can also be prepared by the dehydrohalogenation of **2a** in the presence of PPh_2H (Scheme 2.5, bottom).

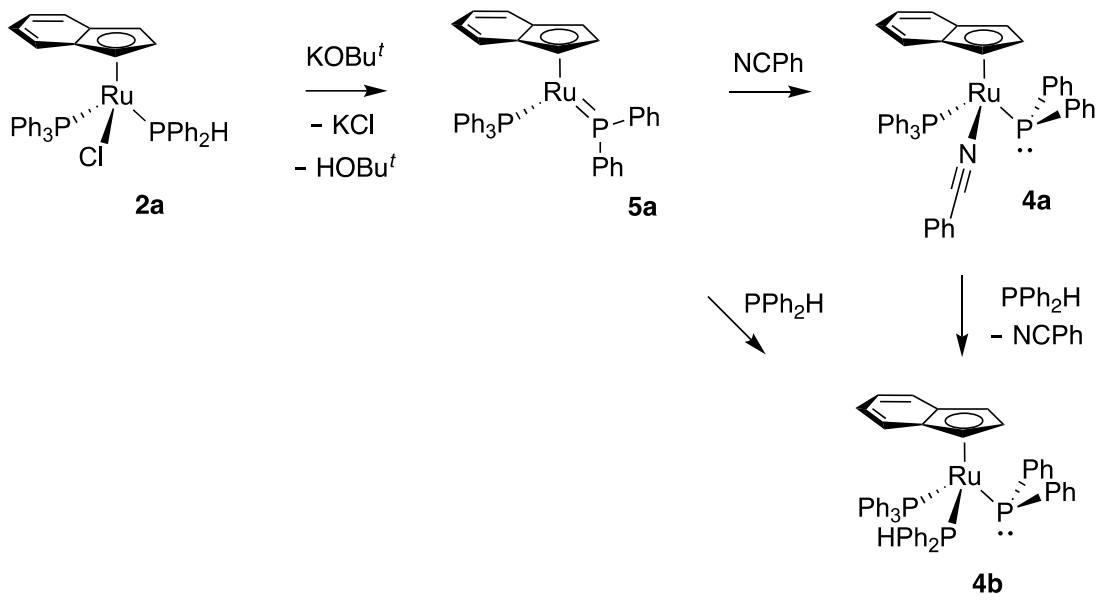

Scheme 2.5. Synthesis of Ru(η^5-indenyl)(PPh_2)(NCPh)(PPh_3) (**4a**) and Ru(η^5-indenyl)(PPh_2)(PPh_2H)(PPh_3) (**4b**) via dehydrohalogenation of Ru(η^5-indenyl)Cl(PPh_2H)(PPh_3) (**2a**).

The structure of **4b** was confirmed and the complex was characterized by 1D NMR (^{1}H, ^{31}P{^{1}H}, ^{31}P, ^{13}C{^{1}H} and ^{13}C DEPT 135) and 2D NMR (^{1}H COSY, ^{1}H/^{31}P{^{1}H}-HSQC, ^{1}H/^{31}P{^{1}H}-HMBC, ^{1}H/^{13}C{^{1}H}-HSQC and ^{1}H/^{13}C{^{1}H}-HMBC) and IR spectroscopy. The synthesis of **4b** is described in section 2.6.2.3. ^{1}H and ^{13}C{^{1}H} NMR data for complex **4b** is summarized in section 2.6.5, Table 2.4 and 2.5. ^{1}H, ^{31}P{^{1}H} and ^{13}C{^{1}H} NMR spectra of **4b** are in Appendix E.

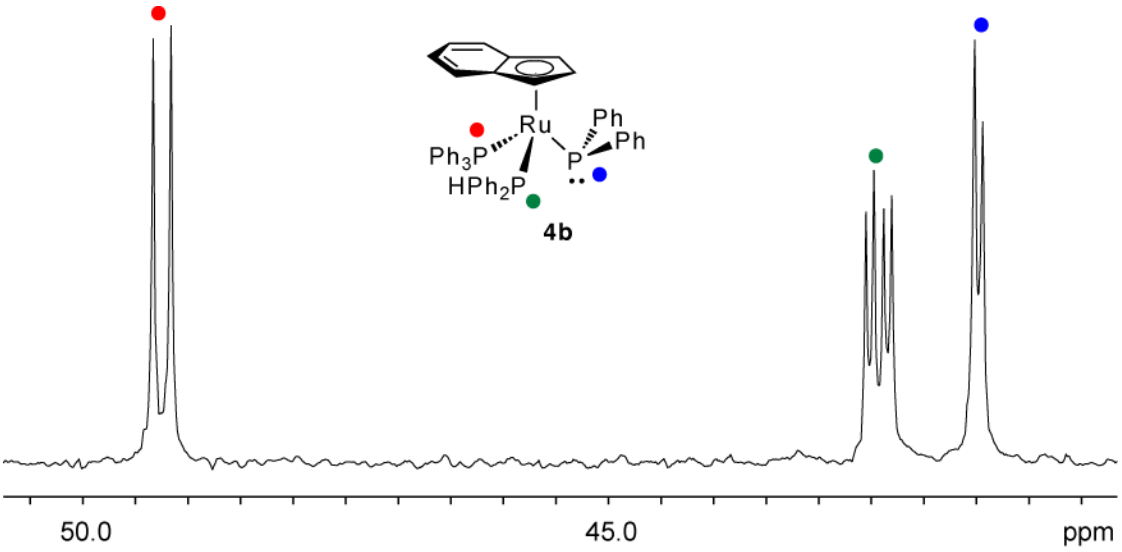

Figure 2.3. $^{31}P\{^{1}H\}$ NMR (202.51 MHz) in d_8-tetrahydrofuran of Ru(η^5-indenyl)(PPh_2)(PPh_2H)(PPh_3) (**4b**).

Complex **4b** has three chemically inequivalent P nuclei. The $^{31}P\{^{1}H\}$ NMR spectrum of **4b** shows a doublet of doublets and two doublets (Figure 2.3). No coupling is observed between the phosphido and PPh_3 ligand. The absence of (or unusually small) $^{2}J_{PP}$ coupling between *pseudo*-tetrahedral terminal phosphido ligands and tertiary phosphine ligands in metal complexes is known. For example, complex **4a** and Ru(η^5-indenyl)(PPh_2)(CO)(PPh_3) (**4c**), which were synthesized by a previous undergraduate student Marc-André Hoyle, have $^{2}J_{PP}$ coupling of 4 and 8 Hz between the coordinated PPh_3 and the PPh_2 ligand, respectively (Figure 2.4). Gladysz *et al.* also reported half-sandwich Ru complexes with *pseudo*-tetrahedral terminal phosphido ligands that also have reduced or no observed $^{2}J_{PP}$ coupling between coordinated tertiary phosphines and terminal phosphido ligands.[23] In **4b**, a $^{2}J_{PP}$ of 15 Hz is observed between the PPh_2H and phosphido ligand, but this is small for typical *cis* $^{2}J_{PP}$ coupling constants. For comparison, a $^{2}J_{PP}$ value of 35 Hz is observed between the PPh_2H and PPh_3 ligand in **4b**. The doublet of doublets is assigned as the coordinated PPh_2H because it has a $^{1}J_{PH}$ coupling of 346 Hz in the ^{31}P NMR

spectrum; in the ^{1}H NMR spectrum there is a doublet with $^{1}J_{PH}$ coupling of 346 Hz corresponding to the hydrogen in the P-H bond.

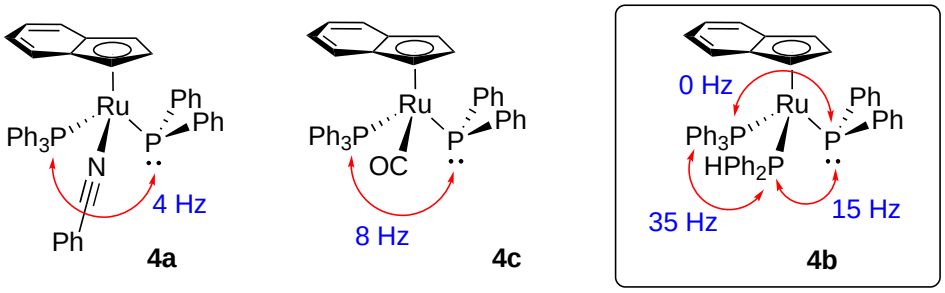

Figure 2.4. $^{2}J_{PP}$ coupling constants of Ru(η^5-indenyl)(PPh_2)(NCPh)(PPh_3) (**4a**), Ru(η^5-indenyl)(PPh_2)(CO)(PPh_3) (**4c**) and Ru(η^5-indenyl)(PPh_2)(PPh_2H)(PPh_3) (**4b**).

2.3.3. Thermolysis of Ru(η^5-indenyl)(PPh_2)(PPh_2H)(PPh_3) (4b)

The PPh_2H ligand in **4b** is strongly bound to Ru relative to the labile NCPh ligand in **4a**. A thermolysis experiment, where a solution of **4b** in d_8-toluene was heated at 60°C, resulted in decomposition of **4b** to the orthometalated product Ru(η^5-indenyl){κ^2-(*o*-C_6H_4)PPh_2}(PPh_2H) (Scheme 2.6). The mechanism for orthometalation involves dissociation of the PPh_2H ligand from **4b**, which generates **5a**. The orthometalated product forms when **5a** undergoes subsequent *ortho* C-H activation of a phenyl substituent in the PPh_3 ligand. The half-life for the thermal decomposition of **4b** was ~ 96 h. An identical thermolysis experiment of **4a**, performed by Marc-André Hoyle, showed that the half-life of decomposition was ~ 4 h; this occurs via dissociation of the NCPh ligand.[22] Since the half-life for orthometalation of **4b** is ~ 24 times longer than the orthometalation of **4a**, the dissociation of PPh_2H from Ru must be slower than the dissociation of NCPh from Ru.

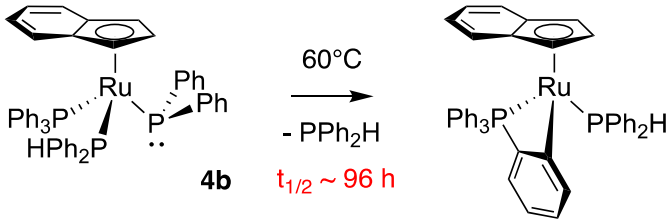

Scheme 2.6. Thermal decomposition of Ru(η^5-indenyl)(PPh_2)(PPh_2H)(PPh_3) (**4b**).

2.3.4. Rationale of Using 3a,b and 4a,b as Catalyst Precursors

Complexes **3a**,**b** and **4a** were chosen as catalyst precursors because each complex represents an entry point into the proposed synthetic hydrophosphination cycle shown in Scheme 2.7, which is a revised synthetic cycle from the one shown in Scheme 2.2, that accounts for using halide-free complexes. Complex **3a** can enter this cycle via substitution of PPh_3 by PPh_2H, which generates **3b**. Complex **3b** is a proposed on-cycle species. Complex **4a** can enter this synthetic cycle via dissociation of NCPh, which generates **5a**. Complex **4b** was also chosen as a complex of interest because **4b** easily forms from **4a** in the presence of PPh_2H.

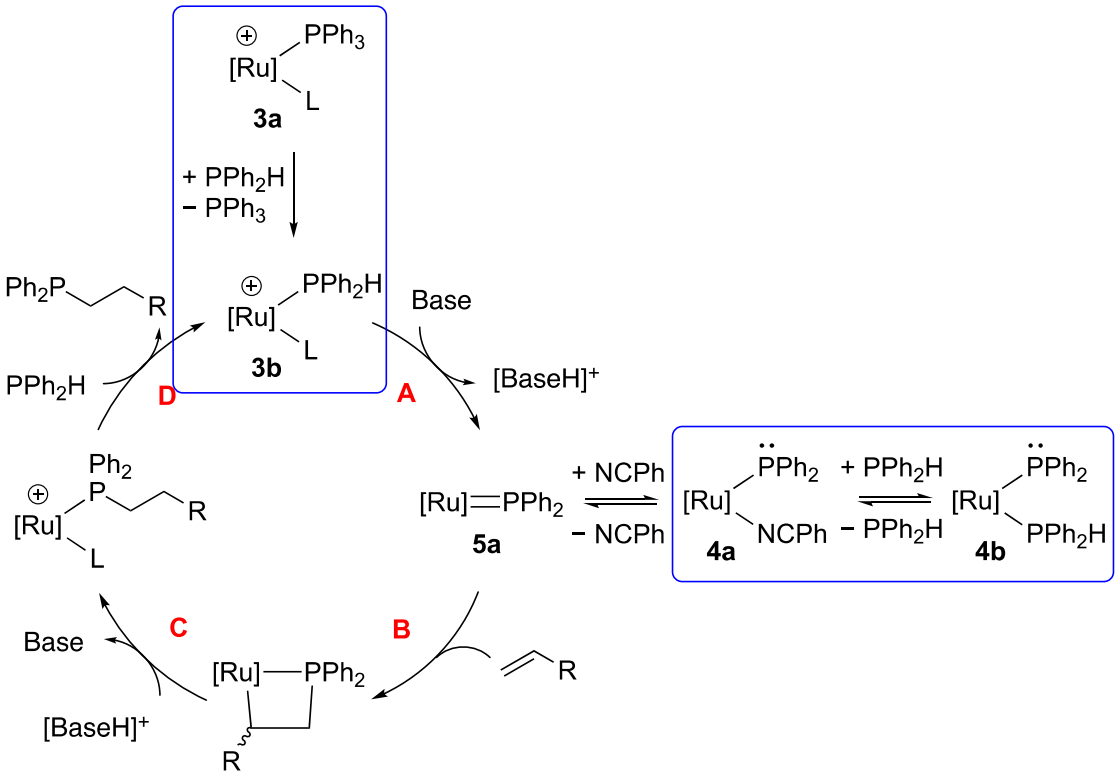

Scheme 2.7. Possible synthetic cycle for the hydrophosphination of alkenes relying on complexes **3a**,**b** and **4a**,**b**.

2.4. Investigation of 3a, 3b, 4a and 4b in Catalytic Hydrophosphination

As mentioned in section 2.3.4, complexes **3a**,**b** and **4a**,**b** provide entry points into the proposed synthetic hydrophosphination cycle (Scheme 2.7). All four complexes are active for the catalytic hydrophosphination of electron-deficient alkenes with PPh_2H. Complexes **3a**,**b** require a base co-catalyst, whereas complexes **4a**,**b** do not require a base co-catalyst. The results presented in this section suggest that an alternative mechanism to the one shown in Scheme 2.7 is operative.

2.4.1. Activity of 3a, 3b, 4a and 4b in Catalytic Hydrophosphination

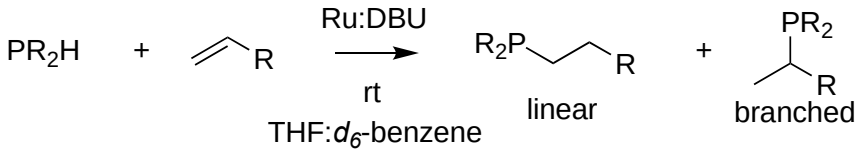

Scheme 2.8. Catalytic hydrophosphination of alkenes with secondary phosphines catalyzed by **3a**, **3b**, **4a** and **4b.**

Complexes **3a**,**b**, and **4a**,**b** were screened for the hydrophosphination of alkenes with secondary phosphines (Scheme 2.8). The catalytic reactions were carried out in 3:1 THF:d_6-benzene solutions in NMR tubes at room temperature with periodic shaking to ensure mixing of the solution. Each reaction used an equimolar amount of PR_2H and alkene with varying amounts of precatalyst and the base co-catalyst DBU. The results are summarized in Table 2.2 and are the average of triplicate runs.

The activities of **3a**,**b**, and **4a**,**b** for catalytic hydrophosphination were measured using quantitative $^{31}P\{^1H\}$ NMR. These $^{31}P\{^1H\}$ NMR experiments were initiated within 15 mins of sample preparation and consisted of 128 scans with a relaxation delay of 55 s to ensure quantification. Each experiment took 2 h 44 s, so the resulting spectra showed time-averaged signal intensities approximately corresponding to the first 1 h of the reaction. The time-averaged conversion over approximately the first 1 h allowed for calculation of the turnover frequency (TOF). The same $^{31}P\{^1H\}$ NMR experiment was used 24 h after sample preparation in order to measure conversions.

All four complexes showed moderate activity under the conditions described. Conversions of 72 - 92% within 24 h to the linear, anti-Markovnikov product (and small amounts of the branched product, Scheme 2.8) were observed when using 10 mol% of precatalyst and base co-catalyst DBU. Complex **4a** had the highest activity of the four complexes studied (entries 1 – 4). In a reaction using a 5 mol% catalyst loading of complex **4a**, a higher TOF, with comparable conversion, was measured (entry 7). In a control reaction with neither Ru precatalyst nor base co-catalyst (entry 5), the linear hydrophosphination product was observed (10% conversion in 24 h), which indicates that a minor thermal background reaction occurs. An additional control experiment, where only base co-catalyst was added to the substrates (entry 6), without Ru precatalyst, showed a mixture of the linear and branched hydrophosphination products in 41% yield. This indicates that a background base-catalyzed hydrophosphination is also possible.

Table 2.2. Reactions Screening the Activity of Complexes 3a, 3b, 4a and 4b in Catalytic Hydrophosphination.[a]

Entry	Complex	Ru:DBU (mol %)	TOF (h^{-1})[b]	Conversion (%)[b]	Linear:Branched
	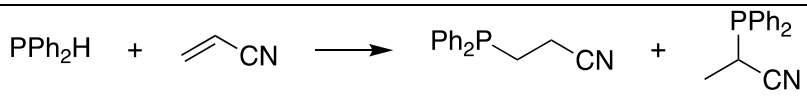				
1	**3a**	10:10	2(0.6)	76(1)	94:6
2	**3b**	10:10	0.9(0.1)	90(4)	98:2
3	**4a**	10:10	7(0.6)	92(6)	87:13
4	**4b**	10:10	2(0.5)	72(5)	92:8
5	-	0:0	-	8(2)	99:trace
6	-	0:10	0.4(0.2)	41(10)	89:11
7	**4a**	5:5	13(1)	73(10)	87:13
8	**3a**	10:0	-	7(3)	99:trace
9	**3b**	10:0	-	1(0)	99:trace
10	**4a**	10:0	5(0)	74(1)	75:25
11	**4b**	10:0	2(0.6)	66(3)	90:10
	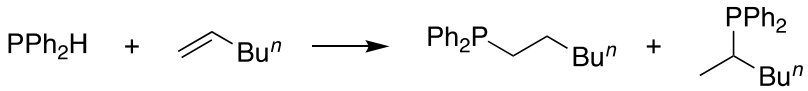				
12	**4a**	10:10	-	trace	-
13	**4a**	10:0	-	trace	-
	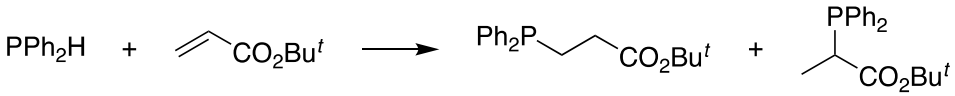				
14	**4a**	10:0	2.9(0.2)	74(3)	99:trace
15	**4b**	10:0	1.7(0.3)	75(4)	99:trace
16	-	0:0	-	8	99:trace
17	-	0:10	-	36	99:trace
	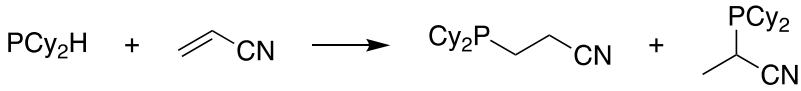				
18	**3a**	10:10	0.7(0.1)	43(12)	99:trace
19	-	0:0	-	trace	-
20	-	0:10	-	trace	-

[a]All reactions were performed at rt in 3:1 THF:d_6-benzene solutions in NMR tubes. [b]Values in ( ) are the standard deviation.

2.4.2. Secondary Phosphines Substrate Scope in Hydrophosphination

Complexes **3b**, **4a** and **4b** have either PPh_2H and/or PPh_2 ligands, so these were only used in hydrophosphination catalysis when PPh_2H was the substrate secondary phosphine. On the other hand, [Ru(η^5-indenyl)(NCPh)$(PPh_3)_2$][$B(C_6F_5)_4$] (**3a**) has two PPh_3 ligands that can be substituted by any secondary phosphine. Thus, **3a** can be applied as a precatalyst for hydrophosphination catalysis with any PR_2H. Complex **3a** was used as a precatalyst with base co-catalyst DBU for the hydrophosphination of acrylonitrile by dicyclohexylphosphine, PCy_2H (Table 2.2, entry 18). The activity of the catalyst system **3a**/DBU and the conversion of this reaction were lower than the analogous reaction with PPh_2H. Control experiments where neither **3a** nor DBU were added (entry 19) showed no conversion. A control experiment where only DBU was added to the substrates, without **3a**, also showed no conversion. These two control experiments confirm that the catalyst system **3a**/DBU is active for the hydrophosphination of acrylonitrile with PCy_2H. This demonstrates that this system can catalyze hydrophosphination of activated alkenes with both alkyl and aromatic phosphines.

2.4.3. Alkene Substrate Scope in Hydrophosphination

Complexes **3a**,**b** and **4a**,**b** are selective for the hydrophosphination of electron-deficient alkenes (acrylonitrile and *tert*-butyl acrylate). Hydrophosphination of 1-hexene using complex **4a** as a precatalyst with and without base co-catalyst was attempted (Table 2.2, entry 12, 13), but no conversion was observed.

The fact that catalysis is only observed with activated, electron-deficient alkenes suggests that a different mechanism to the one shown in Scheme 2.7 is operative. Our proposed mechanism relies on Ru-phosphido complexes/intermediates that can form P-C bonds with alkenes through inner-sphere insertion. As described in section 1.4.2, phosphido ligands on late-metals are nucleophilic, so it is likely that P-C bond formation occurs via outer-sphere, conjugate addition of the phosphido ligands in **4a**,**b** at alkenes (Scheme 2.9). If this mechanism is operative then P-C bond formation would only occur with alkenes that are susceptible to nucleophilic attack (electron-deficient alkenes like acrylonitrile and *tert*-butyl acrylate). No catalysis is observed with 1-hexene because conjugate addition of the phosphido ligand is unlikely to occur at unactivated and electron-rich alkenes. P-C bond formation via conjugate addition of a phosphido ligand at electron-deficient alkenes is known for other late-metal hydrophosphination catalysts (discussed in Chapter 1, section 1.4.2).[24,25,26]

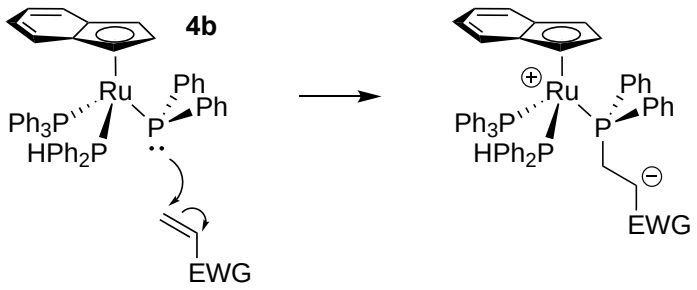

Scheme 2.9. Nucleophilic attack of phosphido ligands at activated, electron-deficient alkenes.

Further support for this outer-sphere, nucleophilic attack mechanism comes from the fact that the metallacycle intermediates proposed in Scheme 2.7 are not observed during

catalysis. In the proposed mechanism described in section 2.2.1, these putative metallacycles (**6**) would form from insertion of alkenes into the Ru-P bond of the coordinatively unsaturated intermediate **5a**. Complex **5a** must form transiently under catalytic conditions in order for substitution to occur; substitution at half-sandwich Ru complexes is dissociative.[27] Thus, if **5a** forms transiently and if the metallacycles are not observed, this must mean that PPh_2H, and possibly NCPh, are much more competitive for coordination at Ru than alkene (Scheme 2.10). If the equilibria in Scheme 2.10 lie heavily towards the coordinatively saturated complexes **4a**,**b**, then alkene addition to **5a** is unlikely. However, the fact that the metallacycles were not observed during catalysis does not necessarily rule out the possibility that such intermediates form.

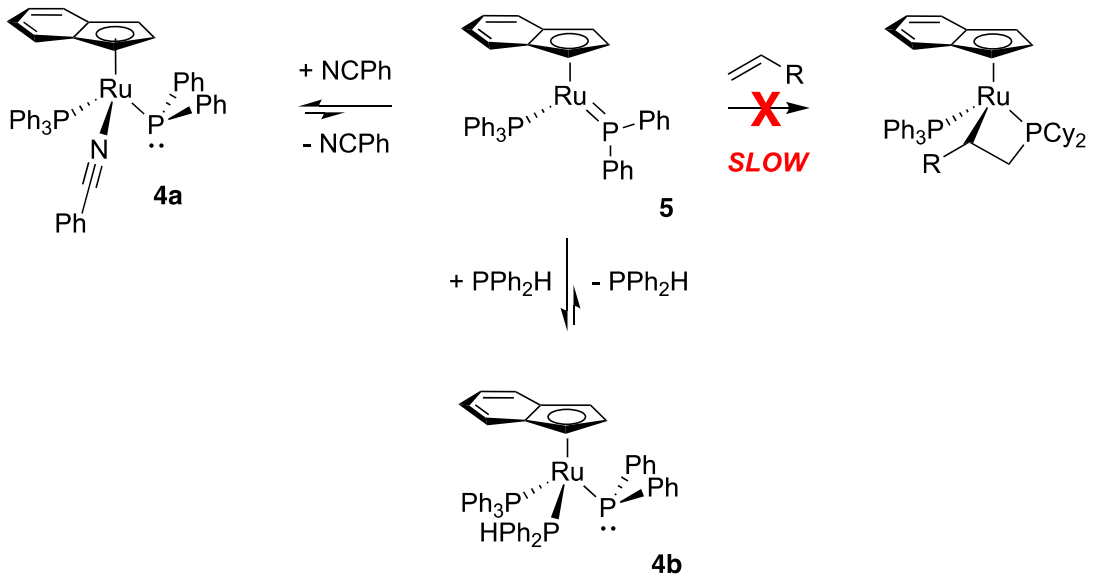

Scheme 2.10. Equilibria occurring under catalytic conditions that prevent formation of metallacycle intermediates.

2.4.4. Proposed Mechanism for Hydrophosphination

A revised proposed mechanism for the hydrophosphination of activated alkenes by PPh_2H using complexes **3a**,**b** and **4a**,**b** is shown in Scheme 2.11. Complex **4b** is the entry point into the active cycle. This proposed cycle relies on conjugate addition of the phosphido ligand in **4b** at alkene, which generates a zwitterionic intermediate (step **A**). The carbanion of this intermediate is quenched by intramolecular proton transfer from coordinated PPh_2H. This generates a Ru-phosphido complex with a coordinated product phosphine (step **B**). Substitution of the product phosphine by PPh_2H is required to regenerate **4b** (step **C**). Complex **4a** can enter this proposed active cycle because complex **4b** readily forms *via* substitution of NCPh in complex **4a** by PPh_2H (step D and discussed section 2.2.2). Complex **3b** enters this proposed cycle via deprotonation of the coordinated PPh_2H (step E), which generates **4a**. Last, **3a** is able to enter this proposed cycle via substitution of PPh_3 in **3a** by PPh_2H (step F), which generates **3b**; subsequent deprotonation generates **4a**.

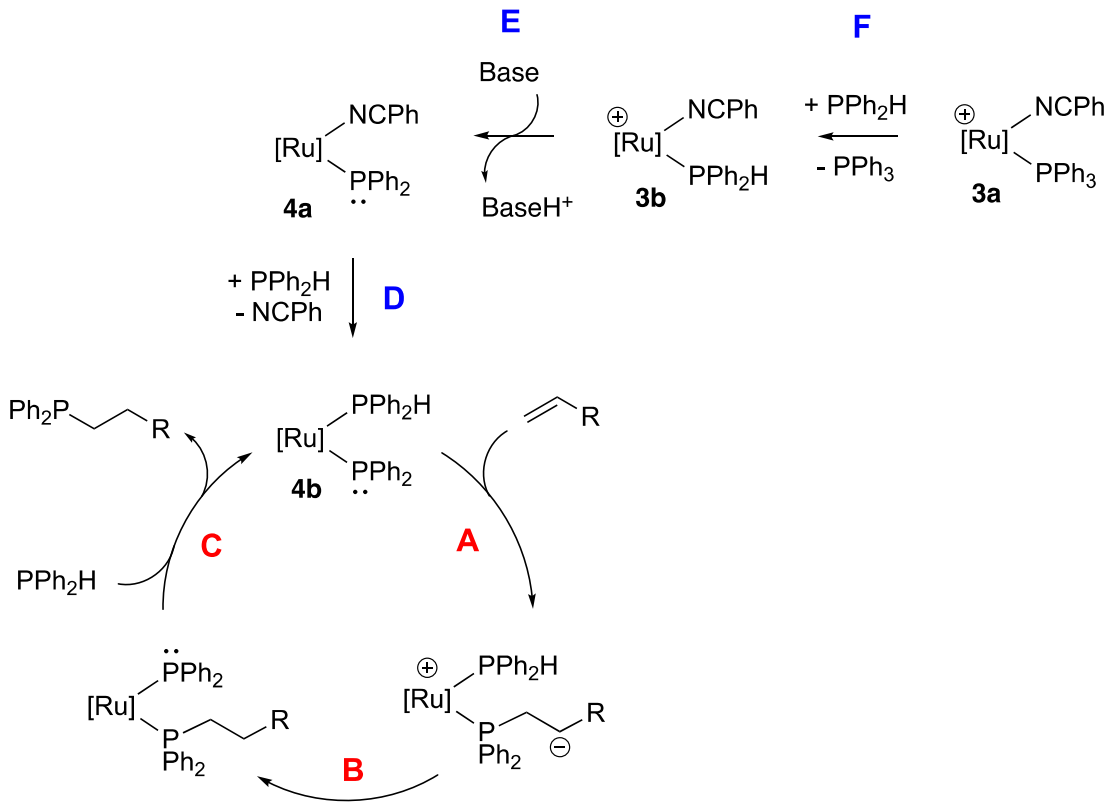

Scheme 2.11. Proposed mechanism for the hydrophosphination of activated alkenes with PPh2H catalyzed by complexes **3a**,**b** and **4a**,**b**.

In this mechanism, the external base is solely used as an initiator for precatalysts **3a**,**b**. The external base initiates catalysis when using **3a**,**b** by deprotonating the Ru-bound PPh_2H, which generates a phosphido ligand (step E). A control experiment where **3a**,**b** were used as precatalysts without adding DBU showed minor conversion, which demonstrates that an external base is needed to initiate catalysis (Table 2.2, entries 8, 9). The minor conversion results from the background thermal hydrophosphination.

A base is not needed to initiate catalysis when using **4a**,**b** because these complexes already contain a phosphido ligand. In the proposed mechanism, the carbanion of the

zwitterionic intermediate (resulting from step A) can deprotonate the Ru-bound PPh_2H (step B). Thus, the carbanion can regenerate a phosphido ligand at Ru, which obviates the need for an external base. A control experiment where **4a**,**b** were used without added DBU (Table 2.2, entries 10, 11) showed comparable activity and conversion to when DBU was added to catalytic reactions where **4a**,**b** were used (entry 3, 4).

The proposed mechanism for hydrophosphination catalyzed by complexes **3a**,**b** and **4a**,**b** shares similarities, but varies from other examples of late-metal hydrophosphination catalysis where metal phosphido complexes are implicated in conjugate addition chemistry (Scheme 2.12; mechanisms discussed in Chapter 1, section 1.4.2). Common to our mechanism and the mechanisms described herein is P-C bond formation via conjugate addition of a phosphido ligand to an electron-deficient alkene, which generates a zwitterionic intermediate. In the Pd-catalyzed hydrophosphination reported by Leung *et al.*, a base co-catalyst is required, which acts as a proton shuttle; NEt_3 deprotonates the P-H bond of Pd-coordinated PPh_2H and redelivers the H^+ to complete the hydrophosphination.[28,29,30,31] In the Pt-catalyzed hydrophosphination reported by Glueck *et al.*, P-H bond activation occurs via oxidation addition of the P-H bond of substrate phosphine to Pt; no base co-catalyst/initiator is needed.[19] The carbanion of the zwitterionic intermediate is quenched by the Pt-H bond to complete the hydrophosphination. Last, the Ru-catalyzed hydrophosphination reported by Morris *et al.* differs from our proposed mechanism.[32] The authors used a coordinatively saturated Ru phosphido complex that has a chelating ancillary ligand, which does not allow for substrate phosphine to coordinate to Ru. Thus, the carbanion of the zwitterionic intermediate can only be quenched by

intermolecular deprotonation of uncoordinated PPh_2H. Unique to our proposed mechanism is that P-H bond activation occurs via intramolecular deprotonation by the carbanion of the zwitterionic intermediate. The indenyl ligand enforces a *cis*-orientation of the P-based ligands, which enables this mechanism.

2.5. Conclusion

Complexes [Ru(η^5-indenyl)(NCPh)$(PPh_3)_2$][$B(C_6F_5)_4$] (**3a**), [Ru(η^5-indenyl)(NCPh)$(PPh_2H)(PPh_3)$][$B(C_6F_5)_4$] (**3b**), Ru(η^5-indenyl)(PPh_2)(NCPh)(PPh_3) (**4a**) and Ru(η^5-indenyl)$(PPh_2)(PPh_2H)(PPh_3)$ (**4b**) are competent catalysts for the hydrophosphination of activated alkenes. The observed selectivity of this system for electron-deficient alkenes suggests that an outer-sphere mechanism involving nucleophilic attack of a phosphido ligand at alkene is operative (Scheme 2.12). Chapter 3 explores and provides evidence for this outer-sphere mechanism through a detailed kinetic and mechanistic analysis of Ru phosphido complexes in hydrophosphination catalysis.

From this study, I found that competitive coordination of substrate phosphine to Ru under catalytic conditions, prevents the proposed inner-sphere mechanism (the equilibrium bifurcating the two cycles in Scheme 2.12). This highlights the importance of coordinative unsaturation of Ru phosphido complexes to allow for alkene insertion, which is the basis of the proposed, inner-sphere hydrophosphination cycle.

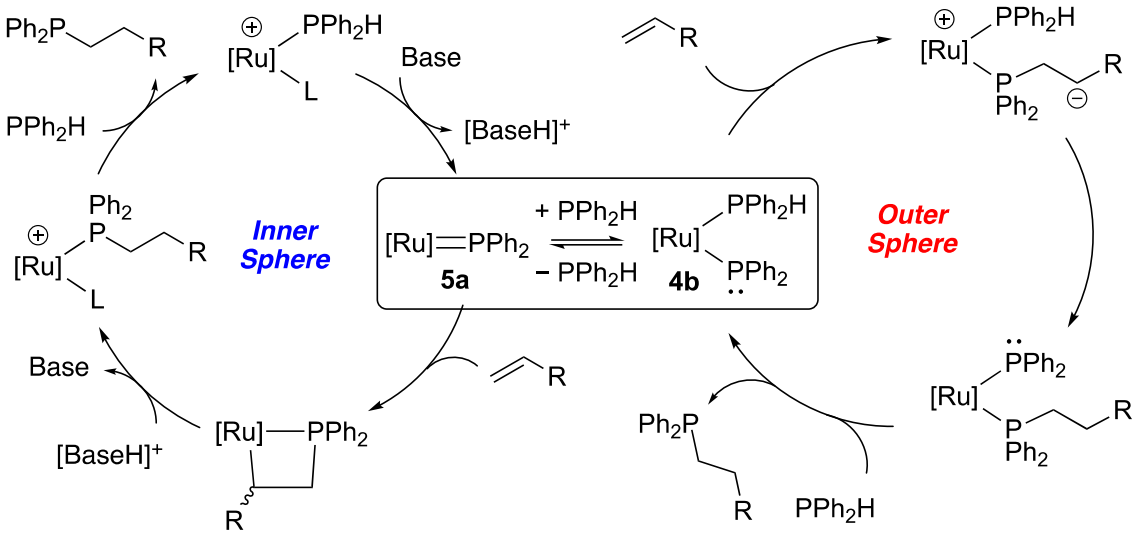

Scheme 2.12. Proposed mechanisms for the inner- (left) and outer-sphere (right) hydrophosphination of alkenes. The two cycles are linked by the equilibrium between **5a** and **4b.**

Accessing this inner-sphere mechanism could potentially allow for the catalytic hydrophosphination of a wider alkene scope, given the breadth of unsaturated substrates that can undergo insertion with **5**. In order to do this, redesigning the catalyst to favour phosphine dissociation could allow for alkene insertion. Furthermore, additional work to identify an appropriate base/conjugate acid pair to act as a proton shuttle is also needed for this inner-sphere cycle.

2.6. Experimental

2.6.1. General Comments

Unless otherwise noted, all reactions and manipulations were performed under nitrogen in a glovebox or using conventional Schlenk techniques. Methanol was distilled from calcium hydride. THF was distilled from sodium/benzophenone under nitrogen and then stored over sodium/benzophenone, and was degassed by three freeze-pump-thaw cycles and vacuum-transferred before use. Dichloromethane, toluene, pentane and hexane were degassed by sparging and then passed through columns of activated alumina in a solvent purification system. Deuterated solvents (Sigma-Aldrich) were stored over sodium/benzophenone (d_6-benzene) or calcium hydride (d_1-chloroform) and then freeze-pump-thaw degassed three times and vacuum-transferred before use, except for d_2-dichloromethane and d_8-THF, which were used as received in 1 g ampules. Unless otherwise specified, reagents were purchased from Sigma-Aldrich Canada and used as received (secondary phosphines, or dried and degassed using established procedures (other reagents). Diphenylphosphine was also purchased from Strem Chemicals as a 10% solution in hexanes; the concentration was checked against a known concentration of triphenylphosphine oxide by $^{31}P\{^{1}H\}$ NMR before use. $K[B(C_6F_5)_4)]$ was purchased from Boulder Scientific Co. and was used as received. Complexes **1**,[11] **2a**[15] and **4a**[18] were prepared according to literature procedures.

NMR spectra were recorded on a Bruker Avance 300 spectrometer operating at 300.27 MHz for ^{1}H and 121.55 MHz for ^{31}P, a Bruker AMX 360 spectrometer operating at 360.13 MHz for ^{1}H and 145.78 MHz for ^{31}P and a Bruker AVANCE 500 spectrometer

operating at 500.27 MHz for ^{1}H, 202.51 MHz for ^{31}P and 125.77 MHz for ^{13}C. Chemical shifts are reported in ppm at ambient temperature. ^{1}H chemical shifts are referenced to residual protonated solvent peak at 7.16 ppm (C_6D_5H). ^{13}C chemical shifts are referenced to C_6D_6 at128.4 ppm and $CDCl_3$ at 77.5 ppm. ^{1}H and ^{13}C chemical shifts are reported relative to tetramethylsilane and ^{31}P chemical shifts are reported relative to 85% H_3PO_4(aq).

Melting/decomposition temperatures were recorded using a Gallenkamp apparatus and are uncorrected. Microanalysis was performed by Canadian Microanalytical Services Ltd., Delta, BC, Canada. IR spectra were recorded for KBr pellets on a PerkinElmer FTIR Spectrum 1000 spectrophotometer. Electrospray ionization mass spectrometry (ESI-MS) was carried out by Rhonda Stoddard (group of Prof. Scott McIndoe) and Dr. Jingwei Luo at the University of Victoria on Waters QTOF Micromass and QTOF II instruments, using the following conditions: capillary voltage 200 V. sample cone voltage 15 V, extraction voltage 0.5 V, source temperature 60 °C, desolvation temperature 120 °C, cone gas 100 L/h, desolvation gas 100 L/h collison energy 2 V.

2.6.2. Preparation of Indenyl Ruthenium Complexes

2.6.2.1. Synthesis of [Ru(η^5-indenyl)(NCPh)(PPh_3)$_2$][$B(C_6F_5)_4$] (3a)

Benzonitrile (0.35 mL, 3.4 mmol) was added to an orange suspension of **1** (0.875 g , 1.13 mmol) and K[$B(C_6F_5)_4$)] (0.809 g, 1.13 mmol) in methanol (25 mL). The resulting orange suspension was stirred for 1 day, during which time it turned yellow with a yellow precipitate. The solution was filtered, and the solid was dried under vacuum. It was then

redissolved in dichloromethane, filtered to remove KCl, and layered with methanol, which gave **3a** as an orange crystalline solid (1.25 g, 70% yield). Anal. Found (calcd for $C_{76}H_{42}NP_2RuBF_{20}$): C., 59.81 (59.94); H., 2.64 (2.78); N., 0.85 (0.92). IR (KBr, cm^{-1}): 2228 (w, ν_{CN}). LR-ESI-MS (CH_2Cl_2, *m/z*):844.35 (M^+, 100%), 741.34 ([M – NCPh]$^+$, 40%). Dec pt: 172-175 °C. $^{31}P\{^1H\}$ NMR (202.55 MHz, d_2-dichloromethane): 46.9 (s, PPh_3).

2.6.2.2. Synthesis of [Ru(η^5-indenyl)(NCPh)(PPh_2H)(PPh_3)][$B(C_6F_5)_4$] (3b)

The procedure described for **3a** was followed, using benzonitrile (0.87 mL, 8.4 mmol), complex **2** (-/982 g, 1.40 mmol), and K[$B(C_6F_5)_4$)] (1.00 g, 1.40 mmol) in methanol (25 mL). The reaction mixture was stirred for 3 days before workup, which gave **3b** as an orange crystalline solid (1.28 g, 63% yield) Anal. Found (calcd for $C_{70}H_{38}NP_2RuBF_{20}$): C., 58.29 (58.11); H., 2.46 (2.65); N., 0.90 (0.97). IR (KBr, cm^{-1}): 2322 (w, ν_{PH}), 2237 (w, ν_{CN}). LR-ESI-MS (CH_2Cl_2, *m/z*): 768.07.35 (M^+, 100%). Dec pt: 173-175 °C. $^{31}P\{^1H\}$ NMR (202.55 MHz, d_2-dichloromethane): 56.3 (d, $^2J_{PP}$ 42 Hz, PPh_3), 35.0 (d, $^2J_{PP}$ 42 Hz, PPh_2H).

2.6.2.3. Synthesis of Ru(η^5-indenyl)(PPh_2)(PPh_2H)(PPh_3) (4b)

KOBu^t (44 mg, 0.40 mmol) was added to an orange solution of **2** (232 mg, 0.33 mmol) and PPh_2H (0.17 mL, 0.99 mmol, 3 equiv) in toluene (30 mL) in a Schlenk flask. The solution turned deep purple and was stirred for 1 h. The solution was then filtered through Celite in a frit to remove KCl and HOBu^t. The solvent was removed from the filtrate under vacuum to give a purple solid, which was washed with pentane (3 × 10 mL)

and dried (190 mg, 68% yield). We have so far been unable to obtain this complex free of minor impurities, thus it has not been submitted for microanalysis. IR (KBr, cm^{-1}): 2310 (w, ν_{PH}). Dec pt: 178-180 °C. $^{31}P\{^{1}H\}$ NMR (202.55 MHz, d_8-THF): 49.1 (d, $^{2}J_{PP}$ 35 Hz, PPh_3), 42.6 (dd, $^{2}J_{PP}$ 35, 15 Hz, PPh_2H), 40.5 (d, $^{2}J_{PP}$ 15 Hz, PPh_2).

2.6.3. Catalyst Screening and Control Reactions

2.6.3.1. General Procedure for Catalytic Reactions

To 1 equiv of precatalyst (0.02 mmol) in a J. Young NMR tube was added 1 equiv of DBU (0.2 mL, 0.1 M in THF), 10 equiv of alkene (0.2 mL, 1.0 M in THF) and 10 equiv of PR_2H (0.2 mL, 1.0 M in THF) and d_6-benzene (0.2 mL). Each reaction was performed in triplicate; conversions and product ratios were determined from relative integration of the product and free secondary phosphine signals in $^{31}P\{^{1}H\}$ NMR spectra obtained using a gated decoupled experiment with a relaxation delay of 55 s.

2.6.3.2. General Procedure for Control Reactions

To 0.2 mL of C_6D_6 in a J. Young NMR tube was added two or more of 0.02 mmol of a Ru precatalyst, 0.2 mL of PR_2H, alkene (1.0 M in THF, 10 equiv), or DBU (0.1 M in THF, 1 equiv). In reactions where one or two reagents were left out the corresponding volume of THF (0.2 or 0.4 mL) was added to maintain the same concentration was would be present in the catalytic reactions described. The reactions were monitored by $^{31}P\{^{1}H\}$ NMR, using the quantitative pulse sequence where necessary.

2.6.4. Thermolysis Reaction of 4b

A solution of **4b** (20 mg, 0.024 mmol) in d_8-toluene was placed in a flame-sealable NMR tube, degassed by three freeze-pump-thaw cycles, and sealed under vacuum. An initial $^{31}P\{^1H\}$ NMR spectrum was obtained. The solution was heated at 60°C in an oil bath and removed periodically for monitoring by $^{31}P\{^1H\}$ NMR. After 96 h, approximately 50% of **4b** had decomposed, giving the orthometalated complex Ru(η^5-indenyl){κ^2-(*o*-C_6H_4)PPh_2}(PPh_2H) as well as free PPh_3 and tentatively assigned Ru(η^5-indenyl)(PPh_2)(PPh_2H)$_2$.

2.6.5. $^{31}P\{^{1}H\}$, ^{1}H and $^{13}C\{^{1}H\}$ NMR Data of Complexes 3a,b and 4b

Table 2.3. 202.51 MHz $^{31}P\{^{1}H\}$ NMR data for complexes **3a,b** and **4b** at 300 K: shift in ppm (multiplicity, 2JPP, Hz).

Compounds	PPh_2	Other
[Ru(η^5-indenyl)(NCPh)(PPh_3)$_2$][$B(C_6F_5)_4$] (3a**)** **CD_2Cl_2**	-	46.9 (s, PPh_3)
[Ru(η^5-indenyl)(NCPh)(PPh_2H)(PPh_3)][$B(C_6F_5)_4$] (3b**)** **$CDCl_3$**	-	56.3 (d, 42) 35.0 (d, 42)
Ru(η^5-indenyl)(PPh_2)(PPh_2H)(PPh_3) (4b**)** **C_4D_8O**	40.5 (d, 15)	49.1 (d, 35) 42.6 (dd, 35, 15)

Table 2.4. 500.27 MHz ^{1}H NMR data for complexes **3a, 3b** and **4b** at 300 K: δ in ppm (multiplicity, RI, J_{avg} or $w_{1/2}$ in Hz, assignment).

Compound	**C_9H_7**				**PPh_3**	**Other**
	H_7, H_4	**H_6, H_5**	**H_2**	**H_3, H_1**		
3a **CD_2Cl_2**	7.14 (d, 7.29, 2H)	7.38 (t, 7.29, 2H)	4.90 (s, 1H)	4.52 (s, 2H)	H_o 7.24 (t, 7.29, 12H) H_m 6.98 (br, 12H) H_p 7.38 (t, 6H)	**NCPh:** H_o 7.31 (m, 2H) H_m 6.83 (m, 2H) H_p 7.64 (t, 7.8, 1H)
3b **$CDCl_3$**	7.50-7.44 (om, 1H, overlapping with $HPPh_2$ H_p and either H_6/H_5) 6.89 (d, 8.3, 1H)	7.50-7.44 (om, 1H, overlapping with $HPPh_2$ H_p and either H7/H4) 7.01-6.91 (om, 1H, overlapping with $HPPh_2$)	4.73 (s, 1H)	4.91 (s, 1H) 4.60 (s, 1H)	H_o 7.09-7.01 (6H, overlapping with HPPh2 peaks) H_m, H_p 7.43-7.35 (9H, overlapping with NCPh and HPPh2 peaks)	**NCPh**: H_o 7.35-7.30 (om, 2H, overlapping with PPh_3 H_m, H_p and $HPPh_2$) H_m 6.78 (d, 7.4, 2H) H_p 7.52 (t, 7.7, 1H) **$HPPh_2$**: H-P 6.22 (dd, 362.7 10.0, 1H) Ph: H_o 7.30-7.24 (om, 4H, overlapping with PPh_3 H_m, H_p and NCPh H_o), H_m 7.01-6.91 (om, 4H, overlapping with PPh3 H_o, and H6/H5), H_p 7.50-7.44 (om, 2H, overlapping with two of H_7/H_6/H_5/H_4)
4b **C_4D_8O**	6.57 (d, 8.4, 1H) 5.42 (d, 8.4, 1H)	7.06 (t, 7.5, 1H) 6.80 (t, 7.5, 1H)	5.72 (s, 1H)	4.83 (s, 1H) 4.07 (s, 1H)	H_o, H_m 7.16-6.87 (br, overlapping with H_5/H_6, 12H) Hp 7.38 - 7.24 (om, 3H)	**$HPPh_2$:** H_o 7.19 (t, 7.1, 2H), 7.38 - 7.24 (om, 2H) H_m 7.41 (t, 8.7, 2H), 7.51 (m, 2H) H_p 7.38 - 7.24 (om, 2H) H-P 6.26 (ddd, 345.7, 10.2, 5.9) **PPh_2**: H_o, H_m 6.78 - 6.65 (br, overlapping with H6/H_5 and P-H, 2H), 6.44 - 6.08 (br, , 2H) H_p 5.82 - 5.53 (br, overlapping with H_2, 1H)

Table 2.5. 125.77 MHz $^{13}C\{^{1}H\}$ NMR data for complexes **3a, 3b** and **4b** at 300 K: δ in ppm (multiplicity, RI, J_{avg} or $w_{1/2}$ in Hz, assignment).

Compound	C_9H_7						PPh_3	Other
	C_6, C_5	C_7, C_4	C_{7a}, C_{3a}	Δδ (C_{7a}, C_{3a})	C_2	C_3, C_1		
3a CD_2Cl_2	131.8 (s)	129.7 (s)	109.6 (s)	-21.1	93.7 (s)	69.0 (s)	C_i 134.5 (s) C_o 128.2 (t, 5) C_m 133.3 (t, 5) C_p 130.3 (s)	**NCPh**: NC 134.3 (s), C_i 111.0 (s), C_o 129.5 (s), C_m 124.3 (s), C_p 134.1 (s) **$B(C_6F_5)_4$**: 149.2 (s), 147.2 (s), 139.2 (s), 137.3 (s), 135.3 (s)
3b $CDCl_3$	131.7 (s) 129.3 (s)	129.0 (s) 124.7 (s)	109.5 (d, 2) 107.7 (s)	-22.1 (av)	93.0 (s)	67.2 (s) 68.9 (d, 6)	C_i 132.5 C_o 133.1 (d, 11) C_m 128.8 (d, 10) C_p 131.0 (d, 2)	**PPh_2H**: C_i 132.4 (s), 132.0 (s), C_o 132.9 (d, 10), 131.4 (d, 10), C_m 129.1 (d, 10), C_p 130.8 (d, 2) **NCPh**: NC 127.7 (s), C_i 110.5 (s), C_o 128.0 (s), C_m 123.6 (s), C_p 134.0 (s) **$B(C_6F_5)_4$**: 149.2 (s), 147.2 (s), 139.2 (s), 137.3 (s), 135.3 (s)
4b C_4D_8O	123.3 (s) 121.0 (s)	126.0 (s) 122.6 (s)	114.5 (s) 107.2 (s)	-19.9 (av)	98.8 (s)	74.4 (d, 11) 72.9 (d, 9)	C_i 133.5 (s) C_o, C_m 127.0 (br s, 29) C_p 128.8 (br s, 23)	**$HPPh_2$**: C_i 135.5 (s), 135.2 (s) C_o 127.8 (s), 127.9 (s) C_m 133.0 (s), 130.0 (s) C_p 131.3 (s), 128.5 (s) **PPh_2**: C_i 139.9 (s), 139.6 (s) C_o 127.9 (s), 128.0 (s) C_m 133.1, 133.0 (s) C_p 131.4 (s), 128.7 (s)

[a] $\Delta\delta(C_{3a,7a}) = \delta(C_{3a,7a}(\eta\text{-indenyl complex})) - \delta(C_{3a,7a}(\eta\text{-sodium indenyl}))$. $\delta(C_{3a,7a})$ for sodium indenyl = 130.7 ppm. [Gamasa, M. P.; Gimeno, J.;Gonzalez-Bernardo, C.; Martin-Vaca, B. M. *Organometallics* **1996**, *15*, 302.]

2.7. References

(1) Belli, R. G.; Burton, K. M. E.; Rufh, S. A.; McDonald, R.; Rosenberg, L. Inner- and Outer-Sphere Roles of Ruthenium Phosphido Complexes in the Hydrophosphination of Alkenes. *Organometallics* **2015**, *34*, 5637–5646.

(2) Derrah, E. J.; Pantazis, D. A.; McDonald, R.; Rosenberg, L. A Highly Reactive Ruthenium Phosphido Complex Exhibiting Ru−P π-Bonding. *Organometallics* **2007**, *26*, 1473–1482.

(3) Burton, K. M. E.; Pantazis, D. A.; Belli, R. G.; McDonald, R.; Rosenberg, L. Alkene Insertions into a Ru–PR2 Bond. *Organometallics* **2016**, *35*, 3970–3980.

(4) Derrah, E. J.; Pantazis, D. A.; McDonald, R.; Rosenberg, L. Concerted [2+2] Cycloaddition of Alkenes to a Ruthenium–Phosphorus Double Bond. *Angew. Chem. Int. Ed.* **2010**, *49*, 3367–3370.

(5) Derrah, E. J.; McDonald, R.; Rosenberg, L. The [2+2] Cycloaddition of Alkynes at a Ru-P *π*-Bond. *Chem. Commun.* **2010**, *46*, 4592–4594.

(6) Rodima, T.; Kaljurand, I.; Pihl, A.; Mäemets, V.; Leito, I.; Koppel, I. A. Acid−Base Equilibria in Nonpolar Media. 2.1 Self-Consistent Basicity Scale in THF Solution Ranging from 2-Methoxypyridine to EtP_1(pyrr) Phosphazene. *J. Org. Chem.* **2002**, *67*, 1873–1881.

(7) Kolthoff, I. M.; Chantooni, M. K.; Bhowmik, S. Dissociation Constants of Uncharged and Monovalent Cation Acids in Dimethyl Sulfoxide. *J. Am. Chem. Soc.* **1968**, *90*, 23–28.

(8) Issleib, K.; Kümmel, R. Alkali-Phosphorverbindungen Und Ihr Reaktives Verhalten : XXX. Zur P-H- Und As-H-Acidität Primärer Und Sekundärer

Phosphine Bzw. Arsine. *J. Organomet. Chem.* **1965**, *3*, 84–91.

(9) Stewart, R. *The Proton: Applications to Organic Chemistry*; Academic Press: Orlando, FL, 1985.

(10) Kaumpees, K; Trummel, A.; Leito, I. Basicities of Strong Bases in Water: A Computational Study. *Croat. Chem. Acta.* **2014**, *87*, 385–395.

(11) Huang, B. B. Sc. (Honours) Thesis, University of Victoria, 2014.

(12) Li, J.-N.; Liu, L.; Fu, Y.; Guo, Q.-X. What Are the PKa Values of Organophosphorus Compounds? *Tetrahedron* **2006**, *62*, 4453–4462.

(13) Abdur-Rashid, K.; Fong, T. P.; Greaves, B.; Gusev, D. G.; Hinman, J. G.; Landau, S. E.; Lough, A. J.; Morris, R. H. An Acidity Scale for Phosphorus-Containing Compounds Including Metal Hydrides and Dihydrogen Complexes in THF: Toward the Unification of Acidity Scales. *J. Am. Chem. Soc.* **2000**, *122*, 9155–9171.

(14) Oro, L. A.; Ciriano, M. A.; Campo, M.; Foces-Foces, C.; Cano, F. H. Indenyl Complexes of Ruthenium(II). Crystal Structure of $[Ru(CO)(PPh_3)_2(\eta^5\text{-}C_9H_7)]ClO_4 \cdot 12CH_2Cl_2$. *J. Organomet. Chem.* **1985**, *289*, 117–131.

(15) Trost, B. M.; Toste, F. D.; Pinkerton, A. B. Non-Metathesis Ruthenium-Catalyzed C−C Bond Formation. *Chem. Rev.* **2001**, *101*, 2067–2096.

(16) Trost, B. M.; Ryan, M. C. Indenylmetal Catalysis in Organic Synthesis. *Angew. Chem. Int. Ed.* **2017**, *56*, 2862–2879.

(17) Bassetti, M.; Marini, S.; Díaz, J.; Gamasa, M. P.; Gimeno, J.; Rodríguez-Álvarez, Y.; García-Granda, S. Synthesis and Properties of the Indenyl Ruthenium(II) Complex $[Ru\{(E)\text{-}\eta^1\text{-}C(C{:}\ CPh)=CHPh\}(\eta^5\text{-}C_9H_7)(\kappa^2\text{-}P\text{-}dppm)]$ (dppm =

Bis(Diphenylphosphino)Methane). An Organometallic Intermediate in the Catalytic Dimerization of Phenylacetylene. *Organometallics* **2002**, *21*, 4815–4822.

(18) Bassetti, M.; Casellato, P.; Gamasa, M. P.; Gimeno, J.; González-Bernardo, C.; Martín-Vaca, B. Insertion Reactions of Alkynes into the Ru−H Bond of Indenylruthenium(II) Hydride Complexes. Mechanism of the Reaction of Phenylacetylene with [RuH(η^5-C_9H_7)(dppm)] (dppm = Bis(Diphenylphosphino)Methane). *Organometallics* **1997**, *16*, 5470–5477.

(19) Derrah, E. J.; Marlinga, J. C.; Mitra, D.; Friesen, D. M.; Hall, S. A.; McDonald, R.; Rosenberg, L. Electronic Control of Conformation in Mixed-Phosphine Complexes of the Ruthenium η^5-Indenyl Fragment. *Organometallics* **2005**, *24*, 5817–5827.

(20) Cadierno, V.; Díez, J.; Pilar Gamasa, M.; Gimeno, J.; Lastra, E. Indenyl Complexes of Group 8 Metals. *Coord. Chem. Rev.* **1999**, *193–195*, 147–205.

(21) Kamigaito, M.; Watanabe, Y.; Ando, T.; Sawamoto, M. A New Ruthenium Complex with an Electron-Donating Aminoindenyl Ligand for Fast Metal-Mediated Living Radical Polymerizations. *J. Am. Chem. Soc.* **2002**, *124*, 9994–9995.

(22) Hoyle, M.-A. M.; Pantazis, D. A.; Burton, H. M.; McDonald, R.; Rosenberg, L. Benzonitrile Adducts of Terminal Diarylphosphido Complexes: Preparative Sources of "Ru═PR2." *Organometallics* **2011**, *30*, 6458–6465.

(23) Giner Planas, J.; Hampel, F.; Gladysz, J. A. Generation and Reactions of Ruthenium Phosphido Complexes [(η^5-C_5H_5)Ru(PR'_3)$_2$(PR_2)]: Remarkably High Phosphorus Basicities and Applications as Ligands for Palladium-Catalyzed

Suzuki Cross-Coupling Reactions. *Chem. Eur. J.* **2005**, *11*, 1402–1416.

(24) Scriban, C.; Glueck, D. S.; Zakharov, L. N.; Kassel, W. S.; DiPasquale, A. G.; Golen, J. A.; Rheingold, A. L. P−C and C−C Bond Formation by Michael Addition in Platinum-Catalyzed Hydrophosphination and in the Stoichiometric Reactions of Platinum Phosphido Complexes with Activated Alkenes. *Organometallics* **2006**, *25*, 5757–5767.

(25) Scriban, C.; Kovacik, I.; Glueck, D. S. A Protic Additive Suppresses Formation of Byproducts in Platinum-Catalyzed Hydrophosphination of Activated Olefins. Evidence for P−C and C−C Bond Formation by Michael Addition. *Organometallics* **2005**, *24*, 4871–4874.

(26) Rosenberg, L. Mechanisms of Metal-Catalyzed Hydrophosphination of Alkenes and Alkynes. *ACS Catal.* **2013**, *3*, 2845–2855.

(27) Belli, R. G.; Wu, Y.; Ji, H.; Joshi, A.; Yunker, L. P. E.; McIndoe, J. S.; Rosenberg, L. Competitive Ligand Exchange and Dissociation in Ru Indenyl Complexes. *Inorg. Chem.* **2019**, *58*, 747–755.

(28) Yang, X.-Y.; Jia, Y.-X.; Tay, W. S.; Li, Y.; Pullarkat, S. A.; Leung, P.-H. Mechanistic Insights into the Role of PC- and PCP-Type Palladium Catalysts in Asymmetric Hydrophosphination of Activated Alkenes Incorporating Potential Coordinating Heteroatoms. *Dalton Trans.* **2016**, *45*, 13449–13455.

(29) Xu, C.; Jun Hao Kennard, G.; Hennersdorf, F.; Li, Y.; Pullarkat, S. A.; Leung, P.-H. Chiral Phosphapalladacycles as Efficient Catalysts for the Asymmetric Hydrophosphination of Substituted Methylidenemalonate Esters: Direct Access to Functionalized Tertiary Chiral Phosphines. *Organometallics* **2012**, *31*, 3022–3026.

(30) Huang, Y.; Pullarkat, S. A.; Li, Y.; Leung, P.-H. Palladacycle-Catalyzed Asymmetric Hydrophosphination of Enones for Synthesis of C*- and P*-Chiral Tertiary Phosphines. *Inorg. Chem.* **2012**, *51*, 2533–2540.

(31) Huang, Y.; Chew, R. J.; Li, Y.; Pullarkat, S. A.; Leung, P.-H. Direct Synthesis of Chiral Tertiary Diphosphines via Pd(II)-Catalyzed Asymmetric Hydrophosphination of Dienones. *Org. Lett.* **2011**, *13*, 5862–5865.

(32) Sues, P. E.; Lough, A. J.; Morris, R. H. Reactivity of Ruthenium Phosphido Species Generated through the Deprotonation of a Tripodal Phosphine Ligand and Implications for Hydrophosphination. *J. Am. Chem. Soc.* **2014**, *136*, 4746–4760.

Chapter 3 Mechanistic Study of the Hydrophosphination of Activated Alkenes Catalyzed by Ru Phosphido Complexes

3.1. Chapter Overview

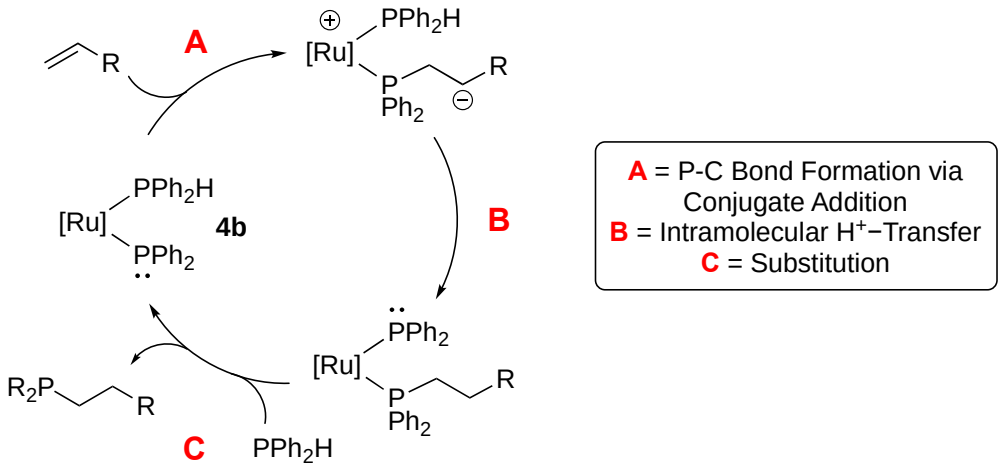

Scheme 3.1. Proposed mechanism for the hydrophosphination of activated alkenes (R = electron withdrawing group) catalyzed by Ru(η^5-indenyl) complexes bearing terminal phosphido ligands.

As described in Chapter Two, Ru complexes bearing phosphido ligands catalyze the hydrophosphination of activated alkenes through an outer sphere mechanism (Scheme 3.1). In this chapter, the reaction kinetics and a detailed mechanistic study of the hydrophosphination of *tert*-butyl acrylate by diphenylphosphine using Ru complexes bearing phosphido ligands as catalysts is described. The complexes studied are Ru(η^5-indenyl)(PPh_2)(NCPh)(PPh_3) (**4a**), Ru(η^5-indenyl)(PPh_2)(PPh_2H)(PPh_3) (**4b**) and Ru(η^5-indenyl)(PPh_2)(CO)(PPh_3) (**4c**). The new complex Ru(η^5-indenyl)(PPh_2)(**P**)$_2$ (**4e**, **P** = $P(Ph_2)CH_2CH_2CO_2Bu^t$) was prepared and characterized. This Chapter includes

contributions from Erick Nuñez Bahena and Dr. Robert McDonald. Supplementary spectra are presented in Appendix E and F.

3.2. Introduction

3.2.1. Mechanisms and Challenges of Late Metal Catalyzed Hydrophosphination

As with all areas of science, the development and advancement of fields can only be achieved through thoroughly understanding the fundamental principles and mechanisms through which they function. This is particularly true in chemistry when studying transition metal-catalyzed reactions. A deep understanding of how the catalyst structure (metal, ligand scaffold) influences the mechanism (rate limiting step, off-cycle processes, catalyst deactivation pathways) and catalytic activity is paramount for guiding the design of robust and highly active catalysts for a given reaction. For hydrophosphination, there are many documented metal catalysts,[1–9] but the field is lacking in detailed mechanistic and kinetic analyses of these catalytic systems. Examples of mechanistic studies on metal-catalyzed hydrophosphination were discussed in section 1.4. In particular, Marks and Glueck delineated the prominent inner-sphere[10–12] and outer-sphere[13,14] mechanisms for hydrophosphination, respectively (described in sections 1.4.1. and 1.4.2, respectively).

Despite the growing number of examples of metal-catalyzed hydrophosphination, further understanding of the mechanisms of these systems is needed in order to address challenges in the field. Common challenges with metal-catalyzed hydrophosphination reactions are the limited substrate scope (both alkene and phosphine)[15] and low activity. Many examples of metal catalysts, or intermediates, for hydrophosphination contain phosphido ligands, which are very nucleophilic, especially when coordinated to late

metals.[16] Thus the mechanism of P-C bond formation in many examples of late metal-catalyzed hydrophosphination typically occurs via conjugate addition of the phosphido ligand at alkene (Scheme 3.1, step A). Notable examples of late metal catalysts for hydrophosphination where P-C bond formation via conjugated addition is proposed include Ru,[17,18] Rh,[19] Pt[13,14] and Pd.[20–25] For this reason, the scope of unsaturated substrates is often limited to activated, electron-deficient alkenes and alkynes. Moreover, diaryl, secondary phosphines (PAr_2H) are overrepresented as substrate phosphine in all examples of metal-catalyzed hydrophosphination. Last, these systems typically have low activities (low turnover frequencies, TOF), which can results from product inhibition or catalyst poisoning by the hydrophosphination product phosphine.

3.2.2. Rationale for Studying the Mechanism of Catalysis by Complex 4

As described in Chapter 2, Ru complexes bearing phosphido ligands catalyze the hydrophosphination of alkenes through an outer sphere mechanism (Scheme 3.1). I proposed that this mechanism was operative based on the fact that catalysis was only observed with electron-deficient substrates. In order to obtain more evidence for this mechanism, I wanted to conduct a detailed study of hydrophosphination catalyzed by these Ru phosphido complexes. This would involve studying the reaction kinetics as well as carefully designing control experiments to probe the putative steps of the proposed mechanism.

The ease of synthesis of a variety of Ru phosphido complexes, Ru(η^5-indenyl)(PPh_2)(L)(PPh_3) (**4**),[26,27] provided the opportunity to conduct a mechanistic and

kinetic analysis of a series of these complexes for the hydrophosphination of activated alkenes. The complexes chosen for this study were **4a**, containing a labile NCPh ligand, **4b**, containing a semi-labile PPh_2H ligand, and **4c**, containing a non-labile CO ligand. I anticipated that studying these complexes would demonstrate if and how simple changes to the catalyst structure would influence the activity or mechanism of catalysis. Initial results from studying complexes **4a**,**b**,**c** showed different catalytic activities by these three complexes (Figure 3.1), which suggests that the seemingly simple modification of a single ancillary ligand can impact catalysis. The insight gained from this mechanistic analysis will guide the design of new metal catalysts as well as help to identify optimal conditions for catalysis.

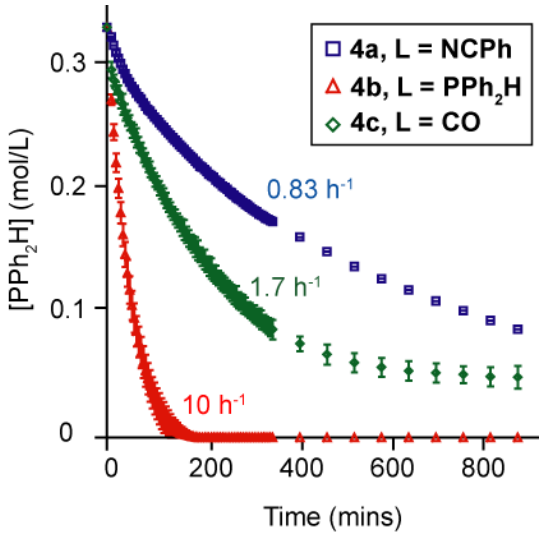

Figure 3.1. Monitoring the hydrophosphination of tert-butyl acrylate with PPh_2H using **4a,b,c** as catalysts precursors by ^1H NMR spectroscopy (C_6D_6, 500.27 MHz).

These reaction profiles (and those presented in this Chapter) were generated from ^1H NMR monitoring of the hydrophosphination of *tert*-butyl acrylate with PPh_2H catalyzed by **4a-c**. This reaction was chosen as the model reaction for this study because *tert*-butyl

acrylate has diagnostic ^{1}H NMR resonances (vinyl and Bu^{t} protons). Using ^{1}H NMR to monitor catalysis and measure activities is advantageous over ^{31}P{^{1}H} NMR (used in Chapter 2) because the experiments are shorter, which allows for many data points to be collected during a reaction (as seen in Figure 3.1).

3.3. Investigating Hydrophosphination Catalysis with Complex 4b

Ru(η^5-indenyl)(PPh_2)(PPh_2H)(PPh_3) (**4b**) was an obvious choice to include in this study because I demonstrated in Chapter 2 that it is a competent catalyst for hydrophosphination and is a proposed on-cycle species. Furthermore, it was the simplest catalyst, with respect to **4a** and **4c**, because it contained the substrate phosphine, PPh_2H coordinated to Ru. In this section the hydrophosphination of *tert*-butyl acrylate with diphenylphosphine (PPh_2H) catalyzed by complex **4b** is described. The reaction rate dependences on the concentration of **4b**, *tert*-butyl acrylate and diphenylphosphine were determined. Monitoring catalysis using **4b** by ^{31}P{^{1}H} NMR showed that the resting state of catalysis is Ru(η^5-indenyl)(PPh_2)(**P**)$_2$ (**4e**, **P** = P($CH_2CH_2CO_2Bu^t$)Ph_2) a complex containing two product phosphine ligands. Furthermore, I determined that this system is susceptible to product inhibition.

3.3.1. Determining the Reaction Rate Dependence on the Concentration of 4b

I determined, using two methods, that the reaction rate dependence on the concentration of **4b** for the hydrophosphination of *tert*-butyl acrylate with PPh_2H is first order. Concentrations of **4b** ranging from 0.0084 – 0.033 M (2.5, 5.0, 7.5 and 10 mol%) were used. All reactions were performed in triplicate.

The first method I used was the initial rates method, which is a traditional method used to determine reaction rate dependences on substrate or catalyst concentrations. This method involves establishing a relationship between the initial rates of a reaction with respect to changes in the concentration of substrate or catalyst. I found that there is a first order dependence of the reaction rate on the concentration of **4b** using the initial rates method (Figure 3.2).

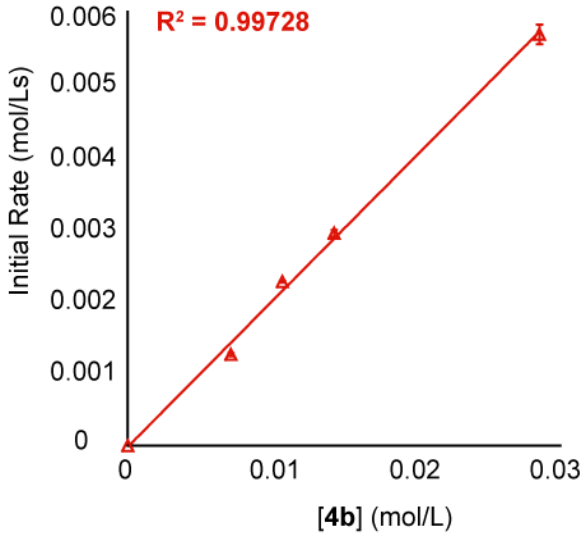

Figure 3.2. First order reaction rate dependence on [**4b**] determined by initial rates method.

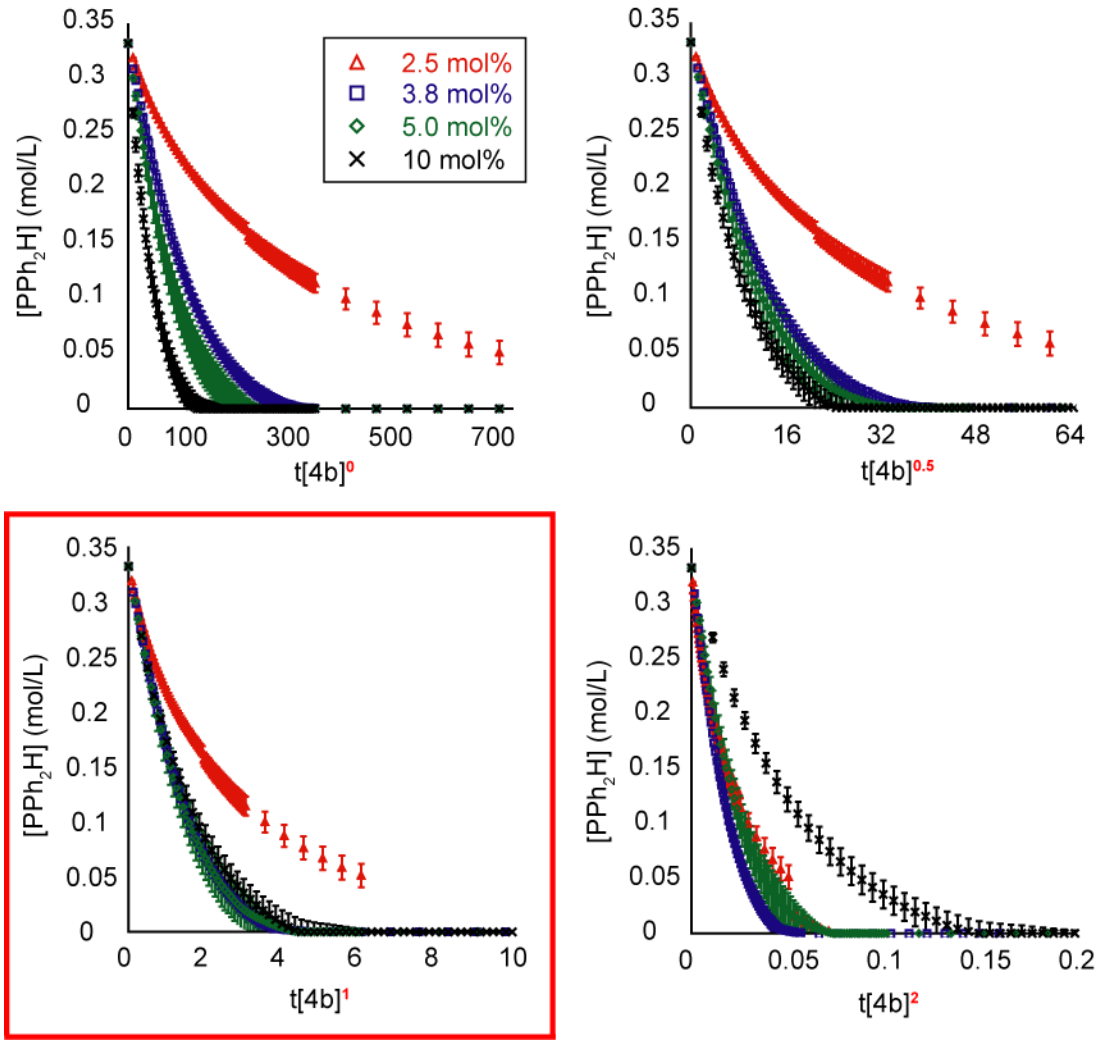

Figure 3.3. Reaction rate dependence on [**4b**] determined by VTNA; at late time points the reaction using 2.5 mol% of **4b** does not fit first order dependence.

The second, new method that I used to determine the reaction rate dependence on the concentration of **4b** is Variable Time Normalization Analysis (VTNA).[28] This method involves plotting the entire reaction profile for reactions using different catalyst concentrations together (Figure 3.3). The time axis is then normalized by multiplying the time by $[cat]^n$, where [cat] is the catalyst concentration for a given reaction and n is an arbitrary number. Assuming that the total catalyst concentration remains constant throughout the reaction, the individual reaction profiles should overlap at a value of n that

represents the rate dependence. As seen in Figure 3.3, a first order dependence on the concentration of **4b** is determined because the reaction profiles for the three reactions using higher concentrations of **4b** (5.0, 7.5 and 10 mol%) overlap at n = 1. However, the reaction where a low concentration of **4b** was used (2.5 mol%) does not overlap with the other reaction profiles at n = 1. The poor overlay could be attributed to either product inhibition or catalyst deactivation at this low catalyst concentration, which will be discussed in detail in section 3.2.2. Since VTNA allows for a direct comparison of all the data points collected, discrepancies, like the poor overlay described, are observed, which would otherwise be missed by exclusively using the initial rates method.

Reactions using the same catalyst loadings of **4b** described above were performed under pseudo-first order conditions (10 equiv of PPh_2H relative to *tert*-butyl acrylate). I determined that there is also a first-order dependence on the concentration of **4b** using VTNA. Under these conditions, the VTNA shows an overlap of all the reaction profiles with different concentrations of **4b** at n = 1 (Figure 3.4), even for the low catalyst concentration reaction (2.5 mol%).

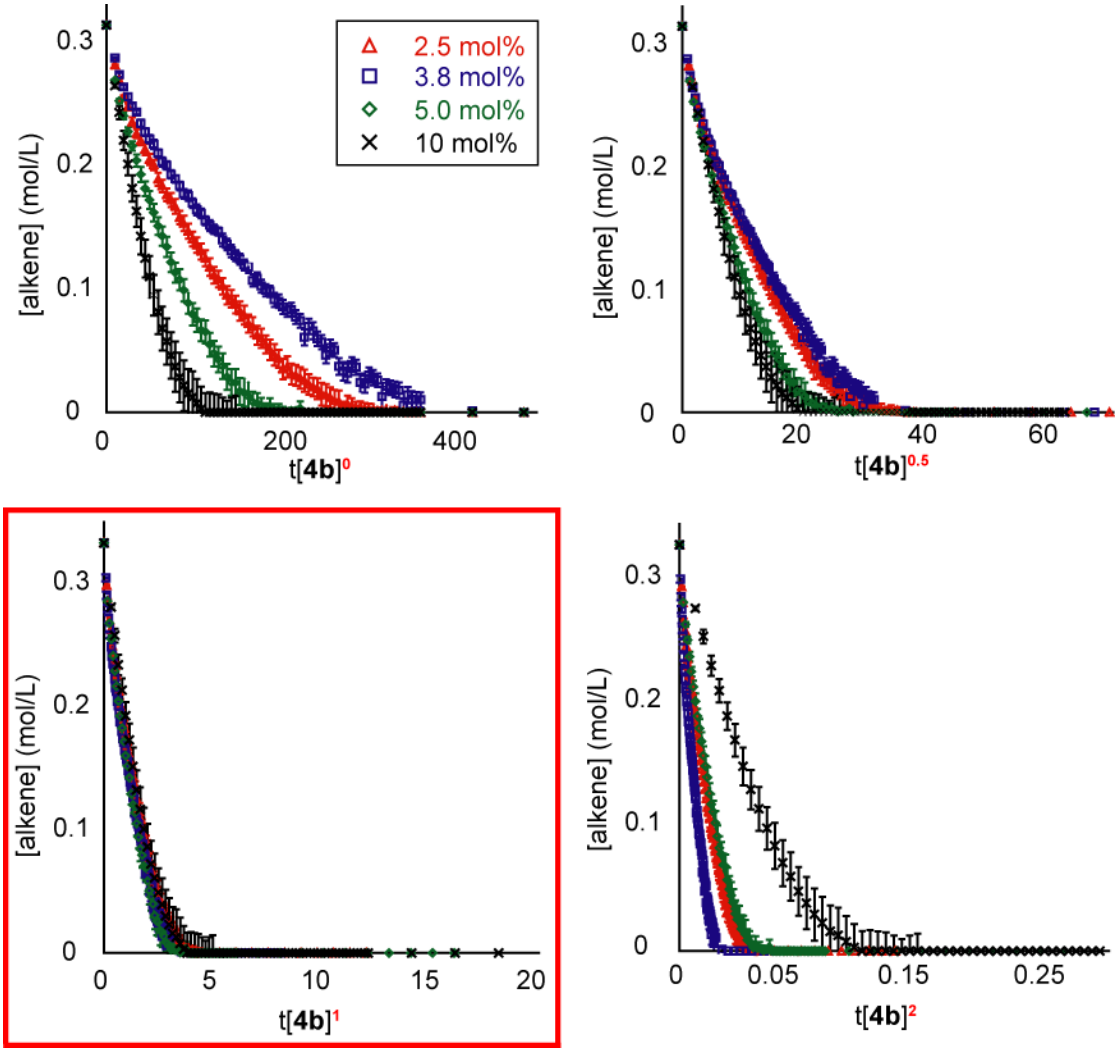

Figure 3.4. First order reaction rate dependence on [**4b**] determined by VTNA under pseudo-first order conditions (excess PPh_2H).

3.3.2. Deducing Product Inhibition Using the "Same Excess "Experiment

As discussed above, the reaction profile of a reaction using a low concentration of **4b** did not overlap with the other reaction profiles of reactions using higher concentrations of **4b** in the VTNA under non-pseudo first order conditions. This suggested that product inhibition or catalyst deactivation could be occurring. Product inhibition is a conceivable issue for metal-catalyzed hydrophosphination because the product phosphines produced are good ligands that can effectively compete with substrates for coordination at the

metal.[29,30] A "same excess" experiment can distinguish whether product inhibition or catalyst deactivation is occurring for a given system by simply comparing the reaction profiles of two to three reactions.[31]

I used the "same excess" method to determine that hydrophosphination catalysis by **4b** is susceptible to product inhibition at low catalyst concentrations (Figure 3.5). Two reactions following the "same excess" protocol were performed: **a** (red plot) and **b** (blue plot). Reaction **b** mimics the conditions of reaction **a** when the reactants are 50% consumed ($t_{1/2}$), but without any product present. When the reaction profile of **b** is time-adjusted to the reaction profile of **a** (Figure 3.5, right), no overlap is observed, which suggests that the rate of the reactions are different at that concentration of the substrates. This indicates either that product inhibition or catalyst deactivation is occurring. To prove that this difference in rate results from product inhibition rather than catalyst deactivation, a third reaction, **c** (green plot), was performed. Reaction **c** is similar to **b**, but the amount of product phosphine that would have formed at $t_{1/2}$ was added to exactly mimic the conditions of reaction **a** at $t_{1/2}$. The reaction profile of **c** after time adjustment more closely matched that of reaction **a**, which indicates that the loss of activity of the catalyst is due to product inhibition. If the profile for reaction **c** had overlapped with reaction **b**, then the loss of activity would result from catalyst deactivation rather than product inhibition, because the presence of product would not have affected the rate.

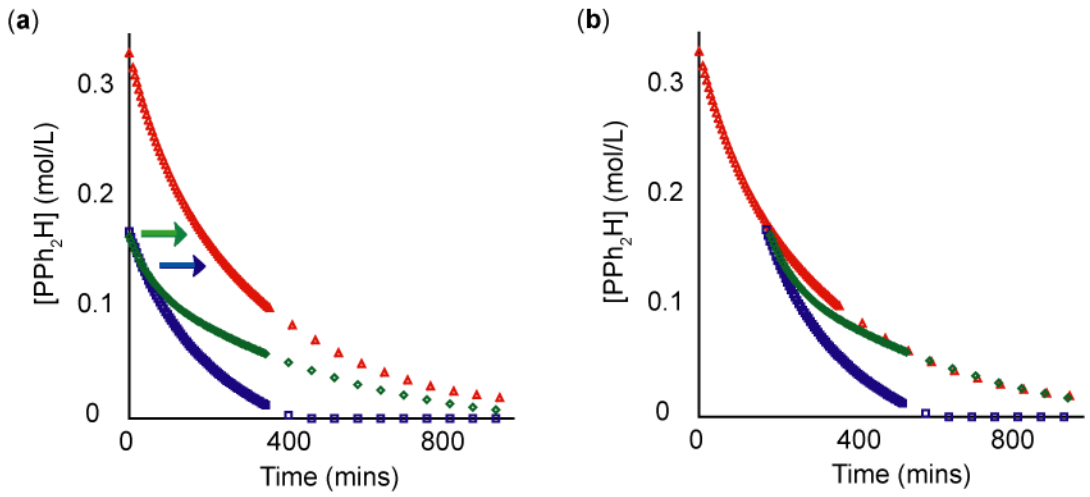

Figure 3.5. Reaction profiles for the hydrophosphination of *tert*-butyl acrylate by PPh_2H following the "same excess" protocol. Profile **a** (red) and **b** (blue) have different initial concentrations of *tert*-butyl acrylate and PPh_2H. Profile **c** (green) has the same initial concentrations as **b** but with added **P** to match the the concentration of **P** in **a**.

Product inhibition likely occurs via competition of the product phosphine, **P**, with the substrate phosphine for coordination at Ru. A key step in the proposed mechanism in Scheme 3.1 involves substitution of Ru-bound **P** by PPh_2H (step C). Substitution at Ru(η^5-indenyl) complexes is known to occur via a dissociative mechanism (Scheme 3.2).[35] At later time points in the catalytic reaction, when [**P**] >> [PPh_2H], the equilibrium of this substitution would lie heavily towards **P**-bound complexes (Scheme 3.2). This effect would be even more pronounced when a low catalyst concentration is used because at later time points, the relative concentration of **P** to catalyst would be higher than in a reaction using a high catalyst concentration. Thus, the poor overlay of the reaction profile of the reaction using a low concentration of **4b** in the VTNA, discussed in section 3.2.1 (Figure 3.3), is attributed to product inhibition.

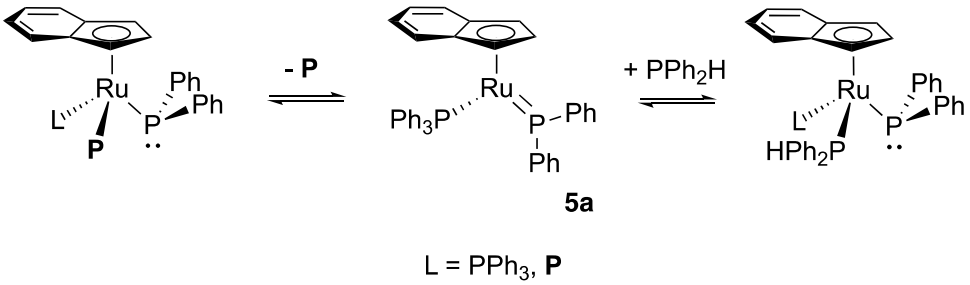

Scheme 3.2. Equilibrium of phosphine substitution at Ru between PPh_2H and the hydrophosphination product phosphine, **P**. This scheme shows the fundamental steps involved in the proposed substitution for catalytic turnover (Scheme 3.1, step C).

Under pseudo-first order conditions, with a large excess of PPh_2H, product inhibition should be prevented because the equilibrium shown in Scheme 3.2 would lie heavily towards PPh_2H-bound complexes. I confirmed that product inhibition is prevented in the presence of excess PPh_2H by performing a "same excess" experiment under pseudo-first order conditions (10 equiv of PPh_2H relative to *tert*-butyl acrylate) (Figure 3.6). Two reactions following the "same excess" protocol were performed: **a** (red plot) and **b** (blue plot). After time adjustment, plot **b** overlaps well with **a**, which suggests that no product inhibition (or catalyst deactivation) occurs under these conditions. This also is consistent with the fact that a first order dependence on the concentration of **4b** is observed at all concentrations under pseudo-first order conditions (as discussed in section 3.2.1).

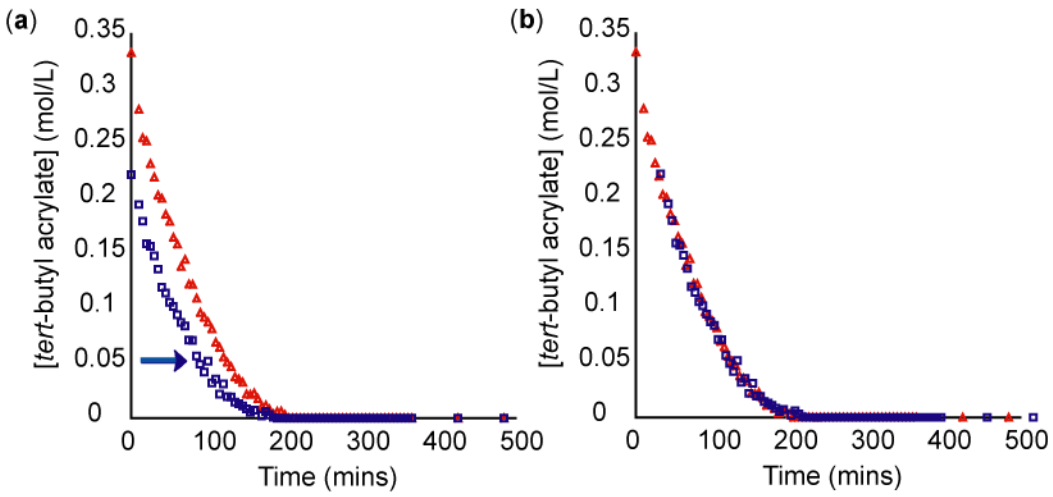

Figure 3.6. Reaction profiles for the hydrophosphination of *tert*-butyl acrylate by PPh_2H following the "same excess" protocol under pseudo-first order conditions. Profile **a** (red) and **b** (blue) have different initial concentrations of *tert*-butyl acrylate and PPh_2H.

3.3.3. Monitoring Hydrophosphination by $^{31}P\{^1H\}$ NMR Using PPh_2H Complex 4b

I used $^{31}P\{^1H\}$ NMR to monitor the hydrophosphination of *tert*-butyl acrylate with PPh_2H catalyzed by **4b** in order to identity the intermediates that form during catalysis (Figure 3.7). This showed that **4b** is completely consumed (**4b** is not present in the initial spectrum collected, ~ 30 mins) and that two new Ru-P species form (Figure 3.7). These new species are the Ru phosphido complexes Ru(η^5-indenyl)(PPh_2)(**P**)$_2$ (**4e**) and Ru(η^5-indenyl)(PPh_2)(**P**)(PPh_3) (**4d**), which both contain the hydrophosphination product, **P**, as a ligand. Complex **4d** only appears during the first couple of turnovers and quickly disappears, while complex **4e** increases in concentration at the expense of **4d** and persists throughout catalysis.

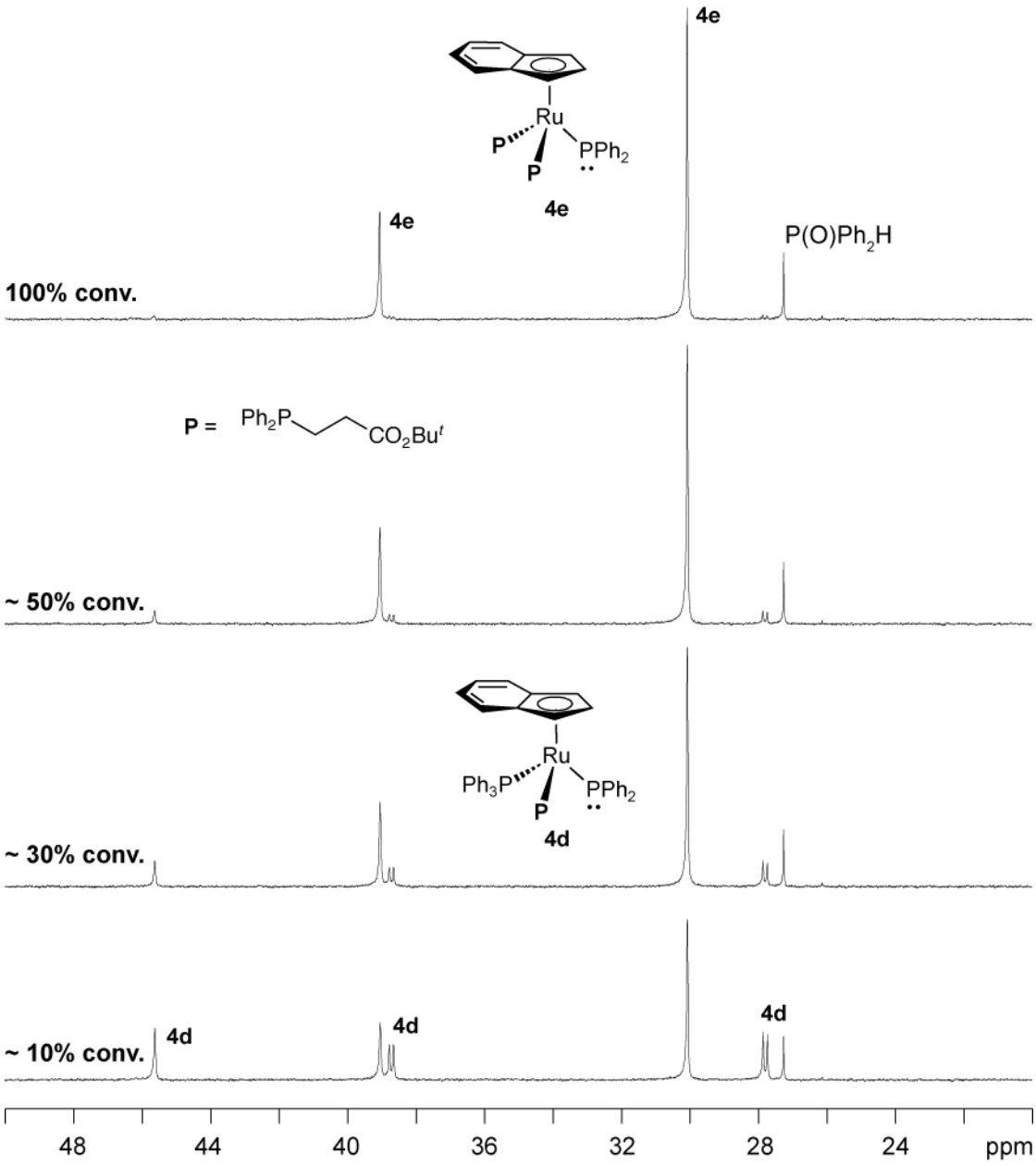

Figure 3.7. Ru-coordinated phosphine/phosphido region of the $^{31}P\{^{1}H\}$ NMR during catalysis under non-pseudo first order conditions using **4b** as the catalyst precursor (145.85 MHz, C_6D_6).

The fact that **4e** is observed as the major species under catalytic conditions suggests that **4e** is the resting state of catalysis when **4b** is used as the precatalyst. Formation of the **P**-bound complexes, **4d**,**e**, as the only species during catalysis suggests that substitution of

P in **4d**,**e** by PPh_2H is rate-limiting (Scheme 3.1, step C). Furthermore, observing **4d**,**e** is consistent with the established product inhibition described in section 3.2.3. Complex **4e** was prepared independently and will be discussed in section 3.4.

3.3.4. Stoichiometric Reactivity of Complex 4b with *tert*-butyl acrylate

I performed stoichiometric reactions of complex **4b** with *tert*-butyl acrylate in order to probe the P-C bond forming step of our proposed mechanism for hydrophosphination. The reactions of complex **4b** with one and two equiv of *tert*-butyl acrylate is presented in this section. The outcomes of these reactions provide evidence for steps A (nucleophilic attack) and B (intramolecular deprotonation) in our proposed mechanism shown in Scheme 3.1.

The reaction of **4b** with one equivalent of *tert*-butyl acrylate gives a mixture of products, of which **4d** (red dots Figure 3.8) is the major product. In this mixture there is also some **4e** (purple dots), the metallacycles Ru(η^5-indenyl)(κ^2-Bu^{t}CO$_2$CHCH$_2$PPh$_2$)(PPh_3) (**6d**, green dots), and Ru(η^5-indenyl)(κ^2-Bu^{t}CO$_2$CHCH$_2$PPh$_2$)(**P**) (**6e**, black dots), PPh_3 and **P**, as well as some unreacted **4b** (blue dots). The final product mixed formed within the time I could collect the $^{31}P\{^1H\}$ NMR spectrum. The complex mixture of products observed demonstrates the variety of substitution reactions that may occur in the presence of PPh_3, PPh_2H and **P**. Complexes **6d**,**e** were identified by the diagnostic ^{31}P chemical shift of P in 4-membered Ru-metallacycles previously reported by our group.[32,33]

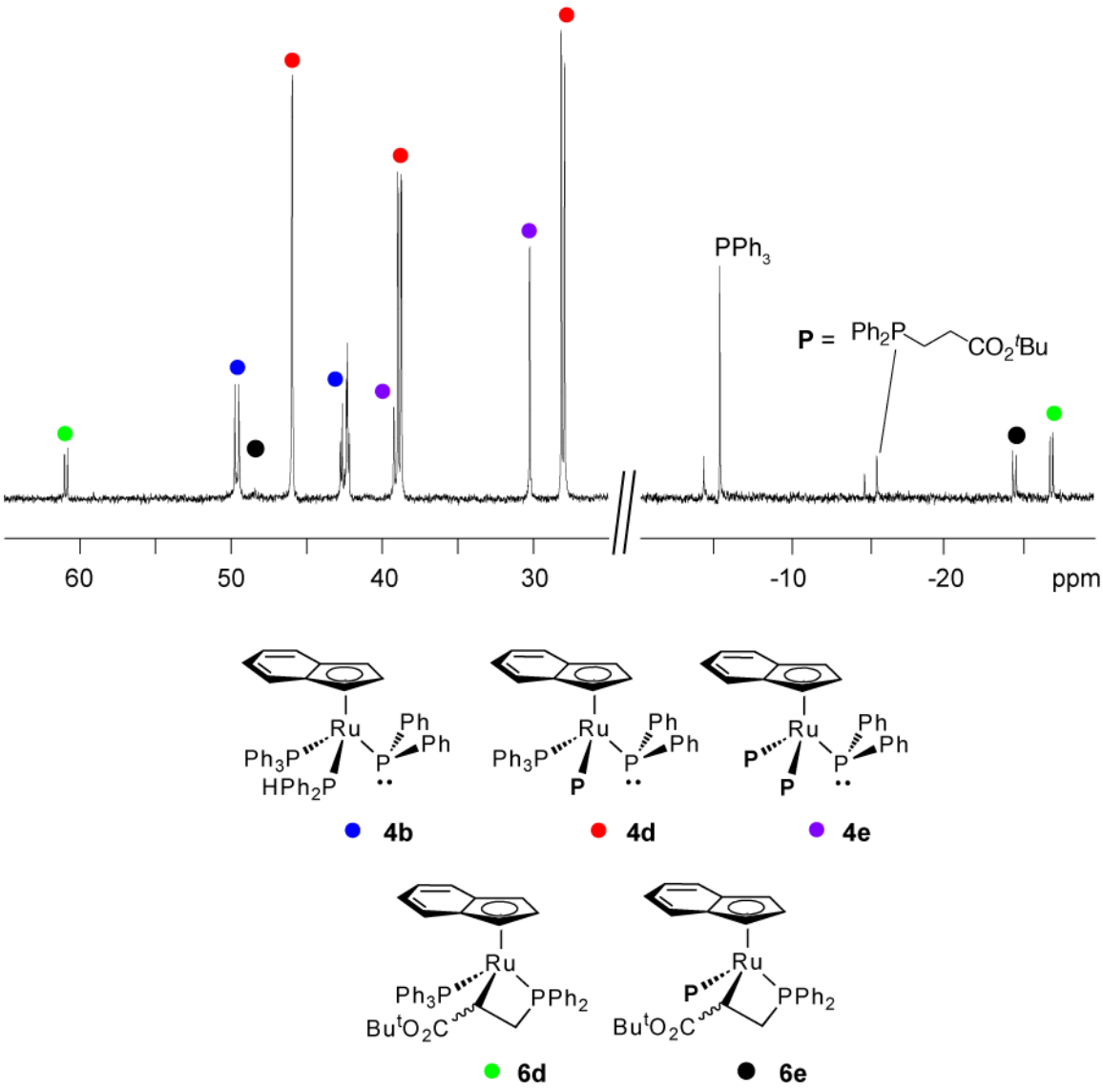

Figure 3.8. $^{31}P\{^{1}H\}$ NMR (121.55 MHz, C_6D_6) spectrum of the reaction of **4b** with one equivalent of *tert*-butyl acrylate.

The proposed mechanism that leads to the product mixture described above is shown in Scheme 3.3. The phosphido ligand in **4b** participates in conjugate addition to *tert*-butyl acrylate. This generates a zwitterionic intermediate, the carbanion of which must be quenched by intramolecular deprotonation of the P-H bond of the coordinated PPh_2H, since this is the only source of H^+ in the reaction mixture. This generates complex **4d**, which

contains the hydrophosphination product phosphine as a ligand. Some unreacted **4b** remains at the end of the reaction because **4d** can react with an additional equivalent of *tert*-butyl acrylate to give complexes **6d**,**e** (Scheme 3.3, bottom, *vide infra*).

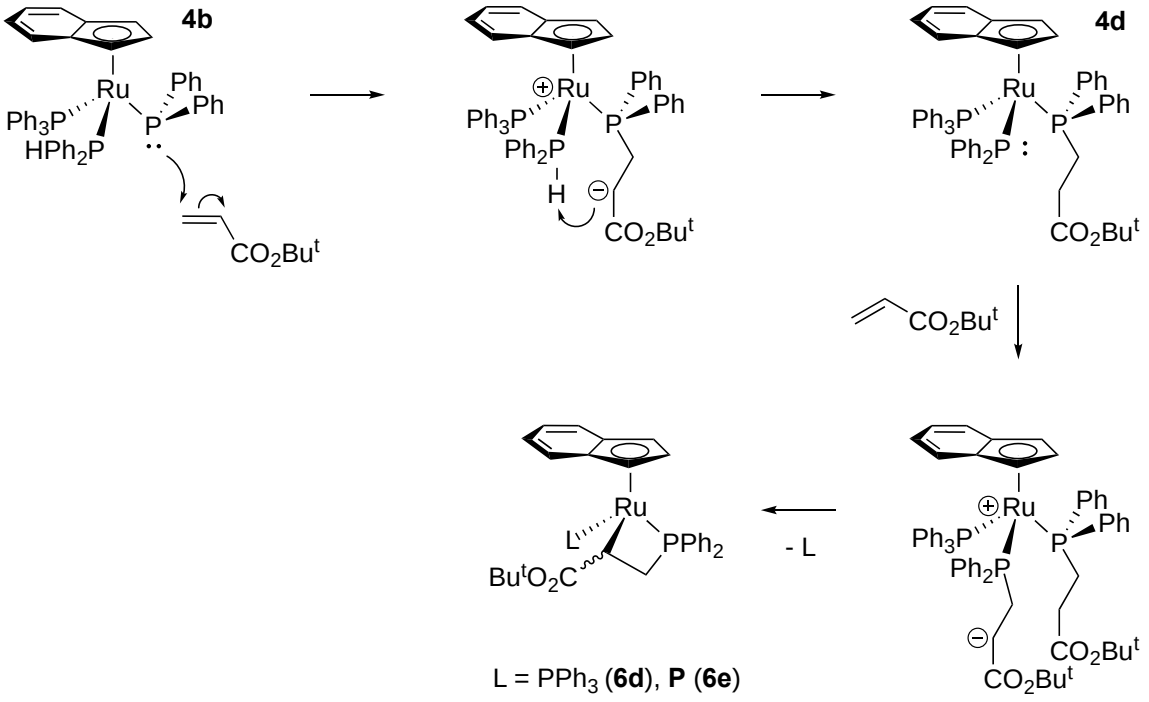

Scheme 3.3. Stoichiometric reaction of **4b** with *tert*-butyl acrylate; reaction with one equiv of *tert*-butyl acrylate results in formation of **4d** (top) and reaction with a second equiv of *tert*-butyl acrylate results in formation of metallacycles **6d**,**e**, PPh_3 and **P** (bottom).

To confirm that complexes **6d**,**e** form from the addition of *tert*-butyl acrylate to **4d**, I performed a reaction where two equiv of *tert*-butyl acrylate were added to **4b**. This gave the metallacycles **6d**,**e** as well as an equivalent of uncoordinated **P** and PPh_3; some minor unidentified species also formed. The reaction was complete within the time I could collect the $^{31}P\{^1H\}$ NMR spectrum. The metallacycles **6d**,**e** form almost exclusively from this reaction because there is no available P-H bond to quench the carbanion of the zwitterionic

intermediate (Scheme 3.3, bottom). Instead, dissociation of either PPh_3 or **P** allows the carbanion to bind to Ru and form the metallacycles.

The metallacycles **6d**,**e** are never observed during catalysis when using **4b** as the precatalyst. This suggests that the phosphido ligand in complex **4d** can participate in nucleophilic attack at an alkene, but that in the presence of excess PPh_2H and **P**, under catalytic conditions, metallacycle formation is prevented. Presumably, dissociation of phosphines from Ru is slower than the rate at which the carbanion is quenched.

3.3.5. Determining the Reaction Rate Dependences on the Concentration of PPh_2H and *tert*-Butyl Acrylate

I determined the reaction rate dependences on the substrate concentrations using a similar VTNA technique to the one described in section 3.2.1.[34] This method normalizes the time between consecutive data points by taking the average of the concentration of the substrate at those points. This removes the kinetic effect of that substrate concentration from the reaction profile and accounts for the changing concentration of the substrate during the reaction.

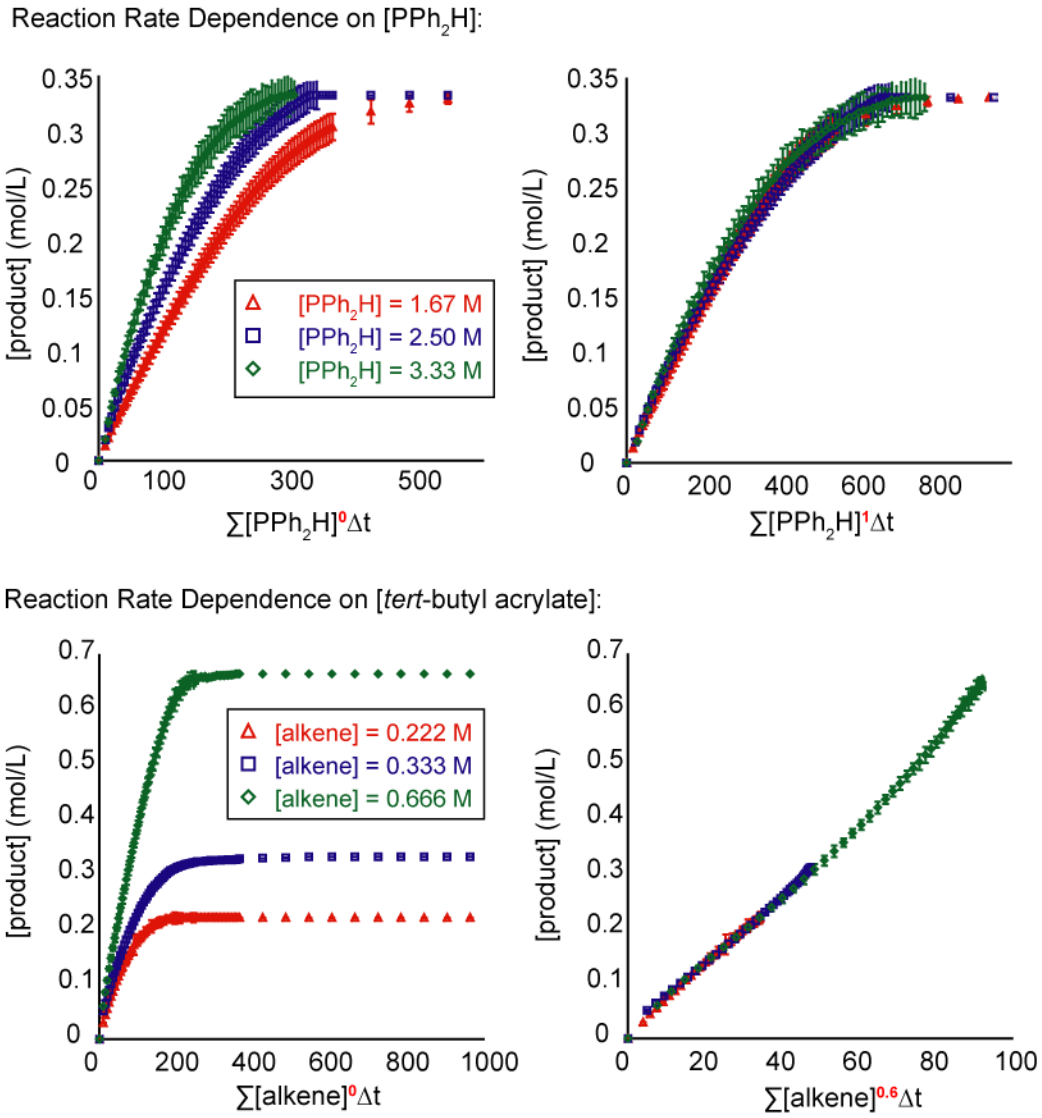

Figure 3.9. Time normalization plots to determine the reaction rate dependences on [PPh_2H] and [*tert*-butyl acrylate] for the hydrophosphination of *tert*-butyl acrylate with PPh_2H catalyzed by complex **4b**, as monitored by ^1H NMR. Top: time normalization for reactions using three different [PPh_2H] showing first order dependence on [PPh_2H] (top, right). Bottom: time normalization for reactions using three different [*tert*-butyl acrylate] showing partial order dependence on [*tert*-butyl acrylate] (bottom, right).

Under pseudo-first order conditions using an excess of PPh_2H, there is a first-order dependence on the PPh_2H concentration and a 0.6-order dependence on *tert*-butyl acrylate concentration (Figure 3.9). The first-order dependence on the PPh_2H concentration is consistent with substitution of Ru-bound **P** by PPh_2H as the rate-limiting step of catalysis

(Scheme 3.1, step C). I anticipated a first-order dependence on the concentration of *tert*-butyl acrylate based on our proposed mechanism (Scheme 3.1). The partial order dependence on the *tert*-butyl acrylate concentration will be discussed further in section 3.4.

3.4. Investigating Hydrophosphination Catalysis with the Product Phosphine Complex 4e

As described in the previous section, Ru(η^5-indenyl)(PPh_2)(**P**)$_2$ (**4e**, **P** = $P(CH_2CH_2CO_2Bu^t)Ph_2$) was observed during the hydrophosphination of *tert*-butyl acrylate with diphenylphosphine catalyzed by precatalyst **4b**. We were motivated to isolate complex **4e** in order to determine if it is a catalytically active intermediate, as well as to study the stoichiometric reactivity of **4e** with the substrates of catalysis. For example, the reaction of **4e** with PPh_2H should provide information on the substitution of **P** in **4e** by PPh_2H (Scheme 3.1, step C).

3.4.1. Synthesis of Ru(η^5-indenyl)(PPh_2){$P(CH_2CH_2CO_2Bu^t)Ph_2$}$_2$ (4e)

Complex **4e** was prepared by a visiting undergraduate summer research student, Erick Nuñez Bahena. It was generated via the dehydrohalogenation of complex **2a** by NaHMDS (sodium hexamethyldisiloxane, Na{$N(SiMe_3)_2$}) in the presence of two equivalents of **P** in toluene (Scheme 3.4). Complex **4e** was isolated as a powder, but it could not be purified because it is extremely soluble, even in non-polar solvents (e.g. pentane, hexane). PPh_3 as well as minor amounts of **4d** and leftover **P** could not be removed from **4e**. Complex **4e** was used, as isolated, for the subsequent reactivity studies because **4d**, PPh_3 and **P** are present during catalysis.

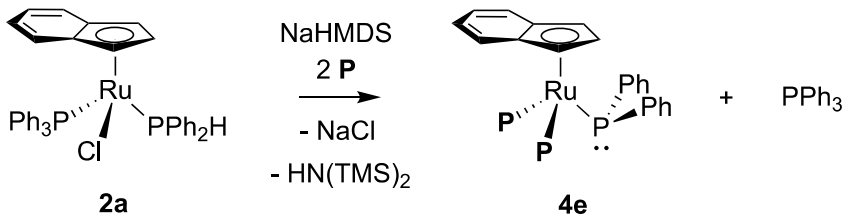

Scheme 3.4. Synthesis of Ru(η^5-indenyl)(PPh_2){$P(CH_2CH_2CO_2Bu^t)Ph_2$}$_2$ (**4e**).

The structure of **4e** was characterized by 1D NMR (^{1}H, ^{31}P{^{1}H}, ^{31}P, ^{13}C{^{1}H} and ^{13}C DEPT 135) and 2D NMR (^{1}H COSY, ^{1}H/^{31}P{^{1}H}-HSQC, ^{1}H/^{31}P{^{1}H}-HMBC, ^{1}H/^{13}C{^{1}H}-HSQC and ^{1}H/^{13}C{^{1}H}-HMBC). Experiment details for the synthesis of **4e** is described in section 3.8.1. The ^{31}P{^{1}H}, ^{1}H and ^{13}C{^{1}H} NMR data are summarized in section 3.8.8, Tables 3.2, 3.3 and 3.4, respectively. ^{1}H, ^{31}P{^{1}H} and ^{13}C{^{1}H} NMR spectra of **4e** are shown in Appendix E.

The ^{31}P{^{1}H} NMR spectrum of **4e** shows a triplet and a doublet at 39.1 and 30.2 ppm, respectively. The triplet resonance corresponds to the phosphido ligand and the doublet corresponds to the two coordinated **P**. No $^1J_{PH}$ coupling is observed in the ^{31}P NMR spectrum, which is consistent with the absence of P-H bonds on these phosphorus ligands. The small $^2J_{PP}$ coupling (3 Hz) between **P** and the phosphido ligand is typical for coupling between *pseudo*-tetrahedral terminal phosphido ligands and tertiary phosphines on a metal complex (discussed in section 2.3.2).

3.4.2. Activity of Complex 4e in Catalytic Hydrophosphination

I found that complex **4e** is a competent catalyst for the hydrophosphination of *tert*-butyl acrylate with PPh_2H, which suggests that it is an on-cycle intermediate. As mentioned

in section 3.2.3, **4e** was observed during catalysis as the resting state for the hydrophosphination of *tert*-butyl acrylate with PPh_2H when catalyst precursor **4b** is used. Catalysis when starting from **4e** is slightly faster than when starting with complex **4b** (Figure 3.10). As discussed in section 3.2.3, complex **4e** is a species that builds up over the course of the hydrophosphination reaction catalyzed by precursor **4b**. The increased rate observed when starting with **4e** may be attributed to the fact that **4e** is an on-cycle intermediate, whereas when starting with **4b** at least two turnovers must occur before **4e** is completely formed.

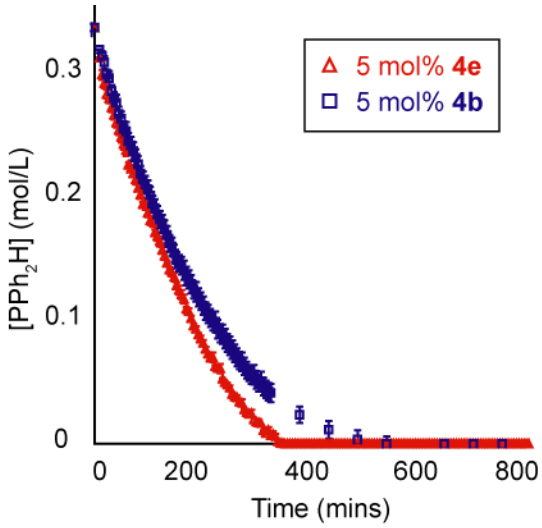

Figure 3.10. Reaction profiles of the hydrophosphination of *tert*-butyl acrylate with PPh_2H using **4b** (blue plot) and **4e** (red plot).

I used $^{31}P\{^1H\}$ NMR to monitor catalysis by **4e**. This showed that complex **4e** is the only species throughout the reaction (Figure 3.11), which confirms that complex **4e** is the resting state of catalysis. Unlike catalysis with **4b** as the precatalyst, complex **4d** is not

observed despite there being an equivalent of PPh_3 present (present from the preparation of **4e**).

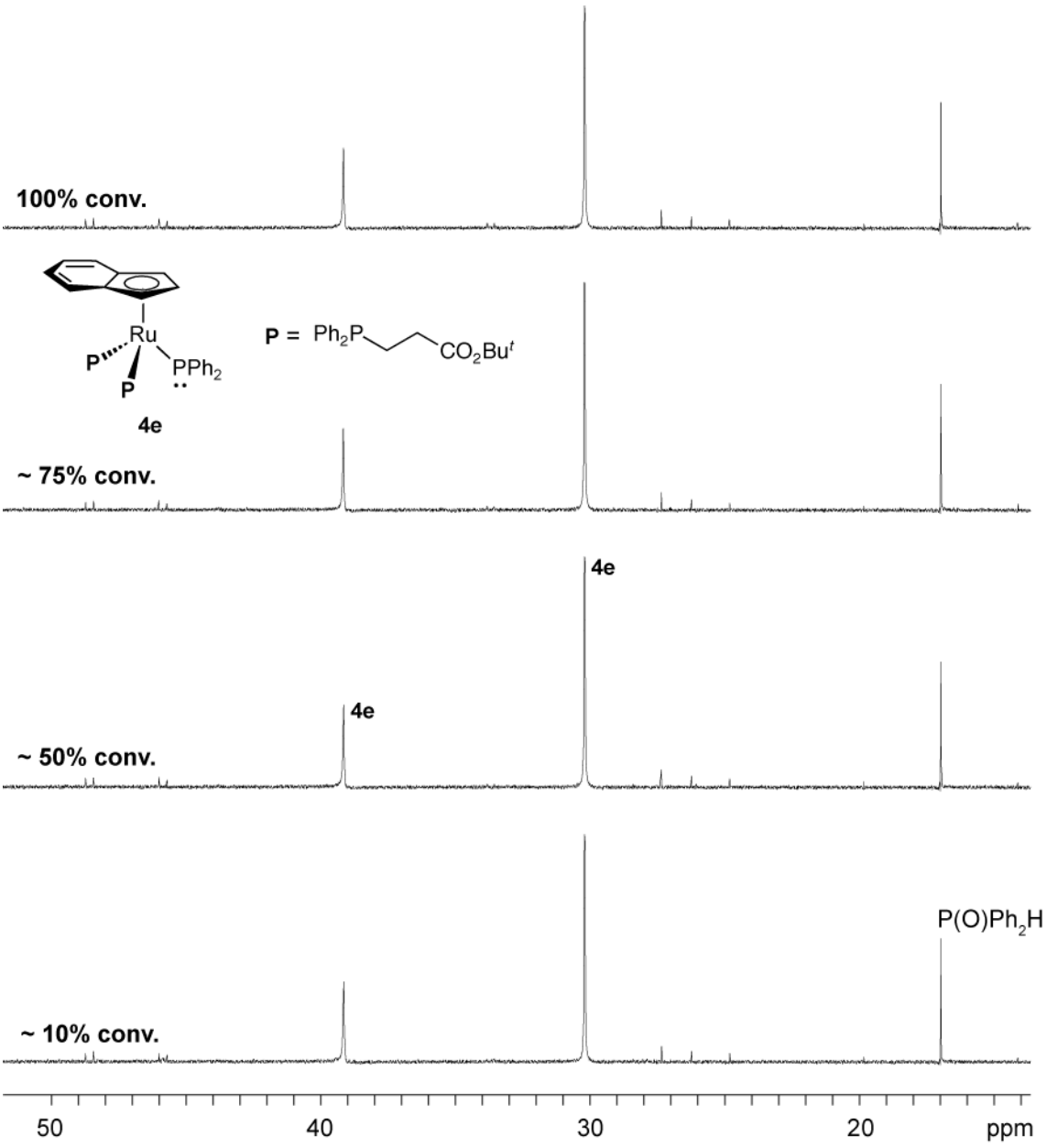

Figure 3.11. Ru-coordinated phosphine/phosphido region of the $^{31}P\{^{1}H\}$ NMR during catalysis under non-pseudo first order conditions using **4e** as the catalyst precursor (145.85 MHz, C_6D_6). Some minor unassigned peaks are observed during catalysis.

3.4.3. Stoichiometric Reactivity of Complex 4e with PPh_2H

Addition of one equiv of PPh_2H to **4e** generates Ru(η^5-indenyl)(PPh_2)(PPh_2H)(**P**) (**4f**) via substitution of **P** by PPh_2H. The substitution takes 24 h to go to completion. The rate of a second reaction using 10 equiv of PPh_2H went to completion at the same rate as the reaction using 1 equiv of PPh_2H, which is consistent with a dissociative mechanism. (The rate of substitution is independent of the PPh_2H concentration because the rate-limiting dissociation of **P** from **4e** must occur before PPh_2H can coordinate to Ru). Dissociative substitution of Ru(η^5-indenyl) complexes is well established.[35,36]

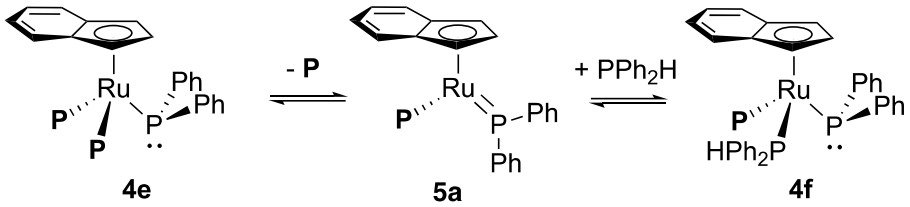

Scheme 3.5. Stoichiometric reaction of **4e** with PPh_2H resulting in formation of Ru(η^5-indenyl)(PPh_2)(PPh_2H){$P(CH_2CH_2CO_2Bu^t)Ph_2$} (**4f**).

The slow substitution of **P** in complex **4e** by PPh_2H is consistent with rate-limiting substitution during catalysis. This is also consistent with **4e** being the observed resting state. In the proposed mechanism in Scheme 3.1, substitution of **P** by PPh_2H is necessary for catalysis to proceed. Complex **4f** is never observed during catalysis, which supports that substitution is rate-limiting. In other words, this suggests that substitution (Scheme 3.1, step C) must be slower than the subsequent conjugate addition of the phosphido ligand in **4f** to alkene (step A).

3.4.4. Stoichiometric Reactivity of Complex 4e with *tert*-butyl acrylate

Addition of one equiv of *tert*-butyl acrylate to complex **4e** results in the formation of the metallacycles **6d**,**e** (~ 1:5 ratio). This reaction takes 4 d to go to completion. These metallacycles can form if the phosphido ligand in **4e** participates in nucleophilic attack at alkene. The carbanion of the zwitterionic intermediate then coordinates to Ru after the dissociation of one coordinated **P** (Scheme 3.6); substitution of **P** by PPh_3 can also occur, which generates **6d**.

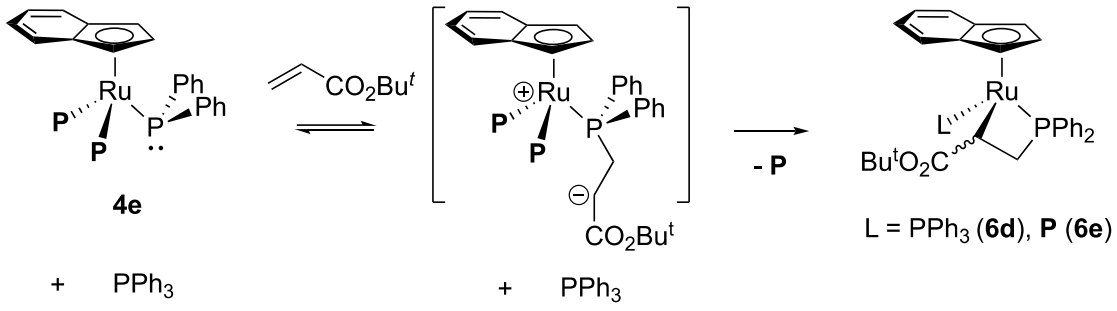

Scheme 3.6. Stoichiometric reaction of **4e** with *tert*-butyl acrylate resulting in formation of metallacycles **6d,e**.

The zwitterionic intermediate in Scheme 3.6 is never observed during this reaction, which suggests that nucleophilic attack of the phosphido ligand in **4e** at alkene must be fast (discussed in section 3.2.4.) and reversible. The zwitterionic intermediate must be forming transiently, but is immediately "trapped" after dissociation of **P** to give the metallacycles. An alternative mechanism to the one shown in Scheme 3.6, where dissociation of **P** from **4e** occurs before addition to the alkene, is excluded because nucleophilic attack at alkene is faster than dissociation (*vide supra* section 3.3.4).

The stoichiometric reaction discussed above points to P-C bond formation that precedes dissociation of **P**, which suggests that under catalytic conditions there could be a competing pathway that also leads to hydrophosphination (Scheme 3.7). In this competing pathway, the carbanion of the zwitterionic intermediate formed after nucleophilic attack (step D) can deprotonate uncoordinated PPh_2H (step E). This would generate a cationic complex containing three coordinated **P** as well as a PPh_2^-. Substitution of **P** by PPh_2^- could regenerate **4e** (step F). This resembles the proposed mechanism for a Ru-catalyzed hydrophosphination that invokes intermolecular deprotonation of PPh_2H (discussed in section 1.4.2, and *vide infra*).[17]

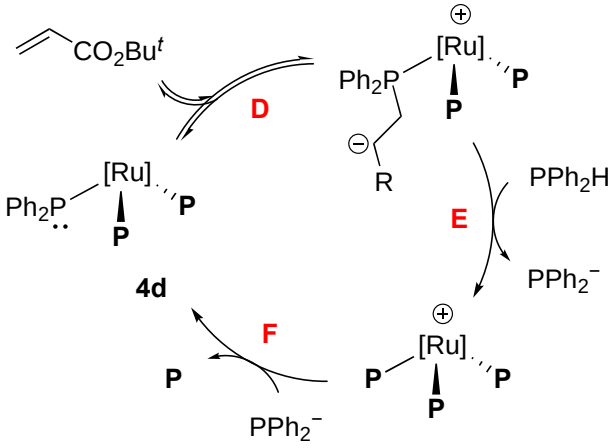

Scheme 3.7. Alternative proposed mechanism for hydrophosphination of *tert*-butyl acrylate.

3.4.5. Sequential Addition of PPh_2H and *tert*-butyl acrylate to Complex 4e

In order to demonstrate the sequential steps of our proposed mechanism, I performed an "order of addition" experiment where PPh_2H, then *tert*-butyl acrylate, were added to **4e**. As stated in section 3.3.4, addition of one equiv of PPh_2H to **4e** results in the formation of

4f via substitution of **P** (Scheme 3.8). After complete conversion of **4e** to **4f**, addition of one equiv of *tert*-butyl acrylate to the reaction mixture regenerated **4e** (Scheme 3.8). Complex **4e** was regenerated within the time I could collect the $^{31}P\{^{1}H\}$ NMR spectrum of the reaction. This sequence of reactions demonstrates that each step of the proposed cycle in Scheme 3.1 is possible.

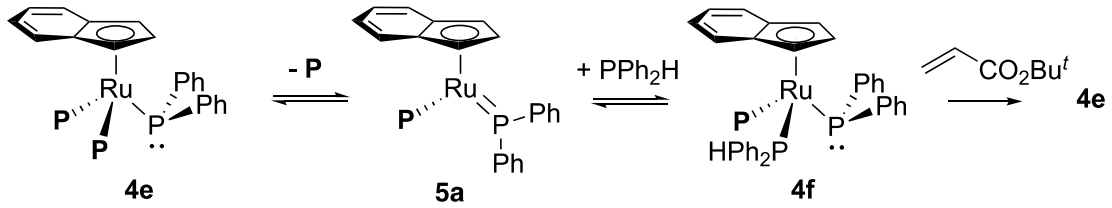

Scheme 3.8. Stoichiometric reaction of **4e** with PPh_2H resulting in **4f** followed by stoichiometric addition of *tert*-butyl acrylate

3.5. Revised Proposed Mechanism for Catalysis by Complexes 4b,e

Based on all the evidence presented in section 3.3. and 3.4, I propose that complexes **4b**,**e** catalyze the hydrophosphination of *tert*-butyl acrylate with PPh_2H via a common mechanism. A revised mechanism is shown in Scheme 3.9, which includes a second cycle involving **4e** (cycle 2). Cycles 1 and 2 are linked by complex **4e**, but arise from the competing reactivity of **4e** with PPh_2H and *tert*-butyl acrylate.

The proposed catalytic cycle 1 relies on substitution of **P** in **4e** by PPh_2H, which generates **4f** (step **A** and **B**); substitution is dissociative, via the coordinatively unsaturated intermediate **5a**. Nucleophilic attack of the phosphido ligand in **4f** at alkene generates a zwitterionic intermediate (step **C**). The carbanion of the zwitterionic intermediate is

quenched by intramolecular proton transfer from the coordinated PPh_2H, which regenerates **4e** (step **D**). This mechanism is supported by the stoichiometric reactivity of **4b** with *tert*-butyl acrylate (steps **C** and **D**), of **4e** with PPh_2H (steps **A** and **B**) and of **4e** with PPh_2H and *tert*-butyl acrylate (steps **A**, **B**, **C** and **D**) discussed in sections 3.2.4, 3.3.3 and 3.3.5, respectively.

The stoichiometric reaction of **4e** with *tert*-butyl acrylate (section 3.3.5) suggests that under catalytic conditions nucleophilic attack of the phosphido ligand in **4e** at alkene could precede dissociation of **P**. This opens the possibility for a competing, productive cycle that involves initial nucleophilic attack of the phosphido ligand in **4e** at alkene (step **E**). The carbanion of the resulting zwitterionic intermediate can deprotonate uncoordinated PPh_2H (step **F**), which generates a cationic complex containing three coordinated **P** as well as uncoordinated PPh_2^-. Substitution of **P** by PPh_2^- would regenerate **4e** (step **G**).

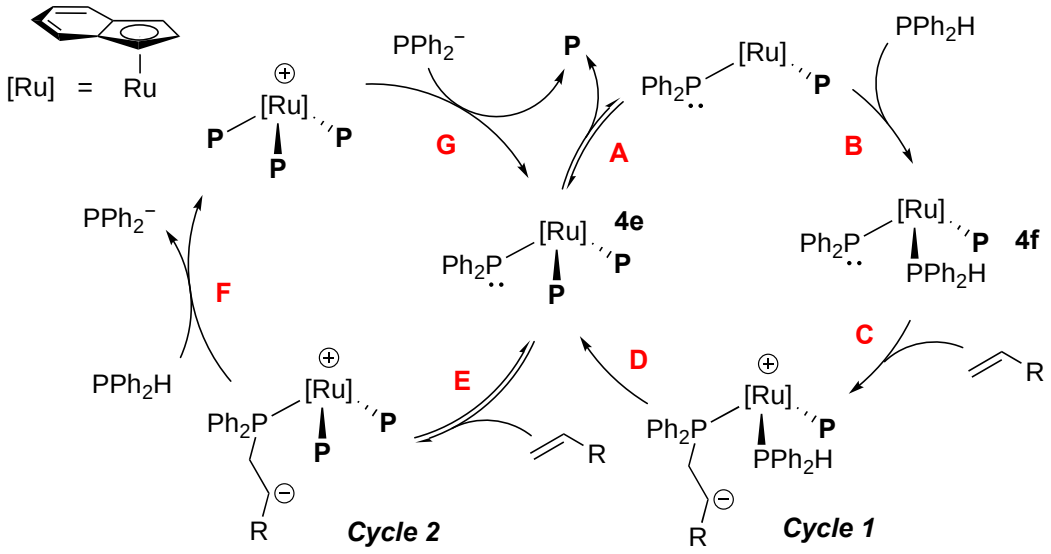

Scheme 3.9. Proposed mechanism for the hydrophosphination of activated alkenes by complexes **4b,e**.

Complex **4e** is the observed resting state of catalysis. This is consistent for both proposed cycles. For cycle 1, dissociation of **P** in **4e** is the rate-limiting step (discussed in section 3.3.4.). The resulting intermediates are quickly consumed by subsequent steps, which regenerates **4e**. For cycle 2, **4e** would also be the resting state if, as proposed, step E is fast and reversible and if step F is rate limiting.

These competing cycles could account for the observed reaction rate dependences on the concentrations of catalyst, PPh_2H and *tert*-butyl acrylate (discussed in sections 3.2.1 and 3.2.5). Both cycles should lead to a first-order dependence on catalyst and PPh_2H concentrations, whereas cycle 2 should also have a first order dependence on the concentration of *tert*-butyl acrylate. The fractional reaction rate dependence observed on the concentration of *tert*-butyl acrylate is 0.6, which could mean that both cycles contribute comparably to the overall rate of the reaction. As will be discussed in Chapter 6, future work involves studying the reaction kinetics of catalysis by complex **4e**, which may provide insight on whether these competing cycles are operative.

3.6. Investigating Hydrophosphination Catalysis with Nitrile Complex 4a

Ru(η^5-indenyl)(PPh_2)(NCPh)(PPh_3) (**4a**) was also included in this study because, as demonstrated in Chapter 2, **4a** is a competent catalyst for hydrophosphination. Complex **4a** contains a labile NCPh ligand, which is easily substituted by PPh_2H to generate **4b**. Therefore, I anticipated that **4a** would participate in catalysis via a similar mechanism to the one proposed for catalysis by **4b**,**e**. The results presented in this section demonstrate that this is true, but also show that NCPh is non-innocent during catalysis. As shown in

section 3.1.1, the activity of catalysis by **4a** is much slower than the activity of catalysis by **4b**. The influence of the benzonitrile ligand, NCPh, in complex **4a** on the catalytic activity is described. Complex Ru(η^5-indenyl)(PPh_2){κ^2-$\underline{P}Ph_2(CH_2CH_2(CO_2Bu^t)C(Ph)\underline{N}H)$}($PPh_3$) (**7a**), an species resulting from an off-cycle process involving NCPh, was independently prepared and characterized.

3.6.1. Monitoring Catalysis by $^{31}P\{^1H\}$ NMR Using Nitrile Complex 4a

$^{31}P\{^1H\}$ NMR monitoring of the hydrophosphination of *tert*-butyl acrylate with PPh_2H using catalyst precursor **4a** shows that complexes **4d**,**e** form during catalysis (the same species observed in catalysis with **4b**). However, a new species identified as Ru(η^5-indenyl)(PPh_2){κ^2-$\underline{P}Ph_2(CH_2CH_2(CO_2Bu^t)C(Ph)\underline{N}H)$}($PPh_3$) (**7a**) and trace amounts of **6d** are also observed, which were not observed in catalysis with **4b**,**e**. Complex **7a** forms initially and persists throughout the catalytic reaction (Figure 3.12). The identification, synthesis and characterization of **7a** is described in sections 3.5.2 and 3.5.3. Similar to what is described in section 3.2.3, complex **4d** only appears during the first two turnovers and quickly disappears, while complex **4e** increases in concentration at the expense of **4d** and persists throughout catalysis. The fact that these same species are observed suggests that complex **4a** participates in the hydrophosphination of alkenes via a similar mechanism to the one described for complexes **4b**,**e** (Scheme 3.9).

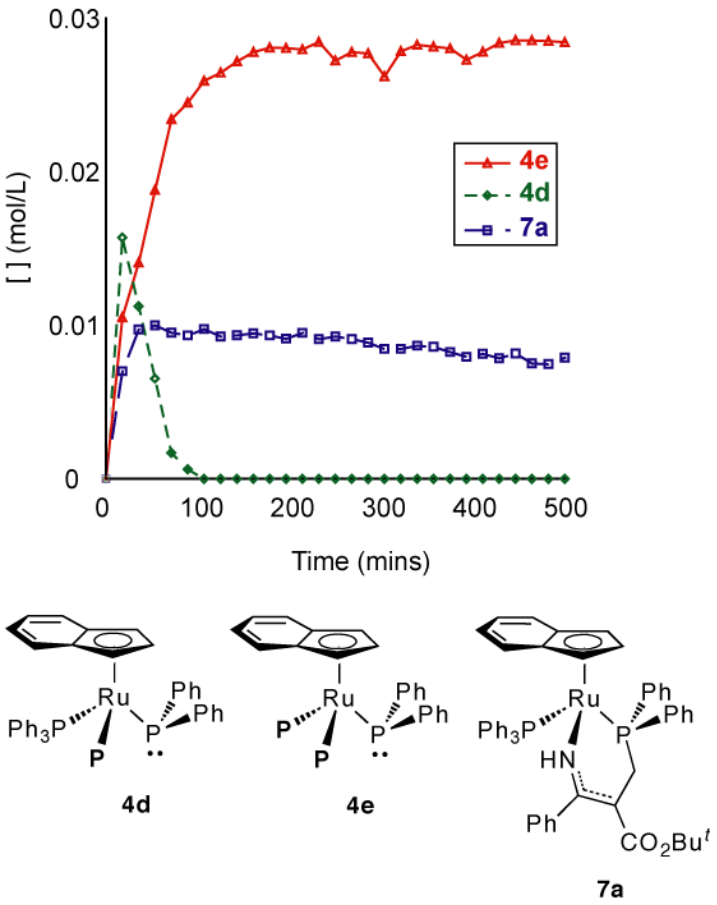

Figure 3.12. Speciation of Ru complexes during the hydrophosphination of *tert*-butyl acrylate with PPh_2H when **4a** is used as the precatalyst, as determined by $^{31}P\{^1H\}$ NMR.

3.6.2. Stoichiometric Reactivity of Complex 4a with *tert*-butyl acrylate

An NMR scale reaction involving the addition of one equiv of *tert*-butyl acrylate to complex **4a** at rt resulted in the formation of complex **6d** (major product) as well as complex **7a** (minor product) (Scheme 3.10). The reaction had gone to completion by the time I collected the ^1H and $^{31}P\{^1H\}$ NMR spectra. Complex **6d** is proposed to form via conjugate addition of the phosphido ligand in **4a** to alkene (Scheme 3.10, top), which generates a zwitterionic intermediate. The carbanion of this zwitterionic intermediate combines with Ru following dissociation of NCPh. Complex **7a** (independent synthesis and characterization described in section 3.5.3) also forms by this conjugate addition

pathway, but the carbanion of the zwitterionic intermediate attacks the coordinated NCPh ligand before dissociation. A subsequent 1,3-proton shift (Scheme 3.10, bottom) generates complex **7a**.

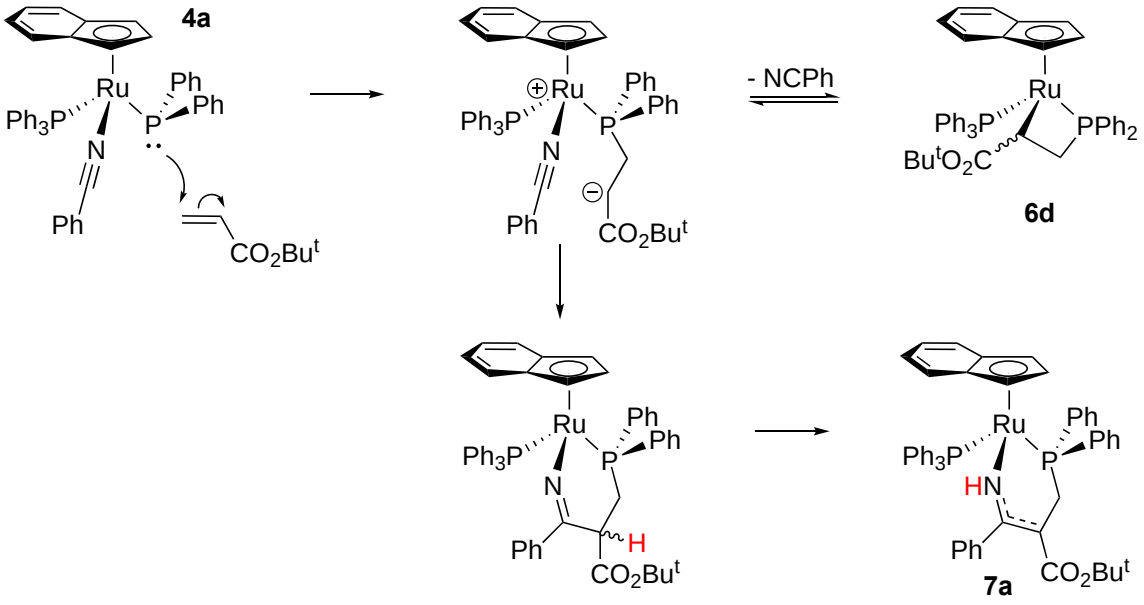

Scheme 3.10. Stoichiometric reaction of **4a** with *tert*-butyl acrylate resulting in formation of **6d** via loss of NCPh (top) and **7a** via nucleophilic attack of the carbanion at the nitrile C (bottom).

An NMR scale reaction where one equiv of *tert*-butyl acrylate was added to complex **4a** at −20°C resulted in the formation of complex **7a** as the major product and complex **6d** as the minor product. As shown in Scheme 3.10, formation of complex **6d** relies on dissociation of the NCPh ligand in order for combination of the carbanion of the zwitterionic intermediate with Ru. The dissociation of NCPh from the zwitterionic intermediate is presumably slower at lower temperatures. This allows for the carbanion of

the zwitterionic intermediate to participate in nucleophilic addition at the coordinated NCPh, which would give more complex **7a** relative to **6d**.

3.6.3. Independent Synthesis and Characterization of Ru(η^5-indenyl)(PPh_2)(κ^2-P(Ph_2)CH_2CH_2(CO_2Bu^t)C(Ph)NH)(PPh_3) (7a)

Complex **7a** was prepared through addition of *tert*-butyl acrylate to complex **4a** in toluene at −20°C. As mentioned in the previous section, this results in complexes **6d** (minor) and **7a** (major). These two complexes have different solubilities in organic solvents, which allowed for separation. Both complexes are slightly and comparably soluble in pentane, but complex **6d** is more soluble in toluene than **7a**. Washing the mixture of products with a 1:10 mixture of toluene:pentane afforded pure complex **7a**, which was crystallized from a saturated pentane solution stored at −30°C.

Single crystals of **7a** were obtained and X-ray diffraction analysis was performed. The resulting structure is shown in Figure 3.13 and selected interatomic bond distances and bond angles are summarized in Table 3.1. The structure shows that there is a *pseudo*-octahedral geometry at Ru with a crystallographic indenyl slip factor of 0.14, which is typical of η^5-coordination of the indenyl ring; this slip factor is described in 2.3.1. In the structure, C9, C10 and N are planar, as the sum of the angles around these atoms are 359.83°, 359.90° and 359.32° respectively. The C9-C10 bond length is 1.389(3) Å, which is slightly longer than a typical C-C double bond. The C10-N bond length is 1.337(3) Å, which is shorter than a typical C-N single bond, but slightly longer than a typical C-N double bond. The planarity of these atoms and the short bond lengths described suggests

that the negative charge in this ligand is delocalized over the N-C10-C9 π-system (as shown in Scheme 3.10).

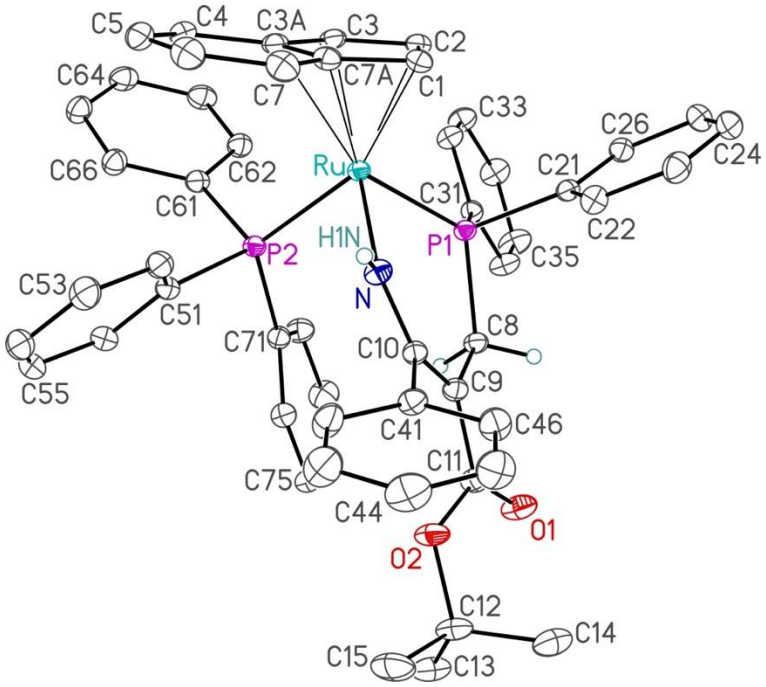

Figure 3.13. Molecular structure of Ru(η^5-indenyl)(PPh_2){κ^2-$\underline{P}Ph_2(CH_2CH_2(CO_2Bu^t)C(Ph)\underline{N}H)$}($PPh_3$) (**7a**). Non-hydrogen atoms are represented by Gaussian ellipsoids at the 30% probability level.

Table 3.1. Selected Interatomic Distances (Å) and Bond Angles (°) for the Molecular Structures of Ru(η^5-indenyl)(PPh_2)(κ^2-P(Ph_2)CH_2CH_2(CO_2Bu^t)C(Ph)NH)(PPh_3) (**7a**).

	7a	
Ru-P1	2.2420(5)	
Ru-P2	2.3059(5)	
Ru-N	2.0855(17)	
C9-C10	1.389(3)	
C10-N	1.337(3)	
Ru-C*	1.918	
Δ	0.14	
P1-Ru-P2	96.705(18)	
P1-Ru-N	84.79(5)	
P2-Ru-N	90.72(5)	
N-C10-C9	126.57(18)	
N-C10-C41	112.33(17)	∑ = 359.90
C41-C10-C9	121.00(17)	
C10-C9-C8	125.24(17)	
C10-C9-C11	124.13(18)	∑ = 359.83
C11-C9-C8	110.46(17)	
Ru-N-C10	138.12(14)	
Ru-N-H1N	111.7(18)	∑ = 359.32
C10-N-H1N	109.5(18)	

[a] C* is centroid of the 5-membered ring of the indenyl ligand. Ru-C* is the distance from Ru to the centroid of the 5-membered ring of the indenyl ligand.

The structure of **7a** was characterized by 1D NMR (^1H, $^{31}P\{^1H\}$, ^{31}P, $^{13}C\{^1H\}$ and ^{13}C DEPT 135) and 2D NMR (^1H COSY, $^1H/^{31}P\{^1H\}$-HSQC, $^1H/^{31}P\{^1H\}$-HMBC, $^1H/^{13}C\{^1H\}$-HSQC and $^1H/^{13}C\{^1H\}$-HMBC), IR spectroscopy and elemental analysis. Experimental details for the synthesis of **7a** is described in section 3.8.2. The $^{31}P\{^1H\}$, ^1H and $^{13}C\{^1H\}$ NMR data of **7a** are summarized in section 3.8.8, Tables 3.2, 3.3 and 3.4, respectively. ^1H, $^{31}P\{^1H\}$ and $^{13}C\{^1H\}$ NMR spectra of **7a** are shown in Appendix E. Crystallographic data for **7a** is in Appendix C.

3.6.4. Activity of Nitrile Complex 4a in Hydrophosphination Catalysis

As discussed in Chapter 2 section 2.2.3, the NCPh ligand in complex **4a** is labile and easily substituted by PPh_2H to generate **4b**. Thus it was expected that as a catalyst precursor, **4a** would be comparable in activity to **4b**,**e**, and would operate through a similar mechanism in catalysis. However, complex **4a** is less active than **4b**,**e** for the hydrophosphination of *tert*-butyl acrylate with PPh_2H (Figure 3.1). The results presented in this section suggest that the lower activity of **4a** is due to the non-innocent behaviour of coordinated and uncoordinated NCPh during catalysis.

The results discussed in sections 3.5.1 and 3.5.2 suggest that the low activity of **4a** results from catalyst deactivation. I determined from monitoring catalysis with **4a** by $^{31}P\{^1H\}$ NMR that some **4a** is initially lost to the irreversible formation of complex **7a**. I performed a "same excess" experiment (technique described in section 3.2.2) that showed that catalyst deactivation occurs when **4a** is used as a catalyst precursor (Figure 3.14). Two reactions following the "same excess" protocol were performed: **a** (blue plot) and **b** (green plot). Reaction **b** is meant to mimic the conditions of reaction **a** at $t_{1/2}$, but without any product present. After time adjustment (Figure 3.14, right), the profile for reaction **b** does not overlap with the profile for reaction **a**, which suggests that either product inhibition or catalyst deactivation occurs under these conditions. A third reaction, **c** (red plot), was performed. Reaction **c** is similar to **b**, but the appropriate amount of product phosphine that would have formed at $t_{1/2}$ was added to exactly mimic the conditions of **a** at $t_{1/2}$. After time adjustment, the profile for reaction **c** overlaps well with the profile for reaction **b**, not **a**, which suggests that catalyst deactivation occurred. This demonstrates that the presence of

P does not account for the loss in activity; if it did, plot **c** would have overlapped with plot **a** like in Figure 3.6. However, plot **c** does not overlap perfectly with **b**, especially at later time points, which is attributed to some product inhibition that is also likely to occur.

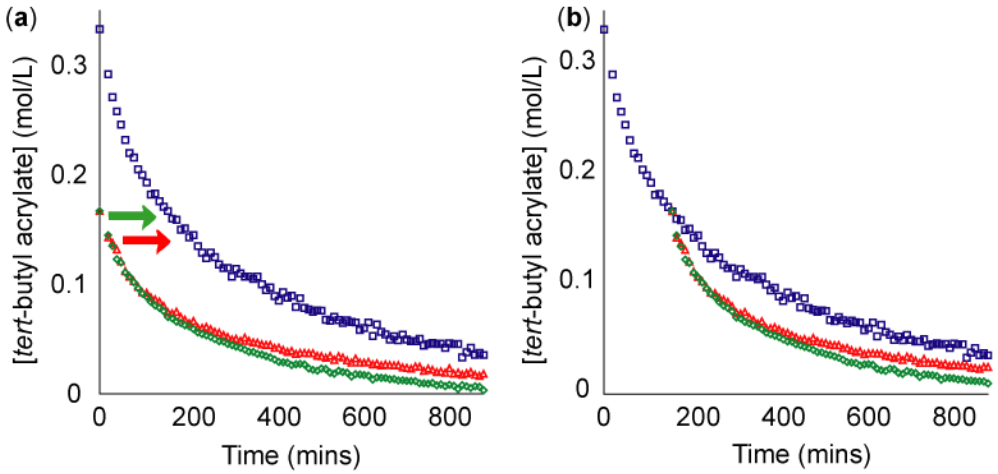

Figure 3.14. Reaction profiles for the hydrophosphination of *tert*-butyl acrylate by PPh_2H following the "same excess" protocol, as monitored by ^1H NMR. Profile **a** (red) and **b** (blue) have different initial concentrations of *tert*-butyl acrylate and PPh_2H. Profile **c** (green) has the same initial concentrations as **b** but with added **P** to match the [**P**] in **a** at $t_{1/2}$.

The portion of **4a** that is converted to **4b** under catalytic conditions results in an equimolar portion of free NCPh in solution during catalysis. This amount of uncoordinated NCPh also influences the overall activity through competition with PPh_2H for coordination at Ru. This is demonstrated through an "order of addition" catalytic experiment where PPh_2H was added to **4a** before *tert*-butyl acrylate to generate **4b** and an equivalent of uncoordinated NCPh *in situ* (Figure 3.15). The presence of a catalytic amount of uncoordinated NCPh reduces the activity of **4b**. As seen in Figure 3.15, the reaction profile for the catalytic reaction using **4b** with an equivalent of NCPh present matches more

closely to the reaction where **4a** was used as the precatalyst than to the reaction where **4b** was used.

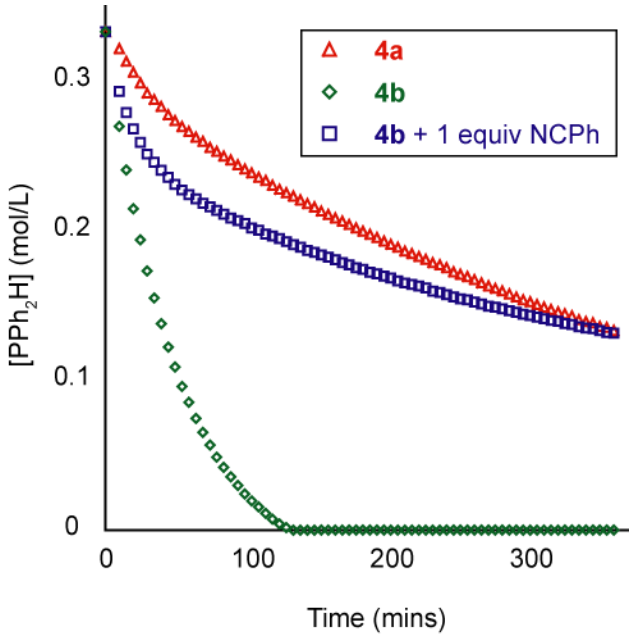

Figure 3.15. Reaction profiles of catalysis using 4a (blue), 4b (green), and 4b with an equiv of NCPh (red).

The competitive coordination of NCPh and ultimately the irreversible formation of **7a** results in the low activity of **4a** (and **4b** in the presence of NCPh). $^{31}P\{^{1}H\}$ NMR monitoring of the "order of addition" catalytic reaction described above shows formation of **4d**,**e** as well as Ru(η^5-indenyl)(PPh_2)(κ^2-P(Ph_2)CH_2CH_2(CO_2Bu^t)C(Ph)NH)(**P**) (**7b**) (Figure 3.16); **7a** is not observed. Complex **7b** was assigned based on the similar $^{31}P\{^{1}H\}$ NMR chemicals shifts to **7a**. Complex **7b** does not form immediately, but builds up over the course of the reaction. Formation of **7b** suggests that NCPh can effectively compete with PPh_2H for coordination at Ru under catalytic conditions, especially at later time points in catalysis when the concentration of PPh_2H is low. The general mechanism for the build-

up of complexes **7** is shown in Scheme 3.11. This is consistent with our study on the substitution of secondary phosphines with **3a** (collaboration with McIndoe group), where we determined that NCPh can compete with tertiary phosphines for coordination at Ru, even at low concentrations relative to phosphines.[35]

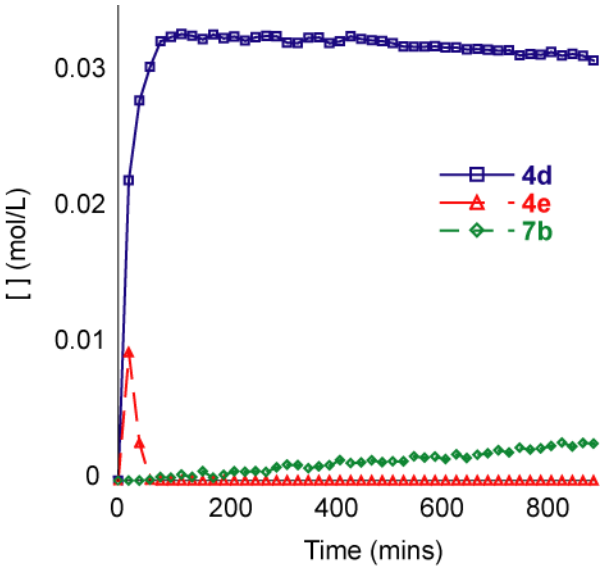

Figure 3.16. Speciation of Ru complexes during the hydrophosphination of *tert*-butyl acrylate with PPh_2H when **4b** is generated *in situ* via addition of PPh_2H to **4a** before *tert*-butyl acrylate (i.e. in the presence on one equiv of NCPh).

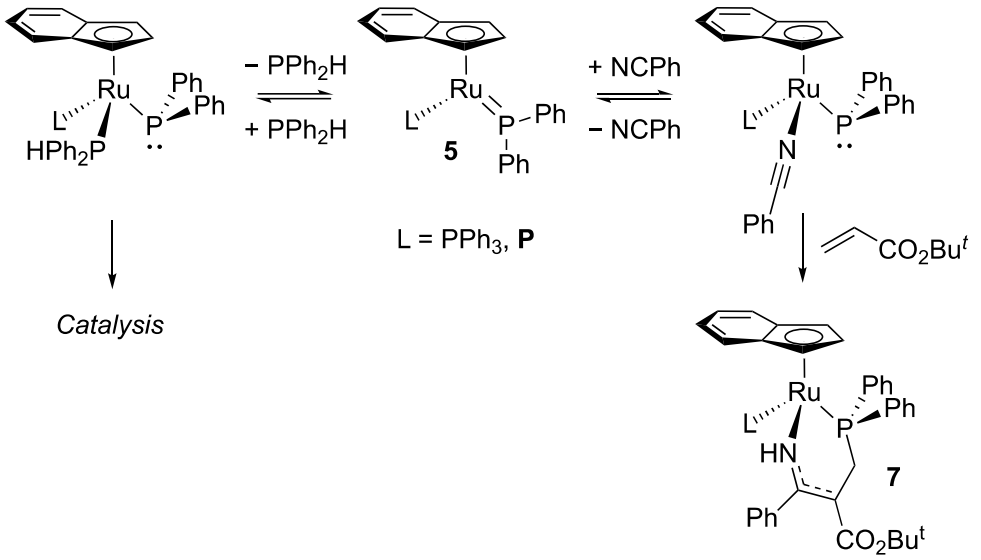

Scheme 3.11. Competition between PPh_2H and NCPh for coordination at Ru. Coordination of NCPh leads to catalyst decomposition to complex **7**.

The non-innocent behaviour of NCPh complicated the determination of the reaction rate dependence on the concentration of **4a** in catalysis. The initial rates method showed a second-order relationship between the concentration of **4a** and the initial rates. The time normalization method also showed a second-order dependence, but since some **4a** is lost in the formation of **7a** under catalytic conditions, the time normalization method is not reliable; it works on the presumption that the catalyst concentrations remains constant throughout catalysis. Typically, first-order reaction rate dependences are observed for catalyst concentrations.[37] Second-order dependences on catalyst concentrations are typically observed when the catalyst is a dimer or an aggregate.

Under pseudo-first order conditions, the non-innocent behaviour of the uncoordinated NCPh in solution is prevented; excess PPh_2H shifts the equilibria away from NCPh-bound complexes towards PPh_2H-bound complexes (Scheme 3.11). Under these

conditions the initial rates and time normalization methods showed a first-order rate dependence on the concentration of **4a**. Furthermore, under these conditions the reaction profiles of catalytic reactions using **4a** as the precatalyst match very well with the reaction profiles of catalytic reactions using **4b** as the precatalyst under the same conditions (Figure 3.17). Complex **4a** is still slightly less active than **4b**. Even under pseudo-first order conditions some **7a** still forms initially when **4a** is used as a precatalyst, which I determined by monitoring catalysis with **4a** under these conditions by $^{31}P\{^{1}H\}$ NMR.

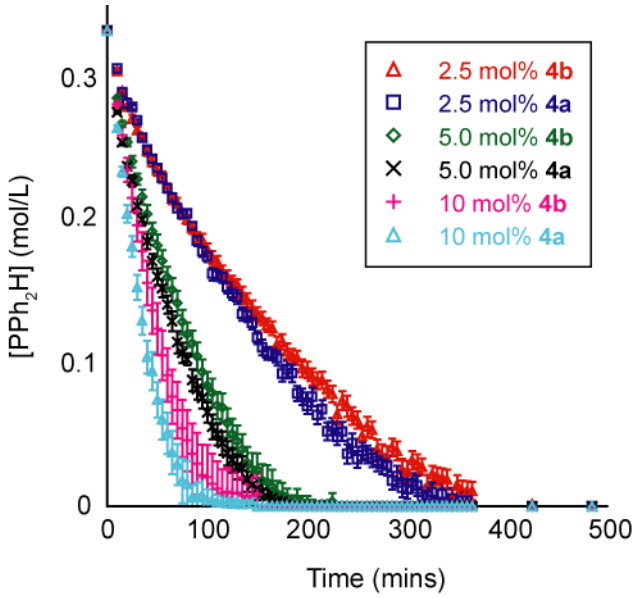

Figure 3.17. Reaction profiles of catalysis, as monitored by ^{1}H NMR, when nitrile complex **4a** and when PPh_2H complex **4b** are used.

3.6.5. Reaction Rate Dependences on the Concentration of PPh_2H and *tert*-Butyl Acrylate

The evidence presented above suggests that **4a** participates in hydrophosphination catalysis via a similar mechanism to complexes **4b**,**e**. Under pseudo-first order conditions using **4a** as the precatalyst, there is a first order dependence on the PPh_2H concentration

and a fractional order (0.55) dependence on the concentration of *tert*-butyl acrylate. These reaction rate dependences are the same as those determined for catalysis using **4b** as the precatalyst under pseudo-first order conditions, which is consistent with **4a** participating in hydrophosphination catalysis via a common mechanism to complexes **4b**,**e**.

3.7. Investigating Hydrophosphination Catalysis with Carbonyl Complex 4c

Ru(η^5-indenyl)(PPh_2)(CO)(PPh_3) (**4c**) is different from complexes **4a**,**b**,**d** in that there is a non-labile CO ligand coordinated to Ru. We were motivated to include **4c** in this study because we anticipated that fully occupying a coordination site at Ru would influence the activity and mechanism of catalysis (the ability of PPh_2H to coordinate to Ru is critical to the mechanism proposed for hydrophosphination by **4a**,**b**,**e**). This is highlighted by the reduced activity of hydrophosphination catalysis by **4c** relative to **4b** shown in Figure 3.1. In this section the hydrophosphination of *tert*-butyl acrylate with PPh_2H catalyzed by catalyst precursor **4c** is investigated. Complex **4c** operates in catalysis through a different mechanism to the one described in Scheme 3.9, which involves an off-cycle process that is not observed in catalysis by complexes **4a**,**b**,**e**.

3.7.1. Proposed Mechanism for Catalysis with Complex 4c

Complex **4c** differs from complexes **4a,b,d** in that there is no readily available coordination site at Ru because of the non-labile CO ligand. This was demonstrated by a previous undergraduate student, Marc-André Hoyle, who showed that complex **4c** does not undergo thermal decomposition to the orthometalated complex Ru(η^5-indenyl){κ^2-(o-C_6H_4)$\underline{P}Ph_2$}(PPh_2H), even when the complex is heated for 5 days at 60°C.

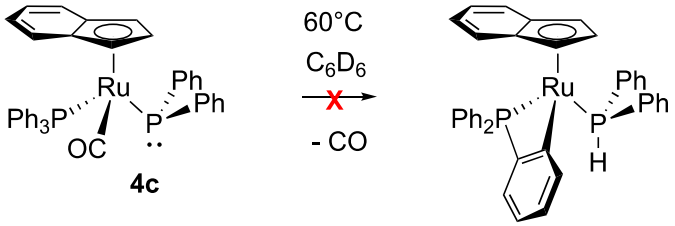

Scheme 3.12. Thermolysis of **4c** at 60°C. Formation of the orthometalated complex is not observed.

The proposed mechanism for catalysis by **4c** (Scheme 3.13) closely resembles the competing cycle proposed for catalysis by **4a**,**b,e** (Scheme 3.9, Cycle 2). After the initial conjugate addition of the phosphido ligand in **4c** at alkene (step A), the carbanion of the zwitterionic intermediate is quenched by intermolecular deprotonation of uncoordinated PPh_2H (step B). This would result in PPh_2^-, which could substitute **P** from Ru to regenerate **4c** (step C). This mechanism differs from the mechanism proposed for catalysis by **4a,b,e** because PPh_2H cannot coordinate to Ru, which prevents the possibility of intramolecular quenching of the zwitterionic intermediate (Scheme 3.9, Cycle 1).

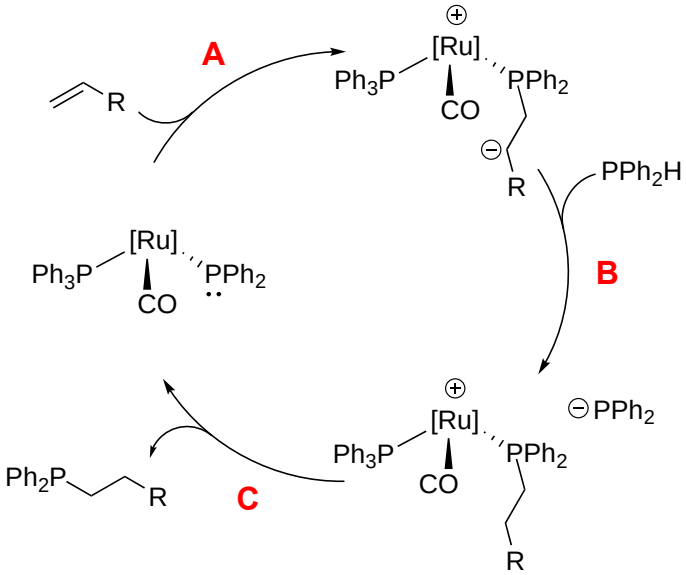

Scheme 3.13. Proposed mechanism for the hydrophosphination of activated alkenes catalyzed by complex **4c**.

This mechanism resembles a proposed mechanism for a reported Ru-catalyzed hydrophosphination.[17] In that report, the catalyst is a half-sandwich Cp*Ru phosphido complex with a bisphosphine ligand that occupies two coordination sites at Ru. The authors propose that the phosphido ligand participates in conjugate addition to acrylonitrile, which generates a zwitterionic intermediate that is quenched by intermolecular proton transfer from free PPh_2H. The argument for intermolecular proton transfer is based on the pK_a of the carbanion (estimated from the pK_a of acetonitrile; pK_a^{DMSO} 31, pK_a^{THF} 35) and free PPh_2H (pK_a^{THF} 38). This Ru complex had high activity (TOF 60 h^{-1}), but quickly deactivated, before the reaction went to completion.

3.7.2. Reactivity of CO Complex 4c with PPh_2H and P

A plausible alternative mechanism for catalysis by **4c** could involve substitution of PPh_3 in **4c** by PPh_2H (Scheme 3.14, step A). If possible, this would generate the complex Ru(η^5-indenyl)(PPh_2)(CO)(PPh_2H) (**9a**). The phosphido ligand in **9a** could then participate in conjugate addition to alkene (step B). Subsequent deprotonation of the coordinated PPh_2H by the carbanion would generate Ru(η^5-indenyl)(PPh_2)(CO)(**P**) (**9b**) (step C), which could undergo substitution by PPh_2H to regenerate **9a** (step D). In order to determine if this mechanism could be possible, I studied the reactivity of complex **4c** with PPh_2H and **P**.

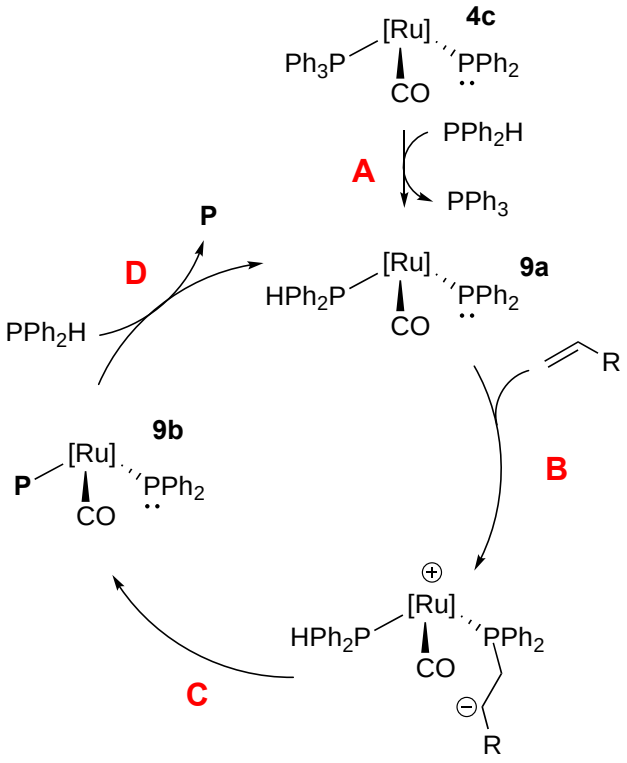

Scheme 3.14. Alternative proposed mechanism for hydrophosphination catalyzed by **4c**.

No reaction is observed when one equiv of PPh_2H is added to **4c** at rt, even after 24 h. Heating this reaction at 60°C for 1 h results in minor substitution of the PPh_3 ligand in **4c** by PPh_2H to generate Ru(η^5-indenyl)(PPh_2)(CO)(PPh_2H) (**9a**), as determined by $^{31}P\{^1H\}$ NMR (Scheme 3.15). Under these conditions the substitution is very slow, with complex **9a** as only a minor product (~ 25% conversion after 24 h at 60°C). After 72 h of heating, complex **4c** and **9a** are gone. In the $^{31}P\{^1H\}$ NMR, a complex mixture of RuP complexes are observed, along with the dehydrocoupled phosphine product, Ph_2P-PPh_2.

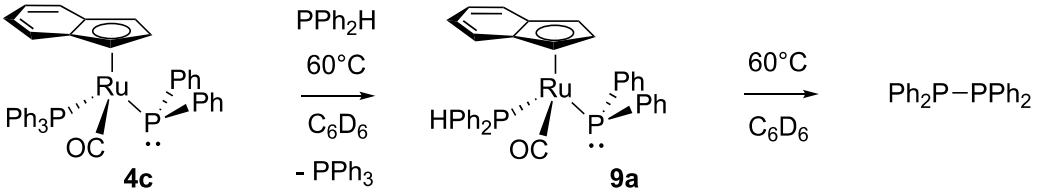

Scheme 3.15. Substitution of PPh_3 in **4c** by PPh_2H at 60°C to give Ru(η^5-indenyl)(PPh_2)(CO)(PPh_2H) (**9a**). Prolonged heating results in the formation of the dehydrocoupled product, Ph_2P-PPh_2.

No reaction is observed when one equiv of **P** is added to **4c** at rt, even after 24 h. Heating this reaction at 60°C results in slow substitution of the PPh_3 ligand in **4c** by **P** to generate Ru(η^5-indenyl)(PPh_2)(CO)(**P**) (**9b**) as determined by $^{31}P\{^1H\}$ NMR (Scheme 3.16). Complex **9b** is completely generated after heating the reaction for 1 week.

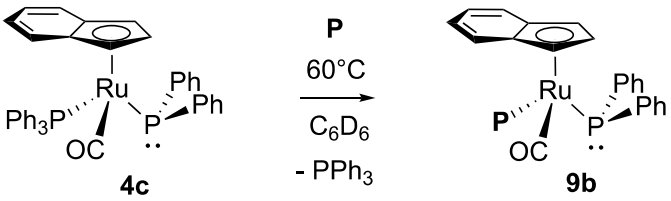

Scheme 3.16. Substitution of PPh_3 in **4c** by PPh_2H at 60°C forming Ru(η^5-indenyl)(PPh_2)(CO)(**P**) (**9b**).

These reactions demonstrate that **4c** does not easily undergo substitution with phosphines. This suggests that the mechanism shown in Scheme 3.14 is not possible under the conditions used for catalysis (rt, 4-6 h, 10 equiv of PPh_2H or **P**).

3.7.3. Evidence for Telomerization of *tert*-Butyl Acrylate in Catalysis with 4c

^{1}H NMR monitoring of hydrophosphination catalysis using **4c** showed that telomerization (hydrophosphination products resulting from addition of multiple equivalents of alkenes) occurs. First, the rate of consumption of *tert*-butyl acrylate was faster than the rate of consumption of PPh_2H under non-pseudo first order conditions (Figure 3.18, 1:1 ratio of PPh_2H:*tert*-butyl acrylate), which is consistent with the multiple alkene additions involved in telomerization. Second, in the ^{1}H NMR spectra of this catalytic reaction, multiple Bu^t resonances are observed, which corresponds to the different chemical environments of the Bu^t in the telomerized products. Third, in the phosphine region of the $^{31}P\{^{1}H\}$ NMR spectrum from this reaction, additional peaks of similar chemical shift to the hydrophosphination product, **P**, are also observed. Based on the work of Glueck, who studied Pt-catalyzed hydrophosphination of electron-deficient alkenes with PAr_2H, these additional phosphine peaks are identified as the telomerized hydrophosphination products.[13] These products represent approximately 5% of all the products formed.

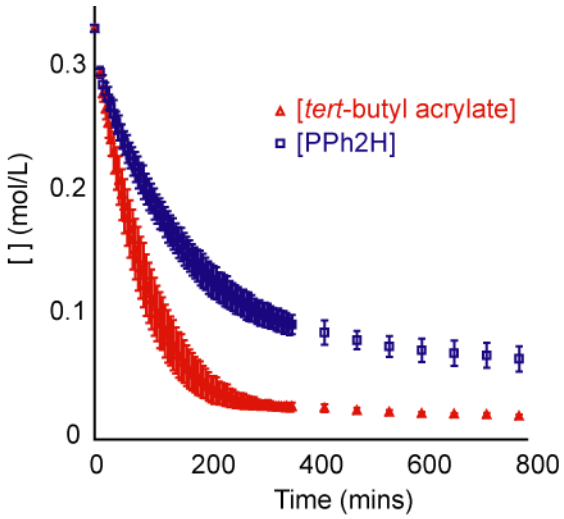

Figure 3.18. Monitoring the hydrophosphination of *tert*-butyl acrylate with PPh_2H using **4c** under non-pseudo first order conditions showing the increased rate of consumption of *tert*-butyl acrylate relative to PPh_2H.

Under pseudo-first order conditions (10 equiv of PPh_2H relative to *tert*-butyl acrylate), telomerization was not observed. In the ^{1}H NMR spectra of this reaction the additional Bu^{t} resonances are absent. A single hydrophosphination product, **P**, is observed in the $^{31}P\{^{1}H\}$ NMR spectrum of this reaction.

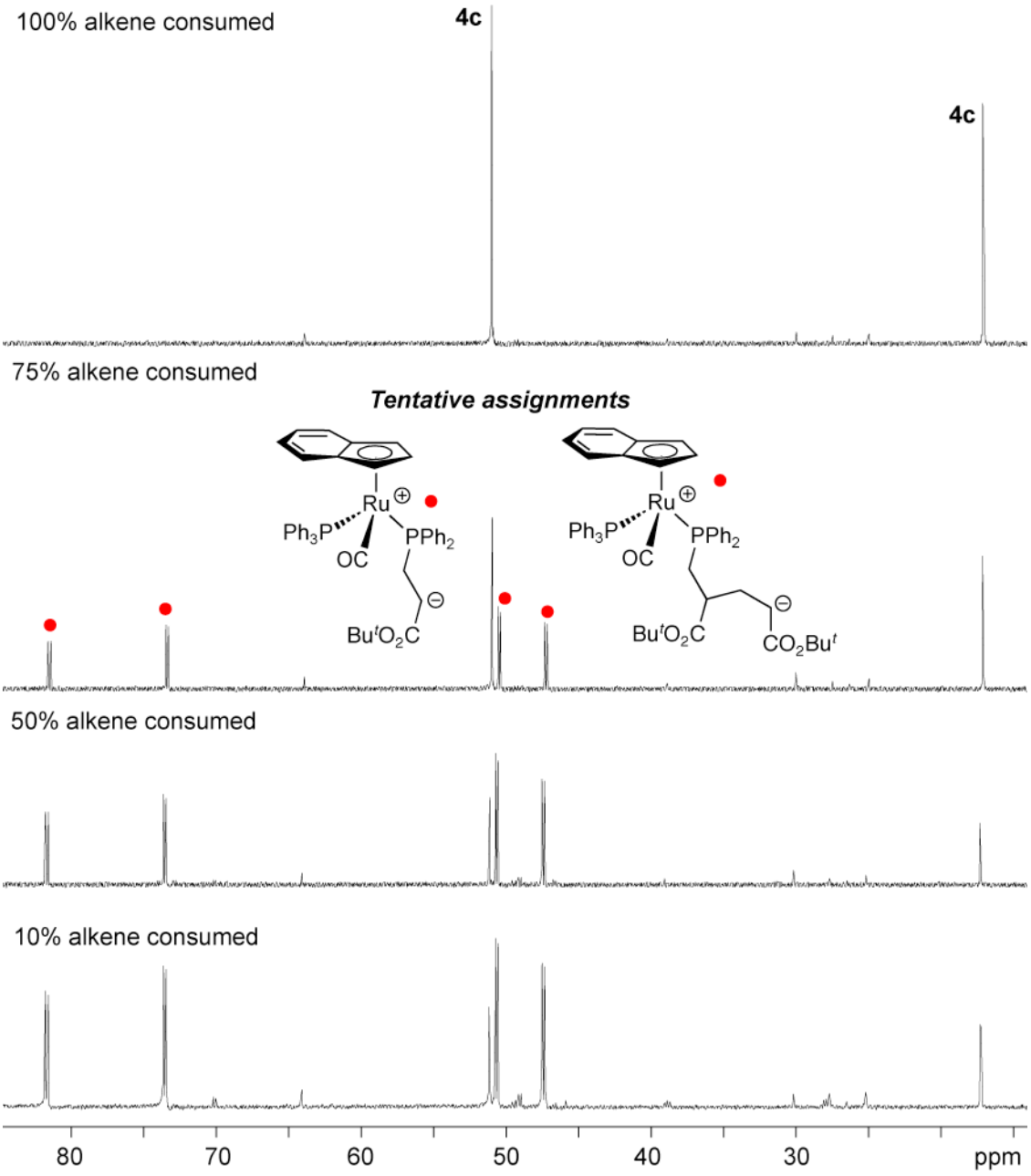

Figure 3.19. Ru phosphine/phosphido region of the $^{31}P\{^{1}H\}$ NMR region during catalysis using **4c** as the catalyst precursor, under non-pseudo first order conditions (145.85 MHz, C_6D_6). Some minor unassigned peaks are also observed during catalysis.

Monitoring hydrophosphination catalysis by $^{31}P\{^{1}H\}$ NMR shows that two new Ru-containing species form during catalysis when **4c** is used (Figure 3.19). Complex **4c** remains present, but at low concentration, throughout the whole catalytic reaction. The two

new Ru-containing complexes form initially, but decrease in concentration as the reaction proceeds. Complex **4c** is fully regenerated by the end of catalysis at the expense of these new species, which are completely consumed. These new Ru-containing intermediates appear as two sets of doublets in the $^{31}P\{^{1}H\}$ NMR spectrum at 73.9 and 50.8 ppm ($^{2}J_{PP}$ 25 Hz) and 82.5 and 47.7 ppm ($^{2}J_{PP}$ 28 Hz). The same speciation of the catalyst is observed under pseudo-first order conditions using an excess of PPh_2H.

ESI-MS analysis of an aliquot from the catalytic reaction mixture showed two Ru-containing cations (Scheme 3.17, bottom). One of these cations had a *m/z* consistent with the product-bound Ru complex [Ru(η^5-indenyl)(CO)(**P**)(PPh_3)]$^+$ (**8a**). The other cation had an *m/z* consistent with an additional equivalent of *tert*-butyl acrylate added to **8a**. In other words, this cation is consistent with a Ru complex that has a product phosphine ligand that would result from the addition of two equivalents of *tert*-butyl acrylate, [Ru(η^5-indenyl)(CO)($PPh_2CH_2CH_2(CO_2Bu^t)CH_2CH_2(COBu^t)$)($PPh_3$)]$^+$ (**8b**). This is consistent with the proposed telomerization.

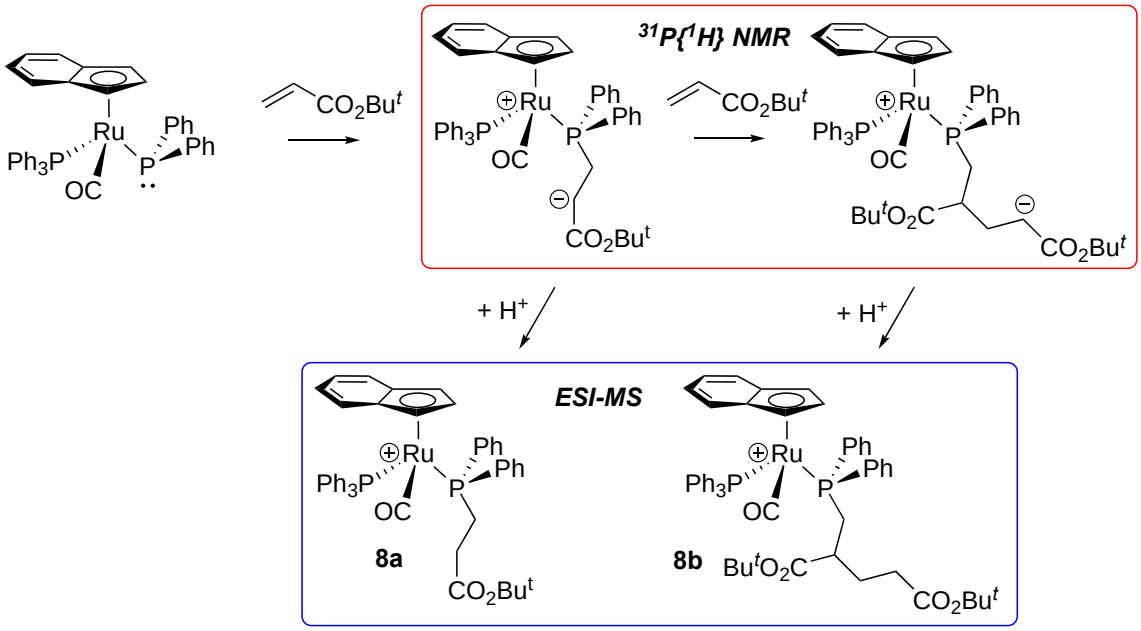

Scheme 3.17. Telomerization of *tert*-butyl acrylate *via* nucleophilic attack of the phosphido ligand in **4c** at the alkene. The zwitterionic intermediates are tentatively assigned as species observed in the $^{31}P\{^{1}H\}$ NMR during catalysis (top). The resulting cations of these zwitterionic intermediates are observed in the ESI-MS during catalysis (bottom).

Addition of one equiv of *tert*-butyl acrylate to complex **4c** results in the same sets of doublets in the $^{31}P\{^{1}H\}$ NMR that were observed during catalysis by **4c**. Unreacted **4c** remains from this stoichiometric reaction. As discussed above, I identified the cations **8a**,**b** from an ESI-mass spectrum of a catalytic mixture. ESI-MS can only observe species with an overall net positive (or negative) charge, like **8a**,**b**, and not zwitterionic species that are overall neutral. Under catalytic conditions there would be PPh_2H as a proton source to quench the zwitterionic intermediates, which would generate **8a**,**b**. Therefore, **8a**,**b** can be detected by ESI-MS. However, in the stoichiometric reaction of *tert*-butyl acrylate with **4c**, there is no proton source to quench the zwitterions. Thus, observing the same sets of doublets by $^{31}P\{^{1}H\}$ NMR in the stoichiometric reaction of complex **4c** with *tert*-butyl

acrylate and in catalysis with **4c**, suggests that these doublets are the corresponding zwitterions of **8a**,**b** (Scheme 3.17, top).

3.7.4. Revised Proposed Mechanism for Catalysis by Complex 4c

A revised proposed mechanism for the hydrophosphination of activated alkenes with PPh_2H catalyzed by **4c** is shown in Scheme 3.18, which accounts for the observed off-cycle telomerization (*vide supra*). Catalysis proceeds via initial conjugate addition of the phosphido ligand in **4c** at alkene (step A). The zwitterionic intermediate is quenched by intermolecular deprotonation of uncoordinated PPh_2H (step B). As discussed in section 3.6.3 the zwitterionic intermediate generated from step A is assigned as the resting state. This suggests that step B is rate limiting. Intermolecular quenching may be slower than the intramolecular quenching described in catalysis with complexes **4a**,**b**,**d** because the P-H bond of coordinated phosphines are more acidic than uncoordinated phosphines. Another argument for the slower intermolecular quenching can be made based on the fact that this would be a bimolecular process, which would be slower than the unimolecular, intramolecular quenching in catalysis with **4a**,**b**,**d**. Moreover, since the zwitterionic intermediate is the proposed resting state, or rather a long-lived intermediate, the carbanion of this intermediate can participate in nucleophilic addition to additional equivalents of alkene, which leads to telomerization (step D). Telomerization competes with step B, both of which are bimolecular processes. Under pseudo-first order conditions using an excess of PPh_2H, the telomerization products are not observed. This suggests that the higher concentration of PPh_2H, relative to the concentration of *tert*-butyl acrylate, increases the rate of step B, which prevents appreciable telomerization.

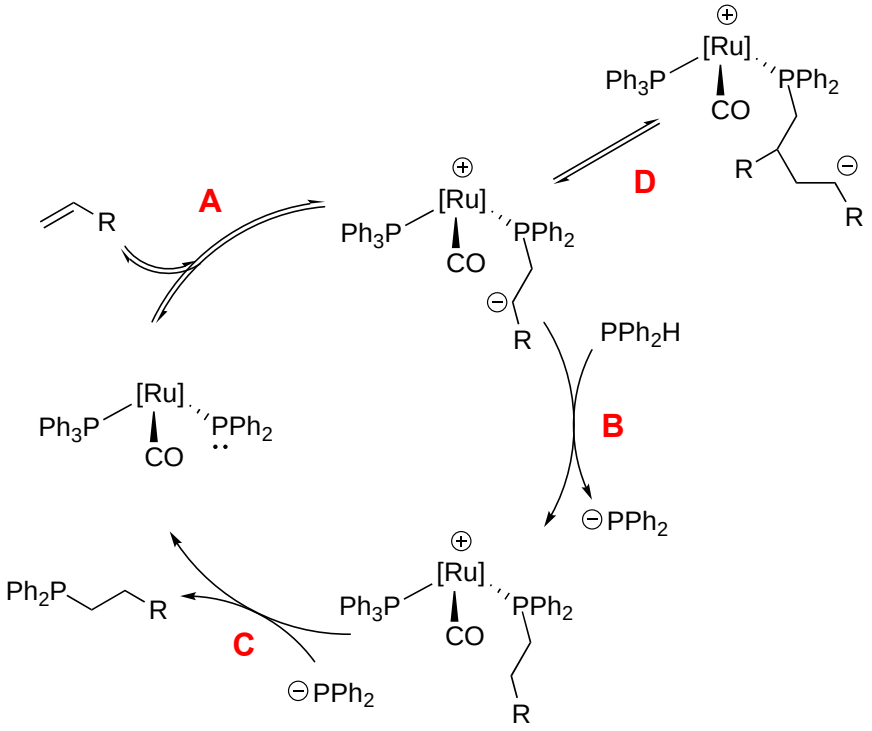

Scheme 3.18. Proposed mechanism for the hydrophosphination of activated alkenes catalyzed by complex **4c**.

Under pseudo-first order conditions there is a first order dependence on the concentration of **4c** and PPh_2H and a partial order (0.5) dependence on the *tert*-butyl acrylate concentration. I determined these using VTNA, as described in section 3.2.1 and 3.2.5. Under pseudo-first order conditions, the experimental rate law when **4c** is used as the catalyst is:

$$\text{rate} = k_{obs}[\mathbf{4c}][PPh_2H][\text{alkene}]^{0.5}$$

The partial order dependence on the concentration of *tert*-butyl acrylate may result from the off-cycle, reversible addition of alkene to the zwitterionic intermediate generated

from step A (step D). Even under pseudo-first order conditions using an excess of PPh_2H, the tentatively-assigned zwitterionic intermediates involved in step D are observed. This demonstrates that this equilibrium (step D) is operative even in the presence of excess PPh_2H. If step D was not occurring, I would have expected a first order dependence on the concentration of *tert*-butyl acrylate. Thus, the concentration of *tert*-butyl acrylate must also have a negative impact on the rate of catalysis via step D.

3.8. Conclusions

The mechanism for the hydrophosphination of *tert*-butyl acrylate with PPh_2H catalyzed by complexes Ru(η^5-indenyl)(PPh_2)(NCPh)(PPh_3) (**4a**), Ru(η^5-indenyl)(PPh_2)(PPh_2H)(PPh_3) (**4b**), Ru(η^5-indenyl)(PPh_2)(CO)(PPh_3) (**4c**) and Ru(η^5-indenyl)(PPh_2)(**P**)$_2$ (**4e**, **P** = $P(CH_2CH_2CO_2Bu^t)Ph_2$) was studied. This investigation revealed the key intermediates, the resting states of catalysis, the off-cycle processes that are operative, and provided evidence for the proposed mechanisms. A particularly substantial conclusion from studying complexes **4b**,**e** is that the substitutional lability of the catalytic intermediates is important for activity. Thus, redesigning the catalyst to increase substitutional lability should result in a more active catalysts for hydrophosphination. This will also presumably diminish the effects of product inhibition (discussed in Chapter 6). A specific result that led to this conclusion was the identification of **4e**, a complex containing two coordinated hydrophosphination product phosphines, as the resting state of catalysis.

Investigating complexes **4a**,**c** in hydrophosphination catalysis also demonstrated how ancillary ligands at the metal can influence catalytic activity and behaviour. Metal catalysts are often designed with easily accessible coordinate sites through the incorporation of labile ligands, but this could potentially also have negative implications on catalysis. For example, in the case of complex **4a**, I showed that having a labile NCPh ligand coordinated to Ru was a liability during catalysis. Although complex **4a** affords **4b** under catalytic conditions**,** which leads to catalysis, the competitive coordination of NCPh and ultimately the irreversible formation of **7** diminishes the catalytic activity. The situation is different for complex **4c**, where fully occupying a coordination site at Ru opened up an off-cycle process (telomerization) that is not observed when using **4a**,**b**,**e** in catalysis.

More generally, the insights gained from studying complexes **4a**,**c** in hydrophosphination catalysis demonstrated how the nucleophilicity of phosphido ligands and of reactive intermediates formed during hydrophosphination (e.g. zwitterions from conjugate addition of phosphido to alkene) can be detrimental to catalysis. The reduced catalytic activity and behaviour of **4a**,**c** relative to **4b**,**e** suggests that it is better to have the substrate phosphine coordinated to Ru, rather than other types of ligands. The coordinated substrate phosphine can quench the nucleophilic intermediates formed during catalysis by intramolecular H^+-transfer, which prevents deleterious reactivity. Interestingly though, under pseudo-first order conditions using excess PPh_2H, all of these complexes have comparable activity (Figure 3.20). Excess PPh_2H, presumably, out-competes NCPh for coordination to Ru in the case of **4a**, which prevents catalyst deactivation, and prevents telomerization in the case of **4c**.

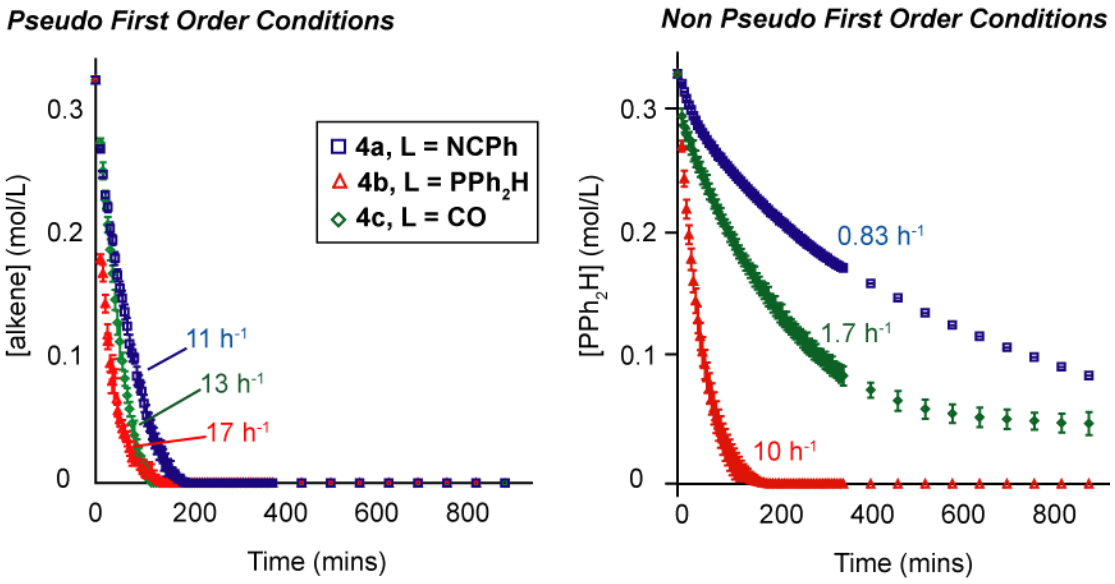

Figure 3.20. Reaction monitoring of the hydrophosphination of *tert*-butyl acrylate with PPh_2H using 10 mol% of **4a-c** under pseudo-first order (left) and non-pseudo first order (right) conditions.

Overall, the work presented in this Chapter demonstrates that valuable information about a catalytic reaction can be gained through rigorous mechanistic and kinetic analyses. This is particularly need in metal-catalyzed hydrophosphination, for which, there are many reported example, but few detailed mechanistic analyses. A thorough understanding of the mechanisms (rate limiting step, off-cycle processes, catalyst deactivation pathways) of metal-catalyzed hydrophosphination will aid in addressing current challenges of the field (section 3.2.1).

3.9. Experimental

See Chapter 2, Section 2.6.1. for general experimental details. *Tert*-butyl acrylate was purchased from Sigma Aldrich. The complexes Ru(η^5-indenyl)(PPh_2)(NCPh)(PPh_3) (**4a**),[26] Ru(η^5-indenyl)(PPh_2)(PPh_2H)(PPh_3) (**4b**)[18] and Ru(η^5-indenyl)(PPh_2)(CO)(PPh_3) (**4c**)[27] and the hydrophosphination product **P**[38] were prepared according to literature procedures. $^{31}P\{^1H\}$ NMR data for complexes **4d**,**e**,**f**, **6d**,**e**, **7a**,**b**, **8a**,**b** and **9a**,**b** is summarized in Table 3.2. ^1H and $^{13}C\{^1H\}$ NMR data of **4e** and **7a** is summarized in Tables 3.3 and 3.4. ^1H, $^{31}P\{^1H\}$ and $^{13}C\{^1H\}$ NMR spectra of **4e** and **7a** are in Appendix E.

3.9.1. Synthesis of Ru(η^5-indenyl)(PPh_2)(P)$_2$ (4e)

The complex Ru(η^5-indenyl)Cl(PPh_2H)(PPh_3) (500 mg, 0.714 mmol) and $P(CH_2CH_2CO_2Bu^t)Ph_2$ (449 mg, mmol, 1.43 mmol, 2 equiv) were dissolved in 10 mL of toluene. $NaN(TMS)_2$ (131 mg, 0.714 mmol) was added. The solution changed colour from orange to purple within 0.5 h. The solution was filtered through celite and the celite was washed with toluene (3 x 5 mL). The solvent was removed from the filtrate under vacuum affording a purple oil, which was triturated with hexanes (3 x 10 mL) to give a purple powder (670 mg, 73% yield, taking into account the residual PPh_3). Due to it being soluble in both hexane and pentane, the product could not be washed to remove the resulting equivalent of PPh_3 or small excess of **P**, nor could it be crystallized. ^1H and $^{13}C\{^1H\}$ NMR characterization of **4e** is summarized Table 3.3 and 3.4.

3.9.2. Synthesis of Ru(η^5-indenyl)(PPh_2){κ^2-$\underline{P}Ph_2(CH_2CH_2(CO_2Bu^t)C(Ph)\underline{N}H)$}($PPh_3$) (7a)

Complex **4a** (500 mg, 0.652 mmol) was dissolved in 10 mL of toluene and the solution was placed in a screw-capped vial and cooled in the glovebox freezer. *Tert*-butyl acrylate (96 μL, 0.65 mmol, 1 equiv) was added to the cooled solution. The solution was allowed to warm to rt and was stirred for 0.5 h. A colour change of the solution from deep red to orange was observed. The solution was transferred to a Schlenk flask and the solvent was removed under vacuum, which gave a red powder that was isolated by vacuum filtration and washed with a 10:1 pentane:toluene mixture. This afforded complex **7a** as a red powder (330 mg, 52% yield). X-ray quality crystals of **6** were isolated from a saturated pentane solution stored at −30°C. M.p. 203-204°C. Anal. Found (calc'd for): C, 70.79 (71.13); H, 5.57 (5.52). ^{1}H and ^{13}C{^{1}H} NMR characterization of **7a** is summarized Table 3.3 and 3.4. Crystallographic data of complex **7a** is presented in Appendix C.

3.9.3. NMR Scale Catalytic Hydrophosphination

Experiments were performed using a standard 5mm NMR tube equipped with a coaxial tube containing 100 μL of a standard solution of $O(SiMe_3)_2$ in C_6D_6. Stock solutions in C_6D_6 were prepared: 1.0 M solutions of both PPh_2H and *tert*-butyl acrylate, 0.1 M solutions of complexes **4a-d**, respectively, and a 0.5 M solution of $O(SiMe_3)_2$. Up to 100 μL of each of the substrate and catalyst solutions were used in order to vary substrate and catalyst concentrations; additional C_6D_6 was added to maintain a constant volume of 350 μL (in addition to the volume displaced by the coaxial tube). Conversion of PPh_2H and *tert*-butyl acrylate to **P** catalyzed by complexes **4a-d** was monitored by ^{1}H NMR (500.13

MHz) at rt using diagnostic signals of the vinyl protons of the alkene, the P-H resonance of PPh_2H and peaks due to the CH_2 groups in the product phosphine. To allow quantitation, each experiment was single scan with a delay of 5 minutes between each experiment for the first 6 hours, and a subsequent delay of 1 hour. All reactions were performed in triplicate.

3.9.4. General Details for Reactions of Complexes 4c, 4e and 7a with PPh_2H

Solid (**4c**: 15 mg, 0.020 mmol; **4e**: 15 mg, 0.020 mmol; **7a**: 15 mg, 0.020 mmol) was dissolved in C_6D_6 and ten equiv of PPh_2H (35 μL, 0.20 mmol) was added. The reactions were monitored by $^{31}P\{^1H\}$ NMR spectroscopy. Unless specified, all reactions were done at rt. $^{31}P\{^1H\}$ NMR spectra are in Appendix F.

3.9.4.1. Reaction of Complex Ru(η^5-indenyl)(PPh_2)(CO)(PPh_3) (4c) with PPh_2H

After 48 h no reaction was observed between **4c** and PPh_2H. Heating for 2 h at 70°C resulted in a minor amount of Ru(η^5-indenyl)(PPh_2)(CO)(PPh_2H) (**9a**). Prolonged heating led to decomposition of **4c** and **9a** along with generation of Ph_2PPPh_2.

3.9.4.2. Reaction of Complex Ru(η^5-indenyl)(PPh_2)(P)$_2$ (4e) with PPh_2H

After 24 h quantitative conversion of complex **4e** to **4f** occurred via substitution of **P** by PPh_2H.

3.9.4.3. Reaction of Ru(η^5-indenyl)(PPh_2)(κ^2-P(Ph_2)CH_2CH_2(CO_2Bu^t)C(Ph)NH)(PPh_3) (7a) with PPh_2H

After 3 d quantitative conversion of complex **7a** to Ru(η^5-indenyl)(PPh_2)(κ^2-P(Ph_2)CH_2CH_2(CO_2Bu^t)C(Ph)NH)(PPh_2H) via substitution of PPh_3 by PPh_2H was observed. Heating the reaction for an additional 3 d at 60 °C resulted in generation of a minor amounts of Ru(η^5-indenyl)(PPh_2)(PPh_2H)$_2$, **P** and some unidentified phosphine products.

3.9.5. General Details for Reactions of Complexes 4a, 4b, 4c and 4e with *tert*-butyl acrylate

Solid (**4a**: 15 mg, 0.020 mmol; **4b**: 15 mg, 0.020 mmol; **4c**: 15 mg, 0.020 mmol; **4e**: 15 mg, 0.020 mmol) was dissolved in C_6D_6 and 1 - 2 equiv of *tert*-butyl acrylate (3 - 6 μL, 0.02 - 0.04 mmol) was added. The reactions were monitored by $^{31}P\{^1H\}$ NMR spectroscopy. Unless specified, all reactions were done at rt. $^{31}P\{^1H\}$ NMR spectra are in Appendix F.

3.9.5.1. Reaction of Ru(η^5-indenyl)(PPh_2)(NCPh)(PPh_3) (4a) with *tert*-butyl acrylate

Within a minute of adding *tert*-butyl acrylate the solution changed colour from dark purple to red. The $^{31}P\{^1H\}$ NMR spectrum collected at ~ 20 min showed complete conversion of **4a** to complexes **6d** and **7a** (~ 2:1 ratio at rt and ~1:2 ratio at −20°C).

3.9.5.2. Reaction of Ru(η^5-indenyl)(PPh_2)(PPh_2H)(PPh_3) (**4b**) with *tert*-butyl acrylate

Within a minute of adding one equiv of *tert*-butyl acrylate the solution changed colour from dark purple to red. The $^{31}P\{^1H\}$ NMR spectrum collected at ~ 20 mins showed some unreacted **4b** as well as complexes **4d**,**e** and **6d**,**e**, PPh_3 and **P**.

3.9.5.3. Reaction of Ru(η^5-indenyl)(PPh_2)(CO)(PPh_3) (**4c**) with *tert*-butyl acrylate

A $^{31}P\{^1H\}$ NMR spectrum collected at ~ 20 mins after addition of *tert*-butyl acrylate to **4c** showed unreacted **4c** as well as the tentatively assigned complexes **8a**,**b**.

3.9.5.4. Reaction of Ru(η^5-indenyl)(PPh_2)(P)$_2$ (**4e**) with *tert*-butyl acrylate

Quantitative conversion of complex **4e** to **6d**,**e** was observed over 4 days. Complex **6d** was a minor product due to the presence of residual PPh_3 left over from the synthesis of **4e**.

3.9.6. General Details for Reactions of Complex 4a-c with P

Solid (**4a**: 15 mg, 0.020 mmol; **4b**: 15 mg, 0.020 mmol; **4c**: 15 mg, 0.020 mmol) was dissolved in C_6D_6 and one equiv of PPh_2H (4 μL, 0.02 mmol) was added. The reactions were monitored by $^{31}P\{^1H\}$ NMR spectroscopy. Unless specified, all reactions were done at rt. $^{31}P\{^1H\}$ NMR spectra are in Appendix F.

3.9.6.1. Reaction of Ru(η^5-indenyl)(PPh_2)(NCPh)(PPh_3) (**4a**) with P

A $^{31}P\{^1H\}$ NMR spectrum collected at ~ 20 mins after addition of **P** to **4a** showed complete conversion of **4a** to complexes **4d**,**e**. A trace amount of **4b** also formed from residual PPh_2H in the isolated **P**.

3.9.6.2. Reaction of Ru(η^5-indenyl)(PPh_2)(PPh_2H)(PPh_3) (**4b**) with P

Over one week $^{31}P\{^1H\}$ NMR spectra showed complete conversion of **4b** to complex **4f** via substitution of PPh_3 by **P**. Since there was residual PPh_2H in the isolated **P** complex Ru(η^5-indenyl)(PPh_2)(PPh_2H)$_2$ began to form after 4 days, presumably via substitution of **P** in complex **4f** by PPh_2H.

3.9.6.3. Reaction of Ru(η^5-indenyl)(PPh_2)(CO)(PPh_3) (**4c**) with P

After 48 h no reaction was observed between **4c** and **P**. Heating for 2 h at 60 °C resulted in the formation of a minor amount of Ru(η^5-indenyl)(PPh_2)(CO)(**P**) (**9b**). Prolonged heating for 7 d led to quantitative conversion of **4c** to **9b** via substitution of PPh_3 by **P** .

3.9.7. Thermolysis of Ru(η^5-indenyl)(PPh_2)(κ^2-P(Ph_2)CH_2CH_2(CO_2Bu^t)C(Ph)NH)(PPh_3) (**7a**)

Complex **7a** (15mg, 0.020 mmol) was dissolved in C_6D_6 and the solution was added to a J Young tube and sealed. Initial ^1H and $^{31}P\{^1H\}$ NMR spectra were collected. The solution was then heated in an oil bath at 60 °C and ^1H and $^{31}P\{^1H\}$ NMR spectra were

collected periodically. After 2 weeks of heating, complex **7a** remained, with only trace amounts of decomposition.

3.9.8. $^{31}P\{^{1}H\}$ NMR Data Table for Compounds 4d,e,f, 6d,e, 7a,b, 8a,b and 9a,b

Table 3.2. 202.51 MHz $^{31}P\{^{1}H\}$ NMR data for complexes **4d,e,f, 6d,e, 7a,b, 8a,b** and **9a,b** at 300 K: shift in ppm (multiplicity, $^{2}J_{PP}$, Hz)

Compound	PPh_2	Other
Ru(η^5-indenyl)(PPh_2)(**P**)(PPh_3) (**4d**)	45.6 (d, 4)	38.7 (dd, 26, 4, PPh_3) 27.9 (26 Hz, **P**)
Ru(η^5-indenyl)(PPh_2)(**P**)$_2$ (**4e**)	39.1 (t, 3)	30.2 (d, 3)
Ru(η^5-indenyl)(PPh_2)(PPh_2H)(**P**) (**4f**)	29.7 (dd, 21, 5)	41.2 (dd, 35, 21, PPh_2H) 35.6 (dd, 35, 5, **P**)
Ru(η^5-indenyl)(κ^2-Bu^{t}CO$_2$CHCH$_2$PPh$_2$)(PPh_3) (**6d**)	-27.0 (d, 25)	61.1 (d, 25)
Ru(η^5-indenyl)(κ^2-Bu^{t}CO$_2$CHCH$_2$PPh$_2$)(**P**) (**6e**)	−24.5 (d, 25)	49.7 (d, 25)
Ru(η^5-indenyl)(PPh_2)(κ^2-P(Ph_2)CH$_2$CH$_2$(CO$_2$Bu^t)C(Ph)NH)(PPh_3) (**7a**)	60.6 (d, 30)	47.2 (d, 4)
Ru(η^5-indenyl)(PPh_2)(κ^2-P(Ph_2)CH$_2$CH$_2$(CO$_2$Bu^t)C(Ph)NH)(**P**) (**7b**)	63.1 (d, 32)	37.4 (d, 32)
[Ru(η^5-indenyl)(CO)(**P**)(PPh_3)]$^+$ (**8a**)	73.9 (d, 25)	51.0 (d, 25)
[Ru(η^5-indenyl)(CO)(PPh_2CH$_2$CH$_2$(CO$_2$Bu^t)CH$_2$CH$_2$(COBu^t))(PPh_3)]$^+$ (**8b**)	81.9 (d, 29)	47.7 (d, 29)
Ru(η^5-indenyl)(PPh_2)(PPh_2H)(CO) (**9a**)	29.1 (d, 16)	37.1 (d, 16)
Ru(η^5-indenyl)(PPh_2)(**P**)(CO) (**9b**)	13.8 (d, 6)	44.1 (d, 6)

*$^{31}P\{^{1}H\}$ NMR chemical shifts reported in C_6D_6.

3.9.9. ^{1}H, $^{13}C\{^{1}H\}$ Data Tables for Isolated Compounds 4e and 7a

Table 3.3. 500.27 MHz ^{1}H NMR data for complexes **4e** and **7a** at 300 K: δ in ppm (multiplicity, RI, J_{avg} or $w_{1/2}$ in Hz, assignment).

	η^5-C_9H_7				
Compound	**H_7,H_4**	**H_6,H_5**	**H_2**	**H_3,H_1**	**Other**
4e C_6D_6	6.23 (dd, $^{3}J_{HH}$ 6.2, $^{4}J_{HH}$ 3.1, 2H)	6.85 (dd, $^{3}J_{HH}$ 6.2 Hz, $^{4}J_{HH}$ 3.1, 2H)	6.28 (td, $^{3}J_{HH}$ 2.8, $^{3}J_{PH}$ 1.4, 1H)	4.72 (d, $^{3}J_{HH}$ 2.8, 2H)	**PPh_2:** 7.84 (m, 5H), 7.15 (m, 5H) **$Ph_2PCH_2CH_2CO_2Bu^t$:** 6.83-6.75 (m, 5H, Ph), 3.00-2.85 (m, 2H, CH_2), 2.20-2.05 (m, 2H, CH_2), 1.85-1.60 (m, 4H, CH_2), 1.29 (s, 18H, Bu^t) 7.11-6.88 (m, overlapping aromatic H, 5H)
7a C_6D_6	7.30-7.20 (1H, overlapping with), 6.49 (d, 8.3)	7.20-7.10 (1H, overlapping with *meta*-H of PPh_2), 6.70 (t, 7.6)	3.76 (s, 1H)	4.83 (s, 1H), 4.63 (s, 1H)	**Metallacycle:** 7.52 (br, 2H, meta-H NCPh) 7.30-7.20 (2H, overlapping with $H_{7/4}$, *ortho*-H NCPh), 7.10-7.01 (m, overlapping with *meta*-H PPh_2, 1H, *para*-H NCPh), 4.01 (dd, 1H, CH_2), 3.96 (s, 1H, N*H*), 1.98 (ddd, 1H, CH_2), 1.24 (s, 9H, Bu^t) **PPh_2:** 7.68 (t, 2H, *ortho*-H), 7.39 (t, 2H, *ortho*-H), 7.20-7.10 (m, *meta*-H overlapping with $H_{6/5}$, 2H), 7.10-7.01 (m, overlapping with *para*-H NCPh, 4H, *meta*- and *para*-Hs) **PPh_3:** 6.84 (t, 6H, *meta*-H), 6.76 (t, 6H, *ortho*-H), 6.91 (t, 3H, *para*-H)

Table 3.4. 125.77 MHz $^{13}C\{^{1}H\}$ NMR data for complexes **4e** and **7a** at 300 K: δ in ppm (multiplicity, RI, J_{avg} or $w_{1/2}$ in Hz, assignment).

	η⁵-C₉H₇						
Compound	**C₆,C₅**	**C₇,C₄**	**C₃ₐ,C₇ₐ**	**Δδ(C₃ₐ,₇ₐ)**	**C₂**	**C₃,C₁**	**Other**
4e C_6D_6	124.5 (s)	122.5 (s)	112.8 (s)	-	97.5 (s)	72.4 (t, $^{2}J_{PC}$ 4)	**PPh_2:** 153.4 (d, $^{1}J_{PC}$ 18 Hz, *ipso*-C), 135.5 (d, $^{2}J_{PC}$ 18 Hz, *ortho*-C) **$Ph_2PCH_2CH_2CO_2Bu^t$:** 171.7 (t, $^{3}J_{PC}$ 5, CCO_2Bu^t), 137.7 (d, $^{1}J_{PC}$ 12, *ipso*-C), 79.3 (s, CMe_3), 32.4 (t, $^{1}J_{PC}$ 4, CH_2), 27.7 (s, Bu^t), 32.4 (d, $^{2}J_{PC}$ 4, CH_2),
7a C_6D_6	127.3 (s), 125. 9 (s)	124.6 (s), 122.3 (s)	112.8 (d, $^{2}J_{PC}$ 4), 108.9 (d, $^{2}J_{PC}$ 6)		66.8 (s)	90.2 (s), 67.4 (d, $^{2}J_{PC}$ 14)	**Metallacycle:** 172.7 (d, $^{2}J_{PC}$ 5, CO_2Bu^t), 169.2 (d, $^{2}J_{PC}$ 8, HN*C*Ph), 149.8 (d, $^{2}J_{PC}$ 2, NCC_{Ph}), 127.6 (s, *para*-C NCPh), 127.4 (s, *ortho* and *meta*-C, NCPh), 81.4 (s, CCO_2Bu^t), 74.9 (s, CMe_3), 28.4 (s, Bu^t), 22.0 (d, $^{2}J_{PC}$ 27, CH_2) **PPh_2:** 142.1 (dd, $^{1}J_{PC}$ 45, $^{3}J_{PC}$ 3, *ipso*-C), 136.9 (dd, $^{1}J_{PC}$ 43, $^{3}J_{PC}$ 4, *ipso*-C), 132.8 (d, $^{2}J_{PC}$ 9, *ortho*-C), 130.9 (d, $^{2}J_{PC}$ 8, *ortho*-C), 129.2 (d, $^{2}J_{PC}$ 2, *para*-C), 128.6 (d, $^{2}J_{PC}$ 2, *para*-C), 127.7 (d, $^{2}J_{PC}$ 9, *meta*-C), 126.6 (d, $^{2}J_{PC}$ 8, *meta*-C) **PPh_3:** 136.3 (dd, $^{1}J_{PC}$ 38, *ipso*-C), 133.7 (d, $^{2}J_{PC}$ 11, *ortho*-C), 128.9 (s, *para*-C), 127.3 (d, $^{2}J_{PC}$ 9, *meta*-C)

3.10. References

(1) Pullarkat, S.; Leung, P.-H. Chiral Metal Complex-Promoted Asymmetric Hydrophosphinations. In *Hydrofunctionalization*; Ananikov, V. P., Tanaka, M., Eds.; Springer Berlin Heidelberg, 2013; pp 145–166.

(2) Glueck, D. Recent Advances in Metal-Catalyzed C–P Bond Formation. In *C-X Bond Formation*; Vigalok, A., Ed.; Springer Berlin Heidelberg, 2010; pp 65–100.

(3) Koshti, V.; Gaikwad, S.; Chikkali, S. H. Contemporary Avenues in Catalytic P-H Bond Addition Reaction: A Case Study of Hydrophosphination. *Coord. Chem. Rev.* **2014**, *265*, 52–73.

(4) Greenhalgh, M. D.; Jones, A. S.; Thomas, S. P. Iron-Catalysed Hydrofunctionalisation of Alkenes and Alkynes. *ChemCatChem* **2015**, *7*, 190–222.

(5) Bezzenine-Lafollée, S.; Gil, R.; Prim, D.; Hannedouche, J. First-Row Late Transition Metals for Catalytic Alkene Hydrofunctionalisation: Recent Advances in C-N, C-O and C-P Bond Formation. *Molecules* **2017**, 1901-1930.

(6) Rodriguez-Ruiz, V.; Carlino, R.; Bezzenine-Lafollee, S.; Gil, R.; Prim, D.; Schulz, E.; Hannedouche, J. Recent Developments in Alkene Hydro-Functionalisation Promoted by Homogeneous Catalysts Based on Earth Abundant Elements: Formation of C-N, C-O and C-P Bond. *Dalton Trans.* **2015**, *44*, 12029–12059.

(7) Pullarkat, S. A. Recent Progress in Palladium-Catalyzed Asymmetric Hydrophosphination. *Synthesis* **2016**, *48*, 493–503.

(8) Trifonov, A. A.; Basalov, I. V; Kissel, A. A. Use of Organolanthanides in the Catalytic Intermolecular Hydrophosphination and Hydroamination of Multiple C–C Bonds. *Dalton Trans.* **2016**, *45*, 19172–19193.

(9) Hill, M. S.; Liptrot, D. J.; Weetman, C. Alkaline Earths as Main Group Reagents in Molecular Catalysis. *Chem. Soc. Rev.* **2016**, *45*, 972–988.

(10) Kawaoka, A. M.; Douglass, M. R.; Marks, T. J. Homoleptic Lanthanide Alkyl and Amide Precatalysts Efficiently Mediate Intramolecular Hydrophosphination/Cyclization. Observations on Scope and Mechanism. *Organometallics* **2003**, *22*, 4630–4632.

(11) Douglass, M. R.; Ogasawara, M.; Hong, S.; Metz, M. V; Marks, T. J. "Widening the Roof": Synthesis and Characterization of New Chiral C1-Symmetric Octahydrofluorenyl Organolanthanide Catalysts and Their Implementation in the Stereoselective Cyclizations of Aminoalkenes and Phosphinoalkenes. *Organometallics* **2002**, *21*, 283–292.

(12) Douglass, M. R.; Marks, T. J. Organolanthanide-Catalyzed Intramolecular Hydrophosphination/Cyclization of Phosphinoalkenes and Phosphinoalkynes. *J. Am. Chem. Soc.* **2000**, *122*, 1824–1825.

(13) Scriban, C.; Glueck, D. S.; Zakharov, L. N.; Kassel, W. S.; DiPasquale, A. G.; Golen, J. A.; Rheingold, A. L. P−C and C−C Bond Formation by Michael Addition in Platinum-Catalyzed Hydrophosphination and in the Stoichiometric Reactions of Platinum Phosphido Complexes with Activated Alkenes. *Organometallics* **2006**, *25*, 5757–5767.

(14) Scriban, C.; Kovacik, I.; Glueck, D. S. A Protic Additive Suppresses Formation of Byproducts in Platinum-Catalyzed Hydrophosphination of Activated Olefins. Evidence for P−C and C−C Bond Formation by Michael Addition. *Organometallics* **2005**, *24*, 4871–4874.

(15) Bange, C. A.; Waterman, R. Challenges in Catalytic Hydrophosphination. *Chem. Eur. J.* **2016**, 12598-12605.

(16) Rosenberg, L. Mechanisms of Metal-Catalyzed Hydrophosphination of Alkenes and Alkynes. *ACS Catal.* **2013**, *3*, 2845–2855.

(17) Sues, P. E.; Lough, A. J.; Morris, R. H. Reactivity of Ruthenium Phosphido Species Generated through the Deprotonation of a Tripodal Phosphine Ligand and Implications for Hydrophosphination. *J. Am. Chem. Soc.* **2014**, *136*, 4746–4760.

(18) Belli, R. G.; Burton, K. M. E.; Rufh, S. A.; McDonald, R.; Rosenberg, L. Inner- and Outer-Sphere Roles of Ruthenium Phosphido Complexes in the Hydrophosphination of Alkenes. *Organometallics* **2015**, *34*, 5637–5646.

(19) Di Giuseppe, A.; De Luca, R.; Castarlenas, R.; Pérez-Torrente, J. J.; Crucianelli, M.; Oro, L. A. Double Hydrophosphination of Alkynes Promoted by Rhodium: The Key Role of an N-Heterocyclic Carbene Ligand. *Chem. Commun.* **2016**, *52*, 5554–5557.

(20) Tay, W. S.; Yang, X.-Y.; Li, Y.; Pullarkat, S. A.; Leung, P.-H. Investigating Palladium Pincer Complexes in Catalytic Asymmetric Hydrophosphination and Hydroarsination. *Dalton Trans.* **2019**, *48*, 4602–4610.

(21) Yang, X.-Y.; Jia, Y.-X.; Tay, W. S.; Li, Y.; Pullarkat, S. A.; Leung, P.-H. Mechanistic Insights into the Role of PC- and PCP-Type Palladium Catalysts in Asymmetric Hydrophosphination of Activated Alkenes Incorporating Potential Coordinating Heteroatoms. *Dalton Trans.* **2016**, *45*, 13449–13455.

(22) Xu, C.; Jun Hao Kennard, G.; Hennersdorf, F.; Li, Y.; Pullarkat, S. A.; Leung, P.-H. Chiral Phosphapalladacycles as Efficient Catalysts for the Asymmetric

Hydrophosphination of Substituted Methylidenemalonate Esters: Direct Access to Functionalized Tertiary Chiral Phosphines. *Organometallics* **2012**, *31*, 3022–3026.

(23) Huang, Y.; Pullarkat, S. A.; Li, Y.; Leung, P.-H. Palladacycle-Catalyzed Asymmetric Hydrophosphination of Enones for Synthesis of C*- and P*-Chiral Tertiary Phosphines. *Inorg. Chem.* **2012**, *51*, 2533–2540.

(24) Huang, Y.; Chew, R. J.; Li, Y.; Pullarkat, S. A.; Leung, P.-H. Direct Synthesis of Chiral Tertiary Diphosphines via Pd(II)-Catalyzed Asymmetric Hydrophosphination of Dienones. *Org. Lett.* **2011**, *13*, 5862–5865.

(25) Lu, Z.; Zhang, H.; Yang, Z.; Ding, N.; Meng, L.; Wang, J. Asymmetric Hydrophosphination of Heterobicyclic Alkenes: Facile Access to Phosphine Ligands for Asymmetric Catalysis. *ACS Catal.* **2019**, *9*, 1457–1463.

(26) Hoyle, M.-A. M.; Pantazis, D. A.; Burton, H. M.; McDonald, R.; Rosenberg, L. Benzonitrile Adducts of Terminal Diarylphosphido Complexes: Preparative Sources of "Ru═PR2." *Organometallics* **2011**, *30*, 6458–6465.

(27) Derrah, E. J.; Pantazis, D. A.; McDonald, R.; Rosenberg, L. A Highly Reactive Ruthenium Phosphido Complex Exhibiting Ru−P π-Bonding. *Organometallics* **2007**, *26*, 1473–1482.

(28) Burés, J. A Simple Graphical Method to Determine the Order in Catalyst. *Angew. Chem. Int. Ed.* **2016**, *55*, 2028–2031.

(29) Douglass, M. R.; Stern, C. L.; Marks, T. J. Intramolecular Hydrophosphination/Cyclization of Phosphinoalkenes and Phosphinoalkynes Catalyzed by Organolanthanides: Scope, Selectivity, and Mechanism. *J. Am. Chem. Soc.* **2001**, *123*, 10221–10238.

(30) Espinal-Viguri, M.; King, A. K.; Lowe, J. P.; Mahon, M. F.; Webster, R. L. Hydrophosphination of Unactivated Alkenes and Alkynes Using Iron(II): Catalysis and Mechanistic Insight. *ACS Catal.* **2016**, *6*, 7892–7897.

(31) Blackmond, D. G. Reaction Progress Kinetic Analysis: A Powerful Methodology for Mechanistic Studies of Complex Catalytic Reactions. *Angew. Chem. Int. Ed.* **2005**, *44*, 4302–4320.

(32) Derrah, E. J.; Pantazis, D. A.; McDonald, R.; Rosenberg, L. Concerted [2+2] Cycloaddition of Alkenes to a Ruthenium–Phosphorus Double Bond. *Angew. Chem. Int. Ed.* **2010**, *49*, 3367–3370.

(33) Burton, K. M. E.; Pantazis, D. A.; Belli, R. G.; McDonald, R.; Rosenberg, L. Alkene Insertions into a Ru–PR2 Bond. *Organometallics* **2016**, *35*, 3970–3980.

(34) Burés, J. Variable Time Normalization Analysis: General Graphical Elucidation of Reaction Orders from Concentration Profiles. *Angew. Chem. Int. Ed.* **2016**, *55*, 16084–16087.

(35) Belli, R. G.; Wu, Y.; Ji, H.; Joshi, A.; Yunker, L. P. E.; McIndoe, J. S.; Rosenberg, L. Competitive Ligand Exchange and Dissociation in Ru Indenyl Complexes. *Inorg. Chem.* **2019**, *58*, 747–755.

(36) Gamasa, M. P.; Gimeno, J.; Gonzalez-Bernardo, C.; Martín-Vaca, B. M.; Monti, D.; Bassetti, M. Phosphine Substitution in Indenyl- and Cyclopentadienylruthenium Complexes. Effect of the H5 Ligand in a Dissociative Pathway. *Organometallics* **1996**, *15*, 302–308.

(37) Blackmond, D. G. Kinetic Profiling of Catalytic Organic Reactions as a Mechanistic Tool. *J. Am. Chem. Soc.* **2015**, *137*, 10852–10866.

(38) Moglie, Y.; González-Soria, M. J.; Martín-García, I.; Radivoy, G.; Alonso, F. Catalyst- and Solvent-Free Hydrophosphination and Multicomponent Hydrothiophosphination of Alkenes and Alkynes. *Green Chem.* **2016**, *18*, 4896–4907.

Chapter 4 Exploring the Viability of Phosphenium Ligands in Metal-Catalyzed Hydrophosphination

4.1. Chapter Overview

In this chapter, the synthesis and reactivity of molybdenum complexes that contain electrophilic phosphenium ligands (PR_2^+) is described. Complexes *cis*-$Mo(CO)_4(PR_2H)_2$ (*cis*-**10a** R = Tol^p, *cis*-**10b** R = Ph) and *fac*-$Mo(CO)_3(PPh_2H)_3$ (*fac*-**11**) were prepared and were used as precursors for the synthesis of complexes *trans*-$[Mo(CO)_4(PTol^p_2H)(PTol^p_2)][B(C_6H_3Cl_2)_4]$ (*trans*-**12a**$[B(C_6H_3Cl_2)_4]$), *trans*-$[Mo(CO)_4(PR_2H)(PR_2)][B(C_6H_3Cl_2)_4]$ (*trans*-**12b**$[B(C_6H_3Cl_2)_4]$) and *trans*-$[Mo(CO)_4(PPh_2H)(PPh_2)][B(C_6H_3Cl_2)_4]$ (*trans*-**13**$[B(C_6H_3Cl_2)_4]$) *via* hydride abstraction. The new complexes *trans*-**12a**,**b**$[B(C_6H_3Cl_2)_4]$ and *trans*-**13**$[B(C_6H_3Cl_2)_4]$ were synthesized, isolated and fully characterized. The reactivity of complexes *trans*-**12a**,**b** and *trans*-**13** relevant to hydrophosphination is described. This Chapter includes contributions from Carly Slusar, Dr. Dimitrios Pantazis and Dr. Robert McDonald. Supplementary spectra are presented in Appendix E, G and H.

4.2. Introduction

A major challenge with metal-catalyzed hydrophosphination is that the substrate scope used is generally limited to electron-deficient alkenes or alkynes.[1] This arises from the fact that many examples of metal-catalyzed hydrophosphination involve intermediates in catalysis that contain phosphido ligands, which are extremely nucleophilic, especially as ligands on late metals.[2] Thus, P-C bond formation typically occurs via conjugate addition of the phosphido ligand to the unsaturated substrate, which is more likely to occur with

electron-deficient substrates; the nucleophilicity of phosphido ligands is also critical for P-C bond formation that occurs via alkene insertion into M-PR_2 bond. Given this general observation and the results of Chapters 2 and 3, we were motivated to develop a new methodology for metal-catalyzed hydrophosphination that allowed for the hydrophosphination of simple and electron-rich alkenes.

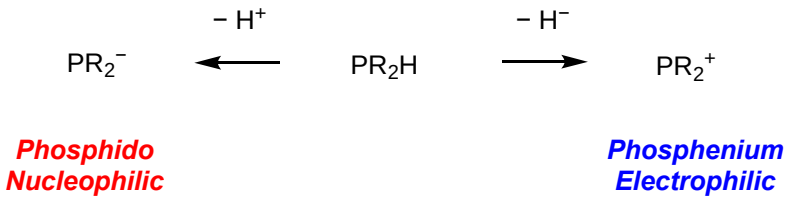

Scheme 4.1. P-H bond activation by deprotonation generating a phosphido (left) and hydride abstraction generating a phosphenium (right).

An unexplored area of metal-catalyzed hydrophosphination is the potential intermediacy of electrophilic phosphenium ligands. Phospheniums ligands are like phosphido ligands in that these are both PR_2 fragments, but are electrophilic rather than nucleophilic (*vide infra*, section 4.2.1). A critical step of hydrophosphination catalysis is P-H bond activation, which can occur through deprotonation or oxidative addition (discussed in Chapter 1). In both of those cases, a PR_2^- is formally delivered to the metal. The P-H bond is non-polar, so *umpolung* (polarity inversion) of P-H bond activation via hydride abstraction could generate metal-bound phospheniums (Scheme 4.1). Phosphenium ligands could form P-C bonds in hydrophosphination through electrophilic addition to unsaturated substrates, which could allow for the hydrophosphination of simple and electron-rich substrates. To the best of my knowledge, no examples of metal-catalyzed

hydrophosphination exist that implicate metal phosphenium complexes or P-H bond activation by hydride abstraction.

4.2.1. Electronic Structure of Phospheniums

Phospheniums (PR_2^+) are cationic, two-coordinate phosphorus species.[3] These differ from phosphido moieties (also a two-coordinate phosphorus species) in that phospheniums are electrophilic and phosphido moieties are nucleophilic (as discussed in Chapter 2 and 3).

An analogy can be drawn between phospheniums and Fischer-type carbenes.[4] In particular, interest in using phospheniums as ligands for metals arises from this comparison since phosphenium ligands have a lone pair of electrons for σ-donation and an empty p-orbital for π-acceptance from the metal (Figure 4.1). Furthermore, phospheniums, like Fischer-type carbenes, usually have π-donating substituents (alkoxide, amide). The interaction between the π-donating substituents and the p_π-orbital of the phosphenium P stabilizes the phosphenium. This interaction also destabilizes the p_π-orbital, which favours a fully occupied σ-orbital. Unlike N-heterocyclic carbenes (NHC), which are stronger σ-donors than π-acceptors, N-heterocyclic phospheniums (NHP^+) are stronger π-acceptors than σ-donors.

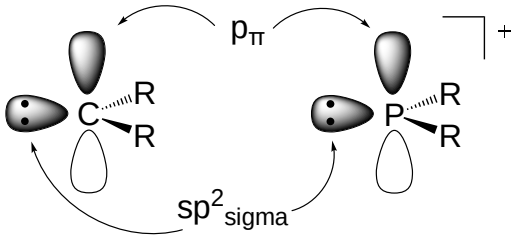

Figure 4.1. Structure and bonding orbitals of a generic Fischer carbene and phosphenium.

4.2.2. First Examples of Phospheniums

The cyclic 1,3-dimethyl-1,3,2-diazaphosphenium was the first example of an isolated, stable phosphenium reported by Fleming *et al* (Figure 4.2).[5] This was followed by Parry *et al* who synthesized the first acyclic phosphenium, bis(dimethylamino)phosphenium.[6] Parry *et al* also reported the first example of a metal complex of a phosphenium ligand (Figure 4.2).[7]

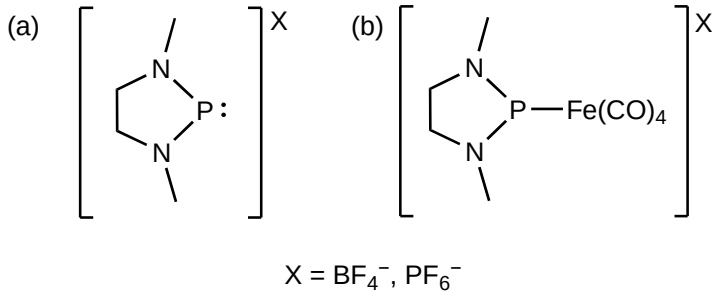

Figure 4.2. First examples of (a) stable phosphenium[5,6] and (b) metal complex with a phosphenium ligand.[7]

4.2.3. Synthesis of Metal-Phosphenium Complexes

There are various methods to synthesize metal-phosphenium complexes (Scheme 4.2).[8] Among them, the most common methods are abstraction of a halide,[9] alkoxide[10] or amide substituent[11] from a coordinated phosphine by Lewis acids[12] (e.g. PF_5, BF_3 or HPF_6). Electrophilic attack (substitution) of a ligand by a phosphenium at a metal centre is also known[7,13] (Scheme 4.2). The first examples of isolated, stable phospheniums (mentioned above) were synthesized through halide abstraction from diaminohalophosphines.

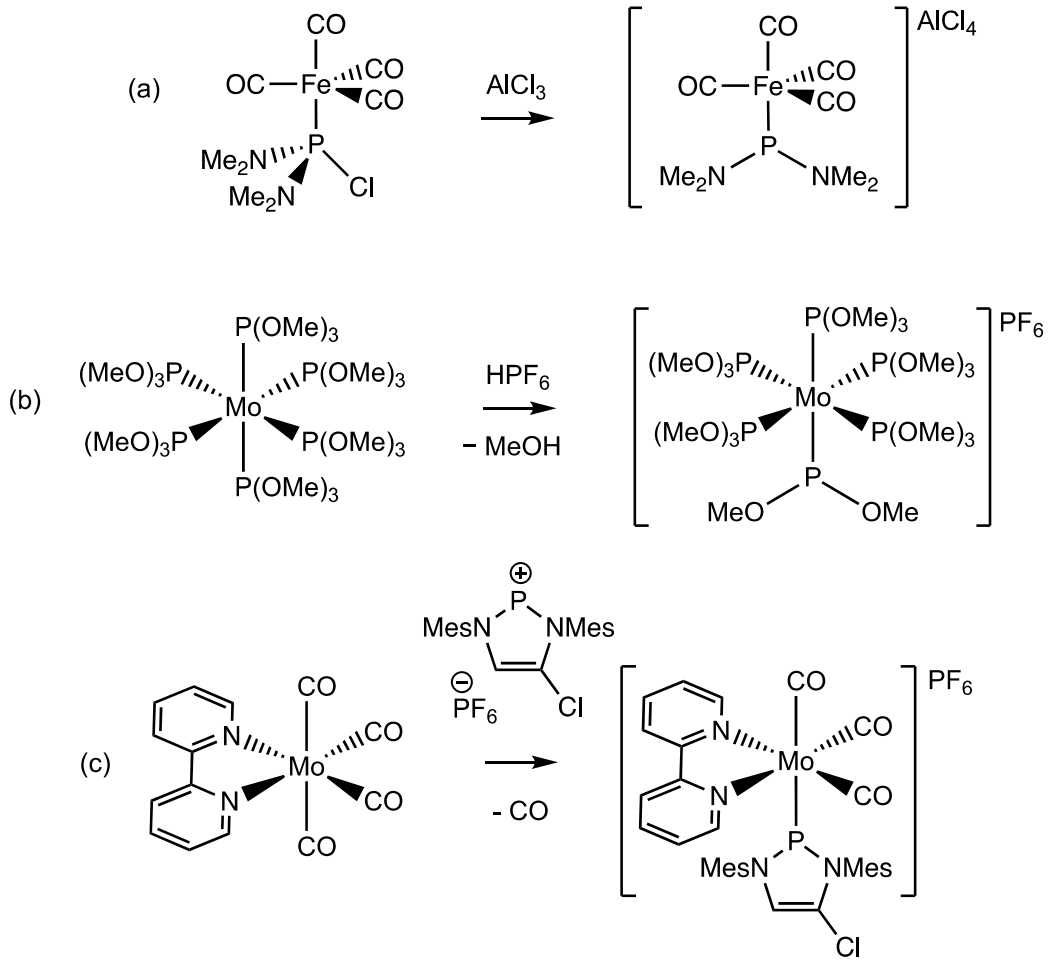

Scheme 4.2. Representative examples of the synthesis of metal complexes bearing phosphenium ligands: (a) halide abstraction,[9] (b) alkoxide abstraction[10] and (c) electrophilic attack.[7,13]

Hydride abstraction of secondary or primary phosphines is an underexplored method of synthesizing phospheniums and metal complexes with phosphenium ligands (Scheme 4.3). The limited examples include hydride abstraction of phosphines that are stabilized by intramolecular coordination of pendant donor groups[14,15,16] (Scheme 4.3).

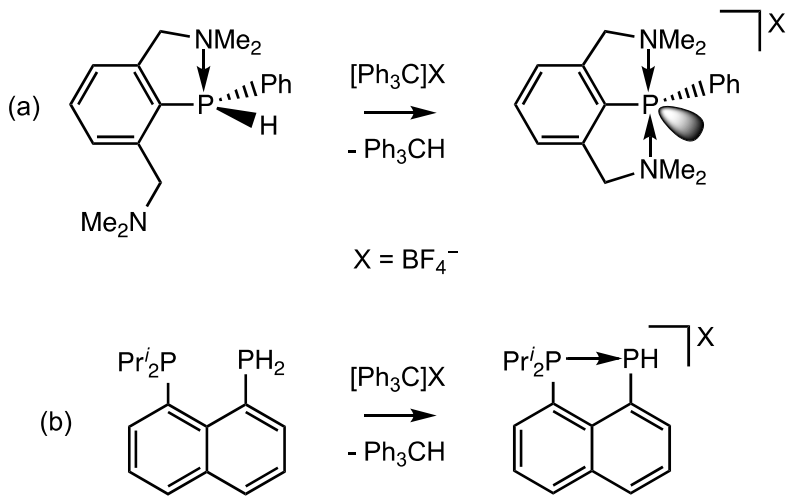

Scheme 4.3. Examples of hydride abstraction of secondary[14,15] and primary phosphines.[16]

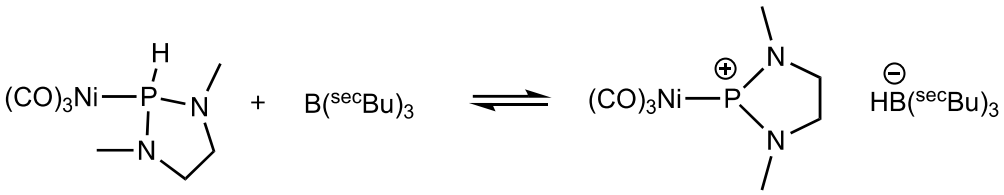

Scheme 4.4. Reversible hydride abstraction of a Ni-bound 1,3-dimethyl-1,3,2-diazaphospholidine by $B(^{sec}Bu)_3$.

One notable example of hydride abstraction from phosphines is the reversible hydride abstraction of a Ni-coordinated 1,3-dimethyl-1,3,2-diazaphospholidine by $B(^{sec}Bu)_3$ reported by Parry *et al.*[17] (Scheme 4.4). The authors attempted to isolate the corresponding phosphenium complex using $[Ph_3C]BF_4$ as a hydride abstraction reagent, but the *in situ* generated phosphenium abstracted a fluoride from the BF_4^- anion.

4.2.4. Reactivity of Phospheniums

Phospheniums are known to behave as electrophiles in reactions with organic substrates. The reactivity of phosphenium moieties with alkenes and alkynes is of particular relevance to hydrophosphination. For example, PR_2^+ species add to 1,3-dienes to give phospholenes,[18,19] as well as to alkynes to give phosphireniums[20,21] (Scheme 4.5). These reactions do not result in hydrophosphination, but exemplify the ability of phosphenium moieties to form P-C bonds with unsaturated substrates.

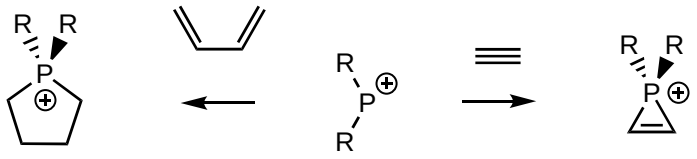

Scheme 4.5. Electrophilic addition of a phosphenium to 1,3-dienes (left) and alkynes (right).

Metal-coordinated phospheniums are also known to act as electrophiles. This is exemplified by the work of Sterenberg *et al* who have shown that phosphenium ligands in W and Fe complexes form P-C bonds with organic substrates through electrophilic C-H bond activation reactions (Scheme 4.6).[22–26] The authors generate phosphenium ligands at metals by chloride abstraction from coordinated chlorophosphines using $AlCl_3$, $GaCl_3$ or AgOTf.

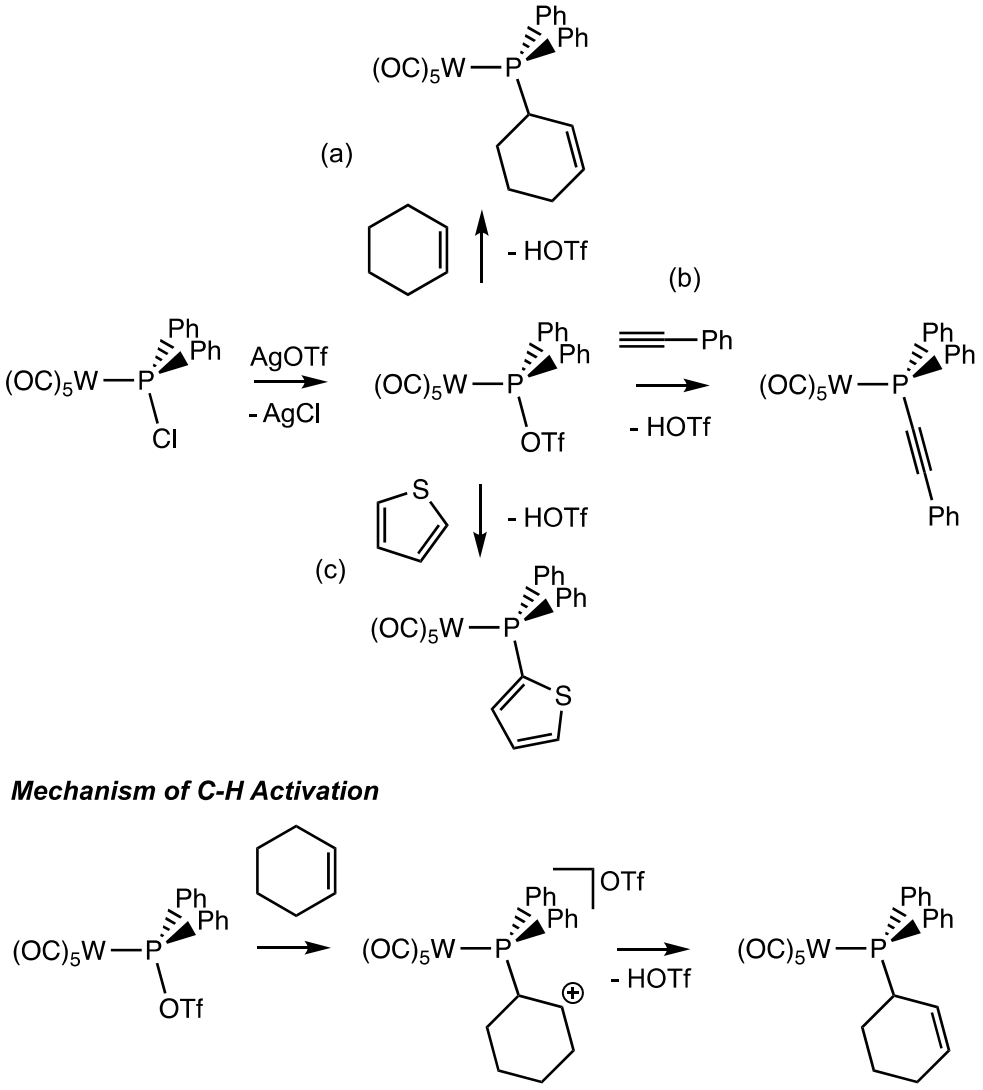

Scheme 4.6. Electrophilic activation of (a) C(sp^3)-H, (b) C(sp^2)-H and (c) C(sp)-H bonds by a tungsten phosphenium complex and the mechanism for C(sp^3)-H (bottom).

4.2.5. Precedent and Proposed Mechanism for Phosphenium Mediated Hydrophosphination

A key aspect of catalytic hydrophosphination is P-H bond activation. As discussed in section 4.2.3, it is possible to generate phosphenium ligands via hydride abstraction from

P-H bonds. Another critical aspect of hydrophosphination is P-C bond formation. As discussed in section 4.2.4. phospheniums can participate in P-C bond formation with unsaturated organic substrates. These reactions of phosphines containing P-H bonds and phospheniums set the precedent for the steps of a putative hydrophosphination mediated by phospheniums, which has not been reported.

Further support for the possibility of a phosphenium-mediated hydrophosphination comes from the work of Gudat,[27] Kinjo[28] and Speed[29,30] who have investigated the reactivity of 1,3,2-diazaphospholenes. They have demonstrated that the P-H bond of 1,3,2-diazaphospholenes can mediate the stoichiometric hydrophosphination of aldehydes, ketones and CO_2 (Scheme 4.7). The regiochemistry of the P-H bond addition of 1,3,2-diazaphospholenes to these carbonyl bonds is consistent with addition of a phosphenium (to the O) and a hydride (to the C). This contrasts the typical reactivity of secondary phosphines with carbonyl containing compounds where nucleophilic attack of the phosphine at the C occurs.[31] Kinjo and Speed have utilized this reactivity of 1,3,2-diazaphospholenes for the catalytic reduction of CO_2, ketones and imines with hydrosilanes and hydroboranes. These examples demonstrate that hydrophosphination via hydride delivery from a P-H bond is a means for the catalytic reduction of organic substrates.

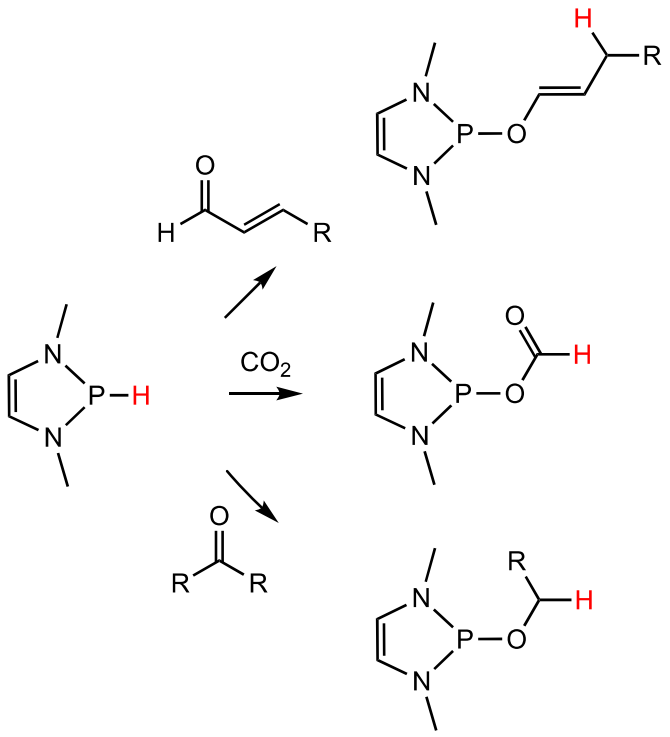

Scheme 4.7. Stoichiometric hydrophosphination of conjugated aldehydes, CO_2 and ketones by 1,3,2-diazaphospholenes.[27,28]

Based on the mechanistic analysis described in Chapter 3 we envisioned an analogous mechanism whereby metal phosphenium complexes (instead of metal phosphido complexes) would participate as intermediates in hydrophosphination (Scheme 4.8). Such a mechanism would require a metal complex that contains both a phosphenium ligand and a secondary phosphine ligand. An unsaturated substrate would undergo nucleophilic addition to the phosphenium ligand (step A), which generates a carbocationic intermediate. Intramolecular hydride transfer from the P-H bond of the coordinated PR_2H would quench the carbocationic intermediate and regenerate a phosphenium ligand at the metal (step B). Substitution of the product phosphine would regenerate the catalyst (step C). This Chapter

describes our efforts to explore the viability of metal phosphenium complexes as intermediates in hydrophosphination and implement this mechanism.

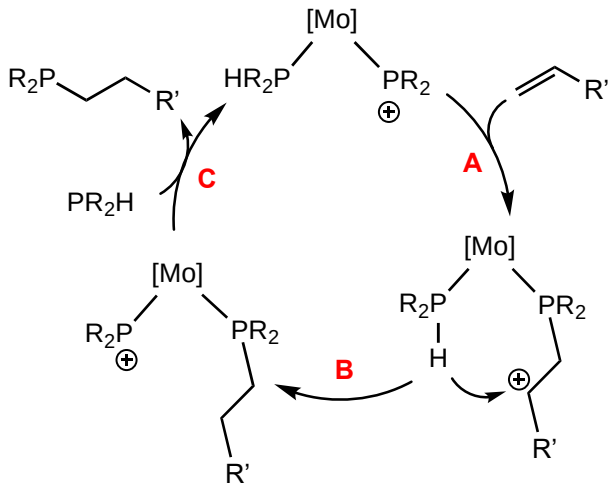

Scheme 4.8. Proposed mechanism for electrophilic hydrophosphination of unsaturated substrates.

4.3. Preparation of $Mo(CO)_4(PR_2H)_2$ and $Mo(CO)_3(PPh_2H)_3$

In this section, the synthesis of complexes *cis*-$Mo(CO)_4(PR_2H)_2$ (*cis*-**10**) and *fac*-$Mo(CO)_3(PPh_2H)_3$ (*fac*-**11**) is described. These complexes are known,[32] but we prepared them from modified literature procedures.[33] Section 4.4 describes the synthesis of *trans*-$[Mo(CO)_4(PTol_2^pH)(PTol_2^p)][B(C_6H_3Cl_2)_4]$ (*trans*-[**12a**][$B(C_6H_3Cl_2)_4$]), *trans*-$[Mo(CO)_4(PR_2H)(PR_2)][B(C_6H_3Cl_2)_4]$ (*trans*-[**12b**][$B(C_6H_3Cl_2)_4$]) and *trans*-$[Mo(CO)_4(PPh_2H)(PPh_2)][B(C_6H_3Cl_2)_4]$ (*trans*-[**13**][$B(C_6H_3Cl_2)_4$]) from *cis*-**10a**, *cis*-**10b** and *fac*-**11**, respectively.

4.3.1. Synthesis of $Mo(CO)_4(PR_2H)_2$

Complexes *cis*-$Mo(CO)_4(PR_2H)_2$ (**10a**, R = Tol^p; **b**, R = Ph; **c**, R = Cy) were prepared from *cis*-$Mo(CO)_4$(piperidine)$_2$ via the addition of two equivalents of a secondary phosphine. Mild heating of this reaction resulted in the formation of *cis*-**10a**,**b**,**c** via the substitution of piperidine by PR_2H (Scheme 4.9). These complexes are known to undergo thermal isomerization to the thermodynamically favoured *trans* complexes,[24] but the mild reaction conditions prevented this isomerization from occurring. Formation of *cis*-**10a-c** was confirmed by ^1H and $^{31}P\{^1H\}$ NMR as well as IR spectroscopy, which agreed with literature values. The synthesis of *cis*-**10a**,**b**,**c** is described in section 4.9.2.

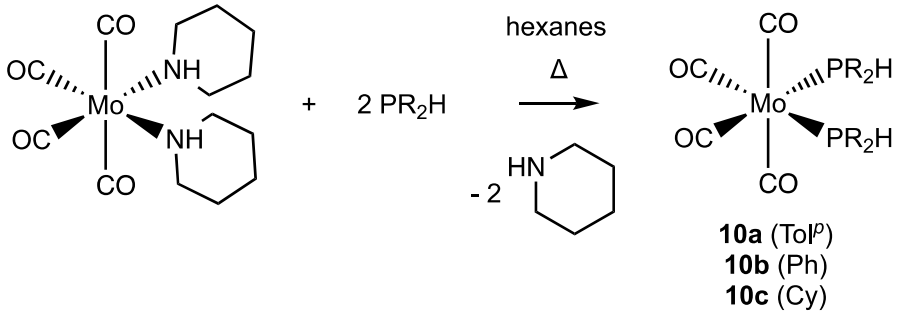

Scheme 4.9. Synthesis of *cis*-$Mo(CO)_4(PTol^p{}_2H)_2$ (**10a**), *cis*-$Mo(CO)_4(PPh_2H)_2$ (**10b**) and *cis*-$Mo(CO)_4(PCy_2H)_2$ (**10c**).

4.3.2. Synthesis of $Mo(CO)_3(PR_2H)_3$

The synthesis of *fac*-$Mo(CO)_3(PPh_2H)_3$ (*fac*-**11**) from *fac*-$Mo(CO)_3(NCMe)_3$ was performed by an undergraduate research student, Carly Slusar. Addition of three equivalents of PPh_2H to *fac*-$Mo(CO)_3(NCMe)_3$ at room temperature in acetonitrile resulted in the substitution of acetonitrile from Mo by PPh_2H to give *fac*-**11** (Scheme 4.10). This

was confirmed by ^{1}H and $^{31}P\{^{1}H\}$ NMR as well as IR spectroscopy, which agreed with literature values. The synthesis of *fac*-**11** is described in section 4.9.3.

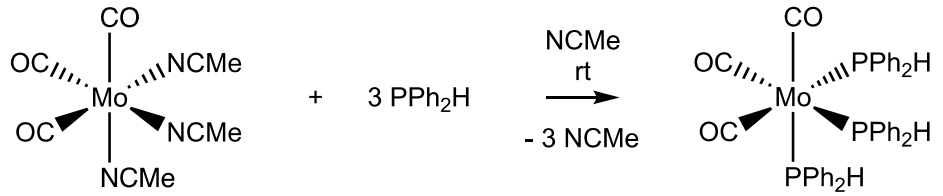

11

Scheme 4.10. Synthesis of *fac*-$Mo(CO)_3(PPh_2H)_3$ (*fac*-**11**).

4.4. Hydride Abstraction from $Mo(CO)_4(PR_2H)_2$ and $Mo(CO)_3(PPh_2H)_3$

In this section, the synthesis of *trans*-$[Mo(CO)_4(PTol_2^pH)(PTol_2^p)][B(C_6H_3Cl_2)_4]$ (*trans*-[**12a**][$B(C_6H_3Cl_2)_4$])), *trans*-$[Mo(CO)_4(PPh_2H)(PPh_2)][B(C_6H_3Cl_2)_4]$ (*trans*-[**12b**][$B(C_6H_3Cl_2)_4$]) and *trans*-$[Mo(CO)_4(PPh_2H)(PPh_2)][B(C_6H_3Cl_2)_4]$ (*trans*-[**13**][$B(C_6H_3Cl_2)_4$]),) via hydride abstraction of coordinated secondary phosphines is described. The characterization of complexes *trans*-[**12a**,**b**][$B(C_6H_3Cl_2)_4$] and *trans*-[**13**][$B(C_6H_3Cl_2)_4$] is described. The X-ray structure and computational analysis of *trans*-**12a** is presented. Experimental details for the synthesis of *trans*-[**12a**,**b**][$B(C_6H_3Cl_2)_4$] and *trans*-[**13**][$B(C_6H_3Cl_2)_4$] are presented in section 4.9.5 and 4.9.6.

4.4.1. Synthesis of *trans*-$[Mo(CO)_4(PR_2H)(PR_2)][B(C_6H_3Cl_2)_4]$ and *trans*-$[Mo(CO)_4(PPh_2H)(PPh_2)][B(C_6H_3Cl_2)_4]$

Compounds *trans*-[**12a**,**b**][$B(C_6H_3Cl_2)_4$] and *trans*-[**13**][$B(C_6H_3Cl_2)_4$] were prepared by addition of one equivalent of the hydride abstracting agent [Ph_3C][$B(C_6H_3Cl_2)$] (orange) to the secondary phosphine complexes *cis*-**10a**,**b** and *fac*-**11** (white to beige) at

room temperature (Scheme 4.11) in dichloromethane, which caused a changed colour to deep green. The reactions were complete within an hour as confirmed by the disappearance of *cis*-**10a**,**b** and *fac*-**11** by $^{31}P\{^{1}H\}$ NMR. The synthesis of *trans*-[**13**][$B(C_6H_3Cl_2)_4$] was performed by undergraduate research student Carly Slusar. Complexes *trans*-[**12a**,**b**][$B(C_6H_3Cl_2)_4$] were crystallized by liquid-liquid diffusion of pentane into a dichloromethane solution of *trans*-[**12a**,**b**][$B(C_6H_3Cl_2)_4$] at room temperature (X-ray diffraction analysis of *trans*-**12a** is discussed below). Complex *trans*-[**13**][$B(C_6H_3Cl_2)_4$] could not be crystallized, but was isolated as a powder.

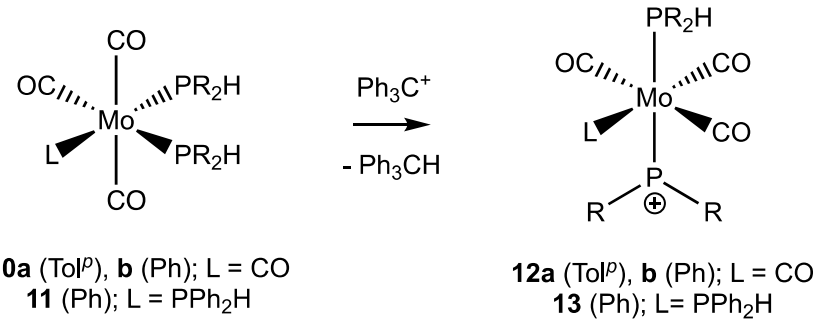

10a (Tol^{p}), **b** (Ph); L = CO
11 (Ph); L = PPh_2H

12a (Tol^{p}), **b** (Ph); L = CO
13 (Ph); L= PPh_2H

Scheme 4.11. Synthesis of complexes *trans*-**12a**,**b** and *trans*-**13**.

No reaction was observed from the addition of [Ph_3C][$B(C_6H_3Cl_2)$] to *cis*-**10c**. This can be rationalized from both steric and electronic arguments. PCy_2H has a larger cone angle (145°) than PPh_2H and $PTol_2^{p}H$ (126°),[34] so for steric reasons, it may be more difficult for hydride abstraction to occur from *cis*-**10c**. The facile hydride abstraction from PPh_2H and $PTol_2^{p}H$, relative to PCy_2H, could result from the resonance stabilization of the resulting phosphenium by the aromatic substituents at P. However, the P-H bond of PCy_2H

could possibly be more hydridic than the P-H bond of PPh_2H and $PTol_2^pH$ because the alkyl substituents at P are more electron-releasing.

4.4.2. Detailed Characterization of [*trans*-$Mo(CO)_4(PR_2H)(PR_2)][B(C_6H_3Cl_2)_4]$ (*trans*-[12a,b][$B(C_6H_3Cl_2)_4$]) and *trans*-$[Mo(CO)_4(PPh_2H)(PPh_2)][B(C_6H_3Cl_2)_4]$ (*trans*-[13][$B(C_6H_3Cl_2)_4$])

The structures of *trans*-**12a**,**b** and *trans*-**13** were characterized by 1D NMR (^1H, $^{31}P\{^1H\}$, ^{31}P, $^{13}C\{^1H\}$ and ^{13}C DEPT 135) and 2D NMR (^1H COSY, $^1H/^{31}P\{^1H\}$-HSQC, $^1H/^{31}P\{^1H\}$-HMBC, $^1H/^{13}C\{^1H\}$-HSQC and $^1H/^{13}C\{^1H\}$-HMBC), IR spectroscopy and elemental analysis. ^1H, $^{31}P\{^1H\}$ and ^{13}C NMR spectra of *trans*-**12a**,**b** and *trans*-**13** are in Appendix E. Crystallographic data for *trans*-[**12a**][$B(C_6H_3Cl_2)_4$] is in Appendix D.

The $^{31}P\{^1H\}$ NMR spectra of complexes **12a**,**b** both show two sets of doublets that are assigned as the *cis*- and *trans*-isomers of **12a**,**b** (Figure 4.3). The downfield peak of each set of doublets (δ: **12a**, 439.1 ppm; **12b**, 440.6 ppm) is assigned as the phosphenium ligand and the upfield peak (δ: **12a**, -7.1 ppm; **12b** -6.2 ppm) is assigned as the coordinated PR_2H. The phosphenium ligand was assigned based on the fact that sp^2-hybridized P nuclei have a diagnostic, huge downfield chemical shift.[35–38] This is true for phosphenium ligands (PR_2^+) and planar, sp^2-hybridized phosphido ligands (PR_2^-). The upfield doublet observed in the $^{31}P\{^1H\}$ NMR for both isomers of **12a**,**b** exhibits a $^1J_{PH}$ coupling (360 Hz) in the ^{31}P NMR spectra, which confirms that these signals are due to the coordinated secondary phosphine. For both complexes **12a**,**b**, the major product is assigned as the *trans* isomer,

based on the large $^{2}J_{PP}$ coupling constants (**12a**, 70 Hz; **12b**, 70 Hz). The $^{2}J_{PP}$ coupling constants for the *cis* isomers of **12a**,**b** are 38 Hz.

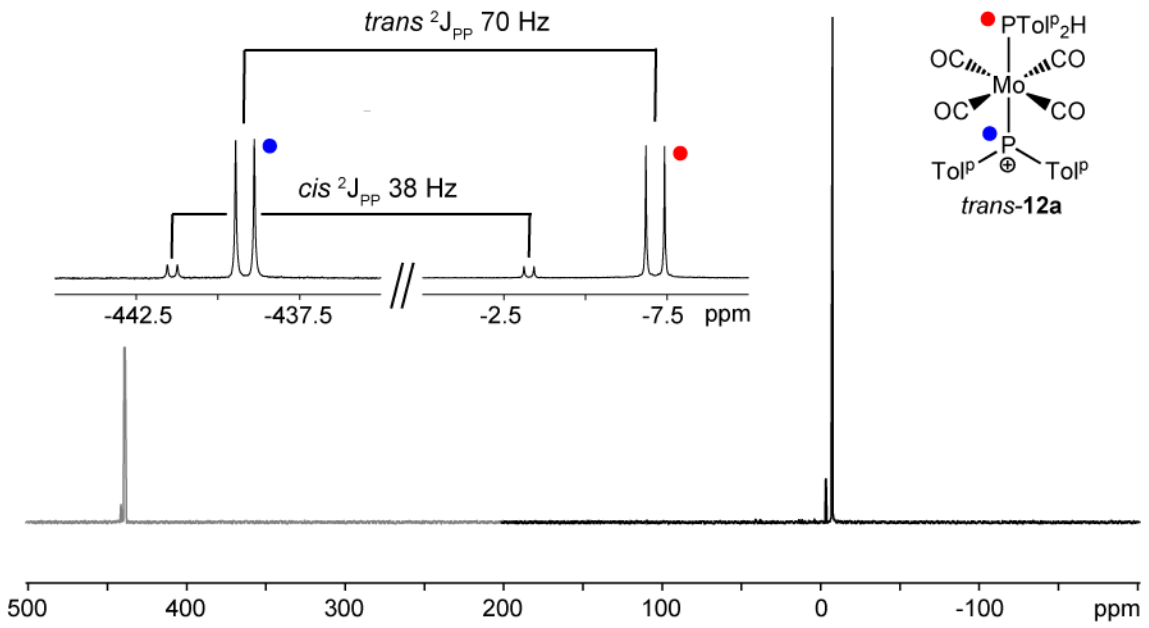

Figure 4.3. $^{31}P\{^{1}H\}$ NMR spectrum (202.51 MHz, CD_2Cl_2) of $[Mo(CO)_4(PTol_2^pH)(PTol_2^p)][B(C_6H_3Cl_2)_4]$ (**12a**$[B(C_6H_3Cl_2)_4]$) showing signals due to the major, *trans*, and minor, *cis*, isomers.

The $^{31}P\{^{1}H\}$ NMR spectrum of complex *trans*-**13** shows three doublet of doublets at 395.4, 6.9 and 3.8 ppm. These doublet of doublets correspond to the phosphenium ligand and two chemically inequivalent PPh_2H ligands, respectively (Figure 4.4). Based on the $^{2}J_{PP}$ coupling constants, one of the coordinated PPh_2H ligands is *cis* to the phosphenium ligand and the other PPh_2H ligand is *trans* to the phosphenium ligand. This accounts for the chemical inequivalence of the two PPh_2H ligands.

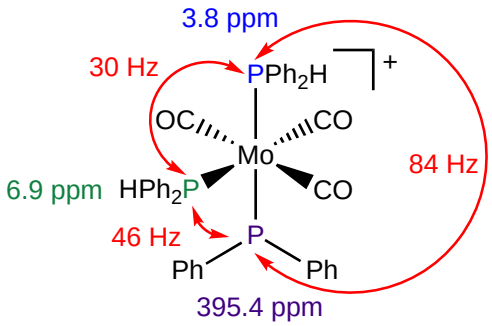

Figure 4.4. Structure of *trans*-**13** labelled with $^{31}P\{^{1}H\}$ NMR chemical shifts and the $^{2}J_{PP}$ coupling constants.

After hydride abstraction of *cis*-**10a**,**b** and *fac*-**11**, **12a**,**b** and **13** undergo an isomerization such that the P-containing ligands are *trans*- and *mer*- respectively (Scheme 4.12). The *trans*- and *mer*- isomers of **12a**,**b** and **13** are likely favoured over the *cis*- and *fac*- isomers because phosphenium ligands are of comparable π-acidity to CO.[39–41] Thus, isomerization occurs such that the strongest π-acid (presumably the phosphenium ligand) is *trans* to the strongest σ-donating ligand (PR_2H). Isomerization of these complexes would require an available vacant coordination site. A proposed mechanism for the isomerization comes from a study on the substitution reactions of tungsten-carbonyl complexes with a trisphosphine ligand.[42] For complexes **12a**,**b** and **13**, this involves a 1,2-shift of the coordinated PR_2H to a CO ligand, isomerization and a subsequent 1,2-shift of PR_2H back to Mo to generate the new isomer (Scheme 4.12). An alternative mechanism that involves dissociation of a PR_2H ligand would also allow isomerization, but is unlikely because free PR_2H would coordinate to the phosphenium ligand if it dissociated from Mo (this will be discussed further in section 4.7.1).

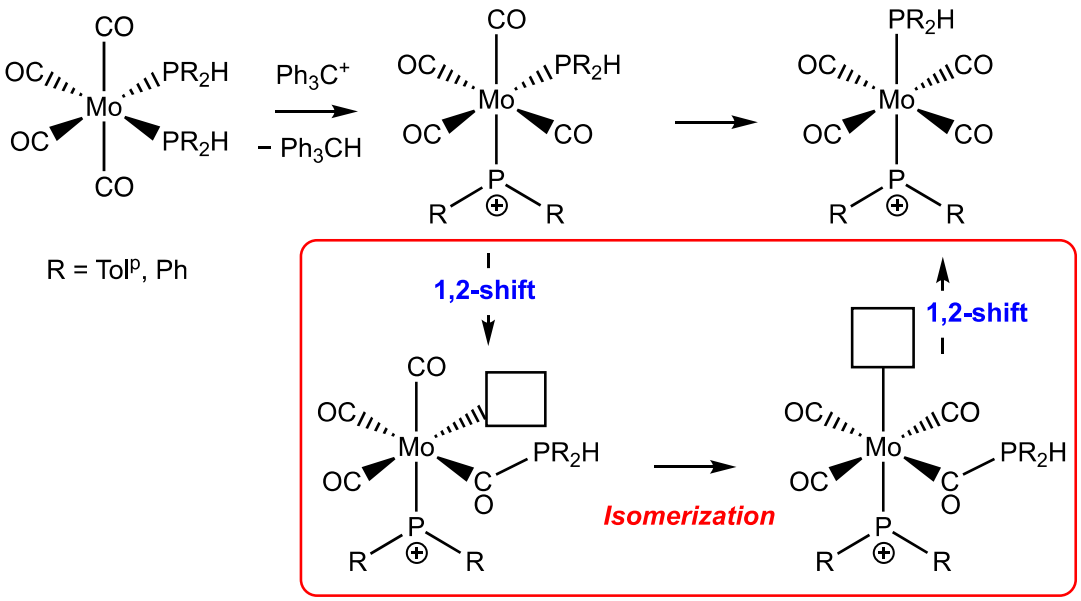

Scheme 4.12. Hydride abstraction from *cis*-**10a,b** and subsequent isomerization from *cis*- to *trans*-**12a,b**.

Single crystals of complex *trans*-**12a**[$B(C_6H_3Cl_2)_4$] were obtained and X-ray diffraction analysis was performed. The resulting molecular structure of *trans*-**12a** is shown in Figure 4.4 and selected interatomic bond distances and bond angles are summarized in Table 4.1. The structure shows the *trans*-isomer of **12a** with an octahedral geometry at Mo. P1 is the phosphorus atom of the coordinated PPh_2H and P2 is the phosphorus atom of the phosphenium ligand. The Mo-P1 bond length, 2.5216(14) Å, is significantly longer than the Mo-P2 bond length, 2.2878(13) Å. The Mo-P2 bond length is consistent with other Mo-P(phosphenium) bond distances. For example, Mo phosphenium complexes reported by Gudat *et al.* have Mo-P bond lengths ranging from 2.2016 – 2.254 Å.[13] The M-P(phosphenium) bond distances are often shorter than the M-P(precursor phosphine) bond lengths,[43] which is attributed to a π-bonding interactions between the metal and phosphenium ligand.[4] The structure of *trans*-**12a** shows that P2 is planar; the

sum of the bond angles around P2 is 360.03°. This is consistent with the diagnostic chemical shift for the phosphenium ligand in the $^{31}P\{^{1}H\}$ NMR, which suggested an sp^2-hybridized P. The short Mo-P2 bond distance and planarity of P2 is also consistent with a π-bonding interaction between Mo and P2.

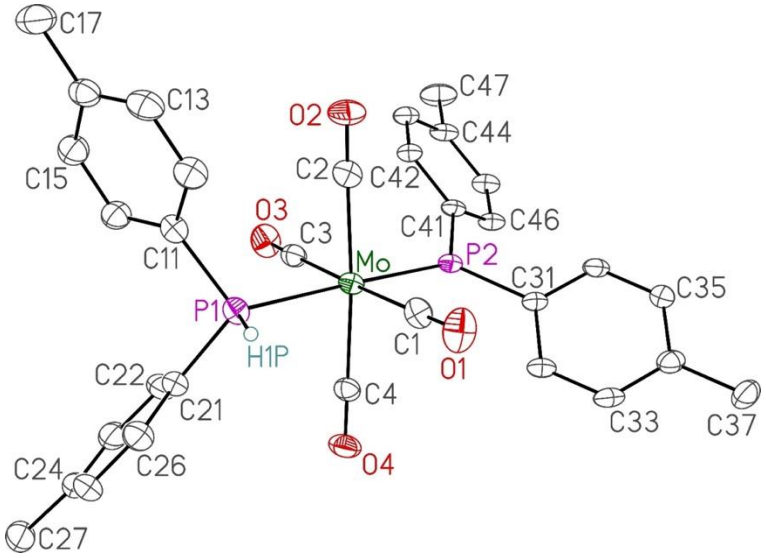

Figure 4.5. Molecular structure of *trans*-$[Mo(CO)_4(PTol_2^pH)(PTol_2^p)]^+$ (*trans*-**12a**). Non-hydrogen atoms are represented by Gaussian ellipsoids at the 30% probability level.

Table 4.1. Selected Interatomic Distances (Å) and Bond Angles (°) for the Molecular Structure of the Cation from *trans*-$[Mo(CO)_4(PTol_2^pH)(PTol_2^p)]^+$ (*trans*-**12a**).

	Å	
Mo-P1	2.5216(14)	
Mo-P2	2.2878(13)	
P1-H1P	1.30(7)	
P1-Mo-P2	177.96(5)	
Mo-P2-C31	125.87(16)	
Mo-P2-C41	125.86(18)	∑ = 360.03°
C31-P2-C41	108.3(2)	

4.4.3. Computational Analysis of *trans*-[Mo(CO)$_4$(PTol$^p{}_2$H)(PTol$^p{}_2$)] (*trans*-12a)

Our collaborator Dr. Dimitrios Pantazis performed the computational analysis of the phosphenium complex *trans*-**12a.** The model was set up using the crystallographic coordinates of *trans*-**12a**. Density functional theory (DFT) was used (density functional B3PW91 with D3BJ dispersion corrections) to perform geometry optimization. The ZORA Hamiltonian was used for inclusion of scalar relativistic effects, with all-electron relativistically recontracted basis sets (ZORA-def2-TZVP(-f) for all atoms except Mo, for which the all-electron "old"-ZORA-TZVP was used). The DFT structure was in good agreement with the crystallographic data for *trans*-**12a**. This method produced Mo-P1 and Mo-P2 bond lengths of 2.518 and 2.285 Å, respectively; these bonds lengths are 2.5216(14) and 2.2878(13) Å, respectively, from the crystallographic data.

Natural Bond Orbital (NBO) analysis produced one σ- and one π-bonding orbital for the Mo−PTol$^p{}_2$ bond in *trans*-**12a** (Figure 4.5). The σ-bonding orbital is polarized towards the phosphenium P (66%) and the π-bonding orbital is polarized towards the Mo (64%). This is consistent with the generally observed coordination mode of phosphenium ligands on metals.[44]

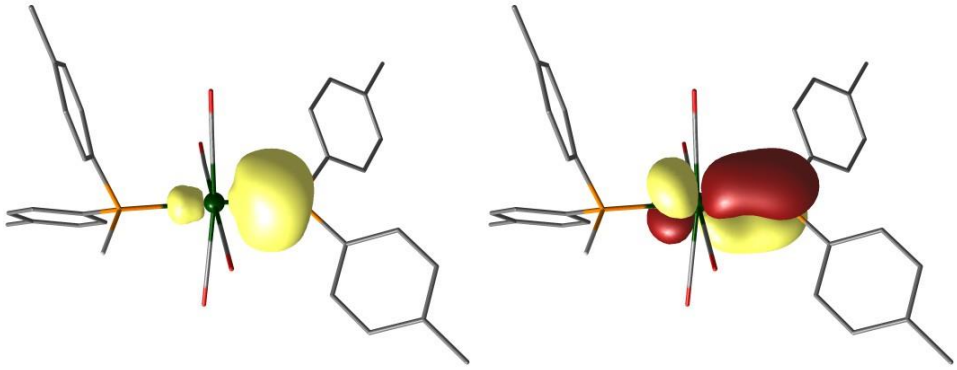

Figure 4.6. The σ- and π-bonding orbitals for the Mo-P(phosphenium) bond in *trans*-**12a** produced from NBO analysis.

Table 4.2. Mayer and Wiberg Bond Order Metrics for Mo-P Bonds in *trans*-**12a**.

	Mayer	**Wiberg**
Mo-PR_2^+	1.31	1.02
Mo-PR_2H	0.76	0.43

The results from two computationally-derived bond order metrics were also consistent with double bond character in the Mo−PTol$^p_2$ bond in *trans*-**12a**; data is summarized in Table 4.2. The Wiberg bond index was obtained from the NBO analysis. This gave values of 1.02 for the Mo−PTol$^p_2$ bond and 0.43 for the Mo−PTol$^p_2$H bond. The computed Mayer bond orders gave values of 1.31 for the Mo−PTol$^p_2$ bond and 0.76 for the Mo−PTol$^p_2$H bond. In both cases, the Mo−PTol$^p_2$ bond order is larger than the bond order for the Mo−PTol$^p_2$H bond. Since we are confident that the Mo−PTol$^p_2$H bond is a single bond, we can confidently say that the Mo−PTol$^p_2$ bond is a double bond. These results complement the X-ray and $^{31}P\{^1H\}$ NMR data, which are consistent with a double bond between Mo and the phosphenium ligand.

The lowest unoccupied molecular orbital (LUMO) of *trans*-**12a** is a π*-orbital of the Mo-P(phosphenium) bond (Figure 4.6). This orbital is delocalized, but has a major contribution from the P of the phosphenium ligand. This is consistent with the known electrophilicity of phosphenium ligands.[45] In section 4.5, reactions that demonstrate the electrophilicity of the phosphenium ligands in complexes **12a**,**b** and **13** are discussed.

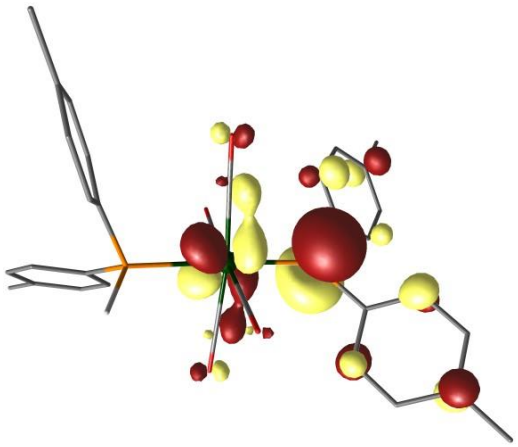

Figure 4.7. The LUMO of *trans*-**12a**.

4.4.4. Attempted Hydride Abstraction with $B(C_6F_5)_3$

Complexes *trans*-**12a**,**b** and *trans*-**13** were prepared via hydride abstraction from coordinated secondary phosphines using $[Ph_3C]^+$. The trityl cation is a very strong hydride-abstracting reagent that irreversibly abstracts hydrides from molecules. For the purpose of exploiting phospheniums in hydrophosphination catalysis, we wanted to identify a weaker Lewis acid than the trityl cation that could perform the hydride abstraction of complexes *cis*-**10a**,**b** and *fac*-**11** reversibly. A candidate was $B(C_6F_5)_3$ because it is a strong Lewis acid that has been employed in many types of catalysis, including dehydrocoupling of primary and secondary phosphines, which involves reversible P-H bond activation via hydride

abstraction.[46] Moreover, $[HB(C_6F_5)_3]^-$ is a much stronger hydride donor than Ph_3CH, which bodes well for using $B(C_6F_5)_3$ as a hydride shuttle.[47]

No reaction occured upon addition of $B(C_6F_5)_3$ to *cis*-**10a** at room temperature as determined by $^{31}P\{^1H\}$ NMR (Scheme 4.13). When the reaction was heated at 60°C, *cis*-**10a** decreased in concentration and two new species formed (singlet at 6.5 ppm and a broad peak at 0.2 ppm in the $^{31}P\{^1H\}$ NMR spectrum). The singlet at 6.5 ppm is tentatively assigned as $Mo(CO)_4(PTol^p{}_2H)$. The broad peak at 0.2 ppm has previously been attributed to the $PTol_2{}^pH$ adduct of $B(C_6F_5)_3$.[48,49] Heating this reaction likely results in dissociation of $PTol_2{}^pH$ from *cis*-**10a**. The uncoordinated $PTol_2{}^pH$ forms an adduct with $B(C_6F_5)_3$. No hydride abstraction is observed presumably because $B(C_6F_5)_3$ is not a strong enough Lewis acid to remove a hydride from the coordinated secondary phosphines in *cis*-**10a**. The $^{31}P\{^1H\}$ NMR spectrum of this reaction is in Appendix H.

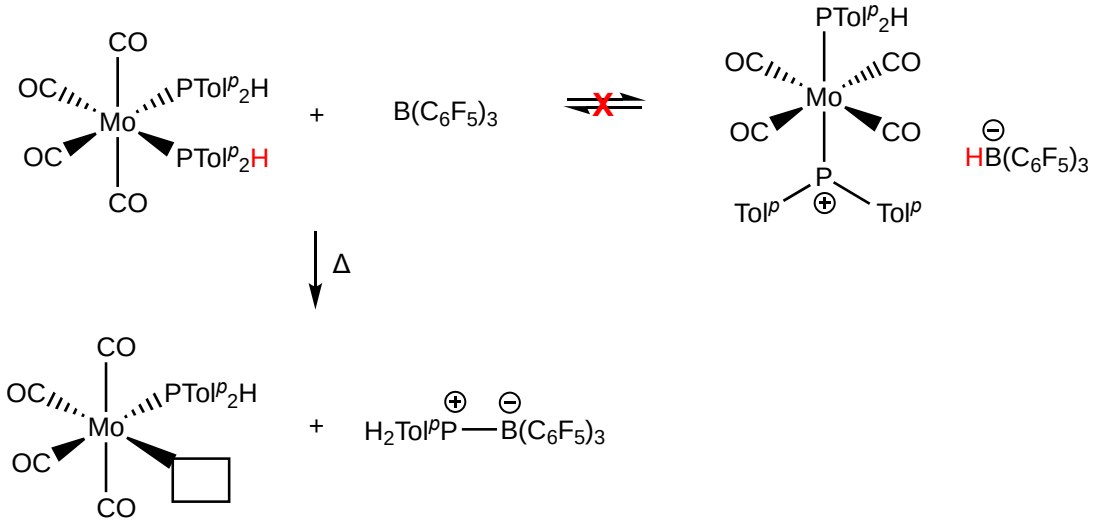

Scheme 4.13. Addition of $B(C_6F_5)_3$ to *cis*-**10a**, which results in $PTol^p{}_2H$ dissociation and adduct formation with $B(C_6F_5)_3$.

4.5. Investigation of the Electrophilicity of the PR_2 Ligands in *trans*-12a,b and *trans*-13

In this section the electrophilicity of phosphenium ligands in metal complexes is discussed, and the electrophilicity of the phosphenium ligands in complexes *trans*-**12a,b** and *trans*-**13** is demonstrated through reactions with $[NBu_4]PF_6$ and MeOH.

4.5.1. Is the PR_2 Ligand in *trans*-12a,b and *trans*-13 an Electrophilic Phosphenium?

Complexes *trans*-**12a,b** and *trans*-**13** were prepared by formally removing a hydride from *cis*-**10a**,**b** and *fac*-**11**, but we wanted to ensure that the PR_2 ligand in these complexes was in fact an electrophilic phosphenium ligand, not a nucleophilic phosphido ligand (Scheme 4.14). The reason for this is that the phosphenium ligand in an M-PR_2 fragment can potentially be reduced to a phosphido ligand by the metal. This can occur if the metal can undergo a two-electron oxidation. This reactivity is highlighted by the work of Thomas *et al.* whom have synthesized various metal complexes bearing an N-heterocyclic phosphenium (NHP^+) ligand. For example, complexes of Pd and Pt bearing an NHP^+ ligand undergo a two-electron redox reaction where oxidation of M^0 to M^{2+} is accompanied by reduction of the NHP^+ ligand to an N-heterocyclic phosphido (NHP^-) ligand; this was confirmed by the observed nucleophilicity of the P-nucleus in the NHP ligand.[50,51] In another example, a Cu(I) complex bearing the same NHP^+ ligand exhibited electrophilic reactivity at the P-nucleus in the NHP ligand, which suggested that the NHP^+ was not reduced by the metal; Cu(I) is less likely to undergo a 2-electron oxidation.[52]

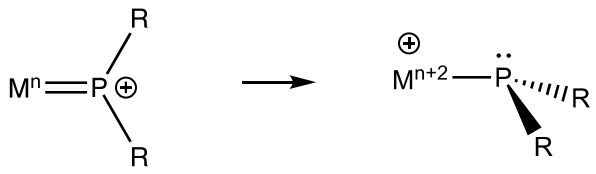

Scheme 4.14. A two-electron redox reaction of a metal-phosphenium complex that results in an oxidized metal with a phosphido ligand.

Sections 4.5.2 and 4.5.3 describe reactivity studies that confirm that the PR_2 ligand in complexes *trans*-**12a,b** and *trans*-**13** are in fact electrophilic phosphenium ligands.

4.5.2. Reaction of *trans*-12a,b with $[NBu_4]PF_6$

Addition of $[NBu_4]PF_6$ to complexes *trans*-**12a,b** results in fluoride abstraction from the PF_6^- of $[NBu_4]PF_6$ by the PR_2 ligand. This confirms that the PR_2 ligands of *trans*-**12a,b** are electrophilic and therefore phosphenium, not phosphido, ligands (Scheme 4.15). During this reaction, the solutions change colour from dark green to brown and a gas evolves from solution, which is presumably PF_5. The $^{31}P\{^1H\}$ NMR spectra from these reactions show two doublets of doublets. The downfield doublet of doublets (δ: R = Tol^p, 205.2 ppm; R = Ph, 201.5 ppm) corresponds to the PR_2F ligand because it exhibits a diagnostic $^1J_{PF}$ coupling constant (R = Tol^p, 861 Hz; R = Ph, 865 Hz). The other doublet of doublets (δ: R = Tol^p, 17.4 ppm; R = Ph, 16.3 ppm) corresponds to the coordinated PR_2H because it shows a $^1J_{PH}$ coupling in the ^{31}P NMR. The upfield doublet of doublets shows a small $^3J_{PF}$ coupling in the $^{31}P\{^1H\}$ NMR. These signals show a $^2J_{PP}$ coupling constant of 70 – 72 Hz, which suggests that the phosphines are *trans* in the resulting complex. $^{31}P\{^1H\}$ NMR spectra are shown in Appendix H.

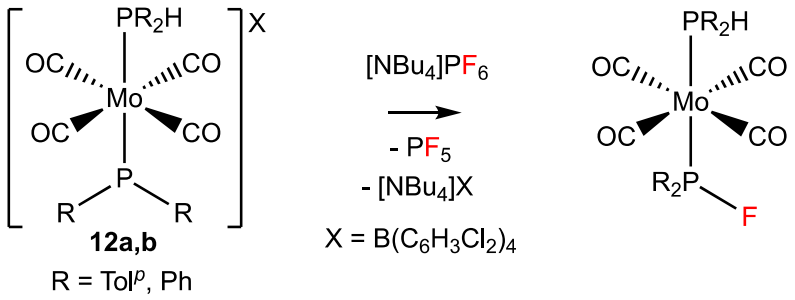

Scheme 4.15. Reaction of $[NBu_4]PF_6$ with *trans*-**12a,b**$[B(C_6H_3Cl_2)_4]$ resulting in fluoride abstraction from PF_6^- by the phosphenium ligands of *trans*-**12a,b**$[B(C_6H_3Cl_2)_4]$.

4.5.3. Reaction of *trans*-12a,b with MeOH

To confirm that the PR_2 ligands in *trans*-**12a** and *trans*-**13** were electrophilic phosphenium ligands, I wanted to compare the reactivity of these complexes with the known reactivity of our group's Ru phosphido complexes. One reaction is the addition of MeOH to the Ru phosphido complexes **5**, which results in the formation of a Ru hydride complexes; this results from deprotonation of MeOH by the phosphido ligand in complex **5**.[53]

Addition of MeOH to complexes *trans*-**12a,b** results in coordination of MeOH to the phosphenium ligand (Scheme 4.16). This is consistent with a phosphenium ligand because many examples of donor stabilized phospheniums are known.[54–56] Upon addition of MeOH to *trans*-**12a,b**, the solutions change colour from dark green to brown. The $^{31}P\{^1H\}$ NMR spectrum shows two doublets. The downfield doublet (δ: R = Tol^p, 148.1 ppm; R = Ph, 147.7 ppm) corresponds to the MeOH-coordinated phosphenium ligand. The upfield doublet (δ: R = Tol^p, 17.2 ppm; R = Ph, 14.9 ppm) corresponds to the coordinated PR_2H ligand. Thus, the different reactivity of *trans*-**12a,b** with MeOH compared to **5** suggests

that the PR_2 ligand in *trans*-**12a,b** is an electrophilic phosphenium. $^{31}P\{^1H\}$ NMR spectra are shown in Appendix H.

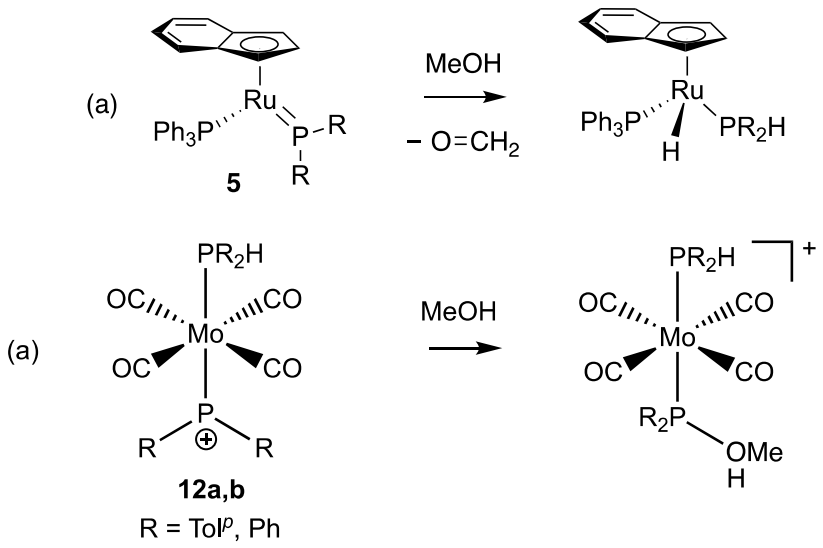

Scheme 4.16. Addition of MeOH to (a) Ru phosphido complex **5** and (b) *trans*-**12a,b**.

4.6. Addition of Unsaturated Substrates to 12a,b and 13

The results presented in section 4.4.1 established that heterolytic P-H bond activation of metal-bound secondary phosphines *via* hydride abstraction is possible. In this section, the other steps of a putative hydrophosphination cycle mediated by metal phosphenium complexes (P-C and C-H bond formation, step A and B, respectively, in Scheme 4.8) are established. The reactions of compounds *trans*-**12a,b** and *trans*-**13** with unsaturated substrates is described and demonstrate that these complexes can mediate the stoichiometric hydrophosphination of alkenes and ketones.

4.6.1. Addition of Alkenes and Ketones to *trans*-12a,b

A variety of unsaturated substrates were added to *trans*-**12a,b** in order to investigate if hydrophosphination would occur. Reactions of *trans*-**12a,b** with styrene, 1-hexene, acetophenone, cyclohexenone, cyclohexanone, or 4-phenyl-3-buten-2-one resulted in complex product mixtures, which were difficult to characterize. This presumably resulted from deleterious reactions of reactive intermediates that form via the addition of these substrates to the phosphenium ligand (*vide infra*). The discussion in this section will focus on the reactivity of *trans*-**12a,b** with 1,1-diphenylethylene and benzophenone, which afforded a single product.

Addition of 1,1-diphenylethylene to *trans*-**12a,b** in CD_2Cl_2 results in complexes containing the coordinated hydrophosphination product, *trans*-$[Mo(CO)_4(PR_2CHCHPh_2)(PR_2)]^+$ (*trans*-**14a,b**) (Scheme 4.17). The reactions had gone to completion within the time I could collect NMR spectra (~20 mins). The $^{31}P\{^1H\}$ NMR spectrum of this reaction using *trans*-**12a** shows a doublet at 18.6 ppm that corresponds to the coordinated hydrophosphination product, $Tol^p{}_2PCH_2CHPh_2$, and a doublet at 434.5 ppm, which is the new phosphenium ligand. No $^1J_{PH}$ coupling is observed in the ^{31}P NMR spectrum of this reaction mixture, which confirms that no P-H bond remains in the product complex. The ^1H NMR shows two resonances corresponding to the methylene and methine protons of the coordinated hydrophosphination product. Complexes **14a**,**b** are assigned as the *trans*-isomers based on the large $^2J_{PP}$ coupling constants (72 Hz).

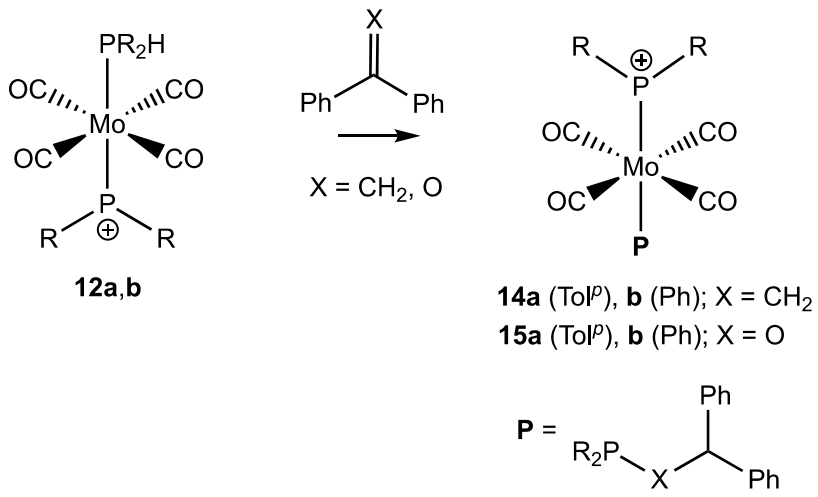

Scheme 4.17. Stoichiometric hydrophosphination of 1,1-diphenylethylene and benzophenone by complexes **12a,b**.

Similar to 1,1-diphenylethylene, addition of benzophenone to *trans*-**12a,b**results in the complexes containing the coordinated hydrophosphination product, *trans*-$[Mo(CO)_4(PR_2OCHPh_2)(PR_2)]^+$ (*trans*-**15a,b**) (Scheme 4.17). The reactions had gone to completion within the time I could collect NMR spectra (~20 mins). The $^{31}P\{^1H\}$ NMR spectrum of this reaction with *trans*-**12a,b** shows a doublet at 132.8 ppm corresponding to the coordinated hydrophosphination product $Tol^p{}_2POCHPh_2$ and a doublet at 440.3 ppm, which is the new phosphenium ligand. No $^1J_{PH}$ coupling is observed in the ^{31}P NMR spectrum, which confirms that no P-H bond remains in the product. The regiochemistry of the hydrophosphination of benzophenone (P-O and C-H bond formation) is consistent with the electrophilic nature of the phosphenium. Complexes **15a**,**b** are assigned as the *trans*-isomers based on the large $^2J_{PP}$ coupling constants (89 Hz).

The well-behaved reactions of 1,1-diphenylethylene and benzophenone with **12a**,**b** relative to the other substrates tested can be attributed to the relative stability of the proposed carbocationic intermediate formed. A proposed mechanism for this hydrophosphination involves nucleophilic addition of the alkene or ketone to the phosphenium ligand, which would generate a carbocation. The resulting carbocation from addition of 1,1-diphenylethylene or benzophenone to the phosphenium should be very stable due to resonance stabilization with the aromatic substituents. A less stable carbocation could possibly undergo deleterious reactions.

4.6.2. Addition of phenylacetylene to *trans*-12a,b and *trans*-13

Addition of phenylacetylene to complexes *trans*-**12a,b** and *trans*-**13** results in addition of phenylacetylene to the phosphenium ligand (Scheme 4.18, complexes **16a**,**b** and **17**). I was unable to obtain X-ray quality crystals of **16a**,**b**[$B(C_6H_3Cl_2)_4$] or **17**[$B(C_6H_3Cl_2)_4$], but the structure of these compounds was determined using 1D NMR (^1H, $^{31}P\{^1H\}$, ^{31}P, $^{13}C\{^1H\}$ and ^{13}C DEPT 135) and 2D NMR (^1H COSY, $^1H/^{31}P\{^1H\}$-HSQC, $^1H/^{31}P\{^1H\}$-HMBC, $^1H/^{13}C\{^1H\}$-HSQC and $^1H/^{13}C\{^1H\}$-HMBC). The full NMR characterization of **16b** is presented here.

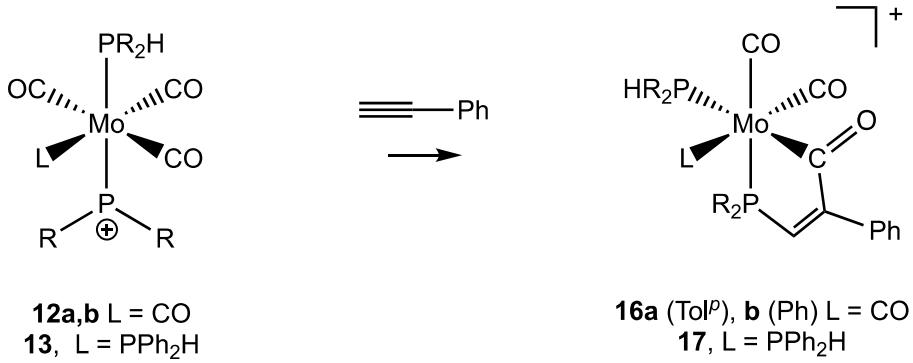

12a,b L = CO
13, L = PPh_2H

16a (Tol^p), **b** (Ph) L = CO
17, L = PPh_2H

Scheme 4.18. Reactions of phenylacetylene with complexes **12a,b** and **13**.

In the $^{31}P\{^{1}H\}$ NMR of complex **16b** a set of doublets is observed at 73.0 and −1.9 ppm. The downfield resonance for **16b** is assigned as the former phosphenium ligand that has formed a P-C bond with phenylacetylene (P, Figure 4.7). The other resonance is assigned as the coordinated PPh_2H ligand (P) because it has a $^{1}J_{PH}$ coupling in the ^{31}P NMR spectrum. The $^{2}J_{PP}$ coupling constant (24 Hz) indicates that the P-containing ligands in **16b** are *cis*.

A doublet is observed at 9.24 ppm in the ^{1}H NMR spectrum of complex **16b**. This downfield H resonance is assigned as the former terminal H of phenylacetylene (H, Figure 4.7). This H resonance shows a two-bond correlation to P in the $^{1}H/^{31}P\{^{1}H\}$-HMBC, which confirms that P-C bond formation occurred between the terminal C of phenylacetylene and the phosphenium P of **12b**. After addition of phenylacetylene to the phosphenium ligand the terminal H of phenylacetylene would be two bonds from P, which accounts for the observed $^{2}J_{PH}$ coupling of 11 Hz. The chemical shift of H is not typical for an olefinic H, but could result from the charge or ring current in this unusual structure.

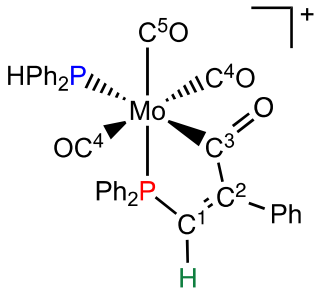

Figure 4.8. Proposed structure of **16b** showing atom labels.

The two alkynyl carbons of phenylacetylene now have chemical shifts characteristic of alkenyl carbons in **16b**, which supports that addition of phenylacetylene to the phosphenium ligand occurred. The H shows a one-bond correlation to a ^{13}C signal at 164.4 ppm in the $^{1}H/^{13}C\{^{1}H\}$-HSQC of **16b**, which is assigned as the terminal C of phenylacetylene that was involved in P-C bond formation with the phosphenium of **12b** (C_1 in Figure 4.7). The H shows a two-bond correlation to a ^{13}C signal at 153.6 ppm in the $^{1}H/^{13}C\{^{1}H\}$-HMBC of **16b**, which corresponds to what was the internal alkynyl carbon of phenylacetylene (C_2 in Figure 4.7). Furthermore, C^1 and C^2 are doublets, in the $^{13}C\{^{1}H\}$ and ^{13}C DEPT 135 NMR spectra of **16b**, due to coupling with P ($^{1}J_{PC}$ 47 Hz for C_1 and $^{2}J_{PC}$ 25 Hz for C_2), which are consistent with expected values.

There are three carbonyl resonances at 266.4 ($^{2}J_{PC}$ 19, 2 Hz), 218.8 ($^{2}J_{PC}$ 26, 11 Hz) and 202.8 ppm ($^{2}J_{PC}$ 9, 7 Hz) in the $^{13}C\{^{1}H\}$ NMR spectrum of **16b**. These all have two $^{2}J_{PC}$ couplings because of the two chemically inequivalent P nuclei in the complex. Observation of only three chemically inequivalent carbonyl Cs supports that **16b** is symmetrical as shown in Figure 4.7 (plane of symmetry defined by C^3, C^5, P, P). One of the carbonyl resonances has an unusual chemical shift at 266.4 ppm, which is very different from the chemical shift of the other two carbonyl ligands, 202.8 and 218.8 ppm; in general this resonance is outside the typical region where CO ligands appear in $^{13}C\{^{1}H\}$ NMR. This resonance is assigned as C^3 in Figure 4.7. The H shows a three-bond correlation to the ^{13}C signal at 266.4 ppm in the $^{1}H/^{13}C\{^{1}H\}$-HMBC. There is not a correlation to the other carbonyls, which is consistent with that fact that these are 4 bonds apart in the proposed structure. Observing a correlation between H and C^3 suggests that these are fewer than 4

bonds apart. Based on this result it is proposed that a C-C bond has also been formed. The resonances at 202.8 and 218.8 ppm are assigned as C^4 and C^5, respectively, based on peak intensity.

A possible mechanism for the addition of phenylacetylene to *trans*-**12a**,**b** is shown in Scheme 4.19. After nucleophilic addition of phenylacetylene to the phosphenium ligand, the generated carbocation undergoes subsequent reactivity with one of the CO ligands to form a C-C bond. This would account for the observed correlation in the $^1H/^{13}C\{^1H\}$-HMBC between H and C_3 because it would be a 3-bond correlation. I could not find any literature precedent for this proposed mechanism.

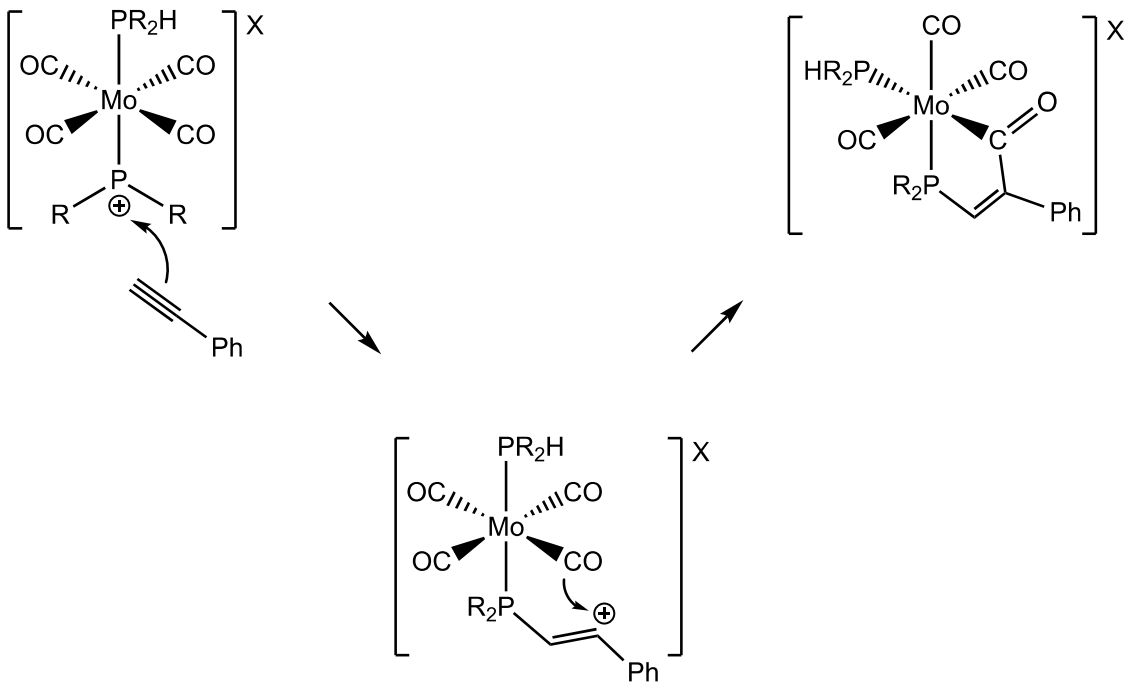

Scheme 4.19. Proposed mechanism for addition of phenylacetylene to *trans*-**12a,b**.

The spectroscopic features of complex **16a** is very similar to those described above for complex **16b**. Complex **17** also has similar spectroscopic features, but differs because **17** has two PPh_2H ligands. In the $^{31}P\{^1H\}$ NMR spectrum of **17** there are three doublet of doublets that result from the presence of two chemically inequivalent PPh_2H ligands.

4.6.3. Addition of Alkenes and Ketones to 13

Addition of excess 1,1-diphenylethylene or benzophenone to *trans*-**13** results in complexes containing two coordinated hydrophosphination product ligands, $[Mo(CO)_3(PPh_2XCHPh_2)_2(PPh_2)]^+$ (**18a** X = CH_2; **18b** X = O) (Scheme 4.20). These reactions, in $CDCl_3$, were monitored by $^{31}P\{^1H\}$ NMR. Initial formation of two isomers of a complex bearing one coordinated hydrophosphination product, one PPh_2H and a phosphenium ligand is observed in these reactions. These intermediates form from an initial hydrophosphination of unsaturated substrate by **13**. A subsequent hydrophosphination of unsaturated substrate is mediated by these intermediates because the additional coordinated PPh_2H is a hydride source, which generates **18a**,**b**. The $^{31}P\{^1H\}$ NMR spectrum of $[Mo(CO)_3(PPh_2CH_2CHPh_2)_2(PPh_2)]^+$ (**18a**) shows an upfield doublet (33.8 ppm, $^2J_{PP}$ 43 Hz) assigned as the two coordinated hydrophosphination products, and a downfield triplet for the phosphenium ligand (380.8 ppm, $^2J_{PP}$ 43 Hz). In these complexes the two product phosphine ligands are both *cis* to the phosphenium ligand (the magnitude of the $^2J_{PP}$ coupling constants observed for **18a**,**b** are consistent with a *cis*-orientation of the P-based ligands). This contrasts the usual preference for the phosphenium ligand to be *trans* to a phosphine ligand, as described above for *trans*-**12a**,**b** and *trans*-**13**. This is

attributed to steric congestion at Mo that disfavours a *cis* orientation of the two bulky hydrophosphination product phosphines.

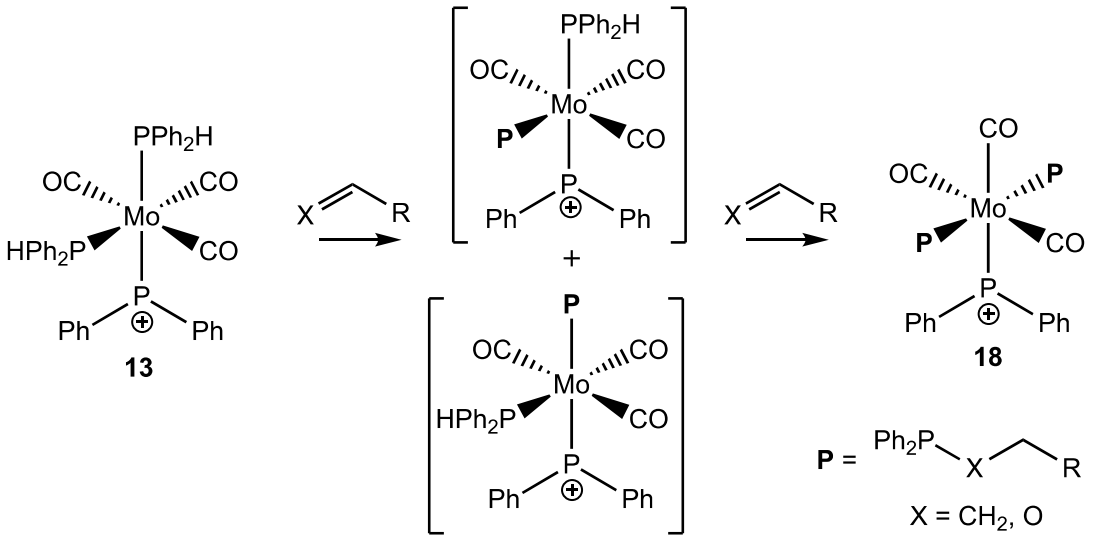

Scheme 4.20. Stoichiometric hydrophosphination of alkenes and ketones mediated by *trans*-**13**.

Complex *trans*-**13** mediates the hydrophosphination of a wide substrate scope. This includes styrene (**18c**), indene (**18d**) and even the simple alkenes like ethylene (**18e**), propene (**18f**), 1-hexene (**18g**) and cyclopentene (**18h**), which are extremely challenging substrates for metal catalyzed hydrophosphination.[1] The ^{1}H, $^{31}P\{^{1}H\}$ and $^{13}C\{^{1}H\}$ NMR assignments of **18a-h** is presented in Table 4.8 and 4.9 in section 4.9.8. Minor amounts of other isomers of **18** are observed in all of these reactions. No reaction is observed upon addition of *trans*-stilbene, cyclohexene or *cis*-butene to **13**. This suggests that internal alkenes bulkier than cyclopentene cannot participate in addition to the phosphenium ligand. Addition of ethyl vinyl ether, an electron-rich alkene, to complex **13** results in a viscous

solution within 5 mins, which suggests that the alkene was polymerized. Cationic polymerization of ethyl vinyl ether is known.[57]

The reactions of *trans*-**13** with styrene and indene are complete within 8 h, whereas the reactions with 1-hexene and cyclopentene are slow and go to completion over 1 week. The increased rate of the reactions with styrene and indene may be attributed to the relatively stable carbocation intermediates that would form from addition of these substrates to the phosphenium ligand of **13**. The reaction with 1,1-diphenylethylene goes to completion with 24 h, which is slower than the reaction with styrene, possibly due to steric reasons. Hydrophosphination of benzophenone is complete within an hour. This fast reaction is attributed to that fact that C=O bonds are better nucleophiles than C=C bonds. The reactions of ethylene and propene were complete within 24 h, which is much faster than the reactions with 1-hexene and cyclopentene, but may be attributed to the large excess of ethylene and propene added to the reactions.

The increased scope of alkenes for hydrophosphination mediated by **13** relative to **12a**,**b** may be attributed to the increased hydricity of the P-H bonds in **13**. Relative to **12a**,**b**, complex **13** has one less CO ligand and one more PPh_2H ligand, which makes Mo more electron-rich, and in turn makes the P-H bonds of the coordinated phosphines in **13** more hydridic than those in **12a**,**b**. Thus, hydride transfer from coordinated PPh_2H to the carbocation intermediates that result from addition of alkenes to the phosphenium ligand in **13** is fast. In the corresponding reactions with **12a**,**b**, hydride transfer is slower allowing for the carbocationic intermediates to undergo deleterious reactions with the CO ligands

(described in section 4.6.1. and 4.6.2. with phenylacetylene). It is worth reiterating that the rate of the addition of alkenes to the phosphenium ligands in **12a**,**b** is faster than for **13**. A more electron-rich Mo would make the phosphenium ligand of **13** less electrophilic, which is consistent with the overall slower hydrophosphination mediated by **13** than by **12a**,**b**.

4.6.4. Mechanism of Phosphenium-Mediated Hydrophosphination

Possible mechanisms for the stoichiometric hydrophosphination of alkenes and ketones by complexes *trans*-**12a**,**b** and *trans*-**13** are shown in Scheme 4.21 and Scheme 4.22. Both pathways involve nucleophilic addition of the unsaturated substrate to the phosphenium ligands in *trans*-**12a**,**b** or *trans*-**13**, which generates a carbocation intermediate. The carbocation can be quenched either by intramolecular hydride transfer from a coordinated PR_2H (Scheme 4.21) or by intermolecular hydride transfer from another complex containing PR_2H (Scheme 4.22). Either pathway would complete the hydrophosphination of the unsaturated substrate and regenerate a phosphenium ligand at Mo. For the intramolecular hydride transfer to occur, the PR_2H ligand likely has to be *cis* to the phosphine ligand with the pendant carbocation, which implies that isomerization must take place.

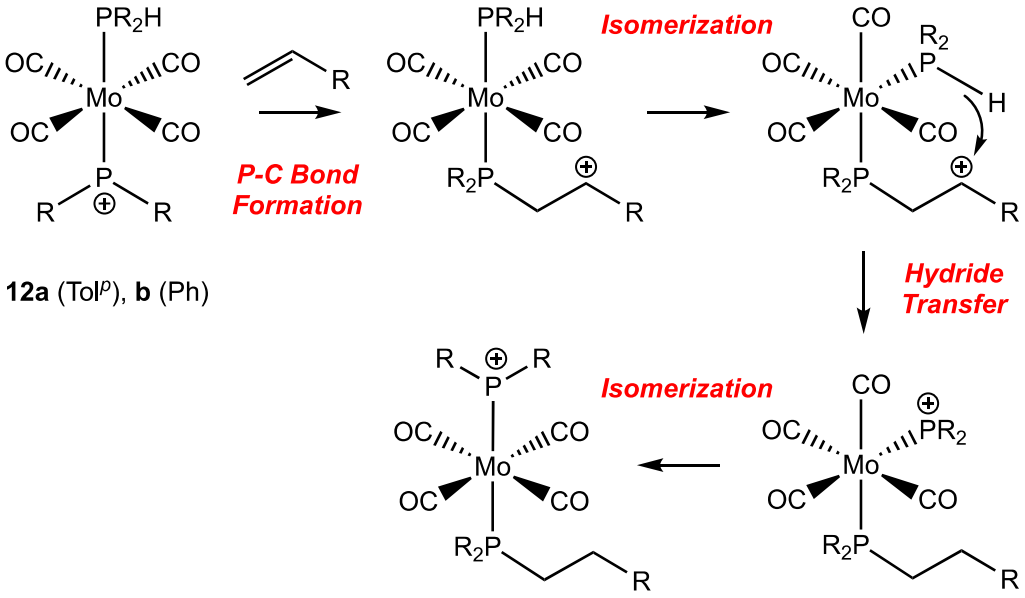

Scheme 4.21. Possible mechanism for the intramolecular stoichiometric hydrophosphination of unsaturated substrates by complexes *trans*-**12a,b**.

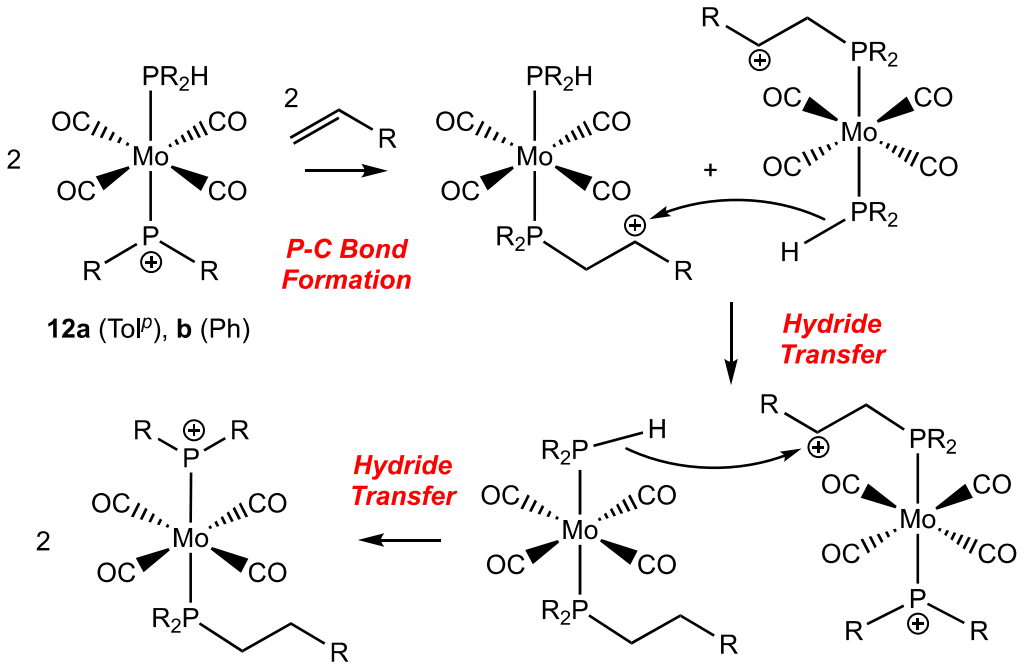

Scheme 4.22. Possible mechanism for the intermolecular stoichiometric hydrophosphination of unsaturated substrates by complexes *trans*-**12a,b**.

To probe which of the two pathways described above is operative, a control experiment where equimolar amounts of *trans*-**12b**, *cis*-**10b** (as an external hydride source) and 1,1-diphenylethylene were added together was performed (Scheme 4.23). If the mechanism is intramolecular, I would expect to see only **14b** with unreacted **10b** as the products (path a). If the mechanism is intermolecular, I would expect to observe **12b** remaining as well as a new neutral complex containing PPh_2H and the hydrophosphination product as ligands, $Mo(CO)_4(Ph_2PCHCH_2Ph_2)(PPh_2H)$ (path b). This new complex would form if a hydride from **10b** quenches the carbocationic intermediate generated from nucleophilic addition of 1,1-diphenylethylene to **12b**. Hydride transfer from **10b** would regenerate **12b**.

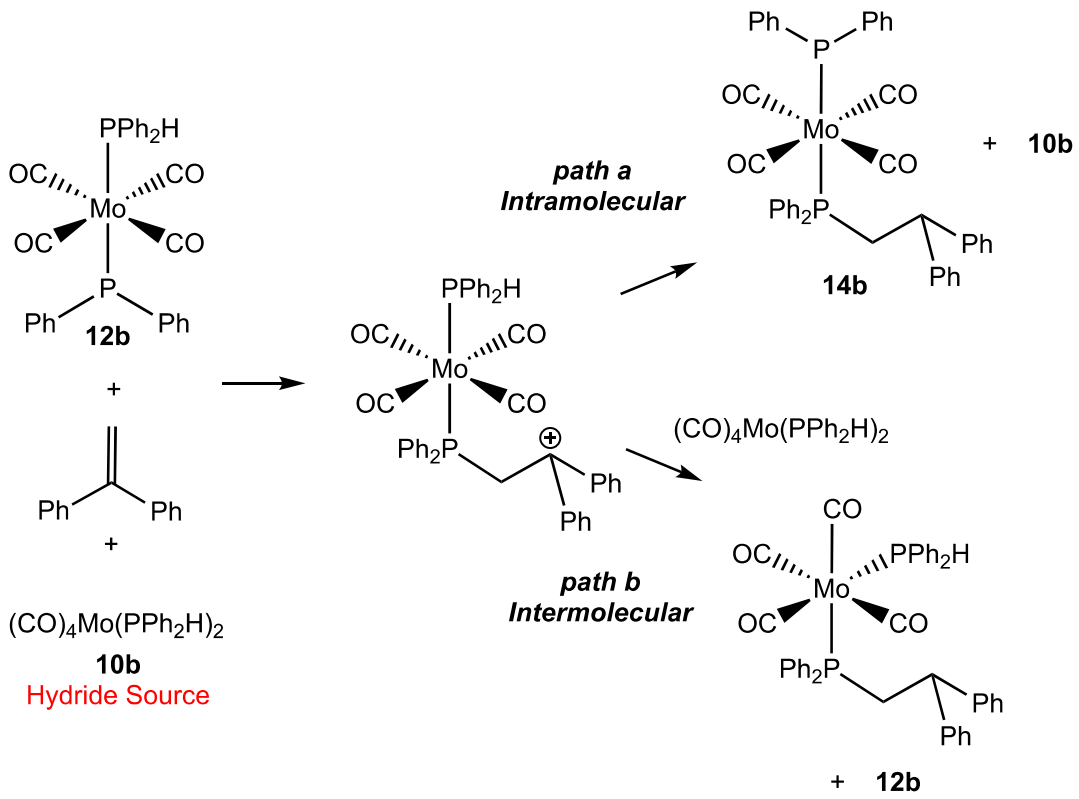

Scheme 4.23. Control experiment to determine if hydride transfer during the hydrophosphination of 1,1-diphenylethylene mediated by *trans*-**12b**$[B(C_6H_3Cl_2)_4]$ is intra- or intermolecular.

The product mixture from the control experiment described above included *trans*-**12b**, *cis*-**10b**, *trans*-**14b** and a new complex tentatively assigned as *cis*-$Mo(CO)_4(Ph_2PCHCH_2Ph_2)(PPh_2H)$. The outcomes of both pathways described are observed, which suggests that both intra- and intermolecular hydride transfer are possible. In the $^{31}P\{^1H\}$ NMR spectrum of this reaction, *cis*-$Mo(CO)_4(Ph_2PCHCH_2Ph_2)(PPh_2H)$ appears as a set of doublets at 31.5 and 18.7 ppm ($^2J_{PP}$ 22 Hz). The doublet at 18.7 ppm exhibits a $^1J_{PH}$ coupling whereas the doublet at 31.5 ppm does not. In the ^1H NMR spectrum of this reaction, two distinct complexes containing the hydrophosphination product phosphine are observed corresponding to *trans*-**14b** and *cis*-$Mo(CO)_4(Ph_2PCHCH_2Ph_2)(PPh_2H)$. It is worth noting, though, that **10b** is a good hydride source and could have biased the reaction towards intermolecular hydride transfer. In the absence of **10b**, intermolecular hydride transfer would have to occur from a phosphenium complex or other cationic intermediate, which would presumably be more difficult. This is consistent with results from another control experiment, where the addition of $[Ph_3C][B(C_6H_3Cl_2)_4]$ to *trans*-**12b** does not result in hydride abstraction of the remaining PPh_2H ligand.

I performed a kinetic analysis on the stoichiometric hydrophosphination of 1,1-diphenylethylene mediated by *trans*-**13** by ^1H NMR and used VTNA to show that there is a first-order dependence on the concentration of both *trans*-**13** and 1,1-diphenylethylene. This could mean either that the nucleophilic addition of 1,1-diphenylethylene to the phosphenium ligand of *trans*-**13** is rate limiting, in which case no information about the hydride transfer step can be determined, or that the hydride transfer step is rate limiting,

but intramolecular. If hydride transfer was rate limiting, but intermolecular, a second order reaction rate dependence would be expected on the concentration of *trans*-**13**. Complexes *trans*-**12a**,**b** could not be used to monitor the hydrophosphination because the reactions were complete before being able to collect the first NMR spectrum.

Overall, the mechanism for the hydrophosphination of unsaturated substrates mediated by *trans*-**12a**,**b** and *trans*-**13** could not be conclusively determined. The control experiment described above suggests that both intra- and intermolecular hydride transfer is possible. The kinetic experiment monitoring the hydrophosphination of 1,1-diphenylethylene mediated by *trans*-**13** also could not conclusively determine the mechanism for hydride transfer.

4.7. Attempted Catalytic Hydrophosphination Using *trans*-12a,b and *trans*-13

The results presented in the previous sections demonstrated that the putative steps of a synthetic cycle for hydrophosphination mediated by metal phosphenium complexes are possible (P-H bond hydride abstraction, P-C bond formation, C-H bond formation). The remaining step to achieve turnover is product phosphine substitution by substrate phosphine (Scheme 4.8, step C). In this section, the reactions of complexes *trans*-**12a**,**b** with secondary phosphines is described. Preliminary efforts to render the stoichiometric hydrophosphination discussed in section 4.6 for turnover or catalysis is described.

4.7.1. Reactions of *trans*-12a,b with PR_2H

Addition of PR_2H to complexes *trans*-**12a**,**b** in CD_2Cl_2 results in coordination of PR_2H to the phosphenium ligand, to generate complexes **19a**,**b** (Scheme 4.24). The $^{31}P\{^1H\}$ NMR spectrum of **19a** shows a doublet of doublets, assigned as the phosphenium ligand, and two doublets, assigned as the two chemically inequivalent $PTol_2^pH$ moieties in the molecule. The doublet of doublets shows a $^1J_{PP}$ coupling (235 Hz) as well as a $^2J_{PP}$ coupling (67 Hz). One of the doublets shows $^1J_{PP}$ coupling, which is assigned as the phosphenium coordinated $PTol_2^pH$. The other doublet is assigned as the Mo-bound $PTol_2^pH$. The two doublets both exhibit a $^1J_{PH}$ coupling in the ^{31}P NMR spectrum, which confirms that these are $PTol_2^pH$ moieties. The phosphenium-bound $PTol^p{}_2H$ and the Mo-bound $PTol^p{}_2H$ do not couple with one another. The relatively large $^2J_{PP}$ coupling (67 Hz) indicates that complex **19a** is the *trans* isomer. A similar $^{31}P\{^1H\}$ NMR spectrum was obtained for complex **19b**.

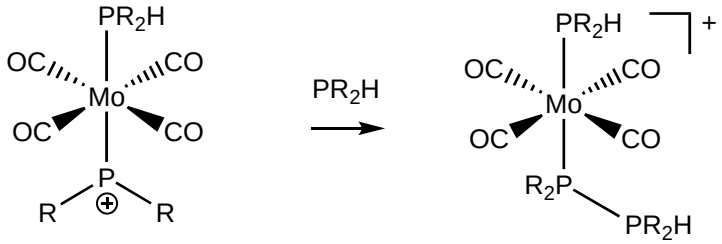

12a,b **19a** (Tol^p), **b** (Ph)

Scheme 4.24. Addition of PR_2H to complexes *trans*-**12a**,**b**, which results in the PR_2H-phosphenium adducts *trans*-**19a**,**b**.

Adduct formation could be problematic for catalysis because it could prevent the nucleophilic addition of unsaturated substrate to the phosphenium ligand (Scheme 4.8, step A). In control experiments where both 1,1-diphenylethylene and PAr_2H were added to *trans*-**12a**,**b**, under stoichiometric and catalytic conditions, only the adducts **19a**,**b** were observed.

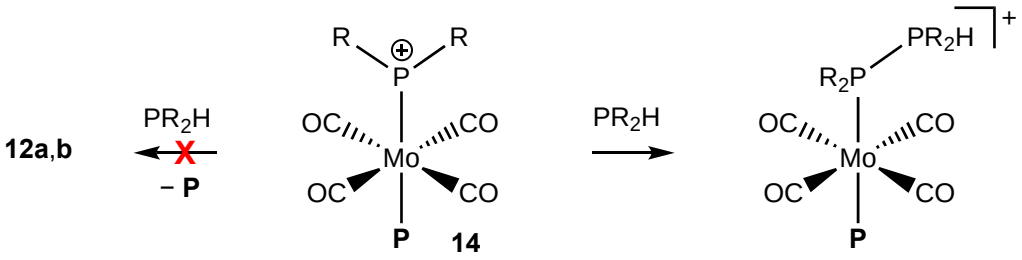

Scheme 4.25. Addition of PR_2H to complexes **14** results in phosphine-phosphenium adduct formation (right) instead of substitution of **P** (left).

In order to achieve catalytic turnover, PR_2H must substitute product phosphine (**P**) from Mo, which would liberate **P** and regenerate **12a,b** or **13** (Scheme 4.8, step C). Addition of PR_2H to phosphenium complexes with **P** as ligands (**14a**,**b**), results in the formation of the corresponding phosphine-phosphenium adducts, $[Mo(CO)_4(\mathbf{P})(PPh_2\{PR_2H\})]$, instead of the desired substitution of **P** by PR_2H (Scheme 4.25).

The results from these control experiments demonstrate the challenges of utilization phosphenium ligands in hydrophosphination. The coordination of substrate phosphine to

the phosphenium ligand and the product phosphine lability need to be addressed in order to achieve turnover and catalysis.

4.8. Conclusions

This Chapter explored the viability of using metal phosphenium complexes for the hydrophosphination of unsaturated substrates. We proposed that metal complexes containing electrophilic phosphenium ligands could allow for the hydrophosphination of simple and electron-rich alkenes because P-C bond formation would likely occur via nucleophilic attack of the alkene at the phosphenium ligand. This is a novel approach to metal-catalyzed hydrophosphination that has never been reported.

Overall, this study is a proof of concept for the viability of metal phosphenium complexes as intermediates in the hydrophosphination of alkenes. I was able to establish the fundamental steps of a putative synthetic hydrophosphination cycle that employs metal phosphenium complexes as intermediates. Moreover, this Chapter demonstrates the synthetic potential of phospheniums to allow for the hydrophosphination of simple and electron-rich alkenes.

From this work, I found that the phosphenium complexes *trans*-[$Mo(CO)_4(PTol_2^pH)(PTol_2^p)$] (*trans*-**12a**), *trans*-[$Mo(CO)_4(PR_2H)(PR_2)$] (*trans*-**12b**) and *trans*-[$Mo(CO)_4(PPh_2H)(PPh_2)$] (*trans*-**13**) mediate the stoichiometric hydrophosphination of unsaturated substrates. Complex **13** mediates the hydrophosphination of a much wider scope of alkenes than **12a**,**b**, which includes simple alkenes such as ethylene, propene, 1-

hexene and cyclopentene. These substrates in particular are extremely challenging substrates for metal-catalyzed hydrophosphination. This difference in scope for the hydrophosphination by **12a**,**b** and **13** demonstrates how tuning the electronic properties and structure of the complexes can drastically influence the reactivity of these complexes for hydrophosphination. In this case, Mo is more electron-rich in **13**, which reduces the electrophilicity of the phosphenium ligand, but increases the hydricity of the P-H bonds of coordinated PPh_2H, relative to **12a**,**b**. Ultimately, demonstrating that these phosphenium complexes can mediate the hydrophosphination of alkenes makes them worthwhile to explore for future studies in metal-catalyzed hydrophosphination.

Attempts to exploit this stoichiometric hydrophosphination for catalysis were conducted, but some challenges were encountered. For example, under catalytic conditions, substrate phosphine (PR_2H) coordinates to the phosphenium ligand of complexes **12a**,**b** and **13**, which prevents alkenes from undergoing electrophilic P-C bond formation with the phosphenium ligands. Another challenge is that these complexes do not easily undergo substitution reactions. In order to achieve turnover, these complexes must be able to undergo substitution in order to release the hydrophosphinated products and regenerate the catalyst. These problems can be addressed through design of the complexes to disfavour substrate phosphine from coordinating to the phosphenium ligand and favour substitution, which will be discussed in Chapter 6.

4.9. Experimental

See Chapter 2, Section 2.6.1. for general experimental details. Complexes *cis*-$Mo(CO)_4(piperidine)_2$[33] and *fac*-$Mo(CO)_3(NCCH_3)_3$[58] were prepared according to literature procedures. Complexes *cis*-$Mo(CO)_4(PTol^p{}_2H)_2$ (**10a**), *cis*-$Mo(CO)_4(PPh_2H)_2$ (**10b**), *cis*-$Mo(CO)_4(PCy_2H)_2$ (**10c**),[40] *fac*-$Mo(CO)_3(PPh_2H)_3$, $Na[B(C_6H_3Cl_2)_4]$[59] and $[Ph_3C][B(C_6H_3Cl_2)]$[60] were prepared according to modified literature procedures.

4.9.1. Synthesis of $Na[B(C_6H_3Cl_2)_4]$

Under nitrogen gas, a 250 mL 3-neck round-bottom flask, equipped with a condenser, stirring bar and a 100 mL dropping funnel, was charged with Mg (2.43 g, 0.10 mol) and $Na[BF_4]$ (2.74 g, 0.025 mol). The apparatus was evacuated and back-filled with nitrogen to remove air, then diethyl ether (10 mL) was added to the flask. 1-Bromo-3,5-dichlorobenzene (22.6 g, 0.10 mol) was added to the dropping funnel and dissolved in diethyl ether (50 mL). A portion (5 mL) of this ether/1-bromo-3,5-dichlorobenzene solution was slowly added to the flask to start the reaction. Once the reaction was initiated, the remaining 1-bromo-3,5-dichlorobenzene solution was added dropwise over 2 h. The reaction was left to stir overnight. The next day, the reaction mixture was added to an aqueous solution of Na_2CO_3 (20 g in 300 mL of water). This solution was filtered and transferred to a separation funnel where the organic phase was removed and the aqueous layer extracted with diethyl ether (2 x 50 mL). The ether extracts were combined and the solvent was removed under vacuum. The resulting yellow oil was triturated with hexanes, which afforded a pale yellow sticky solid. The yellow solid released a white powder upon mixing with water. The white solid was collected in a Buchner funnel and washed with

hexanes (3 x 50 mL) and water (3 x 50 mL). The isolated solid was dried under vacuum overnight at 120 °C. Yield 11 g (90 %).

4.9.2. Synthesis of $[Ph_3C][B(C_6H_3Cl_2)_4]$

In a Schlenk flask, Ph_3CCl (1 g, 3.6 mmol) and $Na[B(C_6H_3Cl_2)_4]$ (2.2 g, 3.6 mmol) were added together and dissolved in dichloromethane. This immediately resulted in a clear orange solution. The reaction was gently heated and stirred for 1 h, which resulted in the formation of a precipitate, NaCl. The solution was filtered. The precipitate was rinsed with dichloromethane (3 x 10 mL) and filtered leaving behind a white solid. The filtrates were combined and the dichloromethane was removed under vacuum, which resulted in an orange powder, $[Ph_3C][B(C_6H_3Cl_2)_4]$. The orange powder was washed with toluene (3x10 mL) to remove any leftover Ph_3CCl and dried. Yield 2.9 g, 93%.

4.9.3. General method for the Synthesis of *cis*-$Mo(CO)_4(PR_2H)_2$ (10a,b)

A Schlenk flask containing *cis*-$Mo(CO)_4(piperidine)_2$ (1.0 g, 2.6 mmol) and PR_2H (2 equiv, 5.3 mmol) in hexanes (20 mL) was gently heated for 1 h in an oil bath. The solution was then allowed to cool and the hexanes was removed under vacuum, which gave a light brown oil. Trituration with hexanes (3 x 20 mL) resulted in precipitation of a beige solid, *cis*-$Mo(CO)_4(PR_2H)_2$**,** which was collected on a Hersch funnel, washed with hexanes (3 x 10 mL) and dried. Quantities of PR_2H used: $PTol_2^pH$ (2 equiv, 5.3 mmol, 1.14 g); PPh_2H (2 equiv 5.3 mmol, 0.92 mL). Yield: **10a**, 1.4 g, 80 %; **10b**, 1.3 g, 84%.

4.9.4. Synthesis of *fac*-$Mo(CO)_3(PPh_2H)_3$ (11)

A Schlenk flask containing *fac*-$Mo(CO)_3(NCCH_3)_3$ (1.0 g, 3.3 mmol) and PPh_2H (3 equiv, 10 mmol, 1.74 mL) in acetonitrile (20 mL) was stirred for 24 h at room temperature. This resulted in the formation of a white precipitate, *fac*-$Mo(CO)_3(PPh_2H)_3$, which was collected in a Hersch funnel and washed with acetonitrile (3 x 5 mL) and dried. Yield 2.2 g, 88%.

4.9.5. General method for the synthesis of *trans*-$[Mo(CO)_4(PR_2H)(PR_2)][B(C_6H_3Cl_2)_4]$ (12a,b)

cis-$Mo(CO)_4(PR_2H)_2$ and $[Ph_3C][B(C_6H_3Cl_2)_4]$ (1 equiv) were added to a Schlenk flask and dissolved in dichloromethane (20 mL). The solution was allowed to stir for 1 h at room temperature. The solution changed colour from orange to dark green/brown. The solvent was removed under vacuum, which resulted in a green/brown solid. The solid was mixed with toluene then collected in a filter frit and washed with toluene (3 x 10 mL) to remove Ph_3CH.

4.9.5.1. Synthesis of *trans*-$[Mo(CO)_4(PTol^p_2H)(PTol^p_2)][B(C_6H_3Cl_2)_4]$ (*trans*-12a$[B(C_6H_3Cl_2)_4]$)

cis-$Mo(CO)_4(PTol^p_2H)_2$ (500 mg, 0.86 mmol) and $[Ph_3C][B(C_6H_3Cl_2)_4]$ (722 mg, 0.86 mmol) were used and the reaction was stirred for 1 h at room temperature. A green powder was obtained. Yield 750 mg, 75%. Melting point: 141°C. IR (KBr, cm^{-1}): 2083, 1989. Anal. Found (calc'd for): C, 54.67 (54.29); H, 3.36 (3.31).

4.9.5.2. Synthesis of *trans*-[Mo(CO)$_4$(PPh$_2$H)(PPh$_2$)][B(C$_6$H$_3$Cl$_2$)$_4$] (*trans*-[12b][B(C$_6$H$_3$Cl$_2$)$_4$])

cis-Mo(CO)$_4$(PTol$^p{}_2$H)$_2$ (500 mg, 0.79 mmol) and [Ph$_3$C][B(C$_6$H$_3$Cl$_2$)$_4$] (658 mg, 0.79 mmol) were used and the reaction was stirred for 1 h at room temperature. A brown/green powder was obtained. Yield 700 mg, 72 %. Melting point: 137°C. IR (KBr, cm^{-1}): 2080, 1988. Microanalysis was not performed on *trans*-[**12b**][B(C$_6$H$_3$Cl$_2$)$_4$] because it could not be purified of an unknown impurity. ^{1}H NMR spectra that shows the impurty is in Appendix E.

4.9.6. Synthesis of *trans*-[Mo(CO)$_3$(PPh$_2$H)$_2$(PPh$_2$)][B(C$_6$H$_3$Cl$_2$)$_4$] (*trans*-[13][B(C$_6$H$_3$Cl$_2$)$_4$])

To a Schlenk flask containing *fac*-Mo(CO)$_3$(PPh$_2$H)$_3$ (500 mg, 0.677 mmol) in dichloromethane (20 mL) [Ph$_3$C][B(C$_6$H$_3$Cl$_2$)$_4$] (1 equiv, 550 mg, 0.677 mmol) was added and the solution was allowed to stir for 1 h at room temperature. The solution changed colour from orange to dark green. Pentane (20 mL) was added to the reaction solution, which resulted in a green oil and light green supernatant. The supernatant (containing the Ph$_3$CH byproduct) was decanted. This was repeated two more times. The solvent was removed under vacuum, which afforded pure *trans*-[**13**][B(C$_6$H$_3$Cl$_2$)$_4$] as a green solid. Yield 800 mg, 88%. Melting point: 135°C. IR (KBr, cm^{-1}): 2090, 2087, 1990, 1985. Anal. Found (calc'd for): C, 56.79 (56.43); H, 3.33 (3.37).

4.9.7. NMR Tube Reactions of *trans*-[12a,b][B($C_6H_3Cl_2$)$_4$] and *trans*-[13][B($C_6H_3Cl_2$)$_4$]

4.9.7.1. Addition of [NBu_4]PF_6 to *trans*-[12a,b][B($C_6H_3Cl_2$)$_4$]

Complex *trans*-[**12a,b**][B($C_6H_3Cl_2$)$_4$] (15 mg, 0.015 mmol) was dissolved in CD_2Cl_2 and [NBu_4^n]PF_6 (6.0 mg, 0.015 mmol) was added, which resulted a colour change of the solution from green to brown. The evolution of a gas was observed upon addition. The reactions were monitored by $^{31}P\{^1H\}$ NMR. $^{31}P\{^1H\}$ NMR spectra are in Appendix H.

4.9.7.2. Addition of MeOH to *trans*-[12a,b][B($C_6H_3Cl_2$)$_4$]

Complex *trans*-[**12a,b**][B($C_6H_3Cl_2$)$_4$] (15 mg, 0.015 mmol) was dissolved in CD_2Cl_2 and MeOH (50 μL) was added, which resulted a colour change of the solution from green to brown. The reactions were monitored by $^{31}P\{^1H\}$ NMR. $^{31}P\{^1H\}$ NMR spectra are in Appendix H.

4.9.7.3. General Procedure for Addition of Unsaturated Substrates to *trans*-[12a,b][B($C_6H_3Cl_2$)$_4$]

In the glovebox, *trans*-**12a,b**[B($C_6H_3Cl_2$)$_4$] (40 mg, 0.034 mmol) was dissolved in CD_2Cl_2 in a vial and alkene or ketone (1 equiv, 0.034 mmol) was added. The dark green solution was transferred to a J Young tube. All reactions were monitored by ^1H and $^{31}P\{^1H\}$ NMR. $^{31}P\{^1H\}$ NMR data for all observed complexes are reported in Table 4.4. Quantities of unsaturated substrates used: 1,1-diphenylethylene, 7 μL, 0.034 mmol; benzophenone, 7 mg, 0.034 mmol.

4.9.7.4. General Procedure for Addition of Unsaturated Substrates to *trans*-[13][B(C$_6$H$_3$Cl$_2$)$_4$]

In the glovebox, *trans*-**13**[B(C$_6$H$_3$Cl$_2$)$_4$] (20 mg, 0.015 mmol) was dissolved in $CDCl_3$ and alkene or ketone (2 equiv, 0.030 mmol) was added. The dark green solution was transferred to a J Young tube. For gaseous alkenes, the dark green solution of *trans*-**13**[B(C$_6$H$_3$Cl$_2$)$_4$] in $CDCl_3$ was transferred to a J Young tube, and degassed via three freeze-pump-thaw cycles. Gaseous alkenes were added into the J Young tube via a Schlenk line. All reactions were monitored by ^{1}H and ^{31}P{^{1}H} NMR. ^{1}H, ^{31}P{^{1}H} and ^{13}C{^{1}H} NMR data for all observed complexes are reported in Table 4.8, 4.5 and 4.9, respectively. Quantities of non-gaseous unsaturated substrates used: 1,1-diphenylethylene, 6 μL, 0.030 mmol; benzophenone, 6 mg, 0.030 mmol; styrene, 4 μL, 0.030 mmol; indene, 4 μL, 0.030 mmol; 1-hexene, 4 μL, 0.030 mmol; cyclopentene, 4 μL, 0.030 mmol. Representative 1D (^{1}H, ^{31}P{^{1}H}and ^{13}C{^{1}H} DEPT 135) and 2D (^{1}H COSY, ^{1}H/^{31}P{^{1}H}-HSQC, ^{1}H/^{31}P{^{1}H}-HMBC, ^{1}H/^{13}C{^{1}H}-HSQC and ^{1}H/^{13}C{^{1}H}-HMBC) spectra for complex **18e** are in Appendix G.

4.9.7.5. Addition of phenylacetylene to *trans*-[12a,b][B(C$_6$H$_3$Cl$_2$)$_4$] and *trans*-[13][B(C$_6$H$_3$Cl$_2$)$_4$]

In the glovebox, *trans*-[**12a,b**][B(C$_6$H$_3$Cl$_2$)$_4$] (17 mg, 0.015 mmol) or *trans*-[**13**][B(C$_6$H$_3$Cl$_2$)$_4$] (20 mg, 0.015 mmol) was dissolved in CD_2Cl_2 or $CDCl_3$ and phenylacetylene (1-2 equiv, 0.015 - 0.030 mmol) was added. This resulted in a colour change of the solution from dark green to red. All reactions were monitored by ^{1}H and ^{31}P{^{1}H} NMR.

4.9.7.6. Addition of PR_2H to *trans*-[12a,b][$B(C_6H_3Cl_2)_4$]

In the glovebox, *trans*-[**12a,b**][$B(C_6H_3Cl_2)_4$] (17 mg, 0.015 mmol) was dissolved in CD_2Cl_2 and PR_2H (1-2 equiv, 0.015 - 0.030 mmol) was added. This resulted in a colour change of the solution from dark green to yellow. All reactions were monitored by ^1H and $^{31}P\{^1H\}$ NMR. $^{31}P\{^1H\}$ NMR spectra are in Appendix H.

4.9.7.7. Addition of PR_2H and Unsaturated Substrates to *trans*-[12a,b][$B(C_6H_3Cl_2)_4$] and *trans*-[13][$B(C_6H_3Cl_2)_4$]

In the glovebox, *trans*-[**12a,b**][$B(C_6H_3Cl_2)_4$] (17 mg, 0.015 mmol) or *trans*-[**13**][$B(C_6H_3Cl_2)_4$] (20 mg, 0.015 mmol) was dissolved in CD_2Cl_2 or $CDCl_3$ and unsaturated substrates (1-2 equiv, 0.015 - 0.030 mmol) were added. This resulted in a colour change of the solution from dark green to yellow. All reactions were monitored by ^1H and $^{31}P\{^1H\}$ NMR. $^{31}P\{^1H\}$ NMR spectra are in Appendix H.

4.9.8. $^{31}P\{^{1}H\}$, ^{1}H and $^{13}C\{^{1}H\}$ NMR Data for 12a,b, 13, 16b and 18a-h

Table 4.3. $^{31}P\{^{1}H\}$ NMR data of complexes **12a,b** and **13** (202.51 MHz).

Compound	PR_2	PR_2H
$[Mo(CO)_4(PTol_2^pH)(PTol_2^p)]$ (*trans*-**12a**)[a]	***trans*:** 439.1 (d, $^2J_{PP}$ 70 Hz) ***cis*:** 441.2 (d, $^2J_{PP}$ 38 Hz)	***trans*:** -7.2 ***cis*:** -3.3
$[Mo(CO)_4(PPh_2H)(PPh_2)]$ (*trans*-**12b**)[a]	***trans*:** 440.6 (d, $^2J_{PP}$ 70 Hz) ***cis*:** 441.6 (d, $^2J_{PP}$ 38 Hz)	***trans*:** -6.2 ***cis*:** -1.9
Trans-$[Mo(CO)_3(PPh_2H)_2(PPh_2)]$ (*trans*-**13**)[b]	395.6 (dd, $^2J_{PP}$ 84, 46 Hz)	7.0 (dd, $^2J_{PP}$ 46, 30 Hz) 4.1 (dd, $^2J_{PP}$ 84, 30 Hz)

[a]NMR sample prepared in CD_2Cl_2; [b]NMR sample prepared in $CDCl_3$

Table 4.4. $^{31}P\{^{1}H\}$ NMR data of complexes **14a,b** and **15a,b** (202.51 MHz, CD_2Cl_2).

P	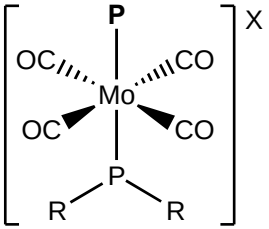	
	R = Ph	**R = Tol^p**
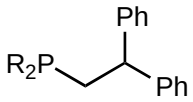 **14a,b**	434.5 (d, $^2J_{PP}$ 72 Hz, PPh_2) 18.6 (d, $^2J_{PP}$ 72 Hz, **P**)	434.5 (d, $^2J_{PP}$ 71 Hz, PPh_2) 18.6 (d, $^2J_{PP}$ 71 Hz, **P**)
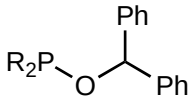 **15a,b**	440.3 (d, $^2J_{PP}$ 88 Hz, PPh_2) 132.8 (d, $^2J_{PP}$ 88 Hz, **P**)	440.3 (d, $^2J_{PP}$ 89 Hz, PPh_2) 132.8 (d, $^2J_{PP}$ 89 Hz, **P**)

Table 4.5. $^{31}P\{^{1}H\}$ NMR data of complexes with coordinated hydrophosphination products resulting from the addition of alkenes and ketones to **13** (202.51 MHz, $CDCl_3$).

	P	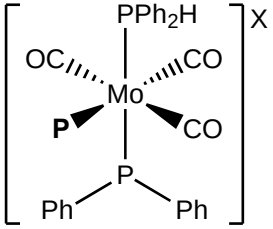	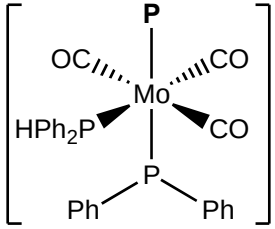	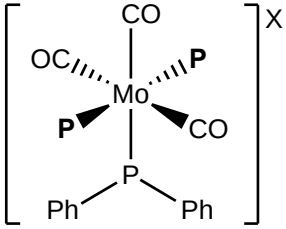
18a	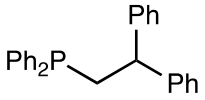	381.6 (dd, $^{2}J_{PP}$ 85, 29 Hz, PPh_2) 27.0 (dd, $^{2}J_{PP}$ 43, 30 Hz, **P**) 6.2 (dd, $^{2}J_{PP}$ 85, 29 Hz, PPh_2H)	387.7 (dd, $^{2}J_{PP}$ 85, 50 Hz, PPh_2) 23.0 (dd, $^{2}J_{PP}$ 85, 29 Hz, **P**) 7.9 (dd, $^{2}J_{PP}$ 50, 29 Hz, PPh_2H)	380.9 (t, $^{2}J_{PP}$ 44 Hz, PPh_2) 33.8 (d, $^{2}J_{PP}$ 44 Hz, **P**)
18b	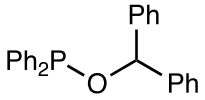	388.7 (dd, $^{2}J_{PP}$ 83, 49 Hz, PPh_2) 136.4 (dd, $^{2}J_{PP}$ 49, 37 Hz, **P**) 5.4 (dd, $^{2}J_{PP}$ 83, 37 Hz, PPh_2H)	392.5 (dd, $^{2}J_{PP}$ 104, 47 Hz, PPh_2) 137.3 (dd, $^{2}J_{PP}$ 104, 35 Hz, **P**) 9.4 (dd, $^{2}J_{PP}$ 47, 35 Hz, PPh_2H)	395.9 (t, $^{2}J_{PP}$ 47 Hz, PPh_2) 144.1 (d, $^{2}J_{PP}$ 47 Hz, **P**)
18c	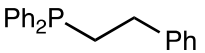	383.0 (dd, $^{2}J_{PP}$ 85, 45 Hz, PPh_2) 23.9 (dd, $^{2}J_{PP}$ 45, 30 Hz, **P**) 6.1 (dd, $^{2}J_{PP}$ 85, 30 Hz, PPh_2H)	388.8 (dd, $^{2}J_{PP}$ 84, 50 Hz, PPh_2) 20.4 (dd, $^{2}J_{PP}$ 84, 29 Hz, **P**) 8.6 (dd, $^{2}J_{PP}$ 50, 29 Hz, PPh_2H)	385.4 (t, $^{2}J_{PP}$ 43 Hz, PPh_2) 30.4 (d, $^{2}J_{PP}$ 43 Hz, **P**)
18d	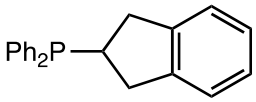	382.2 (dd, $^{2}J_{PP}$ 86, 41 Hz, PPh_2) 39.1 (dd, $^{2}J_{PP}$ 41, 29 Hz, **P**) 6.7 (dd, $^{2}J_{PP}$ 86, 29 Hz, PPh_2H)	388.4 (dd, $^{2}J_{PP}$ 85, 51 Hz, PPh_2) 29.4 (dd, $^{2}J_{PP}$ 85, 51 Hz, **P**) 8.2 (dd, $^{2}J_{PP}$ 51, 29 Hz, PPh_2H)	381. (t, $^{2}J_{PP}$ 42 Hz, PPh_2) 43.9 (d, $^{2}J_{PP}$ 42 Hz, **P**)
18g	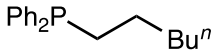	381.7 (dd, $^{2}J_{PP}$ 87, 43 Hz, PPh_2) 24.5 (dd, $^{2}J_{PP}$ 43, 30 Hz, **P**) 6.3 (dd, $^{2}J_{PP}$ 87, 30 Hz, PPh_2H)	386.1 (dd, $^{2}J_{PP}$ 84, 50 Hz, PPh_2) 20.7 (dd, $^{2}J_{PP}$ 84, 29 Hz, **P**) 8.8 (dd, $^{2}J_{PP}$ 50, 29 Hz, PPh_2H)	381.2 (t, $^{2}J_{PP}$ 43 Hz, PPh_2) 31.3 (d, $^{2}J_{PP}$ 43 Hz, **P**)
18h	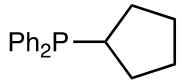	378.1 (dd, $^{2}J_{PP}$ 87, 42 Hz, PPh_2) 37.0 (dd, $^{2}J_{PP}$ 42, 29 Hz, **P**) 7.3 (dd, $^{2}J_{PP}$ 87, 29 Hz, PPh_2H)	384.5 (dd, $^{2}J_{PP}$ 85, 51 Hz, PPh_2) 29.4 (dd, $^{2}J_{PP}$ 85, 29 Hz, **P**) 8.4 (dd, $^{2}J_{PP}$ 51, 29 Hz, PPh_2H)	376.1 (t, $^{2}J_{PP}$ 43 Hz, PPh_2) 42.9 (d, $^{2}J_{PP}$ 43 Hz, **P**)

18f	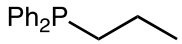	386.1 (dd, $^{2}J_{PP}$, Hz, PPh_2) 24.0 (dd, $^{2}J_{PP}$ 43, 30 Hz, **P**) 6.3 (dd, $^{2}J_{PP}$ 87, 30 Hz, PPh_2H)	369.9 (dd, $^{2}J_{PP}$, Hz, PPh_2) 20.5 (dd, $^{2}J_{PP}$ 84, 29 Hz, **P**) 8.7 (dd, $^{2}J_{PP}$ 50, 29 Hz, PPh_2H)	382.3 (t, $^{2}J_{PP}$ 43 Hz, PPh_2) 30.9 (d, $^{2}J_{PP}$ 43 Hz, **P**)
18e	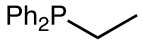	382.3 (dd, $^{2}J_{PP}$ 85, 43 Hz, PPh_2) 23.0 (dd, $^{2}J_{PP}$ 43, 30 Hz, **P**) 6.0 (dd, $^{2}J_{PP}$ 85, 30 Hz, PPh_2H)	385.8 (dd, $^{2}J_{PP}$ 85, 50 Hz, PPh_2) 23.7 (dd, $^{2}J_{PP}$ 85, 30 Hz, **P**) 8.8 (dd, $^{2}J_{PP}$ 50, 30 Hz, PPh_2H)	382.3 (t, $^{2}J_{PP}$ 43 Hz, PPh_2) 34.3 (d, $^{2}J_{PP}$ 43 Hz, **P**)

Table 4.6. ^{1}H NMR Data for **12a,b, 13** and **16b** (500.27 MHz).

Compound	**PR_2**	**PR_2H**	**other**
trans-$[Mo(CO)_4(PTol_2^pH)(PTol_2^p)]$ $[B(C_6H_3Cl_2)_4]$ (**12a**)[a]	7.69 (t, H_o, 4H), 7.46 (d, H_m, 4H), 2.47 (s, *p*-Me, 6H)	7.06 (d, 360 Hz, P<u>H</u>, 1H), 7.53 (dd, H_o, 4H), 7.36 (d, H_m, 4H), 2.42 (s, *p*-Me, 6H)	***cis* isomer:** 2.44 (s, *p*-Me, $PTol_2^p$), 2.38 (s, *p*-Me, $PTol_2^pH$)
trans-$[Mo(CO)_4(PPh_2H)(PPh_2)]$ $[B(C_6H_3Cl_2)_4]$ (**12b**) [a]	8.20 - 7.30 (20 H, overlapping with PPh_2H)	7.13 (d, 361 Hz, P<u>H</u>), 8.20 - 7.30 (20 H, overlapping with PPh_2)	***cis isomer:*** No identifiable peaks
$[Mo(CO)_3(PPh_2H)_2(PPh_2)]$ $[B(C_6H_3Cl_2)_4]$ (**13**) [b]	7.68 (t, $^{2}J_{HH}$ 7.5 Hz, 2H), 7.60 - 7.20 (28H, overlapping with *cis*- and *trans*-PPh_2H)	6.43 (dd, $^{1}J_{PH}$ 350, $^{3}J_{PH}$ 10 Hz, P<u>H</u> of PPh_2H *trans* to PPh_2), 6.59 (dd, $^{1}J_{PH}$ 350, $^{3}J_{PH}$ 11 Hz, P<u>H</u> of PPh_2H *cis* to PPh_2), 7.60 - 7.20 (28H, overlapping with PPh_2)	-
$[Mo(CO)_4(PPh_2H)(PPh_2\{HCCPh\})]$ $[B(C_6H_3Cl_2)_4]$ (**16b**) [a]	7.72 – 7.50 (overlapping with PPh_2H resonances)	7.90 – 7.74 (overlapping peaks, 5H), 7.72 – 7.50 (overlapping with other	9.24 (d, $^{2}J_{PC}$ 10.4 Hz, 1H, PC<u>H</u>), 7.97 (d, $^{3}J_{HH}$ 7.7 Hz, 2H, H_o of PCHCPh), 7.72 – 7.50

	PPh_2 resonances), 7.48 (d, $^1J_{PH}$ 360 Hz, P<u>H</u>)	(overlapping with PPh_2H and PPh_2 resonances)

[a]NMR sample prepared in CD_2Cl_2; [b]NMR sample prepared in $CDCl_3$; [c1]H NMR data for $B(C_6H_3Cl_2)_4$ anion: 7.09 (s, *o*-H, 8H), 6.93 (s, *m*-H, 4H)

Table 4.7. ^{13}C NMR Data for **12a,b, 13** and **16b** (125.79 MHz).

Compound	**PR_2**	**PR_2H**	**other**
Trans-$[Mo(CO)_4(PTol_2^pH)(PTol_2^p)][B(C_6H_3Cl_2)_4]$ (**12a**) [a]	149.1 (s, C_p), 147.0 (d, $^1J_{PC}$ 10 Hz, C_{ipso}), 133.9 (d, $^2J_{PC}$ 10 Hz, C_o), 130.7 (d, $^3J_{PC}$ 10 Hz, C_m), 22.5 (s, *p*-Me)	143.5 (d, $^2J_{PC}$ 2 Hz, C_p), 132.6 (d, $^2J_{PC}$ 12 Hz, C_o), 131.1 (d, $^3J_{PC}$ 11 Hz, C_m), 124.5 (d, $^2J_{PC}$ 12 Hz, C_{ipso}), 21.7 (s, *p*-Me)	**CO:** 204.5 (dd, $^2J_{PC}$ 17, 12 Hz, CO)
Trans-$[Mo(CO)_4(PPh_2H)(PPh_2)][B(C_6H_3Cl_2)_4]$ (**12b**) [a]	148.8 (s, C_{ipso}), 144.0 (s, C_{ipso}), 136.2 (s, C_p), 132.3 (d, $^2J_{PC}$ 11 Hz, C_o), 132.3 (s, C_p), 130.5 (d, $^2J_{PC}$ 11 Hz, C_o), 129.7 (d, $^2J_{PC}$ 10 Hz, C_m), other C_m overlapping with C_o of $B(C_6H_3Cl_2)_4$		**CO:** 203.7 (dd, $^2J_{PC}$ 17, 11 Hz, CO)
Trans-$[Mo(CO)_3(PPh_2H)_2(PPh_2)][B(C_6H_3Cl_2)_4]$ (**13**) [b]	147.7 (s), 134.3 (s, C_o of PPh_2), 132.2 (dd, $^2J_{PC}$ 14, 11 Hz), 131.9 (dd, $^2J_{PC}$ 25, 2 Hz), 129.9 (dd, $^2J_{PC}$ 24, 10 Hz), 129.3 (dd, $^1J_{PC}$ 43, $^3J_{PC}$ 2 Hz, C_{ipso}), 129.2 (s)		**CO:** 212.8 (CO, two chemically equivalent CO *cis*- to all ligands in complexes), 207.4 (CO, *trans*- to one PPh_2H ligand)

	127.5 (dd, $^{1}J_{PC}$ 43, $^{3}J_{PC}$ 3 Hz, C_{ipso}) *due to the unassigned ^{1}H resonances, the aromatic C could not be assigned	
$[Mo(CO)_4(PPh_2H)(PPh_2\{HCCPh\})]$ $[B(C_6H_3Cl_2)_4]$ (**16b**) [a]	132.8 (d, $^{2}J_{PC}$ 12 Hz), 132.2 (d, $^{3}J_{PC}$ 3 Hz), 131.8 (d, $^{2}J_{PC}$ 11 Hz), 130.0 (dd, $^{2}J_{PC}$ 11, $3J_{PC}$ 4 Hz), 129.8 (s) *due to the unassigned ^{1}H resonances, the aromatic C could not be assigned	**$Ph_2CHCPhCO$:** 266.4 (dd, $^{2}J_{PC}$ 19, $^{2}J_{PC}$ 2 Hz, PCHC(Ph)CO), 164.4 (d, $^{1}J_{PC}$ 47 Hz, PCH), 153.6 (d, $^{2}J_{PC}$ 25 Hz, PCHCPh), 144.0 (s, C_{ipso} of CHC(Ph)), 128.4 (s, C_o of CHC(Ph)) **CO:** 218.8 (dd, $^{2}J_{PC}$ 25, $^{2}J_{PC}$ 11 Hz, CO), 202.8 (dd, $^{2}J_{PC}$ 9, $^{2}J_{PC}$ 7 Hz, CO)

[a]NMR sample prepared in CD_2Cl_2; [b]NMR sample prepared in $CDCl_3$; [c] $^{13}C\{^{1}H\}$ NMR data for $B(C_6H_3Cl_2)_4$ anion: 165.1 (q, $^{1}J_{ClC}$ 50 Hz, *m*-C), 133.5 (s, *o*-C), 133.3 (q, $^{1}J_{BC}$ 4 Hz, *ipso*-C), 123.4 (s, *p*-C)

Table 4.8. ^{1}H NMR Data for **18a-h** (500.27 MHz, $CDCl_3$).

Compound	PPh_2	P
$[Mo(CO)_3(PPh_2)(PPh_2CH_2CHPh_2)_2]$ $[B(C_6H_3Cl_2)_4]$ (**18a**)	7.90 – 7.13 (overlapping aromatic resonances for PPh_2, and phosphine ligands)	**Major isomer: $Ph_2PCH_2CHPh_2$:** 3.91 (dt, $^{3}J_{PH}$ 15.7, $^{3}J_{HH}$ 5.8 Hz, PCH_2CH), 3.25 (t, $^{3}J_{HH}$ 5.8 Hz, PCH_2CH, 2H) **Minor Isomers: $Ph_2PCH_2CHPh_2$:** 4.21 (dt, $^{3}J_{PH}$ 15.7, $^{3}J_{HH}$ 5.8 Hz, PCH_2CH), 3.42 (t, $^{3}J_{HH}$ 5.8 Hz, PCH_2CH, 2H), 3.99 (dt, $^{3}J_{PH}$ 15.7, $^{3}J_{HH}$ 5.8 Hz, PCH_2CH), 3.18 (t, $^{3}J_{HH}$ 5.8 Hz, PCH_2CH, 2H), 3.81 (ddt, $^{3}J_{PH}$ 15.1, $^{3}J_{HH}$ 5.6 Hz, PCH_2CH), 3.04 (dd,

		$^{3}J_{HH}$ 5.6, $^{2}J_{HH}$ 3.5 Hz, PC$\underline{H_2}$CH, 1H), 2.95 (dd, $^{3}J_{HH}$ 5.6, $^{2}J_{HH}$ 3.5 Hz, PC$\underline{H_2}$CH, 1H)
$[Mo(CO)_3(PPh_2)(PPh_2OCHPh_2)_2][B(C_6H_3Cl_2)_4]$ (**18b**)	7.90 – 7.13 (overlapping aromatic resonances for PPh_2, and phosphine ligands)	Methine H of **P** overlapping with aromatic protons
$[Mo(CO)_3(PPh_2)(PPh_2CH_2CH_2Ph)_2][B(C_6H_3Cl_2)_4]$ (**18c**)	7.61 (t, $^{3}J_{HH}$ 7.6 Hz, *para* of PPh_2), 7.49 (overlapping H_o and H_m of hydrophosphination ligand, 16H), 7.40 – 7.13 (overlapping aromatic resonances for PPh_2, and phosphine ligands)	**Major isomer: $Ph_2PCH_2CH_2Ph$:** 2.72 (m, PC$\underline{H_2}$, 2H), 2.44 (m, $PCH_2C\underline{H_2}$, 2H) **Minor Isomers: $Ph_2PCH_2CH_2Ph$:** 2.50 (m, 1H), 2.31 (s, 2H), 2.44 (1H overlapping with major isomer)
$[Mo(CO)_3(PPh_2)(PPh_2(indenyl))_2][B(C_6H_3Cl_2)_4]$ (**18d**)	7.03 (dd, $^{3}J_{HH}$ 5.6, $^{4}J_{HH}$ 3.2 Hz, 2H, aromatic H from indenyl), 6.85 (dd, $^{3}J_{HH}$ 5.4, $^{4}J_{HH}$ 3.3 Hz, 2H, aromatic H from indenyl), 7.90 – 7.13 (overlapping aromatic resonances for PPh_2, and phosphine ligands	**Major isomer: Ph_2P(indenyl):** 3.34 (m, 1H, PC$\underline{H}$), 3.02 (m, 2H, PCHC$\underline{H_2}$), 2.85 (m, 2H, PCHC$\underline{H_2}$) **Minor isomer: Ph_2P(indenyl):** overlapping peaks 3.60 – 2.75 ppm
$[Mo(CO)_3(PPh_2)(PPh_2CH_2CH_3)_2][B(C_6H_3Cl_2)_4]$ (**18e**)	7.90 – 7.13 (overlapping aromatic resonances for PPh_2, and phosphine ligands	**Major isomer: $Ph_2PCH_2CH_3$:** 2.43 (m, PC$\underline{H_2}$, 2H), 0.87 (m, $PCH_2C\underline{H_3}$, 3H) **Minor isomer $Ph_2PCH_2CH_3$:** 2.55 (m, PC$\underline{H_2}$, 1H), 2.07 (m, PC$\underline{H_2}$, 1H), 0.73 (dt, $^{3}J_{HH}$ 7.3, $^{3}J_{PH}$ 15.2 Hz, $PCH_2C\underline{H_3}$, 3H)
$[Mo(CO)_3(PPh_2)(PPh_2CH_2CH_2CH_3)_2][B(C_6H_3Cl_2)_4]$ (**18f**)	7.90 – 7.13 (overlapping aromatic resonances for PPh_2, and phosphine ligands	**Major isomer: $Ph_2PCH_2CH_3$:** 2.36 (m, PC$\underline{H_2}$, 2H), 1.18 (m, $PCH_2C\underline{H_2}$, 2H), 0.84 (m, $PCH_2CH_2C\underline{H_3}$, 2H) **Minor isomer $Ph_2PCH_2CH_3$:** 2.55 (m, PC$\underline{H_2}$, 1H), 2.07 (m, PC$\underline{H_2}$, 1H), 0.73 (dt, $^{3}J_{HH}$ 7.3, $^{3}J_{PH}$ 15.2 Hz, $PCH_2C\underline{H_3}$, 3H)
$[Mo(CO)_3(PPh_2)(PPh_2(cyclopentyl))_2][B(C_6H_3Cl_2)_4]$ (**18h**)	7.90 – 7.13 (overlapping aromatic resonances for PPh_2, and phosphine ligands	**Major isomer: Ph_2Pcyclopentyl:** 2.66 (m, PC$\underline{H}$, 1H), 1.77 (m, 2H), 1.29 (m, 4H), 1.05 (m, 2H)

	Minor Isomer: Ph_2Pcyclopentyl: overlapping peaks 3.30 – 0.80 ppm

Table 4.9. $^{13}C\{^1H\}$ NMR data for **18a-h** (125.79 MHz, $CDCl_3$)

Compound	**PPh_2**	**P and CO**
$[Mo(CO)_3(PPh_2)(PPh_2CH_2CHPh_2)_2][B(C_6H_3Cl_2)_4]$ (**18a**)	*due to the unassigned ^1H resonances, the aromatic C could not be assigned	**Major isomer: $PPh_2CH_2CHPh_2$:** 48.4 (s, P<u>C</u>H_2), 41.5 (m, PCH_2<u>C</u>H) **Minor isomer: $PPh_2CH_2CHPh_2$:** 48.1 (dd, $^1J_{PC}$ 31, $^2J_{PC}$ 2 Hz, PCH_2<u>C</u>H), 48.0 (dd, $^1J_{PC}$ 25, $^2J_{PC}$ 5 Hz, PCH_2<u>C</u>H), 39.1 (d, $^2J_{PC}$ 20 Hz, P<u>C</u>H_2CH), 36.3 (d, $^2J_{PC}$ 19 Hz, P<u>C</u>H_2CH) **CO**: 209.2 (s), 214.9 (s)
$[Mo(CO)_3(PPh_2)(PPh_2OCHPh_2)_2][B(C_6H_3Cl_2)_4]$ (**18b**)	*due to the unassigned ^1H resonances, the aromatic C could not be assigned	
$[Mo(CO)_3(PPh_2)(PPh_2CH_2CH_2Ph)_2][B(C_6H_3Cl_2)_4]$ (**18c**)	147.4 (s, C_{ipso} of Ph_2PR), 146.7 (s, C_{ipso} of PPh_2), 139.4 (m, C_{ipso} of CH_2CH_2Ph), 134.0 (s, C_p of CH_2CH_2Ph), 132.1 (dd, $^2J_{PC}$ 10, $^3J_{PC}$ 3 Hz), 131.6 (C_o of hydrophosphination ligand, PPh_2R), 129.5 (t, $^3J_{PC}$ 5 Hz, C_m of CH_2CH_2Ph), 128.9 (s), 128.5 (s), 127.8 (s), 127.7 (s, C_o of CH_2CH_2Ph), 127.7 (d, $^2J_{PC}$ 17 Hz) , 127.0 (m)	**Major isomer: $PPhCH_2CH_2Ph$:** 37.3 (m, P<u>C</u>H_2), 30.4 (s, PCH_2<u>C</u>H_2) **CO**: 209.2 (s), 214.9 (s) **Minor isomer: $PPhCH_2CH_2Ph$:** 35.8 (d, $^1J_{PC}$ 21 Hz), 32.1 (d, $^1J_{PC}$ 19 Hz), 30.2 (dd, $^2J_{PC}$ 22, $^3J_{PC}$ 4 Hz, PCH_2<u>C</u>H_2)
$[Mo(CO)_3(PPh_2)(PPh_2(indenyl))_2][B(C_6H_3Cl_2)_4]$ (**18d**)	148.0 (s, C_i of Ph_2PR), 147.0 (s, C_o of PPh_2), 140.1 (t, $^3J_{PC}$ 4 Hz, quaternary C	**Major isomer: PPh_2(indenyl):** 44.5 (m, P<u>C</u>H), 36.1 (s, PCH<u>C</u>H_2), **CO**: 209.5 (m), 214.4 (m)

	of indenyl substitutent), 127.1 (s, aromatic C of indenyl), 124.2 (s, aromatic C of indenyl), 147.0 (s), 132.4 (t, 5 Hz), 131.9 (s), 129.27 (t, 5 Hz), *due to the unassigned ^{1}H resonances, the aromatic C could not be assigned	
$[Mo(CO)_3(PPh_2)(PPh_2CH_2CH_3)_2][B(C_6H_3Cl_2)_4]$ (**18e**)	147.4 (s, C_i of Ph_2PR), 146.7 (s, C_i of PR_2), 133.4 (s), 133.28 (s), 132.2 (dd, J_{PC} 10, 4 Hz), 131.7 (m), 131.29 (s), 129.3 (m) *due to the unassigned ^{1}H resonances, the aromatic C could not be assigned	**Major isomer: $PPh_2CH_2CH_3$:** 28.9 (m, P<u>C</u>H_2), 8.8 (s, PCH_2<u>C</u>H_3), **CO**: 209.2 (m, CO), 214.9 (m, CO) **Minor isomer: $PPh_2CH_2CH_3$:** 28.3 (d, $^{1}J_{PC}$ 22 Hz, P<u>C</u>H_2), 23.8 (d, $^{1}J_{PC}$ 22 Hz, P<u>C</u>H_2), 8.8 (d, $^{2}J_{PC}$ 5 Hz, PCH_2<u>C</u>H_3), 8.5 (d, $^{2}J_{PC}$ 5 Hz, PCH_2<u>C</u>H_3)
$[Mo(CO)_3(PPh_2)(PPh_2CH_2CH_2CH_3)_2][B(C_6H_3Cl_2)_4]$ (**18f**)	148.0 (s, C_i of Ph_2PR), 146.8 (s, C_i of PR_2), 134.4 (m, Ph C_{ipso} of Ph_2P(propyl)), 132.8 (dd, $^{2}J_{PC}$ 9, $^{4}J_{PC}$ 4 Hz), 132.4 – 131.1 (overlapping peaks), 130.3 – 128.9 (overlapping peaks)	**Major isomer: $PPh_2CH_2CH_2CH_3$**: 37.6 (m, P<u>C</u>H_2), 18.1 (s, PCH_2<u>C</u>H_2), 15.3 (s, PCH_2CH_2<u>C</u>H_3), **CO:** 209.2 (m), 214.9 (m)
$[Mo(CO)_3(PPh_2)(PPh_2(cyclopentyl))_2][B(C_6H_3Cl_2)_4]$ (**18h**)	148.1 (s, C_{ipso} of Ph_2PR), 147.0 (s, C_{ipso} of PPh_2), 136.0 – 134.5, 133.5 – 132.5, 132.3 – 127.5 (overlapping peaks) *due to the unassigned ^{1}H	**Major Isomer: PPh_2(cyclopentyl):** 45.0 (m, P<u>C</u>H), 29.5 (s, PCH(<u>C</u>H_2)), 25.9 (m, PCH(CH_2<u>C</u>H_2))

	resonances, the aromatic C could not be assigned		

Table 4.10. $^{31}P\{^{1}H\}$ NMR data for **19a,b** (202.51MHz, CD_2Cl_2).

	Mo-PR$_2$H	**PR$_2$**	**R$_2$P-PR$_2$H**
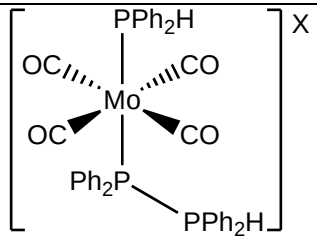	15.4 (br s, $^{1}J_{PH}$ 316 Hz)	82.2 (d, 1J_{PP} 243 Hz)	-3.4 (d, $^{1}J_{PH}$ 425 Hz, $^{1}J_{PP}$ 243 Hz)
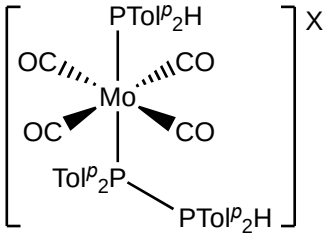	15.4 (br s, $^{1}J_{PH}$ 346 Hz, $^{2}J_{PP}$ 68 Hz)	78.2 (dd, $^{1}J_{PP}$ 235 Hz, $^{2}J_{PP}$ 68 Hz	-4.1 (d, $^{1}J_{PH}$ 443 Hz, $^{1}J_{PP}$ 235 Hz)

4.10. References

(1) Bange, C. A.; Waterman, R. Challenges in Catalytic Hydrophosphination. *Chem. Eur. J.* **2016**, 12598-12605.

(2) Rosenberg, L. Mechanisms of Metal-Catalyzed Hydrophosphination of Alkenes and Alkynes. *ACS Catal.* **2013**, *3*, 2845–2855.

(3) Cowley, A. H.; Kemp, R. A. Synthesis and Reaction Chemistry of Stable Two-Coordinate Phosphorus Cations (Phosphenium ions). *Chem. Rev.* **1985**, *85*, 367–382.

(4) Rosenberg, L. Metal Complexes of Planar PR_2 Ligands: Examining the Carbene Analogy. *Coord. Chem. Rev.* **2012**, *256*, 606–626.

(5) Fleming, S.; Lupton, M. K.; Jekot, K. Synthesis of a Cyclic Fluorodialkylaminophosphine and Its Coordination with Boron Acids. Formation of a Unique Dialkylaminophosphine Cation. *Inorg. Chem.* **1972**, *11*, 2534–2540.

(6) Schultz, C. W.; Parry, R. W. Structure of $[_2((CH_3)_2N)_2PCl].AlCl_3$, $((CH_3)_2N)_3P.((CH_3)_2N)_2PCl.AlCl_3$, and Related Species-Diphosphorus Cations. *Inorg. Chem.* **1976**, *15*, 3046–3050.

(7) Montemayor, R. G.; Sauer, D. T.; Fleming, S.; Bennett, D. W.; Thomas, M. G.; Parry, R. W. Iron Carbonyl Complexes Containing Positively Charged Phosphorus Ligands. *J. Am. Chem. Soc.* **1978**, *100*, 2231–2233.

(8) Nakazawa, H. Transition Metal Complexes Bearing a Phosphenium Ligand. In *Advances in Organometallic Chemistry*; Academic Press, 2004; pp 107–143.

(9) Cowley, A. H.; Kemp, R. A.; Wilburn, J. C. Reaction of (Chlorophosphine)Iron Tetracarbonyl Complexes with Aluminum Chloride. Iron Tetracarbonyl

Complexes of Two-Coordinate Phosphorus Cations. *Inorg. Chem.* **1981**, *20*, 4289–4293.

(10) Nakazawa, H.; Ohta, M.; Miyoshi, K.; Yoneda, H. Reaction of Molybdenum Complexes Containing Phosphite with Boron Trihalides. Formation of Cationic Molybdenum Phosphenium Complexes. *Organometallics* **1989**, *8*, 638–644.

(11) Yamaguchi, Y.; Nakazawa, H.; Itoh, T.; Miyoshi, K. Cationic Phosphenium Complexes of Group 6 Transition Metals. Systematic Approach to Elucidation of Influence of Substituents of the Phosphenium Phosphorus on the Stability of the Complexes. *Bull. Chem. Soc. Jpn.* **1996**, *69*, 983–995.

(12) Muetterties, E. L.; Kirner, J. F.; Evans, W. J.; Watson, P. L.; Abdelmeguid, S.; Tavanaiepour, I.; Day, V. W. Chemistry of Low-Valent Molybdenum Phosphite Complexes: Models of Seven-Coordinate Reaction Intermediates. Proc. Natl. Acad. Sci. U.S.A 75, 1978.

(13) Gudat, D.; Haghverdi, A.; Nieger, M. Complexes with Phosphorus Analogues of Imidazoyl Carbenes: Unprecedented Formation of Phosphenium Complexes by Coordination Induced P−Cl Bond Heterolysis. *J. Organomet. Chem.* **2001**, *617–618*, 383–394.

(14) Bezombes, J.-P.; Carré, F.; Chuit, C.; Corriu, R. J. P.; Mehdi, A.; Reyé, C. Synthesis and Characterization of Functionalized Phosphenium Ions, Stabilized by Two Intramolecular Dative P ← N Bonds. *J. Organomet. Chem.* **1997**, *535*, 81–90.

(15) Carré, F.; Chuit, C.; Corriu, R. J. P.; Mehdi, A.; Reyé, C. N → P Intramolecular Stabilization of Phosphenium Ions and Preparation of Hypercoordinated Phosphanes with Unusual Properties. *J. Organomet. Chem.* **1997**, *529*, 59–68.

(16) Taylor, L. J.; Bühl, M.; Wawrzyniak, P.; Chalmers, B. A.; Woollins, J. D.; Slawin, A. M. Z.; Fuller, A. L.; Kilian, P. Hydride Abstraction and Deprotonation – an Efficient Route to Low Coordinate Phosphorus and Arsenic Species. *Eur. J. Inorg. Chem.* **2016**, *2016*, 659–666.

(17) Snow, S. S.; Jiang, D.-X.; Parry, R. W. Formation of a Nickel Carbonyl Cation Containing a Cyclophosphenium Ligand by Hydride Abstraction. *Inorg. Chem.* **1987**, *26*, 1629–1631.

(18) SooHoo, C. K.; Baxter, S. G. Phosphenium Ions as Dienophiles. *J. Am. Chem. Soc.* **1983**, *105*, 7443–7444.

(19) Cowley, A. H.; Kemp, R. A.; Lasch, J. G.; Norman, N. C.; Stewart, C. A. Reaction of Phosphenium Ions with 1,3-Dienes: A Rapid Synthesis of Phosphorus-Containing Five-Membered Rings. *J. Am. Chem. Soc.* **1983**, *105*, 7444–7445.

(20) Brasch, N. E.; Hamilton, I. G.; Krenske, E. H.; Wild, S. B. π-Ligand Exchange on Phosphenium Ions: Reversible Exchange between Free and Coordinated Alkynes in Phosphirenium Salts. *Organometallics* **2004**, *23*, 299–302.

(21) Unoh, Y.; Hirano, K.; Miura, M. Metal-Free Electrophilic Phosphination/Cyclization of Alkynes. *J. Am. Chem. Soc.* **2017**, *139*, 6106–6109.

(22) King, R. C.; Nilewar, S.; Sterenberg, B. T. Phosphorus-Carbon Bond Forming Reactions of Iron Tetracarbonyl-Coordinated Phosphenium Ions. *J. Organomet. Chem.* **2019**, *880*, 68–74.

(23) Nilewar, S.; Jayaraman, A.; Sterenberg, B. T. Alkyne Insertion into P–C(sp^2) Bonds as a Route to Fused Phospholes: Transition-Metal-Like Reactivity at Phosphorus. *Organometallics* **2018**, *37*, 4699–4710.

(24) Jayaraman, A.; Nilewar, S.; Jacob, T. V; Sterenberg, B. T. Sequential Electrophilic Substitution Reactions of Tungsten-Coordinated Phosphenium Ions and Phosphine Triflates. *ACS Omega* **2017**, *2*, 7849–7861.

(25) Jayaraman, A.; Sterenberg, B. T. Phosphorus–Carbon Bond Forming Reactions of Diphenylphosphenium and Diphenylphosphine Triflate Complexes of Tungsten. *Organometallics* **2016**, *35*, 2367–2377.

(26) Jayaraman, A.; Jacob, T. V; Bisskey, J.; Sterenberg, B. T. Sequential Electrophilic P–C Bond Formation in Metal-Coordinated Chlorophosphines. *Dalton Trans.* **2015**, *44*, 8788–8791.

(27) Burck, S.; Gudat, D.; Nieger, M.; Du Mont, W.-W. P-Hydrogen-Substituted 1,3,2-Diazaphospholenes: Molecular Hydrides. *J. Am. Chem. Soc.* **2006**, *128*, 3946–3955.

(28) Chong, C. C.; Kinjo, R. Hydrophosphination of CO2 and Subsequent Formate Transfer in the 1,3,2-Diazaphospholene-Catalyzed N-Formylation of Amines. *Angew. Chem. Int. Ed.* **2015**, *54*, 12116–12120.

(29) Hynes, T.; Welsh, E. N.; McDonald, R.; Ferguson, M. J.; Speed, A. W. H. Pyridine Hydroboration with a Diazaphospholene Precatalyst. *Organometallics* **2018**, *37*, 841–844.

(30) Adams, M. R.; Tien, C.-H.; Huchenski, B. S. N.; Ferguson, M. J.; Speed, A. W. H. Diazaphospholene Precatalysts for Imine and Conjugate Reductions. *Angew. Chem. Int. Ed.* **2017**, *56*, 6268–6271.

(31) Moiseev, D. V; Marcazzan, P.; James, B. R. Reversible Decomposition of Mono(α-Hydroxy)Phosphines and Their Reaction with α,β-Unsaturated

Aldehydes. *Can. J. Chem.* **2009**, *87*, 582–590.

(32) Campbell, T.; Gibson, A. M.; Hart, R.; Orchard, S. D.; Pope, S. J. A.; Reid, G. Synthesis, Spectroscopic and Structural Characterisation of Chromium(0), Molybdenum(0) and Tungsten(0) Complexes Involving Primary and Secondary Phosphines. *J. Organomet. Chem.* **1999**, *592*, 296–305.

(33) Darensbourg, D. J.; Kump, R. L. A Convenient Synthesis of Cis-Mo(CO)4L2 Derivatives (L = Group 5a Ligand) and a Qualitative Study of Their Thermal Reactivity toward Ligand Dissociation. *Inorg. Chem.* **1978**, *17*, 2680–2682.

(34) Tolman, C. A. Steric Effects of Phosphorus Ligands in Organometallic Chemistry and Homogeneous Catalysis. *Chem. Rev.* **1977**, *77*, 313–348.

(35) Hutchins, L. D.; Paine, R. T.; Campana, C. F. Structure and Bonding in a Phosphenium Ion-Metal Complex, $CH_3NCH_2CH_2N(CH_3)PMo(\eta^5\text{-}C_5H_5)(CO)_2$. An Example of a Molybdenum-Phosphorus Multiple Bond. *J. Am. Chem. Soc.* **1980**, *102*, 4521–4523.

(36) Dahlenburg, L.; Höck, N.; Berke, H. Oligophosphan-Liganden, XXIX. Chelatphosphan-Stabilisierte Rhodium(I)-Komplexe Mit Terminalen Phosphido-Liganden: Synthese, Reaktionen Und Elektronenstruktur. *Chem. Ber.* **1988**, *121*, 2083–2093.

(37) Baker, R. T.; Calabrese, J. C.; Harlow, R. L.; Williams, I. D. New (η^5-C_5Me_5)M(PR_2)x Complexes (M = Tantalum, Molybdenum, and Tungsten): Reversible P-H Bond Activation, sp^3 C-H Bond Activation, and P-C Bond Formation. *Organometallics* **1993**, *12*, 830–841.

(38) Cowley, A. H.; Giolando, D. M.; Nunn, C. M.; Pakulski, M.; Westmoreland, D.;

Norman, N. C. Synthesis and Reactivity of Mononuclear Molybdenum Phosphido Complexes, $[Mo(CO)_2\{P(Cl)R\}(\eta^5\text{-}C_5H_5)][R = CH(SiMe_3)_2$ or $NCMe_2CH_2CH_2CH_2CMe_2]$. X-Ray Crystal Structures of $[Mo(CO)_2\{P(X)(NCMe_2CH_2CH_2CH_2CMe_2)\}(\eta^5\text{-}C_5H_5)](X = Cl$ or $NMe_2)$ and $[Mo_2(CO)_4\{\mu\text{-}P_2[CH(SiMe_3)_2]$. *J. Chem. Soc. Dalton Trans.* **1988**, *8*, 2127–2134.

(39) Hering, C.; Schulz, A.; Villinger, A. On the Synthesis and Reactivity of Highly Labile Pseudohalogen Phosphenium Ions. *Inorg. Chem.* **2013**, *52*, 5214–5225.

(40) Breit, B. Probing New Classes of π-Acceptor Ligands for Rhodium Catalyzed Hydroformylation of Styrene. *J. Mol. Catal. A Chem.* **1999**, *143*, 143–154.

(41) Gudat, D.; Haghverdi, A.; Hupfer, H.; Nieger, M. Stability and Electrophilicity of Phosphorus Analogues of Arduengo Carbenes—An Experimental and Computational Study. *Chem. Eur. J.* **2000**, *6*, 3414–3425.

(42) Van Ausdall, B. R.; Cuddy, M. F.; Southern, J. S.; Wheeler, K. A.; Keiter, E. A.; Treadwell, E. M.; Keiter, R. L. Three Isomers in Equilibrium: Phosphine Exchange of Coordinated and Pendant Phosphines in a Unique Complex, $(OC)_5WL$ (L = 1,2-Bis(Diphenylphosphino)-1-Di-p-Tolylphosphinoethane), and Implications for Understanding the k_2 Term in the Rate Law for Phosphine Substitution in Group 6 Metal Carbonyl Complexes. *Organometallics* **2018**, *37*, 3742–3749.

(43) Nakazawa, H.; Yamaguchi, Y.; Mizuta, T.; Miyoshi, K. Cationic Phosphenium Complexes of Group 6 Transition Metals: Reactivity, Isomerization, and X-Ray Structures. *Organometallics* **1995**, *14*, 4173–4182.

(44) Thomas, C. M.; Hatzis, G. P.; Pepi, M. J. Examining the Effects of Variations in

Ligand Framework and Pnictogen Substitution on the Geometry and Electronic Structure of Metal Complexes of N-Heterocyclic Phosphido Ligands Incorporated into a Diphosphine Pincer Ligand Framework. *Polyhedron* **2018**, *143*, 215–222.

(45) Burck, S.; Gudat, D. Structural Alternatives for the Formation of Halogenophosphine-Phosphenium Complexes. *Inorg. Chem.* **2008**, *47*, 315–321.

(46) Dobrovetsky, R.; Takeuchi, K.; Stephan, D. W. Metal-Free Lewis Acid Mediated Dehydrocoupling of Phosphines and Concurrent Hydrogenation. *Chem. Commun.* **2015**, *51*, 2396–2398.

(47) Heiden, Z. M.; Lathem, A. P. Establishing the Hydride Donor Abilities of Main Group Hydrides. *Organometallics* **2015**, *34*, 1818–1827.

(48) Welch, G. C.; Prieto, R.; Dureen, M. A.; Lough, A. J.; Labeodan, O. A.; Höltrichter-Rössmann, T.; Stephan, D. W. Reactions of Phosphines with Electron Deficient Boranes. *Dalton Trans.* **2009**, *9*, 1559–1570.

(49) Lancaster, S. J.; Mountford, A. J.; Hughes, D. L.; Schormann, M.; Bochmann, M. Ansa-Metallocenes with B−N and B−P Linkages: The Importance of N−H···F−C Hydrogen Bonding in Pentafluorophenyl Boron Compounds. *J. Organomet. Chem.* **2003**, *680*, 193–205.

(50) Pan, B.; Bezpalko, M. W.; Foxman, B. M.; Thomas, C. M. Heterolytic Addition of E-H Bonds across Pt-P Bonds in Pt N-Heterocyclic Phosphenium/Phosphido Complexes. *Dalton Trans.* **2012**, *41*, 9083–9090.

(51) Pan, B.; Xu, Z.; Bezpalko, M. W.; Foxman, B. M.; Thomas, C. M. N-Heterocyclic Phosphenium Ligands as Sterically and Electronically-Tunable Isolobal Analogues of Nitrosyls. *Inorg. Chem.* **2012**, *51*, 4170–4179.

(52) Knight, S. E.; Bezpalko, M. W.; Foxman, B. M.; Thomas, C. M. Coordination of N-Heterocyclic Phosphine- and Phosphenium-Containing Pincer Ligands to Copper(I): Evidence for Reactive Electrophilic Metal–Phosphenium Intermediates. *Inorg. Chim. Acta* **2014**, *422*, 181–187.

(53) Hoyle, M.-A. M.; Pantazis, D. A.; Burton, H. M.; McDonald, R.; Rosenberg, L. Benzonitrile Adducts of Terminal Diarylphosphido Complexes: Preparative Sources of "Ru═PR2." *Organometallics* **2011**, *30*, 6458–6465.

(54) Burford, N.; Ragogna, P. J.; McDonald, R.; Ferguson, M. J. Phosphine Coordination Complexes of the Diphenylphosphenium Cation: A Versatile Synthetic Methodology for P−P Bond Formation. *J. Am. Chem. Soc.* **2003**, *125*, 14404–14410.

(55) Burford, N.; Cameron, T. S.; Ragogna, P. J.; Ocando-Mavarez, E.; Gee, M.; McDonald, R.; Wasylishen, R. E. Phosphine Ligand Exchange at a Phosphine Lewis Acceptor: The First Structural Characterization of Homoleptic Phosphinophosphonium Salts. *J. Am. Chem. Soc.* **2001**, *123*, 7947–7948.

(56) Chitnis, S. S.; Burford, N. Phosphine Complexes of Lone Pair Bearing Lewis Acceptors. *Dalton Trans.* **2015**, *44*, 17–29.

(57) Eismann, U.; Spange, S. Cationic Initiation of Vinyl Ether Polymerization Induced by (4-RC_6H_4)(4-RC_6H_4)RCX in Conjunction with Silica: Producing Highly Head Group Functionalized Polymers. *Macromolecules* **1997**, *30*, 3439–3446.

(58) Tate, D. P.; Knipple, W. R.; Augl, J. M. Nitrile Derivatives of Chromium Group Metal Carbonyls. *Inorg. Chem.* **1962**, *1*, 433–434.

(59) Chaplin, A. B.; Weller, A. S. [B(3,5-$C_6H_3Cl_2$)$_4$]– as a Useful Anion for

Organometallic Chemistry. *Eur. J. Inorg. Chem.* **2010**, *2010*, 5124–5128.

(60) Kulinna, H.; Spaniol, T. P.; Maron, L.; Okuda, J. Cationic Zirconium Hydrides Supported by an NNNN-Type Macrocyclic Ligand: Synthesis, Structure, and Reactivity. *Inorg. Chem.* **2012**, *51*, 12462–12472.

Chapter 5 Investigating the Lewis Acidity of and Hydrosilylation Catalysis by Complexes 12a,b

5.1. Chapter Overview

In this chapter, the Lewis acidity and Lewis acidic reactivity of the phosphenium complexes *trans*-[Mo(CO)$_4$(PTol$_2^p$H)(PTol$_2^p$)][B(C$_6$H$_3$Cl$_2$)$_4$] (*trans*-**12a**[B(C$_6$H$_3$Cl$_2$)$_4$]), *trans*-[Mo(CO)$_4$(PPh$_2$H)(PPh$_2$)][B(C$_6$H$_3$Cl$_2$)$_4$] (*trans*-**12b**[B(C$_6$H$_3$Cl$_2$)$_4$]) is described. A detailed study of the reaction of triethylsilane, HSiEt$_3$, with **12a** is presented, which includes variable temperature (VT) NMR and computational data. The η^1-HSiEt$_3$ adduct of **12a**, [Mo(CO)$_4$(PR$_2$H)(R$_2$P•••H•••SiEt$_3$)][B(C$_6$H$_3$Cl$_2$)$_4$] (**20a**), was identified spectroscopically. Furthermore, I determined that complex **20a** undergoes reversible Si-H bond activation via a deuterium-labelling experiment. A preliminary study on the utility of these phosphenium complexes for the hydrosilylation of unsaturated substrates is described. Mechanistic and kinetic analysis of the hydrosilylation of 1-hexene with HSiEt$_3$ catalyzed by **12b** is discussed. This Chapter includes contributions from Dr. Dimitrios Pantazis. Supplementary spectra are presented in Appendix I.

5.2. Introduction

Hydrosilanes (HSiR$_3$) are ubiquitous chemicals that are widely used as reductants in organic synthesis. Common reactions of hydrosilanes include hydrosilylation of unsaturated substrates,[1–3] homo-[4] and hetero-dehydrocoupling[5] and dealkylative coupling[6] (Scheme 5.1), catalyzed by both transition metals and main group Lewis acids. The

literature on these reactions of hydrosilanes is extensive. This Chapter will specifically focus on main group Lewis acid-catalyzed hydrosilylation.

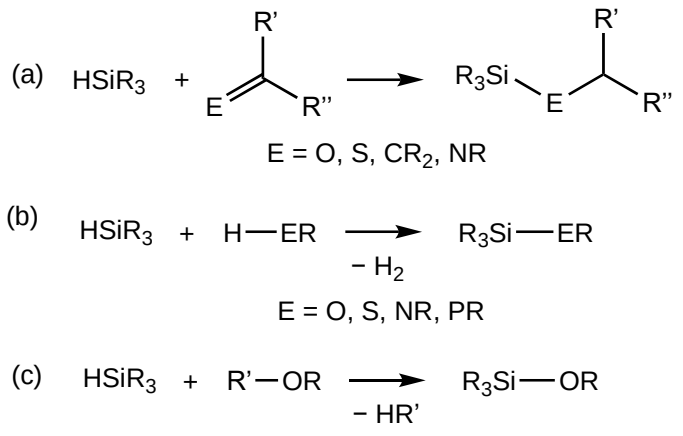

Scheme 5.1. General reactions of hydrosilanes: (a) hydrosilylation, (b) dehydrocoupling and (c) dealkylative coupling.

5.2.1. Lewis Acid Catalyzed Hydrosilylation

An early example of Lewis acid catalyzed hydrosilylation was reported by Yamamoto *et al* where they investigated a variety of Lewis acids for the hydrosilylation of alkynes.[7] The authors found that Al Lewis acids ($AlCl_3$ and $EtAlCl_2$) are efficient catalysts for this reaction. The proposed mechanism involves addition of the C−C multiple bond to the Lewis acid, which generates a zwitterionic intermediate (Scheme 5.2, step A). The carbocation in this intermediate is quenched by a hydride from the substrate silane, which generates a silylium, R_3Si^+ (step B). Subsequent transmetallation generates the hydrosilylation product and regenerates the neutral catalyst (step C).

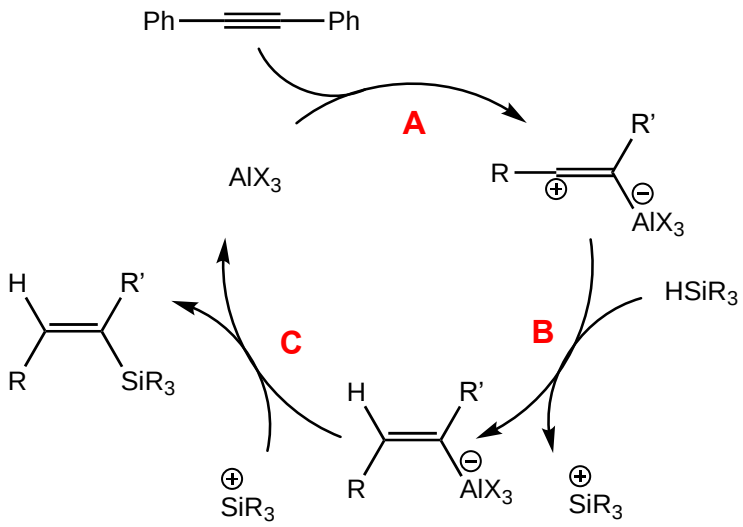

Scheme 5.2. Proposed mechanism for AlR_3-catalyzed hydrosilylation of alkynes.

Lambert *et al* reported a Lewis acid-initiated hydrosilylation using $[Ph_3C][B(C_6F_5)_4]$ (Scheme 5.3).[8,9] In this example, Ph_3C^+ activates triethylsilane, $HSiEt_3$, by irreversible hydride abstraction (step A). This generates a triethylsilylium cation, Et_3Si^+, which is stabilized by the formation of an adduct with the aromatic solvent, $[Et_3Si(arene)]^+$ (e.g. benzene, toluene). Nucleophilic addition of alkenes to Et_3Si^+ generates a carbocation intermediate (step B), which abstracts a hydride from another equivalent of silane (step C). This completes the cycle by regenerating Et_3Si^+. This is an example where the Lewis acid initiates, rather than catalyzes, the hydrosilylation through irreversible Si-H bond activation. The hydrosilylation is catalyzed by the silylium.

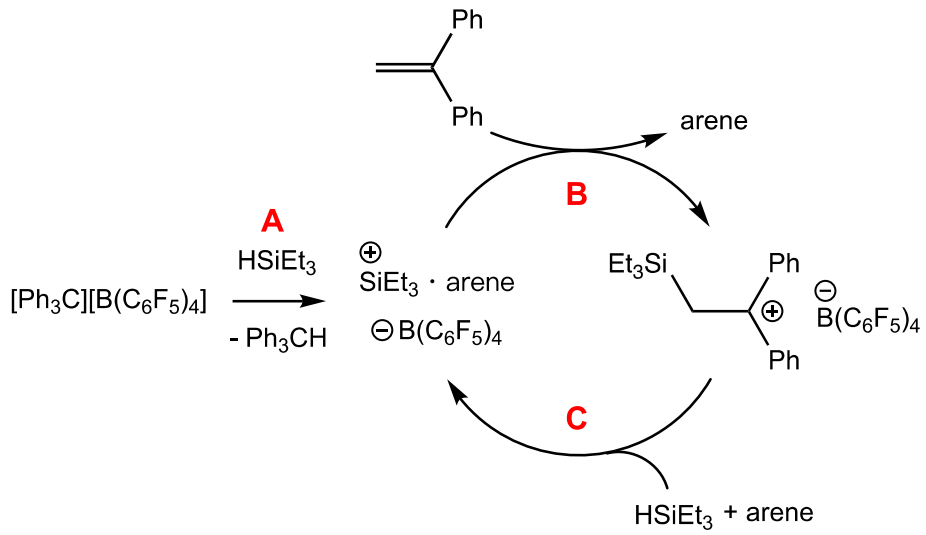

Scheme 5.3. Proposed mechanism for $[Ph_3C][B(C_6F_5)_4]$-initiated hydrosilylation of alkenes.

Since these early examples, growing interest in main group Lewis acid catalysis has led to the widespread use of the Lewis acidic borane tris(pentafluorophenyl)borane, $B(C_6F_5)_3$.[10,11] In particular, $B(C_6F_5)_3$ has been widely used as a Lewis acid catalyst for the hydrosilylation of unsaturated substrates.[12] Notable examples include the work of Piers *et al* who showed that $B(C_6F_5)_3$ can catalyze the hydrosilylation of aromatic aldehydes, ketones, esters and imines.[13–17] Our group extended this strategy to include $B(C_6F_5)_3$-catalyzed hydrosilylation of poly(phenylsilane) and disilanes with alkenes, aldehydes, ketones, imines and thioketones.[6,18,19]

The proposed mechanism of $B(C_6F_5)_3$-catalyzed hydrosilylation (Scheme 5.4) differs from the two mechanisms described above. $B(C_6F_5)_3$ reversibly activates silanes through η^1 coordination of the hydridic Si-H bond to the empty p-orbital of the borane (step A).[20] The Si-H bond is polarized in this adduct such that unsaturated substrates can attack the

nascent electropositive silylium, which generates a carbocation intermediate and $[HB(C_6F_5)_3]^-$ (step B).[21] Subsequent hydride transfer from the borate anion, $[HB(C_6F_5)_3]^-$, to the carbocation generates the hydrosilylation product and regenerates $B(C_6F_5)_3$ (step C).

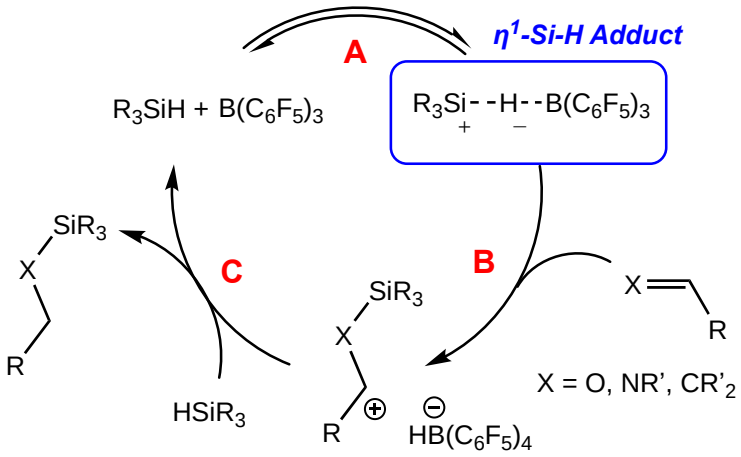

Scheme 5.4. Proposed mechanism for the hydrosilylation of unsaturated substrates by $B(C_6F_5)_3$.

A key intermediate of the proposed mechanism for $B(C_6F_5)_3$-catalyzed hydrosilylation is the η^1-Si-H adduct of the borane. Evidence for this intermediate comes from a report by Piers *et al* where they isolated the η^1-$HSiEt_3$ adduct of a Lewis acidic perfluoroboraindene.[22] A diagnostic spectroscopic feature of this adduct is the diminished $^1J_{SiH}$ coupling of the silane upon coordination to the Lewis acid. This intermediate has been identified for other main group Lewis acid ($Al(C_6F_5)_3$,[23] and described below for $[FP(C_6F_5)_3][B(C_6F_5)_4]$).

5.2.2. P-Based Lewis Acids

Recently, research in the field of main group Lewis acids[24] has extended to P-based compounds.[25] In particular, P(V) Lewis acids have proven to be very efficient catalysts for many Lewis acid-catalyzed reactions. This area has been pioneered by Stephan *et al* who showed that the fluorophosphonium cation $[FP(C_6F_5)_3][B(C_6F_5)_4]$ is a highly active Lewis acid catalyst for hydrosilylation, olefin isomerization, hydrodefluorination, dehydrocoupling and hydrogenation.[26–28] The proposed mechanism for hydrosilylation of alkenes catalyzed by $[FP(C_6F_5)_3][B(C_6F_5)_4]$ closely resembles that of $B(C_6F_5)_3$-catalyzed hydrosilylation (Scheme 5.5). The Si-H bond of hydrosilanes is activated through the formation of an adduct with an empty, low-lying σ^*-orbital of the phosphonium catalyst.

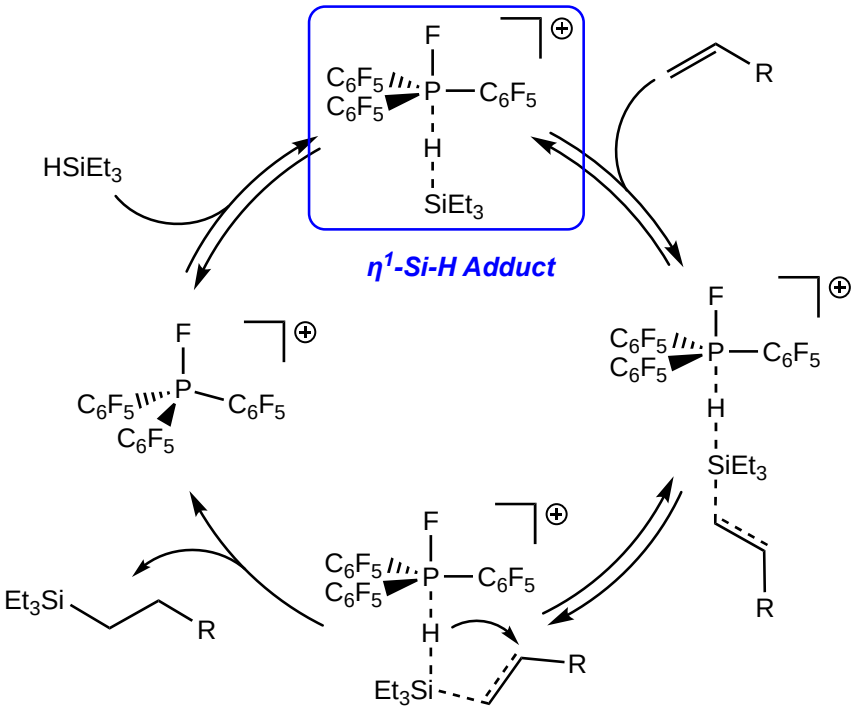

Scheme 5.5. Proposed mechanism for the hydrosilylation of alkenes catalyzed by the fluorophosphonium $[FP(C_6F_5)_3][B(C_6F_5)_4]$.

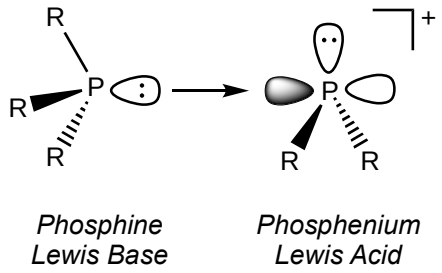

Figure 5.1. General structure of a phosphine-stabilized phosphenium, which demonstrates how a P(III) compound can be a Lewis base (phosphines) or a Lewis acid (phospheniums).

P(III) compounds are traditionally viewed as Lewis bases (ligands for metals) or nucleophiles (Wittig reaction), but many examples of P(III) electrophiles or Lewis acids have been reported.[29] For example, Burford *et al* have studied the electrophilicity of phosphine-stabilized phospheniums (Figure 5.1) and bipyridine-stabilized P(III) cations.[30] Only a few examples exist of P(III) Lewis acids as catalysts, which are largely limited to N-heterocyclic phosphines.[31–33] As discussed in Chapter 4, Gudat has demonstrated the stoichiometric, electrophilic reactivity of 1,3,2-diazaphospholenes, a masked-phosphenium.[34] Recently, Stephan *et al* have utilized bipyridine- and terpyridine-stabilized P(III) dications as Lewis acid catalysts for the hydrosilylation of alkenes, ketones and aldehydes[35] as well as for hydrodefluorination of C-F bonds with hydrosilanes (Scheme 5.6).[36]

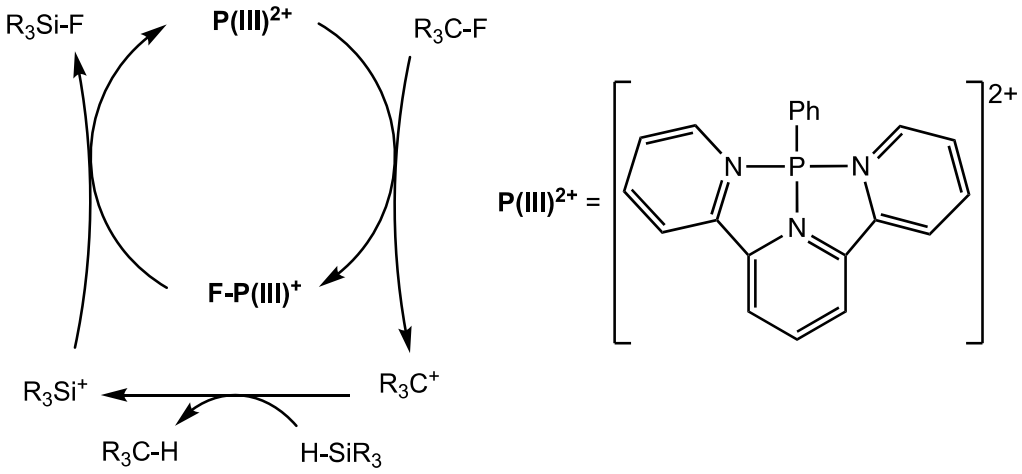

Scheme 5.6. Proposed mechanism for the hydrodefluorination of C-F bonds with hydrosilanes catalyzed by P(III) dications.

5.2.3. Rationale for Investigating Lewis Acidic Reactivity of Complexes 12a,b in Reactions with Hydrosilanes

As described in Chapter 4, phospheniums are electrophilic P(III) species. The electrophilicity of phospheniums arises from the presence of an empty *p*-orbital at P (Figure 5.1). This feature of phospheniums makes them Lewis acids as well. Electrophilicity and Lewis acidity are often used interchangeably, but there is a subtle difference. Electrophilicity is used in discussions of reactivity and kinetics, whereas Lewis acidity refers to thermodynamic properties.[37] Thus, given that phospheniums are Lewis acids, we wanted to investigate the Lewis acidity of complexes **12a**,**b**. Complexes **12a**,**b** are unique because the Lewis acid is coordinated to a metal, which is also Lewis acidic. Furthermore, within the complex there is a coordinated PR_2H, which could act as a hydride source. Thus, studying complexes **12a**,**b** will provide insight on whether the features described above have implications on reactivity of the Lewis acidic phosphenium ligands. Further

motivation for this study comes from the growing literature on P-based Lewis acids, which, as stated above, includes very few examples of P(III) Lewis acid catalysts. Last, the phosphenium ligands of **12a**,**b** are non-donor stabilized P(III) cations, whereas most examples of P(III) cations/Lewis acids are donor stabilized. Demonstrating that complexes **12a**,**b** can be Lewis acid catalysts for hydrosilylation would add a significant contribution to existing literature on P-based Lewis acid catalysis.

5.3. Assessing the Lewis Acidity and Lewis Acidic Reactivity of Complexes 12a,b

In this section, measurement of the Lewis acidity of complexes **12a**,**b** is described. This was measured using two methods. The Gutmann-Beckett Method is an experimental measurement of Lewis acidity and the Global Electrophilicity Index is a computational method. A reactivity study is also presented, which demonstrates that **12a**,**b** are Lewis acidic.

5.3.1. Measuring the Acceptor Number of Complexes 12a,b Using the Gutmann-Becket Method

The Gutmann-Beckett Method is an experimental method for determining the Lewis acidity of a compound.[38–40] It involves measuring the change in the ^{31}P NMR chemical shift of triethylphosphine oxide (TEPO) in the presence of the Lewis acid of interest. The ^{31}P NMR chemical shift of TEPO is very sensitive to the chemical environment because the O of TEPO can coordinate to Lewis acids, which deshields the P nucleus of TEPO. Lewis acidity assessed by this method is characterized by a parameter called the Acceptor Number (AN), which is defined by:

$$AN = 2.21(\delta_{sample} - 41.0)$$

$$= \frac{(\delta_{sample} - 41.0)}{(\delta_{SbCl5} - 41.0)} \text{ x } 100$$

where δ_{sample} is the ^{31}P NMR chemical shift of TEPO in the presence of a Lewis acid and 41.0 is the ^{31}P NMR chemical shift of TEPO in hexane (AN = 0). This measurement is a percentage relative to the chemical shift of TEPO in $SbCl_5$ (AN = 100), 86.14 ppm, which accounts for the 2.21 factor shown in the equation. A higher AN indicates a more Lewis acidic compound.

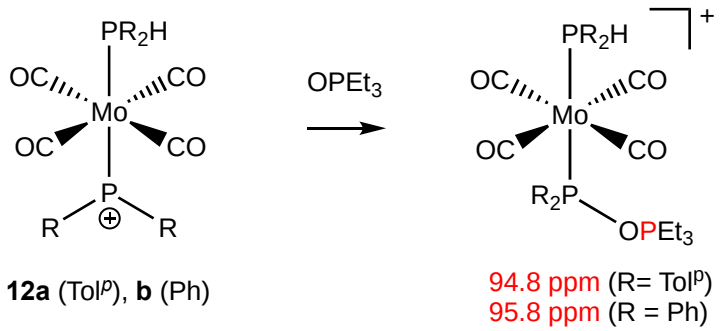

Scheme 5.7. Addition of TEPO to complexes **12a,b**.

As expected, addition of TEPO to complexes **12a**,**b** results in coordination of TEPO to the phosphenium ligands of **12a**,**b** (Scheme 5.7). The ^{31}P{^{1}H} NMR chemical shifts for the phosphenium-coordinated TEPO are 94.8 and 95.8 ppm, which correspond to AN of 119 and 121 for **12a** and **12b**, respectively. These AN values are extremely high compared to other main group Lewis acids like boranes or borenium cations.[41] For example, the commonly used Lewis acid $B(C_6F_5)_3$ has an AN of 82.[42] The AN of **12a** is slightly lower

than **12b**. This is attributed to the more electron-rich and donating *p*-tolyl substituents of **12a** relative to the phenyl substituents of **12b**, which reduces the Lewis acidity of **12a**.

5.3.2. Calculating the Global Electrophilicity Index of Complexes 12a,b

Our computational collaborator Dr. Dimitrios Pantazis calculated the Global Electrophilicity Index (GEI)[43,44] of the phosphenium complexes **12a**,**b**. Computational details are summarized in section 4.4.3. The GEI, ω, is effectively the measure of the ability of a molecule to accept two electrons, defined by:

$$\omega = \mu^2/2\eta = \chi^2/2\eta$$

where μ is the chemical potential, which is the negative of electronegativity (χ), and η is the hardness ($1/\eta$ is softness). Hardness is described as the resistance of the chemical potential to change in the number of electrons.[45,46] This concept relates to hard-soft acid-base theory, which describes the polarizability of acids and bases.[47] The GEI, as well as μ and η, can simply be calculated from the energy of the highest occupied molecular orbital (HOMO) and the lowest unoccupied molecular orbital (LUMO) of a molecule because:

$$\mu = \frac{1}{2}(E_{HOMO} + E_{LUMO})$$

$$\eta = E_{LUMO} - E_{HOMO}$$

From the optimized structures and calculated E_{HOMO} and E_{LUMO} of **12a**,**b** described in section 4.4.3, the GEI for complexes **12a**,**b** were calculated. The GEI for **12a**,**b** are 10.075 and 10.665 eV, respectively. These results are consistent with the Gutmann-Beckett analysis, which showed that **12b** is more Lewis acidic than **12a** (higher GEI means more Lewis acidic). These values are very high, but it is important to note that cationic species will always have higher GEI values than neutral species. For example, the GEI of $B(C_6F_5)_3$, $[FP(C_6F_5)_3]^+$ and Ph_3C^+ are 1.408, 3.622 and 3.982 eV, respectively.

5.3.3. Reaction of Complexes 12a,b with THF

Addition of THF to complexes **12a**,**b** in CD_2Cl_2 results in coordination of THF to the phosphenium ligand and subsequent ring-opening polymerization. In the $^{31}P\{^1H\}$ NMR spectrum of this reaction with **12a**, two doublets are observed at 147.8 and 18.0 ppm ($^2J_{PP}$ 22 Hz). The doublet at 18.0 ppm is due to the coordinated PPh_2H ligand because in the ^{31}P NMR spectrum it exhibits a $^1J_{PH}$ coupling (325 Hz). The doublet at 147.8 ppm does not have a $^1J_{PH}$ coupling. Due to the downfield chemical shift this signal is assigned as the THF-coordinated phosphenium ligand. This chemical shift is consistent with Mo-bound phosphines that contain -OR substituents.[48] Addition of THF to **12b** produced a similar $^{31}P\{^1H\}$ spectrum. In both cases, the solutions had turned into a gel within an hour, which suggests that the THF had polymerized. Presumably this occurs through cationic ring-opening polymerization, initiated via coordination of THF to the phosphenium ligand of complexes **12a**,**b** (Scheme 5.8). Lewis acid-initiated polymerization of THF is known, which proceeds via the coordination of THF to the Lewis acid, similar to what is shown in Scheme 5.8. [49,50] The $^{31}P\{^1H\}$ spectra for these reactions are presented in Appendix I.

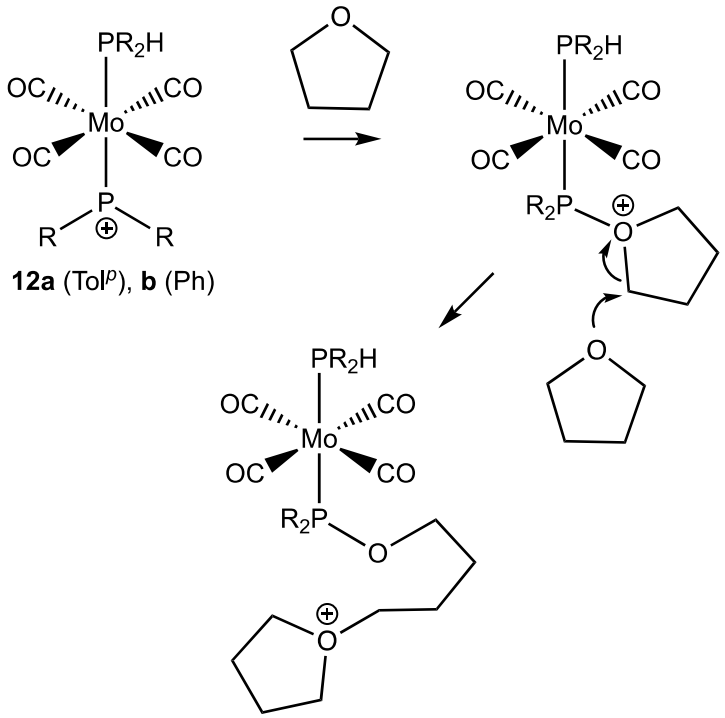

Scheme 5.8. Cationic polymerization of THF initiated by complexes **12a,b**.

5.4. Reactivity of $HSiEt_3$ with Complexes 12a,b

In this section the reactivity of complexes **12a**,**b** with $HSiEt_3$ is described. The results of a variable temperature (VT) NMR study suggest that $HSiEt_3$ forms an η^1-Si-H adduct with the phosphenium ligand of **12a** to give the complex *cis*-$[Mo(CO)_4(PTol^p{}_2H)(Tol^p{}_2P\bullet\bullet\bullet H\bullet\bullet\bullet SiEt_3\})]^+$ (**20a**). Furthermore, the results of a VT NMR study using $DSiEt_3$ suggest that reversible Si-H bond activation occurs via the formation of **20a**.

5.4.1. Addition of $HSiEt_3$ to Complexes 12a,b

Addition of $HSiEt_3$ to complexes **12a**,**b** in CD_2Cl_2 results in a colour change of the solution from dark green to yellow. The ^1H NMR spectra show that the Si-H resonance of $HSiEt_3$ and the P-H resonance of complexes **12a**,**b** are broad. Furthermore, for the reaction of **12a** the resonances for the -CH_3 of the *p*-tolyl substituents of the $PTol^p_2$ and $PTol^p_2H$ ligands have coalesced; these resonances are chemically inequivalent in **12a**. The $^{31}P\{^1H\}$ NMR spectrum shows two overlapping broad resonances from 15 to − 15 ppm (Figure 5.2) and the diagnostic downfield signals of the phosphenium ligands are gone. Additional signals appear in the $P\{^1H\}$ NMR spectrum, which are unassigned (* in Figure 5.2). Based on these NMR experiments, I proposed that $HSiEt_3$ interacts with the phosphenium ligands in **12a**,**b**, possible by forming the η^1-Si-H adducts $[Mo(CO)_4(PR_2H)(R_2P\bullet\bullet\bullet H\bullet\bullet\bullet SiEt_3\})]^+$ (**20a**, R = Tol^p; **20b**, R = Ph). The addition of $HSiEt_3$ to **12b** was monitored by electrospray ionization mass spectrometry (ESI-MS) (performed by graduate student Sofia Donnecke in Prof. Scott McIndoe's group in our department). A positively charged species with an *m/z* and isotope pattern consistent with the sum of **12b** and $HSiEt_3$ (also consistent with **20b**) was observed (Figure 5.3).

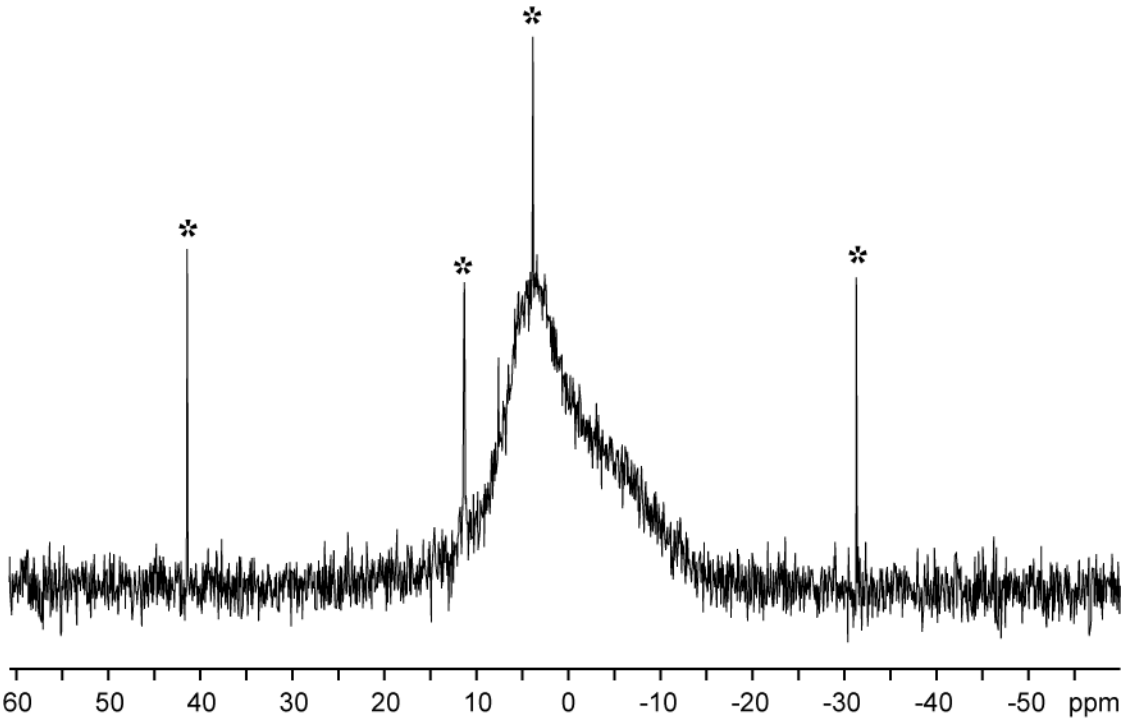

Figure 5.2. $^{31}P\{^{1}H\}$ NMR spectrum of the mixture resulting from the addition of $HSiEt_3$ to **12a** (CD_2Cl_2, 145.85 MHz). Unassigned peaks labelled (*).

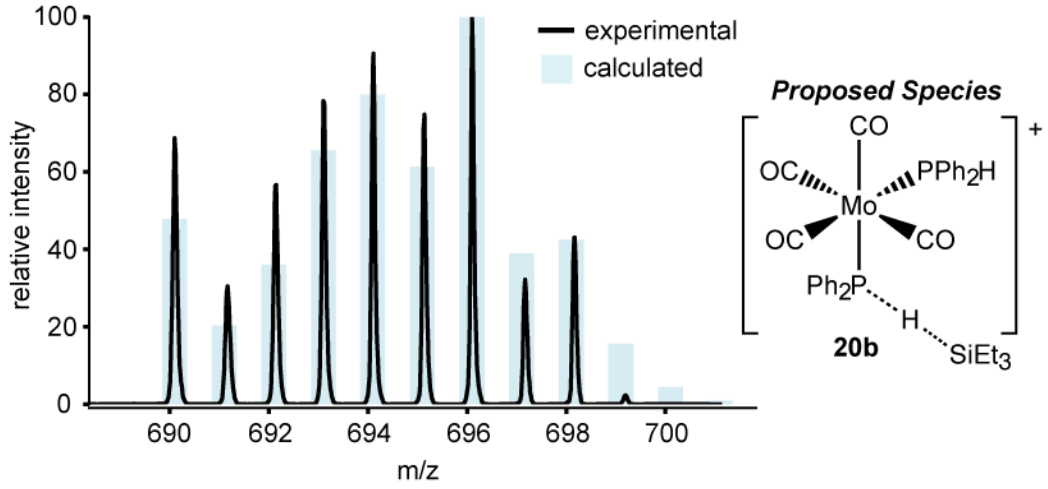

Figure 5.3. Mass spectrum (ESI-MS, positive ion mode) of the reaction solution from the addition of $HSiEt_3$ to complex **12b**. Experimental data (line) and predicted isotope pattern (bars) for $C_{34}H_{37}O_4SiP_2Mo$ (e.g. **12b**•$HSiEt_3$)are overlayed.

5.4.2. Low Temperature NMR Study of the Addition of $HSiEt_3$ and $DSiEt_3$ to 12a,b

This NMR study was conducted in order to investigate the reaction of $HSiEt_3$ with complex **12a**. Based on the ESI-MS data described above, I anticipated that this study would provide additional evidence for the formation of the complex $[Mo(CO)_4(PTol^p{}_2H)(Tol^p{}_2P\bullet\bullet\bullet H\bullet\bullet\bullet SiEt_3\})]^+$ (**20a**). Complex **12a** was chosen for this study because the Me groups of the *p*-tolyl substituents could possibly be diagnostic NMR handles. ^1H and $^{31}P\{^1H\}$ NMR spectra were collected at temperatures ranging from 298 K (room temperature) to 183 K (−90°C). The ^1H NMR spectra from this VT NMR study are shown in Appendix H.

The broad, overlapping $^{31}P\{^1H\}$ signals observed at room temperature for this reaction (Figure 5.2) decoalesce at 238 – 258 K to give two broad peaks that resolve as doublets at 183 K (Figure 5.4, left). In the ^{31}P NMR spectrum at 183 K, both of these doublets exhibit a $^1J_{PH}$ coupling (346 and 344 Hz), which suggests that both P nuclei have a P-H bond. This set of doublets is tentatively assigned as the η^1-$HSiEt_3$ adduct of **12a**, *cis*-**20a**. Complex **20a** is assigned as the cis isomer based on the $^2J_{PP}$ coupling constant (23 Hz). At ~ 218 K, an additional signal assigned as **10a** is observed, which results from a second decoalescence. In the ^1H NMR spectra collected at all temperatures, the signals assigned as the *p*-Me groups in the product complex remain coalesced. Broad peaks assigned as the P-H resonances decoalesce at 218 K to give two sets of signals that are assigned as distinct P-H protons. In complex **20a** there would be one P-H for the coordinated $PTol^p{}_2H$ and another P-H for the $PTol^p{}_2$ involved in the η^1-$HSiEt_3$ adduct.

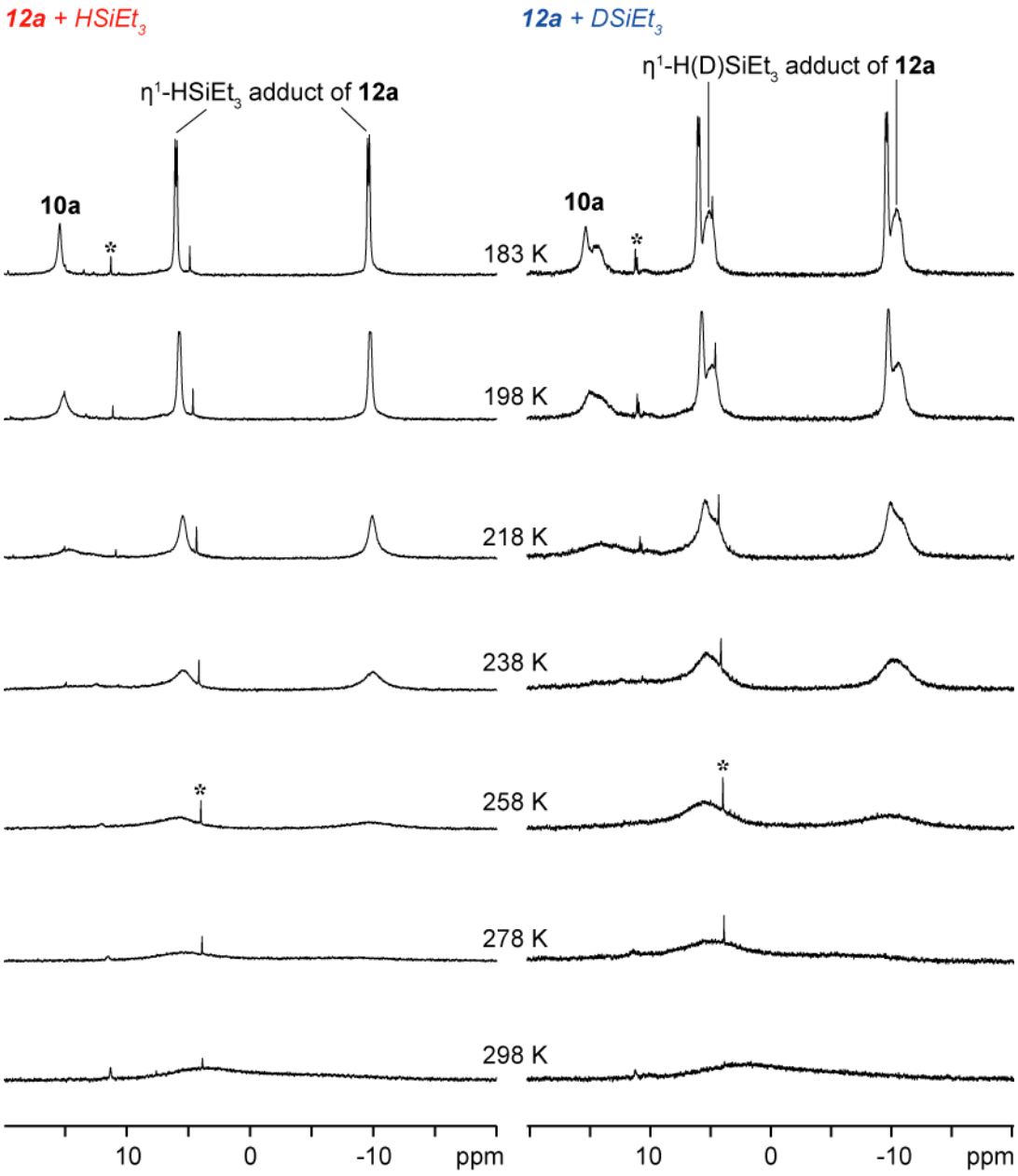

Figure 5.4. $^{31}P\{^{1}H\}$ NMR spectra of the VT NMR experiment used to examine the interaction of **12a** with $HSiEt_3$ (left) and $DSiEt_3$ (right); (CD_2Cl_2, 145.85 MHz). Unassigned peaks labelled (*).

Additional NMR experiments are needed to confirm that **20a** forms via the addition of $HSiEt_3$ to **12a**. For example, a $^{1}H/^{31}P\{^{1}H\}$-HMBC experiment should show a correlation between the methylene protons of the triethylsilyl group to the P nucleus of the P-H-Si

moiety in **20a**. Furthermore, $^{29}Si\{^{1}H\}$ NMR, as well as $^{1}H/^{29}Si\{^{1}H\}$ HSQC/HMBC, is also needed in order to confirm the speciation of $HSiEt_3$ in this reaction. These, as well as additional experiments, will be discussed in Chapter 6.

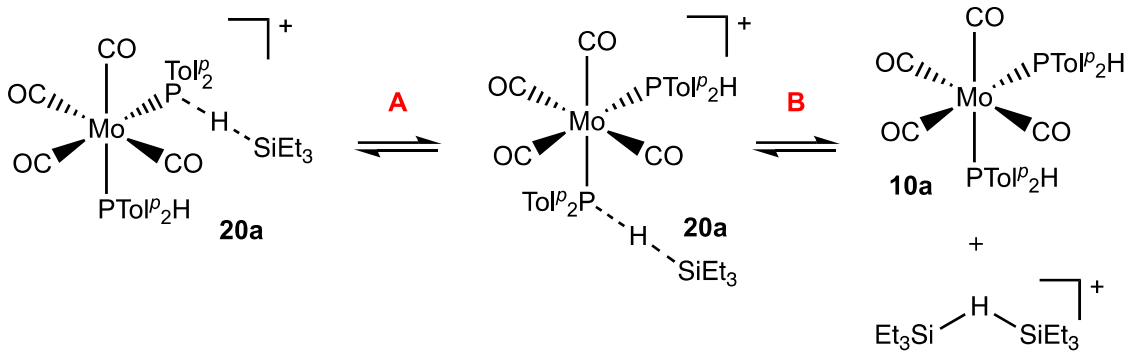

Scheme 5.9. Intra- (A) and intermolecular (B) equilibria involving **20a**.

The two observed decoalescences from this VT NMR study suggests that there are two distinct equilibria that involve **20a** (Scheme 5.9). One of the equilibria is probably an intramolecular process that involves exchange of triethylsilylium, Et_3Si^+, between the two coordinated $PTol^p_2H$ (equilibrium A). The other equilibrium may be an intermolecular process that involves hydride abstraction from $HSiEt_3$, which generates **10a** and $HSiEt_3$-stabilized Et_3Si^+ (equilibrium B). This is proposed to account for the formation of **10a**. It has been established that $^+SiEt_3$, when generated *in situ* through hydride abstraction, can be stabilized by additional equiv of $HSiEt_3$ through the formation of a hydride bridged silylium complex $[Et_3Si\text{-}H\text{-}SiEt_3]^+$.[51] The ^{1}H and $^{31}P\{^{1}H\}$ NMR spectra recorded after allowing the reaction mixture to warm to room temperature were identical to the initial spectra at room temperature, which suggests that this reactivity is reversible.

This same low temperature VT NMR experiment for a sample prepared using deuterium-labelled triethylsilane, $DSiEt_3$, was performed. At room temperature, similar overlapping broad peaks were observed in the $^{31}P\{^1H\}$ NMR spectrum. At 183 K, the same signals were observed as in the reaction with $HSiEt_3$, but new peaks that are assigned as the isotopomers of **20a** and **10a** were also observed (Figure 5.4, right). This suggests that deuterium has incorporated into at the P-H bonds of **20a** and **10a**. The proposed mechanism for this H/D exchange is shown in Scheme 5.10. Deuteride abstraction from $DSiEt_3$, through the formation of *d*$_1$-**20a**, reversibly generates $(CO)_4Mo(PTol^p_2H)(PTol^p_2D)$ (*vide infra*, section 5.4.3) and $[Et_3Si\text{-}H\text{-}SiEt_3]^+$. Triethylsilylium cation, Et_3Si^+, reforms an η^1-adduct with either the coordinated $PTol^p_2H$ or $PTol^p_2D$ of $(CO)_4Mo(PTol^p_2H)(PTol^p_2D)$; essentially, Et_3Si^+ "hops" between the coordinated secondary phosphines, stabilized by either P-H(D) bond.

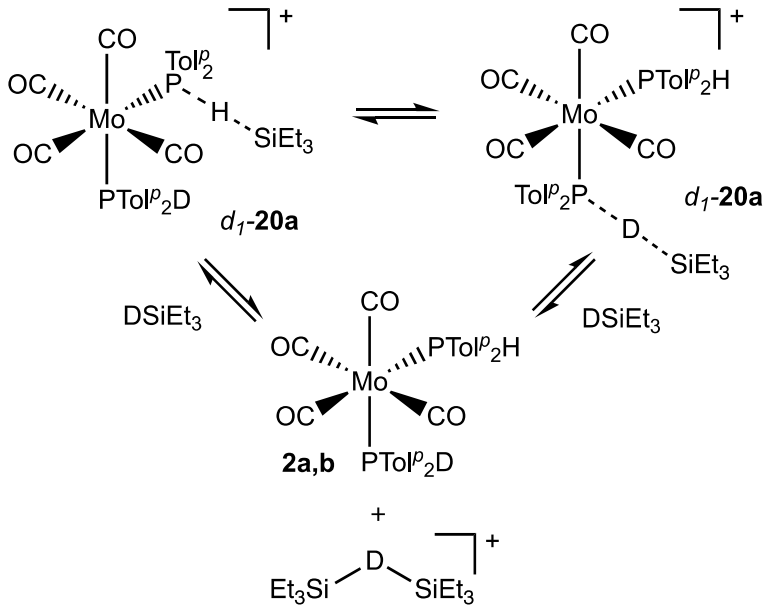

Scheme 5.10. Equilibria involving **20a**, which gives both isotopomers of **20a** when using $DSiEt_3$.

5.4.3. High Temperature NMR Study of the Addition of $HSiEt_3$ and $DSiEt_3$ to 12a,b

This NMR study was conducted in order to further investigate the reaction of $HSiEt_3$ with complex **12a**. In particular, I anticipated that $HSiEt_3$ in **20a** would dissociate at elevated temperatures, which would regenerate **12a** and free $HSiEt_3$. ^{1}H and $^{31}P\{^{1}H\}$ NMR spectra were collected at temperatures ranging from 298 K (room temperature) to 338 K (65°C). The reaction was performed in in C_7D_8/CD_2Cl_2.

The broad $^{31}P\{^{1}H\}$ resonances observed at room temperature for this reaction shift downfield and sharpen upon heating the reaction to 338 K (Figure 5.5). A new signal observed at 338 K is assigned as complex **10a** (Scheme 5.11). This is irreversible, as cooling the solution back to room temperature does not reproduce the initial spectra of this reaction. If, as proposed, Et_3Si^+ forms from **20a** via reversible hydride abstraction, then it must have participated in some other, irreversible reaction at elevated temperatures. One possibility is that Et_3Si^+ participates in electrophilic addition to C_7D_8, which is known to occur with aromatic solvents.[51,52] In the ^{1}H NMR of this reaction, additional ethyl signals are observed, which are assigned as the triethylsilylium adduct of toluene. On the other hand, silylium ions are known to abstract chloride from dichloromethane, which generates $ClSiR_3$.[53,54] The elevated temperatures used for this reaction could increase the rate of decomposition of Et_3Si^+ to Et_3SiCl, which is also irreversible. $^{29}Si\{^{1}H\}$ NMR is needed in order to determine the fate of the Et_3Si^+ in this reaction, which will show whether $[Et_3Si(toluene)]^+$ or $ClSiEt_3$ forms.

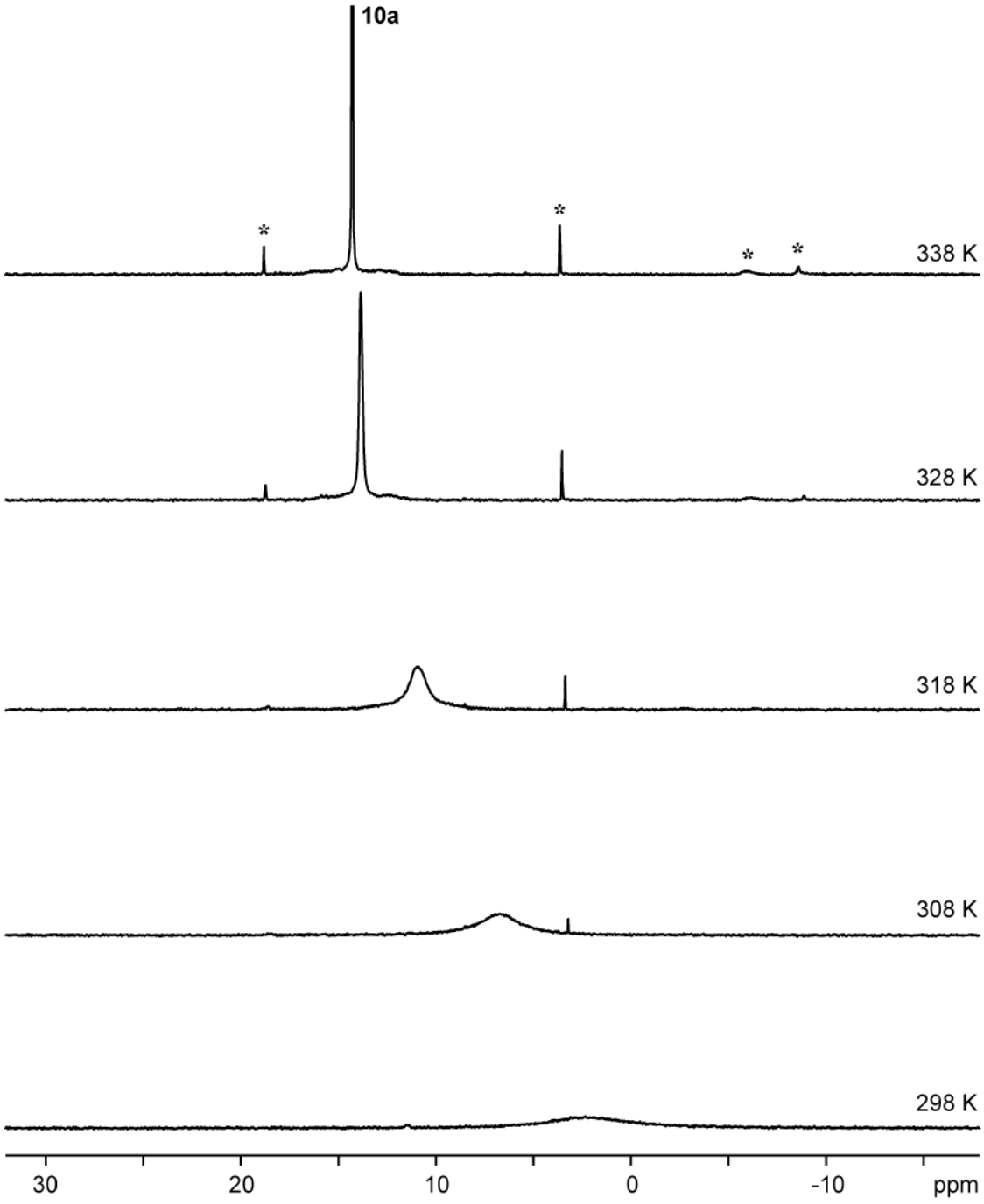

Figure 5.5. $^{31}P\{^{1}H\}$ NMR spectra of the high temperature VT NMR experiment used to examine the interaction of **12a** with $HSiEt_3$ (C_7H_8:CD_2Cl_2 5:1, 145.85 MHz). Unassigned peaks labelled (*).

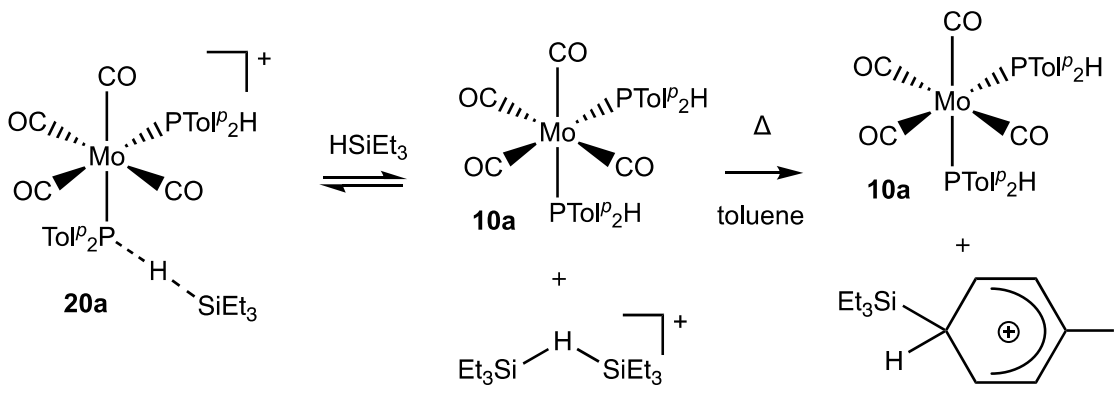

Scheme 5.11. Proposed mechanism for the decomposition of Et_3Si^+ with toluene.

Heating a reaction where two equiv of $DSiEt_3$ was added to complex **12a** at 60°C results in the formation of $Mo(CO)_4(PTol^p_2H)(PTol^p_2D)$. Formation of $Mo(CO)_4(PTol^p_2H)(PTol^p_2D)$ confirms that the silane is the hydride source in these reactions. The $^{31}P\{^1H\}$ NMR spectrum of this reaction shows a triplet of doublets at 13.3 ppm ($^1J_{PD}$ 49, $^2J_{PP}$ 18 Hz) assigned as $PTol^p_2D$ and a doublet at 14.4 ($^2J_{PP}$ 18 Hz) assigned as $PTol^p_2H$.

5.4.4. Computational Analysis of η^1-$HSiEt_3$ Adduct of 12a,b

Complexes **20a**,**b**$[B(C_6H_3Cl_2)_4]$ could not be isolated for crystallographic analysis. In order to study the structure of these complexes our computational collaborator Dr. Dimitrios Pantazis generated, optimized and performed calculations of complex **20b**. General computational details are discussed in section 4.4.3. The *cis*- and *trans*- isomers of **20b** were investigated. As discussed in section 5.4.2, I assigned **20a** as the *cis* isomer based on $^2J_{PP}$ coupling constants, but it is conceivable that isomerization could occur.

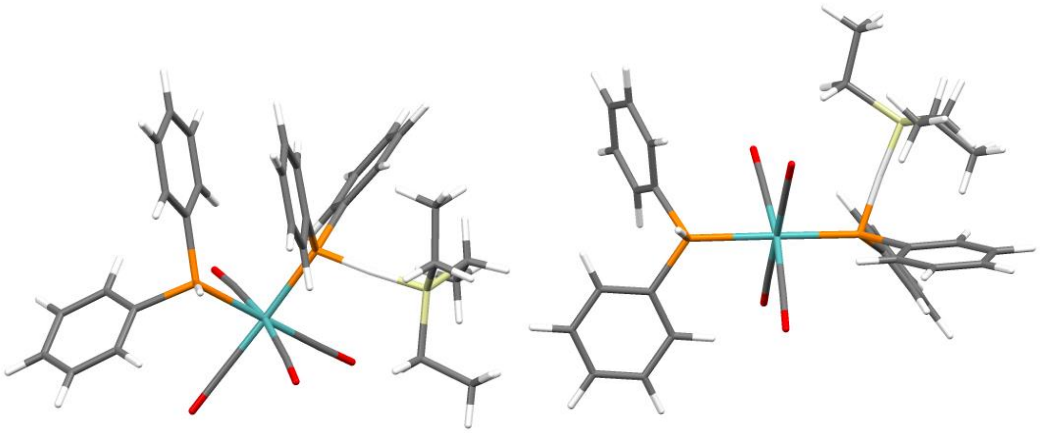

Figure 5.6. Computed and optimized structures of the *cis*- and *trans*- isomers of $[Mo(CO)_4(PPh_2H)(Ph_2P\{HSiEt_3\})]^+$ (**20b**).

The structures of *cis*- and *trans*-**20b** are shown in Figure 5.6 and select bond lengths and angles are summarized in Table 5.1. The P-H bond length of the PPh_2H ligand is shorter than the P-H bond length in the P-H-Si moiety of both cis- and trans-**20b**. The P-H and Si-H bond lengths of the P-H-Si moiety in the calculated structures are significantly different for the two isomers of the adduct. For the *trans*-isomer, the P-H bond length is elongated and the Si-H bond length is shortened relative to the *cis*- isomer. Phospheniums are π-acids, so increasing the electron-density of the metal d-orbital that the phosphenium has a π-interaction with will reduce the Lewis acidity of the phosphenium. This can be rationalized by the electron density at the phosphenium ligands in each isomer. Having the strong σ-donor PPh_2H *trans* to the phosphenium makes the phosphenium in the *trans*-isomer less Lewis acidic than the phosphenium in the *cis*-isomer. This results in a weaker interaction of the phosphenium in the *trans*-isomer with the silane (less activated Si-H bond). The bond angles around P (not including the bond angles with H) in the P-H-Si

moiety deviate only slightly from planarity for *trans*-**20b**, which is also consistent with the weaker interaction with $HSiEt_3$ for this isomer. The P-H-Si bond angle in both *cis*- and *trans*-**20b** are nearly linear, which is consistent with the η^1-binding mode of the adduct.

Table 5.1. Calculated P-H/Si-H bond lengths and angles of the P-H-Si moiety and thermodynamic parameters of $[Mo(CO)_4(PPh_2H)(Ph_2P\{HSiEt_3\})]^+$ (**20b**).

	PPh_2H	**P-H-Si**				**$\Delta H°_{calc}$**	**$\Delta G°_{calc}$**
	P-H (Å)	**P-H (Å)**	**Si-H (Å)**	**P-H-Si (°)**	**$\sum$P°**	**(kcal/mol)**	
Cis-	1.408	1.632	1.620	175.70	338.66	-18.4	-4.0
Trans-	1.410	1.699	1.594	174.06	353.60	-17.1	-1.7

Thermodynamic parameters, $\Delta H°_{calc}$ and $\Delta G°_{calc}$, were also calculated for *cis*- and *trans*-**20b**; these are tabulated in Table 5.1. Formation of both *cis*- and *trans*-**20b** are thermodynamically favourable, but the *cis*-adduct is thermodynamically more favoured than the *trans*-adduct. This observation is consistent with the higher Lewis acidity of the phosphenium ligand in the *cis*-isomer as discussed above, which would result in a stronger adduct with $HSiEt_3$. This is consistent with the VT NMR experiment described in section 5.4.2, where only *cis*-**20a** is observed (based on the $^2J_{PP}$ coupling constants); signals attributed to *trans*-**20a** were not observed.

5.5. Hydrosilylation of Alkenes Catalyzed by 12a,b

As discussed in section 5.1, a mechanism of Lewis acid-catalyzed hydrosilylation involves Si-H bond activation through the formation of η^1-H-Si adducts with the Lewis acid. After I established that **12a**,**b** can activate the Si-H bonds of hydrosilanes through the

formation of the η^1-H-Si adduct **20a**,**b** (section 5.4), I wanted to investigate if complexes **12a**,**b** could be used as hydrosilylation catalysts. Hydrosilylation of 1-hexene with $HSiEt_3$ catalyzed by **12b** was used as a model reaction for studying the reaction kinetics. I determined the reaction rate dependences on the concentrations of **12b**, 1-hexene and $HSiEt_3$. Based on these results, I proposed a mechanism for hydrosilylation catalyzed by **12b**. The scope of unsaturated organic substrates and silanes for this reaction is also described.

5.5.1. Hydrosilylation of 1-hexene with $HSiEt_3$ Catalyzed by 12a,b

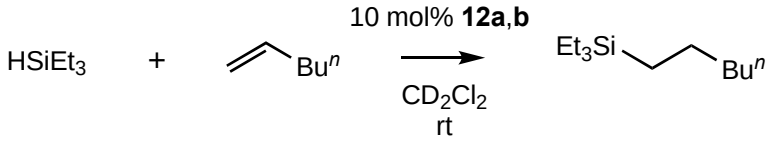

Scheme 5.12. Catalytic hydrosilylation of 1-hexene with $HSiEt_3$ using 10 mol% of **12a**,**b** in CD_2Cl_2 at rt.

A test reaction using 10 mol% of **12b** and equimolar amounts of $HSiEt_3$ and 1-hexene was conducted at room temperature in CD_2Cl_2 (Scheme 5.12). For all hydrosilylation reactions $HSiEt_3$ was always added to **12b** before adding unsaturated substrate, to ensure that **20b** forms first. This order of addition prevents hydrophosphination or P-C bond forming reactions of the unsaturated substrates mediated by **12b**. The anti-Markovnikov hydrosilylation product was identified by ^{1}H NMR. Monitoring this reaction by ^{1}H NMR revealed that catalytic activity ceased after ~ 1 h, which did not result in full conversion to the hydrosilylation product (Figure 5.7, red plot).

The $^{31}P\{^{1}H\}$ NMR spectrum collected during the reaction initially showed the broad resonances associated with complex **20b** (section 5.4). These signals disappear and the signal associated with **10b** appears as the activity of catalysis decreases. The loss of activity is attributed to catalyst deactivation via an irreversible hydride abstraction from $HSiEt_3$, which generates **10b**.

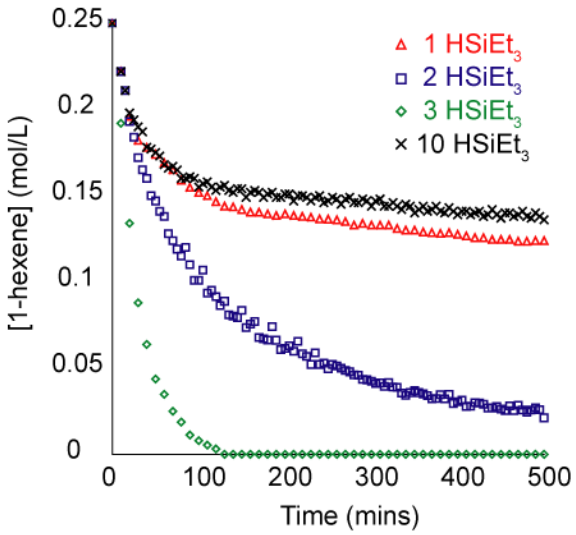

Figure 5.7. Reaction monitoring by ^{1}H NMR of the hydrosilylation of 1-hexene with $HSiEt_3$ catalyzed by **12b** using a 1:1, 2:1, 3:1 and 10:1 ratio of $HSiEt_3$ to 1-hexene.

The activity and conversion of hydrosilylation catalyzed by **12b** is influenced by the number of equivalents of $HSiEt_3$, relative to 1-hexene, used (Figure 5.7). For example, using a 2:1 ratio of $HSiEt_3$ to 1-hexene resulted in higher conversion than the reaction using a 1:1 ratio, but eventually catalytic activity is lost due to catalyst deactivation (blue plot). Under pseudo first order conditions, where a 10:1 ratio of $HSiEt_3$ to 1-hexene is used (black plot), activity is lost after ~ 1 h, due to catalyst deactivation via the formation of **10b**. The optimal ratio of $HSiEt_3$ to 1-hexene for catalysis is 3:1 (green plot). A reaction using 10

mol% of **12a** and a 3:1 ratio of $HSiEt_3$ and 1-hexene conducted at room temperature in CD_2Cl_2 resulted in complete conversion within 3 h. No loss in the activity of the catalysis was observed.

The necessity for multiple equivalents of $HSiEt_3$ to maintain catalytic activity may result from a stabilization of the *in situ* generated $SiEt_3^+$ or the η^1-$HSiEt_3$ adduct **20b** under catalytic conditions by excess $HSiEt_3$. As discussed in section 5.4.3, Et_3Si^+, when generated *in situ* through hydride abstraction, can be stabilized by additional equiv of $HSiEt_3$ through the formation of a hydride-bridged silylium complex $[Et_3Si\text{-}H\text{-}SiEt_3]^+$, which would otherwise undergo decomposition. For example, silylium ions are known to abstract chloride from dichloromethane, which generates $ClSiR_3$. Thus, formation of $[Et_3Si\text{-}H\text{-}SiEt_3]^+$ may prevent decomposition of $SiEt_3^+$ in dichloromethane (solvent used for catalytic reactions). This silylium stabilization may account for the improved catalytic activity in the presence of excess $HSiEt_3$.

Despite the stabilization and improved catalytic activity with multiple equiv of $HSiEt_3$, too large an excess of $HSiEt_3$ (pseudo first order conditions, 10:1 $HSiEt_3$:1-hexene) results in catalyst deactivation to give **10b**. As discussed in section 5.3, complex **20a** reversibly activates the Si-H bond of $HSiEt_3$ (Scheme 5.13). Thus, in the presence of a large excess of $HSiEt_3$ the equilibrium involving reversible Si-H bond activation by **20b** would lie heavily towards $[Et_3Si\text{-}H\text{-}SiEt_3]^+$ and **10b,** which may account for the observed catalyst deactivation.

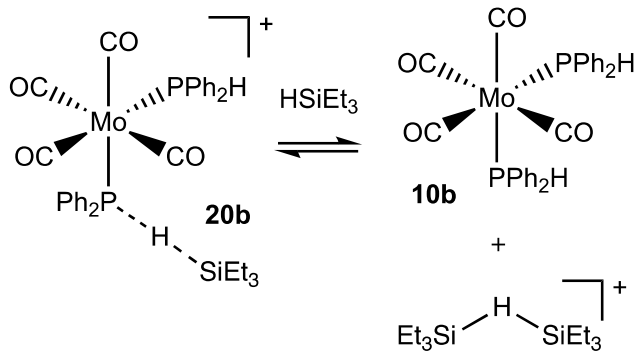

Scheme 5.13. Reversbile Si-H bond activation of $HSiEt_3$ via complex **20b**.

5.5.2. Unsaturated Substrate Scope for Hydrosilylation Catalyzed by 12a,b

Complex **12b** catalyzes the hydrosilylation of unsaturated substrates, which includes some alkenes and ketones and diphenylacetylene with trialkylhydrosilanes (Table 5.2 and in section 5.5.3, Table 5.3). All reactions were performed in CD_2Cl_2 at room temperature using 10 mol% of **12b** and monitored by ^1H NMR; results are summarized in Table 5.2. ^1H NMR data for the hydrosilylation products is presented in section 5.7.8, Table 5.4.

Complex **12b** catalyzes the hydrosilylation of alkenes by $HSiEt_3$. For example, hydrosilylation of 1-hexene by $HSiEt_3$ (entry 1) goes to completion after 3 h. Complex **12b** is very active for the hydrosilylation of styrene and 1,1-diphenylethylene. These reactions reach ~ 60% conversion within 1 h (entry 4 and 5). However, the catalyst deactivates to **10b** within that time. For cyclohexene and cyclopentene (entry 2 and 3), ~ 40% conversion is achieved after 24 h (the catalyst had deactivated to **10b**). No hydrosilylation is observed after 24 h for *trans*-stilbene (entry 6). The hydrosilylation of diphenylacetylene is complete within 30 mins (entry 7). This reaction selectively produces the vinyl silane products even

in the presence of excess $HSiEt_3$, which is consistent with the low or no activity of **12b** for the hydrosilylation of internal alkenes.

Table 5.2. Scope of unsaturated substrates for hydrosilylation by $HSiEt_3$ catalyzed by complex **12b**.[a]

Entry	Substrate	Product	Time (h)	Conversion (%)
		$HSiEt_3$		
1	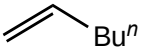	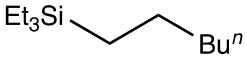	3	>99
2	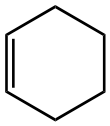	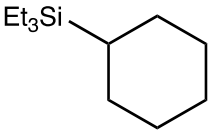	24	40
3		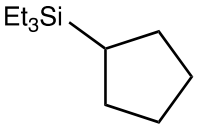	24	40
4	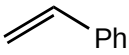	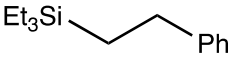	0.5	60
5	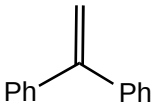	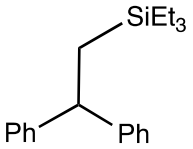	0.5	60
6	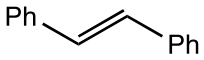	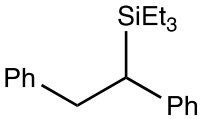	24	0
7	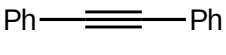	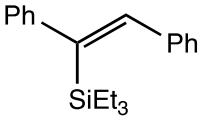	0.5	>99
8	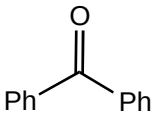	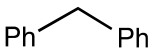	0.5	>99
9	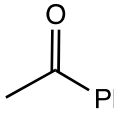	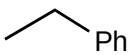	0.5	>99
10	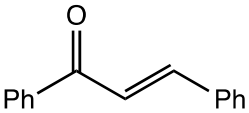	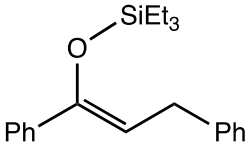	0.5	>99

[a] Reaction conditions: 10 mol% **12b** in CD_2Cl_2 at room temperature, 3:1 $HSiEt_3$:unsaturated substrate. The reactions were monitored and the products were identified by ^1H NMR.

Hydrosilylation of ketones catalyzed by **12b** is very fast and also results in deoxygenation in the presence of excess hydrosilane. Deoxygenation results from over-reduction of the carbonyl bond by a second equiv of silane, which also generates a disiloxane, $R_3SiOSiR_3$. For example, the hydrosilylation of benzophenone with excess $HSiEt_3$ (standard conditions: 3 equiv $HSiEt_3$) catalyzed by **12b** results in complete deoxygenation to diphenylmethane (entry 8). The hydrosilylation of benzophenone in the presence of 1 equiv of $HSiEt_3$ results in an 2:1 ratio of the hydrosilylated ketone and diphenylmethane; the reaction did not reach full conversion as there is unreacted benzophenone and $HSiEt_3$. Deoxygenation of acetophenone to give ethylbenzene was also observed in the presence of excess $HSiEt_3$ (entry 9). Hydrosilylation of *trans*-chalcone selectively forms the silyl enol ether (entry 10) via 1,4-addition. Products resulting from the deoxygenation or reduction of the C-C double bond of *trans*-chalcone are not observed, even in the presence of excess $HSiEt_3$. This result suggests that **12b** can be used as a selective catalyst for the 1,4-hydrosilylation of conjugated ketones.

5.5.3. Silane Substrate Scope for Hydrosilylation Catalyzed by 12a,b

A variety of hydrosilanes were assessed for this reaction (Table 5.3), but hydrosilylation catalysis using complex **12b** was only observed with tertiary alkyl silanes. For example, hydrosilylation of 1-hexene with $HSi(hexyl)_3$ using 10 mol% of **12b** is complete within 4 h at rt in CD_2Cl_2 (Table 5.3, entry 1). No catalysis is observed with $H_2Si(hexyl)_2$, H_2SiPh_2, $HSiMePh_2$ and $HSi(OEt)_3$ because complex **12b** irreversibly abstracts hydride from these silanes under catalytic conditions (entries 2, 3, 4 and 5), which generates **10b**. A possible explanation for this is that H_2SiPh_2 and $HSiMePh_2$ are stronger

hydride donors that $HSiEt_3$[55]. For $HSi(OEt)_3$, other decomposition is also observed, possibly due to reactivity of the phosphenium ligand with the ethoxy groups of $HSi(OEt)_3$. These results highlight that the phosphenium ligand in **12b** is extremely Lewis acidic, which will need to be addressed (e.g. catalyst redesign) to increase the scope of hydrosilanes used for this reaction.

Table 5.3. Scope of hydrosilanes for the hydrosilylation 1-hexene catalyzed by **12b**.[a]

Entry	Silane	Product	Time (h)	Conversion (%)
1	$HSi(hexyl)_3$	$Si(hexyl)_4$	4	>99
2	$H_2Si(hexyl)_2$	$HSi(hexyl)_3$	24	-
3	H_2SiPh_2	$HSiPh_2(hexyl)$	24	-
4	$HSiMePh_2$	$MeSiPh_2(hexyl)$	24	-
5	$HSi(OEt)_3$	$Si(OEt)_3(hexyl)$	24	-

[a] Reaction conditions: 10 mol% **12b** in CD_2Cl_2 at room temperature, 3:1 $HSiEt_3$:1-hexene. The reactions were monitored and the products were identified by ^1H NMR.

5.5.4. Kinetic Analysis of Hydrosilylation Catalyzed by 12a,b

The hydrosilylation of 1-hexene with $HSiEt_3$ was selected as a model reaction to study the kinetics of hydrosilylation catalyzed by **12b**. These reactions were conducted at room temperature in CD_2Cl_2 with a 3:1 ratio of $HSiEt_3$ and 1-hexene to ensure ideal catalytic behaviour and complete conversion to the hydrosilylation product. As described above, $HSiEt_3$ was always added to **12b** before adding 1-hexene, to ensure that **20b** forms instead of products that result from P-C bond formation. The reactions were monitored by ^1H NMR. The data presented is the average of triplicate experiments. Reaction rate dependences on the concentration of the catalyst and substrates were determined using VTNA, described in Chapter 3.

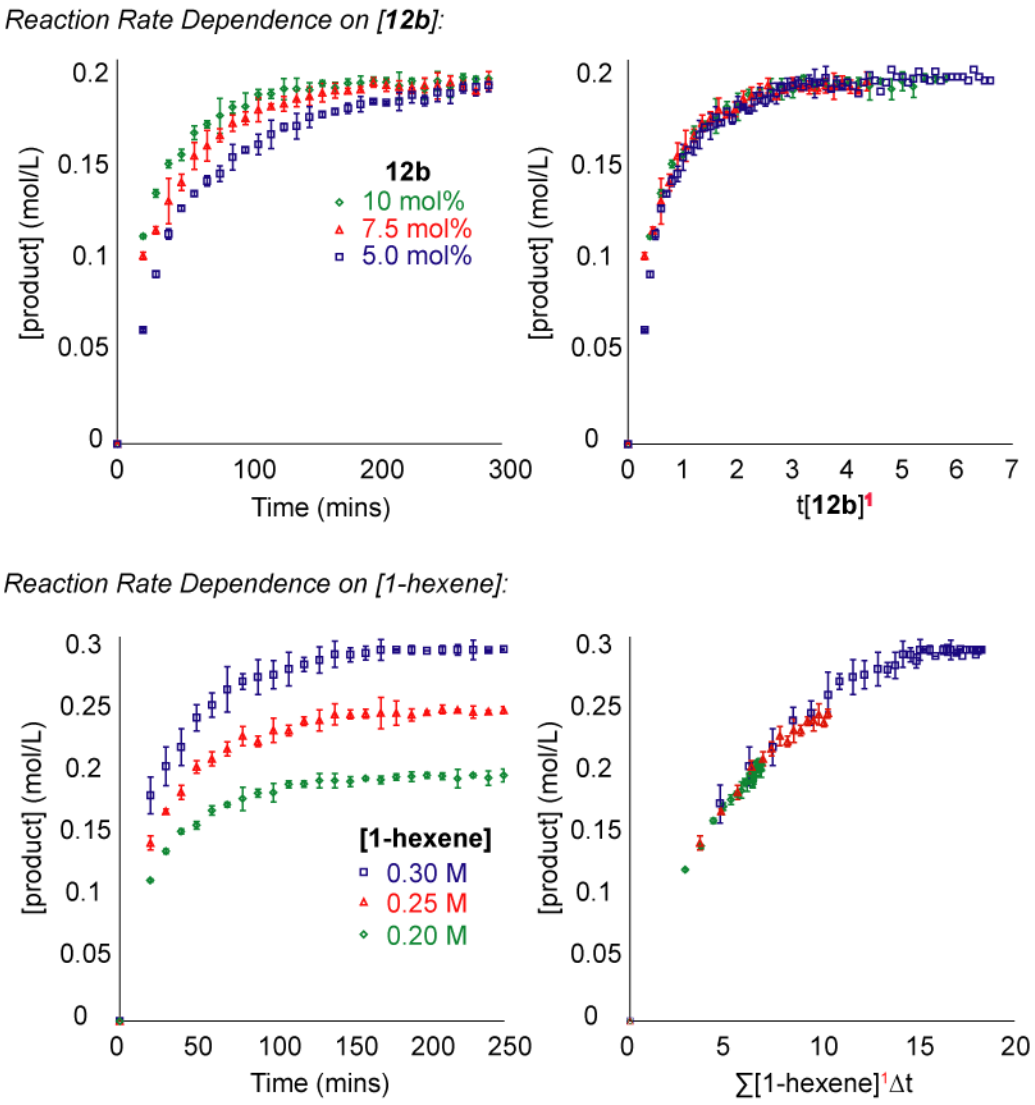

Figure 5.8. Reaction monitoring, using ^{1}H NMR (500.27 MHz), of the hydrosilylation of 1-hexene with $HSiEt_3$ catalyzed by complex 12b. Top left: reactions using three different [12b]. Top right: time normalization shows a first order dependence on [12b]. Bottom left: reactions using three different [1-hexene]. Bottom right: time normalization shows a first order dependence on [1-hexene].

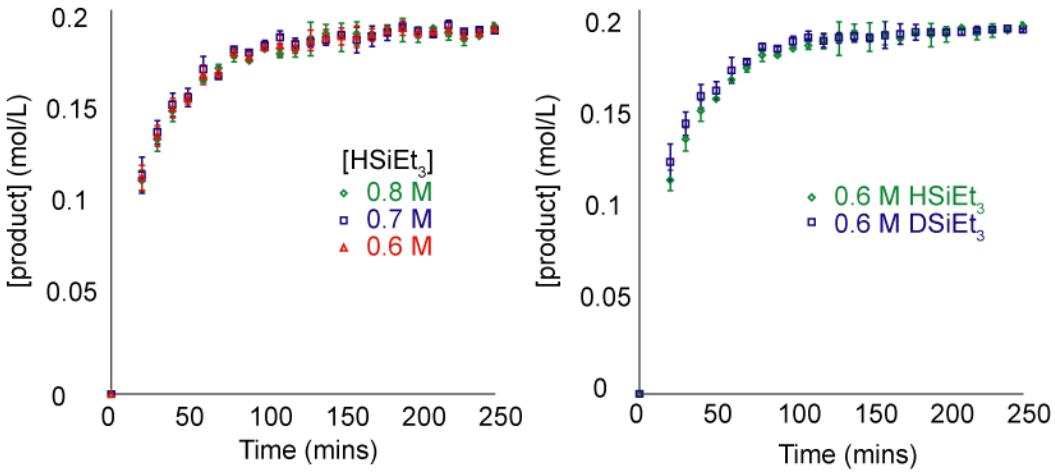

Figure 5.9. Reaction monitoring, using ^{1}H NMR (500.27 MHz), of the hydrosilylation of 1-hexene with $HSiEt_3$ catalyzed by complex 12b. Left: reactions using three different [$HSiEt_3$]; overlap implies a zero order dependence on [$HSiEt_3$]. Right: reactions using 0.6 M of $HSiEt_3$ and $DSiEt_3$; overlap implies no kinetic isotope effect.

A first-order reaction rate dependence on the concentration of **12b** was determined by three reactions using catalyst concentrations of 0.010, 0.015 and 0.020 M (5.0, 7.5 and 10 mol%, respectively) (Figure 5.8, top). This reaction also has a first-order dependence on the concentration of 1-hexene, which was determined by three reactions using 10 mol% of **12b**, but with different 1-hexene concentrations of 0.2, 0.3 and 0.4 M (Figure 5.8, bottom). Three reactions using 10 mol% of **12b**, but with different $HSiEt_3$ concentrations of 0.6, 0.7 and 0.8 M (3, 4 and 5 equivalents relative to 1-hexene, respectively) (Figure 5.9, left) produced identical reaction profiles, which suggests a zero-order reaction rate dependence on the concentration of $HSiEt_3$. Moreover, a reaction using 10 mol% of **12b** and 0.6 M $DSiEt_3$ produced an identical kinetic profile to the corresponding reaction using 0.6 M $HSiEt_3$ (Figure 5.9, right). This shows that there is no kinetic isotope effect on the rate of the reaction, which suggests Si-H bond activation is not involved in the rate-determining step. This is consistent with the zero order dependence on the concentration of $HSiEt_3$. The overall experimental rate law is:

$$\text{Reaction rate} = k_{obs}[\mathbf{12b}][\text{1-hexene}]$$

5.5.5. Proposed Mechanism for the Hydrosilylation of Alkenes Catalyzed by 12a,b

A proposed mechanism for the hydrosilylation of alkenes with $HSiEt_3$ catalyzed by **12b** involves catalyst activation *via* formation of **20b,** the η^1-$HSiEt_3$ adduct of **12b** (Scheme 5.14, step A). In this study, $HSiEt_3$ was always added first to **12b** to prevent P-C bond forming reactions of the unsaturated substrates with **12b**. The broad overlapping peaks in the $^{31}P\{^1H\}$ NMR at room temperature attributed to **20b** (confirmed from the VT NMR study, section 5.4) are the only resonances observed throughout the catalytic reaction, which suggests that **20b** is the resting state. Complex **20b** may be involved in two equilibria. One process is intramolecular (step B) and the other is intermolecular, which generates $[Et_3Si\text{-}H\text{-}SiEt_3]^+$ (step E). After catalyst activation, addition of alkene to the activated hydrosilane generates a carbocation (step C). Subsequent hydride transfer to the carbocation from the activated Si-H bond produces the hydrosilylation product and regenerates **12b** (step D). Introduction of $HSiEt_3$ regenerates **20b** (step A'). The observed zero-order dependence of the reaction rate on the $HSiEt_3$ concentration suggests that this step occurs after the rate determining step. This suggests that step C is rate determining, which is consistent with the fact that **20b** is the observed resting state of catalysis. This mechanism closely resembles the mechanisms of Lewis acid-catalyzed hydrosilylation of unsaturated substrates proposed by Piers,[22,56] Gevorgyan[20] and Oestreich [21]

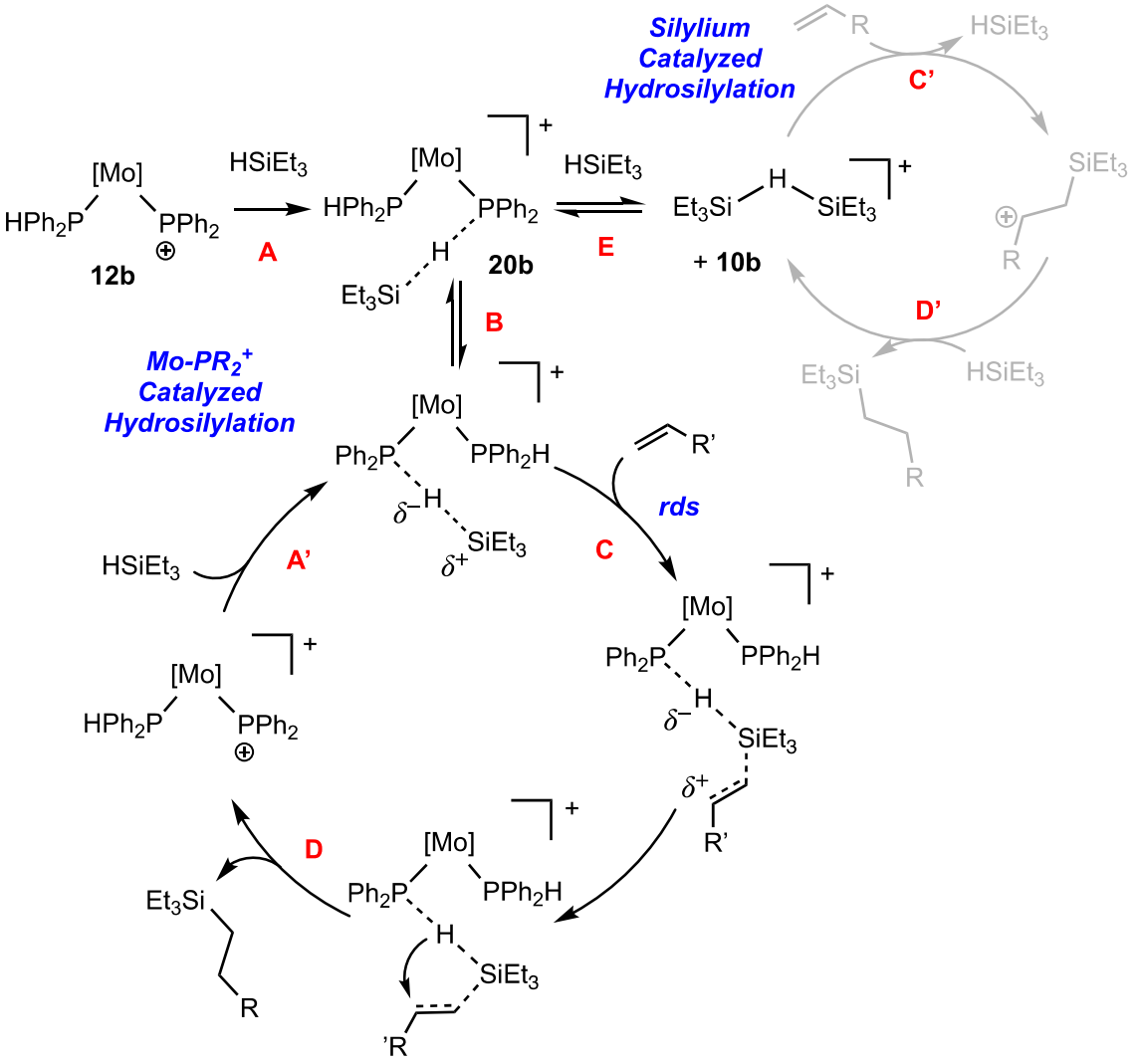

Scheme 5.14. Proposed mechanism for the hydrosilylation of alkenes catalyzed by complex **12b**.

An alternative mechanism is also possible, where complex **12b** acts as an initiator for the hydrosilylation of alkenes. Lewis acid-initiated hydrosilylation typically involves irreversible hydride abstraction from silanes, which generates silyliums that can catalyze the reaction. From the low temperature VT NMR study examining the reactivity of hydrosilanes with **12a** (section 5.3), I determined that complex **12a** can reversibly activate the Si-H bond of $HSiEt_3$, which generates **10a** and, presumably, $[Et_3Si\text{-}H\text{-}SiEt_3]^+$ (step E

in Scheme 5.14). This silylium species could catalyze the hydrosilylation of alkenes if it forms under catalytic conditions. Alkene addition to $[Et_3Si\text{-}H\text{-}SiEt_3]^+$ would generate a carbocation intermediate (Scheme 5.14, step B'), which can be quenched by hydride transfer from $HSiEt_3$ (step C'). This would regenerate $[Et_3Si\text{-}H\text{-}SiEt_3]^+$ in the presence of excess $HSiEt_3$. If this mechanism is operative, the zero-order dependence on the concentration of $HSiEt_3$ can still be accounted for if alkene addition to Et_3Si^+ (step B') is the rate determining step of the cycle. Similar proposed mechanisms have been previously reported for Lewis acid-initiated/silylium-catalyzed hydrosilylation of alkenes. In these cases, a method used to distinguish if a Lewis acid-initiated/silylium-catalyzed mechanism is operative is to compare the reaction rates and product distribution of hydrosilylation using the Lewis acid of interest to $[Ph_3C]^+$-initiated hydrosilylation.[56,57]

A control experiment using $[Ph_3C][B(C_6F_5)_4]$ as an initiator for hydrosilylation was conducted in order to compare an established silylium-catalyzed hydrosilylation to the observed hydrosilylation using complex **12b**. I would expect to see similar reaction rates for hydrosilylation initiated by $[Ph_3C][B(C_6F_5)_4]$ and **12b**, when using the same mol % of each, if **12b** is an initiator rather than a catalyst. A reaction using 10 mol% of $[Ph_3C][B(C_6F_5)_4]$ under the same conditions as catalysis with **12b** (rt, CD_2Cl_2; 3 equiv of $HSiEt_3$ relative to 1-hexene; silane added first to $[Ph_3C][B(C_6F_5)_4]$) was complete within 10 minutes. This contrasts the much slower catalysis mediated by **12b** that is complete within 3 h. The different rates of hydrosilylation initiated by $[Ph_3C][B(C_6F_5)_4]$ and catalyzed with **12b** could mean that **12b** truly is a Lewis acid catalyst for hydrosilylation, but this still does not rule out the possibility that **12b** acts as an initiator. If the silylium-

catalyzed mechanism is operative, but the equilibrium shown in step E (Scheme 5.12) lies towards **20b**, the overall concentration of $[Et_3Si\text{-}H\text{-}SiEt_3]^+$ would remain low throughout the reaction. This could also account for a slower reaction rate compared to the Ph_3C^+-initiated hydrosilylation.

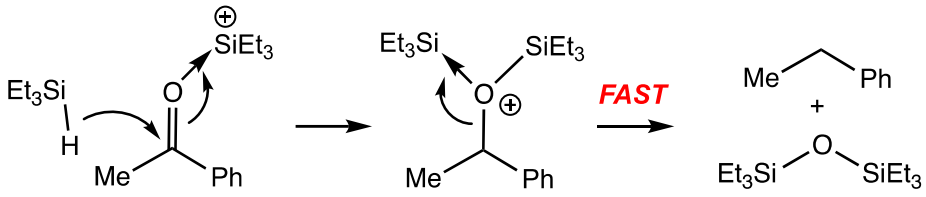

Scheme 5.15. Proposed mechanism for silylium-catalyzed hydrosilylation of acetophenone, which results in the formation of ethylbenzene as the exclusive product via over-reduction of the carbonyl bond.

Exclusive deoxygenation of ketones via hydrosilylation is a telltale sign of a Lewis acid-initiated/silylium-catalyzed hydrosilylation (Scheme 5.15). In a silylium-catalyzed hydrosilylation, silane is the hydride source. Thus, Et_3Si^+ is formed in close proximity to the product of a single hydrosilylation, which then rapidly leads to deoxygenation via formation of $R_3SiOSiR_3$ (Scheme 5.15). If **12b** is an initator, hydrosilylation of ketones mediated by **12b** is expected to give exclusively the deoxygenated product. A comparison of $[Ph_3C]^+$-initiated, **12b**-mediated and $B(C_6F_5)_3$-catalyzed hydrosilylation is shown in Scheme 5.16. A control experiment using 5 mol% of $[Ph_3C][B(C_6F_5)_4]$ to initiate the hydrosilylation of acetophenone with $HSiEt_3$ (1:1 ratio of acetophenone:$HSiEt_3$ used) results in ethylbenzene as the exclusive product. A reaction using 5 mol% of **12b** for the hydrosilylation of acetophenone with $HSiEt_3$ (1:1 ratio of acetophenone:$HSiEt_3$ used) results in a 2:1 ratio of silyl ether:ethylbenzene, with unreacted acetophenone and $HSiEt_3$.

Piers *et al* performed a similar control experiment with $[Ph_3C][B(C_6F_5)_4]$ to determine the mechanism of $B(C_6F_5)_3$-catalyzed hydrosilylation of ketones. The authors found that the silyl ether was the exclusive product when $B(C_6F_5)_3$ is used.[26] The fact that **12b** did not exclusively give the deoxygenated product suggests that **12b** is a catalyst for hydrosilylation, but observing some of the deoxygenated product suggests that **12b** may also initiate the reaction as well (i.e. producing some reactive free Et_3Si^+).

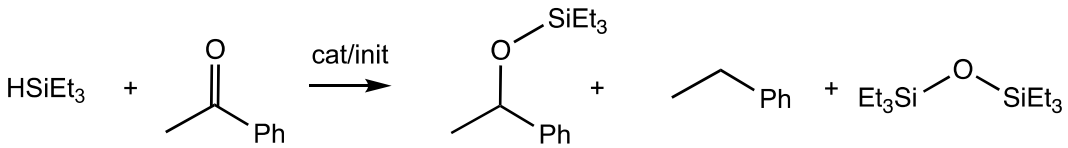

$[Ph_3C][B(C_6F_5)_4]$	0	:	1	:	1
12b	1	:	0.5	:	0.5
$B(C_6F_5)_3$	1	:	0	:	0

Scheme 5.16. Product distribution of the hydrosilylation of benzophenone with $HSiEt_3$ initiated by $[Ph_3C][B(C_6F_5)_4]$ and catalyzed by **12b**.

5.6. Conclusion

Chapter 4 demonstrated that the electrophilicity of the phosphenium ligands in *trans*-$[Mo(CO)_4(PTol_2^pH)(PTol_2^p)][B(C_6H_3Cl_2)_4]$ (*trans*-**12a**$[B(C_6H_3Cl_2)_4]$) and *trans*-$[Mo(CO)_4(PR_2H)(PR_2)][B(C_6H_3Cl_2)_4]$ (*trans*-**12b**$[B(C_6H_3Cl_2)_4]$) could be utilized for hydrophosphination. Building upon that study, we wanted to investigate if these complexes could also be used as Lewis acid catalysts.

I assessed the Lewis acidity of **12a**,**b** by two complementary experimental (Gutmann-Becket method) and computational (GEI) methods. The calculated metrics of **12a**,**b** by these methods show that complexes **12a**,**b** are extremely strong Lewis acids. Complexes **12a**,**b** are even more Lewis acidic than the commonly used Lewis acid $B(C_6F_5)_3$.

The Lewis acidic reactivity of these complexes is most notably demonstrated through the ability of **12a**,**b** to reversibly activate the Si-H bonds of hydrosilanes. I identified the η^1-$HSiEt_3$ adduct of **12a**, $[Mo(CO)_4(PTol_2{}^pH)(PTol_2{}^p\{HSiEt_3\})]$ (**20a**), using a low temperature VT NMR experiment. Computational studies provided support for the formation of complex $[Mo(CO)_4(PPh_2H)(PPh_2{}^p\{HSiEt_3\})]$ (**20b**). η^1-$HSiEt_3$ adducts of main group Lewis acids are critical intermediates in proposed mechanisms for hydrosilylation and other main group Lewis acid-catalyzed reactions of hydrosilanes (e.g. dehydrocoupling, hydrodefluorination etc.).

I exploited the ability of complexes **12a**,**b** to activate the Si-H bonds of silanes for hydrosilylation catalysis. Complex **12b** is a competent catalysts for the hydrosilylation of alkenes, alkynes and ketones with trialkylsilanes. The proposed mechanism for hydrosilylation catalyzed by **12b** resembles the Lewis acid-catalyzed mechanisms proposed by Piers,[23] Gevorgyan[24] and Oestreich.[25] An alternate mechanism, whereby **12b** acts as an initiator could not definitively be ruled out. As I determined based on the VT NMR studies, **12a** can reversibly abstract hydride from $HSiEt_3$, which generates the silylium adduct $[Et_3Si\text{-}H\text{-}SiEt_3]^+$. This silylium species is known to catalyze the hydrosilylation of unsaturated substrates. The extreme Lewis acidity of **12b** resulted in

irreversible hydride abstraction from some hydrosilanes. In those cases no hydrosilylation was observed. Thus, although these complexes have remarkably high Lewis acidities, this may have deleterious implications for catalysis.

Ultimately, this study demonstrates the utility of metal phosphenium complexes as Lewis acid catalysts. This adds a significant contribution to the existing literature on P(III) Lewis acids, which is generally limited to N-heterocyclic phosphines. Furthermore, these are unique catalysts because the Lewis acidity of the phosphenium ligand can be tuned through modifying the electron-density of the metal (e.g. changing the metal or the ligands). This is the first example of a new class of Lewis acid catalysts. Future work and directions on how to extend the breadth of metal phosphenium complexes as Lewis acid catalysts will be discussed in Chapter 6.

5.7. Experimental

See Chapter 2, Section 2.6.1. for general experimental details. See Chapter 4, Section 4.4.3. for general computational details. All hydrosilylation products were identified by ^{1}H NMR based on known literature values (summarized in Table 5.4).[27,58–61] $[Ph_3C][B(C_6F_5)_4]$ was prepared according to a literature procedure.[62] $DSiEt_3$ was prepared according to a modified literature procedure.[63] All substrates were dried and purified according to known literature procedures.

5.7.1. NMR Tube Reactions of 12a,b

5.7.1.1. Addition of THF to 12a,b

12a,**b** (40 mg, 0.034 mmol) was dissolved in CD_2Cl_2 (600 μL) and THF. The reaction was monitored by ^{1}H and $^{31}P\{^{1}H\}$ NMR. $^{31}P\{^{1}H\}$ NMR spectra are in Appendix I.

5.7.1.2. Addition of TEPO to 12a,b

12a,**b** (40 mg, 0.034 mmol) was dissolved in CD_2Cl_2 (600 μL) and TEPO (6 mg, 0.034 mmol) was added. The solution changed colour from dark green to yellow upon addition of TEPO. The reaction was monitored by ^{1}H and $^{31}P\{^{1}H\}$ NMR. $^{31}P\{^{1}H\}$ NMR spectra are in Appendix I.

5.7.2. Synthesis of $DSiEt_3$

Wilkinson's catalyst (40 mg, 0.043 mmol) was added to a 100 mL round bottom flask with a needle valve and a stir bar. Dichloromethane (5 mL) was added and resulted

in an orange solution. $HSiEt_3$ (1.4 mL, 1.0 g, 8.6 mmol) was added to the flask. The solution was degassed via three freeze-pump-thaw cycles and then backfilled with D_2 gas (1 atm). The mixture was stirred for 24 h at room temperature. The flask was brought into a glovebox and the solution was passed through a Florisil column to remove Rh complexes, which resulted in a dichloromethane solution of $DSiEt_3$ (>99% deuteration determined by ^1H NMR). The solution was placed in the glovebox freezer (~ −20°C) uncapped allowing for some dichloromethane to evaporate giving a concentrated $DSiEt_3$ solution. ^1H NMR (500.27 MHz, C_6D_6): 0.89 (t, $^3J_{HH}$ 7.9 Hz, 9H), 0.51 (q, $^3J_{HH}$ 7.9 Hz, 6H).

5.7.3. Procedure for Low Temperature VT NMR Experiments

Complex **12a** (40 mg, 0.043 mmol) was dissolved in CD_2Cl_2 (600 μL) and $HSiEt_3$ (2 equiv, 0.086, 14 μL) was added, which resulted in an immediate colour change of the solution from dark green to yellow. The solution was transferred to a J Young NMR tube. ^1H and $^{31}P\{^1H\}$ spectra were collected at room temperature (298 K). Additional ^1H and $^{31}P\{^1H\}$ spectra were collected at 278, 258, 238, 218, 208, 188 and 183 K. The same procedure was followed when using $DSiEt_3$.

5.7.4. Procedure for High Temperature VT NMR Experiments

Complex **12a** (40 mg, 0.043 mmol) was dissolved in a mixture of C_7H_8 (550 μL) and CD_2Cl_2 (50 μL). $HSiEt_3$ (2 equiv, 0.086, 14 μL) was added, which resulted in an immediate colour change of the solution from dark green to yellow. The solution was transferred to a J Young NMR tube. ^1H and $^{31}P\{^1H\}$ spectra were collected at room

temperature (298 K). Additional ^{1}H and $^{31}P\{^{1}H\}$ spectra were collected at 318, 338, 358 and 378 K. The same procedure was followed when using $DSiEt_3$.

5.7.5. General Procedure for the Hydrosilylation Reactions of 1-Hexene with $HSiEt_3$ Catalyzed by 12b

A 0.05 M solution of **12b** in d_2-dichloromethane (100, 150 or 200 μL) and neat $HSiEt_3$ (48, 64 or 80 μL) were added to a vial. Neat 1-hexene (12, 15 or 18 μL) was added. Additional d_2-dichloromethane was added to maintain a constant volume of 500 μL. This solution was placed in an NMR tube, which was then fitted with a coaxial tube containing a 0.25 M solution of hexamethyldisiloxane in d_2-dichloromethane. The reactions were monitored at room temperature by ^{1}H NMR, collecting single scan experiments every 10 minutes for 4 – 6 h.

5.7.6. Hydrosilylation Initiated by $[Ph_3C][B(C_6F_5)_4]$

$[Ph_3C][B(C_6F_5)_4]$ (5 mg, 6 μmol) was dissolved in CD_2Cl_2 (600 μL). $HSiEt_3$ (54 μL, 0.32 mmol) was added to the solution, which changed colour from yellow to colourless. 1-Hexene (16 μl , 0.11 mmol) or acetophenone (37 mg, 0.32 mmol) was added to the solution, which was then transferred to a J Young NMR tube. The reaction was monitored by ^{1}H NMR. The reaction was complete by the time the first ^{1}H NMR spectrum was collected (30 minutes).

5.7.7. General Procedure for the Hydrosilylation of Unsaturated Substrates

In a glovebox, 200 μL of a 0.05 M solution of **12b** (1 equiv) in CD_2Cl_2 and neat silane were added together. The unsaturated organic substrates were added or dissolved in this solution and additional CD_2Cl_2 was added to maintain a constant volume of 500 μL. Quantities of unsaturated substrates: cyclohexene, 10 μL, 10 equiv; cyclopentene, 9 μL, 10 equiv; styrene, 12 μL, 10 equiv; 1,1-diphenylethylene, 18 μL, 10 equiv; *trans*-stilbene, 18 mg, 10 equiv; diphenylacetylene, 18 mg, 10 equiv; benzophenone, 36 mg, 20 equiv; *trans*-chalcone, 21 mg, 10 equiv. Quantities of silanes: $HSiEt_3$, 48 μL, 30 equiv; $HSi(hexyl)_3$, 107 uL, 30 equiv; $H_2Si(hexyl)_2$, 60 mg, 30 equiv $HSi(OEt)_3$, 55 uL, 30 equiv; H_2SiPh_2, 56 uL, 30 equiv; $HSiMePh_2$, 60 uL, 30 equiv.

5.7.8. ^{1}H NMR data for Hydrosilylation Products

Table 5.4. ^{1}H NMR Data for the Hydrosilylation Products (500.27 MHz, CD_2Cl_2)[27,58-61]

Compound	^{1}H NMR Data	Compound	^{1}H NMR Data
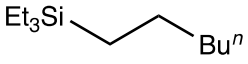	1.30 (m, 8H), 0.94 (t, $^{3}J_{HH}$ 7.9 Hz, 9H, $SiCH_2C\underline{H}_3$), 0.90 (t, $^{3}J_{HH}$ 7.2 Hz, 3H), 0.51 (q, $^{3}J_{HH}$ 7.9 Hz, 6H, $SiC\underline{H}_2CH_3$)	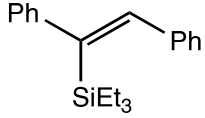	7.37-7.29 (m, 7H, ArH), 7.22 (m, 3H, ArH), 0.82 (t, $^{3}J_{HH}$ 7.9 Hz, 9H, $SiCH_2C\underline{H}_3$), 0.43 (q, $^{3}J_{HH}$ 7.9 Hz, 6H, $SiC\underline{H}_2CH_3$)
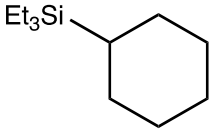	1.68 (m, 5H), 1.18 (m, 5H), 0.90 (t, $^{3}J_{HH}$ 7.9 Hz, 9H, $SiCH_2C\underline{H}_3$), 0.72 (m, 1H), 0.51 (q, $^{3}J_{HH}$ 7.9 Hz, 6H, $SiC\underline{H}_2CH_3$)	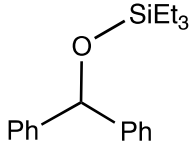	7.44-7.254 (m, 10H, Ar$\underline{H}$), 5.83 (s, 1H, ArC$\underline{H}$), 0.95 (t, $^{3}J_{HH}$ 7.9 Hz, 9H, $SiCH_2C\underline{H}_3$), 0.65 (q, $^{3}J_{HH}$ 7.9 Hz, 6H, $SiC\underline{H}_2CH_3$) **Diphenylmethane:** 7.29 (m, 4H); 7.20 (m, 6H); 3.98 (s, 2H)
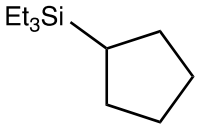	1.27-1.79 (m, 9H), 0.95 (t, $^{3}J_{HH}$ 7.9 Hz, 9H, $SiCH_2C\underline{H}_3$), 0.53 (q, $^{3}J_{HH}$ 7.9 Hz, 6H, $SiC\underline{H}_2CH_3$)	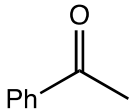	7.37-7.31 (m, 4H, Ph), 7.26-7.22 (m, 1H, Ph), 4.88 (q, 1H, $^{3}J_{HH}$ 6.4 Hz, C$\underline{H}$OSiEt$_3$), 1.45 (d, 3H, $^{3}J_{HH}$ 6.4 Hz, $C\underline{H}_3$), 0.93 (t, $^{3}J_{HH}$ 7.9 Hz, 9H, $SiCH_2C\underline{H}_3$), 0.59 (q, $^{3}J_{HH}$ 7.9 Hz, 6H, $SiC\underline{H}_2CH_3$). **Ethylbenzene**: 7.26 (m, 5H); 2.70 (q, $^{3}J_{HH}$ 8.0 Hz, 2H); 1.29 (t, $^{3}J_{HH}$ 8.0 Hz, 3H)

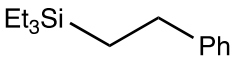	7.11-7.27 (m, 5H, Ph), 2.71 (t, $^{3}J_{HH}$ 8.0 Hz, 2H, $SiCH_2C\underline{H_2}Ph$), 0.98 (t, $^{3}J_{HH}$ 8.0 Hz, 2H, $SiC\underline{H_2}CH_2Ph$), 092 (t, $^{3}J_{HH}$ 8.0 Hz, 9H, $SiCH_2C\underline{H_3}$), 0.66 (q, $^{3}J_{HH}$ 8.0 Hz, 6H, $SiC\underline{H_2}CH_3$)	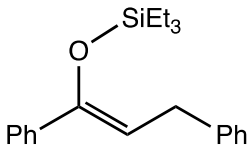	7.64-7.61 (m, 2H, Ph), 7.40-7.36 (m, 8H, Ph), 5.41 (t, $^{3}J_{HH}$ 7.9 Hz, 1H, CH), 3.65 (d, $^{3}J_{HH}$ 7.9 Hz, 2H, CH_2), 1.13 (t, $^{3}J_{HH}$ 7.9 Hz, 9H, $SiCH_2C\underline{H_3}$), 0.82 (q, 6H, $^{3}J_{HH}$ 7.9 Hz, $SiC\underline{H_2}CH_3$) *single isomer observed, based on chemical shifts I have assigned it as the E isomer
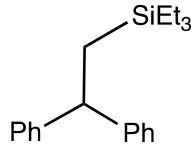	7.18 (m, 8H), 7.05 (m, 2H), 3.99 (t, $^{3}J_{HH}$ 7.9 Hz, 1H, $Ar_2C\underline{H}$), 1.33 (d, $^{3}J_{HH}$ 7.9 Hz, 2H, $Ar_2CHC\underline{H_2}$), 0.75 (t, $^{3}J_{HH}$ 8.1 Hz, 9H, $SiCH_2C\underline{H_3}$), 0.26 (q, $^{3}J_{HH}$ 7.9 Hz, 6H, $SiC\underline{H_2}CH_3$)		

5.8. References

(1) Lipke, M. C.; Liberman-Martin, A. L.; Tilley, T. D. Electrophilic Activation of Silicon–Hydrogen Bonds in Catalytic Hydrosilations. *Angew. Chem. Int. Ed.* **2017**, *56*, 2260–2294.

(2) Waterman, R.; Hayes, P. G.; Tilley, T. D. Synthetic Development and Chemical Reactivity of Transition-Metal Silylene Complexes. *Acc. Chem. Res.* **2007**, *40*, 712–719.

(3) Iglesias, M.; Fernández-Alvarez, F. J.; Oro, L. A. Non-Classical Hydrosilane Mediated Reductions Promoted by Transition Metal Complexes. *Coord. Chem. Rev.* **2019**, *386*, 240–266.

(4) Corey, J. Y. B. T.-A. in O. C. Dehydrocoupling of Hydrosilanes to Polysilanes and Silicon Oligomers: A 30 Year Overview. In *Advances in Organometallic Chemistry*; Academic Press, 2004; pp 1–52.

(5) Waterman, R. Mechanisms of Metal-Catalyzed Dehydrocoupling Reactions. *Chem. Soc. Rev.* **2013**, *42*, 5629–5641.

(6) Lee, P. T. K.; Rosenberg, L. Borane-Catalysed Postpolymerisation Modification of the Si–H Bonds in Poly(Phenylsilane). *Dalton Trans.* **2017**, *46*, 8818–8826.

(7) Sudo, T.; Asao, N.; Gevorgyan, V.; Yamamoto, Y. Lewis Acid Catalyzed Highly Regio- and Stereocontrolled Trans-Hydrosilylation of Alkynes and Allenes. *J. Org. Chem.* **1999**, *64*, 2494–2499.

(8) Lambert, J. B.; Zhao, Y. A Stable β-Silyl Carbocation. *J. Am. Chem. Soc.* **1996**, *118*, 7867–7868.

(9) Lambert, J. B.; Zhao, Y.; Wu, H. β-Silyl and β-Germyl Carbocations Stable at Room Temperature. *J. Org. Chem.* **1999**, *64*, 2729–2736.

(10) Piers, W. E.; Chivers, T. Pentafluorophenylboranes: From Obscurity to Applications. *Chem. Soc. Rev.* **1997**, *26*, 345–354.

(11) Erker, G. Tris(Pentafluorophenyl)Borane: A Special Boron Lewis Acid for Special Reactions. *Dalton Trans.* **2005**, *11*, 1883–1890.

(12) Hackel, T.; McGrath, A. N. Tris(Pentafluorophenyl)Borane-Catalyzed Reactions Using Silanes. *Molecules*. **2019**, *24*, 432-462.

(13) Piers, W. E.; Marwitz, A. J. V; Mercier, L. G. Mechanistic Aspects of Bond Activation with Perfluoroarylboranes. *Inorg. Chem.* **2011**, *50*, 12252–12262.

(14) Blackwell, J. M.; Sonmor, E. R.; Scoccitti, T.; Piers, W. E. $B(C_6F_5)_3$-Catalyzed Hydrosilation of Imines via Silyliminium Intermediates. *Org. Lett.* **2000**, *2*, 3921–3923.

(15) Parks, D. J.; Piers, W. E. Tris(Pentafluorophenyl)Boron-Catalyzed Hydrosilation of Aromatic Aldehydes, Ketones, and Esters. *J. Am. Chem. Soc.* **1996**, *118*, 9440–9441.

(16) Oestreich, M.; Hermeke, J.; Mohr, J. A Unified Survey of Si–H and H–H Bond Activation Catalysed by Electron-Deficient Boranes. *Chem. Soc. Rev.* **2015**, *44*, 2202–2220.

(17) Robert, T.; Oestreich, M. Si−H Bond Activation: Bridging Lewis Acid Catalysis with Brookhart's Iridium(III) Pincer Complex and $B(C_6F_5)_3$. *Angew. Chem. Int. Ed.* **2013**, *52*, 5216–5218.

(18) Lee, P. T. K.; Skjel, M. K.; Rosenberg, L. Borane-Catalyzed Si–H Activation

Routes to Polysilanes Containing Thiolato Side Chains. *Organometallics* **2013**, *32*, 1575–1578.

(19) Lee, P. T. K.; Rosenberg, L. Scope and Selectivity of $B(C_6F_5)_3$-Catalyzed Reactions of the Disilane $(Ph_2SiH)_2$. *J. Organomet. Chem.* **2016**, *809*, 86–93.

(20) Rubin, M.; Schwier, T.; Gevorgyan, V. Highly Efficient $B(C_6F_5)_3$-Catalyzed Hydrosilylation of Olefins. *J. Org. Chem.* **2002**, *67*, 1936–1940.

(21) Mewald, M.; Oestreich, M. Illuminating the Mechanism of the Borane-Catalyzed Hydrosilylation of Imines with Both an Axially Chiral Borane and Silane. *Chem. Eur. J.* **2012**, *18*, 14079–14084.

(22) Houghton, A. Y.; Hurmalainen, J.; Mansikkamäki, A.; Piers, W. E.; Tuononen, H. M. Direct Observation of a Borane–Silane Complex Involved in Frustrated Lewis-Pair-Mediated Hydrosilylations. *Nat. Chem.* **2014**, *6*, 983.

(23) Chen, J.; Chen, E. Y.-X. Elusive Silane–Alane Complex [Si−H···Al]: Isolation, Characterization, and Multifaceted Frustrated Lewis Pair Type Catalysis. *Angew. Chem. Int. Ed.* **2015**, *54*, 6842–6846.

(24) Weicker, S. A.; Stephan, D. W. Main Group Lewis Acids in Frustrated Lewis Pair Chemistry: Beyond Electrophilic Boranes. *Bull. Chem. Soc. Jpn.* **2015**, *88*, 1003–1016.

(25) Bayne, J. M.; Stephan, D. W. Phosphorus Lewis Acids: Emerging Reactivity and Applications in Catalysis. *Chem. Soc. Rev.* **2016**, *45*, 765–774.

(26) Caputo, C. B.; Hounjet, L. J.; Dobrovetsky, R.; Stephan, D. W. Lewis Acidity of Organofluorophosphonium Salts: Hydrodefluorination by a Saturated Acceptor. *Science* **2013**, *341*, 1374−1377.

(27) Pérez, M.; Hounjet, L. J.; Caputo, C. B.; Dobrovetsky, R.; Stephan, D. W. Olefin Isomerization and Hydrosilylation Catalysis by Lewis Acidic Organofluorophosphonium Salts. *J. Am. Chem. Soc.* **2013**, *135*, 18308–18310.

(28) vom Stein, T.; Peréz, M.; Dobrovetsky, R.; Winkelhaus, D.; Caputo, C. B.; Stephan, D. W. Electrophilic Fluorophosphonium Cations in Frustrated Lewis Pair Hydrogen Activation and Catalytic Hydrogenation of Olefins. *Angew. Chem. Int. Ed.* **2015**, *54*, 10178–10182.

(29) Burford, N.; Ragogna, P. J. New Synthetic Opportunities Using Lewis Acidic Phosphines. *J. Chem. Soc. Dalton Trans.* **2002**, *23*, 4307–4315.

(30) Chitnis, S. S.; Burford, N. Phosphine Complexes of Lone Pair Bearing Lewis Acceptors. *Dalton Trans.* **2015**, *44*, 17–29.

(31) Chong, C. C.; Kinjo, R. Hydrophosphination of CO_2 and Subsequent Formate Transfer in the 1,3,2-Diazaphospholene-Catalyzed N-Formylation of Amines. *Angew. Chem. Int. Ed.* **2015**, *54*, 12116–12120.

(32) Adams, M. R.; Tien, C.-H.; Huchenski, B. S. N.; Ferguson, M. J.; Speed, A. W. H. Diazaphospholene Precatalysts for Imine and Conjugate Reductions. *Angew. Chem. Int. Ed.* **2017**, *56*, 6268–6271.

(33) Dunn, N. L.; Ha, M.; Radosevich, A. T. Main Group Redox Catalysis: Reversible P(III)/P(V) Redox Cycling at a Phosphorus Platform. *J. Am. Chem. Soc.* **2012**, *134*, 11330–11333.

(34) Gudat, D. A Very Peculiar Family of N-Heterocyclic Phosphines: Unusual Structures and the Unique Reactivity of 1,3,2-Diazaphospholenes. *Dalton Trans.* **2016**, *45*, 5896–5907.

(35) Andrews, R. J.; Chitnis, S. S.; Stephan, D. W. Carbonyl and Olefin Hydrosilylation Mediated by an Air-Stable Phosphorus(III) Dication under Mild Conditions. *Chem. Commun.* **2019**, *55*, 5599–5602.

(36) Chitnis, S. S.; Krischer, F.; Stephan, D. W. Catalytic Hydrodefluorination of C−F Bonds by an Air-Stable PIII Lewis Acid. *Chem. Eur. J.* **2018**, *24*, 6543–6546.

(37) Anslyn, E. V.; Dougherty, D. A. *Modern Physical Organic Chemistry*; University Science Books: Sausalito, CA, 2006; pp. 288-289.

(38) Mayer, U.; Gutmann, V.; Gerger, W. The Acceptor Number — A Quantitative Empirical Parameter for the Electrophilic Properties of Solvents. *Monatsh. Chem.* **1975**, *106*, 1235–1257.

(39) Gutmann, V. Solvent Effects on the Reactivities of Organometallic Compounds. *Coord. Chem. Rev.* **1976**, *18*, 225–255.

(40) Beckett, M. A.; Strickland, G. C.; Holland, J. R.; Sukumar Varma, K. A Convenient n.m.r. Method for the Measurement of Lewis Acidity at Boron Centres: Correlation of Reaction Rates of Lewis Acid Initiated Epoxide Polymerizations with Lewis Acidity. *Polymer* **1996**, *37*, 4629–4631.

(41) Sivaev, I. B.; Bregadze, V. I. Lewis Acidity of Boron Compounds. *Coord. Chem. Rev.* **2014**, *270–271*, 75–88.

(42) Beckett, M. A.; Brassington, D. S.; Coles, S. J.; Hursthouse, M. B. Lewis Acidity of Tris(Pentafluorophenyl)Borane: Crystal and Molecular Structure of $B(C_6F_5)_3 \cdot OPEt_3$. *Inorg. Chem. Commun.* **2000**, *3*, 530–533.

(43) Jupp, A. R.; Johnstone, T. C.; Stephan, D. W. The Global Electrophilicity Index as a Metric for Lewis Acidity. *Dalton Trans.* **2018**, *47*, 7029–7035.

(44) Jupp, A. R.; Johnstone, T. C.; Stephan, D. W. Improving the Global Electrophilicity Index (GEI) as a Measure of Lewis Acidity. *Inorg. Chem.* **2018**, *57*, 14764–14771.

(45) Parr, R. G.; Pearson, R. G. Absolute Hardness: Companion Parameter to Absolute Electronegativity. *J. Am. Chem. Soc.* **1983**, *105*, 7512–7516.

(46) Parr, R. G.; Szentpály, L. v.; Liu, S. Electrophilicity Index. *J. Am. Chem. Soc.* **1999**, *121*, 1922–1924.

(47) Hartwig, J. *Organotransition Metal Chemistry: From Bonding to Catalysis*; University Science Books: Sausalito, CA, 2010; pp. 177.

(48) Gray, G. M.; Gray, R. J. Synthesis and a Multinuclear NMR Spectroscopic Study of Some $Mo(CO)_5(PPh_2XR)$ (X = O, NH; R = 1-4 Carbon Alkyls) Complexes. Steric Effects on Phosphorus-31 and Molybdenum-95 Chemical Shifts. *Organometallics* **1983**, *2*, 1026–1031.

(49) Pan, B.; Gabbaï, F. P. $[Sb(C_6F_5)_4][B(C_6F_5)_4]$: An Air Stable, Lewis Acidic Stibonium Salt That Activates Strong Element-Fluorine Bonds. *J. Am. Chem. Soc.* **2014**, *136*, 9564–9567.

(50) Zhou, J.; Liu, L. L.; Cao, L. L.; Stephan, D. W. The Arene-Stabilized H5-Pentamethylcyclopentadienyl Arsenic Dication $[(\eta^5\text{-Cp*})As(Toluene)]_2^+$. *Angew. Chem. Int. Ed.* **2019**, *58*, 5407–5412.

(51) Connelly, S. J.; Kaminsky, W.; Heinekey, D. M. Structure and Solution Reactivity of (Triethylsilylium)Triethylsilane Cations. *Organometallics* **2013**, *32*, 7478–7481.

(52) Lambert, J. B.; Zhang, S.; Stern, C. L.; Huffman, J. C. Crystal Structure of a Silyl Cation with No Coordination to Anion and Distant Coordination to Solvent.

Science **1993**, *260*, 1917–1918.

(53) Kira, M.; Hino, T.; Sakurai, H. Chemistry of Organosilicon Compounds. 292. An NMR Study of the Formation of Silyloxonium Ions by Using Tetrakis[3,5-Bis(Trifluoromethyl)Phenyl]Borate as Counteranion. *J. Am. Chem. Soc.* **1992**, *114*, 6697–6700.

(54) Xie, Z.; Manning, J.; Reed, R. W.; Mathur, R.; Boyd, P. D. W.; Benesi, A.; Reed, C. A. Approaching the Silylium (R_3Si^+) Ion: Trends with Hexahalo (Cl, Br, I) Carboranes as Counterions. *J. Am. Chem. Soc.* **1996**, *118*, 2922–2928.

(55) Heiden, Z. M.; Lathem, A. P. Establishing the Hydride Donor Abilities of Main Group Hydrides. *Organometallics* **2015**, *34*, 1818–1827.

(56) Parks, D. J.; Blackwell, J. M.; Piers, W. E. Studies on the Mechanism of $B(C_6F_5)_3$-Catalyzed Hydrosilation of Carbonyl Functions. *J. Org. Chem.* **2000**, *65*, 3090–3098.

(57) Süsse, L.; LaFortune, J. H. W.; Stephan, D. W.; Oestreich, M. Axially Chiral, Electrophilic Fluorophosphonium Cations: Synthesis, Lewis Acidity, and Reactivity in the Hydrosilylation of Ketones. *Organometallics* **2019**, *38*, 712–721.

(58) Koller, J.; Bergman, R. G. Controlled Hydrosilylation of Carbonyls and Imines Catalyzed by a Cationic Aluminum Alkyl Complex. *Organometallics* **2012**, *31*, 2530–2533.

(59) Tran, B. L.; Pink, M.; Mindiola, D. J. Catalytic Hydrosilylation of the Carbonyl Functionality via a Transient Nickel Hydride Complex. *Organometallics* **2009**, *28*, 2234–2243.

(60) Song, Y.-S.; Yoo, B. R.; Lee, G.-H.; Jung, I. N. Lewis Acid-Catalyzed Regio- and

Stereoselective Hydrosilylation of Alkenes with Trialkylsilanes. *Organometallics* **1999**, *18*, 3109–3115.

(61) Bayne, J. M.; Holthausen, M. H.; Stephan, D. W. Pyridinium–Phosphonium Dications: Highly Electrophilic Phosphorus-Based Lewis Acid Catalysts. *Dalton Trans.* **2016**, *45*, 5949–5957.

(62) Scott, V. J.; Çelenligil-Çetin, R.; Ozerov, O. V. Room-Temperature Catalytic Hydrodefluorination of C(sp^3)−F Bonds. *J. Am. Chem. Soc.* **2005**, *127*, 2852–2853.

(63) Fryzuk, M. D.; Rosenberg, L.; Rettig, S. J. Reaction of Primary Silanes with Dinuclear Rhodium Hydride Complexes: Silane Coupling Reactions. *Inorganica Chim. Acta* **1994**, *222*, 345–364.

Chapter 6 Conclusions and Future Work

6.1. Chapter Overview

The work described in this thesis has provided information on the role of metal complexes containing phosphido (PR_2^-) and phosphenium (PR_2^+) ligands in the hydrophosphination of alkenes. This chapter describes future work needed to publish the projects presented in Chapters 3, 4 and 5, as well as future directions for each project. For example, ideas on how to expand the Ru-catalyzed hydrophosphination of activated alkenes to achieve higher catalyst activities and the possibility of asymmetric hydrophosphination (section 6.2) is presented. A proposal on how to take the stoichiometric phosphenium-mediated hydrophosphination toward catalysis is also described (section 6.3). Although outside the scope of hydrophosphination, Chapter 5 described the use of *trans*-$[Mo(CO)_4(PTol_2^pH)(PTol_2^p)][B(C_6H_3Cl_2)_4]$ (**12a**), *trans*-$[Mo(CO)_4(PPh_2H)(PPh_2)][B(C_6H_3Cl_2)_4]$ (**12b**) as Lewis acid catalysts for hydrosilylation. In section 6.4, ideas on how to improve the activity of these phosphenium complexes for hydrosilylation is presented.

6.2. Potential for a Highly Active Catalyst for Asymmetric Hydrophosphination of Activated Alkenes

As described in Chapters 2 and 3, the Ru phosphido complexes Ru(η^5-indenyl)(PPh_2)(NCPh)(PPh_3) (**4a**), Ru(η^5-indenyl)(PPh_2)(PPh_2H)(PPh_3) (**4b**), Ru(η^5-indenyl)(PPh_2)(CO)(PPh_3) (**4c**) and Ru(η^5-indenyl)(PPh_2)(**P**)$_2$ (**4e**, **P** = $P(Ph_2)CH_2CH_2CO_2Bu^t$) catalyze the hydrophosphination of electron-deficient alkenes. I

found that a critical motif of the active catalyst is a Ru complex that contains both a diphenylphosphido ligand and a diphenylphosphine ligand (substrate phosphine, PPh_2H). This motif is conducive to the proposed mechanism, which involves conjugate addition of the phosphido ligand to alkene (Scheme 6.1, Cycle 1, step C) and subsequent intramolecular H^+-transfer from the coordinated secondary phosphine (step D). The work presented in Chapter 3 provided some evidence for a possible competing mechanism that also relies on **4e** (Cycle 2).

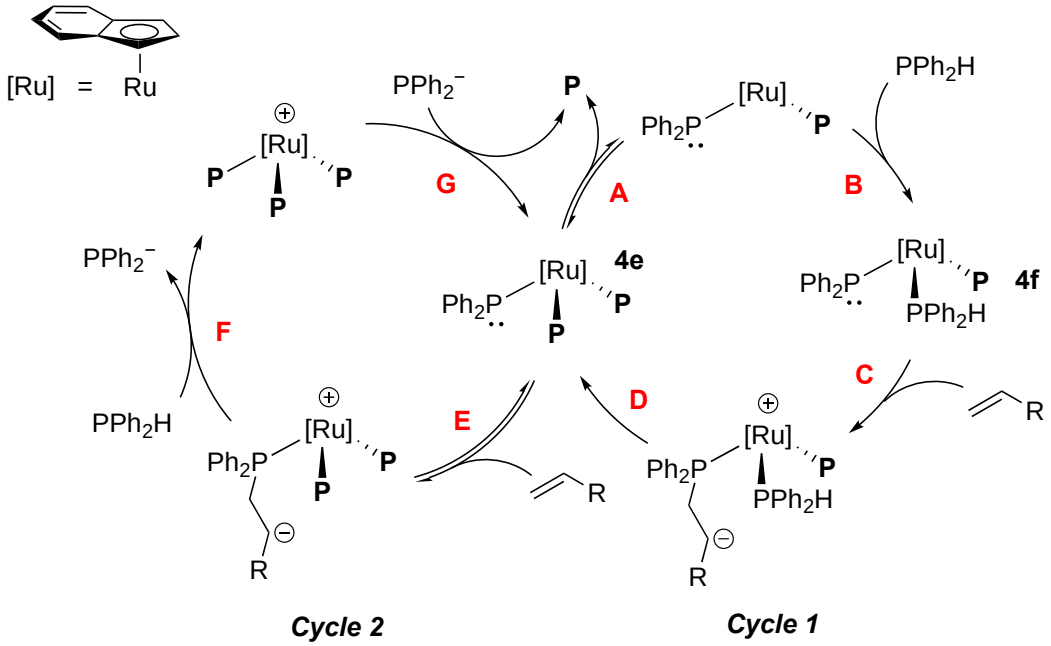

Scheme 6.1. Proposed mechanism for Ru-catalyzed hydrophosphination of activated alkenes.

Through this study, I found that catalysis by complexes **4a**,**b**,**e** is susceptible to product inhibition and that substitution of the hydrophosphination product phosphine from Ru

(Scheme 6.1, step A and B) is rate-limiting. Addressing the product inhibition and slow substitution will ultimately improve catalytic activity for hydrophosphination.

6.2.1. Future Work

Additional experimental work is currently in progress that will be included in the publication on the results presented in Chapter 3. I am currently studying the reaction kinetics of the hydrophosphination of *tert*-butyl acrylate with PPh_2H catalyzed by **4e** since it is the final resting state. Studying complex **4e** directly could provide additional information about the mechanism of catalysis. For example, if only one of the proposed cycles in Scheme 6.1 is operative in catalysis by **4e**, I should observe reaction rate dependences on the substrate concentrations that reflect that (i.e. if only Cycle 1 is operative, there should be a first-order dependence on the PPh_2H concentration and a zero-order dependence on the alkene concentration).

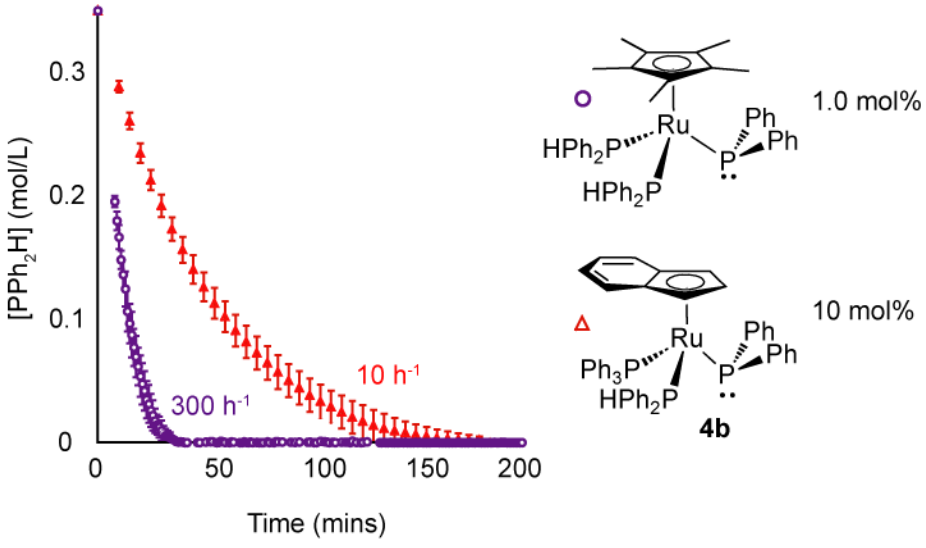

Figure 6.1. Reaction monitoring (^{1}H NMR) of the hydrophosphination of *tert*-butyl acrylate with PPh_2H catalyzed using 1.0 mol% of Ru(η^5-Cp*)(PPh_2)(PPh_2H)$_2$ (purple) and 10 mol% of **4a** (red).

A preliminary study of a new complex Ru(η^5-Cp*)(PPh_2)(PPh_2H)$_2$ (identified by Jin Yang, a graduate student in the Rosenberg group) showed that this complex is extremely active (TOF 300 h^{-1}) for the hydrophosphination of electron-deficient alkenes (Figure 6.1). To the best of my knowledge, this is among the highest reported TOFs for metal-catalyzed alkene hydrophosphination. As mentioned above, increasing substitutional lability at Ru should lead to a highly active catalyst for hydrophosphination because product substitution is rate-limiting for catalysis with **4a**,**b**,**e**. Jin Yang's study of Ru(η^5-Cp*) complexes demonstrated that there is increased substitutional lability for Ru(η^5-Cp*) complexes relative to Ru(η^5-indenyl) complexes.[1] The Cp* ligand encourages substitution by making the Ru centre more electron-rich as well as increasing steric congestion around Ru. Both of these factors favour the dissociative substitution mechanism of half-sandwich Ru complexes.[2] In terms of catalysis, this presumably helps to prevent product inhibition and increases the rate of substitution, which leads to an overall increase in catalytic activity for catalysis by Ru(η^5-Cp*)(PPh_2)(PPh_2H)$_2$ relative to **4a**,**b**,**e**.

Including a preliminary study of hydrophosphination catalyzed by Ru(η^5-Cp*)(PPh_2)(PPh_2H)$_2$ in a publication along with the results of Chapter 3 would beautifully demonstrate how mechanistic insight can guide the design of highly active catalysts. Some additional experiments will be need for this preliminary study (e.g. identifying intermediates by $^{31}P\{^1H\}$ NMR, same excess experiment etc.). These will confirm whether Ru(η^5-Cp*)(PPh_2)(PPh_2H)$_2$ participates in hydrophosphination catalysis via a similar mechanism to the one proposed for complexes **4a**,**b**,**e**. Furthermore, a same excess experiment would verify if product inhibition is prevented in hydrophosphination catalyzed

by Ru(η^5-Cp*)(PPh_2)(PPh_2H)$_2$. An undergraduate summer research student in our group, Hayley Parkin, is currently conducting this work.

6.2.2. Future Directions

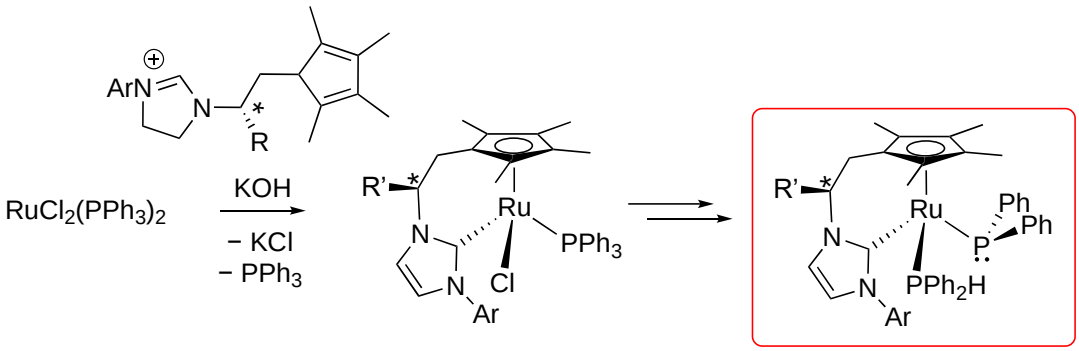

Figure 6.2. Synthesis and structure of a proposed chiral Ru phosphido complex bearing a chelating Cp*/NHC ligand.

A future direction for this project is to develop chiral Ru catalysts for asymmetric hydrophosphination. One possibility to achieve this is to design a catalyst that contains a chelating, chiral half-sandwich ligand.[3,4] In particular, I propose modifying the catalyst to contain a chelating Cp*/N-heterocyclic carbene (NHC) ligand (Figure 6.2).[5] The linkage between the Cp* and NHC moieties presents an opportunity to introduce chirality in the catalyst. Ru complexes of this ligand have been reported.[6] This complex could be prepared following a similar synthetic route to the one I used to prepare Ru(η^5-indenyl)Cl(PPh_3)$_2$ (**1**) (Figure 6.2). The phosphido ligand in the proposed structure would be very basic, which could present challenges in the preparation of this complex. For example, orthometalation of the N-Ar group or deprotonation of the Cp*/NHC linker by the phosphido ligand could occur. These reactions are likely to occur, as our group as shown, for coordinatively unsaturated Ru phosphido complexes. Thus, ensuring that the complex is coordinatively

saturated, as shown in the proposed structure, could prevent these reactions of the phosphido ligand.

This chiral phosphido complex could be even more active than Ru(η^5-Cp*)(PPh_2)(PPh_2H)$_2$. This Cp*/NHC ligand would provide even more electron density and steric congestion at Ru than Cp* because of the added NHC moiety coordinated to Ru; NHCs are strong σ-donors and can offer varying degrees of steric congestion through modifying the aryl (Ar) substituent. We could benchmark the success of this chiral catalyst by comparing the enantioselectivities to those of the asymmetric Pd-catalyzed hydrophosphination of activated alkenes reported by Leung *et al*, which are the highest reported enantioselectivities (> 99%) for hydrophosphination.[7]

6.3. Developing Metal Phosphenium Complexes as Catalysts for Hydrophosphination

The goal of developing metal phosphenium complexes for catalytic hydrophosphination is to widen the alkene substrate scope that participates in hydrophosphination catalysis. As shown in Chapter 2 and 3, late metal complexes that contain phosphido ligands generally catalyze the hydrophosphination of only electron-deficient alkenes because P-C bond formation occurs via conjugate addition of the phosphido to alkene. An electrophilic phosphenium ligand would participate in P-C bond via nucleophilic attack of alkene at phosphenium. This different avenue for P-C bond formation could address the limited substrate scope in metal-catalyzed hydrophosphination.

The work presented in Chapter 4 is a proof of concept that demonstrates the viability of metal phosphenium complexes as intermediates for the hydrophosphination of unsaturated substrates. In particular, the complex *trans*-[$Mo(CO)_3(PPh_2H)_2(PPh_2)$] (*trans*-**13**) mediates the stoichiometric hydrophosphination of a wide scope including simple alkenes such as ethylene, propene, 1-hexene and cyclopentene. These alkenes are traditionally challenging substrates for metal-catalyzed hydrophosphination.[8] Thus, besides demonstrating the viability of this methodology, this work demonstrates the potential of metal phosphenium complexes to mediate new transformations in hydrophosphination.

A proposed mechanism for hydrophosphination mediated by metal complexes with phosphenium ligands is shown in Scheme 6.2. This involves P-C bond formation via nucleophilic attack of alkene at the phosphenium ligand, which generates a carbocationic intermediate (Scheme 6.2, step A). Subsequent hydride transfer from the P-H bond of a coordinated PR_2H generates a new phosphenium complex with the coordinated hydrophosphination product (step B). I demonstrated that steps A and B occur in the absence of substrate phosphine. However, I found that under catalytic conditions, excess PR_2H coordinated to the phosphenium ligand (step D), which prevents P-C bond formation. A control experiment where excess PR_2H was added to a Mo complex containing a phosphenium and a product phosphine as ligands did not result in substitution of the product phosphine from Mo, which is required for turnover (step C). Thus, redesigning the complex to disfavour step D and favour step C is necessary to implement this catalytic hydrophosphination cycle (*vide infra*, section 6.3.2).

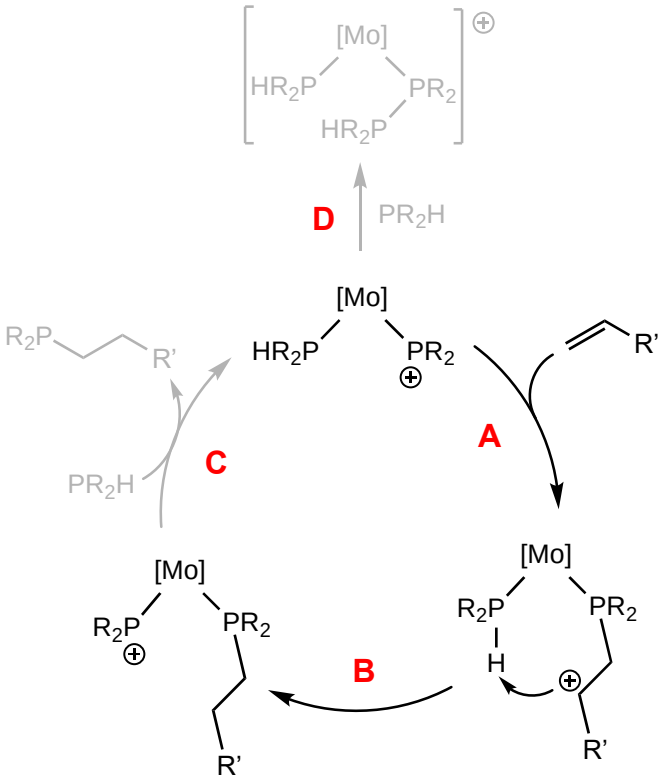

Scheme 6.2. Proposed mechanism for the hydrophosphination of alkenes mediated by metal phosphenium intermediates.

6.3.1. Future work

Additional work is needed in order to prepare the work presented in Chapter 4 for publication. For example, some supplementary work investigating the substrate scope is needed. Of utmost importance is providing additional evidence for the proposed mechanism of hydrophosphination mediated by **12a**,**b** and **13**. First, we need to definitively distinguish if hydride transfer (step B) is intra- or intermolecular, possibly via deuterium labelling experiments. Second, it will be particularly important to provide evidence for the proposed carbocationic intermediate, which results from addition of alkene to the phosphenium ligand (step A). A Hammett analysis[9] of the hydrophosphination of *para*-

substituted styrene derivatives mediated by **13** (Scheme 6.3) would provide such evidence. The *para*-substituents influence the electronics of the styrene derivatives and is defined by a substituent constant, σ; electron withdrawing substituents have high σ, and electron donating substituents have low σ. Plotting the log of the ratio of rate constants (k_X/k_H) for the reactions of styrene derivatives with **13** as a function of σ should produce a linear relationship defined by:

$$\log\left(\frac{k_X}{k_H}\right) = \rho\sigma_X$$

where ρ is the slope. A Hammett analysis would indicate that a carbocationic intermediate forms in the reaction if a linear correlation is observed that has a negative slope (ρ). Alternatively, non-linearity (e.g. if ρ changes) would signify a change in mechanism or rate-determining step among the series of styrenes investigated.

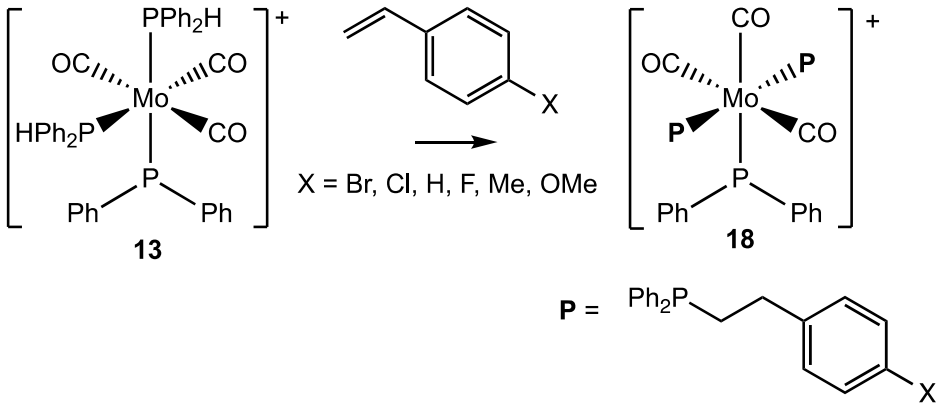

Scheme 6.3. Hydrophosphination of *para*-substituted styrene derivatives mediated by **13**.

6.3.2. Future Directions

As discussed above, catalysis by **12a**,**b** or **13** is precluded by adduct formation at the phosphenium ligands in these complexes with substrate phosphine (Scheme 6.2, step D) and the inhibition of product phosphine substitution (step C). Addressing these challenges may render the system catalytic. In order to do so, I propose modifying the structure of the Mo complex by replacing a CO ligand with a bulky and σ-donating ligand like an NHC (Figure 6.3). This would increase the electron density at Mo, which should favour dissociation of phosphine ligands from Mo and facilitate substitution (step C). If Mo is more electron rich, the phosphenium ligand would also be less electrophilic, which would decrease the strength of the adduct resulting from step D. If the electron density of Mo is further increased by replacing a CO ligand in **12a**,**b** or **13** with an NHC, the P-H bonds of the coordinated PR_2H will become even more hydridic, which will facilitate the hydride transfer of step B. Last, if the NHC is bulky, the increased steric congestion around Mo could also disfavour adduct formation (step D) and favour dissociation of phosphine ligands from Mo (step C). The complexes shown in Figure 6.3 may be prepared from *cis*-$Mo(CO)_4(piperidine)_2$ or *fac*-$Mo(CO)_3(NCMe)_3$. I would first have to prepare the precursor complexes containing PR_2H ligands and an NHC ligand. However, preparing these may not be trivial because a distribution of complexes could form from the addition of PR_2H and NHCs to *cis*-$Mo(CO)_4(piperidine)_2$ or *fac*-$Mo(CO)_3(NCMe)_3$ via ligand redistribution. If this is a problem, I could modify the reactions conditions (e.g. temperature, equivalents of PR_2H or NHC used, order of addition) to hopefully favour formation of the desired complexes.

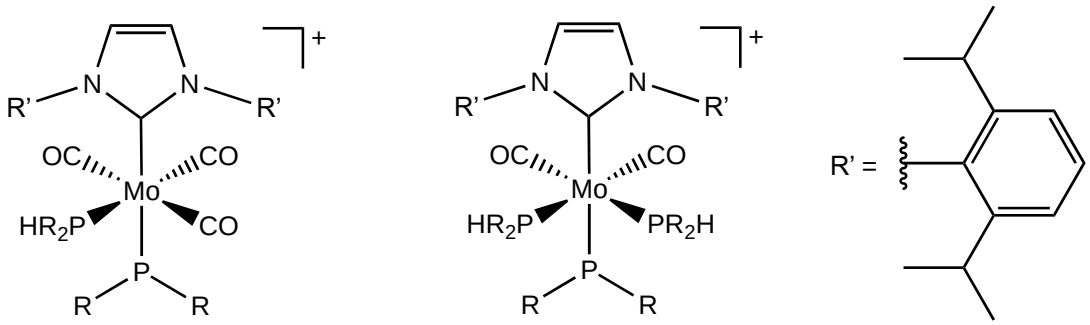

Figure 6.3. Possible structures of Mo-phosphenium complexes with the 1,3-bis(2,6-diisopropylphenyl) NHC ligand.

6.4. Exploring the Utility of Metal Phosphenium Complexes for Lewis Acid Catalyzed Reactions of Hydrosilanes

P-based Lewis acids recently gained traction in the field of main group catalysis, but are limited to P(V) Lewis acids.[10] Few examples of P(III) Lewis acids exist because these are traditionally thought of and used as Lewis bases. As described in Chapter 5, complexes **12a**,**b** are Lewis acids because the phosphenium ligands have a low-lying, empty p-orbital. This offered the opportunity to explore these complexes as P(III) Lewis acid catalysts.

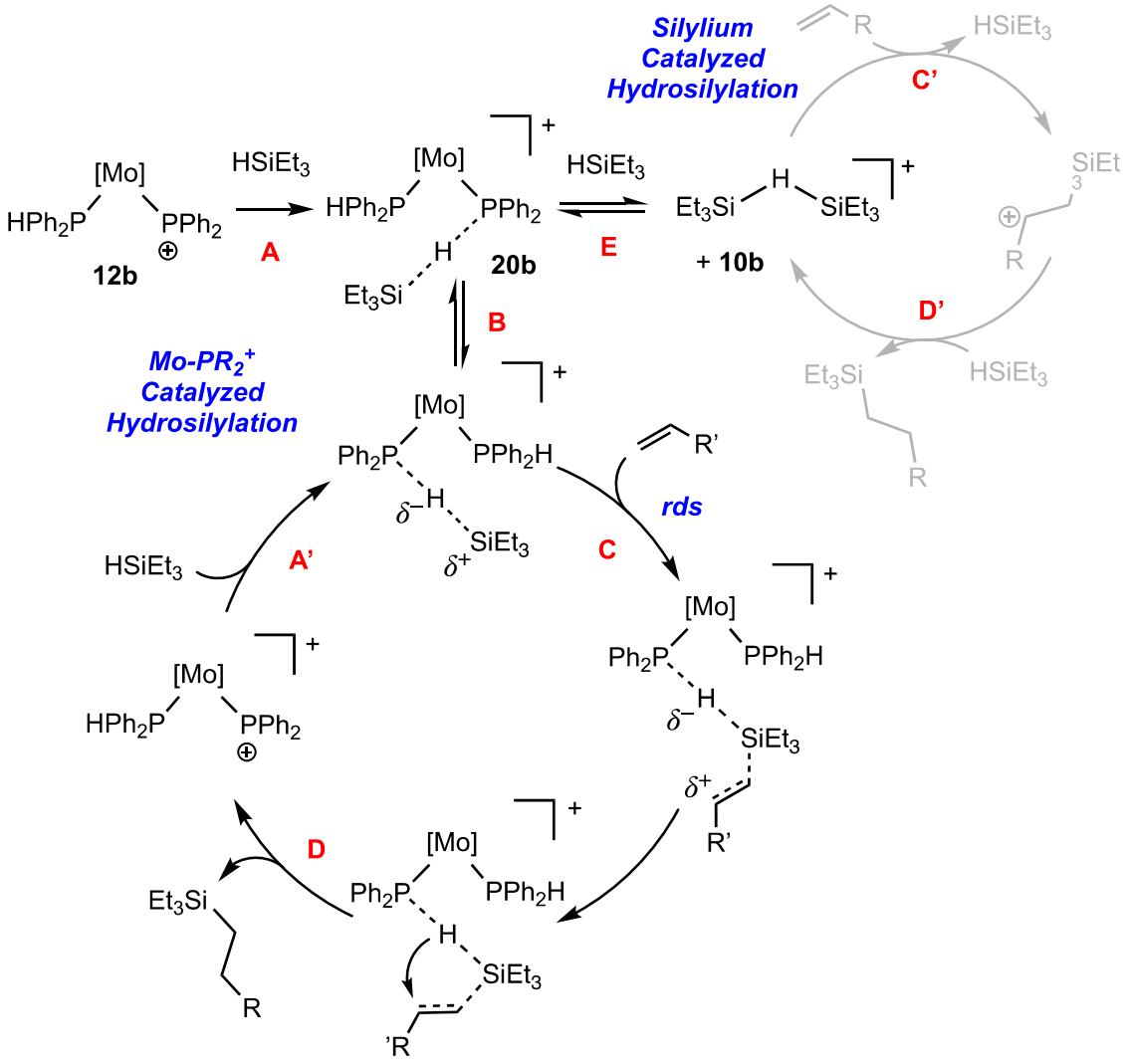

Scheme 6.4. Proposed mechanism for the hydrosilylation of alkenes with $HSiEt_3$ catalyzed by complexes **12a**,**b**.

As discussed in Chapter 5, complex **12b** catalyzes the hydrosilylation of alkenes. The proposed mechanism involves Si-H bond activation by **12b** via the formation of the silane adduct $[Mo(CO)_4(PPh_2H)(Ph_2P{\bullet\bullet\bullet}H{\bullet\bullet\bullet}SiEt_3)]$ (Scheme 6.4, **20b**, step A). Nucleophilic addition of alkene to the activated silane (step C) and subsequent hydride transfer (step D)

generates the hydrosilylation product. A silylium-catalyzed hydrosilylation, where **12b** act as an initiator, could not be ruled out.

6.4.1. Future work

In Chapter 5, the formation of the η^1-$HSiEt_3$ adduct of complex **12a** (**20a**) was tentatively proposed based on a VT NMR experiment. Additional work is needed in order to provide evidence that this species is in fact complex **20a**. Homo- and heteronuclear 2D NMR experiments at low temperature should exhibit the correlations shown in Figure 6.4, if it is in fact the η^1-$HSiEt_3$ adduct of complexes **12a.** For example, a $^1H/^{31}P\{^1H\}$-HMBC experiment should show a correlation between the methylene protons of the triethylsilyl group to the P nucleus of the P-H-Si moiety (red, Figure 6.4). A $^1H/^{31}P\{^1H\}$-HSQC experiment would identify the H of the P-H-Si moiety. Evidence for the proposed intramolecular silylium transfer could be provided by a ^1H EXSY experiment, which could show a correlation between the P-H bond of the PR_2H ligand and the H of the P-H-Si moiety (green). $^{29}Si\{^1H\}$ NMR, as well as $^1H/^{29}Si\{^1H\}$ HSQC/HMBC, is also needed in order to confirm the speciation of $HSiEt_3$ in this reaction, in particular, if $[Et_3Si\text{-}H\text{-}SiEt_3]^+$ forms. Furthermore, line shape analysis of the low temperature VT NMR data will provide the rate constants, which can be used to determine the activation parameters for the dynamic processes of **20a**.

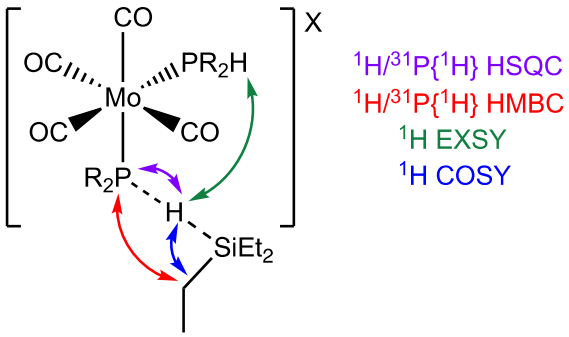

Figure 6.4. Expected 2D NMR correlations for the η^1-$HSiEt_3$ adduct of complexes **12a,b**.

6.4.2. Future Directions

The phosphenium ligands in **12a**,**b** as extremely strong Lewis acids (e.g. AN = 119, 121, respectively, from the Gutmann-Beckett test). This had deleterious implications on the hydrosilylation reported in Chapter 5 (and even for the hydrophosphination reported in Chapter 4). For example, the breadth of silanes used for the hydrosilylation catalyzed by complex **12b** is limited to trialkylsilanes because **12b** irreversibly abstracts a hydride from aromatic silanes, which are better hydride donors than alkyl silanes.[11] Second, under catalytic conditions, deactivation of **12b** to $Mo(CO)_4(PPh_2H)_2$ (**10b**) was frequently observed. Last, the high Lewis acidity of **12b** possibly enables a silylium-catalyzed hydrosilylation via hydride abstraction of silanes. Thus, I propose that a complex with a less Lewis acidic phosphenium ligand could address the issues described above. In order to do so, phosphenium complexes containing strong σ-donating ligands could be used because a more electron-rich metal centre will result in a less Lewis acidic phosphenium ligand. Candidates are the complexes containing NHC ligands shown in Figure 6.3. These are unique catalysts in that the Lewis acidity of the phosphenium ligand can be tuned through modifying the metal centre because the electron density at the metal influences the electrophilicity of the phosphenium ligand.

Utilizing metal phosphenium complexes for other Lewis acid-catalyzed reactions would be a significant contribution to the literature on P(III) Lewis acid catalysis. It would be worthwhile to explore other types of Lewis acid-catalyzed reactions of hydrosilanes using complexes **12a**,**b** or other Mo phosphenium complexes. For example, Lewis acids are known to catalyze the hydrodefluorination of C(sp^3)-F bonds using hydrosilanes[12] as well as catalyze the dehydrocoupling of hydrosilanes to generate Si-E bonds (E = O, N, S, C, P, B).[13] The same issues associated with the high Lewis acidity of **12a**,**b** (described above) may also be problematic in these other reactions, but further emphasizes the need to design a complex with a less Lewis acidic phosphenium ligand.

6.5. References

(1) Yang, J.; Langis-Barsetti, S.; McDonald, R.; Rosenberg, L. Terminal Phosphido Complexes of the Ru(η^5-Cp*) Fragment. *Organometallics*. Under Revision.

(2) Belli, R. G.; Wu, Y.; Ji, H.; Joshi, A.; Yunker, L. P. E.; McIndoe, J. S.; Rosenberg, L. Competitive Ligand Exchange and Dissociation in Ru Indenyl Complexes. *Inorg. Chem.* **2019**, *58*, 747–755. and references therein.

(3) Chai, Z.; Chu, J.; Qi, Y.; Tang, M.; Hou, J.; Yang, G. Half-Sandwich Chiral Rare-Earth Metal Complexes with Linked Tridentate Amido-Indenyl Ligand: Synthesis, Characterization, and Catalytic Properties for Intramolecular Hydroamination. *RSC Adv.* **2017**, *7*, 1759–1765.

(4) Consiglio, G.; Morandini, F. Half-Sandwich Chiral Ruthenium Complexes. *Chem. Rev.* **1987**, *87*, 761–778.

(5) Pontes da Costa, A.; Viciano, M.; Sanaú, M.; Merino, S.; Tejeda, J.; Peris, E.; Royo, B. First Cp*-Functionalized N-Heterocyclic Carbene and Its Coordination to Iridium. Study of the Catalytic Properties. *Organometallics* **2008**, *27*, 1305–1309.

(6) da Costa, A. P.; Mata, J. A.; Royo, B.; Peris, E. Preparation of Cp-Functionalized N-Heterocyclic Carbene Complexes of Ruthenium. Resolution of Chiral Complexes and Catalytic Studies. *Organometallics* **2010**, *29*, 1832–1838.

(7) (a) Yen Wong, E. H.; Jia, Y.-X.; Li, Y.; Pullarkat, S. A.; Leung, P.-H. Catalytic Asymmetric Synthesis of Pt- and Pd-PCP Pincer Complexes Bearing a Para-N Pyridinyl Backbone. *J. Organomet. Chem.* **2018**, *862*, 22–27. (b) Yang, X.-Y.; Tay, W. S.; Li, Y.; Pullarkat, S. A.; Leung, P.-H. Asymmetric 1,4-Conjugate

Addition of Diarylphosphines to α,β,γ,δ-Unsaturated Ketones Catalyzed by Transition-Metal Pincer Complexes. *Organometallics* **2015**, *34*, 5196–5201. (c) Li, X.-R.; Yang, X.-Y.; Li, Y.; Pullarkat, S. A.; Leung, P.-H. Efficient Access to a Designed Phosphapalladacycle Catalyst via Enantioselective Catalytic Asymmetric Hydrophosphination. *Dalton Trans.* **2017**, *46*, 1311–1316.

(8) Bange, C. A.; Waterman, R. Challenges in Catalytic Hydrophosphination. *Chem. Eur. J.* **2016**, *22*, 12598–12605.

(9) Anslyn, E. V.; Dougherty, D. A. *Modern Physical Organic Chemistry*; University Science Books: Sausalito, CA, 2006; pp. 445-451.

(10) Bayne, J. M.; Stephan, D. W. Phosphorus Lewis Acids: Emerging Reactivity and Applications in Catalysis. *Chem. Soc. Rev.* **2016**, *45*, 765–774.

(11) Heiden, Z. M.; Lathem, A. P. Establishing the Hydride Donor Abilities of Main Group Hydrides. *Organometallics* **2015**, *34*, 1818–1827.

(12) Chitnis, S. S.; Krischer, F.; Stephan, D. W. Catalytic Hydrodefluorination of C−F Bonds by an Air-Stable PIII Lewis Acid. *Chem. Eur. J.* **2018**, *24*, 6543–6546.

(13) Melen, R. L. Dehydrocoupling Routes to Element–Element Bonds Catalysed by Main Group Compounds. *Chem. Soc. Rev.* **2016**, *45*, 775–788.

Appendix A X-Ray Crystallographic structure report for [Ru(η^5-indenyl)(NCPh)(PPh_3)$_2$][B(C_6F_5)$_4$] (3a)

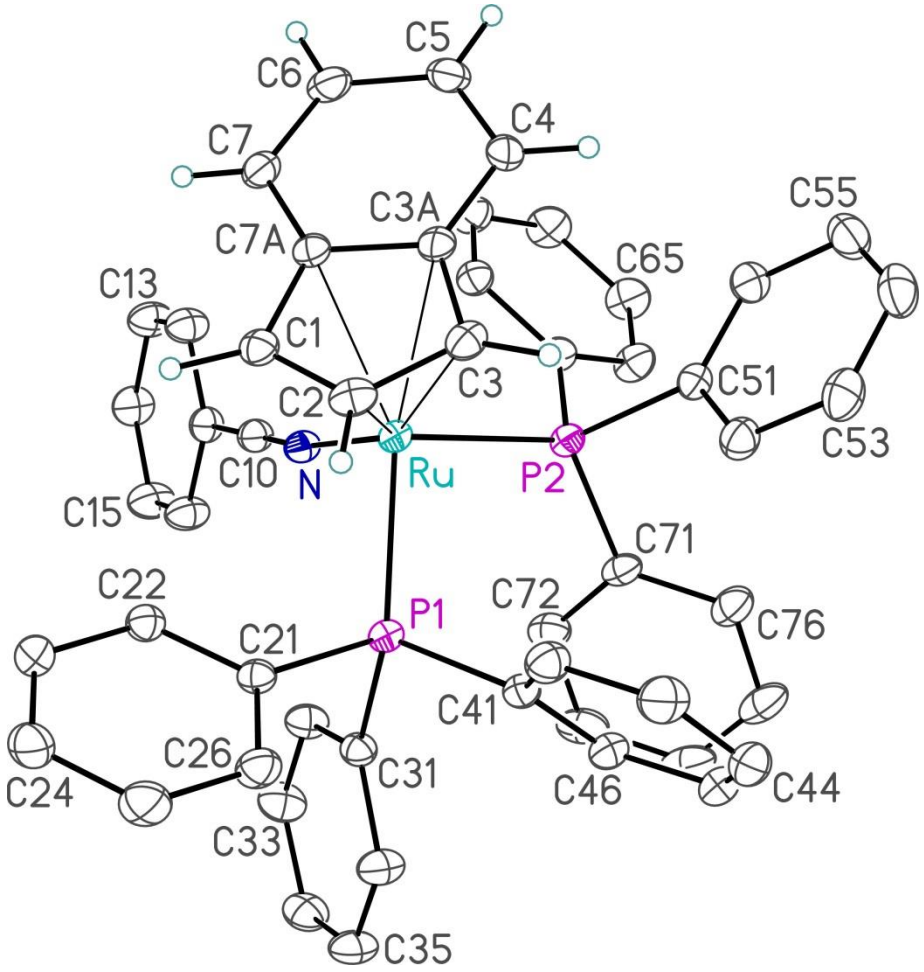

Figure A.1. Perspective view of the molecular structure of the cation from [Ru(η^5-indenyl)(NCPh)(PPh_3)$_2$][B(C_6F_5)$_4$] (**3a**) showing the atom labeling scheme. Non-hydrogen atoms are represented by Gaussian ellipsoids at the 30% probability level. Hydrogen atoms attached to the indenyl group, C8 and C9 are shown with arbitrarily small thermal parameters; phenyl-group hydrogens are not shown.

This structure determination, as well as that of complex **3b** in Appendix B, **7** in Appendix C and **12a** in Appendix D, were carried out by Dr. Robert McDonald at the X-Ray Crystallography Laboratory, Department of Chemistry, University of Alberta, Edmonton, Alberta, Canada T6G 2G2. E-mail: Bob.McDonald@ualberta.ca. Phone: 1-(780)-492-2485.

Table A.1. Crystallographic Experimental Details

A. Crystal Data	
formula	$C_{91}H_{57}BF_{20}NP_2Ru$
formula weight	1718.19
crystal dimensions (mm)	0.24 × 0.22 × 0.15
crystal system	triclinic
space group	$P\bar{1}$ (No. 2)
unit cell parameters[a]	
a (Å)	16.0400 (6)
b (Å)	16.8124 (6)
c (Å)	16.8412 (6)
α (deg)	104.6950 (4)
β (deg)	107.8349 (4)
γ (deg)	108.4208 (4)
V (Å^3)	3780.4 (2)
Z	2
ρ_{calcd} (g cm^{-3})	1.509
μ (mm^{-1})	0.349
B. Data Collection and Refinement Conditions	
diffractometer	Bruker PLATFORM/APEX II CCD[b]
radiation (λ [Å])	graphite-monochromated Mo Kα (0.71073)
temperature (°C)	–80
scan type	ω scans (0.3°) (15 s exposures)
data collection 2θ limit (deg)	56.87
total data collected	35924 (-21 ≤ h ≤ 21, -22 ≤ k ≤ 22, -22 ≤ l ≤ 22)
independent reflections	18521 (R_{int} = 0.0249)
number of observed reflections (*NO*)	15091 [$F_o^2 \geq 2\sigma(F_o^2)$]
structure solution method	intrinsic phasing (*SHELXT-2014*[c])
refinement method	full-matrix least-squares on F^2 (*SHELXL–2014*[d])
absorption correction method	Gaussian integration (face-indexed)
range of transmission factors	1.0000–0.9187
data/restraints/parameters	18521 / 0 / 1000
goodness-of-fit (S)[e] [all data]	1.047
final R indices[f]	
R_1 [$F_o^2 \geq 2\sigma(F_o^2)$]	0.0377
wR_2 [all data]	0.0970
largest difference peak and hole	0.780 and –0.535 e Å^{-3}

[a]Obtained from least-squares refinement of 9994 reflections with 4.60° < 2θ < 52.24°.

[b]Programs for diffractometer operation, data collection, data reduction and absorption correction were those supplied by Bruker.

[c]Sheldrick, G. M. *Acta Crystallogr.* **2015**, *A71*, 3–8.

[d]Sheldrick, G. M. *Acta Crystallogr.* **2015**, *C71*, 3–8.

[e]$S = [\Sigma w(F_o^2 - F_c^2)^2/(n - p)]^{1/2}$ (n = number of data; p = number of parameters varied; $w = [\sigma^2(F_o^2) + (0.0413P)^2 + 1.4346P]^{-1}$ where $P = [\mathrm{Max}(F_o^2, 0) + 2F_c^2]/3$).

[f]$R_1 = \Sigma||F_o| - |F_c||/\Sigma|F_o|$; $wR_2 = [\Sigma w(F_o^2 - F_c^2)^2/\Sigma w(F_o^4)]^{1/2}$.

Table A.2. Atomic Coordinates and Equivalent Isotropic Displacement Parameters

(a) atoms of the [(η^5–indenyl)Ru(NCPh)(PPh_3)$_2$]$^+$ ion

Atom	*x*	*y*	*z*	U_{eq}, Å^2
Ru	0.16331(2)	0.42696(2)	0.18916(2)	0.02368(5)*
P1	0.15243(3)	0.28203(3)	0.16799(3)	0.02488(10)*
P2	0.04216(4)	0.41919(3)	0.24311(3)	0.02677(10)*
N	0.27063(12)	0.49072(11)	0.31770(11)	0.0287(3)*
C1	0.24900(15)	0.47602(13)	0.11607(13)	0.0307(4)*
C2	0.16013(16)	0.40060(14)	0.05416(13)	0.0333(4)*
C3	0.08220(15)	0.42243(14)	0.05663(13)	0.0324(4)*
C3A	0.12383(14)	0.51854(14)	0.11317(13)	0.0300(4)*
C4	0.08262(16)	0.58055(15)	0.13126(15)	0.0361(5)*
C5	0.14340(17)	0.67025(16)	0.18362(17)	0.0413(5)*
C6	0.24507(17)	0.70150(15)	0.22231(16)	0.0403(5)*
C7	0.28735(15)	0.64361(14)	0.20815(14)	0.0343(4)*
C7A	0.22685(14)	0.55088(13)	0.15041(13)	0.0290(4)*
C10	0.33010(15)	0.53785(14)	0.38864(14)	0.0311(4)*
C11	0.39955(14)	0.59528(14)	0.48020(13)	0.0315(4)*
C12	0.43260(17)	0.68901(15)	0.50945(15)	0.0412(5)*
C13	0.49408(18)	0.74292(16)	0.59884(16)	0.0458(6)*
C14	0.52275(17)	0.70431(16)	0.65918(15)	0.0447(5)*
C15	0.49017(18)	0.61139(17)	0.63016(16)	0.0493(6)*
C16	0.42889(17)	0.55633(15)	0.54054(15)	0.0433(5)*
C21	0.22999(14)	0.25578(13)	0.11443(13)	0.0272(4)*
C22	0.32423(14)	0.32228(14)	0.14820(14)	0.0307(4)*
C23	0.39022(16)	0.30589(15)	0.11765(15)	0.0376(5)*
C24	0.36275(18)	0.22309(17)	0.05144(17)	0.0454(6)*
C25	0.26985(19)	0.15623(16)	0.01744(18)	0.0478(6)*
C26	0.20372(17)	0.17178(14)	0.04904(15)	0.0379(5)*
C31	0.19049(14)	0.24092(13)	0.25836(13)	0.0290(4)*
C32	0.25683(16)	0.30110(15)	0.34555(14)	0.0370(5)*
C33	0.29047(18)	0.26981(17)	0.41211(16)	0.0451(5)*
C34	0.25833(18)	0.17791(17)	0.39191(16)	0.0438(5)*
C35	0.19466(18)	0.11725(16)	0.30532(17)	0.0462(6)*
C36	0.16079(17)	0.14796(15)	0.23844(16)	0.0409(5)*

C41	0.02987(14)	0.19440(13)	0.09212(14)	0.0295(4)*
C42	-0.00756(16)	0.17569(14)	-0.00072(15)	0.0376(5)*
C43	-0.10273(18)	0.11358(16)	-0.05718(17)	0.0472(6)*
C44	-0.16247(17)	0.07011(16)	-0.02208(18)	0.0494(6)*
C45	-0.12684(16)	0.08989(15)	0.06963(17)	0.0436(5)*
C46	-0.03169(15)	0.15100(13)	0.12637(15)	0.0350(4)*
C51	-0.07142(14)	0.40356(14)	0.15734(14)	0.0311(4)*
Atom	*x*	*y*	*z*	U_{eq}, Å^2
C52	-0.12244(15)	0.32395(15)	0.07905(15)	0.0380(5)*
C53	-0.20806(17)	0.30938(17)	0.01178(16)	0.0464(6)*
C54	-0.24285(17)	0.37499(19)	0.02159(17)	0.0498(6)*
C55	-0.19316(18)	0.45434(18)	0.09793(18)	0.0480(6)*
C56	-0.10802(16)	0.46859(16)	0.16602(16)	0.0390(5)*
C61	0.07497(15)	0.52446(13)	0.33634(13)	0.0306(4)*
C62	0.15264(15)	0.60415(14)	0.35506(14)	0.0330(4)*
C63	0.17535(17)	0.68509(15)	0.42296(15)	0.0411(5)*
C64	0.12119(18)	0.68708(16)	0.47257(16)	0.0467(6)*
C65	0.04382(19)	0.60819(16)	0.45457(17)	0.0472(6)*
C66	0.02107(17)	0.52733(15)	0.38724(15)	0.0406(5)*
C71	-0.00009(15)	0.33453(13)	0.28940(14)	0.0320(4)*
C72	0.06937(18)	0.32805(15)	0.35748(15)	0.0394(5)*
C73	0.0433(2)	0.26369(17)	0.39400(18)	0.0500(6)*
C74	-0.0530(2)	0.20640(16)	0.36352(19)	0.0524(7)*
C75	-0.1227(2)	0.21404(16)	0.29816(19)	0.0516(7)*
C76	-0.09722(17)	0.27751(15)	0.26047(17)	0.0431(5)*

(b) tetrakis(pentafluorophenyl)borate ion atoms

Atom	*x*	*y*	*z*	U_{eq}, Å^2
F82	0.40937(10)	0.19606(8)	0.86401(8)	0.0420(3)*
F83	0.48913(12)	0.37287(10)	0.96411(10)	0.0596(4)*
F84	0.53128(11)	0.49712(9)	0.88839(12)	0.0637(4)*
F85	0.49521(11)	0.43829(9)	0.70969(12)	0.0586(4)*
F86	0.41495(9)	0.26280(9)	0.60811(9)	0.0434(3)*
F92	0.18941(9)	-0.03890(9)	0.49472(8)	0.0428(3)*
F93	0.20511(11)	-0.09987(10)	0.34164(9)	0.0597(4)*
F94	0.37570(13)	-0.02981(12)	0.32968(10)	0.0662(4)*
F95	0.53512(10)	0.10409(10)	0.47886(10)	0.0506(4)*
F96	0.52277(8)	0.16586(8)	0.63445(9)	0.0401(3)*
F102	0.56446(8)	0.18314(8)	0.81900(9)	0.0397(3)*
F103	0.65136(10)	0.08530(10)	0.87210(10)	0.0534(4)*
F104	0.55491(12)	-0.09806(10)	0.81383(11)	0.0604(4)*
F105	0.36391(11)	-0.18230(9)	0.69406(12)	0.0595(4)*
F106	0.27487(9)	-0.08735(8)	0.63337(9)	0.0405(3)*

F112	0.21501(9)	0.15045(9)	0.56424(8)	0.0410(3)*
F113	0.03483(9)	0.11461(10)	0.54578(9)	0.0477(3)*
F114	-0.03748(9)	0.02848(10)	0.64401(10)	0.0525(4)*
F115	0.07945(10)	-0.01218(9)	0.76609(10)	0.0487(3)*
F116	0.25678(9)	0.01755(8)	0.78206(8)	0.0376(3)*

Atom	*x*	*y*	*z*	U_{eq}, Å^2
C81	0.40950(13)	0.21830(13)	0.73048(13)	0.0288(4)*
C82	0.42980(15)	0.25352(14)	0.82219(14)	0.0329(4)*
C83	0.47058(16)	0.34497(15)	0.87592(16)	0.0405(5)*
C84	0.49202(16)	0.40756(14)	0.83765(18)	0.0428(5)*
C85	0.47314(16)	0.37765(15)	0.74810(18)	0.0413(5)*
C86	0.43185(14)	0.28495(14)	0.69605(14)	0.0322(4)*
C91	0.35449(14)	0.07072(13)	0.57339(13)	0.0296(4)*
C92	0.27714(15)	0.00131(14)	0.49560(14)	0.0329(4)*
C93	0.28328(17)	-0.03243(15)	0.41476(15)	0.0405(5)*
C94	0.36951(19)	0.00273(16)	0.40833(15)	0.0426(5)*
C95	0.44900(17)	0.07020(15)	0.48329(16)	0.0385(5)*
C96	0.44003(15)	0.10145(14)	0.56264(14)	0.0318(4)*
C101	0.41242(14)	0.05421(13)	0.72441(13)	0.0270(4)*
C102	0.50916(14)	0.09223(13)	0.78528(14)	0.0302(4)*
C103	0.55679(15)	0.04308(15)	0.81518(14)	0.0354(5)*
C104	0.50888(17)	-0.04945(16)	0.78513(16)	0.0400(5)*
C105	0.41311(17)	-0.09159(14)	0.72495(16)	0.0380(5)*
C106	0.36867(14)	-0.03997(13)	0.69586(14)	0.0305(4)*
C111	0.24499(14)	0.08205(13)	0.67023(13)	0.0276(4)*
C112	0.18342(15)	0.10728(14)	0.61429(13)	0.0309(4)*
C113	0.09014(15)	0.09044(14)	0.60403(14)	0.0342(4)*
C114	0.05360(15)	0.04766(14)	0.65331(15)	0.0366(5)*
C115	0.11219(15)	0.02556(14)	0.71321(15)	0.0353(5)*
C116	0.20518(14)	0.04245(13)	0.72082(14)	0.0302(4)*
B	0.35492(15)	0.10666(14)	0.67523(15)	0.0262(4)*

(c) solvent benzene atoms

Atom	*x*	*y*	*z*	U_{eq}, Å^2
C11S	0.0386(2)	0.2213(2)	0.79026(19)	0.0582(7)*
C12S	0.0410(2)	0.2683(2)	0.7346(2)	0.0607(7)*
C13S	0.1272(2)	0.3159(2)	0.7336(3)	0.0737(9)*
C14S	0.2114(2)	0.3163(2)	0.7890(3)	0.0810(10)*
C15S	0.2089(2)	0.2696(2)	0.8448(2)	0.0671(8)*
C16S	0.1227(2)	0.2223(2)	0.84529(18)	0.0598(7)*
C21S[a]	0.6739(3)	0.4518(4)	0.2421(2)	0.0646(16)

C22S[a]	0.6953(4)	0.3802(3)	0.2529(3)	0.087(2)
C23S[a]	0.7475(4)	0.3866(3)	0.3390(3)	0.064(4)
C24S[a]	0.7782(4)	0.4645(3)	0.4142(2)	0.0553(15)
C25S[a]	0.7568(3)	0.5361(2)	0.4034(2)	0.0572(14)
C26S[a]	0.7047(3)	0.5297(3)	0.3173(3)	0.0530(13)

Atom	*x*	*y*	*z*	U_{eq}, Å^2
C31S[a]	0.6615(3)	0.3991(4)	0.2127(3)	0.0655(15)
C32S[a]	0.6995(4)	0.3509(3)	0.2572(3)	0.0719(18)
C33S[a]	0.7548(5)	0.3910(4)	0.3503(3)	0.084(5)
C34S[a]	0.7721(5)	0.4793(4)	0.3988(3)	0.102(3)
C35S[a]	0.7341(5)	0.5275(3)	0.3542(4)	0.104(3)
C36S[a]	0.6788(4)	0.4874(3)	0.2612(4)	0.0690(17)
C41S[a]	0.4179(2)	-0.0438(2)	-0.0451(3)	0.0613(15)
C42S[a]	0.4469(3)	0.0459(3)	-0.0376(3)	0.0473(12)
C43S[a]	0.5438(3)	0.10741(19)	0.0115(3)	0.0708(17)
C44S[a]	0.6117(2)	0.0792(3)	0.0532(3)	0.0790(19)
C45S[a]	0.5827(3)	-0.0106(3)	0.0457(3)	0.0643(16)
C46S[a]	0.4858(3)	-0.0721(2)	-0.0035(3)	0.0700(17)

Anisotropically-refined atoms are marked with an asterisk (*). The form of the anisotropic displacement parameter is: $\exp[-2\pi^2(h^2a^{*2}U_{11} + k^2b^{*2}U_{22} + l^2c^{*2}U_{33} + 2klb^*c^*U_{23} + 2hla^*c^*U_{13} + 2hka^*b^*U_{12})]$. [a]Refined with an occupancy factor of 0.5.

Table A.3. Selected Interatomic Distances (Å)

(a) within the [(η^5–indenyl)Ru(NCPh)(PPh_3)$_2$]$^+$ ion

Atom1	Atom2	Distance	Atom1	Atom2	Distance
Ru	P1	2.3123(5)	C22	C23	1.381(3)
Ru	P2	2.3664(5)	C23	C24	1.378(3)
Ru	N	2.0426(17)	C24	C25	1.380(3)
Ru	C1	2.2181(19)	C25	C26	1.388(3)
Ru	C2	2.1844(19)	C31	C32	1.386(3)
Ru	C3	2.1801(19)	C31	C36	1.395(3)
Ru	C3A	2.3515(18)	C32	C33	1.390(3)
Ru	C7A	2.3581(18)	C33	C34	1.375(3)
P1	C21	1.8408(19)	C34	C35	1.373(3)
P1	C31	1.8435(19)	C35	C36	1.389(3)
P1	C41	1.829(2)	C41	C42	1.400(3)
P2	C51	1.835(2)	C41	C46	1.395(3)
P2	C61	1.836(2)	C42	C43	1.387(3)
P2	C71	1.836(2)	C43	C44	1.388(4)
N	C10	1.144(3)	C44	C45	1.379(4)
C1	C2	1.415(3)	C45	C46	1.384(3)
C1	C7A	1.444(3)	C51	C52	1.397(3)
C2	C3	1.419(3)	C51	C56	1.392(3)
C3	C3A	1.453(3)	C52	C53	1.387(3)
C3A	C4	1.419(3)	C53	C54	1.382(4)
C3A	C7A	1.430(3)	C54	C55	1.378(4)
C4	C5	1.368(3)	C55	C56	1.390(3)
C5	C6	1.412(3)	C61	C62	1.392(3)
C6	C7	1.365(3)	C61	C66	1.394(3)
C7	C7A	1.419(3)	C62	C63	1.391(3)
C10	C11	1.436(3)	C63	C64	1.379(3)
C11	C12	1.387(3)	C64	C65	1.384(3)
C11	C16	1.387(3)	C65	C66	1.385(3)
C12	C13	1.376(3)	C71	C72	1.388(3)
C13	C14	1.379(3)	C71	C76	1.392(3)
C14	C15	1.376(3)	C72	C73	1.390(3)
C15	C16	1.382(3)	C73	C74	1.380(4)
C21	C22	1.393(3)	C74	C75	1.374(4)
C21	C26	1.391(3)	C75	C76	1.391(3)

(b) within the tetrakis(pentafluorophenyl)borate ion

Atom1	Atom2	Distance	Atom1	Atom2	Distance
F82	C82	1.350(2)	F84	C84	1.346(2)
F83	C83	1.342(3)	F85	C85	1.353(2)

Atom1	Atom2	Distance	Atom1	Atom2	Distance
F86	C86	1.348(2)	C85	C86	1.391(3)
F92	C92	1.348(2)	C91	C92	1.390(3)
F93	C93	1.350(3)	C91	C96	1.391(3)
F94	C94	1.346(2)	C91	B	1.665(3)
F95	C95	1.351(2)	C92	C93	1.382(3)
F96	C96	1.357(2)	C93	C94	1.372(3)
F102	C102	1.356(2)	C94	C95	1.371(3)
F103	C103	1.344(2)	C95	C96	1.376(3)
F104	C104	1.345(2)	C101	C102	1.391(3)
F105	C105	1.343(2)	C101	C106	1.391(3)
F106	C106	1.361(2)	C101	B	1.653(3)
F112	C112	1.354(2)	C102	C103	1.376(3)
F113	C113	1.346(2)	C103	C104	1.369(3)
F114	C114	1.341(2)	C104	C105	1.372(3)
F115	C115	1.354(2)	C105	C106	1.376(3)
F116	C116	1.356(2)	C111	C112	1.393(3)
C81	C82	1.396(3)	C111	C116	1.389(3)
C81	C86	1.387(3)	C111	B	1.649(3)
C81	B	1.653(3)	C112	C113	1.377(3)
C82	C83	1.381(3)	C113	C114	1.373(3)
C83	C84	1.376(3)	C114	C115	1.367(3)
C84	C85	1.363(3)	C115	C116	1.385(3)

(c) within the solvent benzene molecules

Atom1	Atom2	Distance	Atom1	Atom2	Distance
C11S	C12S	1.373(4)	C31S	C32S	1.390[a]
C11S	C16S	1.375(4)	C31S	C36S	1.390[a]
C12S	C13S	1.369(4)	C32S	C33S	1.390[a]
C13S	C14S	1.383(4)	C33S	C34S	1.390[a]
C14S	C15S	1.371(5)	C34S	C35S	1.390[a]
C15S	C16S	1.363(4)	C35S	C36S	1.390[a]
C21S	C22S	1.390[a]	C41S	C42S	1.390[a]
C21S	C26S	1.390[a]	C41S	C46S	1.390[a]
C22S	C23S	1.390[a]	C42S	C43S	1.390[a]
C23S	C24S	1.390[a]	C43S	C44S	1.390[a]
C24S	C25S	1.390[a]	C44S	C45S	1.390[a]
C25S	C26S	1.390[a]	C45S	C46S	1.390[a]

[a]Distance fixed during refinement.

Table A.4. Selected Interatomic Angles (deg)

(a) within the [(η^5–indenyl)Ru(NCPh)(PPh_3)$_2$]$^+$ ion

Atom1	Atom2	Atom3	Angle	Atom1	Atom2	Atom3	Angle
P1	Ru	P2	98.240(17)	Ru	C1	C7A	76.98(11)
P1	Ru	N	96.82(5)	C2	C1	C7A	107.36(18)
P1	Ru	C1	104.78(5)	Ru	C2	C1	72.54(11)
P1	Ru	C2	87.01(5)	Ru	C2	C3	70.87(11)
P1	Ru	C3	106.66(6)	C1	C2	C3	109.40(18)
P1	Ru	C3A	143.60(5)	Ru	C3	C2	71.20(11)
P1	Ru	C7A	141.38(5)	Ru	C3	C3A	77.84(11)
P2	Ru	N	91.84(5)	C2	C3	C3A	107.19(17)
P2	Ru	C1	153.07(5)	Ru	C3A	C3	65.00(10)
P2	Ru	C2	132.54(6)	Ru	C3A	C4	130.86(14)
P2	Ru	C3	96.82(6)	Ru	C3A	C7A	72.58(11)
P2	Ru	C3A	92.02(5)	C3	C3A	C4	132.93(19)
P2	Ru	C7A	118.91(5)	C3	C3A	C7A	107.42(17)
N	Ru	C1	99.00(7)	C4	C3A	C7A	119.54(19)
N	Ru	C2	134.58(7)	C3A	C4	C5	118.5(2)
N	Ru	C3	153.42(7)	C4	C5	C6	121.7(2)
N	Ru	C3A	117.74(7)	C5	C6	C7	121.4(2)
N	Ru	C7A	92.40(7)	C6	C7	C7A	118.5(2)
C1	Ru	C2	37.50(7)	Ru	C7A	C1	66.41(10)
C1	Ru	C3	63.45(8)	Ru	C7A	C3A	72.08(10)
C1	Ru	C3A	61.11(7)	Ru	C7A	C7	128.78(14)
C1	Ru	C7A	36.61(7)	C1	C7A	C3A	108.09(18)
C2	Ru	C3	37.94(8)	C1	C7A	C7	131.73(19)
C2	Ru	C3A	61.14(7)	C3A	C7A	C7	120.16(18)
C2	Ru	C7A	60.80(7)	N	C10	C11	175.9(2)
C3	Ru	C3A	37.16(7)	C10	C11	C12	120.11(19)
C3	Ru	C7A	61.45(7)	C10	C11	C16	119.61(19)
C3A	Ru	C7A	35.34(7)	C12	C11	C16	120.17(19)
Ru	P1	C21	112.14(6)	C11	C12	C13	119.5(2)
Ru	P1	C31	125.79(7)	C12	C13	C14	120.4(2)
Ru	P1	C41	112.05(6)	C13	C14	C15	120.1(2)
C21	P1	C31	95.92(9)	C14	C15	C16	120.3(2)
C21	P1	C41	105.06(9)	C11	C16	C15	119.5(2)
C31	P1	C41	103.23(9)	P1	C21	C22	117.04(14)
Ru	P2	C51	112.85(7)	P1	C21	C26	124.37(15)
Ru	P2	C61	113.23(7)	C22	C21	C26	118.32(18)
Ru	P2	C71	122.21(7)	C21	C22	C23	121.20(19)
C51	P2	C61	103.16(9)	C22	C23	C24	120.0(2)
C51	P2	C71	102.47(10)	C23	C24	C25	119.7(2)
C61	P2	C71	100.58(9)	C24	C25	C26	120.6(2)
Ru	N	C10	169.95(16)	C21	C26	C25	120.2(2)
Ru	C1	C2	69.96(11)	P1	C31	C32	121.06(15)

Atom1	Atom2	Atom3	Angle	Atom1	Atom2	Atom3	Angle
P1	C31	C36	120.49(16)	C53	C54	C55	120.3(2)
C32	C31	C36	118.12(19)	C54	C55	C56	120.2(2)
C31	C32	C33	121.0(2)	C51	C56	C55	120.5(2)
C32	C33	C34	120.1(2)	P2	C61	C62	120.00(15)
C33	C34	C35	119.8(2)	P2	C61	C66	121.19(16)
C34	C35	C36	120.5(2)	C62	C61	C66	118.77(19)
C31	C36	C35	120.5(2)	C61	C62	C63	120.38(19)
P1	C41	C42	120.61(16)	C62	C63	C64	120.3(2)
P1	C41	C46	120.79(16)	C63	C64	C65	119.8(2)
C42	C41	C46	118.30(19)	C64	C65	C66	120.1(2)
C41	C42	C43	120.5(2)	C61	C66	C65	120.6(2)
C42	C43	C44	120.4(2)	P2	C71	C72	117.58(16)
C43	C44	C45	119.5(2)	P2	C71	C76	123.73(18)
C44	C45	C46	120.6(2)	C72	C71	C76	118.7(2)
C41	C46	C45	120.7(2)	C71	C72	C73	121.0(2)
P2	C51	C52	118.74(16)	C72	C73	C74	119.7(2)
P2	C51	C56	122.80(17)	C73	C74	C75	119.8(2)
C52	C51	C56	118.4(2)	C74	C75	C76	120.8(2)
C51	C52	C53	121.0(2)	C71	C76	C75	119.9(2)
C52	C53	C54	119.6(2)				

(b) within the tetrakis(pentafluorophenyl)borate ion

Atom1	Atom2	Atom3	Angle	Atom1	Atom2	Atom3	Angle
C82	C81	C86	113.16(18)	F92	C92	C91	121.21(18)
C82	C81	B	118.33(17)	F92	C92	C93	115.01(19)
C86	C81	B	128.28(18)	C91	C92	C93	123.8(2)
F82	C82	C81	119.47(17)	F93	C93	C92	120.7(2)
F82	C82	C83	115.64(19)	F93	C93	C94	119.4(2)
C81	C82	C83	124.9(2)	C92	C93	C94	119.9(2)
F83	C83	C82	120.9(2)	F94	C94	C93	120.1(2)
F83	C83	C84	120.2(2)	F94	C94	C95	120.8(2)
C82	C83	C84	118.9(2)	C93	C94	C95	119.0(2)
F84	C84	C83	120.1(2)	F95	C95	C94	119.9(2)
F84	C84	C85	120.7(2)	F95	C95	C96	120.9(2)
C83	C84	C85	119.2(2)	C94	C95	C96	119.2(2)
F85	C85	C84	119.9(2)	F96	C96	C91	119.60(18)
F85	C85	C86	119.7(2)	F96	C96	C95	115.55(18)
C84	C85	C86	120.3(2)	C91	C96	C95	124.8(2)
F86	C86	C81	121.02(18)	C102	C101	C106	112.40(18)
F86	C86	C85	115.44(18)	C102	C101	B	126.73(17)
C81	C86	C85	123.5(2)	C106	C101	B	120.18(17)
C92	C91	C96	113.15(18)	F102	C102	C101	120.91(17)
C92	C91	B	125.95(17)				
C96	C91	B	120.34(17)				

Atom1	Atom2	Atom3	Angle	Atom1	Atom2	Atom3	Angle
F102	C102	C103	114.79(18)	C111	C112	C113	124.95(19)
C101	C102	C103	124.29(19)	F113	C113	C112	120.66(19)
F103	C103	C102	120.2(2)	F113	C113	C114	120.14(19)
F103	C103	C104	119.53(19)	C112	C113	C114	119.20(19)
C102	C103	C104	120.2(2)	F114	C114	C113	121.0(2)
F104	C104	C103	120.6(2)	F114	C114	C115	120.2(2)
F104	C104	C105	120.7(2)	C113	C114	C115	118.75(19)
C103	C104	C105	118.66(19)	F115	C115	C114	119.78(19)
F105	C105	C104	120.2(2)	F115	C115	C116	119.82(19)
F105	C105	C106	120.6(2)	C114	C115	C116	120.39(19)
C104	C105	C106	119.21(19)	F116	C116	C111	120.95(17)
F106	C106	C101	119.27(17)	F116	C116	C115	115.43(18)
F106	C106	C105	115.51(18)	C111	C116	C115	123.62(19)
C101	C106	C105	125.21(19)	C81	B	C91	114.57(16)
C112	C111	C116	112.93(17)	C81	B	C101	112.64(16)
C112	C111	B	119.43(17)	C81	B	C111	102.20(15)
C116	C111	B	127.51(17)	C91	B	C101	100.27(15)
F112	C112	C111	119.03(17)	C91	B	C111	112.51(16)
F112	C112	C113	116.00(18)	C101	B	C111	115.26(15)

(c) within the solvent benzene molecules

Atom1	Atom2	Atom3	Angle	Atom1	Atom2	Atom3	Angle
C12S	C11S	C16S	120.0(3)	C32S	C31S	C36S	120.0[a]
C11S	C12S	C13S	119.9(3)	C31S	C32S	C33S	120.0[a]
C12S	C13S	C14S	119.6(3)	C32S	C33S	C34S	120.0[a]
C13S	C14S	C15S	120.4(3)	C33S	C34S	C35S	120.0[a]
C14S	C15S	C16S	119.6(3)	C34S	C35S	C36S	120.0[a]
C11S	C16S	C15S	120.4(3)	C31S	C36S	C35S	120.0[a]
C22S	C21S	C26S	120.0[a]	C42S	C41S	C46S	120.0[a]
C21S	C22S	C23S	120.0[a]	C41S	C42S	C43S	120.0[a]
C22S	C23S	C24S	120.0[a]	C42S	C43S	C44S	120.0[a]
C23S	C24S	C25S	120.0[a]	C43S	C44S	C45S	120.0[a]
C24S	C25S	C26S	120.0[a]	C44S	C45S	C46S	120.0[a]
C21S	C26S	C25S	120.0[a]	C41S	C46S	C45S	120.0[a]

[a]Angle includes distances fixed during refinement.

Table A.5. Torsional Angles (deg)

Atom1	Atom2	Atom3	Atom4	Angle	Atom1	Atom2	Atom3	Atom4	Angle
P2	Ru	P1	C21	174.51(7)	C7A	Ru	P2	C61	-51.11(9)
P2	Ru	P1	C31	-69.98(8)	C7A	Ru	P2	C71	-171.54(10)
P2	Ru	P1	C41	56.64(7)	P1	Ru	N	C10	176.7(9)
N	Ru	P1	C21	-92.62(8)	P2	Ru	N	C10	-84.8(9)
N	Ru	P1	C31	22.89(9)	C1	Ru	N	C10	70.5(9)
N	Ru	P1	C41	149.51(8)	C2	Ru	N	C10	84.2(9)
C1	Ru	P1	C21	8.59(9)	C3	Ru	N	C10	24.5(10)
C1	Ru	P1	C31	124.11(10)	C3A	Ru	N	C10	8.5(10)
C1	Ru	P1	C41	-109.28(9)	C7A	Ru	N	C10	34.3(9)
C2	Ru	P1	C21	41.93(9)	P1	Ru	C1	C2	64.37(12)
C2	Ru	P1	C31	157.45(10)	P1	Ru	C1	C7A	178.61(10)
C2	Ru	P1	C41	-75.93(9)	P2	Ru	C1	C2	-83.49(16)
C3	Ru	P1	C21	74.79(9)	P2	Ru	C1	C7A	30.74(19)
C3	Ru	P1	C31	-169.69(10)	N	Ru	C1	C2	163.94(12)
C3	Ru	P1	C41	-43.07(9)	N	Ru	C1	C7A	-81.83(12)
C3A	Ru	P1	C21	69.64(11)	C2	Ru	C1	C7A	114.23(17)
C3A	Ru	P1	C31	-174.85(11)	C3	Ru	C1	C2	-37.14(12)
C3A	Ru	P1	C41	-48.23(11)	C3	Ru	C1	C7A	77.09(12)
C7A	Ru	P1	C21	9.92(11)	C3A	Ru	C1	C2	-79.26(13)
C7A	Ru	P1	C31	125.44(11)	C3A	Ru	C1	C7A	34.98(11)
C7A	Ru	P1	C41	-107.94(11)	C7A	Ru	C1	C2	-114.23(17)
P1	Ru	P2	C51	-103.45(7)	P1	Ru	C2	C1	-119.19(11)
P1	Ru	P2	C61	139.82(7)	P1	Ru	C2	C3	122.27(11)
P1	Ru	P2	C71	19.39(9)	P2	Ru	C2	C1	142.36(10)
N	Ru	P2	C51	159.38(8)	P2	Ru	C2	C3	23.83(15)
N	Ru	P2	C61	42.65(8)	N	Ru	C2	C1	-22.56(16)
N	Ru	P2	C71	-77.78(9)	N	Ru	C2	C3	-141.09(12)
C1	Ru	P2	C51	45.23(14)	C1	Ru	C2	C3	-118.54(17)
C1	Ru	P2	C61	-71.49(14)	C3	Ru	C2	C1	118.54(17)
C1	Ru	P2	C71	168.08(14)	C3A	Ru	C2	C1	79.17(12)
C2	Ru	P2	C51	-9.94(10)	C3A	Ru	C2	C3	-39.37(11)
C2	Ru	P2	C61	-126.66(10)	C7A	Ru	C2	C1	38.54(11)
C2	Ru	P2	C71	112.91(11)	C7A	Ru	C2	C3	-80.00(12)
C3	Ru	P2	C51	4.55(9)	P1	Ru	C3	C2	-61.81(12)
C3	Ru	P2	C61	-112.18(9)	P1	Ru	C3	C3A	-174.93(10)
C3	Ru	P2	C71	127.39(10)	P2	Ru	C3	C2	-162.56(11)
C3A	Ru	P2	C51	41.53(9)	P2	Ru	C3	C3A	84.32(11)
C3A	Ru	P2	C61	-75.20(9)	N	Ru	C3	C2	89.28(19)
C3A	Ru	P2	C71	164.37(10)	N	Ru	C3	C3A	-23.8(2)
C7A	Ru	P2	C51	65.62(9)	C1	Ru	C3	C2	36.72(11)

Atom1	Atom2	Atom3	Atom4	Angle
C1	Ru	C3	C3A	-76.41(12)
C2	Ru	C3	C3A	-113.13(16)
C3A	Ru	C3	C2	113.13(16)
C7A	Ru	C3	C2	78.15(12)
C7A	Ru	C3	C3A	-34.97(11)
P1	Ru	C3A	C3	8.20(16)
P1	Ru	C3A	C4	134.37(17)
P1	Ru	C3A	C7A	-111.31(12)
P2	Ru	C3A	C3	-98.64(11)
P2	Ru	C3A	C4	27.5(2)
P2	Ru	C3A	C7A	141.86(11)
N	Ru	C3A	C3	168.21(11)
N	Ru	C3A	C4	-65.6(2)
N	Ru	C3A	C7A	48.71(13)
C1	Ru	C3A	C3	83.28(13)
C1	Ru	C3A	C4	-150.5(2)
C1	Ru	C3A	C7A	-36.23(11)
C2	Ru	C3A	C3	40.21(12)
C2	Ru	C3A	C4	166.4(2)
C2	Ru	C3A	C7A	-79.30(13)
C3	Ru	C3A	C4	126.2(2)
C3	Ru	C3A	C7A	-119.50(17)
C7A	Ru	C3A	C3	119.50(17)
C7A	Ru	C3A	C4	-114.3(2)
P1	Ru	C7A	C1	-2.16(16)
P1	Ru	C7A	C3A	117.66(11)
P1	Ru	C7A	C7	-127.66(16)
P2	Ru	C7A	C1	-164.66(10)
P2	Ru	C7A	C3A	-44.84(13)
P2	Ru	C7A	C7	69.83(19)
N	Ru	C7A	C1	101.90(12)
N	Ru	C7A	C3A	-138.28(12)
N	Ru	C7A	C7	-23.60(19)
C1	Ru	C7A	C3A	119.82(17)
C1	Ru	C7A	C7	-125.5(2)
C2	Ru	C7A	C1	-39.49(12)
C2	Ru	C7A	C3A	80.34(13)
C2	Ru	C7A	C7	-165.0(2)
C3	Ru	C7A	C1	-83.06(13)
C3	Ru	C7A	C3A	36.76(12)
C3	Ru	C7A	C7	151.4(2)
C3A	Ru	C7A	C1	-119.82(17)
C3A	Ru	C7A	C7	114.7(2)
Ru	P1	C21	C22	45.32(16)
Ru	P1	C21	C26	-140.85(16)
C31	P1	C21	C22	-87.29(16)
C31	P1	C21	C26	86.54(19)
C41	P1	C21	C22	167.27(15)
C41	P1	C21	C26	-18.9(2)
Ru	P1	C31	C32	-21.4(2)
Ru	P1	C31	C36	165.27(14)
C21	P1	C31	C32	101.42(18)
C21	P1	C31	C36	-71.91(18)
C41	P1	C31	C32	-151.56(17)
C41	P1	C31	C36	35.11(19)
Ru	P1	C41	C42	71.63(17)
Ru	P1	C41	C46	-102.07(16)
C21	P1	C41	C42	-50.38(18)
C21	P1	C41	C46	135.92(16)
C31	P1	C41	C42	-150.34(17)
C31	P1	C41	C46	35.96(18)
Ru	P2	C51	C52	63.35(17)
Ru	P2	C51	C56	-115.24(17)
C61	P2	C51	C52	-174.10(16)
C61	P2	C51	C56	7.3(2)
C71	P2	C51	C52	-69.93(18)
C71	P2	C51	C56	111.49(18)
Ru	P2	C61	C62	14.10(19)
Ru	P2	C61	C66	-168.38(16)
C51	P2	C61	C62	-108.20(17)
C51	P2	C61	C66	69.32(19)
C71	P2	C61	C62	146.18(17)
C71	P2	C61	C66	-36.3(2)
Ru	P2	C71	C72	52.33(18)
Ru	P2	C71	C76	-128.11(16)
C51	P2	C71	C72	179.87(16)
C51	P2	C71	C76	-0.6(2)
C61	P2	C71	C72	-73.96(17)
C61	P2	C71	C76	105.60(19)
Ru	C1	C2	C3	61.64(13)

Atom1	Atom2	Atom3	Atom4	Angle
C7A	C1	C2	Ru	-68.57(13)
C7A	C1	C2	C3	-6.9(2)
Ru	C1	C7A	C3A	-60.27(13)
Ru	C1	C7A	C7	121.8(2)
C2	C1	C7A	Ru	63.84(13)
C2	C1	C7A	C3A	3.6(2)
C2	C1	C7A	C7	-174.4(2)
Ru	C2	C3	C3A	70.23(13)
C1	C2	C3	Ru	-62.68(13)
C1	C2	C3	C3A	7.5(2)
Ru	C3	C3A	C4	-123.5(2)
Ru	C3	C3A	C7A	60.50(13)
C2	C3	C3A	Ru	-65.68(13)
C2	C3	C3A	C4	170.8(2)
C2	C3	C3A	C7A	-5.2(2)
Ru	C3A	C4	C5	92.6(2)
C3	C3A	C4	C5	-175.0(2)
C7A	C3A	C4	C5	0.6(3)
Ru	C3A	C7A	C1	56.76(13)
Ru	C3A	C7A	C7	-124.98(18)
C3	C3A	C7A	Ru	-55.76(12)
C3	C3A	C7A	C1	1.0(2)
C3	C3A	C7A	C7	179.26(17)
C4	C3A	C7A	Ru	127.61(18)
C4	C3A	C7A	C1	-175.63(17)
C4	C3A	C7A	C7	2.6(3)
C3A	C4	C5	C6	-2.3(3)
C4	C5	C6	C7	0.9(3)
C5	C6	C7	C7A	2.3(3)
C6	C7	C7A	Ru	-94.6(2)
C6	C7	C7A	C1	173.7(2)
C6	C7	C7A	C3A	-4.0(3)
C10	C11	C12	C13	175.6(2)
C16	C11	C12	C13	-0.5(4)
C10	C11	C16	C15	-175.3(2)
C12	C11	C16	C15	0.9(4)
C11	C12	C13	C14	-0.1(4)
C12	C13	C14	C15	0.2(4)
C13	C14	C15	C16	0.2(4)
C14	C15	C16	C11	-0.7(4)
P1	C21	C22	C23	174.45(16)
C26	C21	C22	C23	0.2(3)
P1	C21	C26	C25	-175.13(18)
C22	C21	C26	C25	-1.4(3)
C21	C22	C23	C24	1.2(3)
C22	C23	C24	C25	-1.4(4)
C23	C24	C25	C26	0.3(4)
C24	C25	C26	C21	1.1(4)
P1	C31	C32	C33	-175.57(18)
C36	C31	C32	C33	-2.1(3)
P1	C31	C36	C35	175.65(18)
C32	C31	C36	C35	2.1(3)
C31	C32	C33	C34	0.3(4)
C32	C33	C34	C35	1.5(4)
C33	C34	C35	C36	-1.4(4)
C34	C35	C36	C31	-0.4(4)
P1	C41	C42	C43	-175.63(17)
C46	C41	C42	C43	-1.8(3)
P1	C41	C46	C45	174.91(16)
C42	C41	C46	C45	1.1(3)
C41	C42	C43	C44	0.9(3)
C42	C43	C44	C45	0.7(4)
C43	C44	C45	C46	-1.5(4)
C44	C45	C46	C41	0.5(3)
P2	C51	C52	C53	-179.28(17)
C56	C51	C52	C53	-0.6(3)
P2	C51	C56	C55	178.33(17)
C52	C51	C56	C55	-0.3(3)
C51	C52	C53	C54	0.9(3)
C52	C53	C54	C55	-0.3(4)
C53	C54	C55	C56	-0.5(4)
C54	C55	C56	C51	0.8(4)
P2	C61	C62	C63	177.16(17)
C66	C61	C62	C63	-0.4(3)
P2	C61	C66	C65	-176.90(19)
C62	C61	C66	C65	0.6(3)
C61	C62	C63	C64	0.2(3)
C62	C63	C64	C65	-0.1(4)
C63	C64	C65	C66	0.3(4)
C64	C65	C66	C61	-0.6(4)

Atom1	Atom2	Atom3	Atom4	Angle
P2	C71	C72	C73	-177.99(17)
C76	C71	C72	C73	2.4(3)
P2	C71	C76	C75	178.81(17)
C72	C71	C76	C75	-1.6(3)
C71	C72	C73	C74	-1.2(3)
C72	C73	C74	C75	-0.8(4)
C73	C74	C75	C76	1.6(4)
C74	C75	C76	C71	-0.4(4)
C86	C81	C82	F82	178.41(17)
C86	C81	C82	C83	-1.8(3)
B	C81	C82	F82	3.6(3)
B	C81	C82	C83	-176.66(19)
C82	C81	C86	F86	-178.61(17)
C82	C81	C86	C85	1.9(3)
B	C81	C86	F86	-4.4(3)
B	C81	C86	C85	176.11(19)
C82	C81	B	C91	-167.86(17)
C82	C81	B	C101	-54.1(2)
C82	C81	B	C111	70.2(2)
C86	C81	B	C91	18.2(3)
C86	C81	B	C101	132.0(2)
C86	C81	B	C111	-103.8(2)
F82	C82	C83	F83	0.9(3)
F82	C82	C83	C84	-179.03(19)
C81	C82	C83	F83	-178.9(2)
C81	C82	C83	C84	1.2(3)
F83	C83	C84	F84	-0.3(3)
F83	C83	C84	C85	179.6(2)
C82	C83	C84	F84	179.6(2)
C82	C83	C84	C85	-0.5(3)
F84	C84	C85	F85	1.0(3)
F84	C84	C85	C86	-179.49(19)
C83	C84	C85	F85	-178.9(2)
C83	C84	C85	C86	0.6(3)
F85	C85	C86	F86	-1.4(3)
F85	C85	C86	C81	178.12(19)
C84	C85	C86	F86	179.07(19)
C84	C85	C86	C81	-1.4(3)
C96	C91	C92	F92	177.61(18)
C96	C91	C92	C93	-1.7(3)
B	C91	C92	F92	6.2(3)
B	C91	C92	C93	-173.09(19)
C92	C91	C96	F96	-176.58(17)
C92	C91	C96	C95	2.2(3)
B	C91	C96	F96	-4.7(3)
B	C91	C96	C95	174.13(19)
C92	C91	B	C81	-138.80(19)
C92	C91	B	C101	100.3(2)
C92	C91	B	C111	-22.6(3)
C96	C91	B	C81	50.4(2)
C96	C91	B	C101	-70.5(2)
C96	C91	B	C111	166.55(17)
F92	C92	C93	F93	0.8(3)
F92	C92	C93	C94	-179.19(19)
C91	C92	C93	F93	-179.82(19)
C91	C92	C93	C94	0.2(3)
F93	C93	C94	F94	0.1(3)
F93	C93	C94	C95	-178.9(2)
C92	C93	C94	F94	-179.9(2)
C92	C93	C94	C95	1.1(3)
F94	C94	C95	F95	-0.7(3)
F94	C94	C95	C96	-179.68(19)
C93	C94	C95	F95	178.37(19)
C93	C94	C95	C96	-0.6(3)
F95	C95	C96	F96	-1.3(3)
F95	C95	C96	C91	179.89(18)
C94	C95	C96	F96	177.70(18)
C94	C95	C96	C91	-1.1(3)
C106	C101	C102	F102	178.46(17)
C106	C101	C102	C103	-0.7(3)
B	C101	C102	F102	8.0(3)
B	C101	C102	C103	-171.08(19)
C102	C101	C106	F106	-177.47(16)
C102	C101	C106	C105	1.7(3)
B	C101	C106	F106	-6.4(3)
B	C101	C106	C105	172.77(19)
C102	C101	B	C81	-20.9(3)
C102	C101	B	C91	101.3(2)
C102	C101	B	C111	-137.65(19)
C106	C101	B	C81	169.34(17)

Atom1	Atom2	Atom3	Atom4	Angle	Atom1	Atom2	Atom3	Atom4	Angle
C106	C101	B	C91	-68.4(2)	F113	C113	C114	F114	0.6(3)
C106	C101	B	C111	52.6(2)	F113	C113	C114	C115	-178.74(19)
F102	C102	C103	F103	-1.2(3)	C112	C113	C114	F114	-178.73(19)
F102	C102	C103	C104	-179.30(19)	C112	C113	C114	C115	2.0(3)
C101	C102	C103	F103	178.00(18)	F114	C114	C115	F115	-2.9(3)
C101	C102	C103	C104	-0.1(3)	F114	C114	C115	C116	177.81(19)
F103	C103	C104	F104	1.7(3)	C113	C114	C115	F115	176.43(19)
F103	C103	C104	C105	-178.1(2)	C113	C114	C115	C116	-2.9(3)
C102	C103	C104	F104	179.86(19)	F115	C115	C116	F116	0.9(3)
C102	C103	C104	C105	0.1(3)	F115	C115	C116	C111	-179.08(18)
F104	C104	C105	F105	0.2(3)	C114	C115	C116	F116	-179.78(19)
F104	C104	C105	C106	-179.0(2)	C114	C115	C116	C111	0.2(3)
C103	C104	C105	F105	180.0(2)	C16S	C11S	C12S	C13S	0.3(4)
C103	C104	C105	C106	0.8(3)	C12S	C11S	C16S	C15S	-0.2(4)
F105	C105	C106	F106	-1.8(3)	C11S	C12S	C13S	C14S	-0.2(5)
F105	C105	C106	C101	179.05(19)	C12S	C13S	C14S	C15S	-0.1(6)
C104	C105	C106	F106	177.33(19)	C13S	C14S	C15S	C16S	0.2(5)
C104	C105	C106	C101	-1.8(3)	C14S	C15S	C16S	C11S	0.0(5)
C116	C111	C112	F112	177.06(17)	C26S	C21S	C22S	C23S	0.0[a]
C116	C111	C112	C113	-4.1(3)	C22S	C21S	C26S	C25S	0.0[a]
B	C111	C112	F112	0.9(3)	C21S	C22S	C23S	C24S	0.0[a]
B	C111	C112	C113	179.78(19)	C22S	C23S	C24S	C25S	0.0[a]
C112	C111	C116	F116	-176.93(17)	C23S	C24S	C25S	C26S	0.0[a]
C112	C111	C116	C115	3.1(3)	C24S	C25S	C26S	C21S	0.0[a]
B	C111	C116	F116	-1.2(3)	C36S	C31S	C32S	C33S	0.0[a]
B	C111	C116	C115	178.84(19)	C32S	C31S	C36S	C35S	0.0[a]
C112	C111	B	C81	70.8(2)	C31S	C32S	C33S	C34S	0.0[a]
C112	C111	B	C91	-52.6(2)	C32S	C33S	C34S	C35S	0.0[a]
C112	C111	B	C101	-166.70(17)	C33S	C34S	C35S	C36S	0.0[a]
C116	C111	B	C81	-104.7(2)	C34S	C35S	C36S	C31S	0.0[a]
C116	C111	B	C91	131.9(2)	C46S	C41S	C42S	C43S	0.0[a]
C116	C111	B	C101	17.8(3)	C42S	C41S	C46S	C45S	0.0[a]
F112	C112	C113	F113	1.3(3)	C41S	C42S	C43S	C44S	0.0[a]
F112	C112	C113	C114	-179.40(18)	C42S	C43S	C44S	C45S	0.0[a]
C111	C112	C113	F113	-177.59(18)	C43S	C44S	C45S	C46S	0.0[a]
C111	C112	C113	C114	1.7(3)	C44S	C45S	C46S	C41S	0.0[a]

[a]Angle includes distances fixed during refinement.

Table A.6. Least-Squares Planes

Plane	Coefficients[a]			Defining Atoms with Deviations (Å)[b]			
1	2.968(15)	8.774(14)	-16.124(5)	3.074(6)			
				C1	-0.0304(12)	C2	0.0424(12)
				C3	-0.0371(12)	C3A	0.0180(12)
				C7A	0.0070(12)		
				Ru	-1.8937(9)		

Distance: Ru–C_{cent} = 1.904 Å (C_{cent} = C1–C2–C3–C3A–C7A centroid)

Angles: C_{cent}–Ru–P1 = 120.4°, C_{cent}–Ru–P2 = 121.2°, C_{cent}–Ru–N = 121.9°

2	2.33(2)	10.07(4)	-15.603(18)	3.560(15)			
				C1	C2	C3	
				Ru	-1.834(2)		
3	3.178(16)	8.29(2)	-16.278(6)	2.845(9)			
				C1	0.0033(7)	C3	-0.0033(7)
				C3A	0.0054(11)	C7A	-0.0054(11)
				Ru	-1.8655(12)		
4	3.927(13)	7.293(13)	-16.525(3)	2.402(7)			
				C3A	-0.0045(13)	C4	-0.0132(14)
				C5	0.0145(16)	C6	0.0024(16)
				C7	-0.0197(15)	C7A	0.0205(13)
				Ru	-1.773(2)		

Dihedral angle between planes 2 and 3: 7.3(3)°

Dihedral angle between planes 3 and 4: 3.97(13)°

[a]Coefficients are for the form $ax+by+cz = d$ where x, y and z are crystallographic coordinates.

[b]Underlined atoms were not included in the definition of the plane.

Table A.7. Anisotropic Displacement Parameters (U_{ij}, Å^2)

Atom	U_{11}	U_{22}	U_{33}	U_{23}	U_{13}	U_{12}
Ru	0.02486(8)	0.02159(8)	0.02235(8)	0.00868(6)	0.00920(6)	0.00786(6)
P1	0.0265(2)	0.0221(2)	0.0242(2)	0.00918(19)	0.01020(19)	0.00846(19)
P2	0.0279(2)	0.0232(2)	0.0278(3)	0.0090(2)	0.0130(2)	0.0088(2)
N	0.0309(9)	0.0256(8)	0.0289(9)	0.0123(7)	0.0115(7)	0.0108(7)
C1	0.0361(11)	0.0319(10)	0.0325(10)	0.0170(9)	0.0197(9)	0.0157(9)
C2	0.0469(12)	0.0303(10)	0.0248(10)	0.0126(8)	0.0177(9)	0.0148(9)
C3	0.0324(10)	0.0331(11)	0.0250(10)	0.0146(8)	0.0078(8)	0.0075(9)
C3A	0.0309(10)	0.0343(10)	0.0293(10)	0.0203(9)	0.0131(8)	0.0128(8)
C4	0.0330(11)	0.0444(12)	0.0442(12)	0.0300(10)	0.0184(10)	0.0203(10)
C5	0.0507(14)	0.0411(12)	0.0559(14)	0.0302(11)	0.0318(12)	0.0298(11)
C6	0.0471(13)	0.0256(10)	0.0496(13)	0.0160(10)	0.0241(11)	0.0125(10)
C7	0.0329(11)	0.0295(10)	0.0381(11)	0.0150(9)	0.0153(9)	0.0088(9)
C7A	0.0313(10)	0.0297(10)	0.0308(10)	0.0173(8)	0.0151(8)	0.0124(8)
C10	0.0320(10)	0.0286(10)	0.0317(11)	0.0130(9)	0.0118(9)	0.0123(9)
C11	0.0276(10)	0.0301(10)	0.0270(10)	0.0076(8)	0.0059(8)	0.0089(8)
C12	0.0453(13)	0.0354(12)	0.0327(11)	0.0145(10)	0.0063(10)	0.0138(10)
C13	0.0502(14)	0.0293(11)	0.0393(13)	0.0083(10)	0.0066(11)	0.0105(10)
C14	0.0432(13)	0.0407(13)	0.0290(11)	0.0072(10)	0.0019(10)	0.0107(10)
C15	0.0532(15)	0.0416(13)	0.0365(13)	0.0177(11)	0.0022(11)	0.0144(11)
C16	0.0473(13)	0.0307(11)	0.0368(12)	0.0127(10)	0.0051(10)	0.0113(10)
C21	0.0325(10)	0.0259(9)	0.0266(10)	0.0120(8)	0.0142(8)	0.0135(8)
C22	0.0317(10)	0.0278(10)	0.0313(10)	0.0109(8)	0.0125(8)	0.0125(8)
C23	0.0346(11)	0.0379(12)	0.0464(13)	0.0213(10)	0.0195(10)	0.0162(10)
C24	0.0534(14)	0.0461(13)	0.0580(15)	0.0259(12)	0.0372(13)	0.0291(12)
C25	0.0601(16)	0.0333(12)	0.0556(15)	0.0108(11)	0.0344(13)	0.0222(11)
C26	0.0422(12)	0.0266(10)	0.0411(12)	0.0086(9)	0.0194(10)	0.0120(9)
C31	0.0333(10)	0.0301(10)	0.0304(10)	0.0156(8)	0.0163(8)	0.0159(8)
C32	0.0453(12)	0.0331(11)	0.0334(11)	0.0153(9)	0.0137(10)	0.0186(10)
C33	0.0561(15)	0.0461(13)	0.0321(12)	0.0173(10)	0.0120(11)	0.0254(12)
C34	0.0562(15)	0.0502(14)	0.0431(13)	0.0313(12)	0.0241(12)	0.0309(12)
C35	0.0584(15)	0.0354(12)	0.0528(15)	0.0272(11)	0.0224(12)	0.0226(11)
C36	0.0483(13)	0.0306(11)	0.0384(12)	0.0153(10)	0.0125(10)	0.0144(10)
C41	0.0287(10)	0.0220(9)	0.0332(10)	0.0081(8)	0.0104(8)	0.0100(8)
C42	0.0378(12)	0.0317(11)	0.0362(12)	0.0120(9)	0.0113(9)	0.0114(9)
C43	0.0455(14)	0.0384(13)	0.0373(12)	0.0098(10)	0.0014(10)	0.0132(11)
C44	0.0317(12)	0.0327(12)	0.0613(16)	0.0130(11)	0.0030(11)	0.0072(10)
C45	0.0338(12)	0.0289(11)	0.0602(15)	0.0170(11)	0.0160(11)	0.0082(9)
C46	0.0336(11)	0.0257(10)	0.0412(12)	0.0109(9)	0.0149(9)	0.0098(9)
C51	0.0282(10)	0.0295(10)	0.0362(11)	0.0137(9)	0.0153(9)	0.0106(8)
C52	0.0336(11)	0.0340(11)	0.0391(12)	0.0106(9)	0.0132(9)	0.0106(9)

Atom	U_{11}	U_{22}	U_{33}	U_{23}	U_{13}	U_{12}
C53	0.0355(12)	0.0487(14)	0.0371(13)	0.0112(11)	0.0085(10)	0.0075(11)
C54	0.0346(12)	0.0702(18)	0.0455(14)	0.0284(13)	0.0137(11)	0.0219(12)
C55	0.0438(13)	0.0592(16)	0.0559(15)	0.0295(13)	0.0240(12)	0.0311(12)
C56	0.0376(12)	0.0388(12)	0.0434(13)	0.0163(10)	0.0191(10)	0.0177(10)
C61	0.0348(11)	0.0282(10)	0.0278(10)	0.0097(8)	0.0134(8)	0.0131(8)
C62	0.0349(11)	0.0311(10)	0.0328(11)	0.0120(9)	0.0151(9)	0.0134(9)
C63	0.0429(13)	0.0284(11)	0.0429(13)	0.0088(10)	0.0164(10)	0.0101(10)
C64	0.0575(15)	0.0341(12)	0.0407(13)	0.0024(10)	0.0218(12)	0.0189(11)
C65	0.0611(16)	0.0440(13)	0.0468(14)	0.0141(11)	0.0350(13)	0.0256(12)
C66	0.0473(13)	0.0345(11)	0.0417(12)	0.0124(10)	0.0261(11)	0.0141(10)
C71	0.0421(11)	0.0238(9)	0.0367(11)	0.0126(8)	0.0254(10)	0.0128(9)
C72	0.0512(13)	0.0366(12)	0.0425(12)	0.0192(10)	0.0280(11)	0.0221(11)
C73	0.0786(19)	0.0457(14)	0.0526(15)	0.0304(12)	0.0414(14)	0.0366(14)
C74	0.088(2)	0.0327(12)	0.0651(17)	0.0268(12)	0.0576(16)	0.0295(13)
C75	0.0627(16)	0.0323(12)	0.0643(17)	0.0178(12)	0.0438(15)	0.0101(12)
C76	0.0452(13)	0.0347(12)	0.0522(14)	0.0169(11)	0.0292(12)	0.0117(10)
F82	0.0570(8)	0.0344(7)	0.0352(7)	0.0140(6)	0.0240(6)	0.0157(6)
F83	0.0706(10)	0.0429(8)	0.0456(8)	-0.0025(7)	0.0263(8)	0.0144(7)
F84	0.0633(10)	0.0227(7)	0.0945(12)	0.0056(7)	0.0422(9)	0.0107(7)
F85	0.0652(10)	0.0366(7)	0.0938(12)	0.0411(8)	0.0442(9)	0.0226(7)
F86	0.0496(8)	0.0417(7)	0.0464(8)	0.0278(6)	0.0207(6)	0.0195(6)
F92	0.0312(6)	0.0429(7)	0.0366(7)	0.0039(6)	0.0100(5)	0.0080(6)
F93	0.0625(10)	0.0581(9)	0.0337(7)	-0.0020(7)	0.0107(7)	0.0211(8)
F94	0.0962(12)	0.0771(11)	0.0493(9)	0.0224(8)	0.0501(9)	0.0483(10)
F95	0.0594(9)	0.0555(9)	0.0733(10)	0.0393(8)	0.0506(8)	0.0349(7)
F96	0.0306(6)	0.0398(7)	0.0478(7)	0.0179(6)	0.0174(6)	0.0109(5)
F102	0.0292(6)	0.0286(6)	0.0465(7)	0.0118(6)	0.0063(5)	0.0062(5)
F103	0.0364(7)	0.0564(9)	0.0539(9)	0.0169(7)	0.0030(6)	0.0226(7)
F104	0.0706(10)	0.0571(9)	0.0701(10)	0.0323(8)	0.0246(8)	0.0461(8)
F105	0.0626(9)	0.0269(7)	0.0878(12)	0.0218(7)	0.0291(9)	0.0203(7)
F106	0.0323(6)	0.0270(6)	0.0493(8)	0.0093(6)	0.0122(6)	0.0066(5)
F112	0.0418(7)	0.0531(8)	0.0420(7)	0.0296(6)	0.0214(6)	0.0243(6)
F113	0.0379(7)	0.0612(9)	0.0437(8)	0.0206(7)	0.0104(6)	0.0274(7)
F114	0.0291(7)	0.0587(9)	0.0706(10)	0.0233(8)	0.0247(7)	0.0177(6)
F115	0.0494(8)	0.0514(8)	0.0654(9)	0.0331(7)	0.0403(7)	0.0216(7)
F116	0.0399(7)	0.0413(7)	0.0437(7)	0.0262(6)	0.0218(6)	0.0202(6)
C81	0.0242(9)	0.0268(10)	0.0334(10)	0.0115(8)	0.0113(8)	0.0095(8)
C82	0.0329(11)	0.0275(10)	0.0395(11)	0.0132(9)	0.0175(9)	0.0120(9)
C83	0.0376(12)	0.0333(11)	0.0435(13)	0.0057(10)	0.0178(10)	0.0131(10)
C84	0.0356(12)	0.0211(10)	0.0655(16)	0.0073(10)	0.0243(11)	0.0094(9)

Atom	U_{11}	U_{22}	U_{33}	U_{23}	U_{13}	U_{12}
C85	0.0355(12)	0.0301(11)	0.0683(16)	0.0257(11)	0.0273(11)	0.0156(9)
C86	0.0284(10)	0.0325(11)	0.0401(11)	0.0179(9)	0.0152(9)	0.0144(9)
C91	0.0320(10)	0.0306(10)	0.0302(10)	0.0142(8)	0.0139(8)	0.0156(8)
C92	0.0331(11)	0.0338(11)	0.0335(11)	0.0137(9)	0.0145(9)	0.0153(9)
C93	0.0485(13)	0.0382(12)	0.0303(11)	0.0084(9)	0.0121(10)	0.0212(11)
C94	0.0664(16)	0.0453(13)	0.0357(12)	0.0198(10)	0.0305(12)	0.0352(12)
C95	0.0471(13)	0.0398(12)	0.0536(14)	0.0286(11)	0.0341(12)	0.0275(11)
C96	0.0350(11)	0.0299(10)	0.0358(11)	0.0172(9)	0.0163(9)	0.0154(9)
C101	0.0291(10)	0.0268(9)	0.0269(9)	0.0113(8)	0.0144(8)	0.0109(8)
C102	0.0305(10)	0.0290(10)	0.0318(10)	0.0127(8)	0.0142(8)	0.0116(8)
C103	0.0324(11)	0.0431(12)	0.0321(11)	0.0146(9)	0.0115(9)	0.0198(10)
C104	0.0473(13)	0.0427(13)	0.0458(13)	0.0236(11)	0.0226(11)	0.0303(11)
C105	0.0463(13)	0.0252(10)	0.0476(13)	0.0143(9)	0.0242(11)	0.0169(9)
C106	0.0290(10)	0.0275(10)	0.0333(11)	0.0101(8)	0.0149(8)	0.0097(8)
C111	0.0269(9)	0.0233(9)	0.0276(10)	0.0068(8)	0.0105(8)	0.0082(8)
C112	0.0327(10)	0.0300(10)	0.0279(10)	0.0097(8)	0.0129(8)	0.0120(8)
C113	0.0325(11)	0.0337(11)	0.0320(11)	0.0083(9)	0.0094(9)	0.0164(9)
C114	0.0254(10)	0.0321(11)	0.0449(12)	0.0073(9)	0.0146(9)	0.0097(9)
C115	0.0360(11)	0.0301(10)	0.0425(12)	0.0145(9)	0.0224(10)	0.0112(9)
C116	0.0316(10)	0.0248(9)	0.0334(10)	0.0113(8)	0.0136(9)	0.0112(8)
B	0.0245(10)	0.0240(10)	0.0269(11)	0.0097(9)	0.0104(9)	0.0073(8)
C11S	0.0539(16)	0.0697(19)	0.0558(16)	0.0192(14)	0.0285(14)	0.0309(15)
C12S	0.0567(17)	0.0664(18)	0.0650(18)	0.0236(15)	0.0238(15)	0.0368(15)
C13S	0.078(2)	0.071(2)	0.103(3)	0.052(2)	0.048(2)	0.0456(18)
C14S	0.0538(18)	0.076(2)	0.129(3)	0.054(2)	0.040(2)	0.0321(17)
C15S	0.0568(18)	0.071(2)	0.0671(19)	0.0163(16)	0.0166(15)	0.0375(16)
C16S	0.076(2)	0.075(2)	0.0464(15)	0.0213(14)	0.0354(15)	0.0472(17)

The form of the anisotropic displacement parameter is:

$\exp[-2\pi^2(h^2a^{*2}U_{11} + k^2b^{*2}U_{22} + l^2c^{*2}U_{33} + 2klb^*c^*U_{23} + 2hla^*c^*U_{13} + 2hka^*b^*U_{12})]$

Table A.8. Derived Atomic Coordinates and Displacement Parameters for Hydrogen Atoms

Atom	*x*	*y*	*z*	U_{eq}, Å^2
H1	0.3151	0.4797	0.1263	0.037
H2	0.1534	0.3422	0.0128	0.040
H3	0.0119	0.3827	0.0170	0.039
H4	0.0143	0.5602	0.1075	0.043
H5	0.1165	0.7126	0.1942	0.050
H6	0.2849	0.7642	0.2590	0.048
H7	0.3557	0.6649	0.2363	0.041
H12	0.4129	0.7158	0.4681	0.049
H13	0.5169	0.8071	0.6191	0.055
H14	0.5650	0.7419	0.7208	0.054
H15	0.5099	0.5850	0.6719	0.059
H16	0.4070	0.4922	0.5204	0.052
H22	0.3434	0.3799	0.1930	0.037
H23	0.4545	0.3517	0.1423	0.045
H24	0.4076	0.2121	0.0293	0.054
H25	0.2510	0.0990	-0.0280	0.057
H26	0.1403	0.1249	0.0259	0.045
H32	0.2797	0.3647	0.3600	0.044
H33	0.3357	0.3120	0.4716	0.054
H34	0.2801	0.1565	0.4377	0.053
H35	0.1736	0.0538	0.2911	0.055
H36	0.1171	0.1054	0.1787	0.049
H42	0.0325	0.2058	-0.0252	0.045
H43	-0.1271	0.1007	-0.1202	0.057
H44	-0.2274	0.0271	-0.0609	0.059
H45	-0.1680	0.0613	0.0941	0.052
H46	-0.0080	0.1635	0.1893	0.042
H52	-0.0981	0.2792	0.0718	0.046
H53	-0.2426	0.2546	-0.0408	0.056
H54	-0.3013	0.3653	-0.0245	0.060
H55	-0.2172	0.4994	0.1041	0.058
H56	-0.0746	0.5231	0.2189	0.047
H62	0.1904	0.6033	0.3213	0.040
H63	0.2284	0.7392	0.4352	0.049
H64	0.1369	0.7424	0.5190	0.056
H65	0.0062	0.6095	0.4885	0.057
H66	-0.0317	0.4733	0.3756	0.049
H72	0.1357	0.3682	0.3795	0.047
H73	0.0917	0.2592	0.4398	0.060
H74	-0.0712	0.1618	0.3877	0.063

Atom	*x*	*y*	*z*	U_{eq}, Å^2
H75	-0.1891	0.1755	0.2784	0.062
H76	-0.1460	0.2819	0.2151	0.052
H11S	-0.0213	0.1880	0.7908	0.070
H12S	-0.0171	0.2678	0.6968	0.073
H13S	0.1291	0.3484	0.6951	0.088
H14S	0.2713	0.3491	0.7884	0.097
H15S	0.2669	0.2702	0.8830	0.081
H16S	0.1208	0.1899	0.8839	0.072
H21S	0.6383	0.4474	0.1833	0.078
H22S	0.6743	0.3269	0.2015	0.105
H23S	0.7621	0.3377	0.3464	0.077
H24S	0.8138	0.4689	0.4730	0.066
H25S	0.7778	0.5894	0.4548	0.069
H26S	0.6900	0.5786	0.3099	0.064
H31S	0.6237	0.3718	0.1491	0.079
H32S	0.6876	0.2906	0.2241	0.086
H33S	0.7807	0.3580	0.3807	0.101
H34S	0.8099	0.5066	0.4624	0.123
H35S	0.7459	0.5878	0.3874	0.125
H36S	0.6528	0.5204	0.2307	0.083
H41S	0.3517	-0.0858	-0.0788	0.074
H42S	0.4005	0.0652	-0.0661	0.057
H43S	0.5636	0.1687	0.0166	0.085
H44S	0.6779	0.1212	0.0868	0.095
H45S	0.6291	-0.0299	0.0742	0.077
H46S	0.4660	-0.1334	-0.0086	0.084

[a]Included with an occupancy factor of 0.5.

Appendix B X-Ray Crystallographic structure report for [Ru(η^5-indenyl)(NCPh)(PPh_2H)(PPh_3)][$B(C_6F_5)_4$] (3b).

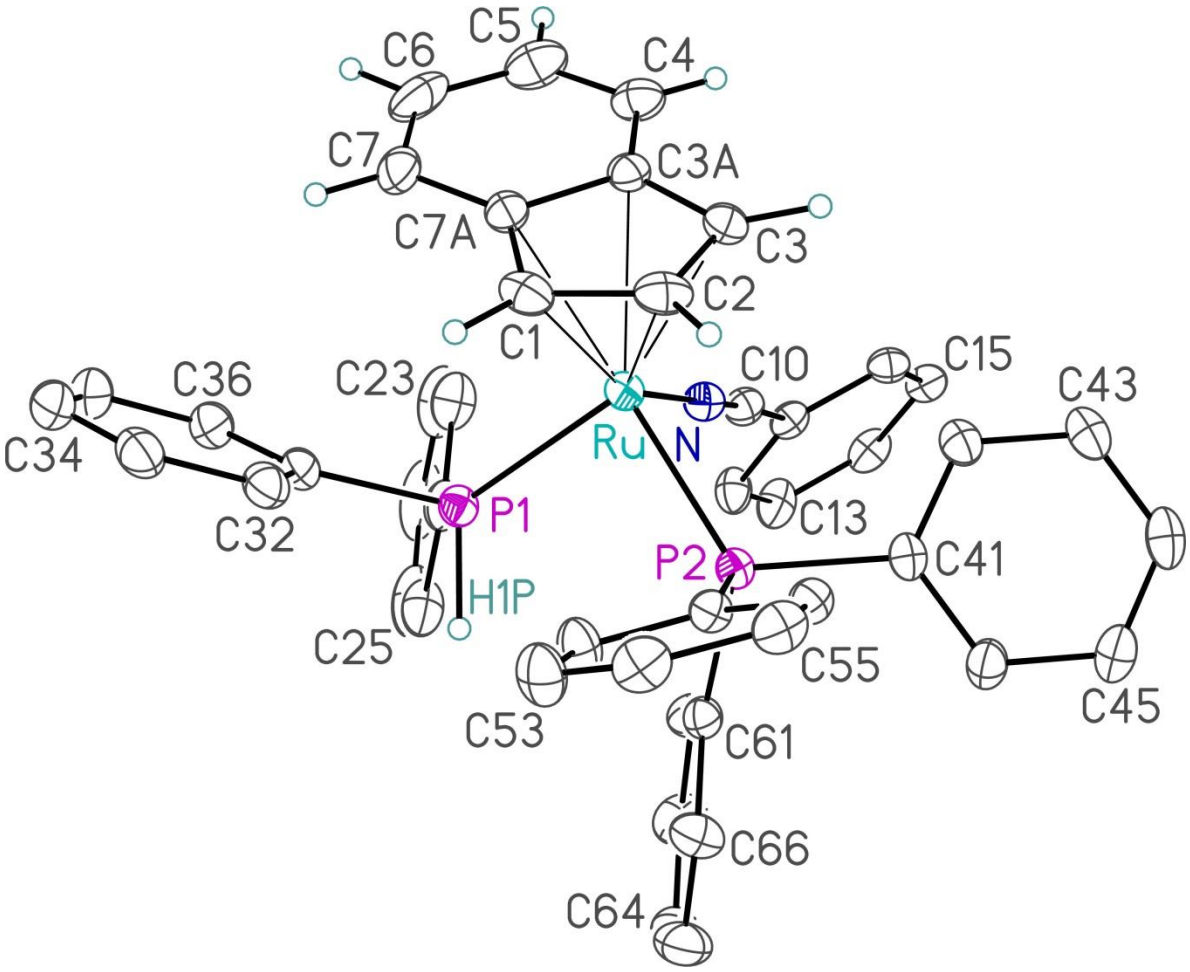

Figure B.1. Perspective view of the molecular structure of the cation from [Ru(η^5-indenyl)(NCPh)(PPh_2H)(PPh_3)][$B(C_6F_5)_4$] (**3b**) showing the atom labeling scheme. Non-hydrogen atoms are represented by Gaussian ellipsoids at the 30% probability level. Hydrogen atoms attached to P1 and the indenyl group are shown with arbitrarily small thermal parameters; phenyl-group hydrogens are not shown.

Table B.1. Crystallographic Experimental Details

A. Crystal Data	
formula	$C_{70}H_{38}BF_{20}NP_2Ru$
formula weight	1446.83
crystal dimensions (mm)	0.37 × 0.22 × 0.21
crystal system	triclinic
space group	$P\bar{1}$ (No. 2)
unit cell parameters[a]	
a (Å)	13.0253 (5)
b (Å)	13.4007 (5)
c (Å)	18.4817 (7)
α (deg)	100.0631 (5)
β (deg)	105.0829 (5)
γ (deg)	94.3895 (5)
V (Å^3)	3041.5 (2)
Z	2
ρ_{calcd} (g cm^{-3})	1.580
μ (mm^{-1})	0.417
B. Data Collection and Refinement Conditions	
diffractometer	Bruker PLATFORM/APEX II CCD[b]
radiation (λ [Å])	graphite-monochromated Mo Kα (0.71073)
temperature (°C)	–80
scan type	ω scans (0.3°) (15 s exposures)
data collection 2θ limit (deg)	56.76
total data collected	27382 (-17 ≤ h ≤ 17, -17 ≤ k ≤ 17, -24 ≤ l ≤ 24)
independent reflections	14662 (R_{int} = 0.0198)
number of observed reflections (*NO*)	12370 [$F_o^2 \geq 2\sigma(F_o^2)$]
structure solution method	Patterson/structure expansion (*DIRDIF–2008*[c])
refinement method	full-matrix least-squares on F^2 (*SHELXL–2014*[d])
absorption correction method	Gaussian integration (face-indexed)
range of transmission factors	0.9823–0.9063
data/restraints/parameters	14662 / 0 / 860
goodness-of-fit (S)[e] [all data]	1.050
final R indices[f]	
R_1 [$F_o^2 \geq 2\sigma(F_o^2)$]	0.0360
wR_2 [all data]	0.0920
largest difference peak and hole	0.848 and –0.744 e Å^{-3}

[a]Obtained from least-squares refinement of 9720 reflections with 4.52° < 2θ < 51.98°.

[b]Programs for diffractometer operation, data collection, data reduction and absorption correction were those supplied by Bruker.

[c]Beurskens, P. T.; Beurskens, G.; de Gelder, R.; Smits, J. M. M.; Garcia-Granda, S.; Gould, R. O. (2008). The *DIRDIF-2008* program system. Crystallography Laboratory, Radboud University Nijmegen, The Netherlands.

[d]Sheldrick, G. M. *Acta Crystallogr.* **2015**, *C71*, 3–8.

[e]$S = [\Sigma w(F_o^2 - F_c^2)^2/(n - p)]^{1/2}$ (n = number of data; p = number of parameters varied; $w = [\sigma^2(F_o^2) + (0.0408P)^2 + 1.1250P]^{-1}$ where $P = [\mathrm{Max}(F_o^2, 0) + 2F_c^2]/3$).

[f]$R_1 = \Sigma||F_o| - |F_c||/\Sigma|F_o|$; $wR_2 = [\Sigma w(F_o^2 - F_c^2)^2/\Sigma w(F_o^4)]^{1/2}$.

Table B.2. Atomic Coordinates and Equivalent Isotropic Displacement Parameters

(a) atoms of [(η^5–indenyl)Ru(NCPh)($PHPh_2$)(PPh_3)]$^+$

Atom	*x*	*y*	*z*	U_{eq}, Å^2
Ru	0.19665(2)	0.37603(2)	0.14376(2)	0.02768(5)*
P1	0.18530(4)	0.20095(4)	0.13535(3)	0.03236(11)*
P2	0.08041(4)	0.39422(4)	0.21775(3)	0.02778(10)*
N	0.32128(13)	0.39952(13)	0.24007(9)	0.0321(4)*
C1	0.11819(17)	0.37494(18)	0.02357(12)	0.0412(5)*
C2	0.10883(17)	0.46924(18)	0.06803(13)	0.0419(5)*
C3	0.21210(17)	0.52308(16)	0.10442(12)	0.0376(5)*
C3A	0.28801(16)	0.46539(16)	0.07786(11)	0.0345(4)*
C4	0.40054(18)	0.4850(2)	0.09427(14)	0.0473(6)*
C5	0.4518(2)	0.4181(3)	0.05858(17)	0.0633(8)*
C6	0.3966(3)	0.3286(3)	0.00661(17)	0.0666(8)*
C7	0.2876(2)	0.30430(19)	-0.00943(13)	0.0526(6)*
C7A	0.23069(18)	0.37343(16)	0.02667(11)	0.0369(5)*
C10	0.39268(16)	0.41138(16)	0.29379(12)	0.0334(4)*
C11	0.47848(15)	0.42137(16)	0.36295(11)	0.0321(4)*
C12	0.50111(19)	0.33410(17)	0.39269(12)	0.0418(5)*
C13	0.5815(2)	0.34358(19)	0.46028(13)	0.0473(6)*
C14	0.63811(17)	0.43789(19)	0.49714(12)	0.0423(5)*
C15	0.61498(16)	0.52429(18)	0.46803(12)	0.0378(5)*
C16	0.53482(15)	0.51679(17)	0.40028(11)	0.0345(4)*
C21	0.30450(19)	0.15317(17)	0.18598(12)	0.0413(5)*
C22	0.4039(2)	0.1898(2)	0.17996(15)	0.0524(6)*
C23	0.4959(2)	0.1526(3)	0.21676(17)	0.0708(9)*
C24	0.4884(3)	0.0811(3)	0.26083(17)	0.0790(11)*
C25	0.3904(3)	0.0457(2)	0.26850(15)	0.0738(10)*
C26	0.2979(2)	0.08090(19)	0.23093(13)	0.0543(6)*
C31	0.14762(18)	0.11941(15)	0.03950(12)	0.0371(4)*

C32	0.04691(19)	0.12141(17)	-0.01019(13)	0.0422(5)*
C33	0.0167(2)	0.06339(19)	-0.08387(14)	0.0509(6)*
C34	0.0858(2)	0.0023(2)	-0.10918(15)	0.0572(7)*
C35	0.1850(2)	-0.00237(19)	-0.06012(15)	0.0565(7)*
C36	0.2160(2)	0.05547(17)	0.01409(14)	0.0461(5)*
C41	0.10964(15)	0.51367(15)	0.28985(11)	0.0317(4)*
C42	0.18934(17)	0.58946(16)	0.29126(12)	0.0380(5)*
C43	0.21339(19)	0.67943(17)	0.34619(13)	0.0437(5)*
C44	0.15733(19)	0.69383(17)	0.40025(13)	0.0452(5)*
C45	0.07915(19)	0.61868(19)	0.40060(14)	0.0472(6)*
C46	0.05464(17)	0.52884(18)	0.34556(13)	0.0416(5)*
C51	-0.05606(15)	0.39129(15)	0.15847(11)	0.0302(4)*
C52	-0.10228(17)	0.29982(17)	0.10699(14)	0.0436(5)*
C53	-0.20183(18)	0.29275(19)	0.05532(14)	0.0493(6)*
C54	-0.25628(16)	0.37706(19)	0.05422(13)	0.0434(5)*
C55	-0.21255(17)	0.46756(18)	0.10487(13)	0.0400(5)*
C56	-0.11207(16)	0.47509(16)	0.15731(12)	0.0335(4)*
C61	0.06325(16)	0.30078(15)	0.27670(12)	0.0340(4)*
C62	0.15326(19)	0.26925(19)	0.32152(13)	0.0455(5)*
C63	0.1442(2)	0.2057(2)	0.37151(14)	0.0552(6)*
C64	0.0446(2)	0.17120(19)	0.37669(15)	0.0558(7)*
C65	-0.0456(2)	0.2005(2)	0.33269(17)	0.0591(7)*
C66	-0.03654(19)	0.26485(18)	0.28259(15)	0.0480(6)*
H1P	0.1140(17)	0.1580(16)	0.1650(12)	0.035(6)

(b) tetrakis(pentafluorophenyl)borate ion atoms

Atom	*x*	*y*	*z*	U_{eq}, Å^2
F72	0.06407(10)	0.07061(10)	0.57445(7)	0.0457(3)*
F73	-0.12532(10)	0.04279(11)	0.60017(9)	0.0567(4)*
F74	-0.15809(11)	0.13337(12)	0.73447(10)	0.0612(4)*
F75	0.00330(12)	0.26548(12)	0.84011(8)	0.0552(4)*
F76	0.19549(10)	0.29412(10)	0.81610(7)	0.0433(3)*
F82	0.35411(11)	0.25392(10)	0.55325(8)	0.0467(3)*
F83	0.40515(12)	0.11598(13)	0.45303(8)	0.0586(4)*
F84	0.37420(12)	-0.08704(12)	0.45528(8)	0.0620(4)*
F85	0.28992(12)	-0.14668(10)	0.56452(9)	0.0574(4)*
F86	0.23671(10)	-0.00988(9)	0.66514(7)	0.0429(3)*
F92	0.13926(10)	0.27482(10)	0.55283(7)	0.0459(3)*
F93	0.11894(12)	0.46523(13)	0.53244(9)	0.0642(4)*
F94	0.22513(14)	0.62805(11)	0.64466(11)	0.0740(5)*
F95	0.35572(13)	0.59440(11)	0.77715(10)	0.0669(4)*
F96	0.37765(10)	0.40641(10)	0.79853(8)	0.0483(3)*
F102	0.26061(11)	0.09626(11)	0.81704(8)	0.0502(3)*

F103	0.43107(14)	0.05555(14)	0.91495(9)	0.0727(5)*
F104	0.63212(13)	0.12290(13)	0.91226(10)	0.0819(6)*
F105	0.65721(11)	0.23710(12)	0.80772(11)	0.0763(5)*
F106	0.48730(10)	0.27974(11)	0.70834(9)	0.0533(4)*
C71	0.14304(15)	0.18098(15)	0.69571(11)	0.0314(4)*
C72	0.05626(16)	0.11907(16)	0.64267(12)	0.0353(4)*
C73	-0.04381(16)	0.10261(17)	0.65500(13)	0.0405(5)*
C74	-0.06169(17)	0.14929(18)	0.72175(14)	0.0435(5)*
C75	0.02002(18)	0.21482(17)	0.77499(13)	0.0398(5)*
C76	0.11846(16)	0.22879(16)	0.76083(11)	0.0347(4)*
C81	0.28831(15)	0.13000(15)	0.61397(11)	0.0324(4)*
C82	0.33335(16)	0.15517(16)	0.55858(12)	0.0362(4)*
C83	0.36271(17)	0.08475(19)	0.50584(12)	0.0426(5)*
C84	0.34781(17)	-0.01728(19)	0.50692(13)	0.0439(5)*
C85	0.30488(17)	-0.04655(16)	0.56149(13)	0.0409(5)*
C86	0.27684(16)	0.02589(16)	0.61256(12)	0.0353(4)*
C91	0.26256(16)	0.32919(16)	0.67526(12)	0.0341(4)*
C92	0.19622(17)	0.35232(17)	0.61011(13)	0.0382(5)*
C93	0.18287(19)	0.45018(19)	0.59864(15)	0.0463(6)*
C94	0.2364(2)	0.53236(18)	0.65504(17)	0.0515(6)*
C95	0.3016(2)	0.51459(18)	0.72130(16)	0.0481(6)*
C96	0.31340(17)	0.41559(16)	0.73046(13)	0.0397(5)*
C101	0.36345(16)	0.19280(15)	0.75741(12)	0.0345(4)*
C102	0.35643(17)	0.13542(17)	0.81194(12)	0.0402(5)*
C103	0.4445(2)	0.11254(19)	0.86425(13)	0.0499(6)*
C104	0.5456(2)	0.1473(2)	0.86332(15)	0.0547(7)*
C105	0.55828(18)	0.20391(18)	0.81087(16)	0.0527(7)*
C106	0.46861(17)	0.22506(16)	0.75957(13)	0.0410(5)*
B	0.26382(18)	0.20920(17)	0.68547(13)	0.0314(5)*

Anisotropically-refined atoms are marked with an asterisk (*). The form of the anisotropic displacement parameter is: $\exp[-2\pi^2(h^2a^{*2}U_{11} + k^2b^{*2}U_{22} + l^2c^{*2}U_{33} + 2klb^*c^*U_{23} + 2hla^*c^*U_{13} + 2hka^*b^*U_{12})]$.

Table B.3. Selected Interatomic Distances (Å)

(a) within [(η^5–indenyl)Ru(NCPh)($PHPh_2$)(PPh_3)]$^+$

Atom1	Atom2	Distance	Atom1	Atom2	Distance
Ru	P1	2.3148(5)	C15	C16	1.389(3)
Ru	P2	2.2889(5)	C21	C22	1.388(4)
Ru	N	2.0310(16)	C21	C26	1.393(3)
Ru	C1	2.187(2)	C22	C23	1.391(3)
Ru	C2	2.196(2)	C23	C24	1.375(5)
Ru	C3	2.229(2)	C24	C25	1.378(5)
Ru	C3A	2.3193(19)	C25	C26	1.387(4)
Ru	C7A	2.314(2)	C31	C32	1.397(3)
P1	C21	1.817(2)	C31	C36	1.393(3)
P1	C31	1.833(2)	C32	C33	1.385(3)
P1	H1P	1.34(2)	C33	C34	1.377(4)
P2	C41	1.839(2)	C34	C35	1.385(4)
P2	C51	1.8228(19)	C35	C36	1.392(3)
P2	C61	1.834(2)	C41	C42	1.388(3)
N	C10	1.148(2)	C41	C46	1.396(3)
C1	C2	1.414(3)	C42	C43	1.390(3)
C1	C7A	1.453(3)	C43	C44	1.379(3)
C2	C3	1.412(3)	C44	C45	1.378(3)
C3	C3A	1.433(3)	C45	C46	1.389(3)
C3A	C4	1.411(3)	C51	C52	1.397(3)
C3A	C7A	1.434(3)	C51	C56	1.385(3)
C4	C5	1.341(4)	C52	C53	1.381(3)
C5	C6	1.409(4)	C53	C54	1.380(3)
C6	C7	1.374(4)	C54	C55	1.375(3)
C7	C7A	1.414(3)	C55	C56	1.396(3)
C10	C11	1.440(3)	C61	C62	1.390(3)
C11	C12	1.396(3)	C61	C66	1.389(3)
C11	C16	1.391(3)	C62	C63	1.382(3)
C12	C13	1.384(3)	C63	C64	1.376(4)
C13	C14	1.378(3)	C64	C65	1.372(4)
C14	C15	1.381(3)	C65	C66	1.391(3)

(b) within the tetrakis(pentafluorophenyl)borate ion

Atom1	Atom2	Distance	Atom1	Atom2	Distance
F72	C72	1.346(2)	F82	C82	1.356(2)
F73	C73	1.350(2)	F83	C83	1.350(3)
F74	C74	1.344(2)	F84	C84	1.346(2)
F75	C75	1.353(2)	F85	C85	1.354(3)
F76	C76	1.355(2)	F86	C86	1.355(2)

F92	C92	1.356(3)	C81	B	1.660(3)
F93	C93	1.346(3)	C82	C83	1.384(3)
F94	C94	1.343(3)	C83	C84	1.371(3)
F95	C95	1.352(3)	C84	C85	1.372(3)
F96	C96	1.349(3)	C85	C86	1.371(3)
F102	C102	1.349(3)	C91	C92	1.387(3)
F103	C103	1.344(3)	C91	C96	1.392(3)
F104	C104	1.350(3)	C91	B	1.652(3)
F105	C105	1.350(3)	C92	C93	1.381(3)
F106	C106	1.352(3)	C93	C94	1.374(4)
C71	C72	1.386(3)	C94	C95	1.367(4)
C71	C76	1.387(3)	C95	C96	1.382(3)
C71	B	1.656(3)	C101	C102	1.387(3)
C72	C73	1.388(3)	C101	C106	1.393(3)
C73	C74	1.367(3)	C101	B	1.658(3)
C74	C75	1.372(3)	C102	C103	1.387(3)
C75	C76	1.379(3)	C103	C104	1.368(4)
C81	C82	1.382(3)	C104	C105	1.365(4)
C81	C86	1.387(3)	C105	C106	1.383(3)

Table B.4. Selected Interatomic Angles (deg)

(a) within [(η^5–indenyl)Ru(NCPh)($PHPh_2$)(PPh_3)]$^+$

Atom1	Atom2	Atom3	Angle	Atom1	Atom2	Atom3	Angle
P1	Ru	P2	92.932(19)	C51	P2	C61	102.26(9)
P1	Ru	N	91.07(5)	Ru	N	C10	178.66(17)
P1	Ru	C1	97.85(6)	Ru	C1	C2	71.53(12)
P1	Ru	C2	131.60(7)	Ru	C1	C7A	75.98(11)
P1	Ru	C3	156.90(6)	C2	C1	C7A	107.57(19)
P1	Ru	C3A	124.42(5)	Ru	C2	C1	70.83(12)
P1	Ru	C7A	95.59(5)	Ru	C2	C3	72.66(12)
P2	Ru	N	89.61(5)	C1	C2	C3	109.26(19)
P2	Ru	C1	112.18(6)	Ru	C3	C2	70.14(11)
P2	Ru	C2	91.08(6)	Ru	C3	C3A	75.10(12)
P2	Ru	C3	105.84(6)	C2	C3	C3A	107.81(19)
P2	Ru	C3A	142.23(5)	Ru	C3A	C3	68.24(11)
P2	Ru	C7A	149.44(6)	Ru	C3A	C4	125.39(15)
N	Ru	C1	155.83(7)	Ru	C3A	C7A	71.79(11)
N	Ru	C2	137.20(8)	C3	C3A	C4	131.4(2)
N	Ru	C3	102.19(7)	C3	C3A	C7A	108.23(18)
N	Ru	C3A	94.61(7)	C4	C3A	C7A	120.4(2)
N	Ru	C7A	119.45(7)	C3A	C4	C5	118.6(2)
C1	Ru	C2	37.64(9)	C4	C5	C6	121.8(3)
C1	Ru	C3	62.90(8)	C5	C6	C7	121.8(2)
C1	Ru	C3A	61.86(7)	C6	C7	C7A	118.0(2)
C1	Ru	C7A	37.54(8)	Ru	C7A	C1	66.48(11)
C2	Ru	C3	37.20(8)	Ru	C7A	C3A	72.17(11)
C2	Ru	C3A	61.13(8)	Ru	C7A	C7	127.20(15)
C2	Ru	C7A	61.65(8)	C1	C7A	C3A	106.89(19)
C3	Ru	C3A	36.66(8)	C1	C7A	C7	133.8(2)
C3	Ru	C7A	61.45(8)	C3A	C7A	C7	119.3(2)
C3A	Ru	C7A	36.04(7)	N	C10	C11	176.3(2)
Ru	P1	C21	116.31(8)	C10	C11	C12	118.60(19)
Ru	P1	C31	117.61(7)	C10	C11	C16	120.27(18)
Ru	P1	H1P	117.4(9)	C12	C11	C16	121.09(18)
C21	P1	C31	103.87(10)	C11	C12	C13	118.9(2)
C21	P1	H1P	98.9(9)	C12	C13	C14	120.2(2)
C31	P1	H1P	99.8(9)	C13	C14	C15	120.8(2)
Ru	P2	C41	114.79(7)	C14	C15	C16	120.1(2)
Ru	P2	C51	110.62(6)	C11	C16	C15	118.87(19)
Ru	P2	C61	120.70(7)	P1	C21	C22	119.28(18)
C41	P2	C51	106.29(9)	P1	C21	C26	121.2(2)
C41	P2	C61	100.55(9)	C22	C21	C26	119.5(2)

Atom1	Atom2	Atom3	Angle	Atom1	Atom2	Atom3	Angle
C21	C22	C23	120.2(3)	C44	C45	C46	120.3(2)
C22	C23	C24	119.7(3)	C41	C46	C45	120.2(2)
C23	C24	C25	120.5(3)	P2	C51	C52	116.58(15)
C24	C25	C26	120.3(3)	P2	C51	C56	124.32(15)
C21	C26	C25	119.7(3)	C52	C51	C56	118.90(18)
P1	C31	C32	119.05(17)	C51	C52	C53	120.8(2)
P1	C31	C36	122.41(18)	C52	C53	C54	119.7(2)
C32	C31	C36	118.5(2)	C53	C54	C55	120.4(2)
C31	C32	C33	120.8(2)	C54	C55	C56	120.2(2)
C32	C33	C34	120.3(2)	C51	C56	C55	120.03(19)
C33	C34	C35	119.7(2)	P2	C61	C62	119.41(16)
C34	C35	C36	120.5(3)	P2	C61	C66	122.51(16)
C31	C36	C35	120.2(2)	C62	C61	C66	117.9(2)
P2	C41	C42	120.44(16)	C61	C62	C63	121.2(2)
P2	C41	C46	120.90(16)	C62	C63	C64	120.0(2)
C42	C41	C46	118.63(19)	C63	C64	C65	120.0(2)
C41	C42	C43	121.0(2)	C64	C65	C66	120.0(2)
C42	C43	C44	119.6(2)	C61	C66	C65	120.8(2)
C43	C44	C45	120.2(2)				

(b) within the tetrakis(pentafluorophenyl)borate ion

Atom1	Atom2	Atom3	Angle	Atom1	Atom2	Atom3	Angle
C72	C71	C76	113.20(18)	C82	C81	B	127.50(18)
C72	C71	B	127.28(18)	C86	C81	B	118.93(18)
C76	C71	B	119.29(17)	F82	C82	C81	121.14(18)
F72	C72	C71	121.35(18)	F82	C82	C83	114.61(19)
F72	C72	C73	115.20(18)	C81	C82	C83	124.2(2)
C71	C72	C73	123.4(2)	F83	C83	C82	120.3(2)
F73	C73	C72	120.2(2)	F83	C83	C84	119.9(2)
F73	C73	C74	119.3(2)	C82	C83	C84	119.8(2)
C72	C73	C74	120.4(2)	F84	C84	C83	120.6(2)
F74	C74	C73	120.9(2)	F84	C84	C85	120.9(2)
F74	C74	C75	120.4(2)	C83	C84	C85	118.5(2)
C73	C74	C75	118.7(2)	F85	C85	C84	120.0(2)
F75	C75	C74	120.0(2)	F85	C85	C86	120.3(2)
F75	C75	C76	120.8(2)	C84	C85	C86	119.7(2)
C74	C75	C76	119.2(2)	F86	C86	C81	119.63(18)
F76	C76	C71	119.08(18)	F86	C86	C85	115.61(19)
F76	C76	C75	115.92(18)	C81	C86	C85	124.7(2)
C71	C76	C75	125.00(19)				
C82	C81	C86	113.01(19)				

Atom1	Atom2	Atom3	Angle	Atom1	Atom2	Atom3	Angle
C92	C91	C96	113.0(2)	F102	C102	C101	121.24(18)
C92	C91	B	120.06(18)	F102	C102	C103	114.7(2)
C96	C91	B	126.46(19)	C101	C102	C103	124.0(2)
F92	C92	C91	118.98(19)	F103	C103	C102	120.5(2)
F92	C92	C93	116.4(2)	F103	C103	C104	120.0(2)
C91	C92	C93	124.6(2)	C102	C103	C104	119.5(2)
F93	C93	C92	120.4(2)	F104	C104	C103	120.2(3)
F93	C93	C94	120.1(2)	F104	C104	C105	120.3(3)
C92	C93	C94	119.5(2)	C103	C104	C105	119.5(2)
F94	C94	C93	120.3(2)	F105	C105	C104	120.5(2)
F94	C94	C95	121.0(3)	F105	C105	C106	120.1(3)
C93	C94	C95	118.7(2)	C104	C105	C106	119.4(2)
F95	C95	C94	119.6(2)	F106	C106	C101	119.56(19)
F95	C95	C96	120.3(2)	F106	C106	C105	116.1(2)
C94	C95	C96	120.1(2)	C101	C106	C105	124.4(2)
F96	C96	C91	120.59(19)	C71	B	C81	113.09(16)
F96	C96	C95	115.4(2)	C71	B	C91	101.95(15)
C91	C96	C95	124.0(2)	C71	B	C101	114.08(17)
C102	C101	C106	113.27(19)	C81	B	C91	114.95(17)
C102	C101	B	126.69(18)	C81	B	C101	99.78(15)
C106	C101	B	119.28(19)	C91	B	C101	113.61(16)

Table B.5. Torsional Angles (deg)

Atom1	Atom2	Atom3	Atom4	Angle	Atom1	Atom2	Atom3	Atom4	Angle
P2	Ru	P1	C21	-110.55(8)	N	Ru	C1	C7A	21.7(3)
P2	Ru	P1	C31	125.38(8)	C2	Ru	C1	C7A	114.29(18)
N	Ru	P1	C21	-20.88(10)	C3	Ru	C1	C2	-36.72(12)
N	Ru	P1	C31	-144.96(9)	C3	Ru	C1	C7A	77.57(13)
C1	Ru	P1	C21	136.58(10)	C3A	Ru	C1	C2	-78.28(13)
C1	Ru	P1	C31	12.51(10)	C3A	Ru	C1	C7A	36.01(12)
C2	Ru	P1	C21	155.40(11)	C7A	Ru	C1	C2	-114.29(18)
C2	Ru	P1	C31	31.32(12)	P1	Ru	C2	C1	-31.54(15)
C3	Ru	P1	C21	104.70(17)	P1	Ru	C2	C3	-149.87(11)
C3	Ru	P1	C31	-19.37(17)	P2	Ru	C2	C1	-126.43(12)
C3A	Ru	P1	C21	75.44(10)	P2	Ru	C2	C3	115.25(13)
C3A	Ru	P1	C31	-48.63(10)	N	Ru	C2	C1	142.98(13)
C7A	Ru	P1	C21	98.84(10)	N	Ru	C2	C3	24.66(18)
C7A	Ru	P1	C31	-25.23(10)	C1	Ru	C2	C3	-118.32(19)
P1	Ru	P2	C41	145.63(7)	C3	Ru	C2	C1	118.32(19)
P1	Ru	P2	C51	-94.11(7)	C3A	Ru	C2	C1	80.39(13)
P1	Ru	P2	C61	25.05(8)	C3A	Ru	C2	C3	-37.93(12)
N	Ru	P2	C41	54.58(8)	C7A	Ru	C2	C1	39.13(12)
N	Ru	P2	C51	174.84(8)	C7A	Ru	C2	C3	-79.20(14)
N	Ru	P2	C61	-66.00(9)	P1	Ru	C3	C2	73.1(2)
C1	Ru	P2	C41	-114.67(9)	P1	Ru	C3	C3A	-42.5(2)
C1	Ru	P2	C51	5.59(9)	P2	Ru	C3	C2	-70.05(13)
C1	Ru	P2	C61	124.75(10)	P2	Ru	C3	C3A	174.32(10)
C2	Ru	P2	C41	-82.62(9)	N	Ru	C3	C2	-163.14(13)
C2	Ru	P2	C51	37.64(9)	N	Ru	C3	C3A	81.23(12)
C2	Ru	P2	C61	156.80(10)	C1	Ru	C3	C2	37.15(14)
C3	Ru	P2	C41	-47.98(9)	C1	Ru	C3	C3A	-78.48(13)
C3	Ru	P2	C51	72.28(9)	C2	Ru	C3	C3A	-115.63(19)
C3	Ru	P2	C61	-168.56(10)	C3A	Ru	C3	C2	115.63(18)
C3A	Ru	P2	C41	-42.45(11)	C7A	Ru	C3	C2	79.79(14)
C3A	Ru	P2	C51	77.81(11)	C7A	Ru	C3	C3A	-35.84(12)
C3A	Ru	P2	C61	-163.03(11)	P1	Ru	C3A	C3	161.27(10)
C7A	Ru	P2	C41	-108.20(12)	P1	Ru	C3A	C4	-72.6(2)
C7A	Ru	P2	C51	12.06(13)	P1	Ru	C3A	C7A	42.20(14)
C7A	Ru	P2	C61	131.22(13)	P2	Ru	C3A	C3	-8.94(16)
P1	Ru	C1	C2	156.74(12)	P2	Ru	C3A	C4	117.17(19)
P1	Ru	C1	C7A	-88.97(12)	P2	Ru	C3A	C7A	-128.01(11)
P2	Ru	C1	C2	60.31(13)	N	Ru	C3A	C3	-104.27(12)
P2	Ru	C1	C7A	174.60(10)	N	Ru	C3A	C4	21.8(2)
N	Ru	C1	C2	-92.6(2)	N	Ru	C3A	C7A	136.67(12)

Atom1	Atom2	Atom3	Atom4	Angle
C1	Ru	C3A	C3	81.56(14)
C1	Ru	C3A	C4	-152.3(2)
C1	Ru	C3A	C7A	-37.50(13)
C2	Ru	C3A	C3	38.50(13)
C2	Ru	C3A	C4	164.6(2)
C2	Ru	C3A	C7A	-80.57(14)
C3	Ru	C3A	C4	126.1(3)
C3	Ru	C3A	C7A	-119.07(18)
C7A	Ru	C3A	C3	119.07(18)
C7A	Ru	C3A	C4	-114.8(2)
P1	Ru	C7A	C1	95.61(12)
P1	Ru	C7A	C3A	-146.17(11)
P1	Ru	C7A	C7	-32.5(2)
P2	Ru	C7A	C1	-9.86(19)
P2	Ru	C7A	C3A	108.36(13)
P2	Ru	C7A	C7	-137.96(18)
N	Ru	C7A	C1	-169.99(12)
N	Ru	C7A	C3A	-51.77(14)
N	Ru	C7A	C7	61.9(2)
C1	Ru	C7A	C3A	118.22(18)
C1	Ru	C7A	C7	-128.1(3)
C2	Ru	C7A	C1	-39.23(13)
C2	Ru	C7A	C3A	78.99(13)
C2	Ru	C7A	C7	-167.3(2)
C3	Ru	C7A	C1	-81.77(14)
C3	Ru	C7A	C3A	36.45(12)
C3	Ru	C7A	C7	150.1(2)
C3A	Ru	C7A	C1	-118.22(18)
C3A	Ru	C7A	C7	113.7(3)
Ru	P1	C21	C22	-45.2(2)
Ru	P1	C21	C26	134.45(17)
C31	P1	C21	C22	85.7(2)
C31	P1	C21	C26	-94.7(2)
Ru	P1	C31	C32	-62.59(18)
Ru	P1	C31	C36	117.21(17)
C21	P1	C31	C32	167.30(17)
C21	P1	C31	C36	-12.9(2)
Ru	P2	C41	C42	6.84(18)
Ru	P2	C41	C46	-171.23(15)
C51	P2	C41	C42	-115.79(17)
C51	P2	C41	C46	66.15(18)
C61	P2	C41	C42	137.99(16)
C61	P2	C41	C46	-40.08(19)
Ru	P2	C51	C52	64.55(17)
Ru	P2	C51	C56	-110.20(17)
C41	P2	C51	C52	-170.23(17)
C41	P2	C51	C56	15.0(2)
C61	P2	C51	C52	-65.24(18)
C61	P2	C51	C56	120.01(18)
Ru	P2	C61	C62	46.6(2)
Ru	P2	C61	C66	-137.92(17)
C41	P2	C61	C62	-80.79(19)
C41	P2	C61	C66	94.7(2)
C51	P2	C61	C62	169.79(18)
C51	P2	C61	C66	-14.7(2)
Ru	C1	C2	C3	62.88(15)
C7A	C1	C2	Ru	-68.06(13)
C7A	C1	C2	C3	-5.2(2)
Ru	C1	C7A	C3A	-61.24(14)
Ru	C1	C7A	C7	119.7(2)
C2	C1	C7A	Ru	65.07(14)
C2	C1	C7A	C3A	3.8(2)
C2	C1	C7A	C7	-175.2(2)
Ru	C2	C3	C3A	66.23(14)
C1	C2	C3	Ru	-61.73(14)
C1	C2	C3	C3A	4.5(2)
Ru	C3	C3A	C4	-118.6(2)
Ru	C3	C3A	C7A	60.94(14)
C2	C3	C3A	Ru	-62.96(14)
C2	C3	C3A	C4	178.4(2)
C2	C3	C3A	C7A	-2.0(2)
Ru	C3A	C4	C5	91.2(3)
C3	C3A	C4	C5	-177.7(2)
C7A	C3A	C4	C5	2.7(3)
Ru	C3A	C7A	C1	57.60(13)
Ru	C3A	C7A	C7	-123.21(19)
C3	C3A	C7A	Ru	-58.72(14)
C3	C3A	C7A	C1	-1.1(2)
C3	C3A	C7A	C7	178.07(18)
C4	C3A	C7A	Ru	120.92(19)

Atom1	Atom2	Atom3	Atom4	Angle
C4	C3A	C7A	C1	178.52(19)
C4	C3A	C7A	C7	-2.3(3)
C3A	C4	C5	C6	-1.1(4)
C4	C5	C6	C7	-1.0(4)
C5	C6	C7	C7A	1.4(4)
C6	C7	C7A	Ru	-88.9(3)
C6	C7	C7A	C1	179.1(2)
C6	C7	C7A	C3A	0.2(3)
C10	C11	C12	C13	-178.2(2)
C16	C11	C12	C13	-0.3(3)
C10	C11	C16	C15	178.12(18)
C12	C11	C16	C15	0.2(3)
C11	C12	C13	C14	-0.2(3)
C12	C13	C14	C15	0.8(4)
C13	C14	C15	C16	-0.9(3)
C14	C15	C16	C11	0.3(3)
P1	C21	C22	C23	-178.5(2)
C26	C21	C22	C23	1.8(4)
P1	C21	C26	C25	179.68(19)
C22	C21	C26	C25	-0.6(4)
C21	C22	C23	C24	-1.7(4)
C22	C23	C24	C25	0.3(4)
C23	C24	C25	C26	0.9(4)
C24	C25	C26	C21	-0.7(4)
P1	C31	C32	C33	177.98(17)
C36	C31	C32	C33	-1.8(3)
P1	C31	C36	C35	-177.82(18)
C32	C31	C36	C35	2.0(3)
C31	C32	C33	C34	0.3(3)
C32	C33	C34	C35	1.2(4)
C33	C34	C35	C36	-1.0(4)
C34	C35	C36	C31	-0.6(4)
P2	C41	C42	C43	-178.97(16)
C46	C41	C42	C43	-0.9(3)
P2	C41	C46	C45	178.70(17)
C42	C41	C46	C45	0.6(3)
C41	C42	C43	C44	0.0(3)
C42	C43	C44	C45	1.1(3)
C43	C44	C45	C46	-1.4(3)
C44	C45	C46	C41	0.5(3)
P2	C51	C52	C53	-174.63(19)
C56	C51	C52	C53	0.4(3)
P2	C51	C56	C55	174.11(16)
C52	C51	C56	C55	-0.5(3)
C51	C52	C53	C54	0.2(4)
C52	C53	C54	C55	-0.8(4)
C53	C54	C55	C56	0.7(3)
C54	C55	C56	C51	0.0(3)
P2	C61	C62	C63	174.5(2)
C66	C61	C62	C63	-1.2(4)
P2	C61	C66	C65	-174.7(2)
C62	C61	C66	C65	0.9(4)
C61	C62	C63	C64	1.0(4)
C62	C63	C64	C65	-0.5(4)
C63	C64	C65	C66	0.2(4)
C64	C65	C66	C61	-0.4(4)
C76	C71	C72	F72	176.73(17)
C76	C71	C72	C73	-3.0(3)
B	C71	C72	F72	2.2(3)
B	C71	C72	C73	-177.44(19)
C72	C71	C76	F76	-177.86(17)
C72	C71	C76	C75	2.6(3)
B	C71	C76	F76	-2.9(3)
B	C71	C76	C75	177.61(19)
C72	C71	B	C81	-17.1(3)
C72	C71	B	C91	106.8(2)
C72	C71	B	C101	-130.3(2)
C76	C71	B	C81	168.67(17)
C76	C71	B	C91	-67.3(2)
C76	C71	B	C101	55.5(2)
F72	C72	C73	F73	-0.9(3)
F72	C72	C73	C74	-178.89(18)
C71	C72	C73	F73	178.77(19)
C71	C72	C73	C74	0.8(3)
F73	C73	C74	F74	2.5(3)
F73	C73	C74	C75	-176.03(19)
C72	C73	C74	F74	-179.57(19)
C72	C73	C74	C75	1.9(3)
F74	C74	C75	F75	-1.3(3)
F74	C74	C75	C76	179.25(19)

Atom1	Atom2	Atom3	Atom4	Angle
C73	C74	C75	F75	177.16(19)
C73	C74	C75	C76	-2.3(3)
F75	C75	C76	F76	0.9(3)
F75	C75	C76	C71	-179.54(18)
C74	C75	C76	F76	-179.64(19)
C74	C75	C76	C71	-0.1(3)
C86	C81	C82	F82	-177.61(17)
C86	C81	C82	C83	1.1(3)
B	C81	C82	F82	-6.4(3)
B	C81	C82	C83	172.25(19)
C82	C81	C86	F86	178.03(17)
C82	C81	C86	C85	-1.0(3)
B	C81	C86	F86	6.0(3)
B	C81	C86	C85	-173.00(19)
C82	C81	B	C71	134.3(2)
C82	C81	B	C91	17.8(3)
C82	C81	B	C101	-104.1(2)
C86	C81	B	C71	-54.9(2)
C86	C81	B	C91	-171.48(17)
C86	C81	B	C101	66.6(2)
F82	C82	C83	F83	-2.0(3)
F82	C82	C83	C84	178.52(18)
C81	C82	C83	F83	179.24(19)
C81	C82	C83	C84	-0.2(3)
F83	C83	C84	F84	-0.6(3)
F83	C83	C84	C85	179.76(19)
C82	C83	C84	F84	178.87(19)
C82	C83	C84	C85	-0.8(3)
F84	C84	C85	F85	0.9(3)
F84	C84	C85	C86	-178.80(19)
C83	C84	C85	F85	-179.47(19)
C83	C84	C85	C86	0.8(3)
F85	C85	C86	F86	1.3(3)
F85	C85	C86	C81	-179.62(18)
C84	C85	C86	F86	-178.98(18)
C84	C85	C86	C81	0.1(3)
C96	C91	C92	F92	-177.95(18)
C96	C91	C92	C93	1.8(3)
B	C91	C92	F92	-5.1(3)
B	C91	C92	C93	174.70(19)
C92	C91	C96	F96	177.49(18)
C92	C91	C96	C95	-1.4(3)
B	C91	C96	F96	5.2(3)
B	C91	C96	C95	-173.7(2)
C92	C91	B	C71	-68.1(2)
C92	C91	B	C81	54.6(2)
C92	C91	B	C101	168.67(18)
C96	C91	B	C71	103.7(2)
C96	C91	B	C81	-133.6(2)
C96	C91	B	C101	-19.5(3)
F92	C92	C93	F93	-2.2(3)
F92	C92	C93	C94	178.62(19)
C91	C92	C93	F93	178.06(19)
C91	C92	C93	C94	-1.2(3)
F93	C93	C94	F94	0.2(3)
F93	C93	C94	C95	-179.3(2)
C92	C93	C94	F94	179.44(19)
C92	C93	C94	C95	-0.1(3)
F94	C94	C95	F95	-0.2(3)
F94	C94	C95	C96	-179.0(2)
C93	C94	C95	F95	179.4(2)
C93	C94	C95	C96	0.5(3)
F95	C95	C96	F96	2.5(3)
F95	C95	C96	C91	-178.5(2)
C94	C95	C96	F96	-178.6(2)
C94	C95	C96	C91	0.3(3)
C106	C101	C102	F102	-178.71(19)
C106	C101	C102	C103	0.6(3)
B	C101	C102	F102	-8.8(3)
B	C101	C102	C103	170.5(2)
C102	C101	C106	F106	178.47(19)
C102	C101	C106	C105	-0.6(3)
B	C101	C106	F106	7.7(3)
B	C101	C106	C105	-171.4(2)
C102	C101	B	C71	18.0(3)
C102	C101	B	C81	-102.9(2)
C102	C101	B	C91	134.3(2)
C106	C101	B	C71	-172.67(18)
C106	C101	B	C81	66.5(2)
C106	C101	B	C91	-56.4(2)

Atom1	Atom2	Atom3	Atom4	Angle
F102	C102	C103	F103	-0.1(3)
F102	C102	C103	C104	179.1(2)
C101	C102	C103	F103	-179.4(2)
C101	C102	C103	C104	-0.3(4)
F103	C103	C104	F104	1.2(4)
F103	C103	C104	C105	179.1(2)
C102	C103	C104	F104	-177.9(2)
C102	C103	C104	C105	0.0(4)

Atom1	Atom2	Atom3	Atom4	Angle
F104	C104	C105	F105	-0.7(4)
F104	C104	C105	C106	177.8(2)
C103	C104	C105	F105	-178.5(2)
C103	C104	C105	C106	-0.1(4)
F105	C105	C106	F106	-0.2(3)
F105	C105	C106	C101	178.9(2)
C104	C105	C106	F106	-178.7(2)
C104	C105	C106	C101	0.4(4)

Table B.6. Least-Squares Planes

Plane	Coefficients[a]				Defining Atoms with Deviations (Å)[b]			
1	0.920(13)	8.293(11)	-16.170(9)	2.863(5)				
					C1	-0.0263(12)	C2	0.0282(13)
					C3	-0.0186(12)	C3A	0.0021(12)
					C7A	0.0145(12)		
					Ru	-1.8885(9)		

Distance: Ru–C_{cent} = 1.893 Å (C_{cent} = C1–C2–C3–C3A–C7A centroid)

Angles: C_{cent}–Ru–P1 = 124.4°, C_{cent}–Ru–P2 = 124.1°, C_{cent}–Ru–N = 124.8°

2	1.67(4)	7.959(19)	-16.529(17)	2.793(7)				
					C1	C2	C3	
					Ru	-1.847(2)		
3	0.641(18)	8.394(11)	-16.033(11)	2.849(6)				
					C1	-0.0037(7)	C3	0.0038(7)
					C3A	-0.0061(12)	C7A	0.0060(12)
					Ru	-1.8713(12)		
4	0.544(13)	8.682(10)	-15.773(9)	2.954(5)				
					C3A	0.0154(15)	C4	-0.0115(17)
					C5	-0.002(2)	C6	0.0107(19)
					C7	-0.0063(17)	C7A	-0.0067(15)
					Ru	-1.850(2)		

Dihedral angle between planes 2 and 3: 4.84(19)°

Dihedral angle between planes 3 and 4: 1.61(14)°

[a]Coefficients are for the form $ax+by+cz = d$ where x, y and z are crystallographic coordinates.

[b]Underlined atoms were not included in the definition of the plane.

Table B.7. Anisotropic Displacement Parameters (U_{ij}, Å^2)

Atom	U_{11}	U_{22}	U_{33}	U_{23}	U_{13}	U_{12}
Ru	0.02646(8)	0.02821(9)	0.02823(8)	0.00843(6)	0.00511(6)	0.00519(6)
P1	0.0359(3)	0.0295(3)	0.0328(3)	0.0083(2)	0.0090(2)	0.0081(2)
P2	0.0265(2)	0.0263(2)	0.0300(2)	0.00637(19)	0.00572(19)	0.00572(18)
N	0.0291(8)	0.0342(9)	0.0351(9)	0.0105(7)	0.0095(7)	0.0072(7)
C1	0.0409(11)	0.0447(13)	0.0325(11)	0.0183(10)	-0.0033(9)	-0.0051(9)
C2	0.0384(11)	0.0489(13)	0.0471(12)	0.0298(11)	0.0118(9)	0.0135(10)
C3	0.0471(12)	0.0303(10)	0.0387(11)	0.0130(9)	0.0138(9)	0.0053(9)
C3A	0.0392(11)	0.0358(11)	0.0287(9)	0.0087(8)	0.0095(8)	0.0011(9)
C4	0.0375(11)	0.0619(16)	0.0426(12)	0.0139(11)	0.0115(10)	-0.0025(11)
C5	0.0456(14)	0.091(2)	0.0624(17)	0.0222(16)	0.0253(13)	0.0119(14)
C6	0.084(2)	0.082(2)	0.0614(17)	0.0278(16)	0.0514(16)	0.0405(18)
C7	0.088(2)	0.0412(13)	0.0340(12)	0.0090(10)	0.0242(12)	0.0115(13)
C7A	0.0483(12)	0.0364(11)	0.0251(9)	0.0101(8)	0.0070(8)	0.0027(9)
C10	0.0319(10)	0.0367(11)	0.0339(10)	0.0089(8)	0.0111(8)	0.0076(8)
C11	0.0290(9)	0.0400(11)	0.0292(9)	0.0086(8)	0.0091(8)	0.0102(8)
C12	0.0514(13)	0.0357(12)	0.0357(11)	0.0051(9)	0.0069(10)	0.0129(10)
C13	0.0613(15)	0.0456(13)	0.0385(12)	0.0132(10)	0.0102(11)	0.0293(12)
C14	0.0368(11)	0.0605(15)	0.0299(10)	0.0107(10)	0.0057(9)	0.0181(10)
C15	0.0318(10)	0.0475(13)	0.0327(10)	0.0075(9)	0.0076(8)	0.0023(9)
C16	0.0318(10)	0.0408(11)	0.0344(10)	0.0145(9)	0.0099(8)	0.0065(8)
C21	0.0505(13)	0.0377(12)	0.0348(11)	0.0058(9)	0.0072(9)	0.0199(10)
C22	0.0473(13)	0.0556(15)	0.0497(14)	0.0041(12)	0.0051(11)	0.0231(12)
C23	0.0529(16)	0.078(2)	0.0636(18)	-0.0110(16)	-0.0048(13)	0.0338(15)
C24	0.089(2)	0.077(2)	0.0493(16)	-0.0091(15)	-0.0184(15)	0.0593(19)
C25	0.118(3)	0.0554(17)	0.0409(14)	0.0067(12)	0.0012(16)	0.0475(19)
C26	0.0805(18)	0.0434(14)	0.0378(12)	0.0099(10)	0.0086(12)	0.0239(13)
C31	0.0471(12)	0.0273(10)	0.0370(11)	0.0058(8)	0.0132(9)	0.0015(9)
C32	0.0493(13)	0.0359(12)	0.0395(12)	0.0099(9)	0.0090(10)	0.0002(10)
C33	0.0627(15)	0.0423(13)	0.0395(12)	0.0086(10)	0.0047(11)	-0.0098(12)
C34	0.084(2)	0.0457(15)	0.0387(13)	0.0021(11)	0.0203(13)	-0.0087(13)
C35	0.0779(19)	0.0396(14)	0.0546(15)	-0.0005(11)	0.0306(14)	0.0036(12)
C36	0.0564(14)	0.0369(12)	0.0471(13)	0.0079(10)	0.0181(11)	0.0065(10)
C41	0.0316(9)	0.0283(10)	0.0308(10)	0.0036(8)	0.0015(8)	0.0077(8)
C42	0.0429(11)	0.0334(11)	0.0344(11)	0.0076(9)	0.0049(9)	0.0034(9)
C43	0.0487(13)	0.0319(11)	0.0419(12)	0.0067(9)	-0.0011(10)	0.0019(9)
C44	0.0489(13)	0.0350(12)	0.0392(12)	-0.0021(9)	-0.0056(10)	0.0140(10)
C45	0.0436(12)	0.0493(14)	0.0429(12)	-0.0045(10)	0.0092(10)	0.0132(11)
C46	0.0358(11)	0.0398(12)	0.0453(12)	-0.0031(10)	0.0119(9)	0.0050(9)
C51	0.0263(9)	0.0315(10)	0.0336(10)	0.0080(8)	0.0079(8)	0.0066(7)
C52	0.0348(11)	0.0345(11)	0.0531(13)	-0.0003(10)	0.0028(10)	0.0075(9)

Atom	U_{11}	U_{22}	U_{33}	U_{23}	U_{13}	U_{12}
C53	0.0356(11)	0.0470(14)	0.0524(14)	-0.0038(11)	0.0004(10)	0.0007(10)
C54	0.0269(10)	0.0587(15)	0.0416(12)	0.0108(11)	0.0033(9)	0.0077(10)
C55	0.0351(11)	0.0466(13)	0.0435(12)	0.0165(10)	0.0115(9)	0.0171(9)
C56	0.0332(10)	0.0339(11)	0.0343(10)	0.0078(8)	0.0097(8)	0.0073(8)
C61	0.0387(10)	0.0298(10)	0.0349(10)	0.0062(8)	0.0121(8)	0.0069(8)
C62	0.0447(12)	0.0549(15)	0.0417(12)	0.0193(11)	0.0128(10)	0.0111(11)
C63	0.0663(16)	0.0630(17)	0.0466(14)	0.0284(13)	0.0173(12)	0.0253(13)
C64	0.085(2)	0.0401(13)	0.0530(15)	0.0201(11)	0.0293(14)	0.0131(13)
C65	0.0631(16)	0.0513(15)	0.0736(18)	0.0244(14)	0.0315(14)	0.0023(13)
C66	0.0446(13)	0.0445(13)	0.0581(15)	0.0192(11)	0.0149(11)	0.0032(10)
F72	0.0390(7)	0.0493(8)	0.0362(7)	-0.0051(6)	-0.0021(5)	0.0042(6)
F73	0.0310(6)	0.0519(8)	0.0711(10)	0.0056(7)	-0.0072(6)	-0.0017(6)
F74	0.0393(7)	0.0684(10)	0.0888(11)	0.0339(9)	0.0273(7)	0.0113(7)
F75	0.0642(9)	0.0646(9)	0.0477(8)	0.0144(7)	0.0288(7)	0.0204(7)
F76	0.0448(7)	0.0457(7)	0.0318(6)	-0.0024(5)	0.0046(5)	0.0036(6)
F82	0.0554(8)	0.0412(7)	0.0518(8)	0.0149(6)	0.0242(6)	0.0111(6)
F83	0.0596(9)	0.0786(11)	0.0458(8)	0.0132(7)	0.0250(7)	0.0217(8)
F84	0.0621(9)	0.0631(10)	0.0522(8)	-0.0139(7)	0.0125(7)	0.0252(8)
F85	0.0666(9)	0.0312(7)	0.0622(9)	-0.0034(6)	0.0040(7)	0.0113(6)
F86	0.0484(7)	0.0330(7)	0.0456(7)	0.0093(5)	0.0097(6)	0.0036(5)
F92	0.0465(7)	0.0523(8)	0.0371(7)	0.0113(6)	0.0047(6)	0.0132(6)
F93	0.0646(9)	0.0752(11)	0.0734(10)	0.0465(9)	0.0275(8)	0.0337(8)
F94	0.0943(12)	0.0405(8)	0.1163(14)	0.0349(9)	0.0609(11)	0.0318(8)
F95	0.0801(11)	0.0310(7)	0.0887(12)	-0.0075(7)	0.0381(9)	-0.0045(7)
F96	0.0454(7)	0.0385(7)	0.0491(8)	-0.0040(6)	0.0027(6)	-0.0015(6)
F102	0.0501(8)	0.0604(9)	0.0458(7)	0.0252(7)	0.0122(6)	0.0124(7)
F103	0.0856(12)	0.0821(12)	0.0491(9)	0.0298(8)	0.0002(8)	0.0303(9)
F104	0.0619(10)	0.0699(11)	0.0783(11)	-0.0012(9)	-0.0362(8)	0.0240(8)
F105	0.0308(7)	0.0567(10)	0.1203(15)	0.0025(10)	-0.0043(8)	0.0010(7)
F106	0.0367(7)	0.0479(8)	0.0747(10)	0.0142(7)	0.0142(7)	0.0014(6)
C71	0.0310(9)	0.0306(10)	0.0299(9)	0.0084(8)	0.0020(8)	0.0049(8)
C72	0.0349(10)	0.0328(11)	0.0337(10)	0.0058(8)	0.0014(8)	0.0079(8)
C73	0.0283(10)	0.0366(11)	0.0504(13)	0.0127(10)	-0.0023(9)	0.0032(8)
C74	0.0325(11)	0.0460(13)	0.0592(14)	0.0240(11)	0.0149(10)	0.0102(9)
C75	0.0443(12)	0.0427(12)	0.0389(11)	0.0148(10)	0.0157(9)	0.0152(10)
C76	0.0365(10)	0.0337(11)	0.0313(10)	0.0069(8)	0.0044(8)	0.0050(8)
C81	0.0291(9)	0.0316(10)	0.0315(10)	0.0028(8)	0.0017(8)	0.0058(8)
C82	0.0341(10)	0.0346(11)	0.0383(11)	0.0069(9)	0.0061(8)	0.0085(8)
C83	0.0360(11)	0.0562(15)	0.0344(11)	0.0052(10)	0.0086(9)	0.0127(10)
C84	0.0364(11)	0.0498(14)	0.0359(11)	-0.0074(10)	0.0006(9)	0.0168(10)

Atom	U_{11}	U_{22}	U_{33}	U_{23}	U_{13}	U_{12}
C85	0.0379(11)	0.0325(11)	0.0419(12)	-0.0009(9)	-0.0033(9)	0.0104(9)
C86	0.0322(10)	0.0350(11)	0.0334(10)	0.0043(8)	0.0009(8)	0.0066(8)
C91	0.0322(10)	0.0332(11)	0.0386(11)	0.0063(9)	0.0123(8)	0.0077(8)
C92	0.0373(11)	0.0397(12)	0.0435(12)	0.0113(10)	0.0174(9)	0.0116(9)
C93	0.0457(12)	0.0519(14)	0.0587(14)	0.0284(12)	0.0285(11)	0.0234(11)
C94	0.0580(15)	0.0351(12)	0.0822(19)	0.0231(13)	0.0446(14)	0.0202(11)
C95	0.0506(13)	0.0320(12)	0.0681(16)	0.0039(11)	0.0321(12)	0.0048(10)
C96	0.0383(11)	0.0330(11)	0.0492(13)	0.0039(9)	0.0174(10)	0.0045(9)
C101	0.0336(10)	0.0297(10)	0.0333(10)	-0.0010(8)	0.0015(8)	0.0058(8)
C102	0.0409(11)	0.0396(12)	0.0337(11)	0.0017(9)	0.0016(9)	0.0100(9)
C103	0.0582(15)	0.0454(13)	0.0364(12)	0.0042(10)	-0.0041(10)	0.0176(11)
C104	0.0464(14)	0.0451(14)	0.0500(14)	-0.0069(11)	-0.0179(11)	0.0165(11)
C105	0.0317(11)	0.0352(12)	0.0716(17)	-0.0076(12)	-0.0075(11)	0.0038(9)
C106	0.0344(11)	0.0310(11)	0.0483(13)	-0.0007(9)	0.0012(9)	0.0038(9)
B	0.0305(11)	0.0299(11)	0.0303(11)	0.0039(9)	0.0037(9)	0.0035(9)

The form of the anisotropic displacement parameter is:

$\exp[-2\pi^2(h^2a^{*2}U_{11} + k^2b^{*2}U_{22} + l^2c^{*2}U_{33} + 2klb^*c^*U_{23} + 2hla^*c^*U_{13} + 2hka^*b^*U_{12})]$

Table B.8. Derived Atomic Coordinates and Displacement Parameters for Hydrogen Atoms

Atom	*x*	*y*	*z*	U_{eq}, Å^2
H1	0.0573	0.3241	-0.0107	0.049
H2	0.0398	0.4954	0.0709	0.050
H3	0.2285	0.5929	0.1377	0.045
H4	0.4392	0.5444	0.1298	0.057
H5	0.5274	0.4315	0.0686	0.076
H6	0.4359	0.2838	-0.0180	0.080
H7	0.2515	0.2429	-0.0437	0.063
H12	0.4620	0.2693	0.3670	0.050
H13	0.5977	0.2849	0.4813	0.057
H14	0.6937	0.4435	0.5432	0.051
H15	0.6540	0.5889	0.4944	0.045
H16	0.5187	0.5758	0.3798	0.041
H22	0.4091	0.2406	0.1506	0.063
H23	0.5636	0.1764	0.2115	0.085
H24	0.5513	0.0559	0.2862	0.095
H25	0.3863	-0.0030	0.2997	0.089
H26	0.2303	0.0559	0.2358	0.065
H32	-0.0015	0.1631	0.0068	0.051
H33	-0.0519	0.0657	-0.1171	0.061
H34	0.0655	-0.0365	-0.1600	0.069
H35	0.2323	-0.0453	-0.0772	0.068
H36	0.2839	0.0513	0.0475	0.055
H42	0.2281	0.5797	0.2541	0.046
H43	0.2681	0.7307	0.3465	0.052
H44	0.1726	0.7557	0.4373	0.054
H45	0.0419	0.6284	0.4386	0.057
H46	0.0003	0.4776	0.3459	0.050
H52	-0.0648	0.2418	0.1075	0.052
H53	-0.2327	0.2301	0.0207	0.059
H54	-0.3244	0.3726	0.0183	0.052
H55	-0.2508	0.5251	0.1042	0.048
H56	-0.0821	0.5377	0.1922	0.040
H62	0.2222	0.2918	0.3177	0.055
H63	0.2067	0.1859	0.4023	0.066
H64	0.0384	0.1271	0.4108	0.067
H65	-0.1143	0.1768	0.3364	0.071
H66	-0.0994	0.2845	0.2520	0.058

Appendix C X-Ray Crystallographic structure report for Ru(η^5-indenyl)(PPh_2)(κ^2-P(Ph_2)CH_2CH_2(CO_2Bu^t)C(Ph)NH)(PPh_3) (7a)

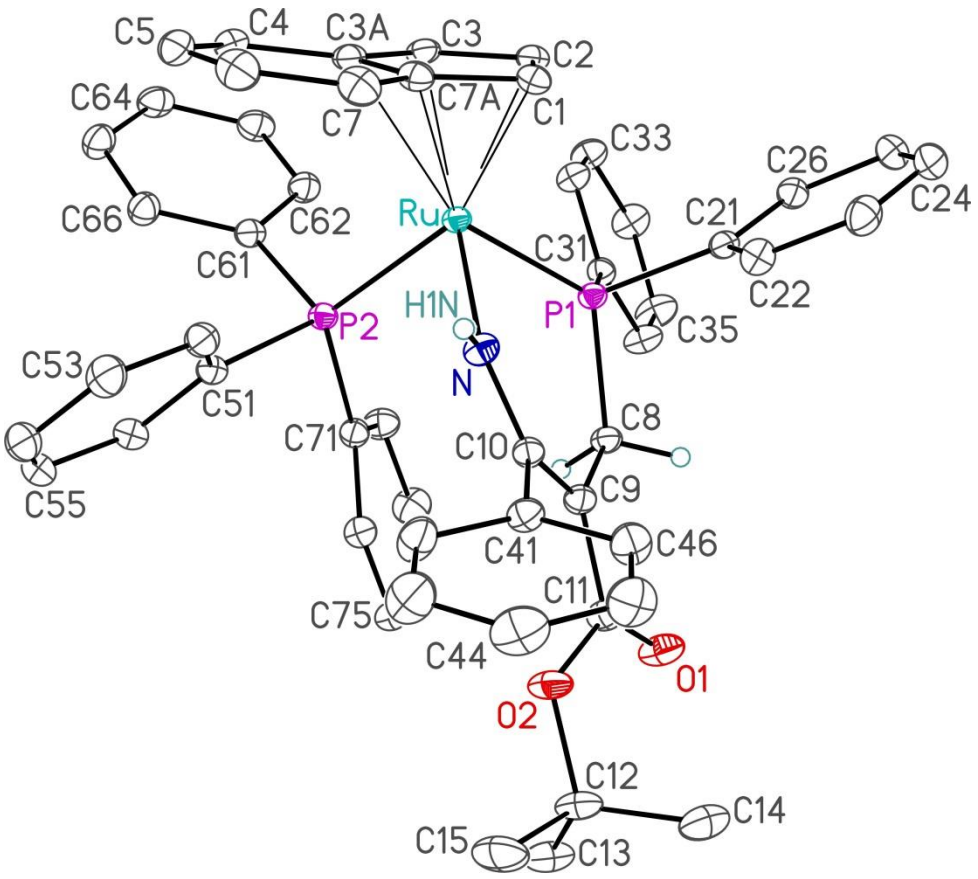

Figure C.1. Perspective view of the molecular structure of Ru(η^5-indenyl)(PPh_2)(κ^2-P(Ph_2)CH_2CH_2(CO_2Bu^t)C(Ph)NH)(PPh_3) (**7a**) showing the atom labeling scheme. Non-hydrogen atoms are represented by Gaussian ellipsoids at the 30% probability level. Hydrogen atoms attached to the N and C8 are shown with arbitrarily small thermal parameters; all other hydrogens are not shown.

Table C.1. Crystallographic Experimental Details

A. Crystal Data	
formula	$C_{53}H_{49}NO_2P_2Ru$
formula weight	894.94
crystal dimensions (mm)	0.23 × 0.10 × 0.03
crystal system	triclinic
space group	$P\bar{1}$ (No. 2)
unit cell parameters[a]	
a (Å)	10.56450 (19)
b (Å)	12.82609 (19)
c (Å)	16.5677 (2)
α (deg)	84.9715 (6)
β (deg)	85.7571 (8)
γ (deg)	74.5055 (8)
V (Å^3)	2152.04 (6)
Z	2
ρ_{calcd} (g cm^{-3})	1.381
μ (mm^{-1})	3.981
B. Data Collection and Refinement Conditions	
diffractometer	Bruker D8/APEX II CCD[b]
radiation (λ [Å])	Cu Kα (1.54178) (microfocus source)
temperature (°C)	–100
scan type	ω and ϕ scans (1.0°) (5 s exposures)
data collection 2θ limit (deg)	147.86
total data collected	15311 (-11 ≤ h ≤ 12, -15 ≤ k ≤ 15, -20 ≤ l ≤ 20)
independent reflections	8367 (R_{int} = 0.0207)
number of observed reflections (*NO*)	7820 [$F_o^2 \geq 2\sigma(F_o^2)$]
structure solution method	Patterson/structure expansion (*DIRDIF–2008*[c])
refinement method	full-matrix least-squares on F^2 (*SHELXL–2014*[d])
absorption correction method	Gaussian integration (face-indexed)
range of transmission factors	0.8762–0.5717
data/restraints/parameters	8367 / 0 / 536
goodness-of-fit (S)[e] [all data]	1.055
final R indices[f]	
R_1 [$F_o^2 \geq 2\sigma(F_o^2)$]	0.0280
wR_2 [all data]	0.0738
largest difference peak and hole	1.925 and –0.449 e Å^{-3}

[a]Obtained from least-squares refinement of 9878 reflections with 5.36° < 2θ < 146.84°.

[b]Programs for diffractometer operation, data collection, data reduction and absorption correction were those supplied by Bruker.

[c]Beurskens, P. T.; Beurskens, G.; de Gelder, R.; Smits, J. M. M.; Garcia-Granda, S.; Gould, R. O. (2008). The *DIRDIF-2008* program system. Crystallography Laboratory, Radboud University Nijmegen, The Netherlands.

[d]Sheldrick, G. M. *Acta Crystallogr.* **2015**, *C71*, 3–8.

[e]$S = [\Sigma w(F_o^2 - F_c^2)^2/(n - p)]^{1/2}$ (n = number of data; p = number of parameters varied; $w = [\sigma^2(F_o^2) + (0.0364P)^2 + 0.9228P]^{-1}$ where $P = [\mathrm{Max}(F_o^2, 0) + 2F_c^2]/3$).

[f]$R_1 = \Sigma||F_o| - |F_c||/\Sigma|F_o|$; $wR_2 = [\Sigma w(F_o^2 - F_c^2)^2/\Sigma w(F_o^4)]^{1/2}$.

Table C.2. Atomic Coordinates and Equivalent Isotropic Displacement Parameters

Atom	*x*	*y*	*z*	U_{eq}, Å^2
Ru	0.14667(2)	0.12173(2)	0.17413(2)	0.01968(5)*
P1	0.09922(5)	0.27899(4)	0.09777(3)	0.02034(10)*
P2	0.30136(5)	0.16080(4)	0.24922(3)	0.02137(10)*
O1	-0.09396(18)	0.58873(12)	0.21946(10)	0.0400(4)*
O2	-0.13396(17)	0.50173(12)	0.33978(9)	0.0355(4)*
N	-0.00438(18)	0.20116(14)	0.25302(10)	0.0262(3)*
C1	0.0376(2)	0.01918(16)	0.12268(12)	0.0279(4)*
C2	0.1440(2)	0.03197(16)	0.06823(12)	0.0273(4)*
C3	0.2660(2)	-0.01606(15)	0.10560(12)	0.0263(4)*
C3A	0.2351(2)	-0.06920(15)	0.18197(12)	0.0254(4)*
C4	0.3160(2)	-0.13782(16)	0.24050(13)	0.0294(4)*
C5	0.2573(3)	-0.18200(17)	0.30610(14)	0.0356(5)*
C6	0.1192(3)	-0.15770(19)	0.31832(14)	0.0378(5)*
C7	0.0380(2)	-0.08998(19)	0.26393(14)	0.0344(5)*
C7A	0.0946(2)	-0.04644(16)	0.19298(12)	0.0275(4)*
C8	0.0388(2)	0.40204(15)	0.15148(11)	0.0238(4)*
C9	-0.0464(2)	0.39712(16)	0.22873(12)	0.0255(4)*
C10	-0.0677(2)	0.30297(16)	0.26864(11)	0.0243(4)*
C11	-0.0948(2)	0.50411(17)	0.25929(13)	0.0294(4)*
C12	-0.2034(3)	0.60177(18)	0.37770(15)	0.0377(5)*
C13	-0.1134(3)	0.6760(2)	0.37945(18)	0.0466(6)*
C14	-0.3292(3)	0.6561(2)	0.33483(18)	0.0474(6)*
C15	-0.2346(3)	0.5596(2)	0.46387(16)	0.0538(7)*
C21	-0.0335(2)	0.28369(15)	0.03105(12)	0.0240(4)*
C22	-0.1537(2)	0.27082(17)	0.06650(13)	0.0301(4)*
C23	-0.2563(2)	0.27234(18)	0.01826(15)	0.0359(5)*
C24	-0.2399(3)	0.28480(19)	-0.06570(15)	0.0374(5)*
C25	-0.1217(3)	0.29738(19)	-0.10131(14)	0.0363(5)*
C26	-0.0193(2)	0.29738(16)	-0.05352(12)	0.0286(4)*

C31	0.2236(2)	0.31183(16)	0.02436(11)	0.0230(4)*
C32	0.3095(2)	0.22742(16)	-0.01577(12)	0.0283(4)*
C33	0.3956(2)	0.24797(18)	-0.07844(14)	0.0334(5)*
C34	0.3977(2)	0.35329(19)	-0.10241(15)	0.0368(5)*
C35	0.3154(3)	0.43765(19)	-0.06214(16)	0.0412(6)*
C36	0.2285(2)	0.41752(17)	0.00071(14)	0.0334(5)*
C41	-0.1767(2)	0.30780(16)	0.33366(12)	0.0277(4)*
C42	-0.1482(3)	0.2592(2)	0.41053(14)	0.0413(6)*
C43	-0.2501(3)	0.2588(2)	0.46923(16)	0.0520(7)*
C44	-0.3790(3)	0.3056(2)	0.45093(17)	0.0490(7)*
C45	-0.4073(3)	0.3521(2)	0.37453(17)	0.0453(6)*
C46	-0.3068(2)	0.3533(2)	0.31579(14)	0.0363(5)*
C51	0.2879(2)	0.12312(16)	0.35862(12)	0.0255(4)*
C52	0.2008(2)	0.06293(17)	0.38804(13)	0.0297(4)*
C53	0.1950(3)	0.0274(2)	0.46985(14)	0.0391(5)*
C54	0.2774(3)	0.0508(2)	0.52223(14)	0.0420(6)*
C55	0.3649(3)	0.11107(19)	0.49376(14)	0.0388(5)*
C56	0.3698(2)	0.14746(17)	0.41279(13)	0.0323(5)*
C61	0.4690(2)	0.08088(16)	0.22173(12)	0.0250(4)*
C62	0.5202(2)	0.09262(17)	0.14197(13)	0.0301(4)*
C63	0.6436(2)	0.03048(19)	0.11754(14)	0.0354(5)*
C64	0.7168(2)	-0.04784(19)	0.17055(15)	0.0361(5)*
C65	0.6663(2)	-0.06229(19)	0.24884(15)	0.0361(5)*
C66	0.5445(2)	0.00191(17)	0.27482(13)	0.0309(4)*
C71	0.3170(2)	0.30020(16)	0.25123(12)	0.0254(4)*
C72	0.3967(2)	0.34347(18)	0.19454(14)	0.0338(5)*
C73	0.3958(3)	0.45240(19)	0.19280(16)	0.0407(5)*
C74	0.3172(3)	0.51861(18)	0.24826(16)	0.0406(6)*
C75	0.2371(2)	0.47703(18)	0.30465(15)	0.0365(5)*
C76	0.2361(2)	0.36848(17)	0.30629(13)	0.0304(4)*
H1N	-0.047(3)	0.154(2)	0.2802(18)	0.044(8)

Anisotropically-refined atoms are marked with an asterisk (*). The form of the anisotropic displacement parameter is: $\exp[-2\pi^2(h^2a^{*2}U_{11} + k^2b^{*2}U_{22} + l^2c^{*2}U_{33} + 2klb^*c^*U_{23} + 2hla^*c^*U_{13} + 2hka^*b^*U_{12})]$.

Table C.3. Selected Interatomic Distances (Å)

Atom1	Atom2	Distance	Atom1	Atom2	Distance
Ru	P1	2.2420(5)	C21	C22	1.403(3)
Ru	P2	2.3059(5)	C21	C26	1.399(3)
Ru	N	2.0855(17)	C22	C23	1.388(3)
Ru	C1	2.222(2)	C23	C24	1.389(3)
Ru	C2	2.1870(19)	C24	C25	1.384(4)
Ru	C3	2.2250(19)	C25	C26	1.387(3)
Ru	C3A	2.3720(19)	C31	C32	1.396(3)
Ru	C7A	2.355(2)	C31	C36	1.391(3)
P1	C8	1.8205(19)	C32	C33	1.384(3)
P1	C21	1.834(2)	C33	C34	1.380(3)
P1	C31	1.831(2)	C34	C35	1.382(3)
P2	C51	1.840(2)	C35	C36	1.390(3)
P2	C61	1.841(2)	C41	C42	1.385(3)
P2	C71	1.842(2)	C41	C46	1.385(3)
O1	C11	1.222(3)	C42	C43	1.397(3)
O2	C11	1.367(2)	C43	C44	1.378(4)
O2	C12	1.466(2)	C44	C45	1.369(4)
N	H1N	0.92(3)	C45	C46	1.389(3)
N	C10	1.337(3)	C51	C52	1.388(3)
C1	C2	1.424(3)	C51	C56	1.400(3)
C1	C7A	1.445(3)	C52	C53	1.394(3)
C2	C3	1.431(3)	C53	C54	1.378(4)
C3	C3A	1.442(3)	C54	C55	1.389(4)
C3A	C4	1.420(3)	C55	C56	1.383(3)
C3A	C7A	1.436(3)	C61	C62	1.401(3)
C4	C5	1.366(3)	C61	C66	1.397(3)
C5	C6	1.412(4)	C62	C63	1.386(3)
C6	C7	1.371(3)	C63	C64	1.382(3)
C7	C7A	1.418(3)	C64	C65	1.382(3)
C8	C9	1.516(3)	C65	C66	1.390(3)
C9	C10	1.389(3)	C71	C72	1.393(3)
C9	C11	1.452(3)	C71	C76	1.398(3)
C10	C41	1.510(3)	C72	C73	1.392(3)
C12	C13	1.517(4)	C73	C74	1.380(4)
C12	C14	1.522(4)	C74	C75	1.382(4)
C12	C15	1.526(3)	C75	C76	1.393(3)

Table C.4. Selected Interatomic Angles (deg)

Atom1	Atom2	Atom3	Angle	Atom1	Atom2	Atom3	Angle
P1	Ru	P2	96.705(18)	C11	O2	C12	120.69(17)
P1	Ru	N	84.79(5)	Ru	N	C10	138.12(14)
P1	Ru	C1	105.21(6)	Ru	N	H1N	111.7(18)
P1	Ru	C2	90.75(5)	C10	N	H1N	109.5(18)
P1	Ru	C3	112.70(5)	Ru	C1	C2	69.85(11)
P1	Ru	C3A	148.58(5)	Ru	C1	C7A	76.68(12)
P1	Ru	C7A	141.71(5)	C2	C1	C7A	106.93(19)
P2	Ru	N	90.72(5)	Ru	C2	C1	72.48(11)
P2	Ru	C1	157.15(6)	Ru	C2	C3	72.51(11)
P2	Ru	C2	137.68(6)	C1	C2	C3	109.58(18)
P2	Ru	C3	102.44(6)	Ru	C3	C2	69.64(11)
P2	Ru	C3A	96.74(5)	Ru	C3	C3A	77.38(11)
P2	Ru	C7A	121.56(5)	C2	C3	C3A	107.00(19)
N	Ru	C1	97.52(8)	Ru	C3A	C3	66.25(10)
N	Ru	C2	131.51(8)	Ru	C3A	C4	129.84(14)
N	Ru	C3	156.25(7)	Ru	C3A	C7A	71.65(11)
N	Ru	C3A	123.25(7)	C3	C3A	C4	132.0(2)
N	Ru	C7A	95.27(7)	C3	C3A	C7A	107.97(18)
C1	Ru	C2	37.67(8)	C4	C3A	C7A	119.93(19)
C1	Ru	C3	63.29(8)	C3A	C4	C5	118.7(2)
C1	Ru	C3A	60.97(7)	C4	C5	C6	121.6(2)
C1	Ru	C7A	36.67(7)	C5	C6	C7	121.3(2)
C2	Ru	C3	37.85(8)	C6	C7	C7A	119.0(2)
C2	Ru	C3A	60.71(7)	Ru	C7A	C1	66.65(11)
C2	Ru	C7A	60.87(7)	Ru	C7A	C3A	72.98(11)
C3	Ru	C3A	36.37(7)	Ru	C7A	C7	127.40(15)
C3	Ru	C7A	61.01(7)	C1	C7A	C3A	108.24(18)
C3A	Ru	C7A	35.36(7)	C1	C7A	C7	132.4(2)
Ru	P1	C8	116.66(6)	C3A	C7A	C7	119.3(2)
Ru	P1	C21	110.34(6)	P1	C8	C9	118.05(14)
Ru	P1	C31	119.82(6)	C8	C9	C10	125.24(17)
C8	P1	C21	103.57(9)	C8	C9	C11	110.46(17)
C8	P1	C31	103.27(9)	C10	C9	C11	124.13(18)
C21	P1	C31	100.95(9)	N	C10	C9	126.57(18)
Ru	P2	C51	114.85(7)	N	C10	C41	112.33(17)
Ru	P2	C61	111.86(7)	C9	C10	C41	121.00(17)
Ru	P2	C71	121.59(7)	O1	C11	O2	122.10(19)
C51	P2	C61	101.47(9)	O1	C11	C9	124.29(19)
C51	P2	C71	100.40(9)	O2	C11	C9	113.47(18)
C61	P2	C71	104.18(9)	O2	C12	C13	110.53(19)

Atom1	Atom2	Atom3	Angle	Atom1	Atom2	Atom3	Angle
O2	C12	C14	110.1(2)	C44	C45	C46	120.4(3)
O2	C12	C15	102.28(19)	C41	C46	C45	120.5(2)
C13	C12	C14	112.7(2)	P2	C51	C52	119.67(16)
C13	C12	C15	109.9(2)	P2	C51	C56	121.54(16)
C14	C12	C15	110.8(2)	C52	C51	C56	118.66(19)
P1	C21	C22	118.42(15)	C51	C52	C53	120.7(2)
P1	C21	C26	122.91(16)	C52	C53	C54	120.0(2)
C22	C21	C26	118.7(2)	C53	C54	C55	120.0(2)
C21	C22	C23	120.4(2)	C54	C55	C56	120.1(2)
C22	C23	C24	120.2(2)	C51	C56	C55	120.5(2)
C23	C24	C25	119.9(2)	P2	C61	C62	118.97(16)
C24	C25	C26	120.3(2)	P2	C61	C66	123.04(16)
C21	C26	C25	120.6(2)	C62	C61	C66	117.77(19)
P1	C31	C32	118.29(15)	C61	C62	C63	121.0(2)
P1	C31	C36	123.24(15)	C62	C63	C64	120.6(2)
C32	C31	C36	118.16(18)	C63	C64	C65	119.1(2)
C31	C32	C33	121.17(19)	C64	C65	C66	120.8(2)
C32	C33	C34	120.1(2)	C61	C66	C65	120.7(2)
C33	C34	C35	119.5(2)	P2	C71	C72	122.30(16)
C34	C35	C36	120.7(2)	P2	C71	C76	118.79(16)
C31	C36	C35	120.4(2)	C72	C71	C76	118.58(19)
C10	C41	C42	120.1(2)	C71	C72	C73	120.7(2)
C10	C41	C46	120.64(19)	C72	C73	C74	120.2(2)
C42	C41	C46	119.1(2)	C73	C74	C75	119.8(2)
C41	C42	C43	119.9(2)	C74	C75	C76	120.4(2)
C42	C43	C44	120.4(2)	C71	C76	C75	120.3(2)
C43	C44	C45	119.7(2)				

Table C.5. Torsional Angles (deg)

Atom1	Atom2	Atom3	Atom4	Angle	Atom1	Atom2	Atom3	Atom4	Angle
P2	Ru	P1	C8	-58.65(8)	C7A	Ru	P2	C61	69.75(9)
P2	Ru	P1	C21	-176.43(7)	C7A	Ru	P2	C71	-166.43(10)
P2	Ru	P1	C31	67.08(7)	P1	Ru	N	C10	-21.2(2)
N	Ru	P1	C8	31.47(9)	P2	Ru	N	C10	75.5(2)
N	Ru	P1	C21	-86.32(8)	C1	Ru	N	C10	-125.9(2)
N	Ru	P1	C31	157.20(9)	C2	Ru	N	C10	-107.5(2)
C1	Ru	P1	C8	127.86(10)	C3	Ru	N	C10	-160.2(2)
C1	Ru	P1	C21	10.08(9)	C3A	Ru	N	C10	174.0(2)
C1	Ru	P1	C31	-106.41(9)	C7A	Ru	N	C10	-162.7(2)
C2	Ru	P1	C8	163.10(10)	P1	Ru	C1	C2	70.73(12)
C2	Ru	P1	C21	45.32(9)	P1	Ru	C1	C7A	-175.35(11)
C2	Ru	P1	C31	-71.17(9)	P2	Ru	C1	C2	-92.41(17)
C3	Ru	P1	C8	-165.16(10)	P2	Ru	C1	C7A	21.5(2)
C3	Ru	P1	C21	77.05(9)	N	Ru	C1	C2	157.35(12)
C3	Ru	P1	C31	-39.44(10)	N	Ru	C1	C7A	-88.72(13)
C3A	Ru	P1	C8	-173.43(12)	C2	Ru	C1	C7A	113.93(18)
C3A	Ru	P1	C21	68.79(12)	C3	Ru	C1	C2	-37.38(12)
C3A	Ru	P1	C31	-47.70(13)	C3	Ru	C1	C7A	76.55(13)
C7A	Ru	P1	C8	123.38(11)	C3A	Ru	C1	C2	-78.65(13)
C7A	Ru	P1	C21	5.60(11)	C3A	Ru	C1	C7A	35.28(12)
C7A	Ru	P1	C31	-110.89(11)	C7A	Ru	C1	C2	-113.93(18)
P1	Ru	P2	C51	136.27(7)	P1	Ru	C2	C1	-114.36(11)
P1	Ru	P2	C61	-108.77(7)	P1	Ru	C2	C3	127.74(11)
P1	Ru	P2	C71	15.05(8)	P2	Ru	C2	C1	144.82(10)
N	Ru	P2	C51	51.43(8)	P2	Ru	C2	C3	26.92(15)
N	Ru	P2	C61	166.39(8)	N	Ru	C2	C1	-30.66(16)
N	Ru	P2	C71	-69.80(9)	N	Ru	C2	C3	-148.55(12)
C1	Ru	P2	C51	-60.10(16)	C1	Ru	C2	C3	-117.90(17)
C1	Ru	P2	C61	54.86(17)	C3	Ru	C2	C1	117.90(17)
C1	Ru	P2	C71	178.67(16)	C3A	Ru	C2	C1	79.41(13)
C2	Ru	P2	C51	-125.18(10)	C3A	Ru	C2	C3	-38.49(11)
C2	Ru	P2	C61	-10.22(11)	C7A	Ru	C2	C1	38.68(12)
C2	Ru	P2	C71	113.59(11)	C7A	Ru	C2	C3	-79.22(13)
C3	Ru	P2	C51	-108.66(9)	P1	Ru	C3	C2	-58.99(12)
C3	Ru	P2	C61	6.30(9)	P1	Ru	C3	C3A	-172.74(10)
C3	Ru	P2	C71	130.12(10)	P2	Ru	C3	C2	-161.81(11)
C3A	Ru	P2	C51	-72.19(8)	P2	Ru	C3	C3A	84.44(12)
C3A	Ru	P2	C61	42.77(9)	N	Ru	C3	C2	76.0(2)
C3A	Ru	P2	C71	166.59(9)	N	Ru	C3	C3A	-37.8(2)
C7A	Ru	P2	C51	-45.20(9)	C1	Ru	C3	C2	37.20(12)

Atom1	Atom2	Atom3	Atom4	Angle
C1	Ru	C3	C3A	-76.54(13)
C2	Ru	C3	C3A	-113.75(18)
C3A	Ru	C3	C2	113.75(18)
C7A	Ru	C3	C2	78.81(13)
C7A	Ru	C3	C3A	-34.94(12)
P1	Ru	C3A	C3	12.92(18)
P1	Ru	C3A	C4	138.79(16)
P1	Ru	C3A	C7A	-107.14(13)
P2	Ru	C3A	C3	-101.85(12)
P2	Ru	C3A	C4	24.0(2)
P2	Ru	C3A	C7A	138.08(11)
N	Ru	C3A	C3	162.83(12)
N	Ru	C3A	C4	-71.3(2)
N	Ru	C3A	C7A	42.77(14)
C1	Ru	C3A	C3	83.49(14)
C1	Ru	C3A	C4	-150.6(2)
C1	Ru	C3A	C7A	-36.58(12)
C2	Ru	C3A	C3	40.09(13)
C2	Ru	C3A	C4	166.0(2)
C2	Ru	C3A	C7A	-79.98(13)
C3	Ru	C3A	C4	125.9(3)
C3	Ru	C3A	C7A	-120.07(18)
C7A	Ru	C3A	C3	120.07(18)
C7A	Ru	C3A	C4	-114.1(2)
P1	Ru	C7A	C1	7.26(17)
P1	Ru	C7A	C3A	126.50(11)
P1	Ru	C7A	C7	-119.22(19)
P2	Ru	C7A	C1	-170.38(10)
P2	Ru	C7A	C3A	-51.13(13)
P2	Ru	C7A	C7	63.1(2)
N	Ru	C7A	C1	95.52(13)
N	Ru	C7A	C3A	-145.23(12)
N	Ru	C7A	C7	-31.0(2)
C1	Ru	C7A	C3A	119.25(17)
C1	Ru	C7A	C7	-126.5(3)
C2	Ru	C7A	C1	-39.76(12)
C2	Ru	C7A	C3A	79.49(13)
C2	Ru	C7A	C7	-166.2(2)
C3	Ru	C7A	C1	-83.32(13)
C3	Ru	C7A	C3A	35.93(11)
C3	Ru	C7A	C7	150.2(2)
C3A	Ru	C7A	C1	-119.25(17)
C3A	Ru	C7A	C7	114.3(3)
Ru	P1	C8	C9	-34.13(18)
C21	P1	C8	C9	87.29(17)
C31	P1	C8	C9	-167.78(16)
Ru	P1	C21	C22	57.27(17)
Ru	P1	C21	C26	-121.44(16)
C8	P1	C21	C22	-68.30(17)
C8	P1	C21	C26	112.99(17)
C31	P1	C21	C22	-174.99(16)
C31	P1	C21	C26	6.30(18)
Ru	P1	C31	C32	34.99(19)
Ru	P1	C31	C36	-151.55(17)
C8	P1	C31	C32	166.79(17)
C8	P1	C31	C36	-19.7(2)
C21	P1	C31	C32	-86.28(18)
C21	P1	C31	C36	87.2(2)
Ru	P2	C51	C52	8.13(19)
Ru	P2	C51	C56	-176.19(15)
C61	P2	C51	C52	-112.71(17)
C61	P2	C51	C56	62.97(18)
C71	P2	C51	C52	140.35(17)
C71	P2	C51	C56	-43.97(19)
Ru	P2	C61	C62	60.76(18)
Ru	P2	C61	C66	-113.72(17)
C51	P2	C61	C62	-176.32(17)
C51	P2	C61	C66	9.2(2)
C71	P2	C61	C62	-72.35(18)
C71	P2	C61	C66	113.16(18)
Ru	P2	C71	C72	-88.17(19)
Ru	P2	C71	C76	85.20(17)
C51	P2	C71	C72	143.92(19)
C51	P2	C71	C76	-42.71(19)
C61	P2	C71	C72	39.1(2)
C61	P2	C71	C76	-147.48(17)
C12	O2	C11	O1	13.4(3)
C12	O2	C11	C9	-170.9(2)
C11	O2	C12	C13	-66.6(3)
C11	O2	C12	C14	58.6(3)

Atom1	Atom2	Atom3	Atom4	Angle
C11	O2	C12	C15	176.4(2)
Ru	N	C10	C9	1.1(4)
Ru	N	C10	C41	177.42(16)
Ru	C1	C2	C3	63.47(13)
C7A	C1	C2	Ru	-68.39(13)
C7A	C1	C2	C3	-4.9(2)
Ru	C1	C7A	C3A	-61.46(14)
Ru	C1	C7A	C7	120.1(2)
C2	C1	C7A	Ru	63.76(13)
C2	C1	C7A	C3A	2.3(2)
C2	C1	C7A	C7	-176.1(2)
Ru	C2	C3	C3A	69.07(13)
C1	C2	C3	Ru	-63.44(14)
C1	C2	C3	C3A	5.6(2)
Ru	C3	C3A	C4	-123.1(2)
Ru	C3	C3A	C7A	59.72(14)
C2	C3	C3A	Ru	-63.81(12)
C2	C3	C3A	C4	173.1(2)
C2	C3	C3A	C7A	-4.1(2)
Ru	C3A	C4	C5	91.2(2)
C3	C3A	C4	C5	-176.1(2)
C7A	C3A	C4	C5	0.8(3)
Ru	C3A	C7A	C1	57.51(13)
Ru	C3A	C7A	C7	-123.83(19)
C3	C3A	C7A	Ru	-56.39(13)
C3	C3A	C7A	C1	1.1(2)
C3	C3A	C7A	C7	179.79(18)
C4	C3A	C7A	Ru	126.01(18)
C4	C3A	C7A	C1	-176.48(17)
C4	C3A	C7A	C7	2.2(3)
C3A	C4	C5	C6	-2.5(3)
C4	C5	C6	C7	1.1(4)
C5	C6	C7	C7A	1.9(3)
C6	C7	C7A	Ru	-93.9(3)
C6	C7	C7A	C1	174.8(2)
C6	C7	C7A	C3A	-3.5(3)
P1	C8	C9	C10	9.5(3)
P1	C8	C9	C11	-175.01(15)
C8	C9	C10	N	9.8(4)
C8	C9	C10	C41	-166.1(2)
C11	C9	C10	N	-165.0(2)
C11	C9	C10	C41	19.0(3)
C8	C9	C11	O1	16.1(3)
C8	C9	C11	O2	-159.52(18)
C10	C9	C11	O1	-168.3(2)
C10	C9	C11	O2	16.0(3)
N	C10	C41	C42	59.7(3)
N	C10	C41	C46	-115.4(2)
C9	C10	C41	C42	-123.8(2)
C9	C10	C41	C46	61.1(3)
P1	C21	C22	C23	-179.12(16)
C26	C21	C22	C23	-0.4(3)
P1	C21	C26	C25	178.21(16)
C22	C21	C26	C25	-0.5(3)
C21	C22	C23	C24	1.1(3)
C22	C23	C24	C25	-1.0(3)
C23	C24	C25	C26	0.1(3)
C24	C25	C26	C21	0.6(3)
P1	C31	C32	C33	172.54(18)
C36	C31	C32	C33	-1.3(3)
P1	C31	C36	C35	-172.4(2)
C32	C31	C36	C35	1.1(4)
C31	C32	C33	C34	0.0(4)
C32	C33	C34	C35	1.5(4)
C33	C34	C35	C36	-1.6(4)
C34	C35	C36	C31	0.3(4)
C10	C41	C42	C43	-176.6(2)
C46	C41	C42	C43	-1.4(4)
C10	C41	C46	C45	176.3(2)
C42	C41	C46	C45	1.1(4)
C41	C42	C43	C44	0.6(5)
C42	C43	C44	C45	0.4(5)
C43	C44	C45	C46	-0.7(4)
C44	C45	C46	C41	-0.1(4)
P2	C51	C52	C53	175.81(17)
C56	C51	C52	C53	0.0(3)
P2	C51	C56	C55	-174.97(17)
C52	C51	C56	C55	0.8(3)
C51	C52	C53	C54	-0.8(4)
C52	C53	C54	C55	0.9(4)

Atom1	Atom2	Atom3	Atom4	Angle	Atom1	Atom2	Atom3	Atom4	Angle
C53	C54	C55	C56	-0.2(4)	C64	C65	C66	C61	1.5(4)
C54	C55	C56	C51	-0.7(3)	P2	C71	C72	C73	173.38(19)
P2	C61	C62	C63	-177.00(17)	C76	C71	C72	C73	0.0(3)
C66	C61	C62	C63	-2.2(3)	P2	C71	C76	C75	-174.37(17)
P2	C61	C66	C65	174.68(18)	C72	C71	C76	C75	-0.8(3)
C62	C61	C66	C65	0.1(3)	C71	C72	C73	C74	1.0(4)
C61	C62	C63	C64	2.7(4)	C72	C73	C74	C75	-1.3(4)
C62	C63	C64	C65	-1.0(4)	C73	C74	C75	C76	0.6(4)
C63	C64	C65	C66	-1.1(4)	C74	C75	C76	C71	0.5(4)

Table C.6. Least-Squares Planes

Plane	Coefficients[a]				Defining Atoms with Deviations (Å)[b]			
1	2.448(10)	11.554(5)	8.455(14)	1.330(3)				
					C1	0.0211(12)	C2	-0.0310(12)
					C3	0.0285(12)	C3A	-0.0153(12)
					C7A	-0.0033(12)		
					<u>Ru</u>	1.9079(9)		

Distance: Ru–C_{cent} = 1.918 Å (C_{cent} = C1–C2–C3–C3A–C7A centroid)

Angles: C_{cent}–Ru–P1 = 123.9º, C_{cent}–Ru–P2 = 126.1º, C_{cent}–Ru–N = 123.9º

2	2.395(12)	11.897(13)	7.48(4)	1.235(5)				
					C1	C2	C3	
					<u>Ru</u>	1.866(2)		
3	2.452(10)	11.414(8)	8.805(19)	1.395(4)				
					C1	-0.0037(7)	C3	0.0037(7)
					C3A	-0.0060(11)	C7A	0.0060(11)
					<u>Ru</u>	1.8872(12)		
4	2.697(9)	11.122(6)	9.479(12)	1.586(4)				
					C3A	0.0034(14)	C4	0.0132(14)
					C5	-0.0146(16)	C6	-0.0011(16)
					C7	0.0175(15)	C7A	-0.0183(14)
					<u>Ru</u>	1.814(2)		

Dihedral angle between planes 2 and 3: 5.3(2)º

Dihedral angle between planes 3 and 4: 3.21(14)º

[a]Coefficients are for the form $ax+by+cz = d$ where x, y and z are crystallographic coordinates.

[b]Underlined atoms were <u>not</u> included in the definition of the plane.

Table C.7. Anisotropic Displacement Parameters (U_{ij}, Å^2)

Atom	U_{11}	U_{22}	U_{33}	U_{23}	U_{13}	U_{12}
Ru	0.02132(9)	0.01762(8)	0.01948(7)	-0.00310(5)	0.00073(5)	-0.00396(5)
P1	0.0224(2)	0.0187(2)	0.0188(2)	-0.00230(16)	0.00146(17)	-0.00388(16)
P2	0.0235(3)	0.0203(2)	0.0203(2)	-0.00289(16)	0.00037(17)	-0.00555(17)
O1	0.0536(11)	0.0244(7)	0.0374(8)	-0.0034(6)	0.0141(7)	-0.0064(7)
O2	0.0481(10)	0.0257(7)	0.0303(8)	-0.0090(6)	0.0118(7)	-0.0068(7)
N	0.0267(9)	0.0229(8)	0.0282(8)	-0.0011(6)	0.0031(7)	-0.0064(7)
C1	0.0307(12)	0.0251(9)	0.0304(10)	-0.0067(8)	-0.0059(8)	-0.0092(8)
C2	0.0363(12)	0.0213(9)	0.0246(9)	-0.0067(7)	-0.0033(8)	-0.0057(8)
C3	0.0314(11)	0.0195(9)	0.0261(9)	-0.0070(7)	0.0028(8)	-0.0029(7)
C3A	0.0316(11)	0.0188(9)	0.0263(9)	-0.0058(7)	-0.0006(8)	-0.0063(7)
C4	0.0335(12)	0.0224(9)	0.0307(10)	-0.0046(8)	-0.0022(8)	-0.0034(8)
C5	0.0493(15)	0.0256(10)	0.0309(11)	0.0008(8)	-0.0053(9)	-0.0082(9)
C6	0.0513(15)	0.0355(12)	0.0323(11)	0.0025(9)	0.0012(10)	-0.0237(10)
C7	0.0364(13)	0.0363(11)	0.0358(11)	-0.0026(9)	0.0005(9)	-0.0196(9)
C7A	0.0319(12)	0.0240(9)	0.0293(10)	-0.0056(8)	-0.0014(8)	-0.0110(8)
C8	0.0275(11)	0.0205(9)	0.0219(9)	-0.0033(7)	0.0021(7)	-0.0042(7)
C9	0.0247(10)	0.0270(10)	0.0224(9)	-0.0043(7)	0.0027(7)	-0.0029(7)
C10	0.0220(10)	0.0268(9)	0.0220(9)	-0.0046(7)	0.0008(7)	-0.0025(7)
C11	0.0301(12)	0.0283(10)	0.0279(10)	-0.0051(8)	0.0061(8)	-0.0052(8)
C12	0.0431(14)	0.0298(11)	0.0385(12)	-0.0145(9)	0.0134(10)	-0.0068(9)
C13	0.0474(16)	0.0361(12)	0.0573(16)	-0.0221(11)	0.0104(12)	-0.0102(11)
C14	0.0410(15)	0.0386(13)	0.0590(16)	-0.0173(11)	0.0101(12)	-0.0032(10)
C15	0.070(2)	0.0515(16)	0.0375(13)	-0.0170(12)	0.0201(13)	-0.0131(14)
C21	0.0262(11)	0.0197(9)	0.0244(9)	-0.0029(7)	-0.0010(7)	-0.0030(7)
C22	0.0281(12)	0.0303(10)	0.0312(10)	0.0004(8)	0.0002(8)	-0.0076(8)
C23	0.0279(12)	0.0332(11)	0.0466(13)	-0.0004(9)	-0.0044(9)	-0.0083(9)
C24	0.0368(14)	0.0329(11)	0.0438(13)	-0.0051(9)	-0.0138(10)	-0.0078(9)
C25	0.0418(14)	0.0381(12)	0.0275(10)	-0.0058(9)	-0.0082(9)	-0.0052(10)
C26	0.0305(12)	0.0285(10)	0.0248(10)	-0.0035(7)	-0.0013(8)	-0.0036(8)
C31	0.0225(10)	0.0251(9)	0.0211(8)	-0.0022(7)	0.0003(7)	-0.0060(7)
C32	0.0295(11)	0.0234(9)	0.0300(10)	-0.0013(8)	0.0046(8)	-0.0053(8)
C33	0.0293(12)	0.0317(11)	0.0361(11)	-0.0052(9)	0.0103(9)	-0.0048(8)
C34	0.0316(13)	0.0379(12)	0.0395(12)	-0.0009(9)	0.0119(9)	-0.0110(9)
C35	0.0437(15)	0.0285(11)	0.0497(14)	0.0003(10)	0.0141(11)	-0.0121(10)
C36	0.0370(13)	0.0232(10)	0.0381(11)	-0.0044(8)	0.0099(9)	-0.0070(8)
C41	0.0287(11)	0.0262(9)	0.0264(9)	-0.0016(7)	0.0047(8)	-0.0061(8)
C42	0.0379(14)	0.0431(13)	0.0311(11)	0.0044(9)	0.0075(10)	0.0049(10)
C43	0.0583(18)	0.0538(16)	0.0316(12)	0.0082(11)	0.0156(12)	-0.0015(13)
C44	0.0432(16)	0.0523(15)	0.0484(14)	-0.0057(12)	0.0229(12)	-0.0135(12)
C45	0.0283(14)	0.0555(15)	0.0525(15)	-0.0074(12)	0.0060(11)	-0.0126(11)

Atom	U_{11}	U_{22}	U_{33}	U_{23}	U_{13}	U_{12}
C46	0.0299(13)	0.0426(12)	0.0354(11)	-0.0033(9)	0.0024(9)	-0.0087(9)
C51	0.0290(11)	0.0235(9)	0.0229(9)	-0.0036(7)	-0.0008(7)	-0.0044(7)
C52	0.0321(12)	0.0288(10)	0.0271(10)	-0.0017(8)	-0.0003(8)	-0.0064(8)
C53	0.0454(15)	0.0371(12)	0.0315(11)	0.0038(9)	0.0050(10)	-0.0089(10)
C54	0.0582(17)	0.0380(12)	0.0233(10)	0.0006(9)	-0.0006(10)	-0.0029(11)
C55	0.0488(15)	0.0362(12)	0.0286(11)	-0.0081(9)	-0.0091(10)	-0.0024(10)
C56	0.0372(13)	0.0303(10)	0.0295(10)	-0.0069(8)	-0.0035(9)	-0.0073(9)
C61	0.0234(11)	0.0244(9)	0.0277(9)	-0.0049(7)	-0.0006(7)	-0.0062(7)
C62	0.0306(12)	0.0296(10)	0.0285(10)	-0.0038(8)	0.0007(8)	-0.0049(8)
C63	0.0325(13)	0.0391(12)	0.0342(11)	-0.0112(9)	0.0066(9)	-0.0079(9)
C64	0.0255(12)	0.0360(11)	0.0457(13)	-0.0136(10)	0.0006(9)	-0.0034(9)
C65	0.0297(13)	0.0326(11)	0.0432(12)	-0.0026(9)	-0.0064(9)	-0.0021(9)
C66	0.0291(12)	0.0307(10)	0.0311(10)	-0.0016(8)	-0.0012(8)	-0.0050(8)
C71	0.0260(11)	0.0227(9)	0.0284(9)	-0.0021(7)	-0.0044(8)	-0.0071(7)
C72	0.0376(13)	0.0281(10)	0.0371(11)	-0.0037(8)	0.0030(9)	-0.0122(9)
C73	0.0451(15)	0.0317(12)	0.0495(14)	0.0011(10)	-0.0014(11)	-0.0185(10)
C74	0.0501(16)	0.0225(10)	0.0516(14)	-0.0023(9)	-0.0120(11)	-0.0111(9)
C75	0.0398(14)	0.0265(10)	0.0408(12)	-0.0087(9)	-0.0074(10)	-0.0011(9)
C76	0.0308(12)	0.0280(10)	0.0316(10)	-0.0041(8)	-0.0033(8)	-0.0054(8)

The form of the anisotropic displacement parameter is:
$\exp[-2\pi^2(h^2a^{*2}U_{11} + k^2b^{*2}U_{22} + l^2c^{*2}U_{33} + 2klb^*c^*U_{23} + 2hla^*c^*U_{13} + 2hka^*b^*U_{12})]$

Table C.8. Derived Atomic Coordinates and Displacement Parameters for Hydrogen Atoms

Atom	x	y	z	U_{eq}, Å^2
H1	-0.057629	0.040947	0.110677	0.033
H2	0.135270	0.064244	0.011084	0.033
H3	0.355906	-0.022457	0.079535	0.032
H4	0.409084	-0.152711	0.234179	0.035
H5	0.310798	-0.230247	0.344417	0.043
H6	0.081692	-0.188853	0.365129	0.045
H7	-0.054767	-0.072503	0.273659	0.041
H8A	0.115967	0.425886	0.164971	0.029
H8B	-0.012063	0.459107	0.113477	0.029
H13A	-0.161267	0.742343	0.404945	0.056
H13B	-0.036890	0.638889	0.410666	0.056
H13C	-0.083959	0.694576	0.323875	0.056
H14A	-0.374850	0.722863	0.360596	0.057
H14B	-0.307453	0.673755	0.277616	0.057
H14C	-0.386347	0.606789	0.338672	0.057

H15A	-0.281896	0.620690	0.495415	0.065
H15B	-0.289363	0.509202	0.462084	0.065
H15C	-0.152436	0.521934	0.489452	0.065
H22	-0.164988	0.261020	0.123828	0.036
H23	-0.337861	0.264840	0.042726	0.043
H24	-0.309825	0.284694	-0.098605	0.045
H25	-0.110706	0.306041	-0.158719	0.044
H26	0.061200	0.306771	-0.078454	0.034
H32	0.308835	0.154601	0.000235	0.034
H33	0.453330	0.189459	-0.105004	0.040
H34	0.455274	0.367704	-0.146233	0.044
H35	0.318230	0.510122	-0.077587	0.049
H36	0.172212	0.476293	0.027706	0.040
H42	-0.059599	0.226255	0.423320	0.050
H43	-0.230368	0.226098	0.522095	0.062
H44	-0.447946	0.305576	0.491138	0.059
H45	-0.496155	0.383598	0.361647	0.054
H46	-0.327414	0.385701	0.262947	0.044
H52	0.144589	0.045754	0.352036	0.036
H53	0.134229	-0.012884	0.489491	0.047
H54	0.274368	0.025681	0.577833	0.050
H55	0.421564	0.127333	0.529954	0.047
H56	0.429196	0.189323	0.393773	0.039
H62	0.469544	0.143927	0.104076	0.036
H63	0.678114	0.041844	0.063872	0.043
H64	0.800753	-0.091141	0.153420	0.043
H65	0.715367	-0.116793	0.285365	0.043
H66	0.512269	-0.008016	0.329236	0.037
H72	0.452307	0.298177	0.156695	0.041
H73	0.449596	0.481214	0.153280	0.049
H74	0.318073	0.592541	0.247708	0.049
H75	0.182292	0.522786	0.342534	0.044
H76	0.180188	0.340736	0.344982	0.036

Appendix D X-Ray Crystallographic structure report for [*trans*-$Mo(CO)_4(PTol_2^pH)(PTol_2^p)][B(C_6H_3Cl_2)_4]$ (12a)

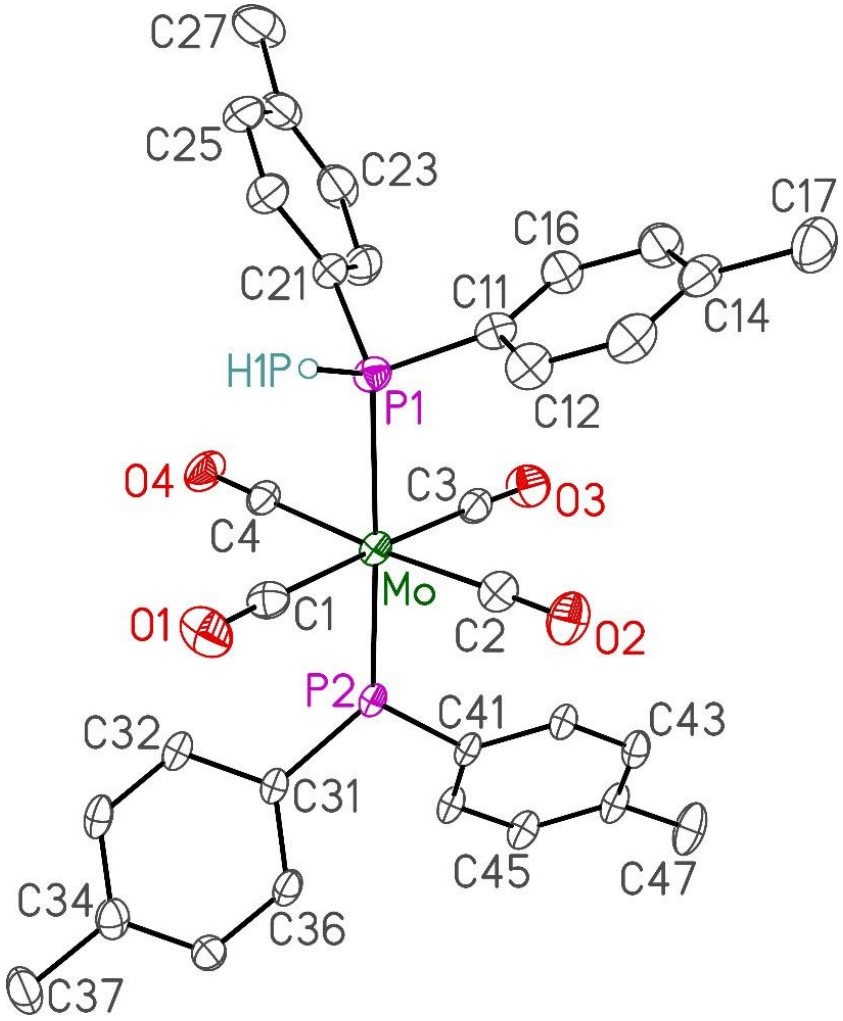

Figure D.1. Perspective view of the molecular structure of [*trans*-$Mo(CO)_4(PTol_2^pH)(PTol_2^p)][B(C_6H_3Cl_2)_4]$ (**12a**) showing the atom labeling scheme. Non-hydrogen atoms are represented by Gaussian ellipsoids at the 30% probability level. The hydrogen atom attached to P1 is shown with arbitrarily small thermal parameters; all other hydrogens are not shown.

Table D.1. Crystallographic Experimental Details

A. Crystal Data	
formula	$C_{57}H_{43}BCl_{10}MoO_4P_2$
formula weight	1315.10
crystal dimensions (mm)	0.30 × 0.13 × 0.04
crystal system	triclinic
space group	$P\bar{1}$ (No. 2)
unit cell parameters[a]	
a (Å)	9.2232(2)
b (Å)	14.2035(3)
c (Å)	23.4365(7)
α (deg)	89.3731(16)
β (deg)	80.2402(19)
γ (deg)	80.7490(15)
V (Å^3)	2986.01(13)
Z	2
ρ_{calcd} (g cm^{-3})	1.463
μ (mm^{-1})	6.776
B. Data Collection and Refinement Conditions	
diffractometer	Bruker D8/APEX II CCD[b]
radiation (λ [Å])	Cu Kα (1.54178) (microfocus source)
temperature (°C)	–100
scan type	ω and ϕ scans (1.0°) (5 s exposures)
data collection 2θ limit (deg)	147.76
total data collected	21096 (-11 ≤ h ≤ 11, -17 ≤ k ≤ 17, -25 ≤ l ≤ 27)
independent reflections	11620 (R_{int} = 0.0440)
number of observed reflections (*NO*)	9382 [$F_o^2 \geq 2\sigma(F_o^2)$]
structure solution method	Patterson/structure expansion (*DIRDIF–2008*[c])
refinement method	full-matrix least-squares on F^2 (*SHELXL–2014*[d])
absorption correction method	Gaussian integration (face-indexed)
range of transmission factors	0.8515–0.2353
data/restraints/parameters	11620 / 0 / 684
goodness-of-fit (S)[e] [all data]	1.102
final R indices[f]	
R_1 [$F_o^2 \geq 2\sigma(F_o^2)$]	0.0628
wR_2 [all data]	0.1702
largest difference peak and hole	1.119 and –1.249 e Å^{-3}

[a]Obtained from least-squares refinement of 9881 reflections with 7.44° < 2θ < 146.86°.

[b]Programs for diffractometer operation, data collection, data reduction and absorption correction were those supplied by Bruker.

[c]Beurskens, P. T.; Beurskens, G.; de Gelder, R.; Smits, J. M. M.; Garcia-Granda, S.; Gould, R. O. (2008). The *DIRDIF-2008* program system. Crystallography Laboratory, Radboud University Nijmegen, The Netherlands.

[d]Sheldrick, G. M. *Acta Crystallogr.* **2015**, *C71*, 3–8.

[e]$S = [\Sigma w(F_o^2 - F_c^2)^2/(n - p)]^{1/2}$ (n = number of data; p = number of parameters varied; $w = [\sigma^2(F_o^2) + (0.0628P)^2 + 9.2010P]^{-1}$ where $P = [\mathrm{Max}(F_o^2, 0) + 2F_c^2]/3$).

[f]$R_1 = \Sigma||F_o| - |F_c||/\Sigma|F_o|$; $wR_2 = [\Sigma w(F_o^2 - F_c^2)^2/\Sigma w(F_o^4)]^{1/2}$.

Table D.2. Atomic Coordinates and Equivalent Isotropic Displacement Parameters

(a) atoms of [trans–Mo(CO)$_4${PH(p-tolyl)$_2$}{P(p-tolyl)$_2$}]$^+$

Atom	*x*	*y*	*z*	U_{eq}, Å^2
Mo	0.11494(4)	0.17165(3)	0.29421(2)	0.03217(12)*
P1	-0.11646(15)	0.21754(9)	0.36895(6)	0.0366(3)*
P2	0.32219(13)	0.13463(7)	0.22453(5)	0.0290(2)*
O1	-0.0544(5)	0.2762(4)	0.1976(2)	0.0650(13)*
O2	0.0146(5)	-0.0276(3)	0.2708(2)	0.0593(12)*
O3	0.2996(5)	0.0639(3)	0.3843(2)	0.0593(12)*
O4	0.2091(5)	0.3696(3)	0.3263(2)	0.0560(11)*
C1	0.0034(6)	0.2394(4)	0.2324(3)	0.0422(12)*
C2	0.0471(6)	0.0431(4)	0.2796(3)	0.0418(12)*
C3	0.2321(6)	0.1028(4)	0.3531(2)	0.0404(12)*
C4	0.1749(6)	0.2998(4)	0.3148(2)	0.0383(11)*
C11	-0.1995(6)	0.1177(4)	0.4018(2)	0.0386(11)*
C12	-0.2872(7)	0.0718(4)	0.3711(3)	0.0495(14)*
C13	-0.3412(7)	-0.0077(4)	0.3940(3)	0.0540(16)*
C14	-0.3129(7)	-0.0452(4)	0.4467(3)	0.0489(14)*
C15	-0.2243(8)	0.0010(5)	0.4760(3)	0.0537(15)*
C16	-0.1693(7)	0.0812(4)	0.4540(3)	0.0463(13)*
C17	-0.3718(9)	-0.1319(5)	0.4710(4)	0.070(2)*
C21	-0.1081(7)	0.2948(4)	0.4291(2)	0.0419(12)*
C22	0.0104(8)	0.2804(4)	0.4581(3)	0.0527(15)*
C23	0.0100(10)	0.3350(5)	0.5071(3)	0.0643(19)*
C24	-0.1091(11)	0.4048(5)	0.5276(3)	0.071(2)*
C25	-0.2250(10)	0.4212(5)	0.4971(3)	0.071(2)*
C26	-0.2275(8)	0.3670(4)	0.4485(3)	0.0580(16)*
C27	-0.1134(14)	0.4618(6)	0.5820(4)	0.107(4)*
C31	0.3633(5)	0.1977(3)	0.1595(2)	0.0305(10)*
C32	0.2960(5)	0.2944(3)	0.1576(2)	0.0338(10)*
C33	0.3106(6)	0.3433(3)	0.1067(3)	0.0402(12)*

C34	0.3900(7)	0.2997(4)	0.0558(3)	0.0425(12)*
C35	0.4581(7)	0.2046(4)	0.0574(2)	0.0432(12)*
C36	0.4448(6)	0.1545(3)	0.1082(2)	0.0366(11)*
C37	0.4005(9)	0.3540(5)	0.0004(3)	0.0606(18)*
C41	0.4688(5)	0.0361(3)	0.2256(2)	0.0312(10)*
C42	0.4339(6)	-0.0454(3)	0.2559(2)	0.0337(10)*
C43	0.5442(6)	-0.1210(3)	0.2632(2)	0.0377(11)*
C44	0.6930(6)	-0.1172(3)	0.2405(3)	0.0402(12)*
C45	0.7278(6)	-0.0367(3)	0.2098(3)	0.0409(12)*
C46	0.6183(6)	0.0389(3)	0.2025(2)	0.0361(11)*
C47	0.8126(8)	-0.1995(4)	0.2493(4)	0.063(2)*
H1P	-0.225(8)	0.265(5)	0.346(3)	0.07(2)

(b) tetrakis(3,5-dichlorophenyl)borate ion atoms

Atom	*x*	*y*	*z*	U_{eq}, Å^2
Cl1	0.72755(16)	0.39540(9)	0.05259(7)	0.0481(3)*
Cl2	0.57337(16)	0.27072(8)	0.26852(6)	0.0437(3)*
Cl3	-0.13651(16)	0.47920(11)	0.29309(8)	0.0565(4)*
Cl4	-0.0051(2)	0.56232(13)	0.06731(8)	0.0629(4)*
Cl5	0.08026(18)	0.85465(10)	0.39103(7)	0.0532(4)*
Cl6	0.59799(19)	0.62785(11)	0.40718(7)	0.0610(4)*
Cl7	0.7829(3)	0.80287(13)	0.09500(10)	0.0846(7)*
Cl8	0.2052(3)	0.96099(11)	0.11532(11)	0.0913(7)*
C51	0.4733(5)	0.5254(3)	0.1952(2)	0.0297(10)*
C52	0.5483(6)	0.5046(3)	0.1388(2)	0.0331(10)*
C53	0.6327(5)	0.4158(3)	0.1232(2)	0.0338(10)*
C54	0.6438(5)	0.3422(3)	0.1621(2)	0.0344(11)*
C55	0.5663(5)	0.3620(3)	0.2176(2)	0.0331(11)*
C56	0.4818(5)	0.4502(3)	0.2351(2)	0.0305(10)*
C61	0.1968(5)	0.5995(3)	0.2025(2)	0.0311(10)*
C62	0.1017(5)	0.5623(3)	0.2474(2)	0.0336(10)*
C63	-0.0229(6)	0.5268(3)	0.2361(3)	0.0395(12)*
C64	-0.0602(6)	0.5268(4)	0.1813(3)	0.0450(14)*
C65	0.0323(6)	0.5650(4)	0.1378(3)	0.0405(12)*
C66	0.1583(6)	0.5999(3)	0.1476(2)	0.0357(11)*
C71	0.3527(5)	0.6622(3)	0.2795(2)	0.0296(9)*
C72	0.2333(6)	0.7314(3)	0.3057(2)	0.0335(10)*
C73	0.2306(6)	0.7679(3)	0.3605(2)	0.0370(11)*
C74	0.3422(6)	0.7384(3)	0.3928(2)	0.0395(12)*
C75	0.4572(6)	0.6706(3)	0.3674(3)	0.0401(12)*

C76	0.4652(6)	0.6337(3)	0.3119(2)	0.0343(11)*
C81	0.4060(6)	0.7146(3)	0.1726(2)	0.0327(10)*
C82	0.5554(7)	0.7222(3)	0.1531(3)	0.0420(12)*
C83	0.5946(8)	0.7991(4)	0.1208(3)	0.0534(16)*
C84	0.4905(10)	0.8725(4)	0.1070(3)	0.062(2)*
C85	0.3423(10)	0.8669(4)	0.1280(3)	0.0587(19)*
C86	0.2995(7)	0.7897(3)	0.1598(3)	0.0437(13)*
B	0.3575(6)	0.6262(3)	0.2128(2)	0.0285(10)*

(c) solvent dichloromethane atoms

Atom	*x*	*y*	*z*	U_{eq}, Å^2
Cl1S	0.8399(4)	0.0581(3)	0.0590(2)	0.177(2)*
Cl2S	1.0413(5)	0.1900(3)	0.0624(2)	0.1671(17)*
C1S	0.9211(13)	0.1465(7)	0.0227(5)	0.108(4)*

Anisotropically-refined atoms are marked with an asterisk (*). The form of the anisotropic displacement parameter is: $\exp[-2\pi^2(h^2a^{*2}U_{11} + k^2b^{*2}U_{22} + l^2c^{*2}U_{33} + 2klb^*c^*U_{23} + 2hla^*c^*U_{13} + 2hka^*b^*U_{12})]$.

Table D.3. Selected Interatomic Distances (Å)

(a) within [trans–Mo(CO)$_4${PH(p-tolyl)$_2$}{P(p-tolyl)$_2$}]$^+$

Atom1	Atom2	Distance	Atom1	Atom2	Distance
Mo	P1	2.5216(14)	C21	C22	1.368(9)
Mo	P2	2.2878(13)	C21	C26	1.396(8)
Mo	C1	2.059(6)	C22	C23	1.393(8)
Mo	C2	2.073(6)	C23	C24	1.379(12)
Mo	C3	2.041(6)	C24	C25	1.372(13)
Mo	C4	2.070(5)	C24	C27	1.510(9)
P1	C11	1.821(6)	C25	C26	1.387(10)
P1	C21	1.816(6)	C31	C32	1.418(6)
P1	H1P	1.30(7)	C31	C36	1.396(7)
P2	C31	1.775(5)	C32	C33	1.372(8)
P2	C41	1.786(4)	C33	C34	1.385(8)
O1	C1	1.127(7)	C34	C35	1.399(7)
O2	C2	1.124(7)	C34	C37	1.499(8)
O3	C3	1.124(7)	C35	C36	1.378(8)
O4	C4	1.136(6)	C41	C42	1.404(7)
C11	C12	1.404(7)	C41	C46	1.400(7)
C11	C16	1.377(8)	C42	C43	1.387(7)
C12	C13	1.373(9)	C43	C44	1.394(8)
C13	C14	1.389(9)	C44	C45	1.397(8)
C14	C15	1.395(8)	C44	C47	1.510(7)
C14	C17	1.494(9)	C45	C46	1.381(7)
C15	C16	1.380(9)			

(b) within the tetrakis(3,5-dichlorophenyl)borate ion

Atom1	Atom2	Distance	Atom1	Atom2	Distance
Cl1	C53	1.740(6)	C55	C56	1.390(6)
Cl2	C55	1.753(5)	C61	C62	1.407(7)
Cl3	C63	1.753(6)	C61	C66	1.391(7)
Cl4	C65	1.745(6)	C61	B	1.644(7)
Cl5	C73	1.757(5)	C62	C63	1.392(7)
Cl6	C75	1.751(5)	C63	C64	1.383(8)
Cl7	C83	1.749(7)	C64	C65	1.381(9)
Cl8	C85	1.746(7)	C65	C66	1.388(7)
C51	C52	1.394(7)	C71	C72	1.411(6)
C51	C56	1.413(6)	C71	C76	1.394(7)
C51	B	1.652(6)	C71	B	1.642(7)
C52	C53	1.389(6)	C72	C73	1.385(7)
C53	C54	1.382(7)	C73	C74	1.387(7)
C54	C55	1.382(8)	C74	C75	1.370(7)

Atom1	Atom2	Distance	Atom1	Atom2	Distance
C75	C76	1.393(7)	C82	C83	1.384(8)
C81	C82	1.398(8)	C83	C84	1.374(10)
C81	C86	1.396(7)	C84	C85	1.387(11)
C81	B	1.635(7)	C85	C86	1.391(8)

(c) within the solvent dichloromethane molecule

Atom1	Atom2	Distance	Atom1	Atom2	Distance
Cl1S	C1S	1.709(12)	Cl2S	C1S	1.750(13)

Table D.4. Selected Interatomic Angles (deg)

(a) within [trans–Mo(CO)$_4${PH(p-tolyl)$_2$}{P(p-tolyl)$_2$}]$^+$

Atom1	Atom2	Atom3	Angle	Atom1	Atom2	Atom3	Angle
P1	Mo	P2	177.96(5)	C13	C14	C17	122.2(6)
P1	Mo	C1	89.18(16)	C15	C14	C17	120.9(7)
P1	Mo	C2	89.92(17)	C14	C15	C16	121.4(6)
P1	Mo	C3	92.95(16)	C11	C16	C15	120.8(5)
P1	Mo	C4	86.57(15)	P1	C21	C22	121.1(4)
P2	Mo	C1	89.00(16)	P1	C21	C26	119.9(5)
P2	Mo	C2	91.07(17)	C22	C21	C26	118.9(6)
P2	Mo	C3	88.87(16)	C21	C22	C23	120.6(7)
P2	Mo	C4	92.50(15)	C22	C23	C24	121.0(8)
C1	Mo	C2	92.4(2)	C23	C24	C25	118.1(6)
C1	Mo	C3	177.9(2)	C23	C24	C27	121.5(9)
C1	Mo	C4	89.7(2)	C25	C24	C27	120.4(9)
C2	Mo	C3	87.5(2)	C24	C25	C26	121.7(7)
C2	Mo	C4	175.9(2)	C21	C26	C25	119.6(7)
C3	Mo	C4	90.6(2)	P2	C31	C32	118.2(4)
Mo	P1	C11	114.95(17)	P2	C31	C36	123.5(3)
Mo	P1	C21	118.7(2)	C32	C31	C36	117.9(5)
Mo	P1	H1P	112(3)	C31	C32	C33	120.6(5)
C11	P1	C21	105.2(3)	C32	C33	C34	121.2(5)
C11	P1	H1P	102(3)	C33	C34	C35	118.6(5)
C21	P1	H1P	102(3)	C33	C34	C37	120.1(5)
Mo	P2	C31	125.87(16)	C35	C34	C37	121.3(6)
Mo	P2	C41	125.86(18)	C34	C35	C36	121.0(5)
C31	P2	C41	108.3(2)	C31	C36	C35	120.8(4)
Mo	C1	O1	178.3(5)	P2	C41	C42	117.9(4)
Mo	C2	O2	177.9(6)	P2	C41	C46	123.6(4)
Mo	C3	O3	178.1(5)	C42	C41	C46	118.2(4)
Mo	C4	O4	179.2(5)	C41	C42	C43	121.1(5)
P1	C11	C12	119.2(5)	C42	C43	C44	120.3(5)
P1	C11	C16	121.7(4)	C43	C44	C45	118.7(5)
C12	C11	C16	118.9(6)	C43	C44	C47	119.9(5)
C11	C12	C13	119.3(6)	C45	C44	C47	121.4(5)
C12	C13	C14	122.7(5)	C44	C45	C46	121.2(5)
C13	C14	C15	116.9(6)	C41	C46	C45	120.5(5)

(b) within the tetrakis(3,5-dichlorophenyl)borate ion

Atom1	Atom2	Atom3	Angle	Atom1	Atom2	Atom3	Angle
C52	C51	C56	116.6(4)	C56	C51	B	120.3(4)
C52	C51	B	122.3(4)	C51	C52	C53	121.8(5)

Atom1	Atom2	Atom3	Angle	Atom1	Atom2	Atom3	Angle
Cl1	C53	C52	119.5(4)	Cl5	C73	C74	118.1(4)
Cl1	C53	C54	118.5(4)	C72	C73	C74	122.6(5)
C52	C53	C54	122.0(5)	C73	C74	C75	116.3(5)
C53	C54	C55	116.2(4)	Cl6	C75	C74	118.2(4)
Cl2	C55	C54	118.3(3)	Cl6	C75	C76	119.1(4)
Cl2	C55	C56	118.3(4)	C74	C75	C76	122.7(5)
C54	C55	C56	123.4(5)	C71	C76	C75	121.3(5)
C51	C56	C55	119.9(5)	C82	C81	C86	116.8(5)
C62	C61	C66	116.7(4)	C82	C81	B	121.9(4)
C62	C61	B	121.1(4)	C86	C81	B	121.1(5)
C66	C61	B	121.6(5)	C81	C82	C83	121.1(6)
C61	C62	C63	120.6(5)	Cl7	C83	C82	119.3(5)
Cl3	C63	C62	119.0(5)	Cl7	C83	C84	118.3(5)
Cl3	C63	C64	118.5(4)	C82	C83	C84	122.4(6)
C62	C63	C64	122.5(6)	C83	C84	C85	116.7(6)
C63	C64	C65	116.5(5)	Cl8	C85	C84	118.9(5)
Cl4	C65	C64	118.4(4)	Cl8	C85	C86	118.9(6)
Cl4	C65	C66	119.2(5)	C84	C85	C86	122.2(6)
C64	C65	C66	122.2(5)	C81	C86	C85	120.7(6)
C61	C66	C65	121.5(5)	C51	B	C61	102.8(3)
C72	C71	C76	116.1(4)	C51	B	C71	113.2(4)
C72	C71	B	119.4(4)	C51	B	C81	112.0(4)
C76	C71	B	124.3(4)	C61	B	C71	112.3(4)
C71	C72	C73	120.9(5)	C61	B	C81	112.3(4)
Cl5	C73	C72	119.2(4)	C71	B	C81	104.7(3)

(c) within the solvent dichloromethane molecule

Atom1	Atom2	Atom3	Angle
Cl1S	C1S	Cl2S	111.1(7)

Table D.5. Torsional Angles (deg)

Atom1	Atom2	Atom3	Atom4	Angle
Mo	P1	C11	C12	-78.8(5)
Mo	P1	C11	C16	96.1(5)
C21	P1	C11	C12	148.8(5)
C21	P1	C11	C16	-36.3(5)
Mo	P1	C21	C22	-44.0(6)
Mo	P1	C21	C26	139.5(5)
C11	P1	C21	C22	86.4(6)
C11	P1	C21	C26	-90.1(5)
Mo	P2	C31	C32	23.2(4)
Mo	P2	C31	C36	-149.4(3)
C41	P2	C31	C32	-157.8(4)
C41	P2	C31	C36	29.5(5)
Mo	P2	C41	C42	27.6(5)
Mo	P2	C41	C46	-146.4(4)
C31	P2	C41	C42	-151.4(4)
C31	P2	C41	C46	34.6(5)
P1	C11	C12	C13	175.4(5)
C16	C11	C12	C13	0.4(9)
P1	C11	C16	C15	-175.1(5)
C12	C11	C16	C15	-0.2(9)
C11	C12	C13	C14	0.0(10)
C12	C13	C14	C15	-0.6(9)
C12	C13	C14	C17	-179.8(6)
C13	C14	C15	C16	0.9(9)
C17	C14	C15	C16	-180.0(6)
C14	C15	C16	C11	-0.5(10)
P1	C21	C22	C23	-174.6(5)
C26	C21	C22	C23	1.9(10)
P1	C21	C26	C25	175.3(5)
C22	C21	C26	C25	-1.3(10)
C21	C22	C23	C24	-0.2(10)
C22	C23	C24	C25	-2.1(11)
C22	C23	C24	C27	177.6(7)
C23	C24	C25	C26	2.8(11)
C27	C24	C25	C26	-177.0(7)
C24	C25	C26	C21	-1.1(11)
P2	C31	C32	C33	-172.8(4)
C36	C31	C32	C33	0.3(7)
P2	C31	C36	C35	172.2(4)
C32	C31	C36	C35	-0.4(7)
C31	C32	C33	C34	0.6(8)
C32	C33	C34	C35	-1.2(8)
C32	C33	C34	C37	178.2(5)
C33	C34	C35	C36	1.1(8)
C37	C34	C35	C36	-178.4(6)
C34	C35	C36	C31	-0.3(8)
P2	C41	C42	C43	-173.9(4)
C46	C41	C42	C43	0.5(7)
P2	C41	C46	C45	173.8(4)
C42	C41	C46	C45	-0.3(7)
C41	C42	C43	C44	0.1(8)
C42	C43	C44	C45	-0.9(8)
C42	C43	C44	C47	179.3(5)
C43	C44	C45	C46	1.1(8)
C47	C44	C45	C46	-179.1(5)
C44	C45	C46	C41	-0.5(8)
C56	C51	C52	C53	-2.8(7)
B	C51	C52	C53	-173.0(4)
C52	C51	C56	C55	2.2(6)
B	C51	C56	C55	172.5(4)
C52	C51	B	C61	89.6(5)
C52	C51	B	C71	-149.2(4)
C52	C51	B	C81	-31.1(6)
C56	C51	B	C61	-80.2(5)
C56	C51	B	C71	41.1(6)
C56	C51	B	C81	159.1(4)
C51	C52	C53	Cl1	-178.3(4)
C51	C52	C53	C54	1.9(7)
Cl1	C53	C54	C55	-180.0(3)
C52	C53	C54	C55	-0.2(7)
C53	C54	C55	Cl2	178.8(3)
C53	C54	C55	C56	-0.5(7)
Cl2	C55	C56	C51	-179.9(3)
C54	C55	C56	C51	-0.5(7)
C66	C61	C62	C63	0.8(6)
B	C61	C62	C63	-170.4(4)
C62	C61	C66	C65	-0.1(6)
B	C61	C66	C65	171.1(4)
C62	C61	B	C51	90.0(5)
C62	C61	B	C71	-31.9(5)

Atom1	Atom2	Atom3	Atom4	Angle
C62	C61	B	C81	-149.5(4)
C66	C61	B	C51	-80.8(5)
C66	C61	B	C71	157.3(4)
C66	C61	B	C81	39.7(5)
C61	C62	C63	Cl3	178.9(3)
C61	C62	C63	C64	-0.5(7)
Cl3	C63	C64	C65	180.0(4)
C62	C63	C64	C65	-0.6(7)
C63	C64	C65	Cl4	177.3(4)
C63	C64	C65	C66	1.4(7)
Cl4	C65	C66	C61	-177.0(3)
C64	C65	C66	C61	-1.1(7)
C76	C71	C72	C73	0.0(7)
B	C71	C72	C73	-175.8(5)
C72	C71	C76	C75	1.4(7)
B	C71	C76	C75	176.9(5)
C72	C71	B	C51	-163.3(4)
C72	C71	B	C61	-47.6(5)
C72	C71	B	C81	74.5(5)
C76	C71	B	C51	21.3(6)
C76	C71	B	C61	137.0(4)
C76	C71	B	C81	-100.9(5)
C71	C72	C73	Cl5	179.5(4)
C71	C72	C73	C74	-0.8(8)

Atom1	Atom2	Atom3	Atom4	Angle
Cl5	C73	C74	C75	179.9(4)
C72	C73	C74	C75	0.2(8)
C73	C74	C75	Cl6	-177.9(4)
C73	C74	C75	C76	1.2(8)
Cl6	C75	C76	C71	177.1(4)
C74	C75	C76	C71	-2.1(8)
C86	C81	C82	C83	-2.5(8)
B	C81	C82	C83	-177.9(5)
C82	C81	C86	C85	1.4(8)
B	C81	C86	C85	176.8(5)
C82	C81	B	C51	-35.0(6)
C82	C81	B	C61	-150.0(4)
C82	C81	B	C71	88.0(5)
C86	C81	B	C51	149.8(4)
C86	C81	B	C61	34.8(6)
C86	C81	B	C71	-87.2(5)
C81	C82	C83	Cl7	-177.5(4)
C81	C82	C83	C84	1.4(9)
Cl7	C83	C84	C85	179.8(5)
C82	C83	C84	C85	0.9(9)
C83	C84	C85	Cl8	176.7(5)
C83	C84	C85	C86	-2.0(9)
Cl8	C85	C86	C81	-177.8(4)
C84	C85	C86	C81	0.9(9)

Table D.6. Anisotropic Displacement Parameters (U_{ij}, Å^2)

Atom	U_{11}	U_{22}	U_{33}	U_{23}	U_{13}	U_{12}
Mo	0.0319(2)	0.02778(19)	0.0371(2)	-0.00330(14)	-0.00883(15)	-0.00214(14)
P1	0.0344(6)	0.0386(6)	0.0360(7)	-0.0025(5)	-0.0087(5)	0.0001(5)
P2	0.0310(6)	0.0207(5)	0.0357(7)	-0.0021(4)	-0.0088(5)	-0.0022(4)
O1	0.042(2)	0.094(4)	0.058(3)	0.019(3)	-0.020(2)	0.004(2)
O2	0.064(3)	0.046(2)	0.077(3)	-0.006(2)	-0.024(2)	-0.023(2)
O3	0.061(3)	0.067(3)	0.049(3)	0.006(2)	-0.023(2)	0.008(2)
O4	0.060(3)	0.038(2)	0.069(3)	-0.0156(19)	0.000(2)	-0.0140(18)
C1	0.031(3)	0.050(3)	0.043(3)	-0.004(2)	-0.006(2)	-0.001(2)
C2	0.038(3)	0.044(3)	0.046(3)	-0.002(2)	-0.016(2)	-0.004(2)
C3	0.047(3)	0.032(2)	0.041(3)	-0.003(2)	-0.007(2)	-0.004(2)
C4	0.036(3)	0.032(2)	0.044(3)	-0.003(2)	-0.004(2)	0.000(2)
C11	0.032(2)	0.044(3)	0.040(3)	-0.006(2)	-0.008(2)	-0.004(2)
C12	0.044(3)	0.056(3)	0.054(4)	-0.004(3)	-0.019(3)	-0.011(3)
C13	0.045(3)	0.055(3)	0.068(4)	-0.014(3)	-0.020(3)	-0.011(3)
C14	0.041(3)	0.043(3)	0.061(4)	-0.011(3)	-0.003(3)	-0.005(2)
C15	0.060(4)	0.055(3)	0.050(4)	-0.001(3)	-0.013(3)	-0.015(3)
C16	0.050(3)	0.049(3)	0.045(3)	-0.001(2)	-0.016(3)	-0.016(3)
C17	0.070(5)	0.050(4)	0.092(6)	-0.006(4)	-0.010(4)	-0.019(3)
C21	0.050(3)	0.034(2)	0.039(3)	-0.003(2)	-0.001(2)	-0.005(2)
C22	0.071(4)	0.041(3)	0.048(4)	-0.008(2)	-0.015(3)	-0.008(3)
C23	0.105(6)	0.053(4)	0.043(4)	-0.001(3)	-0.014(4)	-0.034(4)
C24	0.127(7)	0.045(3)	0.040(4)	-0.009(3)	0.013(4)	-0.038(4)
C25	0.097(6)	0.040(3)	0.061(5)	-0.013(3)	0.024(4)	-0.008(3)
C26	0.060(4)	0.045(3)	0.062(4)	-0.004(3)	0.006(3)	-0.001(3)
C27	0.194(12)	0.071(5)	0.055(5)	-0.026(4)	0.029(6)	-0.072(7)
C31	0.031(2)	0.021(2)	0.041(3)	-0.0001(17)	-0.011(2)	-0.0030(17)
C32	0.030(2)	0.022(2)	0.050(3)	-0.0029(19)	-0.013(2)	-0.0014(17)
C33	0.046(3)	0.022(2)	0.058(3)	0.002(2)	-0.022(3)	-0.0069(19)
C34	0.052(3)	0.034(2)	0.048(3)	0.003(2)	-0.020(3)	-0.015(2)
C35	0.059(3)	0.035(3)	0.038(3)	-0.002(2)	-0.010(2)	-0.012(2)
C36	0.045(3)	0.022(2)	0.044(3)	-0.0035(19)	-0.011(2)	-0.0041(19)
C37	0.092(5)	0.048(3)	0.051(4)	0.017(3)	-0.028(4)	-0.022(3)
C41	0.036(2)	0.0179(19)	0.040(3)	-0.0037(17)	-0.010(2)	-0.0001(17)
C42	0.036(3)	0.022(2)	0.043(3)	-0.0012(18)	-0.008(2)	-0.0042(18)
C43	0.046(3)	0.024(2)	0.047(3)	0.0002(19)	-0.017(2)	-0.008(2)
C44	0.042(3)	0.023(2)	0.059(4)	-0.003(2)	-0.022(3)	-0.003(2)
C45	0.036(3)	0.029(2)	0.059(4)	-0.005(2)	-0.012(2)	-0.004(2)
C46	0.037(3)	0.020(2)	0.051(3)	-0.0028(19)	-0.012(2)	-0.0020(18)
C47	0.053(4)	0.033(3)	0.106(6)	0.001(3)	-0.035(4)	0.004(3)
Cl1	0.0513(8)	0.0355(6)	0.0522(8)	-0.0095(5)	0.0013(6)	-0.0013(5)

Atom	U_{11}	U_{22}	U_{33}	U_{23}	U_{13}	U_{12}
Cl2	0.0533(7)	0.0239(5)	0.0590(8)	0.0068(5)	-0.0254(6)	-0.0047(5)
Cl3	0.0356(7)	0.0589(8)	0.0750(11)	-0.0014(7)	-0.0032(7)	-0.0138(6)
Cl4	0.0616(9)	0.0741(10)	0.0598(10)	-0.0157(8)	-0.0320(8)	-0.0075(8)
Cl5	0.0589(9)	0.0405(7)	0.0518(9)	-0.0118(6)	-0.0047(6)	0.0125(6)
Cl6	0.0670(10)	0.0568(8)	0.0621(10)	-0.0160(7)	-0.0378(8)	0.0112(7)
Cl7	0.0909(14)	0.0514(9)	0.1013(16)	-0.0210(9)	0.0380(12)	-0.0366(9)
Cl8	0.132(2)	0.0336(7)	0.1125(17)	0.0237(9)	-0.0495(15)	0.0018(9)
C51	0.031(2)	0.0209(19)	0.041(3)	-0.0018(17)	-0.015(2)	-0.0068(17)
C52	0.039(3)	0.0192(19)	0.044(3)	-0.0018(18)	-0.016(2)	-0.0063(18)
C53	0.029(2)	0.027(2)	0.047(3)	-0.0072(19)	-0.011(2)	-0.0037(18)
C54	0.032(2)	0.021(2)	0.052(3)	-0.0069(19)	-0.015(2)	-0.0016(17)
C55	0.032(2)	0.0205(19)	0.052(3)	0.0000(19)	-0.021(2)	-0.0054(17)
C56	0.030(2)	0.0216(19)	0.043(3)	-0.0011(18)	-0.012(2)	-0.0061(17)
C61	0.030(2)	0.0164(18)	0.046(3)	-0.0054(17)	-0.012(2)	0.0042(16)
C62	0.028(2)	0.025(2)	0.048(3)	-0.0046(19)	-0.012(2)	-0.0006(17)
C63	0.030(2)	0.029(2)	0.059(4)	-0.005(2)	-0.009(2)	-0.0023(19)
C64	0.033(3)	0.033(2)	0.072(4)	-0.015(2)	-0.024(3)	0.001(2)
C65	0.038(3)	0.034(2)	0.051(3)	-0.012(2)	-0.021(2)	0.005(2)
C66	0.037(3)	0.025(2)	0.044(3)	-0.0068(19)	-0.011(2)	0.0013(18)
C71	0.033(2)	0.0185(18)	0.039(3)	0.0006(17)	-0.009(2)	-0.0077(17)
C72	0.037(3)	0.022(2)	0.041(3)	-0.0011(18)	-0.010(2)	-0.0016(18)
C73	0.041(3)	0.022(2)	0.046(3)	-0.0050(19)	-0.005(2)	-0.0013(19)
C74	0.055(3)	0.031(2)	0.035(3)	-0.0044(19)	-0.012(2)	-0.008(2)
C75	0.046(3)	0.030(2)	0.048(3)	-0.004(2)	-0.019(2)	-0.005(2)
C76	0.035(2)	0.024(2)	0.046(3)	-0.0048(19)	-0.012(2)	-0.0054(18)
C81	0.046(3)	0.0177(19)	0.036(3)	-0.0050(17)	-0.011(2)	-0.0047(18)
C82	0.055(3)	0.023(2)	0.049(3)	-0.007(2)	-0.006(3)	-0.011(2)
C83	0.078(4)	0.031(3)	0.050(4)	-0.014(2)	0.009(3)	-0.026(3)
C84	0.116(6)	0.026(3)	0.045(4)	-0.001(2)	-0.004(4)	-0.024(3)
C85	0.104(6)	0.018(2)	0.057(4)	0.002(2)	-0.027(4)	-0.005(3)
C86	0.060(4)	0.023(2)	0.049(3)	-0.001(2)	-0.017(3)	-0.003(2)
B	0.032(3)	0.018(2)	0.037(3)	-0.0019(18)	-0.011(2)	0.0000(18)
Cl1S	0.117(3)	0.175(4)	0.193(4)	0.080(3)	0.049(3)	0.028(2)
Cl2S	0.190(4)	0.141(3)	0.173(4)	-0.020(3)	-0.084(3)	0.023(3)
C1S	0.121(9)	0.067(5)	0.122(9)	-0.015(6)	0.008(7)	0.001(6)

The form of the anisotropic displacement parameter is:

$\exp[-2\pi^2(h^2a^{*2}U_{11} + k^2b^{*2}U_{22} + l^2c^{*2}U_{33} + 2klb^*c^*U_{23} + 2hla^*c^*U_{13} + 2hka^*b^*U_{12})]$

Table D.7. Derived Atomic Coordinates and Displacement Parameters for Hydrogen Atoms

Atom	*x*	*y*	*z*	U_{eq}, Å^2
H12	-0.308919	0.095535	0.334928	0.059
H13	-0.400367	-0.038162	0.372841	0.065
H15	-0.201377	-0.023135	0.511935	0.064
H16	-0.109886	0.111570	0.475021	0.056
H17A	-0.470564	-0.112887	0.494500	0.084
H17B	-0.303943	-0.165608	0.495208	0.084
H17C	-0.379514	-0.174210	0.439256	0.084
H22	0.093671	0.232764	0.444564	0.063
H23	0.092964	0.323887	0.526794	0.077
H25	-0.305826	0.470993	0.509673	0.085
H26	-0.309849	0.378944	0.428554	0.070
H27A	-0.107837	0.528532	0.572109	0.128
H27B	-0.028562	0.435590	0.600656	0.128
H27C	-0.206545	0.458431	0.608619	0.128
H32	0.240268	0.325675	0.191966	0.041
H33	0.265460	0.408302	0.106381	0.048
H35	0.514369	0.174027	0.022928	0.052
H36	0.491614	0.089843	0.108291	0.044
H37A	0.411995	0.419802	0.008184	0.073
H37B	0.309453	0.354158	-0.015977	0.073
H37C	0.486772	0.323524	-0.027200	0.073
H42	0.332941	-0.048731	0.271647	0.040
H43	0.518357	-0.175559	0.283769	0.045
H45	0.828642	-0.033941	0.193518	0.049
H46	0.644609	0.093123	0.181709	0.043
H47A	0.768526	-0.257773	0.256188	0.075
H47B	0.856985	-0.185618	0.282820	0.075
H47C	0.889912	-0.208331	0.214692	0.075
H52	0.541403	0.552413	0.110347	0.040
H54	0.701369	0.281459	0.151323	0.041
H56	0.430002	0.459922	0.273704	0.037
H62	0.122686	0.561315	0.285695	0.040
H64	-0.145094	0.501890	0.174107	0.054
H66	0.219665	0.624502	0.116149	0.043
H72	0.153648	0.753252	0.285473	0.040
H74	0.338964	0.763804	0.430381	0.047
H76	0.549121	0.588348	0.295842	0.041
H82	0.631395	0.673844	0.162292	0.050
H84	0.518653	0.924483	0.084297	0.074
H86	0.196666	0.788142	0.173013	0.052
H1SA	0.842683	0.199267	0.015347	0.130
H1SB	0.977828	0.121215	-0.015237	0.130

Appendix E NMR Spectra of Isolated Compounds

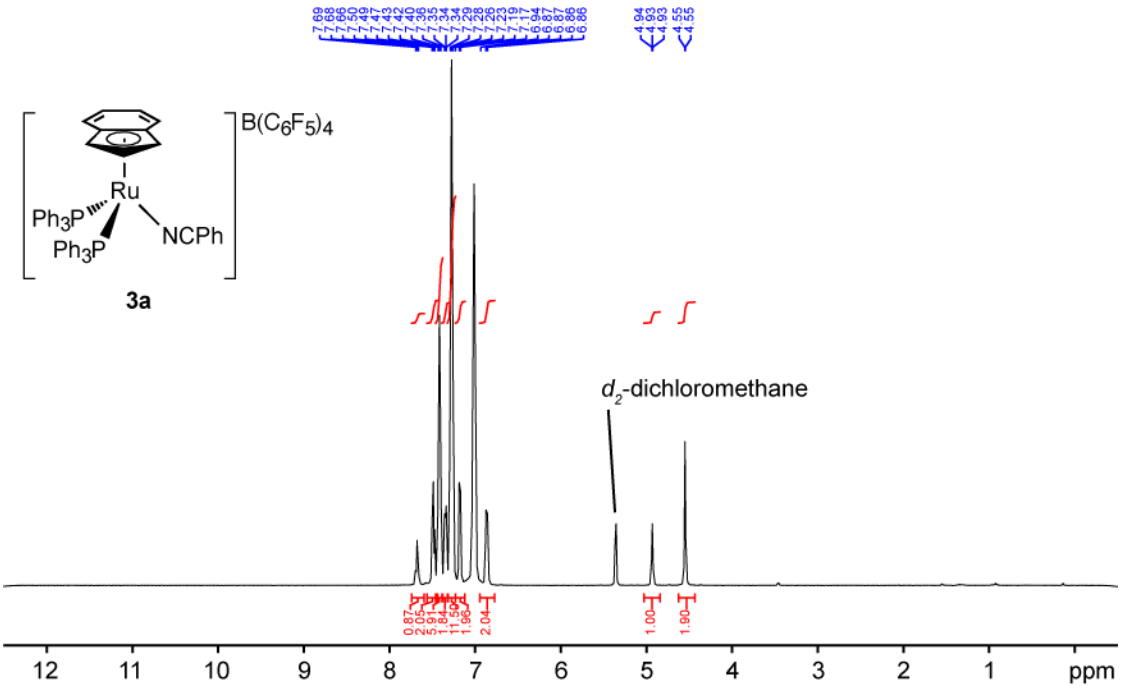

Figure E.1 ^{1}H NMR spectrum (500.27 MHz, d_2-dichloromethane) of complex **3a**.

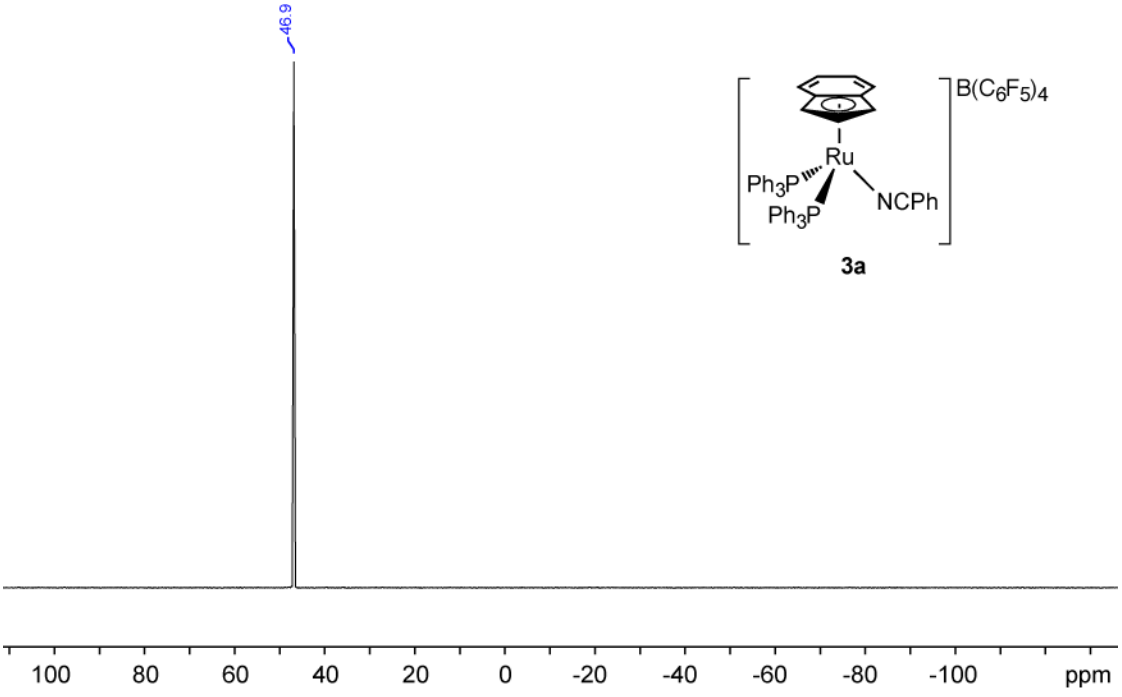

Figure E.2 ^{31}P{^{1}H} NMR spectrum (202.51 MHz, d_2-dichloromethane) of complex **3a**.

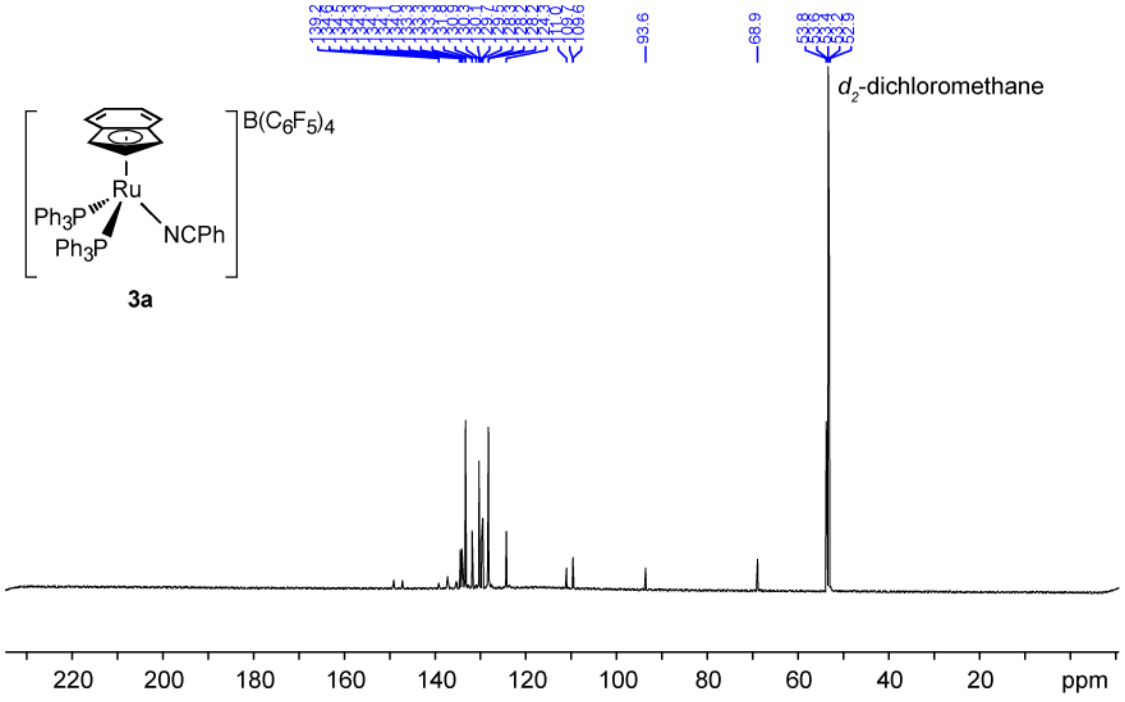

Figure E.3 $^{13}C\{^{1}H\}$ NMR spectrum (125.79 MHz, d_2-dichloromethane) of complex **3a**.

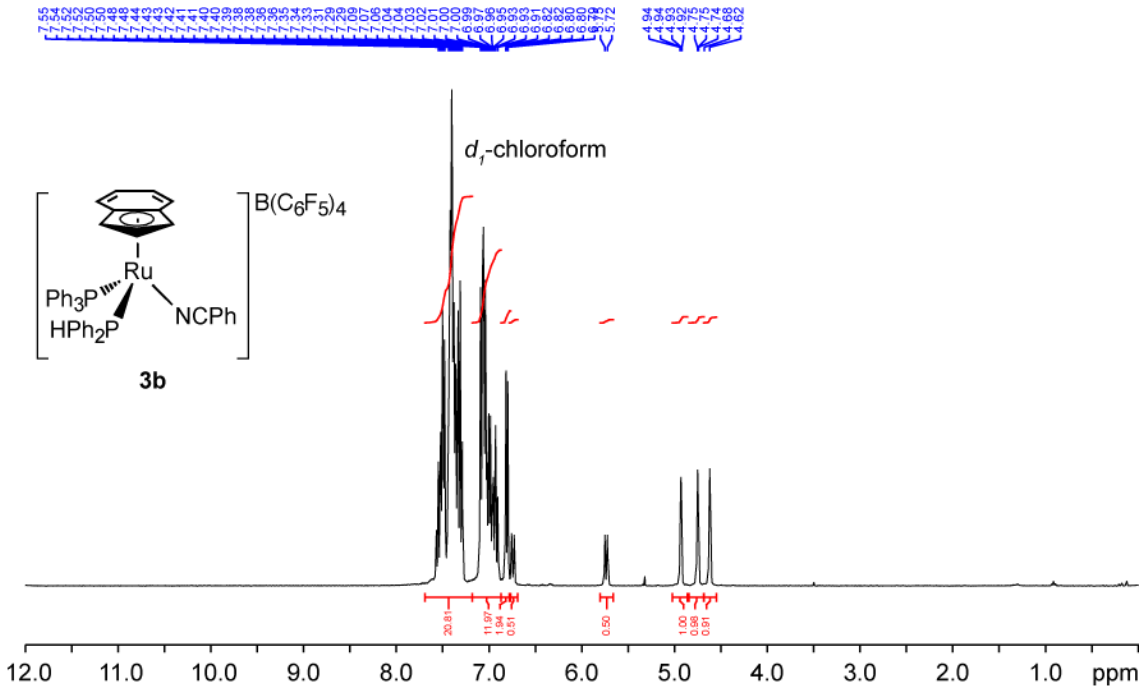

Figure E.4 ^{1}H NMR spectrum (500.27 MHz, d_1-chloroform) of complex **3b**.

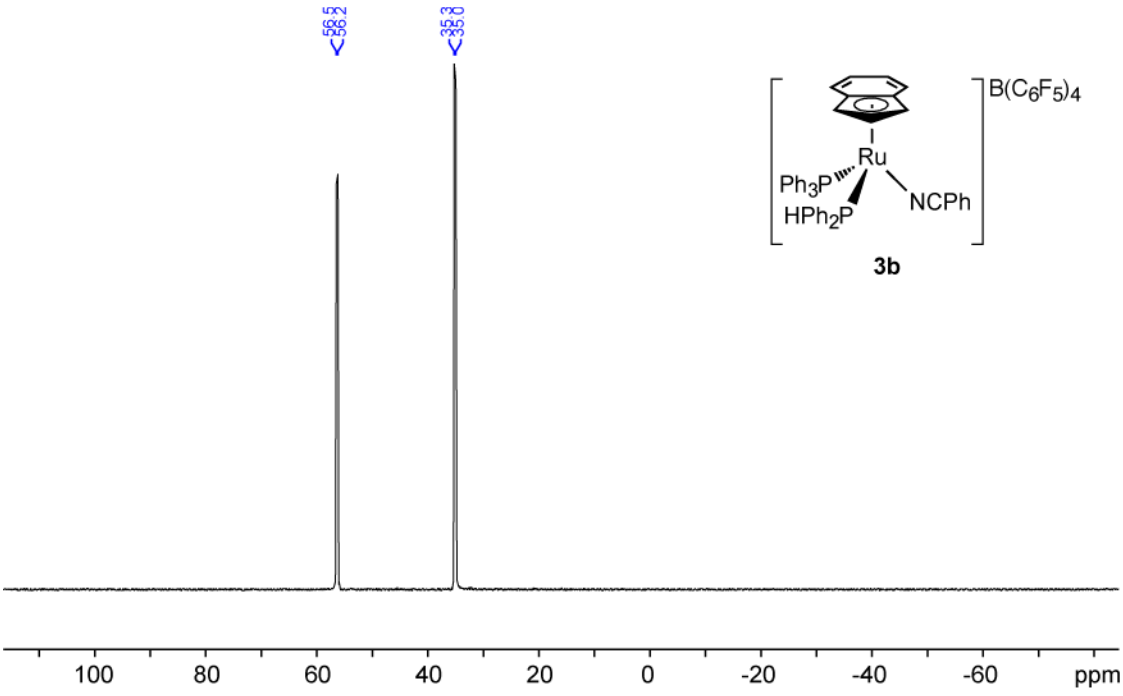

Figure E.5 $^{31}P\{^{1}H\}$ NMR spectrum (202.51 MHz, d_1-chloroform) of complex **3b**.

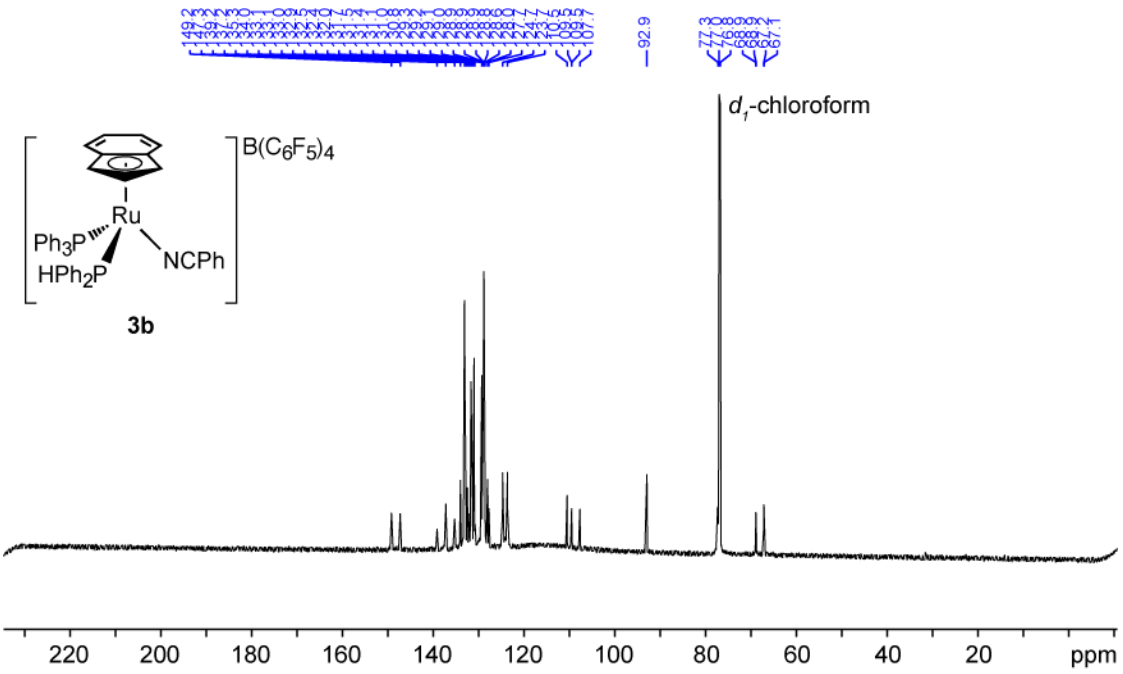

Figure E.6 $^{13}C\{^{1}H\}$ NMR spectrum (125.79 MHz, d_1-chloroform) of complex **3b**.

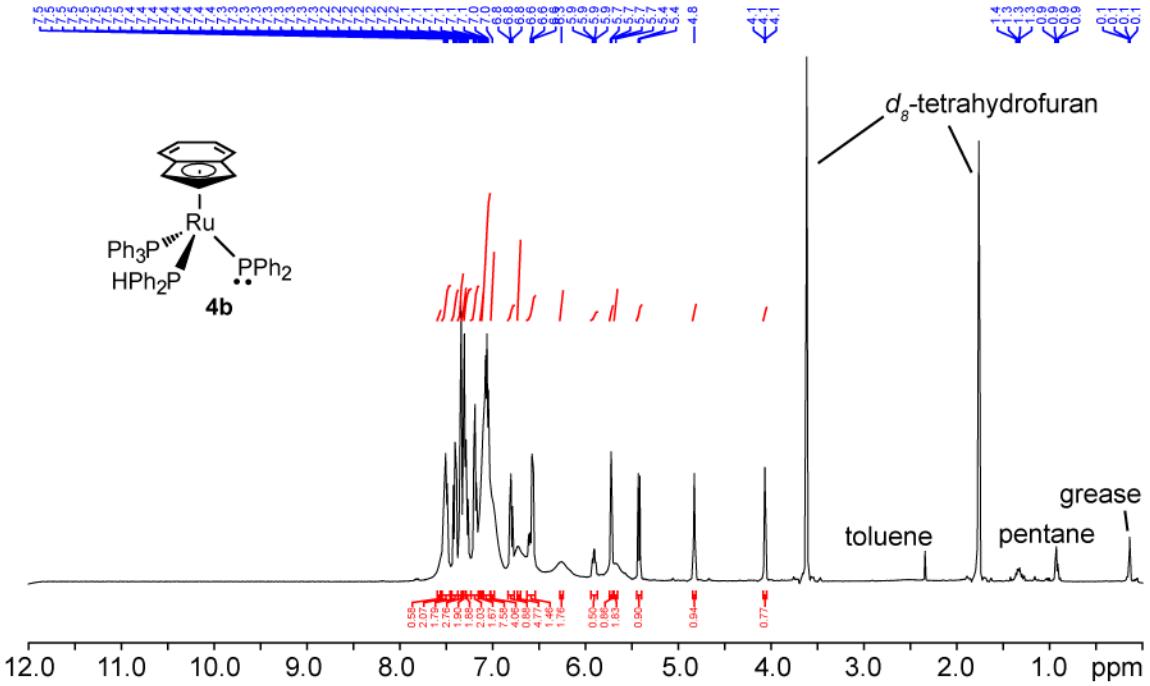

Figure E.7 ^{1}H NMR spectrum (500.27 MHz, C_6D_6) of complex **4b**.

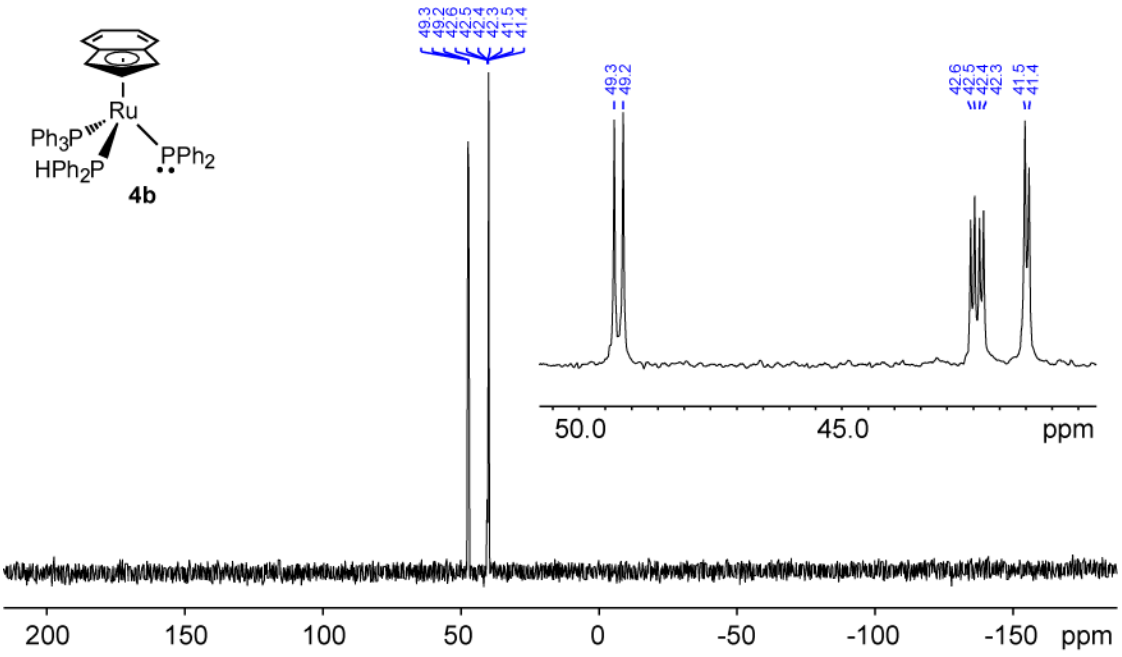

Figure E.8 ^{31}P{^{1}H} NMR spectrum (202.51 MHz, C_6D_6) of complex **4b**.

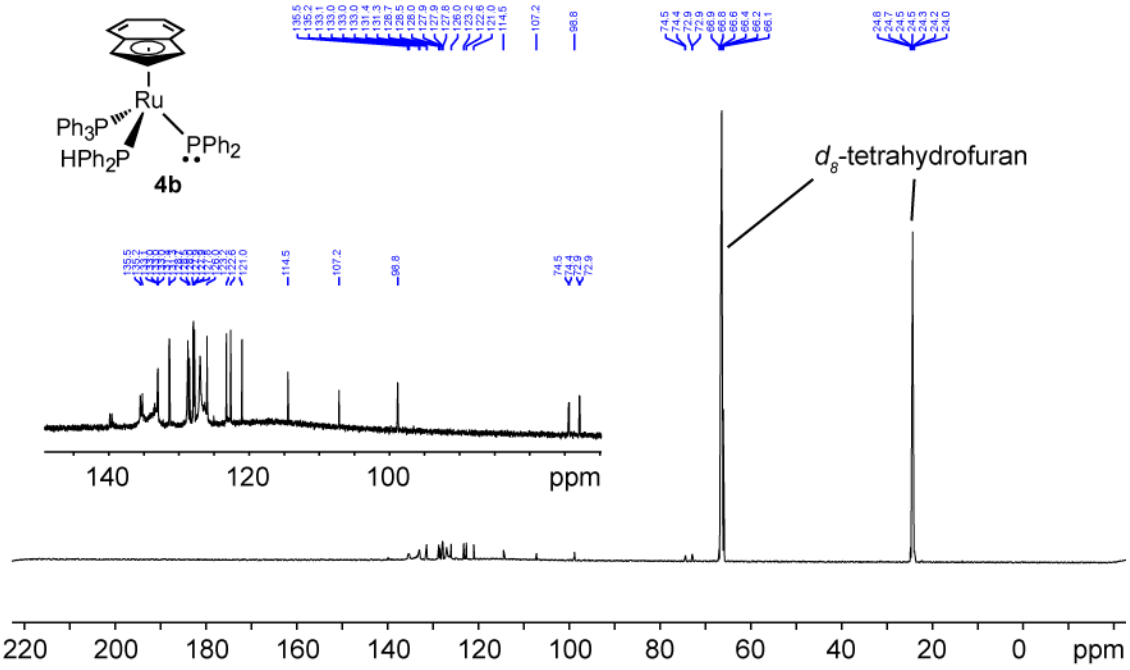

Figure E.9 $^{13}C\{^{1}H\}$ NMR spectrum (125.79 MHz, C_6D_6) of complex **4b**.

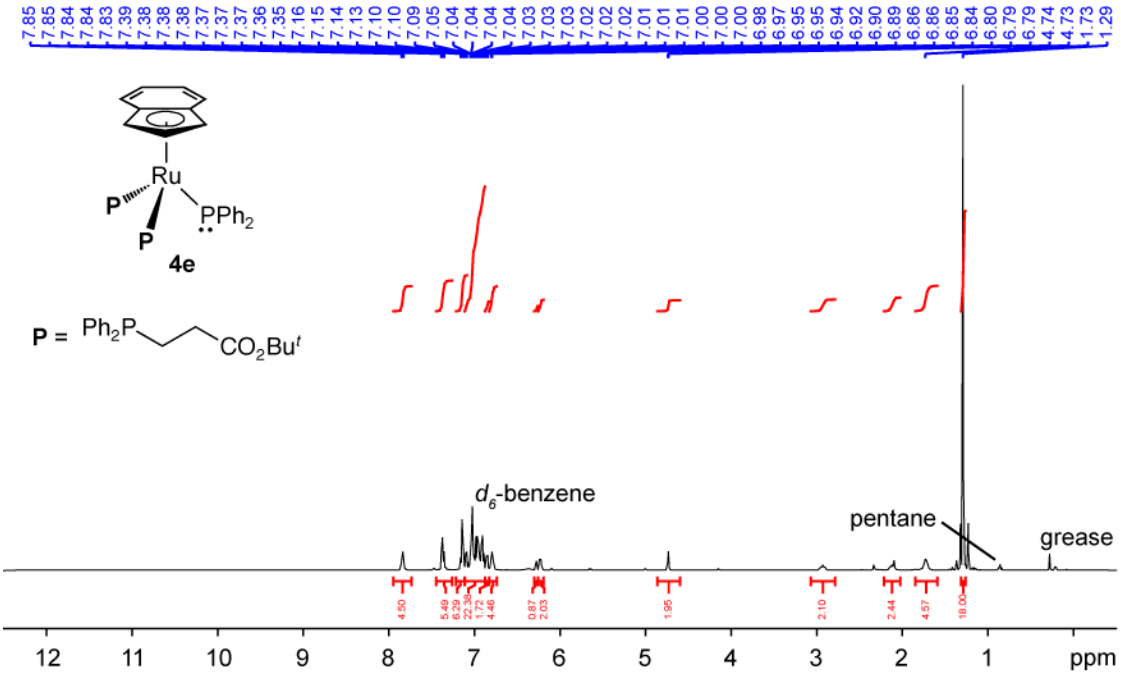

Figure E.10 ^{1}H NMR spectrum (500.27 MHz, C_6D_6) of complex **4e**.

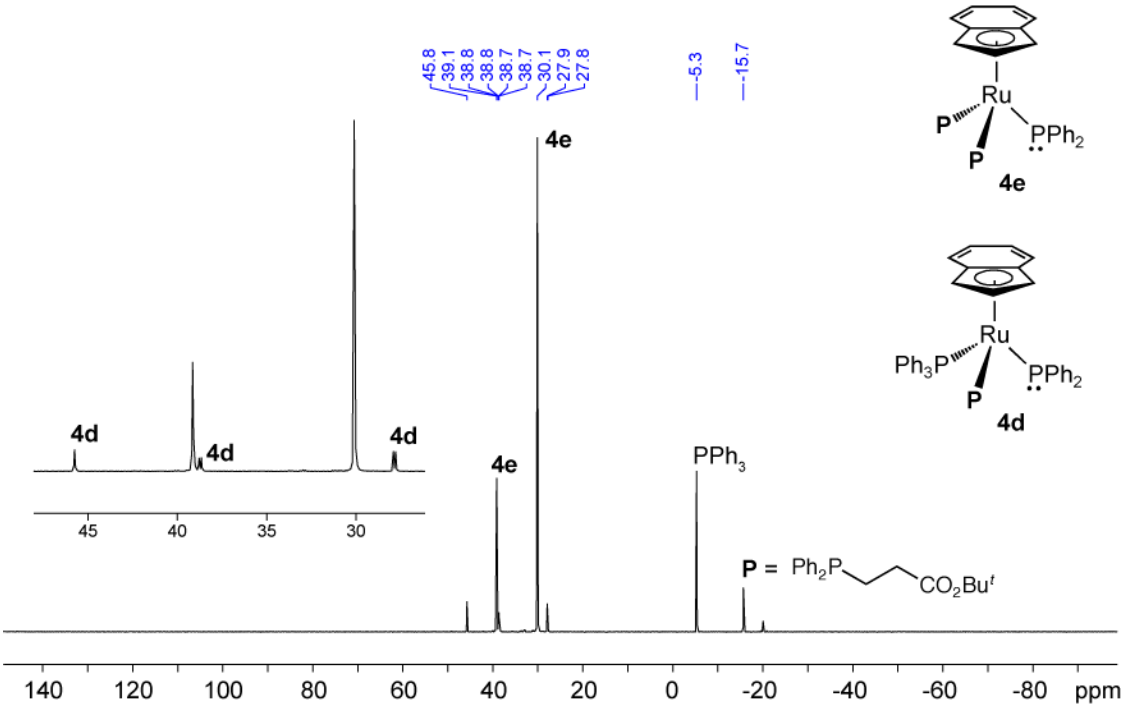

Figure E.11 $^{31}P\{^{1}H\}$ NMR spectrum (202.51 MHz, C_6D_6) of complex **4e**.

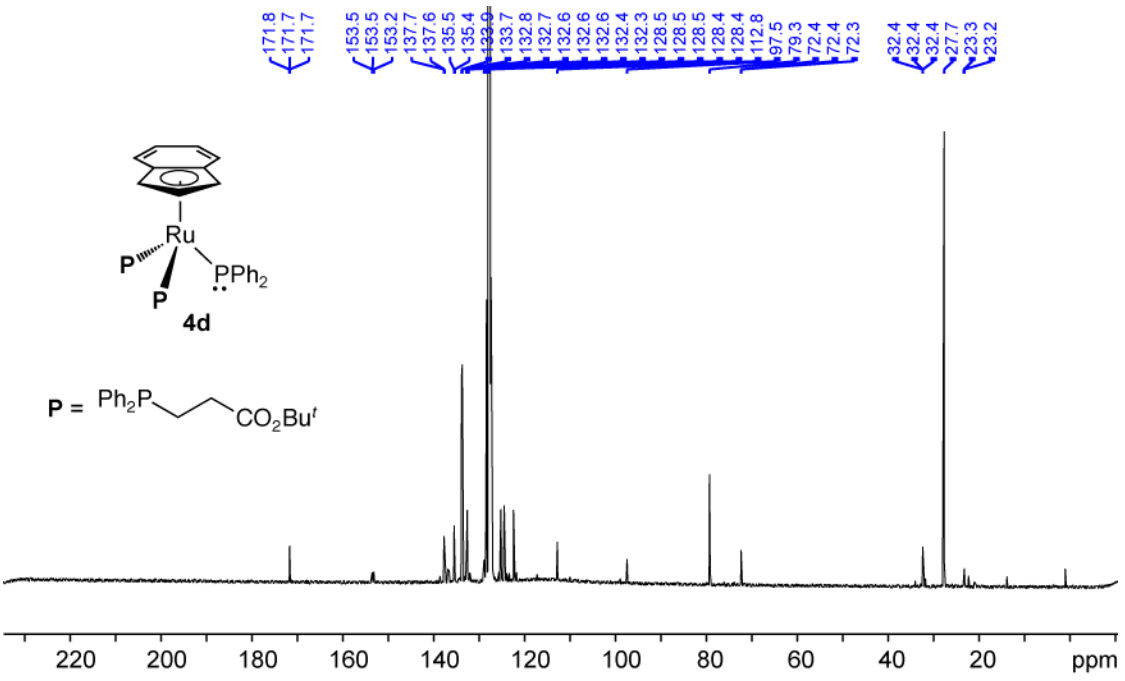

Figure E.12 $^{13}C\{^{1}H\}$ NMR spectrum (125.79 MHz, C_6D_6) of complex **4e**.

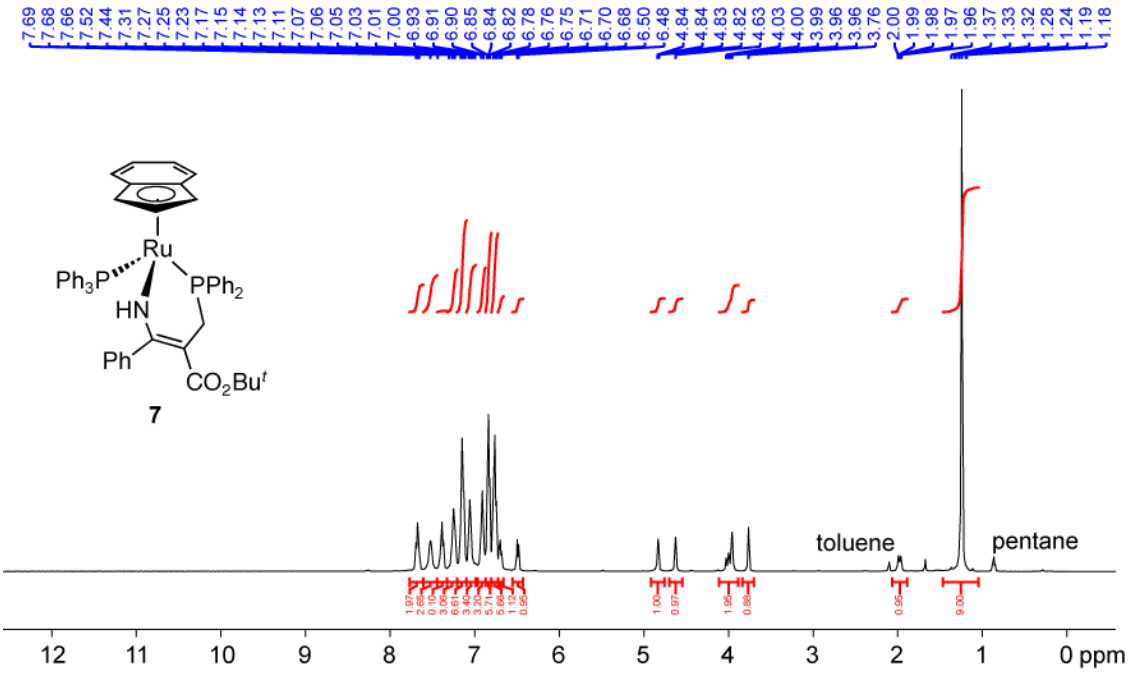

Figure E.13 ^{1}H NMR spectrum (500.27 MHz, C_6D_6) of complex **7a**.

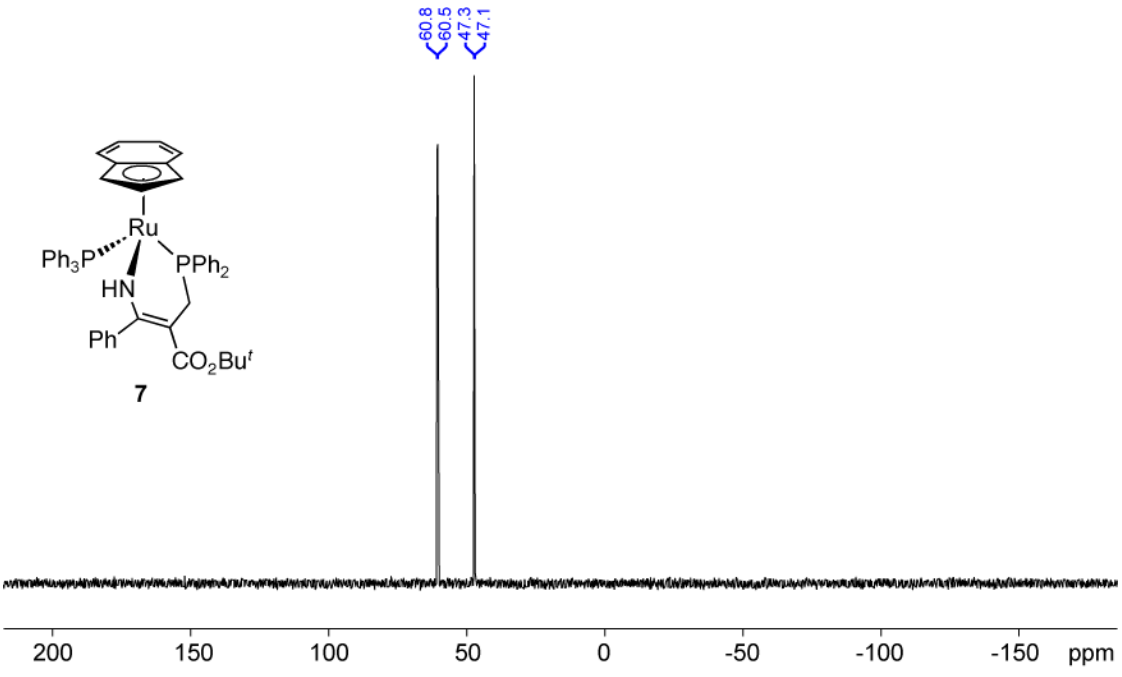

Figure E.14 $^{31}P\{^{1}H\}$ NMR spectrum (202.51 MHz, C_6D_6) of complex **7a**.

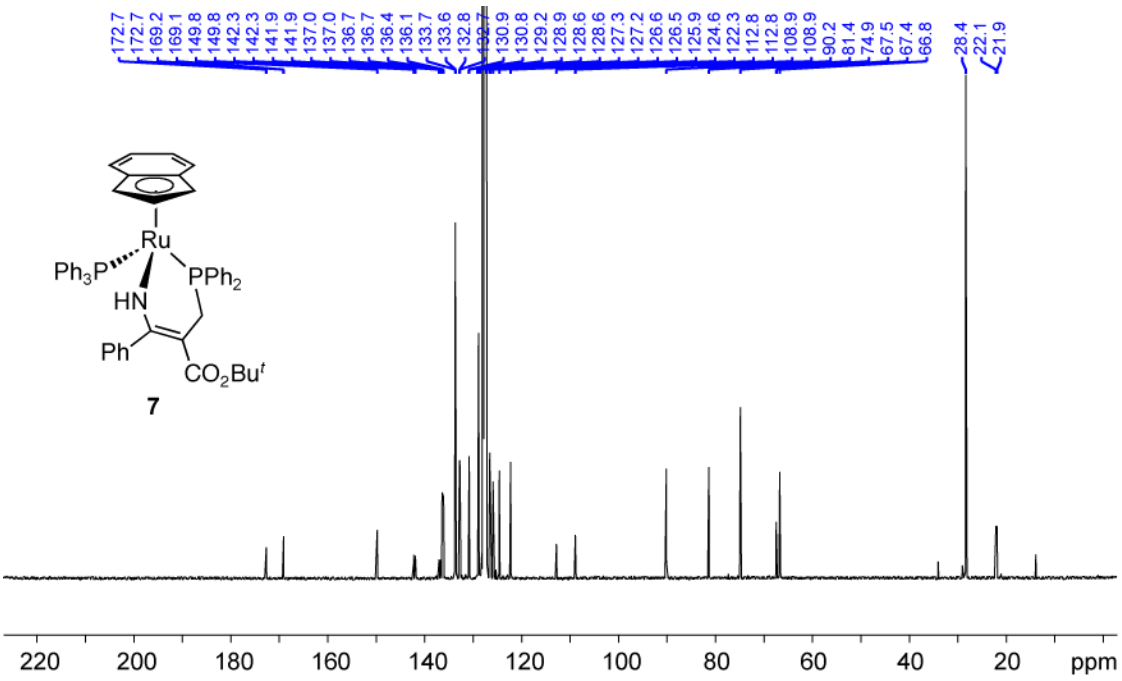

Figure E.15 $^{13}C\{^{1}H\}$ NMR spectrum (125.79 MHz, C_6D_6) of complex **7a**.

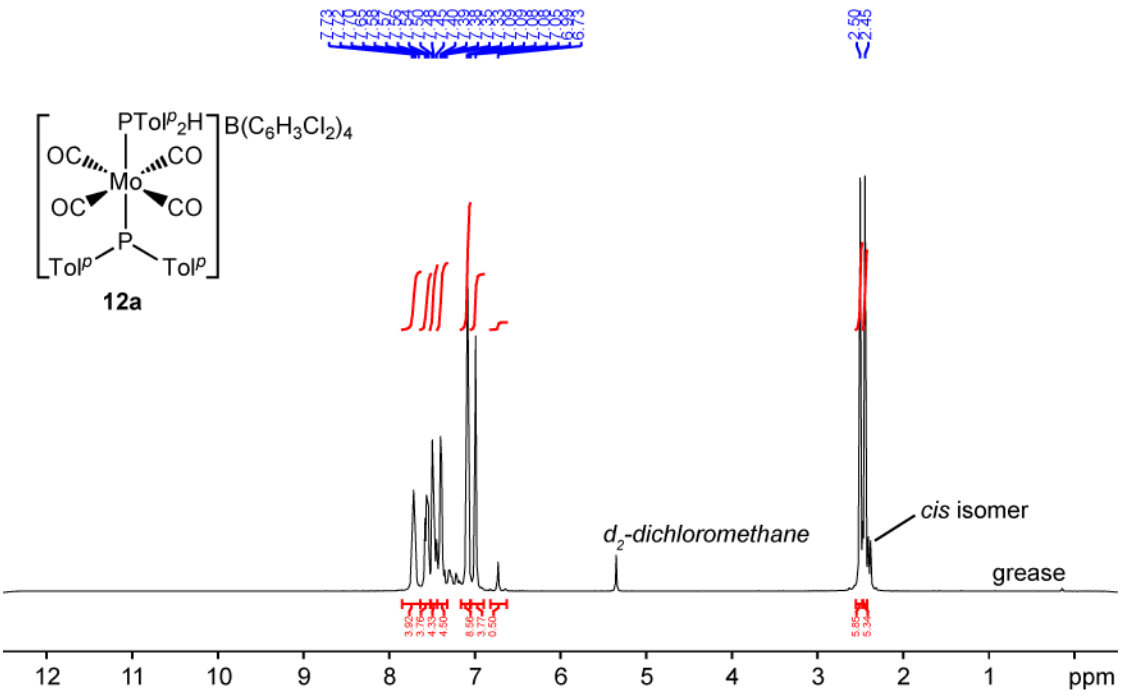

Figure E.16 ^{1}H NMR spectrum (500.27 MHz, CD_2Cl_2) of complex *trans*-**12a**[$B(C_6H_3Cl_2)_4$].

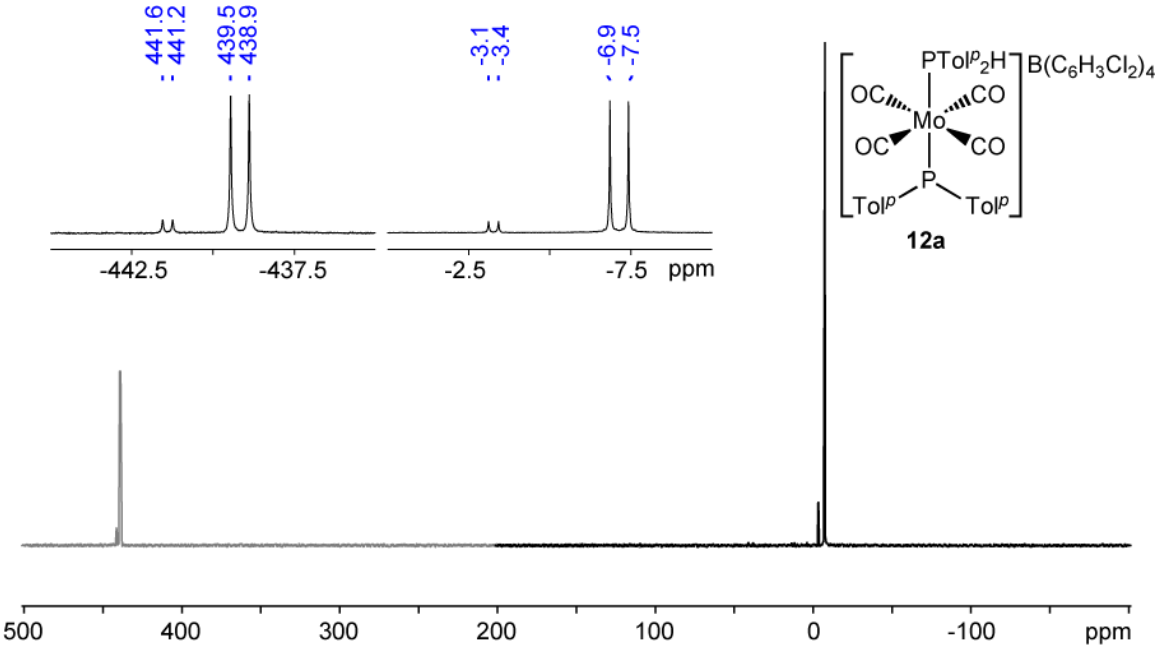

Figure E.17 $^{31}P\{^1H\}$ NMR spectrum (202.51 MHz, CD_2Cl_2) of complex *trans*-**12a**[$B(C_6H_3Cl_2)_4$].

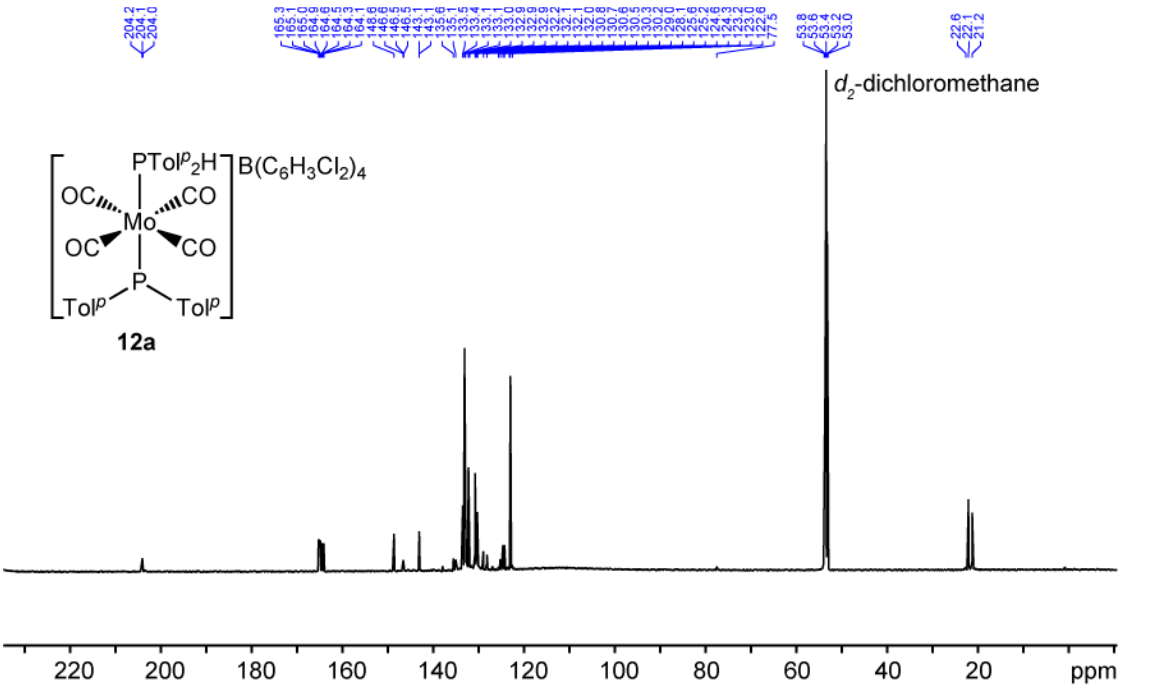

Figure E.18 $^{13}C\{^1H\}$ NMR spectrum (125.79 MHz, CD_2Cl_2) of complex *trans*-**12a**[$B(C_6H_3Cl_2)_4$].

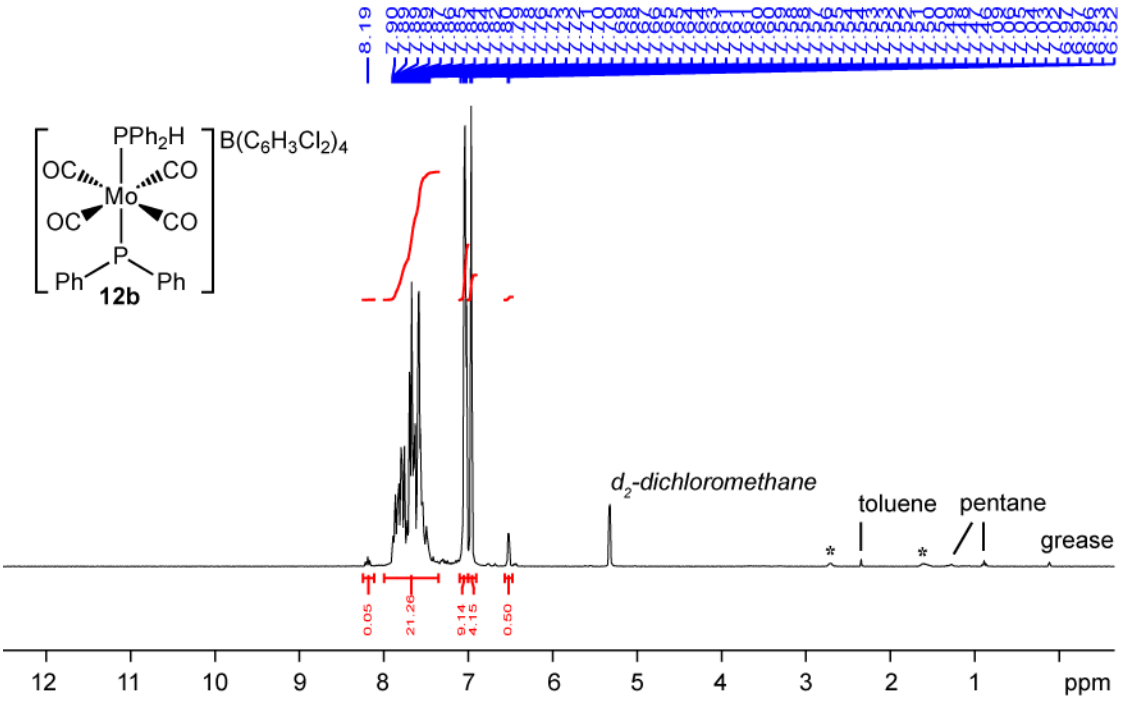

Figure E.19 ^{1}H NMR spectrum (500.27 MHz, CD_2Cl_2) of complex *trans*-**12b**[$B(C_6H_3Cl_2)_4$].

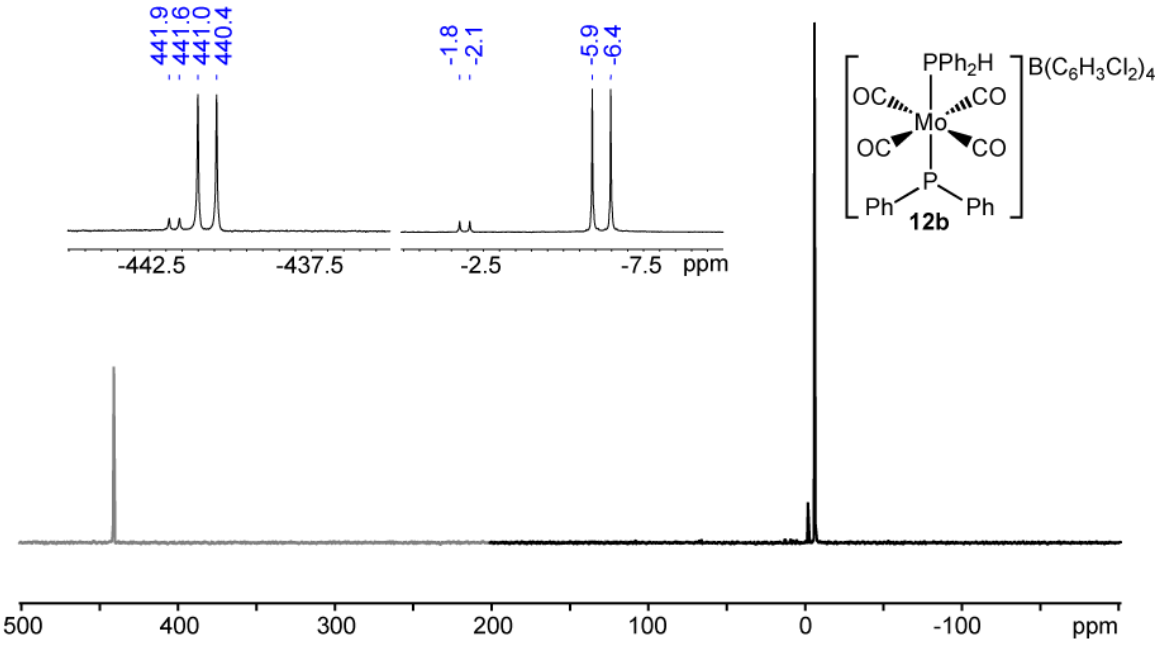

Figure E.20 ^{31}P{^{1}H} NMR spectrum (202.51 MHz, CD_2Cl_2) of complex *trans*-**12b**[$B(C_6H_3Cl_2)_4$].

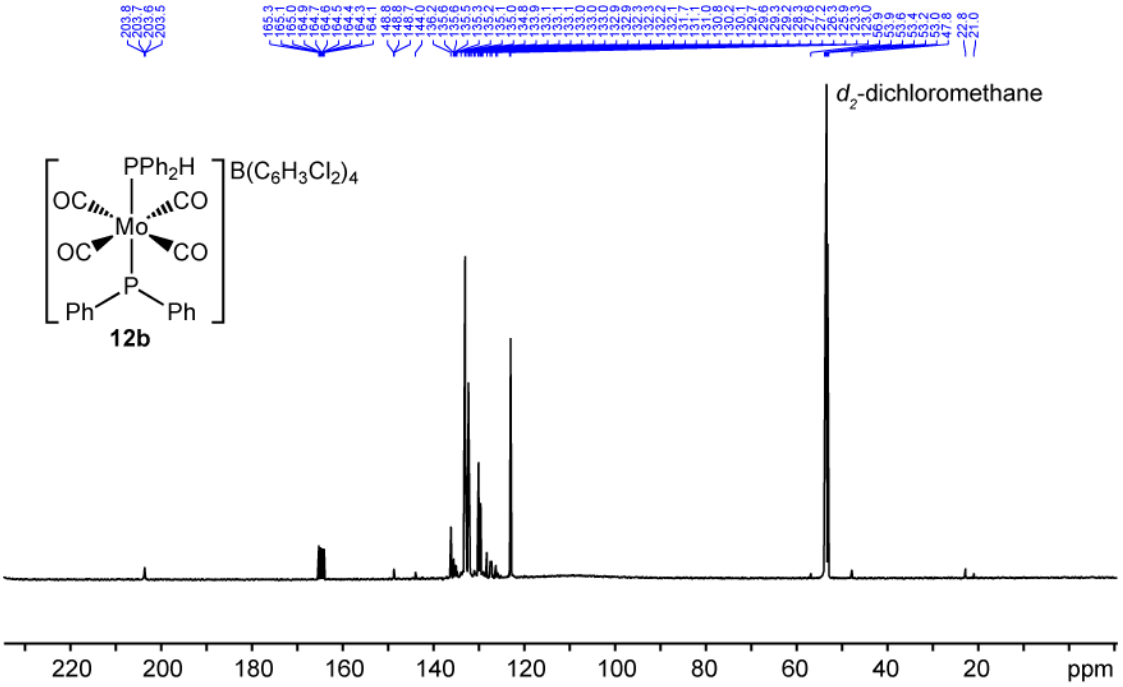

Figure E.21 $^{13}C\{^{1}H\}$ NMR spectrum (125.79 MHz, CD_2Cl_2) of complex *trans*-**12b**$[B(C_6H_3Cl_2)_4]$.

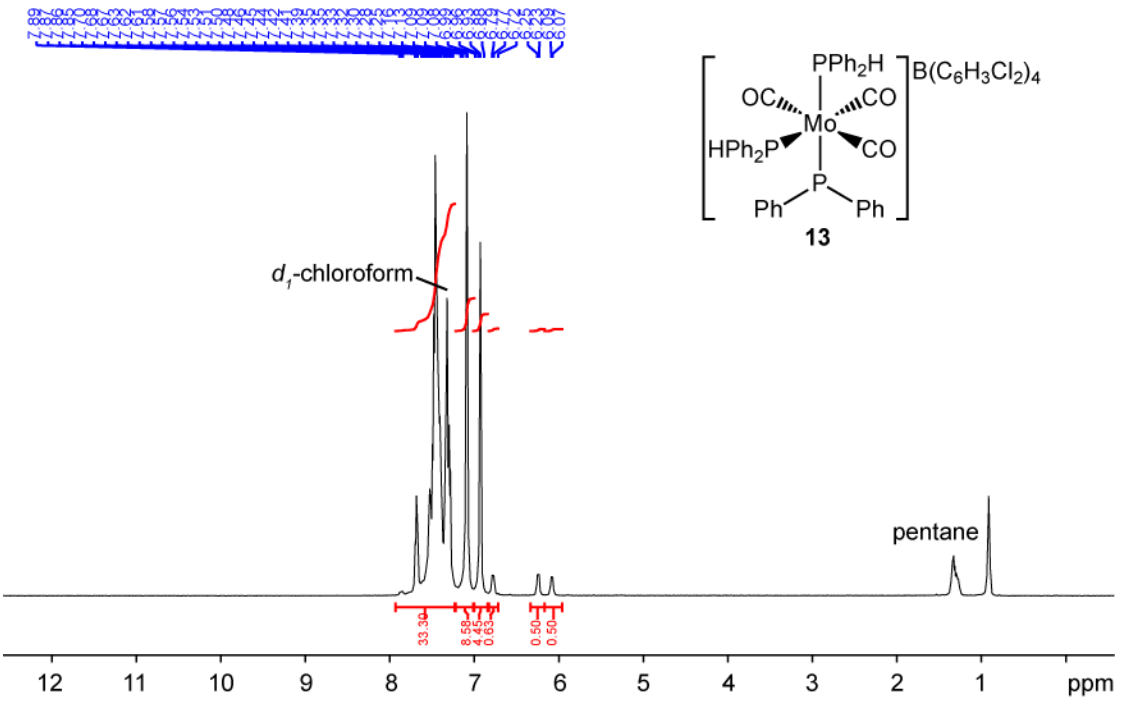

Figure E.22 ^{1}H NMR spectrum (500.27 MHz, $CDCl_3$) of complex *trans*-**13**$[B(C_6H_3Cl_2)_4$.

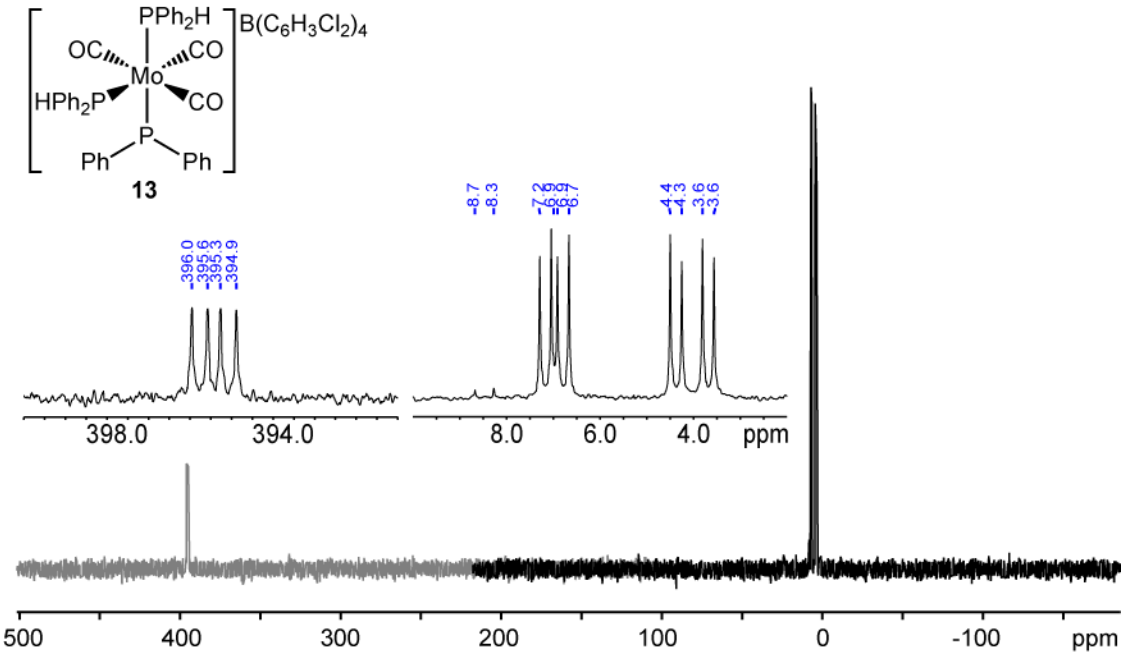

Figure E.23 $^{31}P\{^{1}H\}$ NMR spectrum (202.51 MHz, $CDCl_3$) of complex *trans*-**13**[$B(C_6H_3Cl_2)_4$.

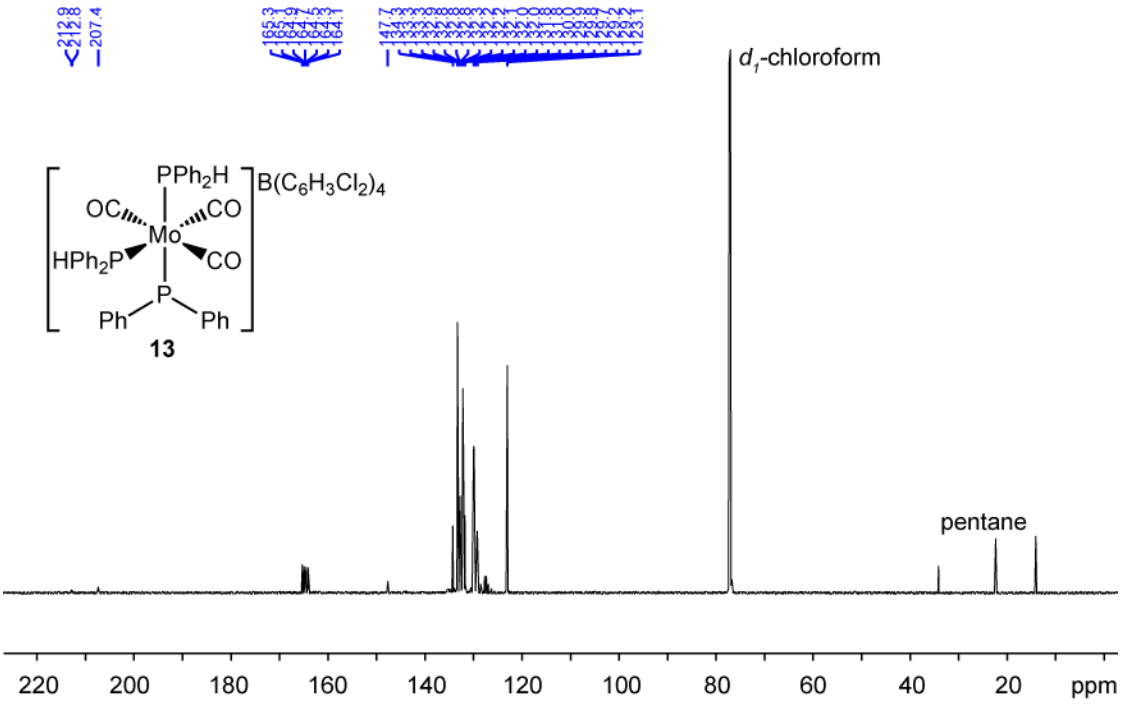

Figure E.24 $^{13}C\{^{1}H\}$ NMR spectrum (125.79 MHz, $CDCl_3$) of complex *trans*-**13**[$B(C_6H_3Cl_2)_4$.

Appendix F $^{31}P\{^{1}H\}$ NMR Spectra of Control Experiments in Chapter 3

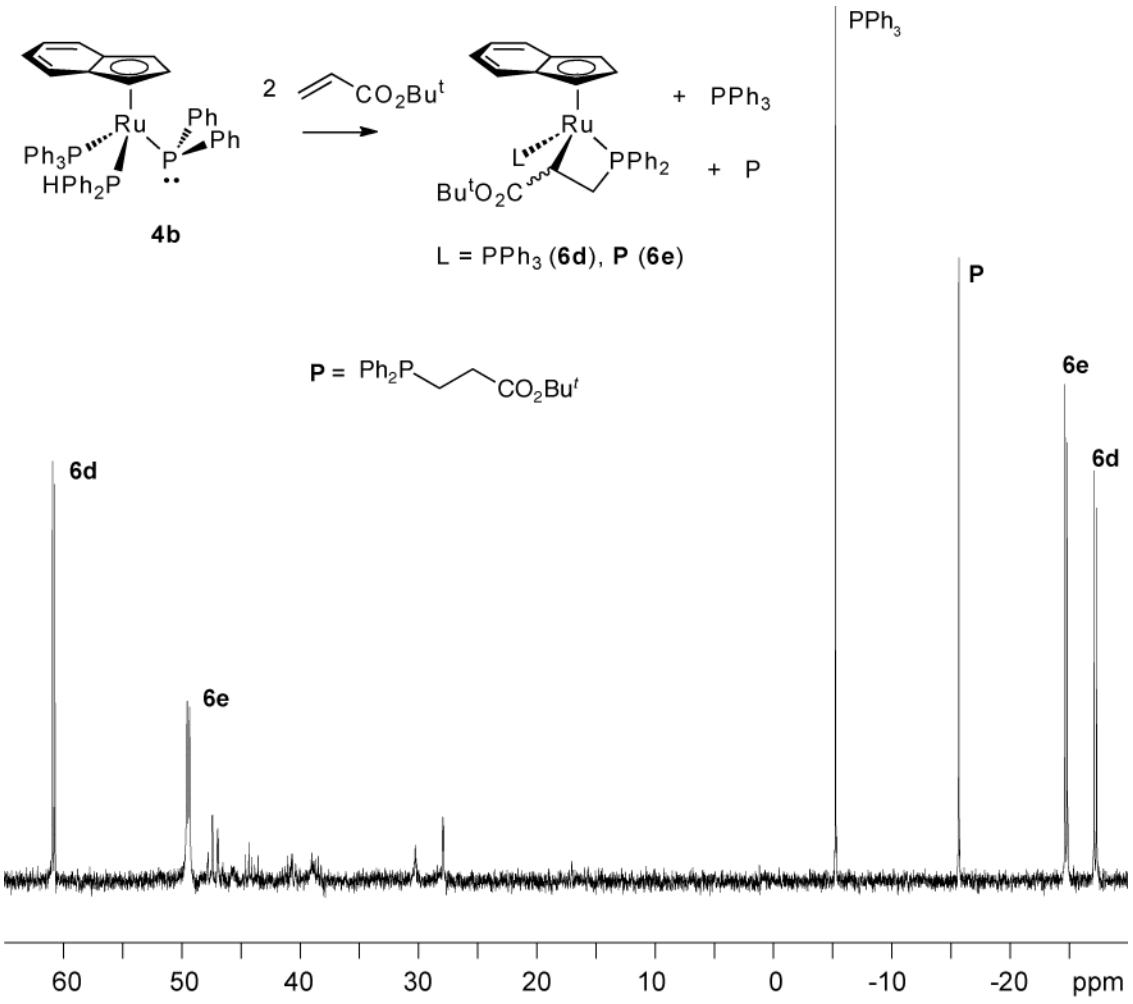

Figure F.1. From section 3.2.4: $^{31}P\{^{1}H\}$ NMR (121.55 MHz, C_6D_6) spectrum of the addition of *tert*-butyl acrylate to complex **4b** , which results in the formation of complexes **6d**,**e** PPh_3 and **P**.

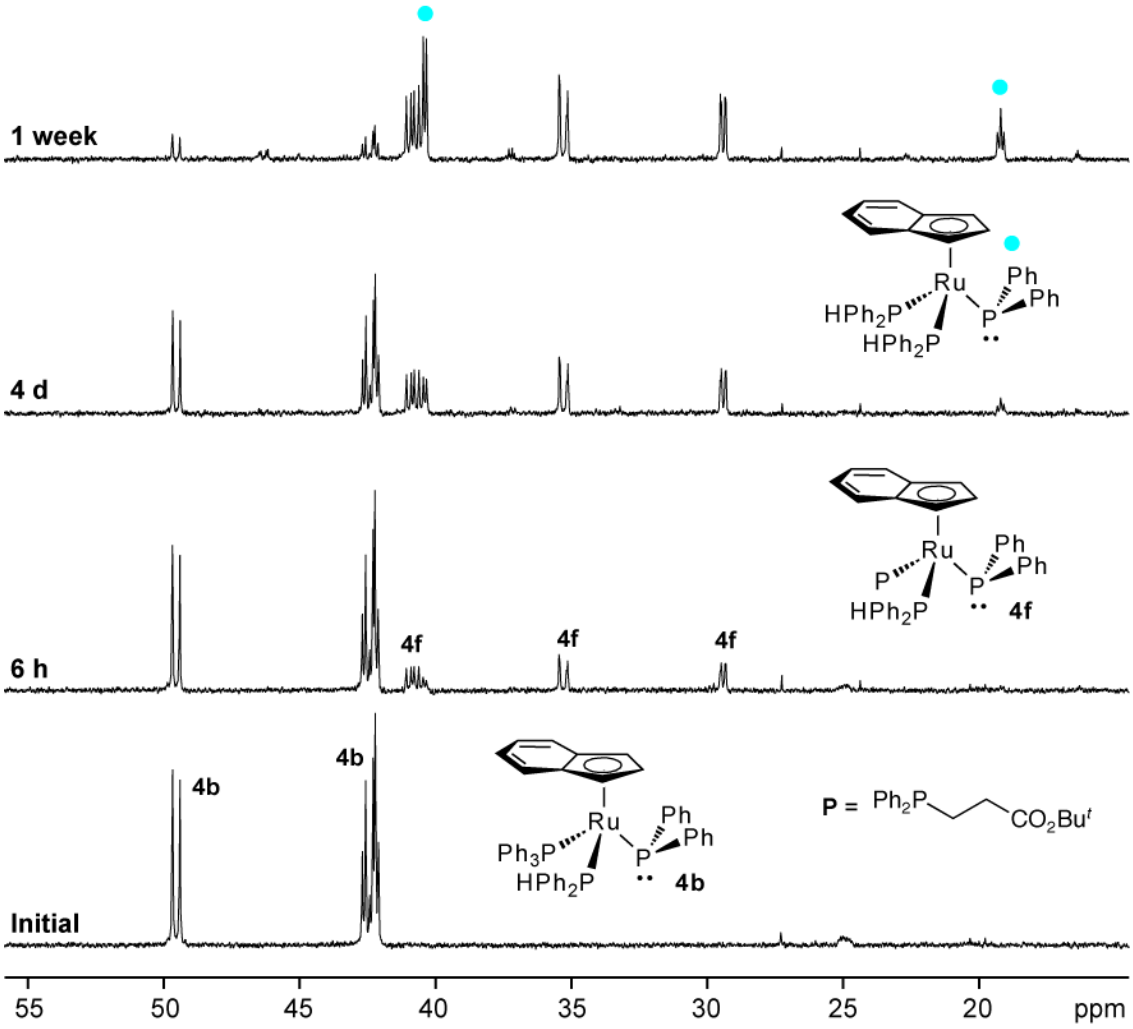

Figure F.2. $^{31}P\{^{1}H\}$ NMR (121.55 MHz, C_6D_6) spectra of the addition of **P** to complex **4b**, which results in the formation of complex **4f**. Additional substitution is observed after 1 week to give the tentatively assigned complex Ru(η^5-indenyl)(PPh_2)(PPh_2H)$_2$.

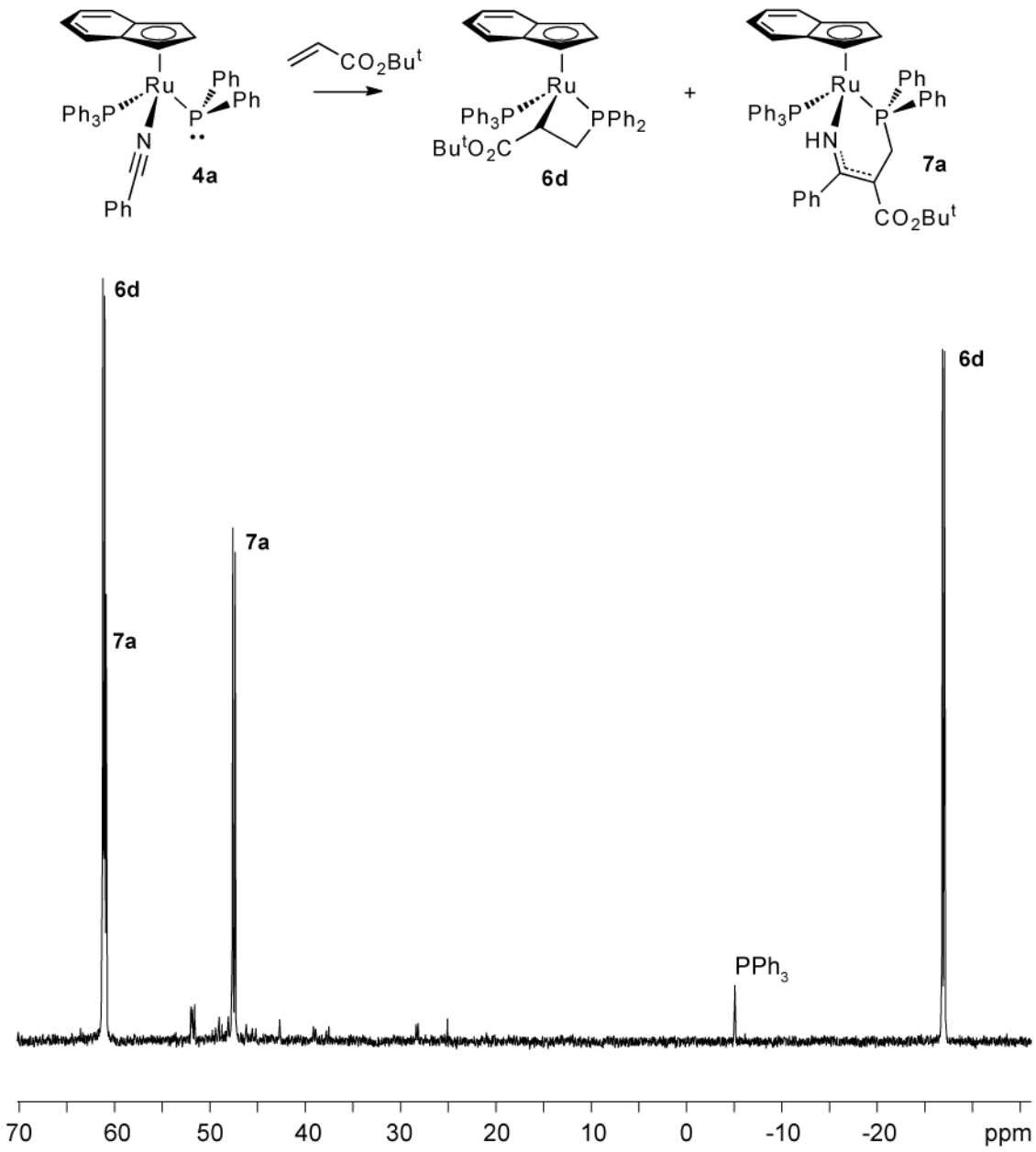

Figure F.3. From section 3.5.2: $^{31}P\{^{1}H\}$ NMR (121.55 MHz, C_6D_6) spectrum of the addition of *tert*-butyl acrylate to complex **4a**, which results in the formation of complex**es 6d** and **7a**. Some minor unassigned products also formed.

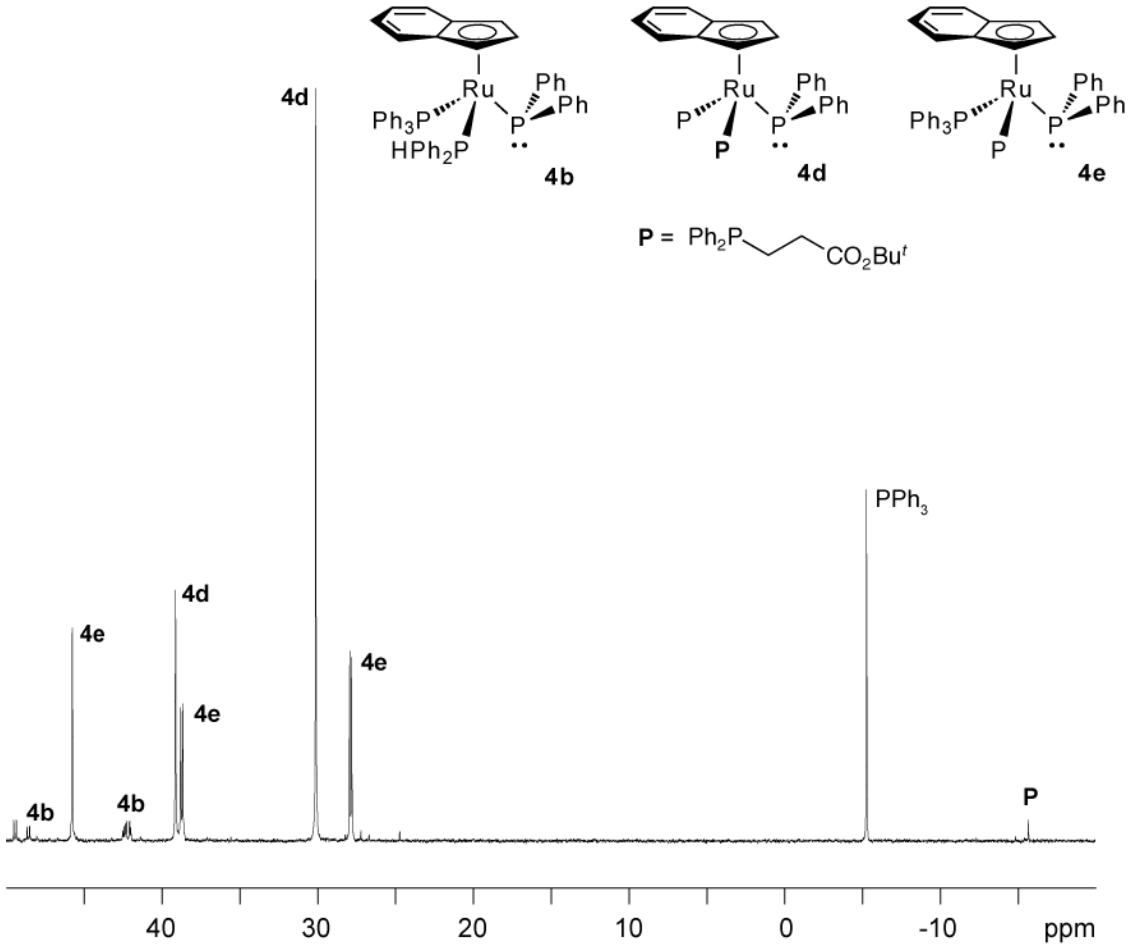

Figure F.4. $^{31}P\{^{1}H\}$ NMR (121.55 MHz, C_6D_6) spectrum of the addition of **P** to complex **4a**, which results in the formation of complexes **4d**,**e**, PPh_3 and minor amounts of **4b**.

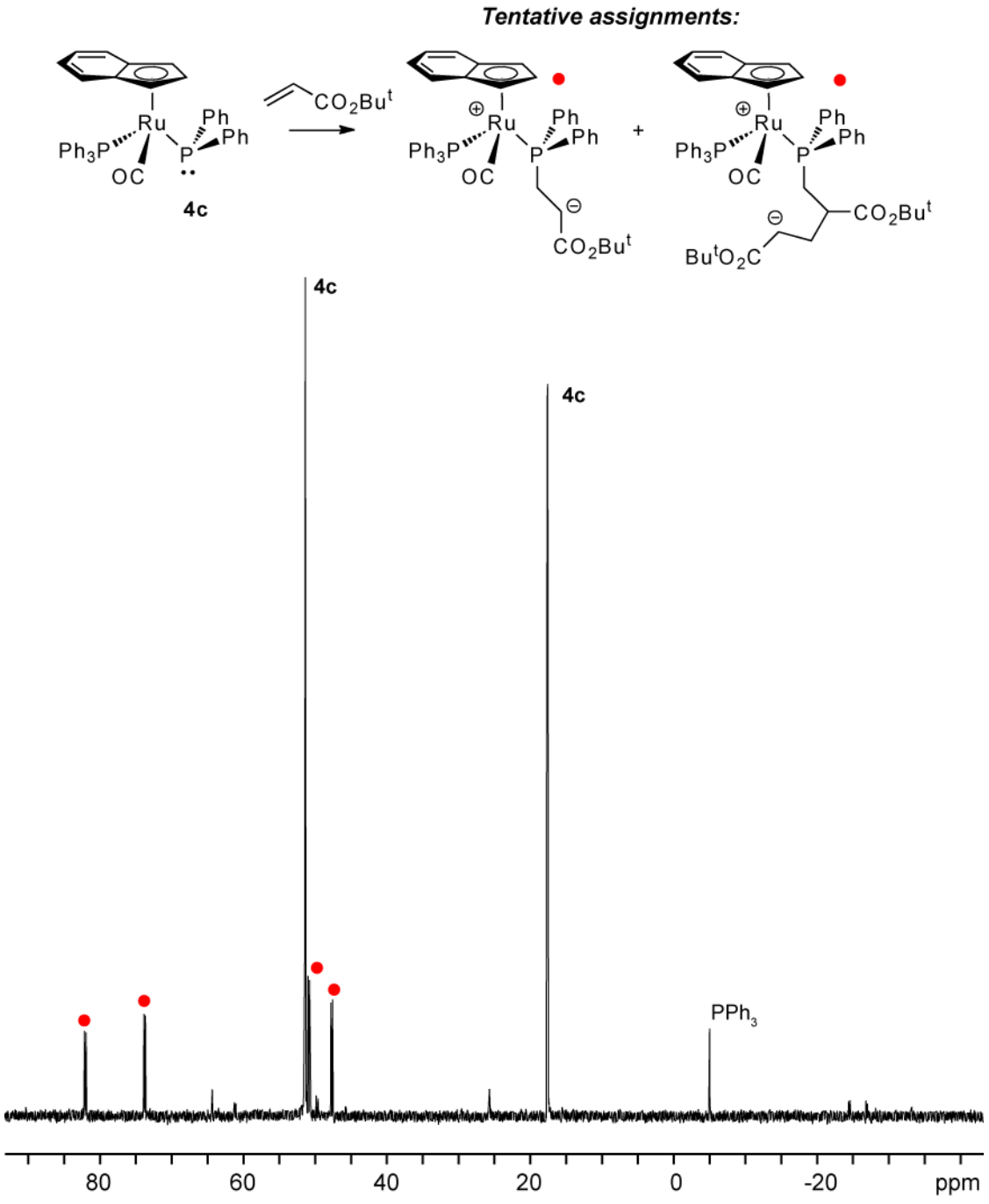

Figure F.5. From section 3.6.3: $^{31}P\{^{1}H\}$ NMR (121.55 MHz, C_6D_6) spectrum of the addition of *tert*-butyl acrylate to complex **4c**, which results in the formation of the tentatively assigned complexes shown and unreacted **4c**.

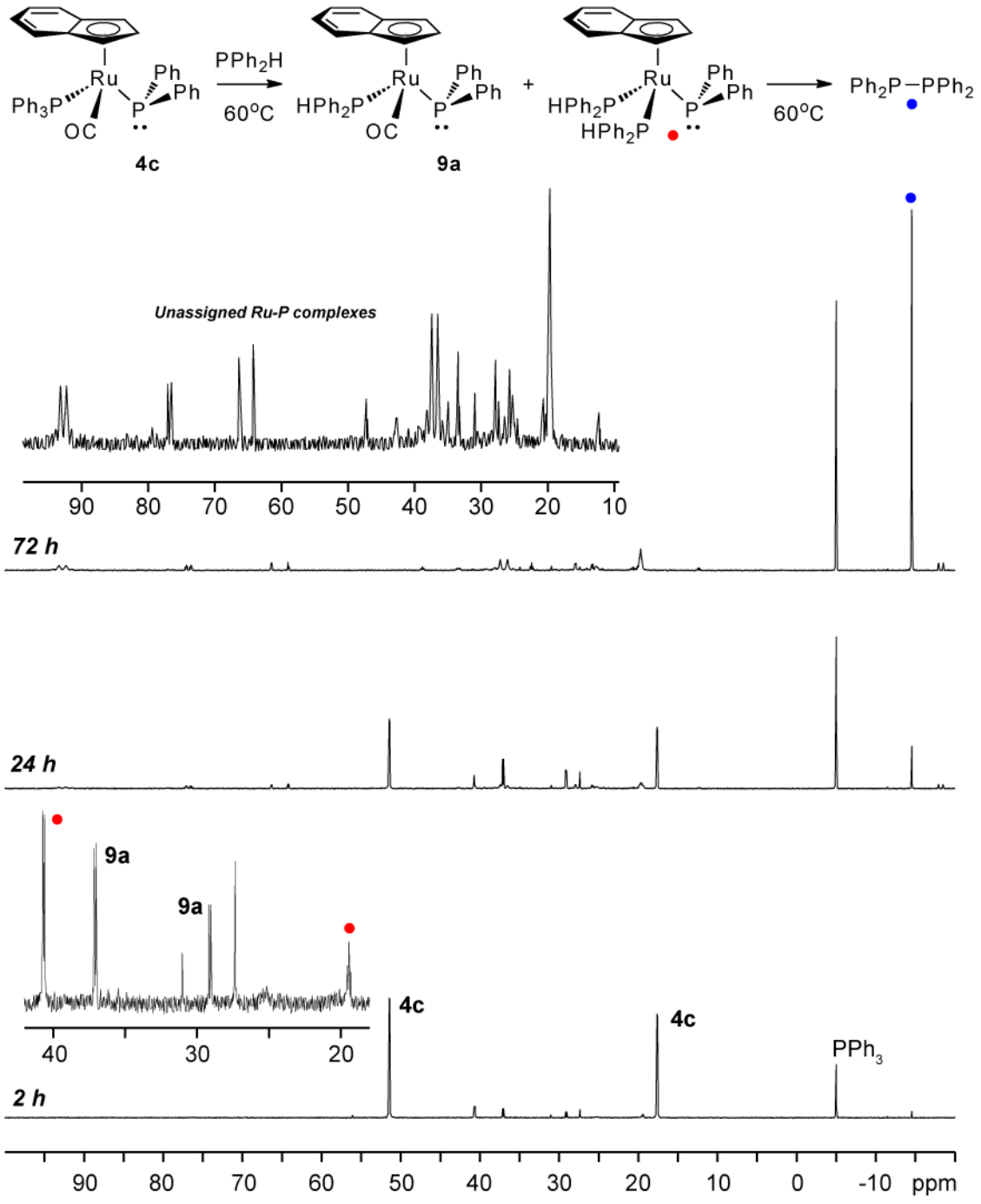

Figure F.6. $^{31}P\{^{1}H\}$ NMR (121.55 MHz, C_6D_6) spectra of the addition of PPh_2H to complex **4c** at 60°C, which results in the initial formation of complex **9a**. Prolonged heating results in the formation of Ph_2P-PPh_2 and a complex mixture of unassigned Ru-P compounds.

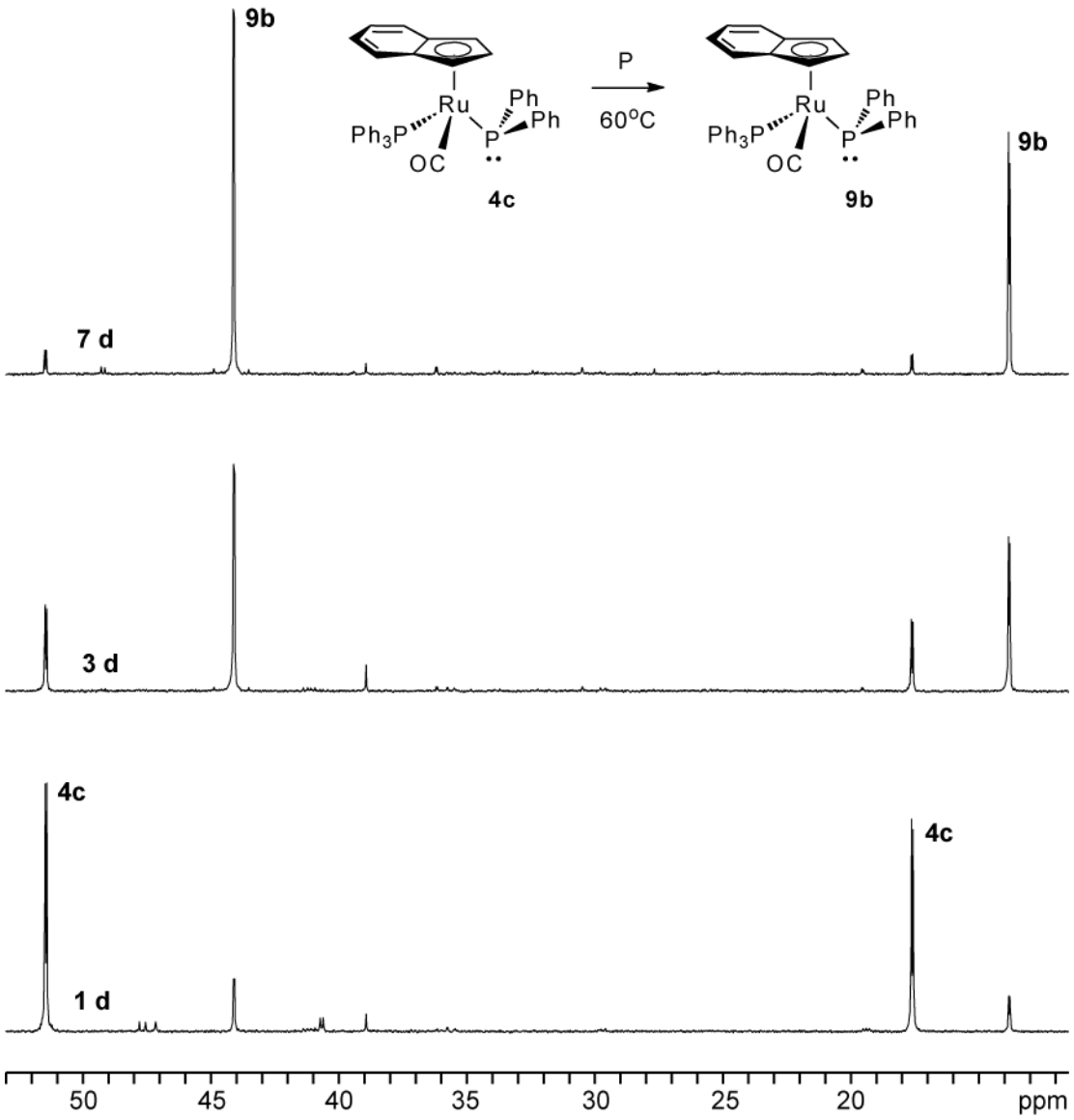

Figure F.7. $^{31}P\{^{1}H\}$ NMR (121.55 MHz, C_6D_6) spectra of the addition of **P** to complex **4c** at 60°C, which results in the formation of complex **9b**.

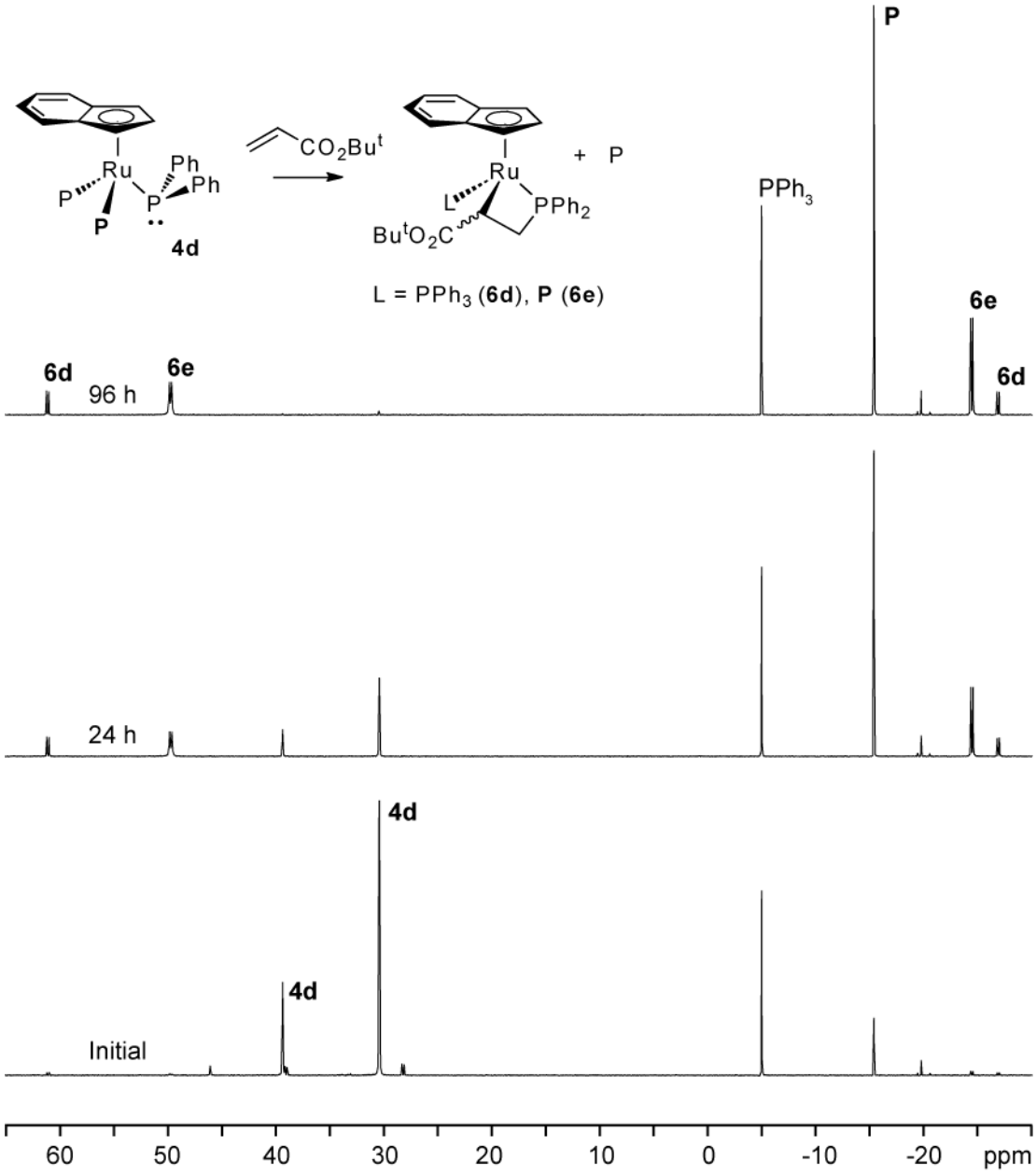

Figure F.8. From section 3.3.4: $^{31}P\{^{1}H\}$ NMR (121.55 MHz, C_6D_6) spectra of the addition of *tert*-butyl acrylate to complex **4d**, which results in the formation of complexes **6d**,**e** and **P**.

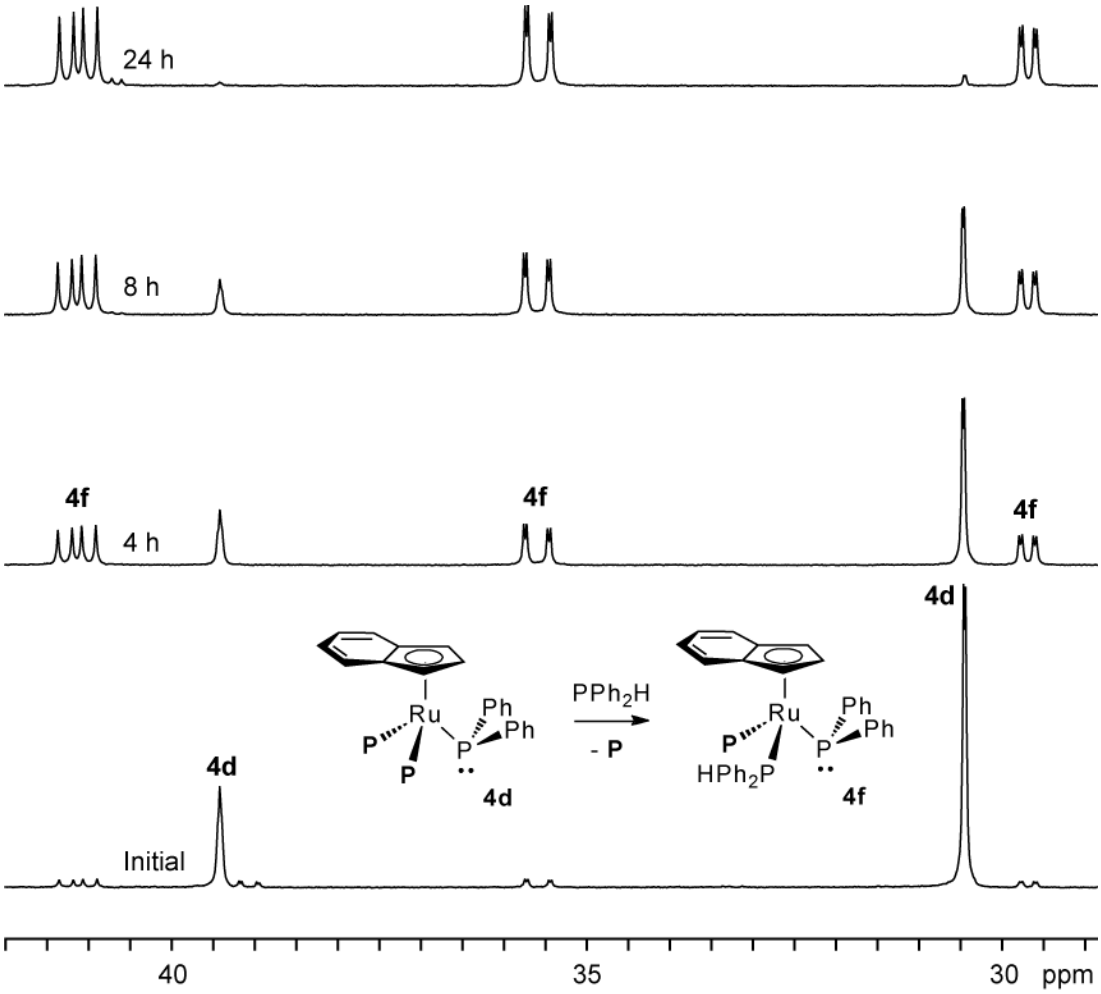

Figure F.9. From section 3.3.3: $^{31}P\{^{1}H\}$ NMR (121.55 MHz, C_6D_6) spectra of the addition of PPh_2H to complex **4d**, which results in the formation of complex **4f**.

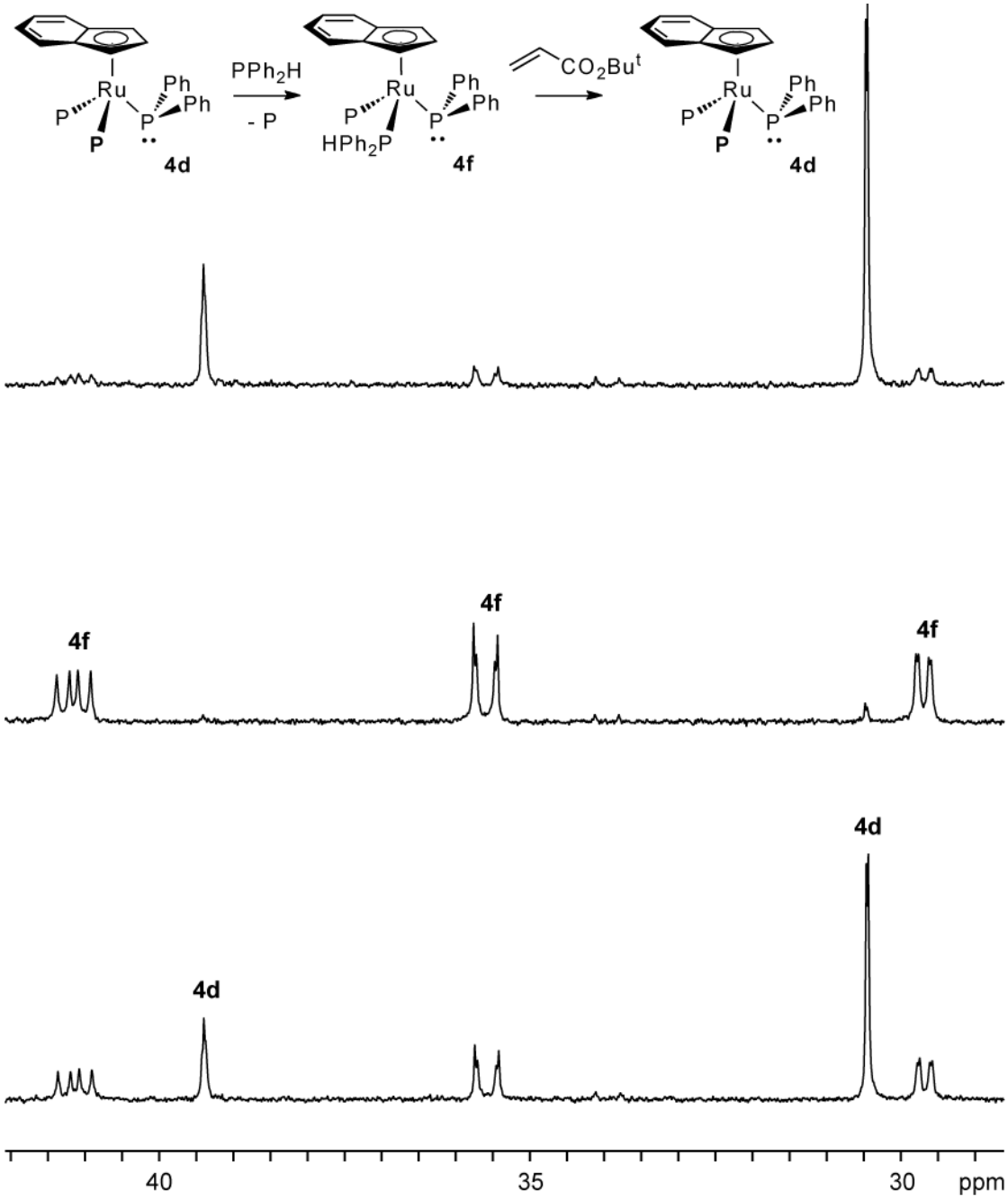

Figure F.10. From section 3.3.5: $^{31}P\{^{1}H\}$ NMR (121.55 MHz, C_6D_6) spectra of the addition of PPh_2H to complex **4d**, which results in the formation of complex **4f**. Subsequent addition of *tert*-butyl acrylate to **4f** regenerates **4d**.

Appendix G **Representative NMR Spectra for the Characterization of [Mo(CO)$_3$(PPh$_2$)(Ph$_2$PCH$_2$CH$_3$)$_2$] (18e)**

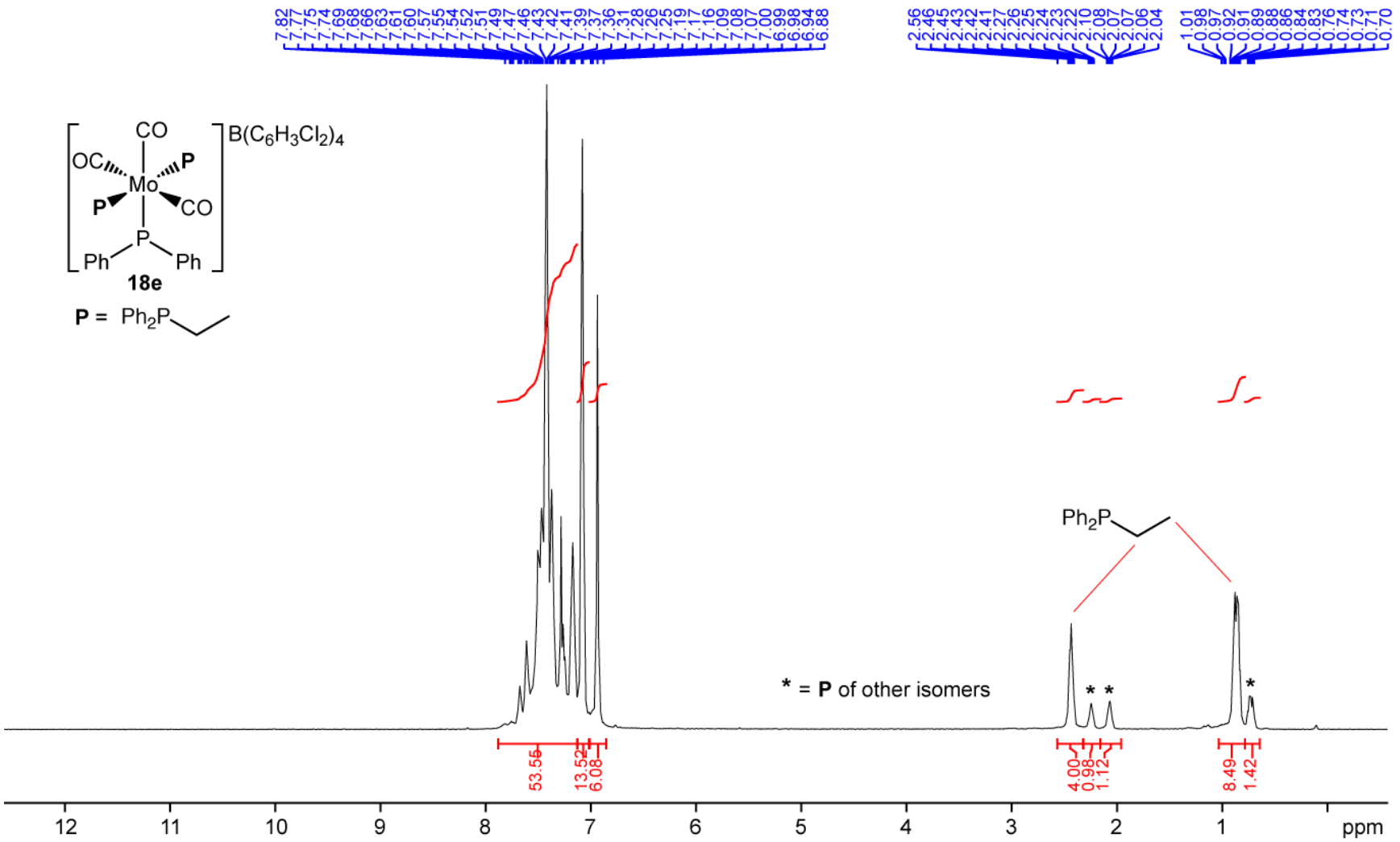

Figure G.1. ^{1}H NMR spectrum of [Mo(CO)$_3$(PPh$_2$)(Ph$_2$PCH$_2$CH$_3$)$_2$] (**18e**) (500.27 MHz, CDCl$_3$).

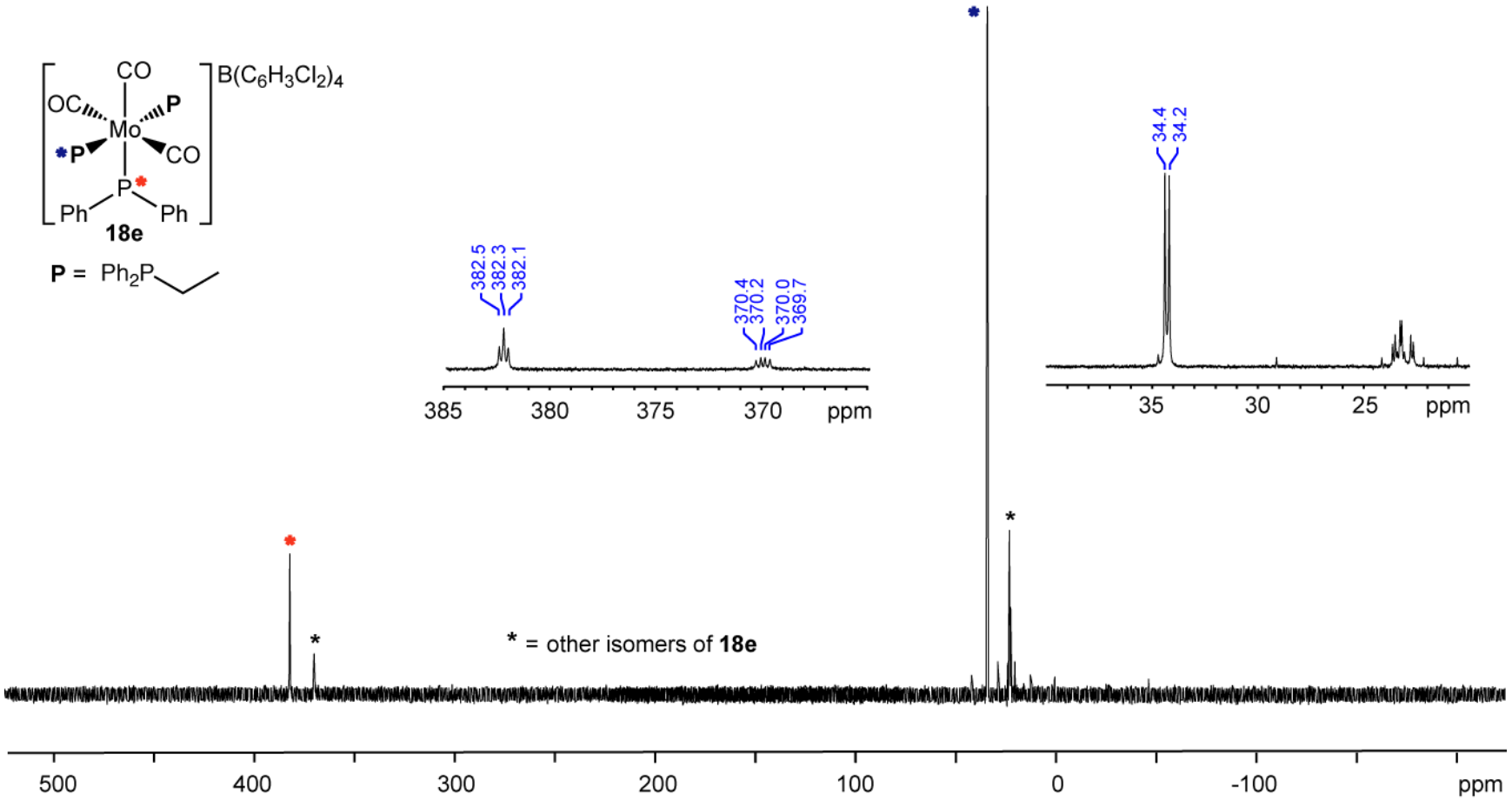

Figure G.2. $^{31}P\{^{1}H\}$ NMR spectrum of $[Mo(CO)_3(PPh_2)(Ph_2PCH_2CH_3)_2]$ (**18e**) (202.51 MHz, $CDCl_3$).

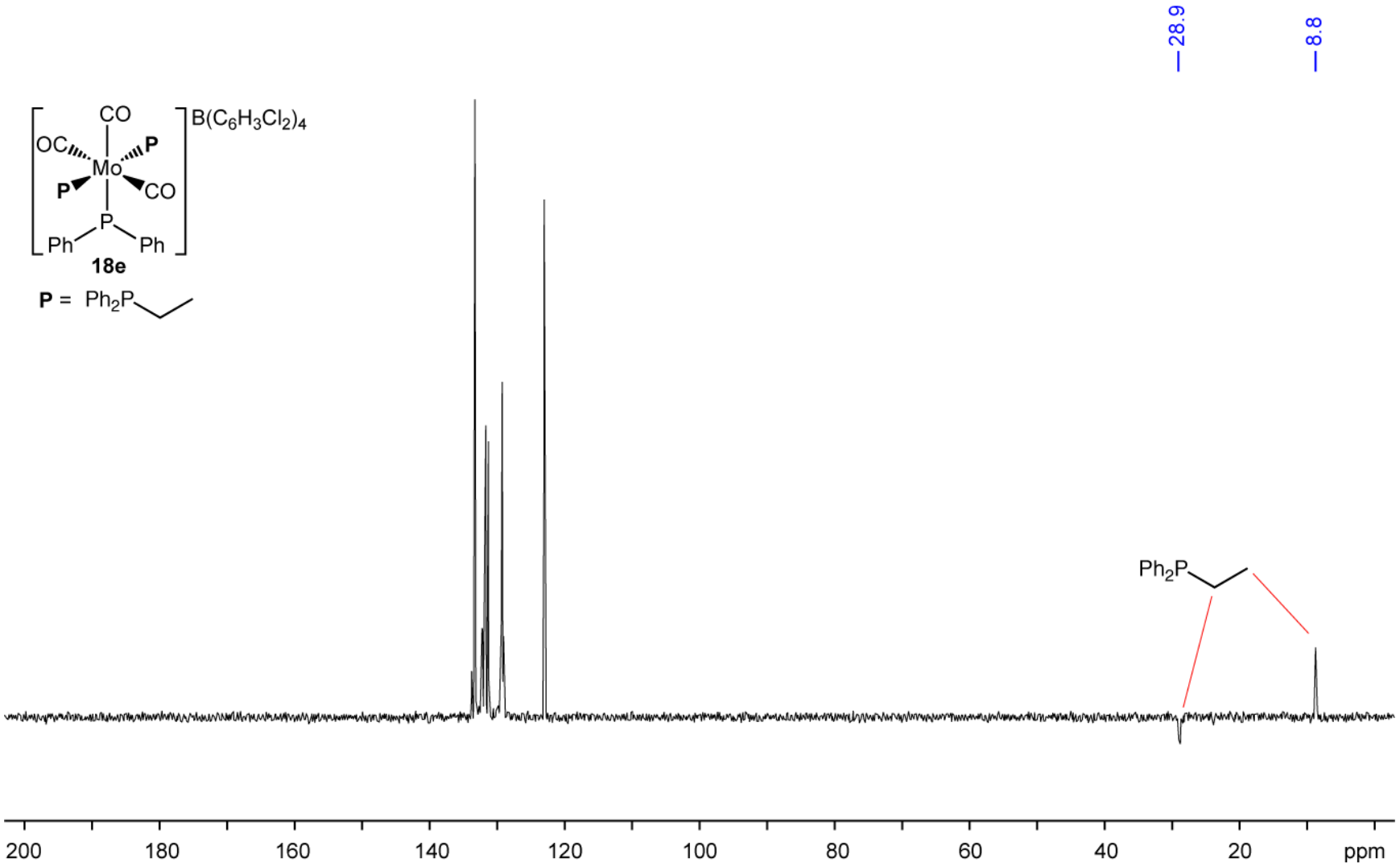

Figure G.3. $^{13}C\{^{1}H\}$ DEPT 135 NMR spectrum of $[Mo(CO)_3(PPh_2)(Ph_2PCH_2CH_3)_2]$ (**18e**) (125.79 MHz, $CDCl_3$).

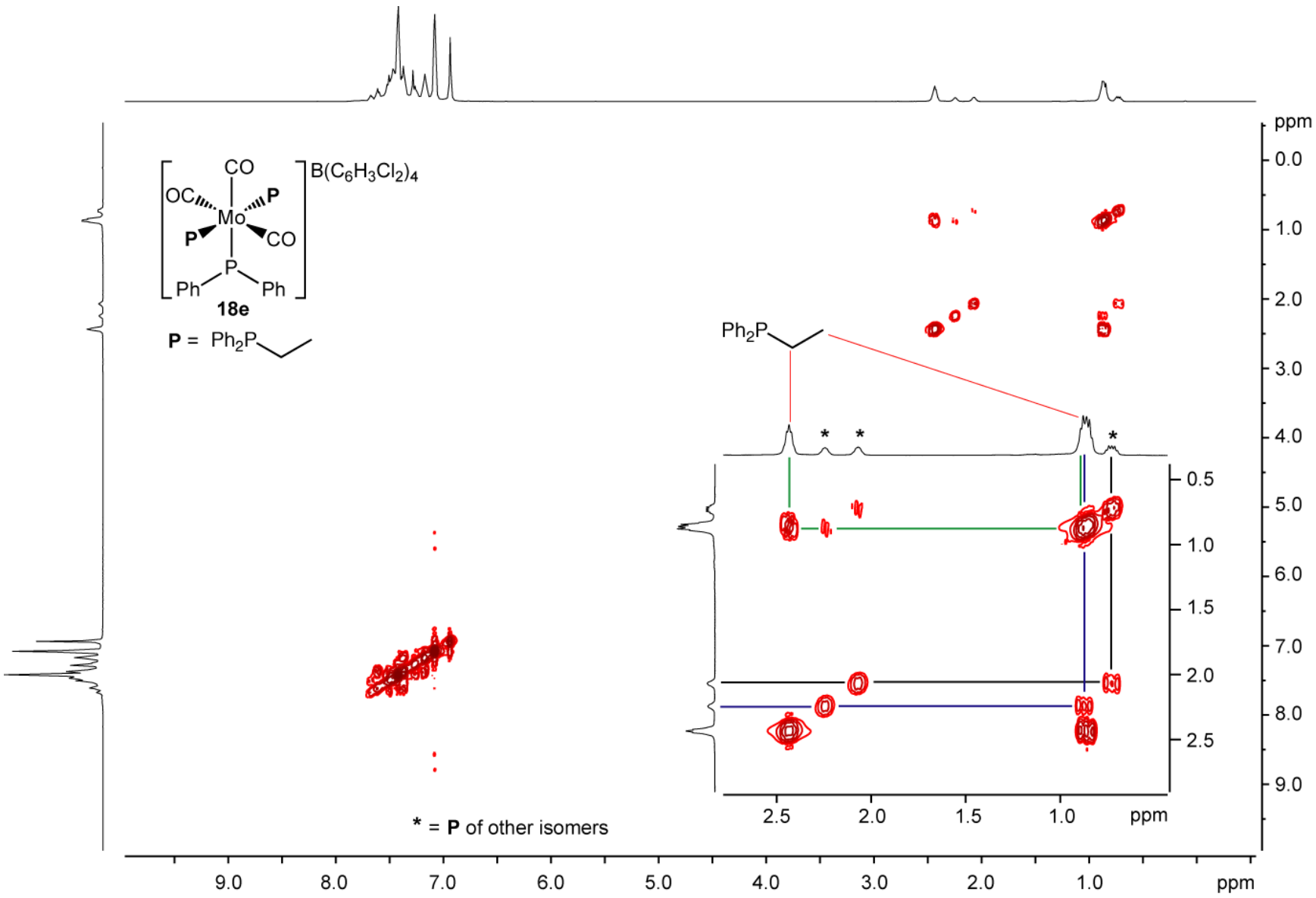

Figure G.4. ^{1}H-COSY NMR spectrum of $[Mo(CO)_3(PPh_2)(Ph_2PCH_2CH_3)_2]$ (**18e**) (500.27 MHz, $CDCl_3$).

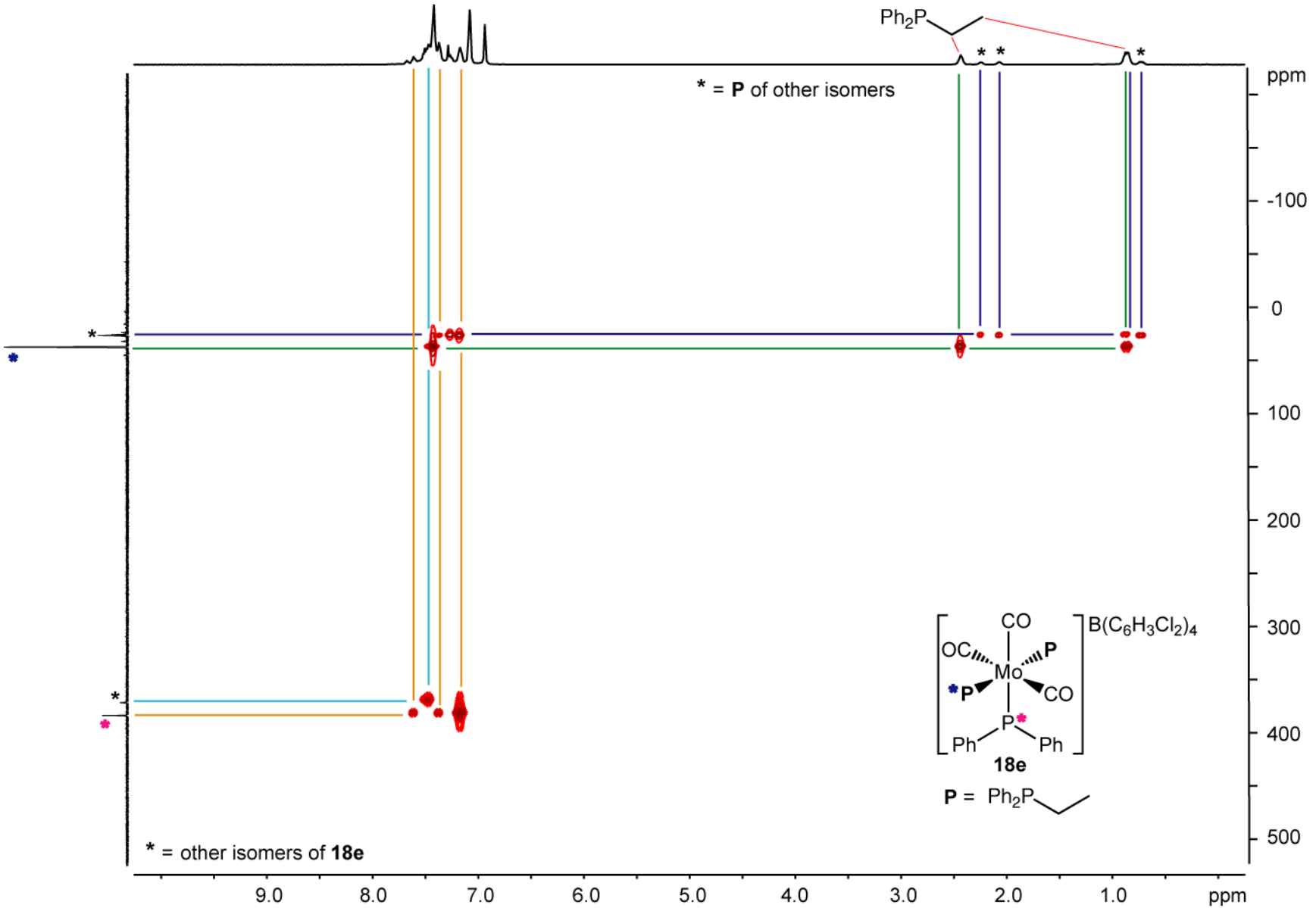

Figure G.5. $^{1}H/^{31}P\{^{1}H\}$-HMBC NMR spectrum of $[Mo(CO)_3(PPh_2)(Ph_2PCH_2CH_3)_2]$ (**18e**) (500.27 MHz, $CDCl_3$).

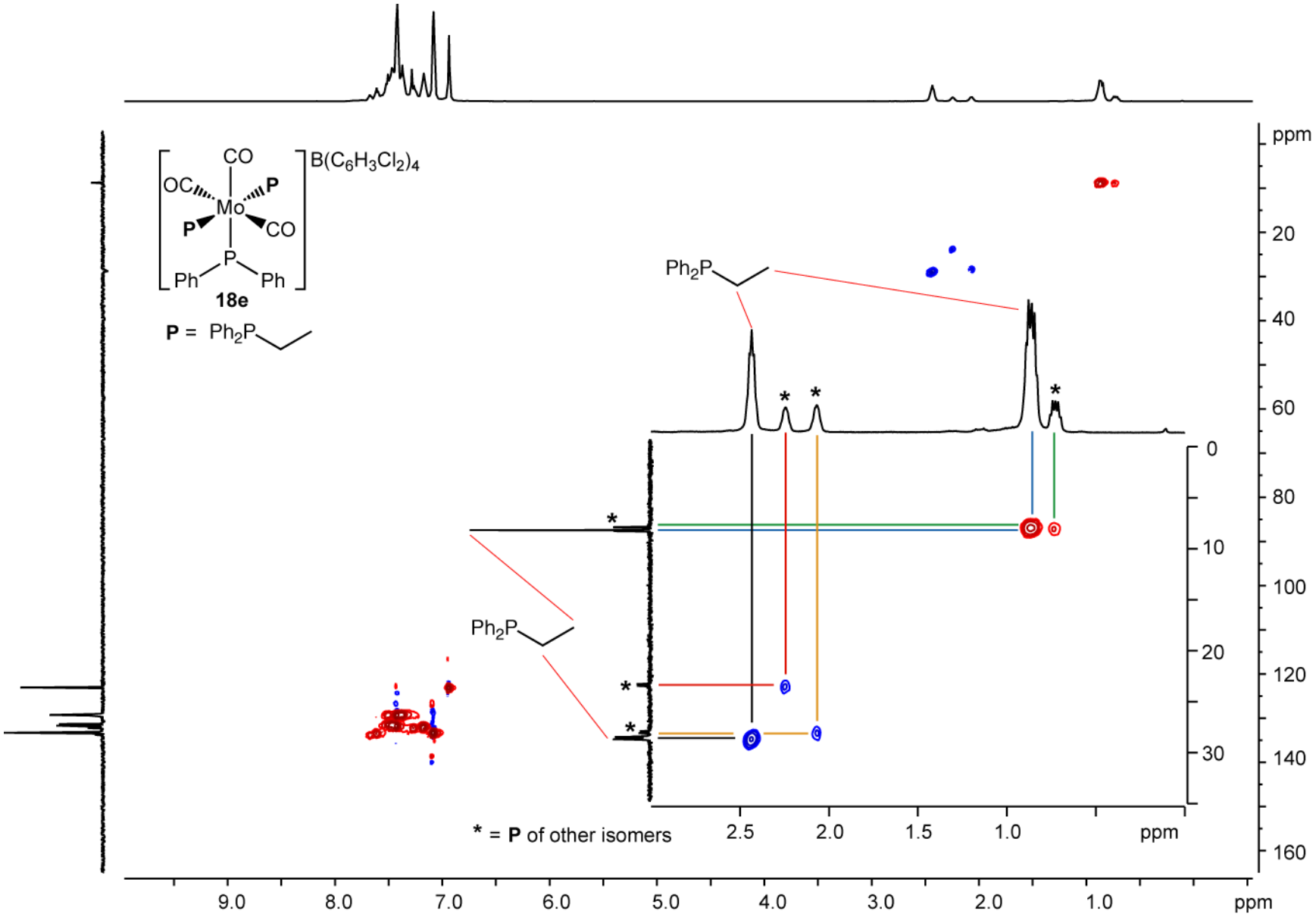

Figure G.6. $^{1}H/^{13}C\{^{1}H\}$-HSQC NMR spectrum of $[Mo(CO)_3(PPh_2)(Ph_2PCH_2CH_3)_2]$ (**18e**) (500.27 MHz, $CDCl_3$).

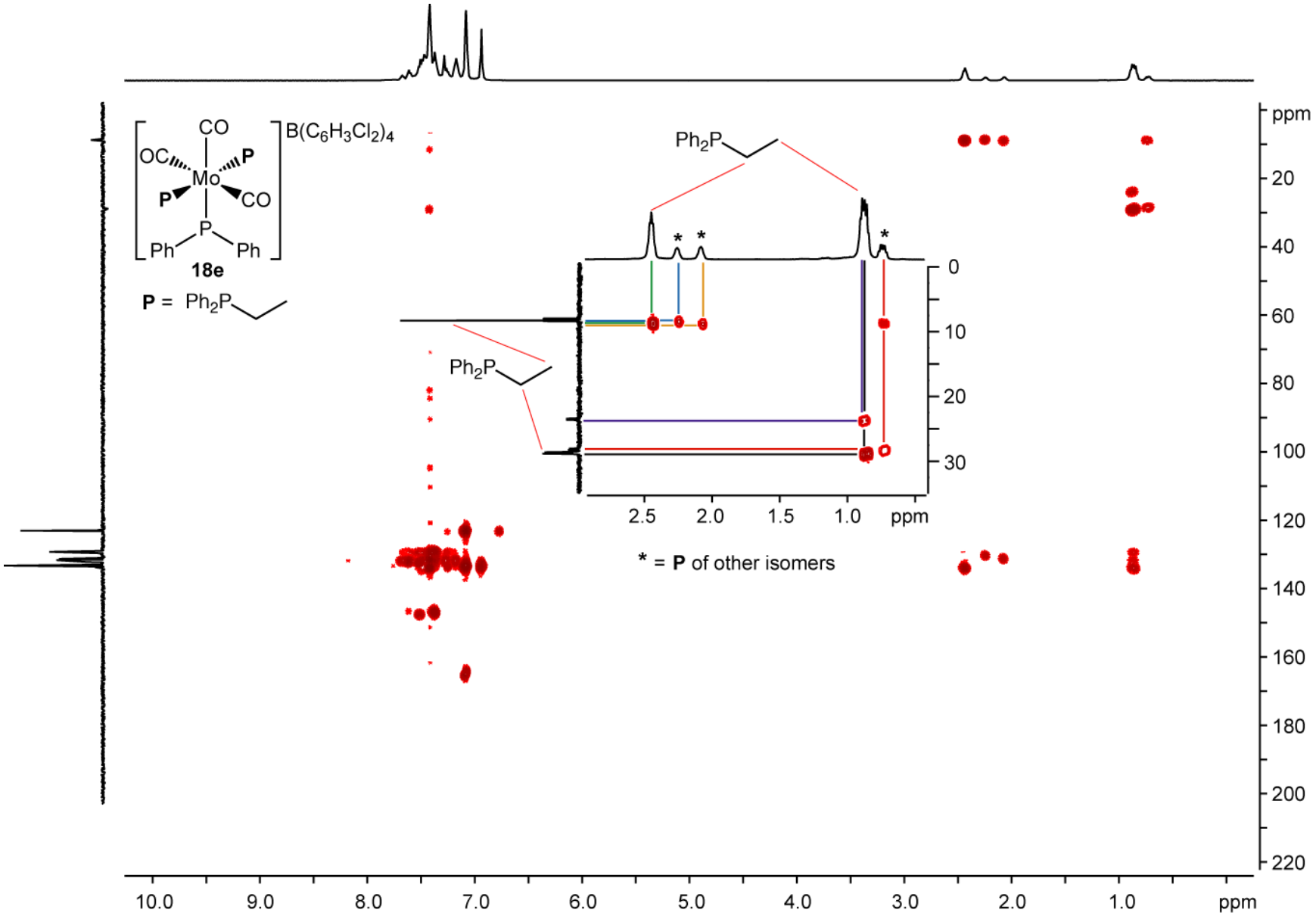

Figure G.7. $^{1}H/^{13}C\{^{1}H\}$-HMBC NMR spectrum of $[Mo(CO)_3(PPh_2)(Ph_2PCH_2CH_3)_2]$ (**18e**) (500.27 MHz, $CDCl_3$).

Appendix H $^{31}P\{^{1}H\}$ NMR Spectra of Experiments from Chapter 4

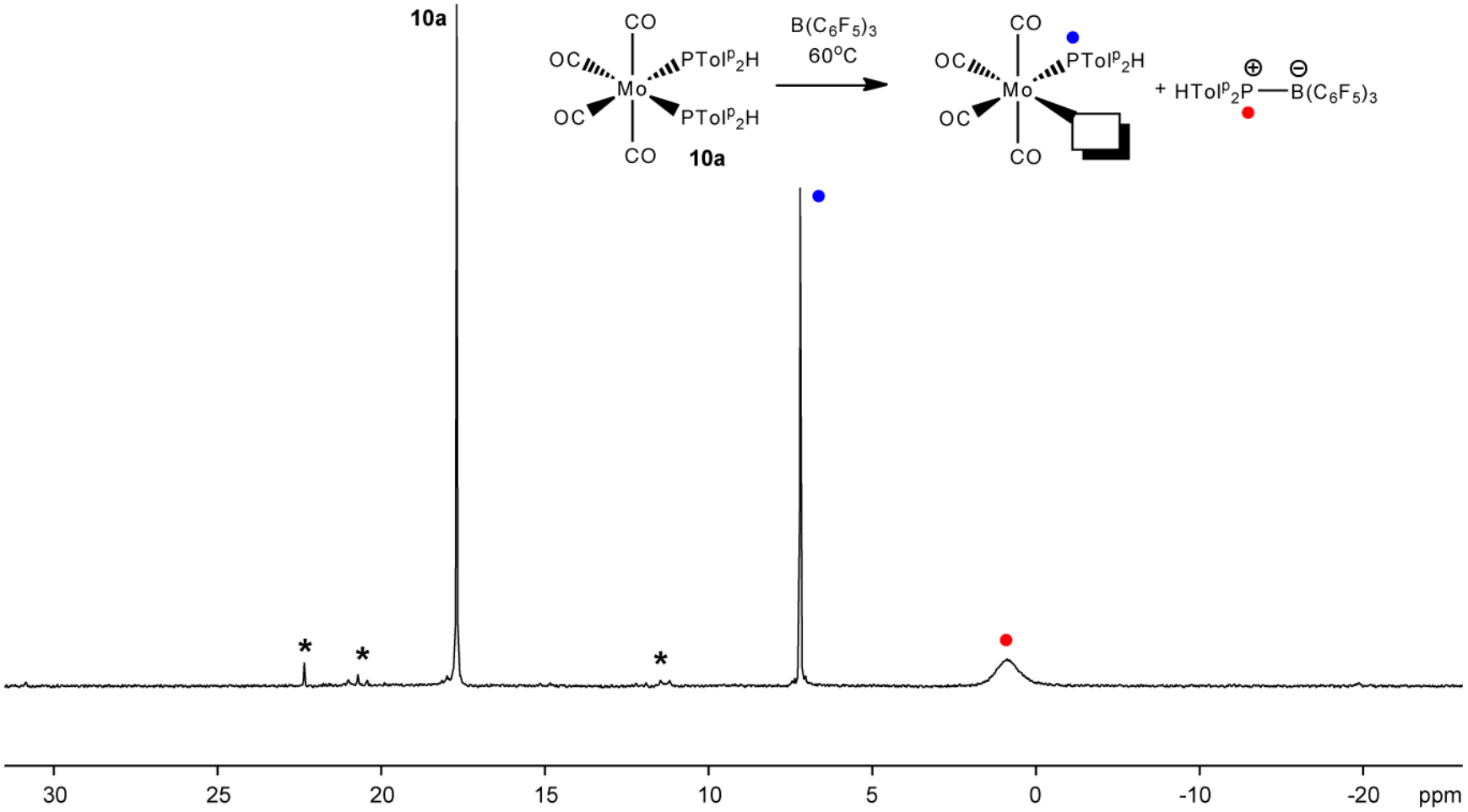

Figure H.1. $^{31}P\{^{1}H\}$ NMR spectrum (202.51 MHz, CD_2Cl_2) from the addition of $B(C_6F_5)_3$ to *trans*-**12a**[$B(C_6H_3Cl_2)_4$]. Reaction was heated at 60°C for 1 h. Unassigned peak labelled (*).

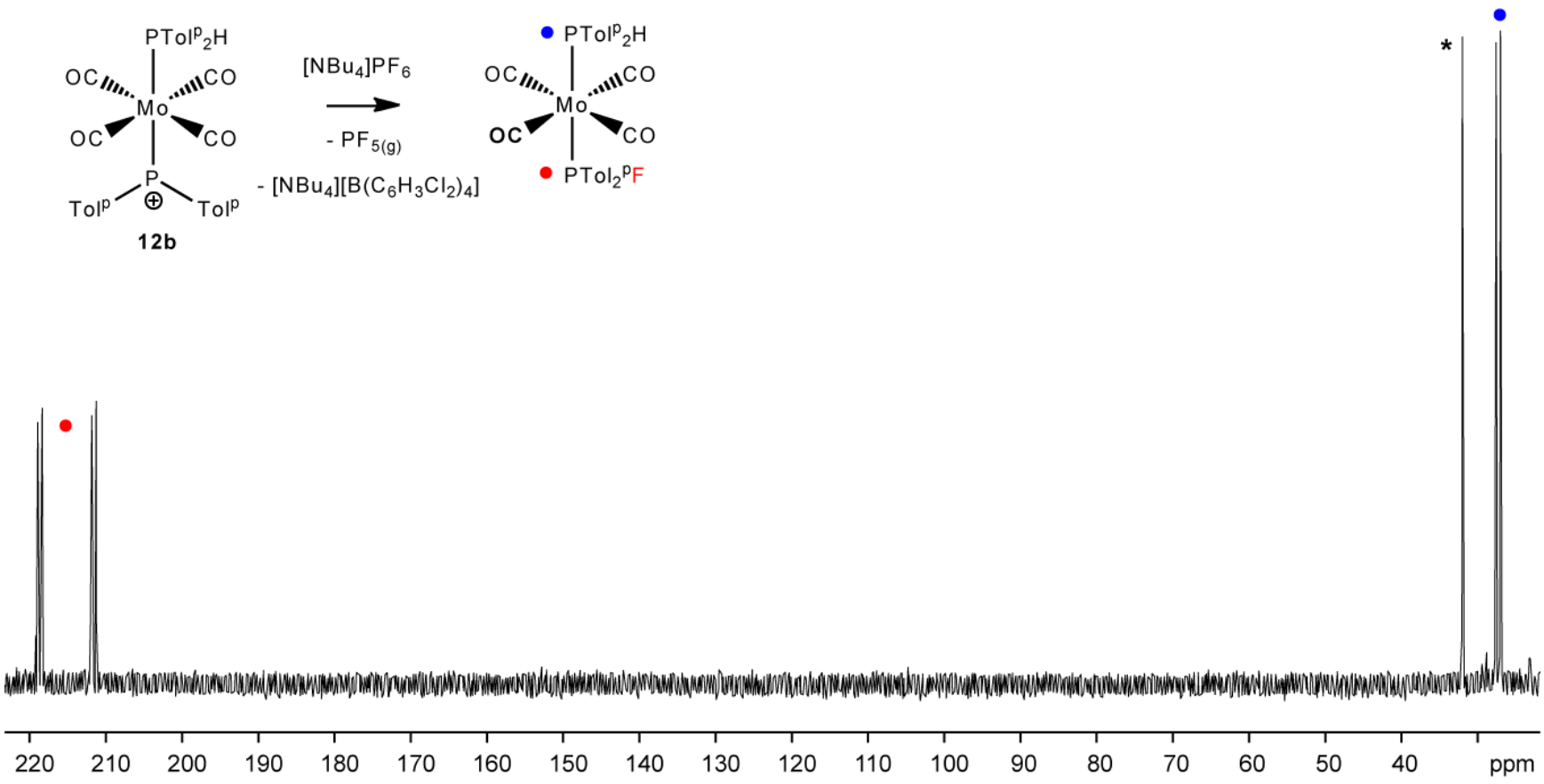

Figure H.2. $^{31}P\{^{1}H\}$ NMR spectrum (202.51 MHz, CD_2Cl_2) from the addition of [NBu$^n_4$][PF_6] to *trans*-**12a**[$B(C_6H_3Cl_2)_4$]. Unassigned peak labelled (*).

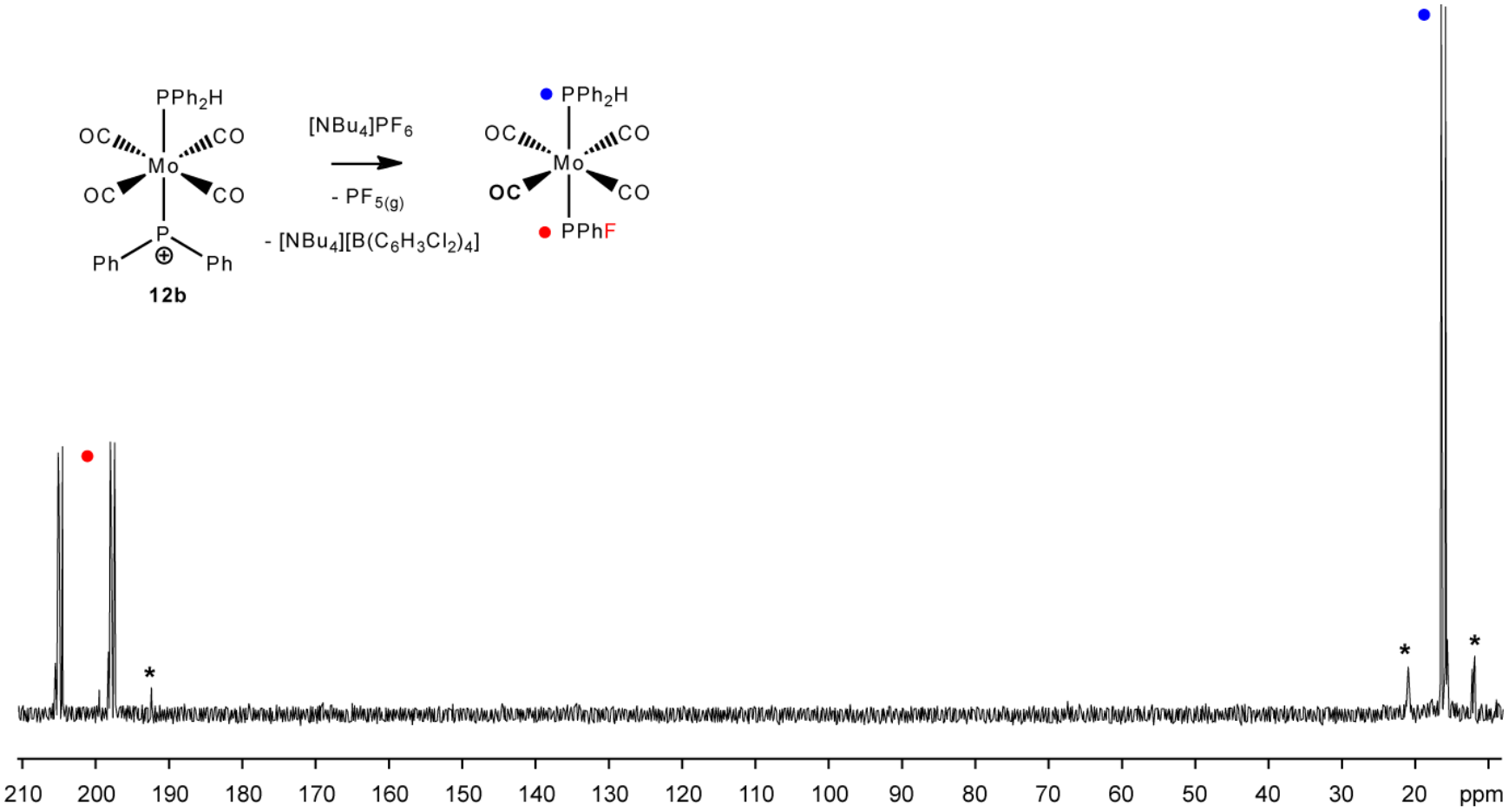

Figure H.3. $^{31}P\{^{1}H\}$ NMR spectrum (202.51 MHz, CD_2Cl_2) from the addition of $[NBu^n_4][PF_6]$ to *trans*-**12a**$[B(C_6H_3Cl_2)_4]$. Unassigned peaks are labelled (*).

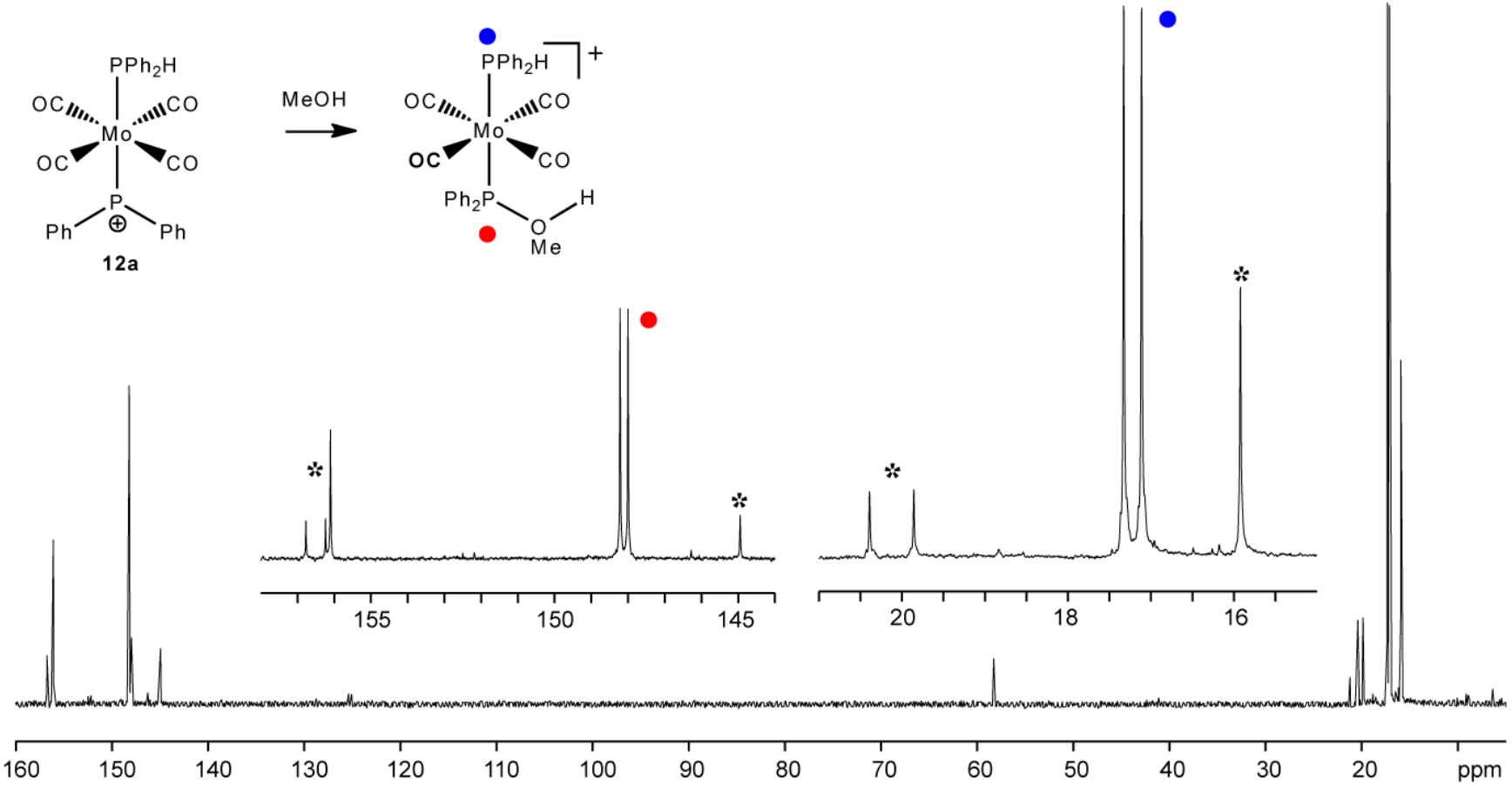

Figure H.4. $^{31}P\{^{1}H\}$ NMR spectrum (202.51 MHz, CD_2Cl_2) from the addition of methanol (MeOH) to *trans*-**12b**$[B(C_6H_3Cl_2)_4]$. Unassigned peaks are labelled (*).

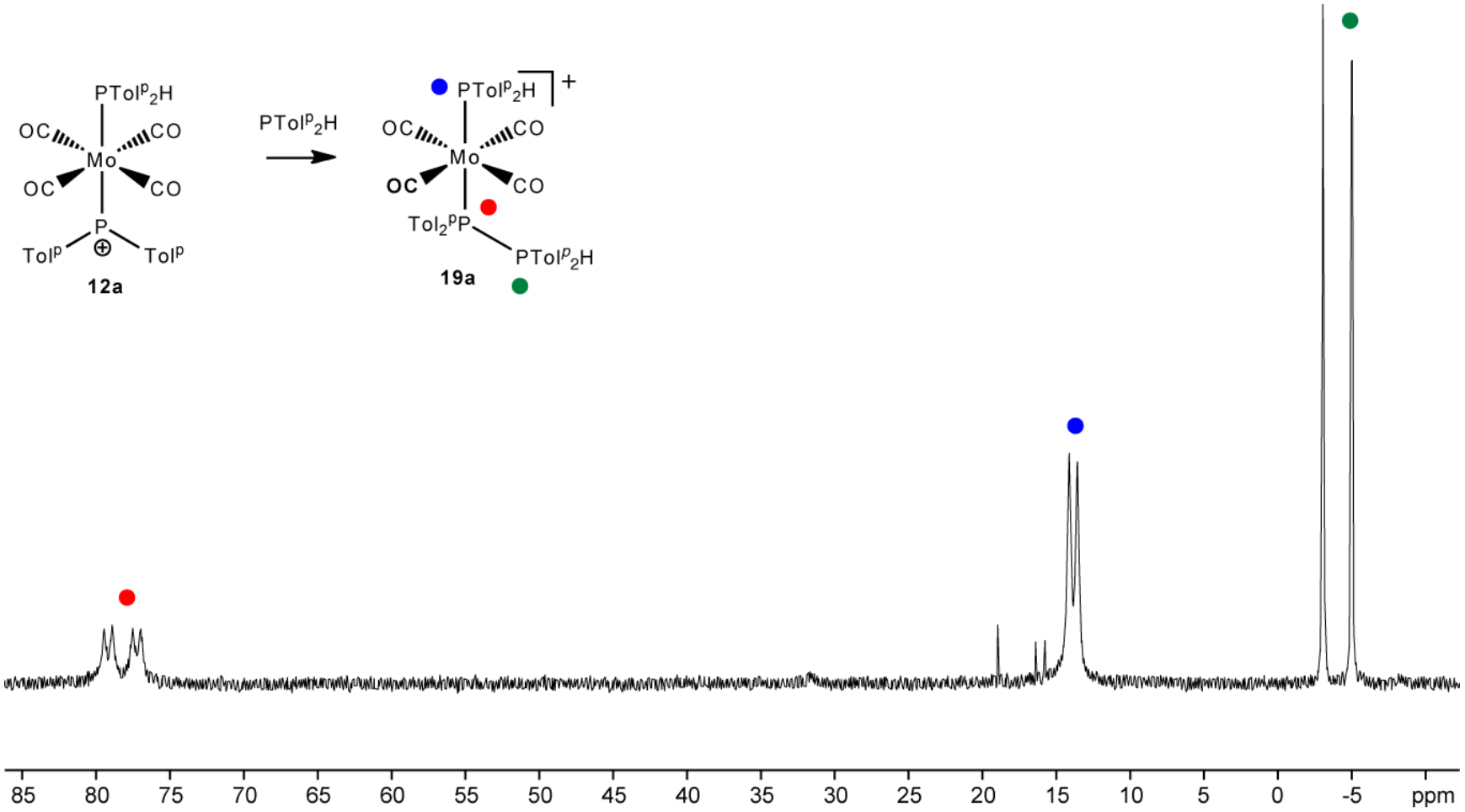

Figure H.5. $^{31}P\{^{1}H\}$ NMR spectrum (202.51 MHz, CD_2Cl_2) from the addition of one equiv of PTol$^p_2$H to *trans*-**12a**[$B(C_6H_3Cl_2)_4$].

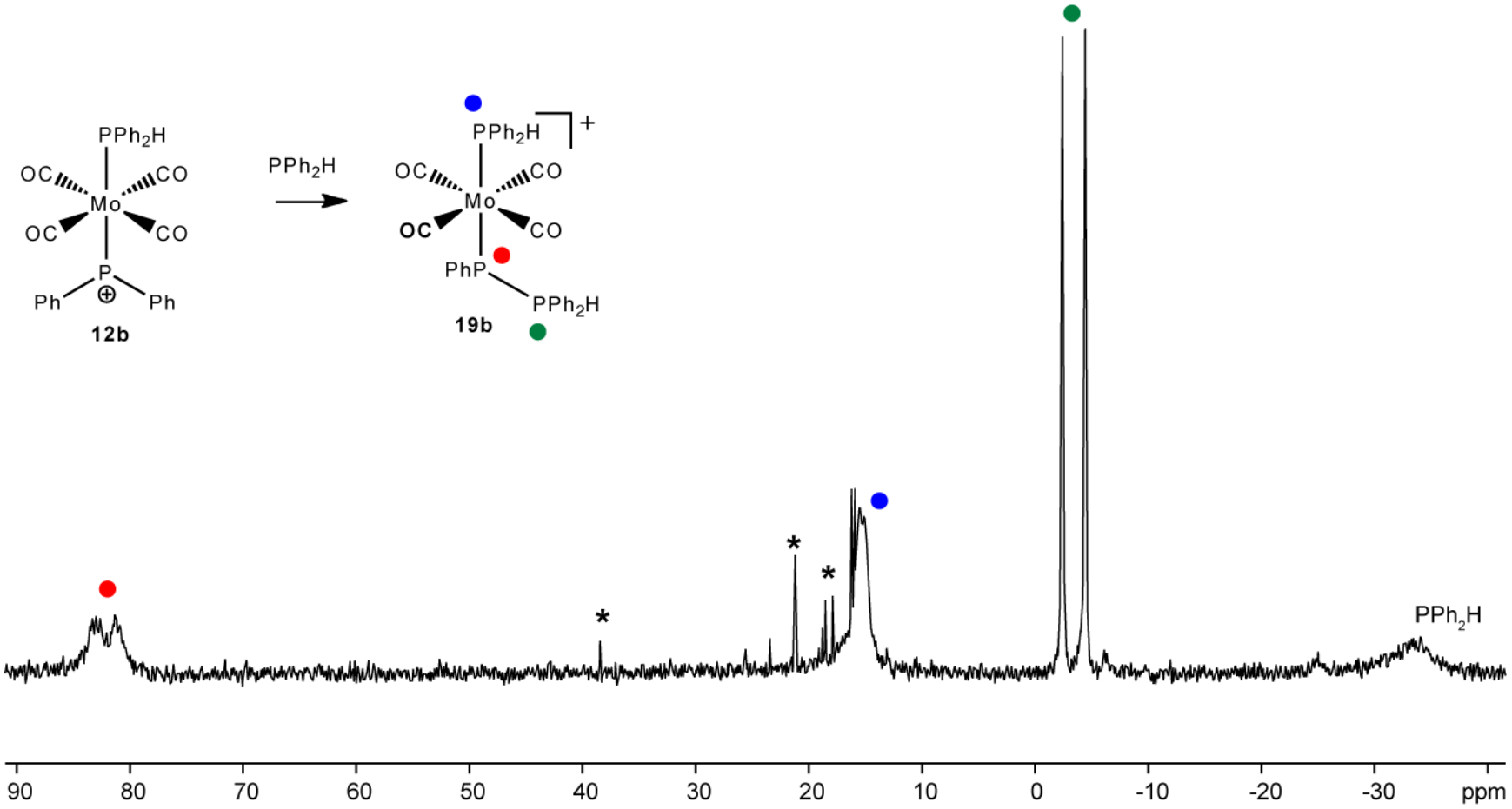

Figure H.6. $^{31}P\{^{1}H\}$ NMR spectrum (202.51 MHz, CD_2Cl_2) from the addition of one equiv of PPh_2H to *trans*-**12b**$[B(C_6H_3Cl_2)_4]$. Unassigned peaks are labelled (*).

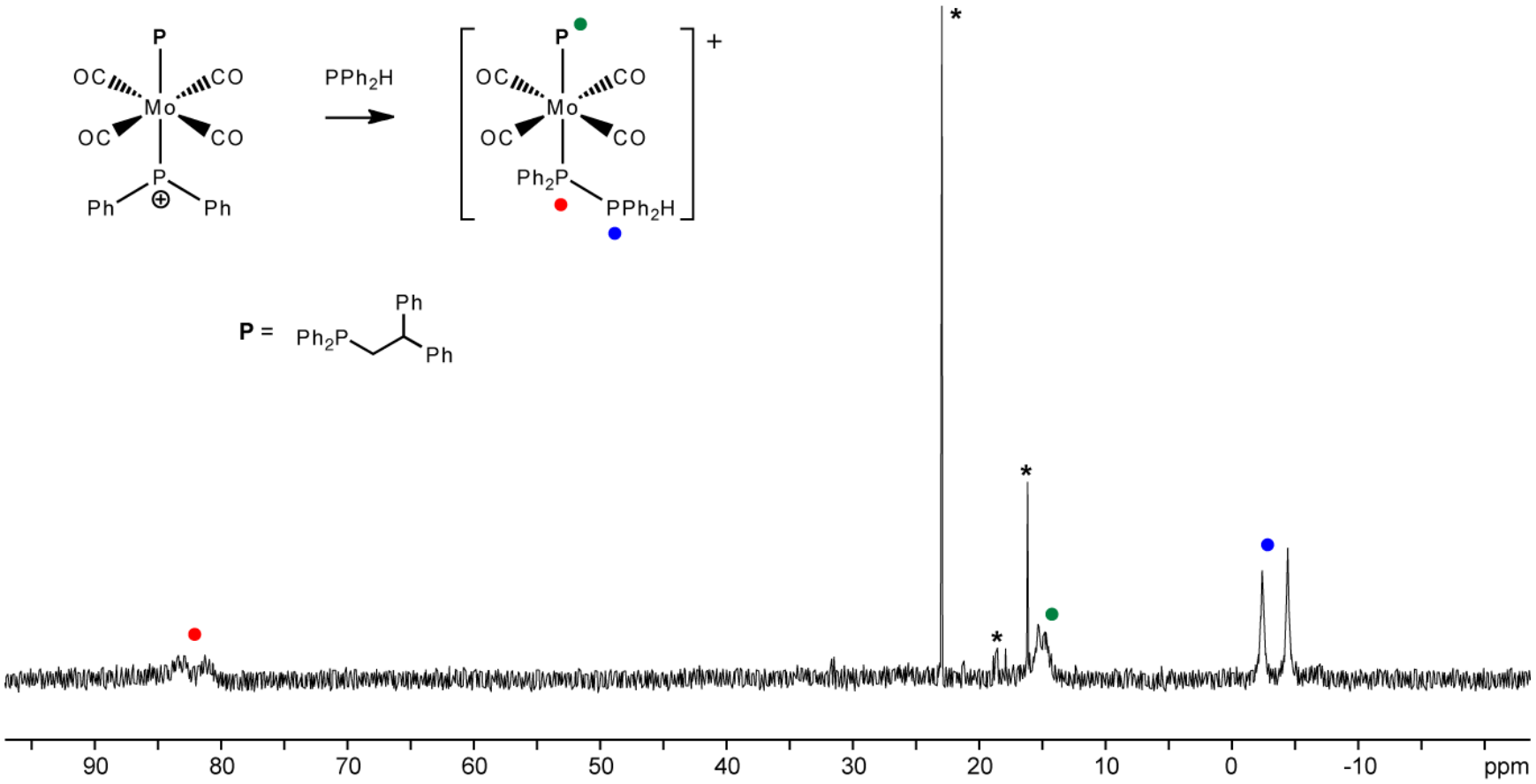

Figure H.7. $^{31}P\{^{1}H\}$ NMR spectrum (202.51 MHz, CD_2Cl_2) from the addition of one equiv of PPh_2H to *trans*-$Mo(CO)_4$(**P**)(PPh_2) (**P** = $P(CH_2CHPh_2)Ph_2$) (*trans*-**14b)**, which was generated in situ from the additions of 1,1-diphenylethylene to *trans*-**12b**. Unassigned peaks are labelled (*).

Appendix I ^{1}H and $^{31}P\{^{1}H\}$ NMR Spectra of Experiments from Chapter 5

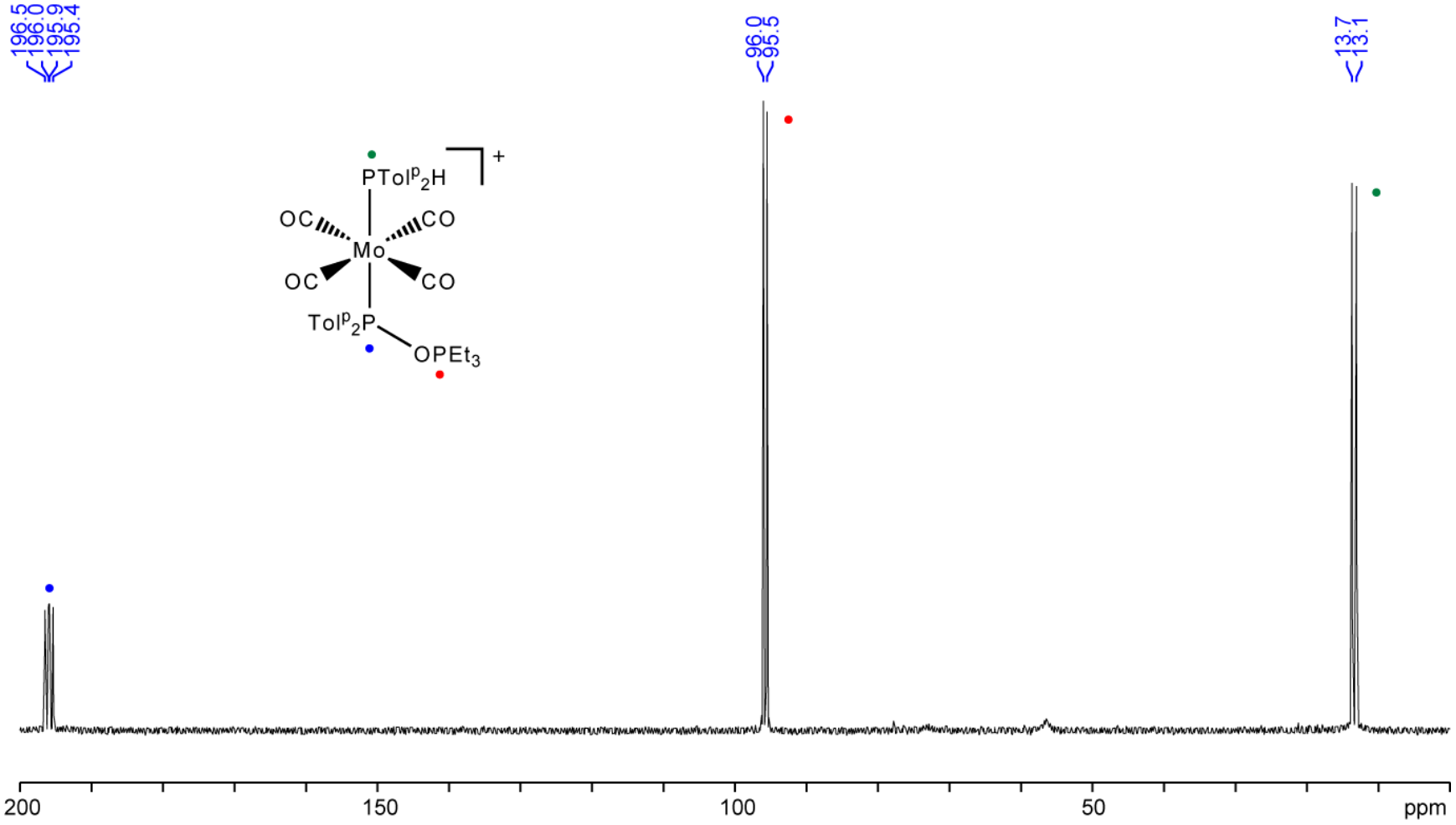

Figure I.1. $^{31}P\{^{1}H\}$ NMR spectrum (202.51 MHz, CD_2Cl_2) from the Gutmann-Beckett Lewis Acidity test on *trans*-**12a**[$B(C_6H_3Cl_2)_4$].

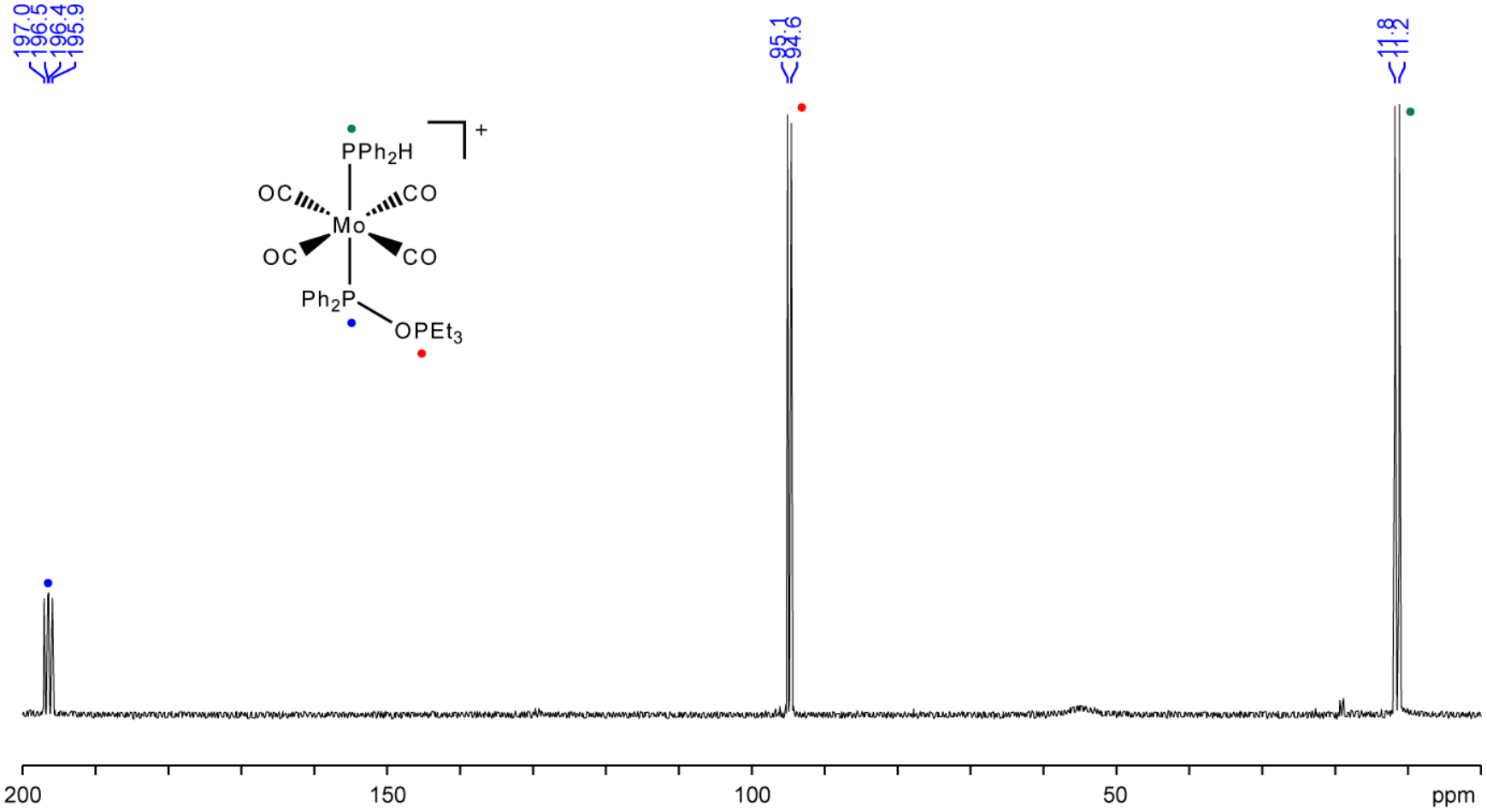

Figure I.2. $^{31}P\{^{1}H\}$ NMR spectrum (202.51 MHz, CD_2Cl_2) from the Gutmann-Beckett Lewis Acidity test on *trans*-**12b**[$B(C_6H_3Cl_2)_4$].

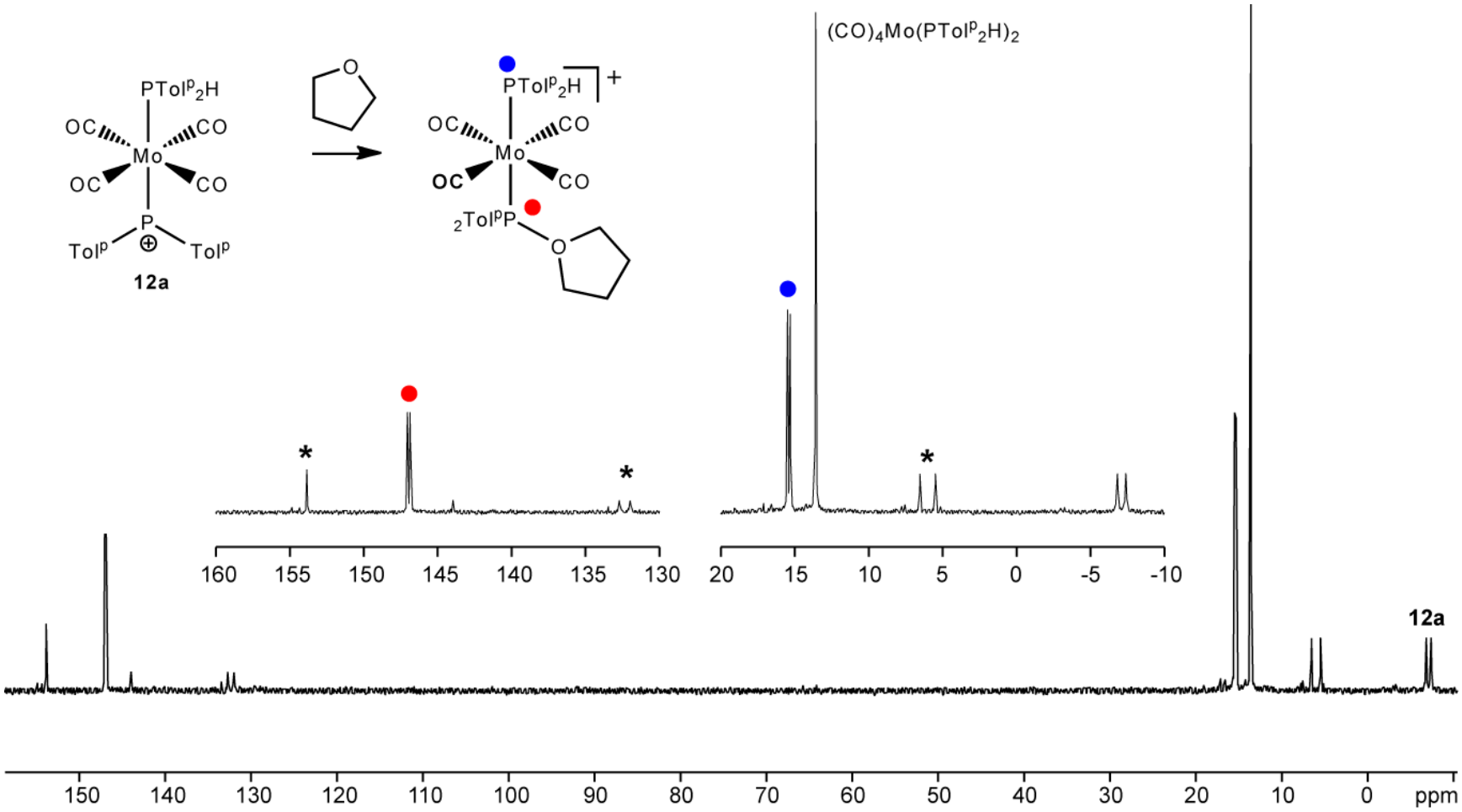

Figure I.3. $^{31}P\{^1H\}$ NMR spectrum (202.51 MHz, CD_2Cl_2) from the addition of tetrahydrofuran to *trans*-**12a**[$B(C_6H_3Cl_2)_4$].

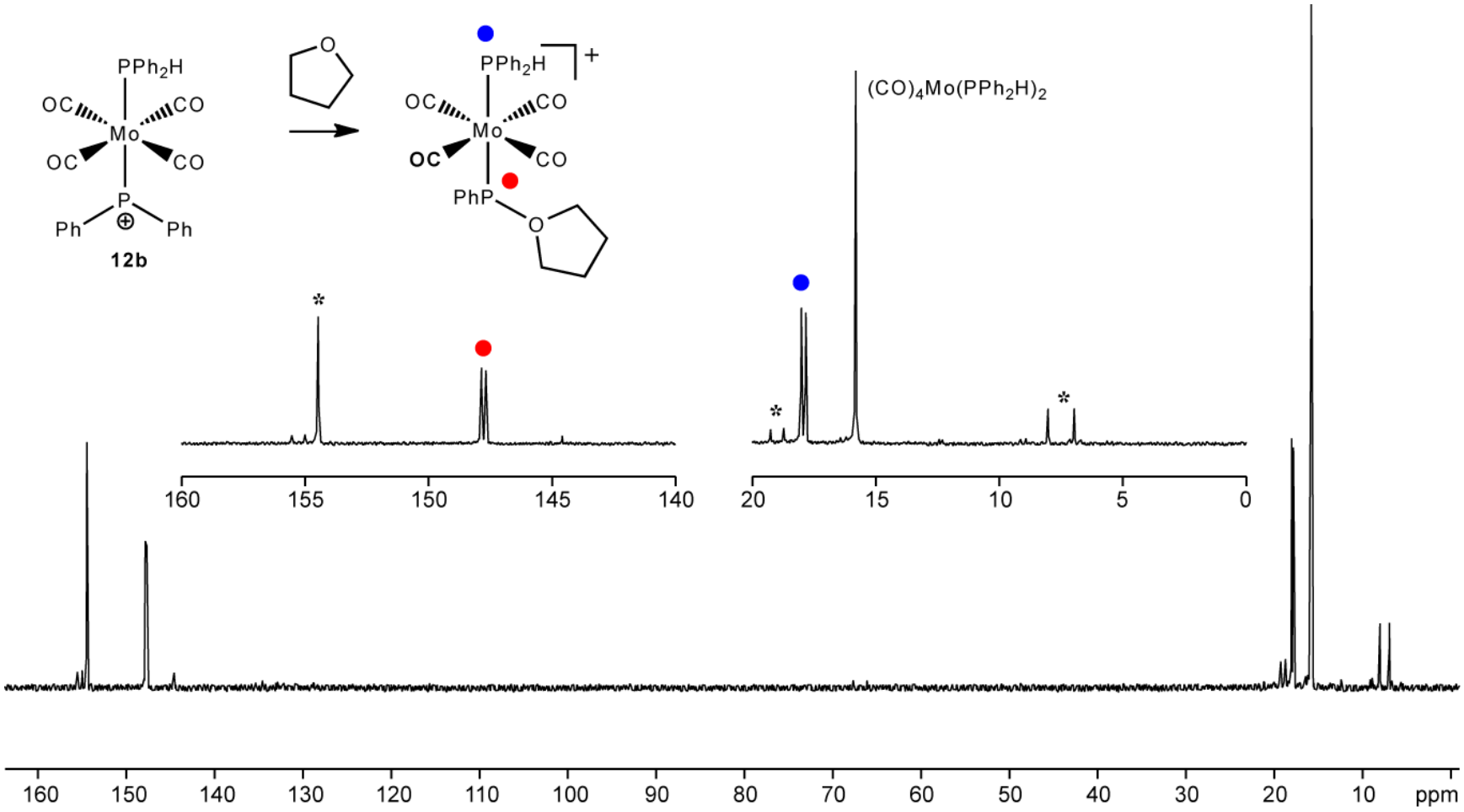

Figure I.4. $^{31}P\{^{1}H\}$ NMR spectrum (202.51 MHz, CD_2Cl_2) from the addition of tetrahydrofurn to *trans*-**12b**[$B(C_6H_3Cl_2)_4$].

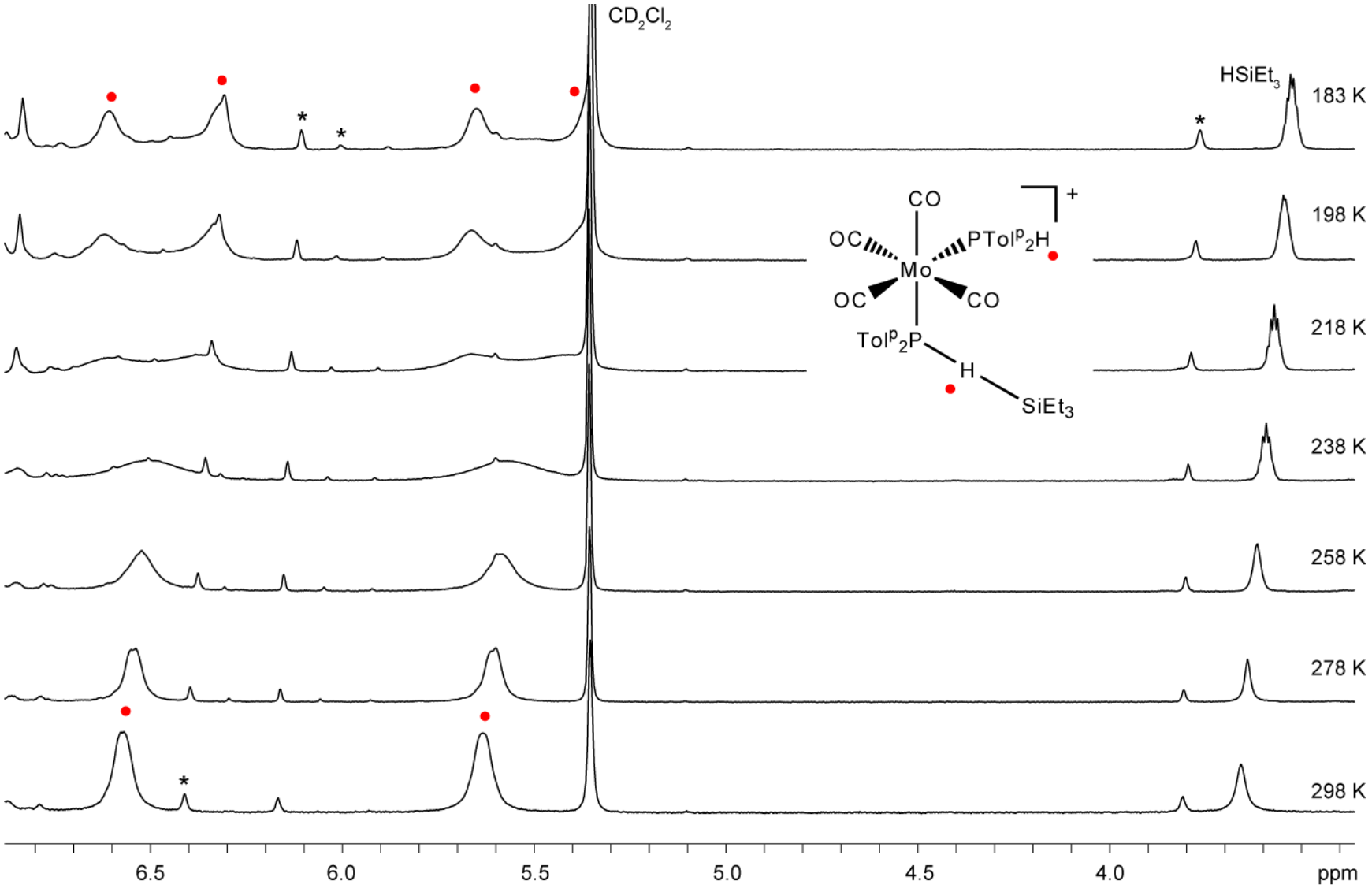

Figure I.5. ^{1}H NMR spectra (360.29 MHz, CD_2Cl_2) from the low temperature VT NMR experiment used to examine the interaction of **12a** with $HSiEt_3$. Two equiv of $HSiEt_3$ were used. Unassigned peaks are labelled (*). Stacked spectra show the decoalescence of the resonance assigned as P-*H* to give two distinct P-*H*.

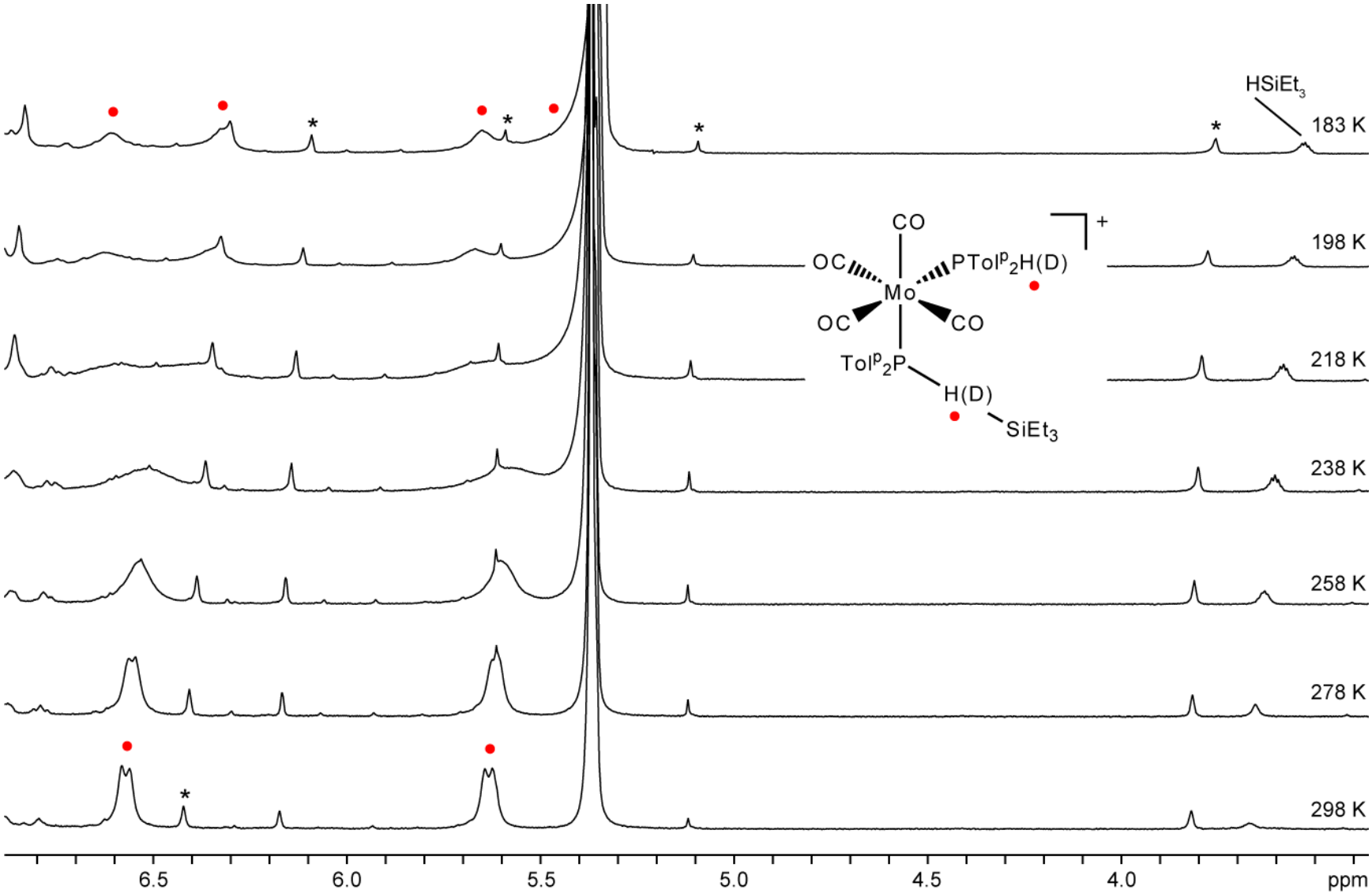

Figure I.6. ^{1}H NMR spectra (360.29 MHz, CD_2Cl_2) the from the low temperature VT NMR experiment used to examine the interaction of **12a** with $HSiEt_3$. Two equiv of $DSiEt_3$ were used. Unassigned peaks are labelled (*). Stacked spectra show the decoalescence of the resonance assigned as P-*H* to give two distinct P-*H*.

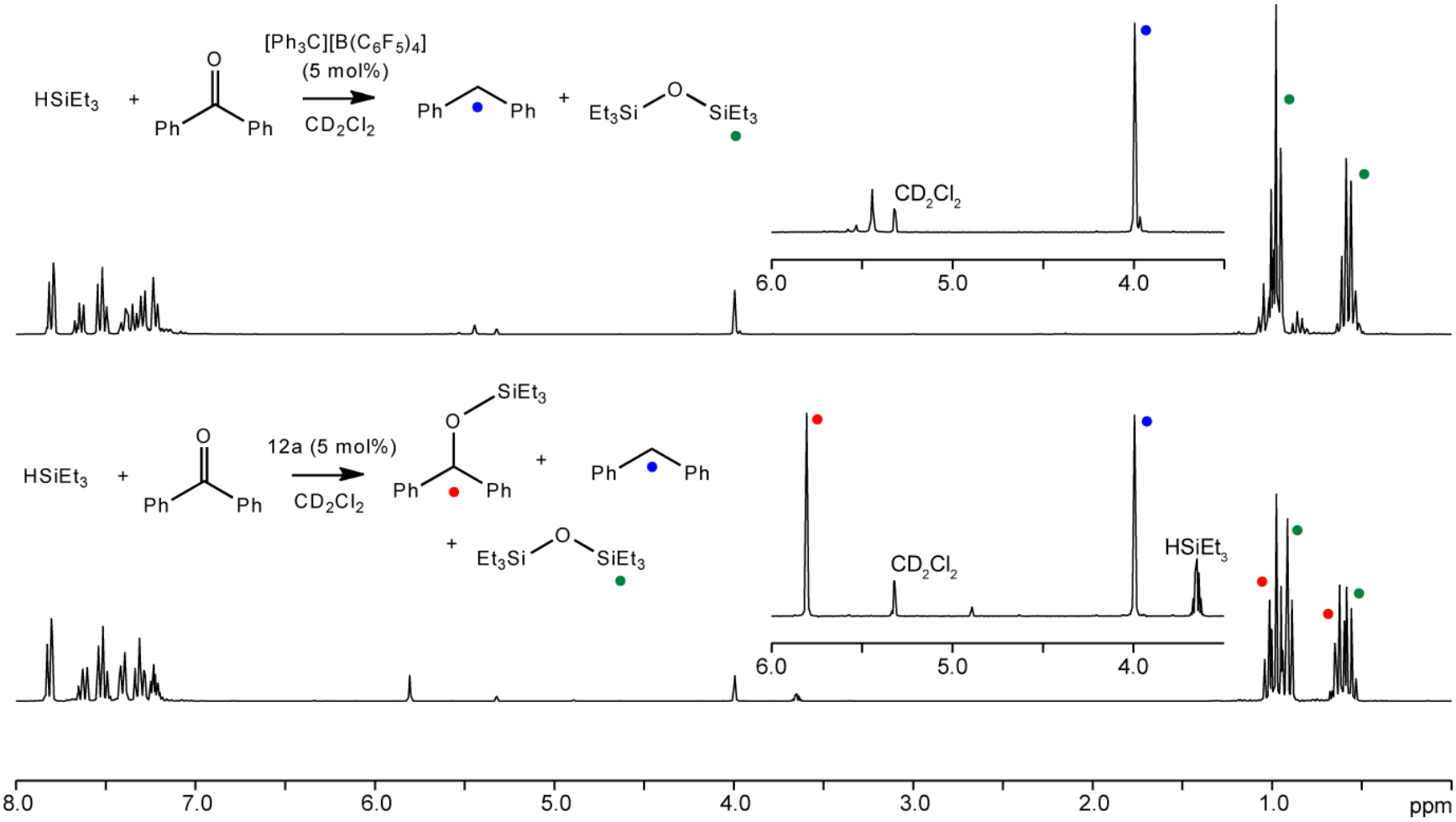

Figure I.7. ^{1}H NMR spectra (500.27 MHz, CD_2Cl_2) of the hydrosilylation of benzophenone with $HSiEt_3$ initiated by $[Ph_3C]\{B(C_6F_5)_4\}]$ (top) and catalyzed by *trans*-**12b**$[B(C_6H_3Cl_2)_4]$ (bottom). Trityl-initiated hydrosilylation results in exclusive deoxygenation of benzophenone. Hydrosilylation catalyzed by *trans*-**12b**$[B(C_6H_3Cl_2)_4]$ results in partial deoxygenation of benzophenone.